Insights into vitamin B_{12} production, acquisition, and use by marine microbes

By

Erin Marie Bertrand
B.S., Bates College, 2005

Submitted in partial fulfillment of the requirements for the degree of
Doctor of Philosophy
at the
MASSACHUSETTS INSTITUTE OF TECHNOLOGY
and the
WOODS HOLE OCEANOGRAPHIC INSTITUTION

February 2012

Signature of Author_____
Joint Program in Oceanography
Massachusetts Institute of Technology
and Woods Hole Oceanographic Institution
(September 21, 2011)

Certified by_____
Dr. Mak A. Saito
Thesis Supervisor

Accepted by_____
Dr. Roger Summons
Chair, Joint Committee for Chemical Oceanography
Woods Hole Oceanographic Institution

Insights into vitamin B_{12} production, use, and acquisition by marine microbes

by

Erin Marie Bertrand

Submitted to the Department of Marine Chemistry and Geochemistry,
Massachusetts Institute of Technology- Woods Hole Oceanographic Institution
Joint Program in Chemical Oceanography on September 21, 2011
In partial fulfillment of the requirements for the degree of
Doctor of Philosophy

Abstract

The distribution and magnitude of marine primary production helps determine the ocean's role in global carbon cycling. Constraining factors that impact this productivity and elucidating selective pressures that drive the composition of marine microbial communities are thus essential aspects of marine biogeochemistry. Vitamin B_{12}, also known as cobalamin, is a cobalt containing organometallic micronutrient produced by some bacteria and archaea and required by many eukaryotic phytoplankton for methionine biosynthesis and regeneration. Although the potential for vitamin B_{12} availability to impact primary production and phytoplankton species composition has long been recognized, the lack of molecular-level tools for studying B_{12} production, use and acquisition has limited inquiry into the role of the vitamin in marine biogeochemical processes. This thesis describes the development of such tools and implements them for the study of B_{12} dynamics in an Antarctic shelf ecosystem.

Nucleic acid probes for B_{12} biosynthesis genes were designed and used to identify a potentially dominant group of B_{12} producers in the Ross Sea. The activity of this group was then verified by mass spectrometry-based peptide measurements. Then, possible interconnections between iron and B_{12} dynamics in this region were identified using field-based bottle incubation experiments and vitamin uptake measurements, showing that iron availability may impact both B_{12} production and consumption. Changes in diatom proteomes induced by low B_{12} and low iron availability were then examined and used to identify a novel B_{12} acquisition protein, CBA1, in diatoms. This represents the first identification of a B_{12} acquisition protein in eukaryotic phytoplankton. Transcripts encoding CBA1 were detected in natural phytoplankton communities, confirming that B_{12} acquisition is an important part of phytoplankton molecular physiology. Selected reaction monitoring mass spectrometry was used to measure the abundance of CBA1 and methionine synthase proteins in diatoms cultures, revealing distinct protein abundance patterns as a function of B_{12} availability. These peptide measurements were implemented to quantify methionine synthase proteins in McMurdo Sound, revealing that there is both B_{12} utilization and starvation in natural diatom communities and that these peptide measurements hold promise for revealing the metabolic status of marine ecosystems with respect to vitamin B_{12}.

Thesis Supervisor: Mak A. Saito
Title: Associate Scientist, Woods Hole Oceanographic Institution

Acknowledgments

The work described in this thesis was supported by a National Science Foundation (NSF) Graduate Research Fellowship (2007037200) and an Environmental Protection Agency STAR Fellowship (F6E20324), the WHOI Ocean Life Institute, the WHOI Ocean Ventures Fund, the MIT Houghton Fund, NSF awards ANT 0732665, OCE 0752291, OPP 0440840, OCE 0327225, OCE 0452883, OCE 0723667, OCE 1031271, and OCE 0928414, the Center for Environmental Bioinorganic Chemistry at Princeton, the Center for Microbial Oceanography: Research and Education (CMORE), the Australian Research Council and the Gordon and Betty Moore Foundation.

I am tremendously grateful for the time I've spent working with and learning from my advisor Mak Saito. Mak has encouraged and supported me at every step. His quiet expectations made me believe that I could become a good scientist and made me feel like my aspirations were worth having. His positive, patient leadership, particularly at sea and on the ice, are an inspiration. Mak has taught me a great deal about bridging disciplines, both philosophically and practicality.

It has been a privilege to work with the other members of the Saito Lab. Thanks to Dawn Moran for all her help and support along the way. I have learned a great deal from Dawn's careful technique, which lent itself so well to trace metal biogeochemistry whether she likes it or not. I thank Abigial Noble for being a great labmate and cohort member and for helping me to grow as a person and as a scientist. I am also indebted to Anne Thompson, Tyler Goepfert and Alysia Cox for assistance along the way, and particularly to Matt McIlvin for his assistance with mass spectrometry during my final data gathering push. I am grateful to have had the opportunity to learn from the late Vladimir Bulygin. In your memory Vlad, I will always try to read, think, and *then* do the experiment.

I am indebted to Andy Allen for lots of helpful advice along the way, for support in the field, and for his patience with my often ignorant questions. I am also grateful for help and advice from Ben Van Mooy. I owe thanks to Sonya Dyhrman for helpful discussions and insights, particularly when it came to the about the value of nutrient limitation biomarkers. I am indebted to Dianne Newman for her practical and insightful advice along the way and I am grateful that Cathy Drennan opened her doors to me and my project; her advice and direction have been invaluable.

Rachel Narehood Austin remains a trusted mentor and friend. I thank her for all the advice and encouragement she has provided me with over the past nine years and particularly for helping me find my passion in molecular environmental research.

I am privileged to have been a student at WHOI, where staff and scientists have open doors and are excited to help students wherever they can. I particularly need to thank Liz Kujawinski and Karen Casciotti for their willingness to answer my questions and provide advice along the way. Van Mooy lab members, particularly Helen Fredricks, have been tremendously

helpful with mass spectrometry questions and coordination. I thank John Waterbury, Freddy Valois, Tracy Mincer, Carl Lamborg, Dan Repeta and their labs for making Watson 1st floor a fantastic place to work. The administrative professionals I have worked with at WHOI, including Mary Zawoysky, Sheila Clifford, Donna Mortimer, and Sue Tomeo are truly amazing- this place would not run nearly as well without their efforts.

I am grateful to Meg Tivey and Mark Kurz for their efforts as education coordinators and Ed Boyle for his work as Joint Program Director. The Academic Programs office, including Julia Westwater, Marsha Gomes, Tricia Morin Gebbie, Ronni Schwartz, Christine Charette, Valerie Caron, Michelle McCafferty, and Dean Yoder do so much to make this program great, and I am grateful for their tireless efforts on behalf of Joint Program students.

I am indebted to Brett Neilan and his lab at the University of New South Wales for taking me in despite the fact that I am American and for introducing me to molecular biology. I am grateful Young Jae Jeon, Falicia Goh, Tim Salmon and the other members of the Neilan Lab for all their advice and assistance.

I have sailed and done field work with a number of people from whom I have learned a great deal and to whom I owe thanks. These include Chief Scientist Jack DiTullio, Dave Hutchins, Julie Rose, Pete Sedwick, Maeve Lohan, Phil Tortell, Rob Dunbar, Walker Smith, Peter Lee, Ana Aguilar-Islas, Clint Hare, Sasha Tozzi and the rest of the CORSACS 1 and 2 science parties as well as Jeff Hoffman, Laure-Anne Ventouras, and Sam Wilson. I am also indebted to Chris Dupont and Jing Bai at the Venter Institute for collaboration on protein overexpression in diatoms.

I am fortunate to have had some fantastic officemates in Watson 115 through these years. To Anne Thompson, Mar Nieto Cid, Jamie Becker, Travis Meador, Kathleen Munson, Rene Boiteau, and Chris Follett- thank you for support, encouragement, distractions and beer/coffee breaks. There are a number of Joint Program students to whom I owe thanks for advice, discussions, and support, including Louie Wurch, Laura Hmelo, Caitlin Frame, Dan Rogers, Erin Banning, Naomi Levine, Dreux Chappell, Kim Popendorf, Carly Buchwald, Steph Owens, Abby Heithoff, Dan Ohnemus, Jeff Kaeli, Carter Esch, Dave Griffith, Eoghan Reeves, James Saenz, Maya Bhatia, Andrea Burke, Emily Roland, and Casey Saenger. I am grateful to other friends, from Woods Hole and beyond, for support, diversion, and inspiration. These include Alex Dorsk, Justin Ossolinski, Elissa Schuett, Andrew Rose, Erika Barko Fairlie, Christina Maki, Aaron Strong, Marselle Alexander-Ozinskas, Chris Richards, Sarah Sherman Stokes, Caitlin Vincent Eaton, and Kate Batchelder.

And to my family. Thank you for everything. You encouraged me to explore, understand, and make as many potions in the backyard as I wanted. I wouldn't have been here without you all. I cannot thank you enough for supporting me, believing in me, and helping me keep my feet on the ground.

Table of Contents

List of Tables

List of Figures

Appendix A

Appendix B

Appendix D

Appendix E

1. Introduction

1.1 Overview

Oxygenic photosynthesis is the major pathway for organic matter production in virtually all ecosystems and consumes carbon dioxide (CO_2) globally at a rate of $\sim 10^{18}$ g C year^{-1} (Field et al. 1998). In marine systems microscopic phytoplankton, including cyanobacteria as well as eukaryotic algae, conduct photosynthesis in irradiated surface waters; their activity amounts to roughly half of global net primary production (Field et al. 1998). This process supplies organic carbon to the rest of the marine food web, including to many bacteria and archaea. Through respiration and heterotrophy, these bacteria and archaea are agents of organic matter remineralization and thus carbon dioxide production. Bacteria and archaea also synthesize compounds that are required for growth by eukaryotic phytoplankton. This mutualism is coupled with competition for potentially growth limiting resources like iron and, in some cases, the production of allelopathic compounds to control the growth of other microbial groups. These

opposing dynamics result in complicated, poorly characterized interactions between trophic groups which are also profoundly impacted by the physiochemical speciation and behavior of nutritional resources and biomolecules in the ocean.

Vitamin B_{12}, also known as cobalamin, is among those compounds that eukaryotic phytoplankton rely on bacteria and archaea to supply. B_{12} is a cobalt-containing organometallic micronutrient believed to be produced only by select bacteria and archaea (Roth et al. 1996, Martens et al. 2002), and required by humans and other metazoans, by an estimated half of all eukaryotic phytoplankton (Croft et al. 2005, Tang et al. 2010) and by some bacteria that cannot make it themselves (Rodionov et al. 2003, Zhang et al. 2009). B_{12} conducts elegant chemistry that centers around its cobalt atom and provides the biochemical capacity for methylation and rearrangement reactions. As such, B_{12} lays the foundation for connections between the growth of prokaryotic and eukaryotic organisms and between cobalt chemistry and essential biological functions. B_{12} is also of interest because it potentially provides a window into the biochemistry that occurred on the ancient Earth and because the utility of B_{12} in modern organisms reflects chemical constraints in past environments, as detailed below. Vitamin B_{12} is thus a molecule of significant interest to many fields of study, including marine biogeochemistry.

Given the B_{12} requirement for growth in some eukaryotic phytoplankton species, the vitamin is in a position to influence two of the major questions that interest marine biogeochemists: (1) what controls the distribution and magnitude of organic matter production in the oceans and (2) what factors contribute to the existence of vast, variable phylogenetic and functional diversity of planktonic organisms in the oceans (classically referred to as the paradox

of the plankton (Hutchinson 1961)). B_{12}'s potential importance in marine systems has long been recognized (Cowey 1956, Droop 1957, Menzel & Spaeth 1962), but in-depth inquiry into the role of B_{12} in these two broad questions has been hampered by a lack of understanding of which organisms require vitamin B_{12} and how much of the vitamin they need relative to the amount available to them. The answers to these questions remain out of reach without an understanding of the molecular mechanisms behind B_{12} use and acquisition in marine microbes as well as knowledge of controls on marine vitamin B_{12} production. This thesis takes steps towards illuminating these unknowns and sets the stage for future study, using molecular-level modes of inquiry, into the role of B_{12} in shaping oceanic productivity and planktonic species composition.

1.2 History and Chemistry of Vitamin B_{12}

Vitamin B_{12} is one of the most well-studied compounds in chemistry. It was discovered as the antidote to the human medical condition 'pernicious anemia,' in 1926. Its structure remained unknown for 30 years until Dorothy Crowfoot Hodgkin and colleagues applied the then emerging technology of x-ray crystallography to the problem (Hodgkin et al. 1956). This discovery resulted in the award of a Nobel Prize in Chemistry to Dr. Hodgkin, one of only three women to receive the award to date. The resulting structure is shown in Figure 1, and contains a corrin ring with a centrally-coordinated cobalt ion, similar to the porphyrin ring found in iron-containing, biologically ubiquitous, heme. The axial ligands of B_{12} are a benzimidazole ring and a variable R group that can be a cyanide, hydroxyl, methyl, or deoxyadenosyl group. The methyl and adenosyl versions are used by enzymes. It is the controllable reactivity of the resulting Co-C

bonds between the central cobalt ion and these axial groups that imparts catalytic activity on the vitamin. When B_{12} catalyzes reactions, cobalt is reduced from the stable Co(III) state through Co(II) to Co(I). The Co(I) state acts both as a reductant and as a nucleophile, allowing the B_{12} to attack carbon atoms from other molecules to generate its active forms (Schrauzer & Deutsch 1969, Lexa & Savant 1983, Drennan et al. 1994). The Co-C bonds in B_{12} compounds are weak compared to C-C bonds, but strong compared to other metal-C bonds, making them sufficiently labile for conducting interesting chemistry. These Co-C bonds can break in two ways, through either the creation of a carbon radical or carbocation intermediate. The radicals and cations generated allow B_{12} to conduct chemistry such as group transfer (as in methylases like methionine synthase; carbocation intermediate) and hydrogen atom abstraction (as in ribonucleotide reductase; radical intermediate) (Pratt 1972, Halperin 1985).

It has been suggested that B_{12} is an ancient molecule that, despite its complex synthesis and structure, may have abiotic origins (Eschenmoser, 1988). B_{12} may then have functioned in the metabolisms of the earliest forms of life and, through its capacity for ribonucleotide reduction, provided a crucial link in the transition from RNA-based to DNA-based life (Benner et al 1989). Though the chemistry of B_{12} is strikingly complex and powerful, all the biological reactions enabled by B_{12} can, in the modern environment, be accomplished by other means. Many of these replacement reactions use iron and manganese enzymes instead. These alternative iron and manganese enzymes, however, require molecular oxygen for activity. This has led some to hypothesize that use of vitamin B_{12} is, in evolutionary and geologic terms, becoming less important and that perhaps the vitamin was most useful to biology in a world where methane and

molecular hydrogen were abundant and molecular oxygen was scarce (Frausto da Silva & Williams 1991). The rise of atmospheric oxygen 2.3 billion years ago (Bekker et al. 2004) would thus mark the beginning of the possibility for evolution of these metabolisms that replace vitamin B_{12}. If it is true that eukaryotic diversification occurred after Earth's major oxygenation events (Anbar & Knoll 2002), the diminishment of B_{12} use after oxygenation is supported by evidence from modern genomes showing that B_{12}-utilizing proteins are much more abundant in prokaryotic proteomes compared to eukaryotic ones (Dupont et al. 2006). However, despite the existence of alternative enzymes that circumvent vitamin B_{12} requirements, enzymes using B_{12} have been retained in many marine eukaryotic microbial genomes. This suggests that in addition to illuminating B_{12}'s potentially important role in modern marine biogeochemistry, continued study of B_{12} use, production and acquisition may provide further insight into major earth history events and long-term evolutionary processes.

1.3. B_{12} in the modern ocean

Early workers showed that many marine algae have an absolute B_{12} requirement and hypothesized that B_{12} availability could influence marine primary production and phytoplankton species composition (Cowey 1956, Droop 1957, Menzel & Spaeth 1962, Guillard & Cassie 1963, Carlucci & Bowes 1970, Swift & Taylor 1972, Swift 1981). More recent field work suggests that vitamin B_{12} availability does in fact impact phytoplankton growth and community composition in many areas of the ocean. This has been demonstrated in the Ross Sea (Bertrand et al. 2007) Appendix 1, the Antarctic Peninsula sector of the Southern Ocean (Panzeca et al. 2006), the

North Pacific (Koch et al. 2011), and Long Island embayments (Sañudo-Wilhelmy et al. 2006, Gobler et al. 2007).

In the ocean, vitamin B_{12} has a nutrient-like profile and is thought to be present in sub-picomolar quantities (Figure 2). Measurement techniques for B_{12} in seawater remained restricted to bioassays (Menzel & Spaeth 1962) until solid phase extraction, high pressure liquid chromatography methods were developed (Okbamichael & Sañudo-Wilhelmy 2004). These methods still require large volumes of seawater and do not distinguish between B_{12} with different axial R groups. Mass spectrometry detection methods are currently being developed to increase sensitivity of this measurement and resolve different forms of the vitamin (Sañudo-Wilhelmy, unpublished; Saito, Tabersky and Bertrand, unpublished). However, the halflife of B_{12} in the surface ocean with respect to photodegradation alone is approximately 4 days (Carlucci et al. 1969). Given this reactivity, along with what may be presumed to be rapid changes in production and consumption rates as a function of biological activity, B_{12} concentrations alone may not be an informative measure of the impact of vitamin B_{12} on marine biogeochemical processes.

1.4. Vitamin B_{12} production

Either through cycling of the microbial loop (Azam 1998, Karl 2002, Droop 2007) or through direct symbiotic interaction (Croft et al. 2005), some portion of the bacterial and archaeal community must be the ultimate source of vitamin B_{12} to phytoplankton. Biosynthesis of vitamin B_{12} requires over 30 enzymatic steps and appreciable amounts of energy, carbon, nitrogen, and transition metals including cobalt, zinc and in some cases iron (Roth et al., 1996; Raux et al.,

2000). The genetic potential for vitamin B_{12} production remains largely uncharacterized in any marine environment. This is in part because 16s rRNA profiling, which is commonly used for bacterial community structure analysis, does not provide information about vitamin B_{12} production potential, since the presence of the biosynthesis pathway among bacterial and archaeal lineages is widespread and extremely variable. An exception to this are the marine cyanobacteria, where all available sequenced genomes appear to contain the B_{12} biosynthetic pathway (Rodionov et al. 2003), and a range of strains have been shown to produce significant amounts of B_{12} (Bonnet et al. 2010). Given their abundance in many marine environments (Partensky et al. 1999), cyanobacteria are likely a major source of vitamin B_{12} in the ocean. The identity of other groups that contribute significantly to oceanic B_{12} production remains unclear, however, and is of particular important in regions with small cyanobacterial populations such as the Southern Ocean and Arctic regions.

1.5. B_{12} demand and acquisition in eukaryotic phytoplankton

Vitamin B_{12} requirements in eukaryotic phytoplankton arise primarily from its use in the enzyme methionine synthase (Croft et al. 2005, Helliwell et al. 2011), which is responsible for regenerating methionine from homocysteine and 5-methyltetrahydrofolate (Banerjee & Matthews 1990). Some eukaryotic phytoplankton genomes encode only one version of this enzyme, MetH, which uses B_{12} as an intermediate methyl group carrier (Goulding et al. 1997), while others encode both MetH and MetE, an enzyme that accomplishes the same reaction without cobalamin but at much lower efficiency (Gonzalez et al. 1992). In eukaryotic phytoplankton, the lack of MetE

results in an absolute B_{12} requirement. There appear to be no phylogenetic relationships between algae that require the vitamin (Helliwell et al. 2011). Even species-level differences in B_{12} requirements have been observed (Tang et al. 2010), making it difficult to discern, using current techniques for phytoplankton identification and classification, whether a community is dominated by B_{12}-requiring phytoplankton. It is notable that the use of and requirement for B_{12} may thus create niche dimensions within algal groups that are not currently considered.

The biochemical mechanism through which phytoplankton acquire vitamin B_{12} from their environment has yet to be elucidated. Within the completely sequenced eukaryotic phytoplankton genomes, there are no genes homologous to known vitamin B_{12} binding or transport proteins (Croft et al. 2006). Despite this, and since the vitamin is present in such low concentrations in the ocean, a high affinity uptake system would be advantageous. Given that phytoplankton without absolute B_{12} requirements still possess enzymes that use B_{12}, we would expect species both with and without this absolute requirement to utilize a high affinity uptake system.

1.6. Summary

Neither B_{12} production nor B_{12} requirements in marine microbes can be tracked using existing descriptors of marine microbial community composition. Thus, the production of and demand for B_{12} may create previously overlooked niche dimensions within marine microbial communities. This means that new methodology is required to determine the B_{12} production and consumption capacities of marine microbial communities and assess their impact on marine

biogeochemical processes. This thesis takes steps toward that end, with the majority of its contributions being enabled by mass spectrometry-based proteomics. Chapter 2 identifies a group of putatively B_{12} producing bacteria in the Ross Sea of Antarctica and shows that they are actively producing B_{12} biosynthesis protein (Bertrand et al. 2011a). Chapter 3 shows that vitamin B_{12} and iron metabolism are linked in an Antarctic shelf ecosystem, and that B_{12} uptake rate measurements may provide insight into the metabolic status of primary producers with respect to vitamin B_{12} (Bertrand et al. 2011b). Chapter 4 uses shotgun proteomics to identify a new protein involved in B_{12} acquisition by eukaryotic phytoplankton, and Chapter 5 identifies quantitative protein abundance profiles that reflect B_{12} utilization and starvation in diatoms, both in culture and in natural populations.

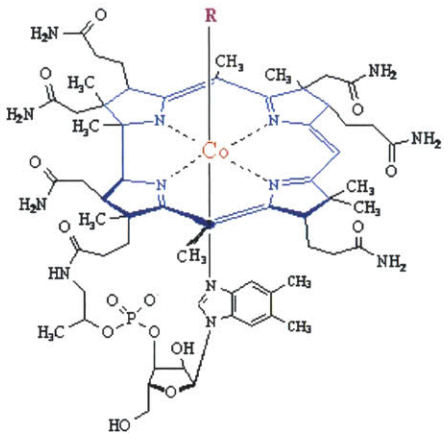

Figure 1: The structure of vitamin B_{12} contains a corrin ring (blue) with a centrally-coordinated cobalt (III) ion. The axial ligands are a benzimidazole ring and a variable R group (pink) that can typically be a cyanide ion, a hydroxyl group, a methyl group, or an adenosyl group.

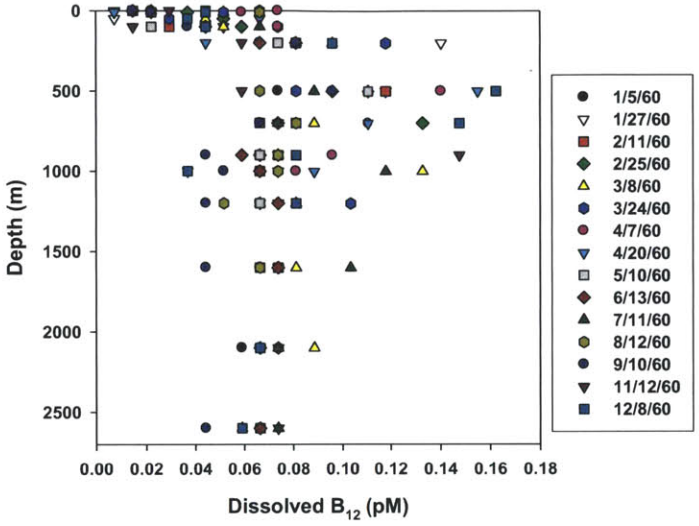

Figure 2: Time series of depth profiles of vitamin B_{12} concentration, measured by bioassay off Bermuda, compiled from Menzel and Spaeth, 1962. Vitamin B_{12} displays a nutrient- like profile, and is present at exceedingly low concentrations.

References

Anbar AD, Knoll AH (2002) Proterozoic ocean chemistry and evolution: A bioinorganic bridge? *Science* 297:1137-1142

Azam F (1998) Microbial control of oceanic carbon flux: The plot thickens. *Science* 280:694-696

Banerjee RG, Matthews RV (1990) Cobalamin- dependent methionine synthase. *The FASEB Journal* 4:1449-1459

Bekker A, Holland HD, Wang PL, Rumble Dand others (2004) Dating the rise of atmospheric oxygen. *Nature* 427:117-120

Benner, SA, Ellington, AD, Tauer, A (1989) Modern metabolism as a palimpsest of the RNA world. *Proc of the Nat Acad of Sci* 86 7054-7058

Bertrand EM, Saito MA, Jeon YJ, Neilan BA (2011a) Vitamin B_{12} biosynthesis gene diversity in the ross sea: The identification of a new group of putative polar B_{12}-biosynthesizers *Environmental Microbiology* 13:1285-1298

Bertrand EM, Saito MA, Lee PA, Dunbar RB, Sedwick PN, DiTullio GR (2011b) Iron limitation of a springtime bacterial and phytoplankton community in the ross sea: Implications for vitamin B_{12} nutrition. *Frontiers in Aquatic Microbiology.* 2(106)

Bertrand EM, Saito MA, Rose JM, Riesselman CR and others (2007) Vitamin B_{12} and iron co-limitation of phytoplankton growth in the ross sea. Limnology and Oceanography 52

Bonnet S, Webb EA, Panzeca C, Karl DM, Capone DG, Sanudo-Wilhelmy SA (2010) Vitamin B_{12} excretion by cultures of the marine cyanobacteria *Crocosphaera* and *Synechococcus*. *Limnol and Oceanog* 55:1959-1964

Carlucci AF, Bowes PM (1970) Production of vitamin B_{12}, thiamine, and biotin by phytoplankton. *Journal of Phycology* 6:351-357

Carlucci AF, Silbernagel SB, McNally PM (1969) The influence of temperature and solar radiation on persistence of vitamin B_{12}, thiamine, and biotin in seawater. *Journal of Phycology* 5:302-305

Cowey CB (1956) A preliminary investigation of the variaton of vitamin B12 in oceanic and coastal waters. *J Mar Biol Ass UK* 35:609-620

Croft MT, Lawrence AD, Raux-Deery E, Warren MJ, Smith AG (2005) Algae acquire vitamin B12 through a symbiotic relationship with bacteria. *Nature* 438:90-93

Croft MT, Warren MJ, Smith AG (2006) Algae need their vitamins. *Eukaryotic Cell* 5:1175-1184

Drennan CL, Matthews RG, Ludwig ML (1994) Cobalamin-dependent methoionine synthase: The structure of a methylcobalamin-binding fragment and implicatiosn for other B_{12}-dependent enzymes. *Curr Op in Struct Biol* 4:919-929

Droop MR (1957) Vitamin B_{12} in marine ecology. Nature 180:1041-1042

Droop MR (2007) Vitamins, phytoplankton and bacteria: Symbiosis or scavenging? *Journal of Plankton Research* 29:107-113

Dupont CL, Yang S, Palenik B, Bourne PE (2006) Modern proteomes contain putative imprints of ancient shifts in trace metal geochemistry. *Proc Natl Acad Sci* 103:17822-17827

Eschenmoser A (1988) Vitamin B_{12}: Experiments Concerning the Origin of Its Molecular Structure. *Angew. Chem. Int. Ed. Eng.* 27, 5-39

Field CB, Behrenfeld MJ, Randerson JT, Falkowski P (1998) Primary production in the biosphere: Integrating terrestrial and oceanic componants. *Science* 281:237-240

Frausto da Silva JJR, Williams RJP (1991) The biological chemistry of the elements, Vol. Clarendon Press, Oxford

Gobler CJ, Norman C, Panzeca C, Taylor GT, Sanudo-Wilhelmy SA (2007) Effect of B-vitamins and inorganic nutrients on algal bloom dynamics in a coastal ecosystem. *Aquat Microb Ecol* 49:181-194

Gonzalez JC, Banerjee RV, Huang S, Sumner JS, Matthews RG (1992) Comparison of cobalamin-independant and cobalamin-dependant methionine synthases from *E. coli*: Two solutions to the same chemical problem. *Biochemistry* 31:6045-6056

Goulding CW, Postigo D, Matthews RG (1997) Cobalamin-dependent methionine synthase is a modular protein with distinct regions for homocysteine, methyltetrahydrofolate, cobalamin and adenosylmethionine. *Biochemistry* 36:8082-8091

Guillard R, Cassie V (1963) Minimum cyanocobalamin requirements of some marine centric diatoms. *Limnology and Oceanography* 8:161-165

Halperin J (1985) Mechanisms of coenzyme B12-dependant rearrangements. *Science* 227:869-875.

Helliwell KE, Wheeler GL, Leptos KC, Goldstein RE, Smith AG (2011) Insights into the evolution of vitamin B_{12} auxotrophy from sequenced algal genomes. *Mol Biol and Evolution*

Hodgkin DC, Kamper J, Mackay M, Pickworth J, Trueblood KN, White JG (1956) Structure of vitamin B_{12}. *Nature* 178:64-66

Hutchinson GE (1961) The paradox of the plankton. *American Naturalist* 95:137-145

Karl DM (2002) Nutrient dynamics in the deep blue sea. *Trends in Microbiol* 10:410-418

Koch F, Marcoval MA, Panzeca C, Bruland KW, Sanudo-Wilhelmy SA, Gobler CJ (2011) The effect of vitamin B_{12} on phytoplankton growth and community structire in the gulf of alaska. *Limnol and Oceanog* 56:1023-1034

Lexa D, Savant JM (1983) The electrochemistry of vitamin B12. *Acc Chem Res* 16:235-243

Martens JH, Bargv H, Warren MJ, Jan D (2002) Microbial production of vitamin B_{12}. *Appl Microbiol Biotechnol* 58:275-285

Menzel DW, Spaeth JP (1962) Occurrence of vitamin B_{12} in the sargasso sea. *Limnol Oceanogr* 7:151-154

Okbamichael M, Sañudo-Wilhelmy SA (2004) A new method for the determination of vitamin B_{12} in seawater. *Analytica Chimica Acta* 517:33-38

Panzeca C, Tovar-Sanchez A, Agusti S, Reche I, Duarte M, Taylor GT, Sanudo-Wilhelmy SA (2006) B vitamins as regulators of phytoplankton dynamics. *EOS* 87

Partensky F, Hess WR, Vaulot D (1999) *Prochlorococcus*, a marine photosynthetic prokaryote of global significance. *Microbiology and Molecular Biology Reviews* 63:106-127

Pratt JM (1972) Inorganic chemistry of vitamin B12. , Vol. Academic Press, London

Rodionov DA, Vitreschak AG, Mironov AA, Gelfand MS (2003) Comparative genomics of the vitamin b_{12} metabolism and regulation in prokaryotes. *J Biol Chem* 278:41148-41159

Roth JR, Lawrence JG, Bobik TA (1996) Cobalamin (coenzyme B_{12}): Synthesis and biological significance. *Annu Rev Microbiol* 50:137-181

Sañudo-Wilhelmy SA, Okbamichael M, Gobler CJ, Taylor GT (2006) Regulation of phytoplankton dynamics by vitamin B12. *Geophysical Research Letters* 33

Schrauzer GN, Deutsch E (1969) Reactions of cobalt(i) supernucleophiles. The alkylation of vitamin B12s, cobaloximes (i), and related compounds. . *J Am Chem Soc* 91:3341-3350

Swift D (1981) Vitamin levels in the gulf of maine and ecological significance of vitamin B12 there. *Journal of Marine Research* 39:375-403

Swift DG, Taylor WR (1972) Growth of vitamin B12 - limited cultures: *Thalassiosira pseudonana, Monochyrsis lutheri,* and *Isochrysis galbana. J Phycol* 10:385-391

Tang YZ, Koch F, Gobler CJ (2010) Most harmful algal bloom species are vitamin B1 and B_{12} auxotrophs. *Proceedings of the National Academies of Sciences* 107:20756-20761

Zhang Y, Rodionov DA, Gelfand MS, Gladyshev VN (2009) Comparative genomics analysis of nickel, cobalt, and vitamin b_{12} utilization. *BMC Genomics* 10

Chapter 2:

Vitamin B_{12} biosynthesis gene diversity in the Ross Sea: the identification of a new group of putative polar B_{12}-biosynthesizers

Vitamin B_{12} biosynthesis gene diversity in the Ross Sea: the identification of a new group of putative polar B_{12}-biosynthesizers. *Environmental Microbiology.* E.M Bertrand, M.A. Saito, Y.J. Jeon, B.A. Neilan. 2011. 13(5), 1285–1298.

Environmental Microbiology (2011)

doi:10.1111/j.1462-2920.2011.02428.x

Vitamin B_{12} biosynthesis gene diversity in the Ross Sea: the identification of a new group of putative polar B_{12} biosynthesizers

Erin M. Bertrand,[1,2,3]* Mak A. Saito,[2] Young Jae Jeon[3] and Brett A. Neilan[3,4]

[1]*MIT/WHOI Joint Program in Chemical Oceanography, Woods Hole, MA 02543, USA.*

[2]*Marine Chemistry and Geochemistry Department, Woods Hole Oceanographic Institution, Woods Hole, MA 02543, USA.*

[3]*School of Biotechnology and Biomolecular Sciences, University of New South Wales, Sydney, New South Wales 2052, Australia.*

[4]*Australian Centre for Astrobiology, University of New South Wales, Sydney, New South Wales 2052, Australia.*

Summary

Vitamin B_{12}, a cobalt-containing micronutrient, has been shown to limit phytoplankton growth in the Ross Sea of the Southern Ocean. However, B_{12} biosynthesis potential in this environment remains uncharacterized. Select bacteria and archaea synthesize B_{12} while many phytoplankton require it for growth. Low ratios of bacterial biomass production to primary productivity and high concentrations of labile cobalt in Antarctic surface water suggest that factors controlling bacterial growth rather than cobalt availability may determine vitamin production rates here. In order to assess B_{12} biosynthesis potential, degenerate polymerase chain reaction primers were designed to target the genetic locus *cbiA/cobB*, encoding cobyrinic acid a,c-diamide synthase, a B_{12} biosynthesis protein. Sequencing the DNA compliment of Ross Sea 16S rRNA (see *Supporting information*) allowed targeting of *cbiA/cobB* probes to dominant bacterial groups. *CbiA/cobB* DNA sequences were successfully identified in clone libraries from the Ross Sea. To our knowledge, this study represents the first targeted molecular characterization of environmental B_{12} biosynthesis potential. A newly identified group of *cbiA/cobB* sequences dominated the diversity of the sequences retrieved; their expression was confirmed via mass spectrometry-based peptide detection. These sequences seem to have originated from a previously undescribed group of bacteria that could dominate the B_{12} biosynthesizing community in polar systems.

Received 30 September, 2010; accepted 6 January, 2011. *For correspondence. E-mail ebertrand@whoi.edu; Tel. (+61) 508 289 2835; Fax (+61) 508 457 2075.

Introduction

Vitamin B_{12}, cobalamin, is produced by select archaea and bacteria (Rodionov *et al.*, 2003) and is required for growth of some bacteria and archaea (Roth *et al.*, 1996), as well as approximately half of all eukaryotic phytoplankton (Croft *et al.*, 2005). Either through cycling of the microbial loop (Karl, 2002; Droop, 2007) or through direct symbiotic interaction (Croft *et al.*, 2005), bacteria and archaea must be the ultimate source of vitamin B_{12} for auxotrophic eukaryotic phytoplankton. Therefore, in areas of the ocean where vitamin B_{12} availability has been shown to be a factor in determining phytoplankton growth and community composition, elucidating controls on bacterial production of vitamin B_{12} is crucial for understanding primary production. These regions, as shown through previous investigations, include the Ross Sea (Bertrand *et al.*, 2007) as well as the Antarctic Peninsula sector of the Southern Ocean (Panzeca *et al.*, 2006), Long Island embayments (Sañudo-Wilhelmy *et al.*, 2006; Gobler *et al.*, 2007), the Sargasso Sea (Menzel and Spaeth, 1962) and the Gulf of Maine (Swift, 1981). In the Ross Sea in particular, vitamin B_{12} has only been shown to limit phytoplankton growth where bacterial populations are small, suggesting that the dynamics of bacterial growth play a large role in determining patterns of vitamin limitation of phytoplankton growth in polar seas (Bertrand *et al.*, 2007).

Vitamin B_{12} production rates must be influenced, in part, by bacterial growth, which in the marine water column is thought to be impacted by temperature, dissolved organic matter (DOM) availability and in some cases the availability of nitrogen or iron. However, B_{12} biosynthesis rates must also be a function of the proportion of the bacterial community contributing to vitamin biosynthesis. Additionally, because cobalt is required for B_{12} biosynthesis, cobalt availability has the potential to limit vitamin B_{12} production. Cobalt is present in the marine water column in picomolar

concentrations (Saito and Moffett, 2002) and in fact, there is evidence that vitamin B_{12} production in surface waters of the North Atlantic may be limited by cobalt availability (Panzeca *et al.*, 2008).

The Ross Sea is home to massive phytoplankton blooms (Smith and Nelson, 1985) and rapid rates of biomass export out of the surface ocean (DiTullio *et al.*, 2000; Buesseler *et al.*, 2001). Primary production in this region has been shown to be controlled by iron availability as well as irradiance (Martin *et al.*, 1990; Sedwick *et al.*, 2000; Coale *et al.*, 2003) and vitamin B_{12} availability (Bertrand *et al.*, 2007). Ratios of bacterial biomass production to primary production in the Ross Sea are exceedingly low (Ducklow *et al.*, 2000; 2001), suggesting that sources of B_{12} relative to sinks might be smaller here than in other regions of the ocean. Cyanobacterial populations in the Ross Sea are extremely small (Marchant *et al.*, 1987; Caron *et al.*, 2000); given the dominance of these organisms in the temperate and tropical oceans (Partensky *et al.*, 1999; Scanlan and West, 2002) and the fact that marine cyanobacteria are known to produce vitamin B_{12} (Bonnet *et al.*, 2010), the Ross Sea and other polar regions are likely missing a large source of B_{12} that is available in other locations. Bacterial growth in the Southern Ocean has been observed to be limited by the availability of DOM (Ducklow *et al.*, 2001; Hall and Safi, 2001; Oliver *et al.*, 2004), iron (Pakulski *et al.*, 1996), and combined iron and DOM (Church *et al.*, 2000). Because vitamin B_{12} production rates must be determined, in part, by bacterial growth, iron and DOM availability may thus impact rates of vitamin production.

One approach to investigate factors regulating B_{12} biosynthesis rates is to develop molecular biological tools to assess and monitor vitamin production potential by characterizing the portion of the bacterial community capable of vitamin biosynthesis. Biosynthesis of vitamin B_{12} requires a large number of enzymatic steps, involving over 30 biosynthesis genes (Roth *et al.*, 1996; Raux *et al.*, 2000). *In silico* analyses of sequenced microbial genomes reveal that the genetic potential to synthesize the vitamin is widespread throughout most bacterial and archaeal phyla (Rodionov *et al.*, 2003). However, not all members of a given taxonomic group possess the genetic machinery for B_{12} biosynthesis (Rodionov *et al.*, 2003), making it difficult to draw conclusions about the B_{12} biosynthesis potential of a microbial community based on traditional taxonomic assessment of its composition. For instance, of the forty-five strains of *Vibrio* with sequenced genomes, only two (*Vibrio splendidus* LGP32 and *Vibrio* MED222) have the genetic machinery for *de novo* B_{12} biosynthesis (E. Bertrand, unpubl. obs.). Therefore, when a *Vibrio* strain is identified in an environmental sample by 16S rRNA gene sequencing, it is not possible to infer whether that strain is capable of B_{12} biosynthesis. As a result, the genetic potential for vitamin B_{12} production remains almost entirely uncharacterized in the Ross Sea or any other environment.

There are currently five bacterioplankton strains isolated from Antarctic seawater with fully sequenced genomes (as of July 2010). *Pseudoalteromonas haloplanktis TAC125* (Medigue *et al.*, 2005) and *Shewanella frigidimarina* NCIMB 400 possess genes encoding the B_{12}-requiring enzyme methionine synthase (MetH) as well as a B_{12} uptake system and the last few genes in the biosynthesis pathway, rendering these strains capable of B_{12} scavenging and salvaging, but not *de novo* synthesis. Draft genomes of the Antarctic marine strains *Agreia* PHSC20C1 and *Polaribacter irgensii* 23-P contain no B_{12} biosynthesis related genes, and no genes encoding known B_{12}-dependent enzymes while the draft genome of *Psychroflexus torques* ATCC 70755 seems to contain at least a partial B_{12} uptake system as well as genes encoding the vitamin B_{12}-requiring enzymes methionine synthase (MetH) and ribonucleotide reductase (RNR II). Although limited in scope, these genomes are currently the only molecular insight into bacterial B_{12} metabolism in the Antarctic Southern Ocean. Because none of these genomes contain the potential for *de novo* biosynthesis, they provide no information regarding the identity of primary vitamin biosynthesizers in this vast region.

In order to further characterize cycling and sources of B_{12} in the Ross Sea, a set of DNA probes were developed to profile B_{12} biosynthesis genetics in the bacterial communities of the Ross Sea. The genes *cbiA* and *cobB*, which encode cobyrinic acid a,c-diamide synthase, were targeted as a marker for vitamin B_{12} biosynthesis potential. Cobyrinic acid a,c-diamide synthase is comprised of two domains – one ATP binding domain and one glutamine amidotransferase domain (Debussche *et al.*, 1990; Galperin and Grishin, 2000). The gene products catalyse the amidation of two sites on the corrin ring of vitamin B_{12} (Fresquet *et al.*, 2004).

Functional gene diversity has been profiled using this approach for many genes critical to biogeochemical cycles, e.g. ammonia monooxygenase and dissimilatory sulfate reductase (Wagner *et al.*, 1998; Hansel *et al.*, 2008), but has yet to be applied to vitamin biosynthesis. The development of these probes has elucidated the importance of particular taxonomic groups in specific processes (Francis *et al.*, 2005) has led to a better understanding of the processes controlling biogeochemical fluxes and has also opened further avenues for research (Church *et al.*, 2005; Steward *et al.*, 2005). This study investigates diversity of a gene involved in vitamin B_{12} biosynthesis, verifies the presence of the protein it encodes, and places these measurements in the context of bacterial abundance as well as cobalt concentrations and lability in the Ross Sea of the Southern Ocean.

Results and discussion

Relevant characteristics of study site

Bacterial abundance and cobalt concentrations and speciation from station NX 19 in the Ross Sea are shown in Table 1. Bacterial abundance was relatively low for marine environments, but was among the higher values observed in the Ross Sea (Ducklow, 2000) and fell within the range of bacterial abundance in which vitamin limitation of primary productivity was previously observed (Bertrand *et al.*, 2007). Total cobalt concentrations were approximately 30 pM throughout the upper 100 m of the water column at this station. These values were within the range of cobalt concentrations previously observed in the ocean [~5–100 pM; (Saito and Moffett, 2002)]. Most importantly, labile cobalt (Co'), the fraction that is thought to be bioavailable, was present at approximately 10 pM throughout the upper water column. These concentrations were at least an order of magnitude larger than other measurements of surface water Co' outside of upwelling regions, suggesting that cobalt bioavailability at this study location is higher than in other areas of the surface ocean (Saito and Moffett, 2001; Saito *et al.*, 2004; 2005; 2010). When considered together with the low bacterial biomass production to primary production ratios observed in this region (Ducklow, 2000), these cobalt speciation data suggested that bacterial metabolism rather than cobalt availability may control the rates of vitamin production in the Ross Sea as bioavailable Co is present in high concentrations. This reinforces the importance of elucidating which bacterial groups are responsible for vitamin production in this region and what factors control their growth and activity.

Table 1. Bacterial abundance and cobalt concentrations from station NX 19.

Depth (m)	Bacteria (10^5 cells ml^{-1})	total dissolved cobalt (pM)	labile cobalt (pM)	Per cent labile (%)
20	1.87	30.6	12.1	39.6
40	2.25	34.6	13.3	38.4
60	1.41	31.9	9.8	30.9
100	1.44	34.1	11.4	33.5

Bacterial abundance was among the higher values observed in the Ross Sea, although this was relatively low when compared with other marine environments. Total cobalt and labile cobalt, the fraction that is thought to be most bioavailable, are also shown. Labile cobalt concentrations here were among the highest surface water values observed using this method. These data show that cobalt availability in these waters was high relative to other marine waters and suggests that cobalt availability is less likely to control the rate of vitamin B_{12} production in the Ross Sea compared with other marine environments.

Design and application of degenerate primers targeting B_{12} synthesis genes

In this study, several essential genes coding for enzymes involved in vitamin B_{12} biosynthesis were initially targeted for DNA probe development including *cbiA/cobB* encoding cobyrinic acid a,c-diamide synthase, *cbiC/cobH* encoding precorrin-8x methylmutase, and *cobT* encoding nicotinate mononucleotide:5,6-dimethylbenzimidazole phosphoribosyltransferase. Each of these genes represent a potential biomarker for vitamin biosynthesis because: (i) when they are present in fully sequenced bacterial and archaeal genomes, the complete B_{12} biosynthesis pathway is also present and (ii) the genes are homologous in both the oxygen-requiring (*cobB, cobH, cobT*) and non-oxygen-requiring pathways for vitamin synthesis (*cbiA, cbiC, cobT*), and thus one set of probes could be designed to target both versions of the biosynthesis pathway. However, attempts to design probes to target the full diversity of these genes as represented in the National Center for Biotechnology Information non-redundant (NCBI nr) database failed because of the high degeneracy of the primers designed. This high degree of degeneracy was required because of extensive diversity between homologous sequences. The B_{12} biosynthesis pathway is one of the most ancient metabolisms (Raux *et al.*, 1999) and the sequences of the associated biosynthesis genes are highly divergent (Rodionov *et al.*, 2003).

CbiA/cobB is among the most highly conserved genes in the B_{12} biosynthesis pathway, making it more conducive to DNA probe design. Because initial probe design targeting the full diversity of these sequences in the NCBI nr database failed, clone libraries were created from the amplified DNA complement of 16S rRNA genes from the Ross Sea and sequencing was performed in order to identify the major taxonomic groups present (see *Supporting information*). The major groups identified in this study (Alpha- and Gammaproteobacteria and Bacteroidetes; Fig. S1, Table S1) were similar to those found in other 16S rRNA gene library sequencing studies in pristine Antarctic surface waters (Webster *et al.*, 2004; Gentile *et al.*, 2006; Murray and Grzymski, 2007). Degenerate primers were then successfully designed to target *cbiA/cobB* genes in the Alpha- and Gammaproteobacteria and Bacteroidetes based on *cbiA/ cobB* sequences from these groups in the NCBI nr database.

Application of cbiA/cobB primers

Figure 1 shows the conserved domains in the CbiA/CobB protein and the genomic loci targeted by the primers designed in this study. These primers were applied to

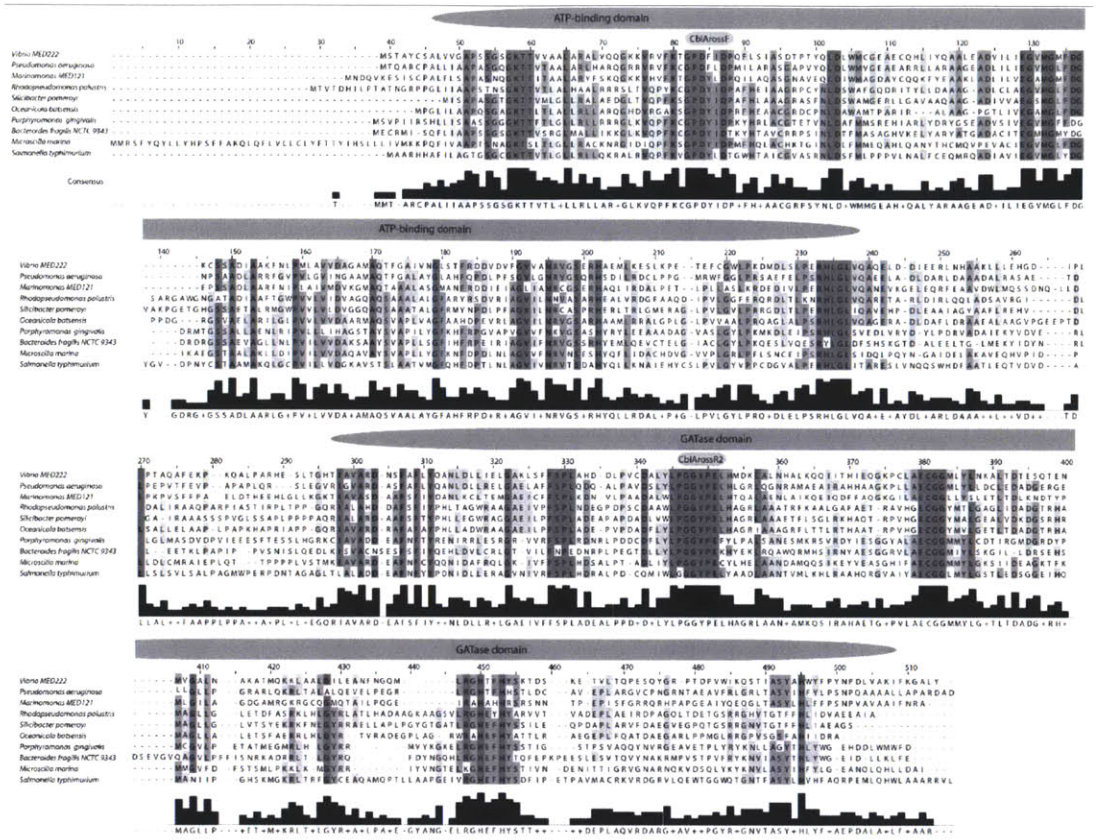

Fig. 1. A Clustal X multiple alignment of CbiA/CobB amino acid sequences from representatives of the Alpha- and Gammaproteobacteria and the Bacteroidetes groups obtained from the NCBI nr database. The alignment was used to design the B_{12} biosynthesis gene primers used in this study. The most highly conserved regions of the alignment are highlighted in the darkest colours. The location of the primers (CbiArossF and CbiArossR2) are denoted by the light gray ovals above the sequence. The conserved functional domains of the protein, one ATP binding domain and one glutamine amidotransferase domain (Debussche *et al.*, 1990; Galperin and Grishin, 2000), are denoted by darker gray ovals above the sequence.

samples from station NX19, taken at four depths within the upper water column. The libraries created using these primers contained 10–30% *cbiA* sequences along with a variety of sequences from other genes that were amplified as a result of primer degeneracy. Only the sequences homologous to *cbiA/cobB*, as determined by blastx (Altschul *et al.*, 1990) searches against the NCBI nr database, were used for further analyses. From this location, 20 different operational taxonomic units (95% similarity) were recovered from 29 sequences. The results are shown in Fig. 2, reported as a neighbour-joining tree of partial amino acid sequences. The tree is rooted to a sequence of CTP synthetase (PyrG) from *Marinomonas* sp. PyrG catalyses the ATP-dependent amidation of dUTP to form dCTP and is thought to be ancestral to CbiA and CobB (Leipe *et al.*, 2002). This tree also includes sequences recovered via a blastp search of the sequence CbiA20m167 against NCBI nr and the Community Cyberinfrastructure for Advanced Microbial Ecology Research & Analysis (CAMERA) all metagenomic open reading frame peptides database (Seshadri *et al.*, 2007) on 19 July 2010 using default parameters. Sequences with the lowest *E*-value blastp results are included in Fig. 2. This tree also includes sequences from eukaryotic algal genomes (*Ostreococcus lucimarinus* and *Fragilariopsis cylindrus*, obtained from the Joint Genome Institute's genome portal) that align with bacterial CbiA/CobB. The currently sequenced eukaryotic algal genomes with blastp homologues to CbiA/CobB sequences (those in Fig. 2 as well as *Ostreococcus tauri, Micromonas sp.* and *Chlorella* sp.)

do not appear to contain full canonical B_{12} biosynthesis pathways, although the genome of *Fragilariopsis cylindrus* appears to contain more potentially B_{12} biosynthesis related proteins than any other eukaryotic algal genome currently available. The significance of the presence of these partial vitamin biosynthesis pathways has yet to be investigated.

Analysis of Group RSB_{12} sequences

Seventy per cent of the CbiA/CobB sequences retrieved in this study, while homologous to known CbiA/CobB sequences, fell into a distinct group herein referred to as Group RSB_{12} (Fig. 2). The best blastp matches in NCBI nr to Group RSB_{12} sequences were included in this tree but did not fall within Group RSB_{12} (CbiA from *Oceanospirillum* sp. MED92; EAR62324.1); it is evident that this group has no sequenced or otherwise characterized representatives. There are also very few representatives of this group in available metagenomic sequencing databases (Table 2); no sequences from the HOT, BATS or GOS databases in CAMERA fell into this group. There was one sequence from Newcomb Bay of the Antarctic Southern Ocean that exactly matched a sequence from this clone library and fell into Group RSB_{12}. There were also short sequence reads from the Norwegian Fjords that were very similar to a portion of the Group RSB_{12} sequence, but as these were so short, it was difficult to accurately include them in the Fig. 2 tree and thus determine if they belong to this new group. The lack of Group RSB_{12} sequence homologues in current databases is perhaps due to the lack of polar metagenome sequence data and the limited genomic sequencing of polar-derived cultured isolates. The complete lack of Group RSB_{12} sequences in tropical, subtropical and subpolar metagenomic databases along with its dominance in this clone library suggested that Group RSB_{12} could be a major contributor to the B_{12}-biosynthesizing community particular to polar regions. While the broad phylogenetic groupings of bacteria found in the Antarctic marine water column are shared with other planktonic ecosystems, there are some species or specific groups that are thought to be predominantly associated with polar systems, including *P. irgensii* as well as some uncultivated gammaproteobacterial species (Murray and Grzymski, 2007). There is thus some precedent for the increased frequency of specific phylogenetic groups in polar regions, as may be the case for organisms encoding Group RSB_{12} sequences.

It is notable that *Fragilariopsis cylindrus* appears to possess multiple copies of CbiA/CobB-like genes and that one clusters close to Group RSB_{12} (Fig. 2). The CbiA/CobB sequences recovered in this study are not likely eukaryotic, as the sample from which the original DNA was extracted was 2 μm prefiltered. In addition, the 16S sequencing results in Fig. S1 suggest that there was only a small amount of eukaryotic DNA available in these samples because about 10% of the sequences retrieved appear to be eukaryotic in origin. Additionally, within the three longer Antarctic metagenomic reads that contain sequences in Group RSB_{12} (Table 2), one read contains a partial gene sequence encoding corrinoid adenosyltransferase BtuR/CobO/CobP adjacent to the *cbiA* sequence. This is evidence that this group of RSB_{12} CbiA – encoding sequences was not isolated from eukaryotes as in many bacterial genomes, B_{12} biosynthesis genes are adjacent to each other (Rodionov *et al.*, 2003), while in eukaryotic genomes they are not (E. Bertrand, unpubl. obs.).

It was of interest to identify the taxonomic group from which the Group RSB_{12} sequences originate. Although the primers to target these genes were designed to target only Alpha- and Gammaproteobacteria and the Bacteroidetes, they were not designed to specifically exclude other groups. Therefore, the identities of the bacteria possessing these sequences cannot be narrowed down on this basis. The Group RSB_{12} sequences clearly clustered with partial CbiA/CobB sequences from Gammaproteobacteria (Fig. 2). However, given the extensive lateral gene transfer that has occurred with B_{12} biosynthesis genes, it is not possible to definitively confirm that Group RSB_{12} sequences originate from a Gammaproteobacterial group. Within the three longer metagenomic reads that contain sequences similar to Group RSB_{12} (Table 2), one also has a partial gene sequence encoding corrinoid adenosyltransferase BtuR/CobO/CobP. The best blastx matches to this sequence in the NCBI nr database were also all from Gammaproteobacteria, further suggesting that Group RSB_{12} may be Gammaproteobacterial in origin.

Additional insights into the novel origin of this vitamin biosynthesis gene could potentially be achieved by determining the guanine and cytosine (G + C) content and codon usage of the clone library sequences. The mean G + C content of the *cbiA/cobB* sequences from GroupRSB_{12} was 48.9% with a standard deviation of 1.2%. If the per cent G + C content of individual protein coding genes reflects the G + C content of the genomes in which they reside (Muto and Osawa, 1987), then the G + C content of this sequence may be useful in ruling out certain groups of bacteria as sources of these sequences. Unfortunately, no firm conclusions could be made about the origin of these *cbiA/cobB* sequences because their G + C content was in no way unusual, and it is possible that the partial sequences available for these *cbiA/cobB* genes are not long enough to be representative of the entire genomes of organisms from which they originate.

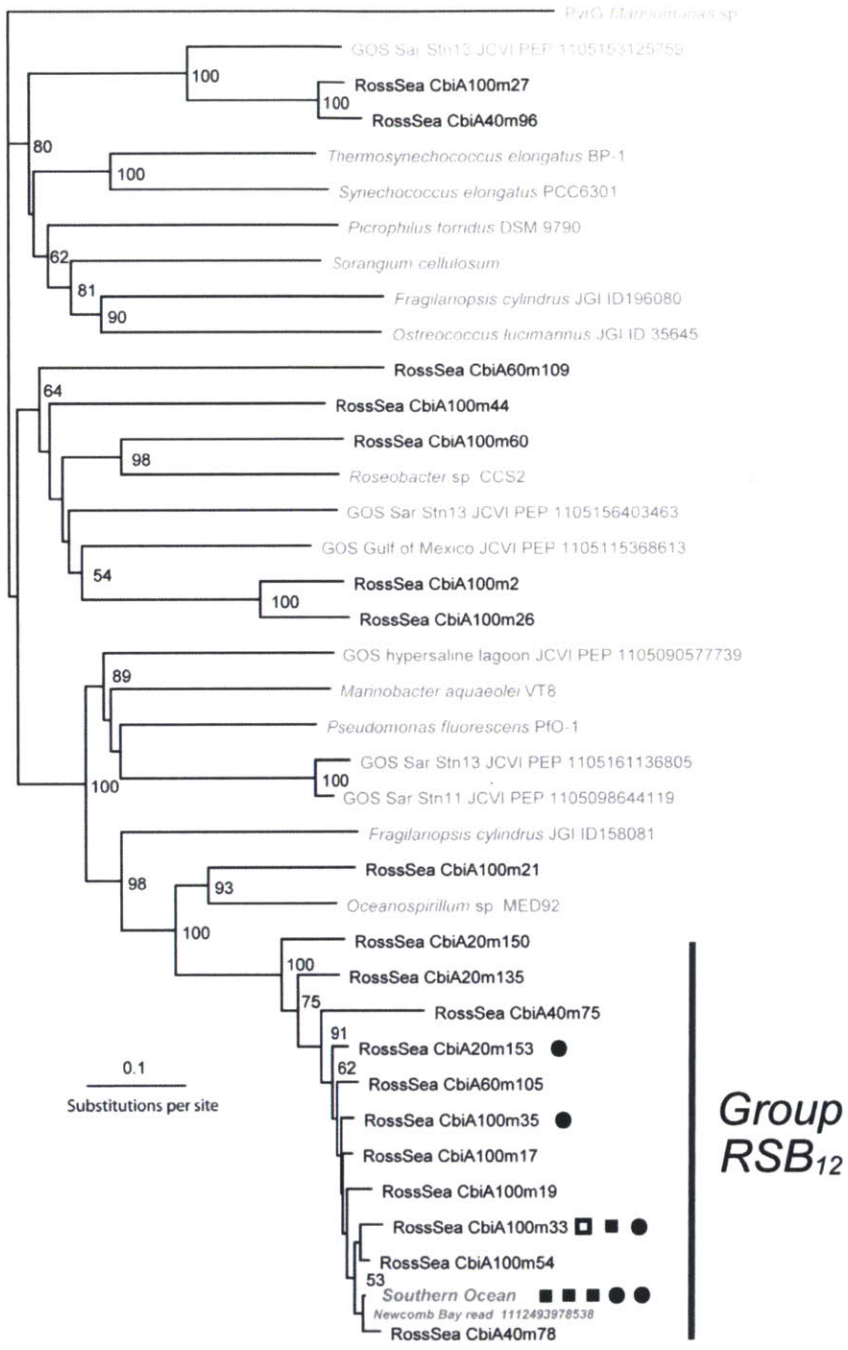

Fig. 2. Neighbour-joining tree of partial CbiA amino acid sequences obtained from the Ross Sea. Sequences obtained in this study from station NX19, 20–100 m depth, are shown in black. One representative of sequence groups with > 95% identity at the nucleic acid level is shown. Each symbol next to a sequence name indicates one additional sequence obtained from the Ross Sea belonging to that group. Closed squares denote that the additional sequence came from 100 m, circles from 20 m, and the open square from 40 m depth. The tree is rooted to a sequence of CTP synthetase (PyrG) from *Marinomonas* sp. PyrG is thought to be ancestral to CbiA and CobB (Leipe *et al.*, 2002). Bootstrap values > 50%, calculated from 4000 replicates, are shown as per cent. Reference sequences from NCBI, the Global Ocean Sequencing dataset, eukaryotic genome sequences from JGI's genome portal, and meta sequence data from the CAMERA database (in gray), including the closest representatives to all environmental samples recovered are shown. Twenty different operational taxonomic units (95% sequence similarity at the nucleic acid level) were recovered from 29 clone sequences. Seventy per cent of the sequences retrieved fell into a distinct group herein referred to as Group RSB_{12} while the others grouped with sequences represented in available the genomic and metagenomic databases.

Confirmation of expression of Group RSB_{12} CbiA proteins – peptide biomarkers

In order to evaluate whether Group RSB_{12} CbiA proteins were expressed in the Ross Sea, we attempted to detect peptides coded for by these sequences using two separate mass spectrometry-based approaches. We conducted global metaproteomic analyses employing reverse phase liquid chromatography coupled to linear ion trap mass spectrometry via electrospray ionization on samples from the Ross Sea. Peptides representing the RSB_{12} sequences or other CbiA/CobB sequences were not detected, perhaps because of the inability of these global proteomic approaches to detect low abundance components of complex mixtures (data not shown). As an alternative, we employed a targeted proteomic approach using reverse phase liquid chromatography separation coupled to triple quadropole mass spectrometry with selected reaction monitoring (SRM) using stable isotopically labelled peptide reference standards. SRM is a type of tandem mass spectrometry, meaning that it detects a parent molecular ion and isolates it, then fragments it and detects resulting fragment ions. This method is much more sensitive than the global ion trap mass spectrometry approach in part because only a narrow range of masses are assayed by the mass spectrometer, increasing the likelihood that low abundance components of complex mixtures can be detected.

Three tryptic peptides – peptides produced in the digestion of intact proteins with the enzyme trypsin – were identified as potential biomarkers for Group RSB_{12} proteins (Table 3). These are coded for by over 70% of the Group RSB_{12} DNA sequences detected in this study, not encoded by any other known sequences (confirmed via a NCBI nr database search on 15 July, 2010 and a search of JGI eukaryotic algal sequences not yet deposited in GenBank), and are also theoretically observable via the mass spectrometry techniques applied here. As shown in Fig. 3, one of these three peptides was detected via SRM mass spectrometry in a Ross Sea protein sample (peptide sequence: HLGLVQAHEVR). There were three pieces of evidence supporting the claim this peptide from the Group RSB_{12} CbiA protein was detected. First, the retention time at which the peak for the native peptide identified here was the same as the synthetic, isotopically labelled standard version. Second, the product distribution patterns (relative peak heights of fragment ions) at this time point were the same for the standard as for the native peptide. Third, this signal was only observed in the protein gel slice that corresponded to the molecular weight of CbiA proteins (43–50 kDa). In addition, none of these peptides were detected in samples of *Crocosphaera watsonii* peptides, which served as a negative control as its genome sequence does not encode these peptides. These data suggest that the CbiA protein encoded by Group RSB_{12} sequences is expressed in the Ross Sea, but that it is among the lower abundance proteins. These data also confirm the potential of targeted proteomic assays, when directed by detailed nucleic acid sequencing information, to confirm the metabolic activity of particular groups of organisms in complex environmental samples.

This study shows that there is a previously unidentified group of *cbiA/cobB* vitamin B_{12} biosynthesis genes in the Ross Sea of the Southern Ocean that actively produce protein. However, because there are many other proteins required for vitamin biosynthesis, this work does not prove that the organisms expressing Group RSB_{12} sequences can or do produce vitamin B_{12}. Even though currently sequenced bacterial genomes that possess *cbiA/cobB* sequences also contain the entire vitamin B_{12} biosynthesis pathway, the fact that only one of many involved genes was documented here is especially important in light of the fact that some eukaryotic algal genomes appear to possess *cbiA/cobB*-like sequences without the rest of the B_{12} biosynthesis pathway. Hence, this study has identified a putative new group of vitamin B_{12} biosynthesizers in the Southern Ocean. Further study will be required to link this new group of gene sequences to specific microbes and verify that they in fact produce the vitamin. Once the bacteria encoding Group RSB_{12} sequences have been identified, these organisms must then be isolated, cultured and manipulated in the laboratory to prove that they do in fact produce vitamin B_{12}.

Once the vitamin biosynthesizing role of these bacteria is confirmed, the distribution, activity and biogeochemical constraints on their growth can be studied to yield insight into controls on B_{12} production. Further study should also

Table 2. Metagenomic sequence reads similar to group RSB_{12}.

Database	Number of blastn hits ($E < 1e-5$)	Read IDs for read $E < 1e-5$	*E*-value	Read length (bp)	Location	Lat	Long
Antarctic Aquatic	3	NCBI_READ_1112493978538	0	902	Newcomb Bay, Antarctica	66.27	110.533
		NCBI_READ_1112533230382[a]	4.09E-122	1003	Antarctic Open Water	63.891	112.073
		NCBI_READ_1112493887005	1.24E-26	1013	Newcomb Bay, Antarctica	66.27	110.533
Marine Metagenome from Coastal Waters project at Plymouth Marine Laboratory	4	PML_READ_00281253	3.35E-123	249	Norwegian Fjord	60.269	5.222
		PML_READ_00287170	3.35E-123	249	Norwegian Fjord	60.269	5.222
		PML_READ_00261281	3.35E-123	249	Norwegian Fjord	60.269	5.222
		PML_READ_00343394	1.12E-116	248	Norwegian Fjord	60.269	5.222
BATS: all Metagenomic 454 reads	0	n/a	n/a	n/a	n/a	n/a	n/a
HOT: all metagenomic sequence reads	0	n/a	n/a	n/a	n/a	n/a	n/a
GOS: all metagenomic sequence reads	0	n/a	n/a	n/a	n/a	n/a	n/a

a. Read also includes a partial cobalamin adenosyltransferase (*btuR/cobO/cobP*) encoding sequence, with best blastx identities to gammaproteobacterial adenosyltransferases.
Databases in CAMERA were searched via blastn for matches to sequence CbiA20m167, employing default parameters. There were no blastn matches to group RSB_{12} sequences in available tropical or subtropical sequencing data and only a few matches were found in the small amount of available polar sequencing data. Possible matches, although on very short reads, were found in sequencing data from sub-polar fjords.

identify other vitamin producers and quantify their relative contributions to vitamin availability in the coastal Antarctic Southern Ocean. The relationships between the distributions of these bacteria, their vitamin biosynthesis protein expression and other bacterial groups and processes will lend insight into how vitamin B_{12} availability and production may also impact bacterial population dynamics. Measuring the abundance and distribution of peptides like those targeted in this study may prove to be an effective method for determining biological activity in a range of geochemically relevant processes in addition to vitamin biosynthesis.

Summary

Factors controlling vitamin B_{12} availability remain largely unknown. In order to determine B_{12} supply to phytoplankton, the rate at which the vitamin is transferred from the particulate to the dissolved pool must be determined. This flux will be a function of bacterial community composition; biosynthesis rate within that population; the rate of population turnover by grazing, viral lysis, and other factors, and the efficiency of the microbial loop. Characterizing the microbial community that produces vitamin B_{12} represents a starting point from which to explore this question.

Primers targeting *cbiA/cobB* were successfully designed and applied to DNA samples from the water column of the Ross Sea. These primers are capable of amplifying *cbiA/cobB* genes in the major groups of bacteria found by 16S rRNA gene sequence analysis at this study site (see *Supporting information*). This study was therefore restricted to detecting functional gene sequences specifically targeted by these primers and as a result was limited to observing only partial diversity of *cbiA/cobB* genes in the Ross Sea. Most of the *cbiA* sequences retrieved fell into a distinct group, Group RSB_{12}, which is not represented in most nucleic acid sequence databases. We hypothesize that this group represents an important subset of B_{12} biosynthesizers in polar regions and probably originates from members of the Gammaproteobacterial lineage. Detection of peptides characteristic of Group RSB_{12} CbiA confirmed the expression of these proteins. These sequences comprise the first molecular description of vitamin B_{12} biosynthesis potential in the Ross Sea, where limitation of phytoplankton growth by vitamin availability has been observed (Bertrand *et al.*, 2007).

Experimental procedures

Sample collection

Whole water samples were collected at 20, 40, 60 and 100 m depths at Station NX19 (30 November, 2006; 76.5°S,

Table 3. Peptides tested as potential Group RSB_{12} biomarkers, the per cent of the Group RSB_{12} sequences coding for each peptide, the peptide sequence for the native and synthetic heavy isotopically labelled versions and the selected reaction monitoring (SRM) reactions.

In % of Group RSB_{12}	Peptide name	Peptide sequence	Parent m/z	Product m/z	Collision energy (V)
75	CbiA_RSB12_1 native	DPEVSLPER	521.264	601.330	19
				401.214	20
				175.119	34
				700.399	21
	CbiA_RSB12_1 heavy	DPEVS[L_C13N15]PER	525.044	608.348	19
				401.214	20
				175.119	34
				707.413	21
85	CbiA_RSB12_2 native	HLGLVQAHEVR	629.854	1008.559	28
				838.453	31
				739.386	27
				1121.643	28
	CbiA_RSB12_2 heavy	HLG[L_C13N15]VQAHEVR	633.363	1015.576	28
				838.453	31
				739.386	27
				1128.660	28
70	CbiA_RSB12_3 native	LLQGTTIGIAR	571.848	788.463	23
				416.262	25
				916.521	23
				175.119	39
	CbiA_RSB12_3 heavy	L[L_C13N15]QGTTIGIAR	575.357	788.463	23
				416.262	25
				916.521	23
				175.119	39

SRMs are described by the mass to charge (m/z) ratios indicative of the particular parent and product ions and collision energies designed to detect the peptides. Collision energy, a measure of the energy applied to the gas that collides with parent ions in the mass spectrometer to produce fragmentation, was optimized to most efficiently generate each product ion.

174.3°W) in the Ross Sea on the CORSACS2 cruise. Water was collected in 10 l trace metal clean Go-Flo bottles (General Oceanics, FL, USA). For DNA samples, approximately 500 ml of water per sample was 2 μm prefiltered and then passed through a 0.2 μm polyethersulfone membrane filter that was retained for DNA extraction and stored at −80°C. Water from the same sampling events was used to count bacterial abundance and quantify total cobalt and labile cobalt concentrations through electrochemical techniques. Protein samples were collected in the Ross Sea on the CORSACS1 cruise (NBP0601) from two stations. For the Station 1 sample (21 December, 2006; 61.4°S, 178.2°W; Southern Ocean, not Ross Sea), 20 l was collected from 10 m depth using a trace metal clean diaphragm pumping system (Bruland *et al.*, 2005), filtered onto a 0.4 μm polycarbonate filter and stored dry at −80°C. For the Station NX 8 sample (12 January 2006; 77.3°S, 175.4°W; Ross Sea) 9 l of water from 10 m and 9 l of water from 30 m was collected as above using Go-Flo bottles and filtered onto a 0.4 μm nitrocellulose filter and stored dry at −80°C. Bacteria and archaea were enumerated using a DAPI (4,6-diamidino-2-phenylindole) staining method (Porter and Feig, 1980).

Cobalt total concentration and speciation measurements

Total cobalt and cobalt speciation analyses were performed by adsorptive cathodic stripping voltammetry using a Metrohm 663 hanging mercury drop electrode and Eco-Chemie Autolab III as described previously (Saito and Moffett, 2002; Saito *et al.*, 2004). Briefly, cobalt total measurements were made by first UV-irradiating the seawater for 1 h to destroy the strong organic ligands that bind cobalt. Seawater (9.25 ml) was then analysed with 0.2 mM dimethylglyoxime, 0.113 M sodium nitrite and 2.5 mM N-(2-hydroxyethyl)piperazine-N-(3-propanesulfonic acid), as cobalt-ligand, catalyst and buffer respectively. Cathodic stripping voltammetry analysis included a deposition step for 90 s at −0.6 V, and linear sweep stripping from −0.6 V to −1.4 V at 10 V s^{-1} with successive 25 pM standard $CoCl_2$ additions. Cobalt speciation was measured similarly but without UV-irradiation and with overnight equilibration with the dimethylglyoxime ligand. Labile cobalt is that which binds to this competitor ligand under the experimental conditions.

DNA extraction

Filter membranes were suspended in a 100 mM NaCl, 100 mM Tris, 1 mM NaCitrate, 5 mM $CaCl_2$, 25 mM EDTA buffer at pH 8 in the presence of 0.2% w/v pyrophosphate and 0.4 mg ml^{-1} Poly A and incubated at 37°C for 1 h. Five mg ml^{-1} lysozyme, 0.3% w/v SDS, 2 mg ml^{-1} proteinase K, were added and the samples were incubated for 30 min at 50°C after which the SDS concentration was increased to 5%. Samples were then lysed by three freeze-thaw cycles in liquid nitrogen for 5 min and at 60°C until heated through. DNA was extracted twice, each with one volume of 24:24:1 phenol: chloroform: isoamyl-alcohol and then precipitated

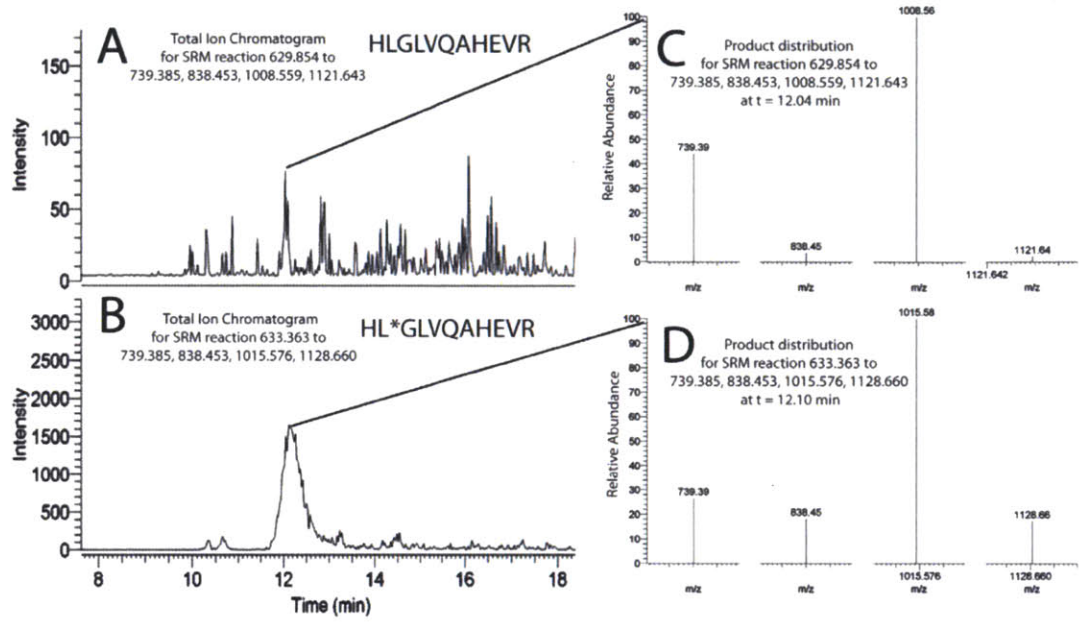

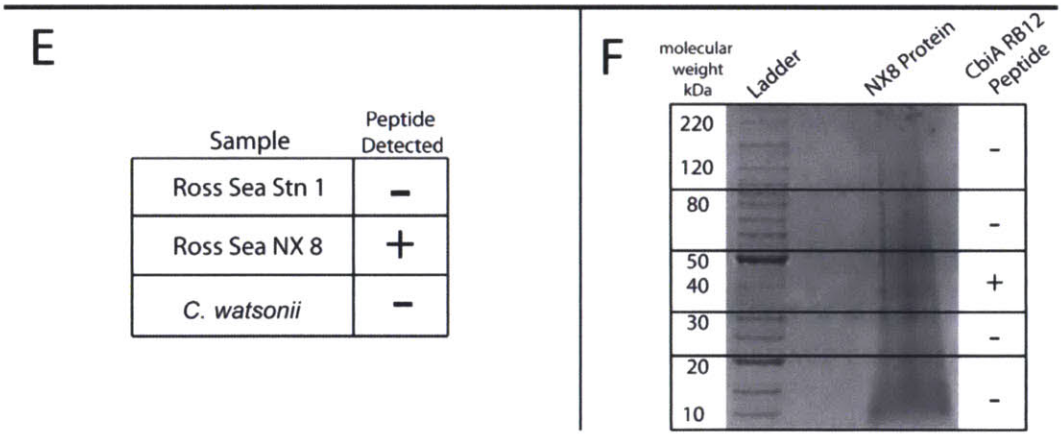

Fig. 3. Evidence supporting the detection of Group RSB_{12} peptide HLGLVQAHEVR in a Ross Sea protein sample. A shows the total ion chromatogram for the selected reaction monitoring of the native peptide HLGLVQAHEVR (parent ion doubly charged with m/z 629.854 is isolated and fragmented into product ions 1008.559, 838.453, 739.386 and 1121.643) while B shows the selected reaction monitoring of the corresponding heavy labelled peptide (parent ion m/z 633.363 to product ions 1008.559, 838.453, 739.385 and 1128.660). Total ion chromatograms represent the sum of the diagnostic product (fragment ion) intensities created upon fragmenting the isolated parent ions. C shows the product ion distribution at a retention time of 12.1 min for the native peptide while D shows a similar product distribution for the heavy labelled peptide in that same time span. E shows that this peptide was identified in the station NX8 sample, but not the Station 1 sample or the *Crocosphaera* control, while F shows that the peptide was only detected in the SDS-PAGE fraction of the station NX8 protein sample containing the mass range that should include the CbiA protein.

three times each with one volume of isopropanol and 0.1 volume of 3 M sodium acetate at pH 5.2 at –20°C for 1 h to overnight and then spun at 12 000 *g* at 4°C for 20 min. Pellets were rinsed once with 70% ethanol and then resuspended in water for further analyses.

Initial B_{12} biosynthesis gene primer designs

DNA probe design was attempted for *cbiA/cobB* and *cbiC/cobH* genes with the goal of targeting all the diversity of these genes as represented in the NCBI nr database. Probes

tested for *cbiA/cobB* include CbiAF (5′-GGTCCTGAYTW YHTNGA-3′), CbiAF2 (5′-GGTCCNGAYTWYHTNGA-3′), CbiAR2 (5′-TAAYTSNGGRWANCCNCC-3′) and CbiAR (5′-TTGTCCTSCRCAYTCNSC-3′). Probes tested for *cbiC/cobH* include CbiCF (5′-GGTAACGCNCCNACNGC-3′) and CbiCR (5′-TGGACRAANCCNACNGG-3′). DNA probes were also designed to target *cobT* sequences from the NCBI nr database from the major groups found by 16S rRNA gene profiling in pristine Antarctic surface waters (Alpha- and Gammaproteobacteria and the Bacteroidetes groups; see *Supporting information*). The resulting probes were CobTrossF (5′-TTTGCNGSNRAYCAYGG-3′) and CobTrossR (5′-TGYTT TSCNAYCATYTCNCC-3′). These probes were tested with DNA samples from NX19, as well as positive control DNA from *Microcystis aeruginosa* PCC 7806 and negative control DNA from *Escherichia coli* under a range of conditions (variations on 94°C for 4 min, 80°C for 2 min (hot start), 10 to 35 cycles of 94°C for 20 s, 45 to 55°C for 30 s and 72°C for 60 s; and 72°C for 7 min).

Final CbiA primer design and application

DNA probes were designed from *cbiA/cobB* sequences from the NCBI nr database based on the major taxonomic groups found by 16S rRNA gene profiling at site NX19 (Alpha- and Gammaproteobacteria and the Bacteroidetes group; see *Supporting information*). The resulting primers were used: CbiArossF (5′-GGTCCNGAYTWYHTNGA-3′) and CbiArossR2 (5′-TAATTCNGGRTANCCNCC-3′) with the following DNA amplification protocol: 94°C for 4 min, 80°C for 2 min (hot start), 35 cycles of 94°C for 20 s, 53°C for 30 s and 72°C for 60 s; and 72°C for 7 min. The products were gel-purified, subjected to 15 additional amplification cycles and cloned into competent *E. coli* DH5 alpha using the pGEM-T-Easy vector (Promega).

Sequencing and phylogenetic analyses

Sequencing was performed using the BigDye Terminator V3.1 cycle sequencing kit. Sequencing of polymerase chain reaction products was performed using both amplification primers (described above) with electrophoresis and reading carried out using an Applied Biosystems 3730 DNA Analyzer (Applied Biosystems) at either the Ramaciotti Center (University of New South Wales) or by Northwoods DNA. Sequences were edited in FinchTV. Subsequent analyses of *cbiA/cob* partial sequences were conducted on a 650 bp region. Multiple alignments of the translated partial CbiA/CobB amino acid sequences were performed using Clustal X (Version 1.83) (Thompson *et al.*, 1994). Phylogenetic reconstruction of the newly identified partial CbiA/CobB sequences was done using genetic distance methods based on all identified prokaryotic phyla. Bootstrap resampling with 1000 to 4000 iterations was also performed (Neilan *et al.*, 2002). Reference strains were obtained from the NCBI nr database. Fastgroup II (Yu *et al.*, 2006) was used to estimate the number of different sequences detected. These sequence data have been submitted to the GenBank database under accession numbers HQ326507 to HQ326535.

Protein extraction and digestion

Protein was extracted from filters by incubating them on ice for 15 min in 15 ml of extraction buffer (0.1 M Tris HCl, pH 7.5; 5% glycerol, 1% SDS, 10 mM EDTA) with periodic gentle vortexing, then heating to 92–98°C in a water bath for 15 min, gently vortexing for 1 min, then mixing in hybridization oven at 20°C for 2 h, with gentle vortexing for 30 s every 30 min. The extraction buffer was then collected and centrifuged at 7000 r.p.m. at 10°C for 20 min. The supernatant was collected, filtered with a 5 μm filter needle and concentrated via ultrafiltering in a Vivaspin 65 000 Da molecular weight cut-off PES membrane in a centrifugal concentrator spinning at 7000 r.p.m. at 10°C until volume was reduced to ~1 ml (~3 h). Protein was precipitated overnight at −20°C in 5 volumes of ice cold 50% acetone, 50% methanol with 0.5 mM HCl. Samples were spun at 13 000 rcf at 4°C for 20 min; pellets were aspirated and then dried at room temperature in a speedvac and resuspended in 100 μl of extraction buffer.

Protein was separated into five size fractions using SDS-PAGE and then digested into tryptic peptides according to Kinter and Sherman (Kinter and Sherman, 2000). Briefly, 15 μl of protein sample was mixed with 15 μl SDS PAGE loading buffer (0.1 M Tris, pH 7.5, 25% glycerol, 0.14 M SDS, 3 mM bromphenol blue), heated to 95°C for 8 min and proteins were then applied to a 4–20% Tris HCl pre-cast Ready Gel (Bio-Rad) for separation by SDS PAGE. Approximately 15 μg of total protein per sample was applied to the gel, as determined by Bovine Serum Albumin-calibrated DC protein Assay (Bio-Rad). Gels were stained using Coomassie Blue, destained and imaged. Gel lanes containing each protein sample were cut into 5 slices (Fig. 3F, corresponding to >100 kDa, 55–100 kDa, 35–55 kDa, 20–35 kDa and <20 kDa). The slices were cut into roughly 1 mm^3 cubes and washed repeatedly with 50% 25 mM NH_4HCO_3, pH 8 50% acetonitrile until completely destained, then dehydrated with 100% acetonitrile. The proteins were reduced using 10 mM dithiothreotol, then alkylated with 55 mM iodoacetamide. Slices were then dehydrated with 100% acetonitrile, dried and rehydrated on ice with trypsin (Promega modified sequencing grade; 1 μg per gel slice) in 25 mM NH_4HCO_3, pH 8. The digest was conducted for 16 h at 37°C. Peptides were then extracted into 5% formic acid, 50% acetonitrile, 45% water and brought to 20 μl final volume and stored at −80°C until analysis.

Peptide biomarker analysis via SRM mass spectrometry

Biomarker peptides for Group RSB_{12} were identified for detection by SRM. In SRM, parent ions of the correct mass for the peptides of interest are detected and isolated in the mass spectrometer within a narrow mass window. Those ions are then fragmented and the intensity of specific characteristic ions produced in the fragmentation (product ions) are quantified. To be identified positively as the analyte of interest using SRM mass spectrometry, the compound must be detected with the same parent mass and the relative magnitude of the characteristic product ions detected must be the same as an authentic standard. In this case, stable isotopically labelled versions of the peptides of interest serve as internal authentic reference standards and can be included in

the same liquid chromatographic separation as the peptides from field samples. The combination of high parent mass resolution, the identification of multiple fragment ions in correct relative magnitude, and having the correct retention time relative to an authentic standard should greatly reduce the likelihood for false positive identifications.

Peptides chosen as SRM-based biomarkers were present in most Group RSB_{12} sequences and not in other CbiA sequences detected in this study or in other protein sequences in the NCBI nr and envr_nr databases (as of 15 July, 2010). They were also in the mass range of 800–2400 Da and lacking methionine or cysteine to facilitate mass spectrometry analysis. Heavy isotope-labelled versions of the biomarker peptides were obtained from Sigma-Aldrich (Stemmann *et al.*, 2001) and handled according to the manufacturer's instructions. Heavy and native sequences of peptides, their parent and product ions monitored, and collision energies are shown in Table 3. Each gel slice (two protein samples, five slices each) was analysed in triplicate. Whole-cell tryptic digests of *C. watsonii*, a marine cyanobacteria that does not contain Group RSB_{12} peptides based on its genome, was used as a negative control. The cyanobacterial sample was processed similarly to the field samples described above except without SDS-PAGE separation. To prepare samples for mass spectrometry analysis, 150 fmol of each heavy labelled peptide was added to approximately 1 μg of protein and the mixture was brought to 50 μl with 2% acetonitrile and 0.1% formic acid for injection.

Selected reaction monitoring analyses were performed on a Thermo Vantage TSQ triple quadrupole mass spectrometer with a Michrom Advance captive spray ion source. The SRM reactions were validated through tuning the mass spectrometer on the heavy labelled peptides described above, introduced by direct infusion, to select the most abundant transitions for monitoring and to optimize the collision energies (Table 3). Q1 operated in 0.2 FWHM (full width at half maximum) resolution while Q3 operated in 0.7 FWHM resolution. All SRMs were monitored over the full chromatographic separation. Reverse phase chromatographic separation consisted of a peptide Cap Trap in-line with a reversed phase Magic C18 AQ column (0.2 × 50 mm, 3 mm particle size, 200 Å pore size) on a Paradigm MS4 HPLC system at a flow rate of 4 μl min^{-1} with a gradient from 5% buffer B then to 45% buffer B over 25 min and to 95% buffer B in 10 min where A was 0.1% formic acid (Michrom) in water (Fisher LC/MS Optima) and B was 0.1% formic acid in acetonitrile (Fisher LC/MS Optima).

Acknowledgements

We are indebted to Falicia Goh, Tim Salmon and other members of the Neilan Lab at UNSW for technical assistance and helpful discussions. We thank Tyler Goepfert for assistance in collecting field samples, Abigail Noble for assistance with cobalt analyses and to Dan Rogers and Erin Banning for assistance with data analysis and helpful discussions. Thanks to Vladimir V. Bulygin for technical assistance with peptide analyses and to Andrew Allen for helpful discussions regarding eukaryotic and metagenomic sequences. Special thanks to the Captain, Crew, and Raytheon Marine and Science Technical Staff of the R/V N.B. Palmer and CORSACS science parties including Chief Scientist Jack DiTullio. This research was supported by NSF grants OPP-0440840, OCE-0327225, OCE-0452883, OPP-0732665, OCE-0752291, The Center for Environmental Bioinorganic Chemistry at Princeton, The Center for Microbial Oceanography: Research and Education (CMORE), the Australian Research Council, and EPA STAR and NSF Graduate Research Fellowships to EMB.

References

Altschul, S.F., Gish, W., Miller, W., Myers, E.W., and Lipman, D.J. (1990) Basic local alignment search tool. *J Mol Biol* **215:** 403–410.

Bertrand, E.M., Saito, M.A., Rose, J.M., Riesselman, C.R., Lohan, M.C., and Noble, A.E *et al.* (2007) Vitamin B_{12} and iron co-limitation of phytoplankton growth in the Ross Sea. *Limnol Oceanogr* **52:** 1079–1093.

Bonnet, S., Webb, E.A., Panzeca, C., Karl, D.M., Capone, D.G., and Sanudo-Wilhelmy, S.A. (2010) Vitamin B_{12} excretion by cultures of the marine cyanobacteria *Crocosphaera* and *Synechococcus*. *Limnol Oceanogr* **55:** 1959–1964.

Bruland, K.W., Rue, E.L., Smith, G.J., and DiTullio, G.R. (2005) Iron, macronutrients and diatom blooms in the Peru Upwelling regime: brown and blue waters of Peru. *Mar Chem* **93:** 81–103.

Buesseler, K., Ball, L., Andrews, J., Cochran, J.K., Hirschberg, D., and Bacon, M.P *et al.* (2001) Upper ocean export of particulate organic carbon and biogenic silica in the Southern ocean along 107.1W. *Deep Sea Res Part II Top Stud Oceanogr* **48:** 4275–4297.

Caron, D.A., Dennett, M.A., Lonsdale, D.J., Moran, D.M., and Shalapyonok, L. (2000) Microzooplankton herbivory in the Ross Sea, Antarctica. *Deep Sea Res Part II Top Stud Oceanogr* **47:** 3249–3272.

Church, M.J., Hutchins, D.A., and Ducklow, H.W. (2000) Limitation of bacterial growth by dissolved organic matter and iron in the Southern Ocean. *Appl Environ Microbiol* **66:** 455–466.

Church, M.J., Short, C.M., Jenkins, B.D., Karl, D.M., and Zehr, J.P. (2005) Temporal patterns of nitrogenase gene (*nifH*) expression in the oligotrophic North Pacific Ocean. *Appl Environ Microbiol* **71:** 5362–5370.

Coale, K.H., Wang, X., Tanner, S.J., and Johnson, K.S. (2003) Phytoplankton growth and biological response to iron and zinc addition in the Ross Sea and Antarctic Circumpolar Current along 170W. *Deep Sea Res Part II Top Stud Oceanogr* **50:** 635–653.

Croft, M.T., Lawrence, A.D., Raux-Deery, E., Warren, M.J., and Smith, A.G. (2005) Algae acquire vitamin B12 through a symbiotic relationship with bacteria. *Nature* **438:** 90–93.

Debussche, L., Thibaut, D., Cameron, B., Crouzet, J., and Blanche, F. (1990) Purification and Characterization of Cobyrinic Acid *a,c*-Diamide Synthase from *Pseudomonas denitrificans*. *J Bacteriol* **172:** 6239–6244.

DiTullio, G., Grebmeier, J.M., Arrigo, K.R., Lizotte, M.P., Robinson, D.H., and Leventer, A., *et al.* (2000) Rapid and early export of Phaeocystis antarctica blooms in the Ross Sea, Antarctica. *Nature* **404:** 595–598.

Droop, M.R. (2007) Vitamins, phytoplankton and bacteria: symbiosis or scavenging? *J Plankton Res* **29:** 107–113.

Ducklow, H. (2000) Bacterial Production and Biomass in the Oceans. In *Microbial Ecology of the Oceans*. Kirchman, D. (ed.). New York, USA: Wiley-Liss, pp. 85–120.

Ducklow, H.W., Dickson, M.-L., Kirchman, D.L., Steward, G., Orchardo, J., Marra, J., and Azam, F. (2000) Constraining bacterial production, conversion effciency and respirationin the Ross Sea, Antarctica, January–February, 1997. *Deep Sea Res Part II Top Stud Oceanogr* **47:** 3227–3247.

Ducklow, H.W., Carlson, C.A., Church, M., Kirchman, D.L., Smith, D., and Steward, G. (2001) The seasonal development of the bacterioplankton bloom in the Ross Sea, Antarctica, 1994–1997. *Deep Sea Res Part II Top Stud Oceanogr* **48:** 4199–4221.

Francis, C.A., Roberts, K.J., Beman, M.J., Santoro, A.E., and Oakley, B.B. (2005) Ubiquity and diversity of ammonia-oxidizing archaea in water columns and sediments of the ocean. *Proc Natl Acad Sci USA* **102:** 14683–14688.

Fresquet, V., Williams, L., and Raushel, F.M. (2004) Mechanism of Cobyrinic Acid a,c-Diamide Synthetase from *Salmonella typhimurium* LT2. *Biochem* **43:** 10619–10627.

Galperin, M.Y., and Grishin, N.V. (2000) The synthetase domains of cobalamin biosynthesis amidotransferases CobB and CobQ belong to a new family of ATP-dependent amidoligases, related to dethiobiotin synthetase. *Proteins* **41:** 238–247.

Gentile, G., Giuliano, L., D'Auria, G., Smedile, F., Azzaro, M., Domenico, M., and Yakimov, M.M. (2006) Study of bacterial communities in Antarctic coastal waters by a combination of 16S rRNA and 16S rDNA sequencing. *Environ Microbiol* **8:** 2150–2161.

Gobler, C.J., Norman, C., Panzeca, C., Taylor, G.T., and Sanudo-Wilhelmy, S.A. (2007) Effect of B-vitamins and inorganic nutrients on algal bloom dynamics in a coastal ecosystem. *Aquat Microb Ecol* **49:** 181–194.

Hall, J.A., and Safi, K. (2001) The impact of in situ Fe fertilization on the microbial food web in the Southern Ocean. *Deep Sea Res Part II Top Stud Oceanogr* **48:** 2591–2613.

Hansel, C.M., Fendorf, S., Jardine, P.M., and Francis, C.A. (2008) Changes in bacterial and archaeal community structure and functional diversity along a geochemically variable soil profile. *Appl Environ Microbiol* **74:** 1620–1633.

Karl, D.M. (2002) Nutrient dynamics in the deep blue sea. *Trends Microbiol* **10:** 410–418.

Kinter, M., and Sherman, M. (2000) *Protein Sequencing and Identification Using Tandem Mass Spectrometry*. New York, USA: John Wiley & Sons.

Leipe, D.D., Wolf, Y.I., Koonin, E.V., and Aravind, L. (2002) Classification and Evolution of P-loop GTPases and Related ATPases. *J Mol Biol* **317:** 41–72.

Marchant, H.J., Davidson, A.T., and Wright, S. W. (1987) The distribution and abundance of chroococcoid cyanobacteria in the Southern Ocean. *Proc NIPR Symp Polar Biol* **1:** 1–9.

Martin, J.H., Fitzwater, S.E., and Gordon, R.M. (1990) Iron deficiency limits phytoplankton productivity in Antarctic waters. *Global Biogeochem Cycles* **4:** 5–12.

Medigue, C., Krin, E., Pascal, G., Barbe, V., Bernsel, A., Bertin, P., *et al.* (2005) Coping with cold: the genome of the versatile marine Antarctica bacterium *Pseudoalteromonas haloplanktis* TAC125. *Genome Res* **15:** 1325–1335.

Menzel, D.W., and Spaeth, J.P. (1962) Occurrence of vitamin B_{12} in the Sargasso Sea. *Limnol Oceanogr* **7:** 151–154.

Murray, A.E., and Grzymski, J.J. (2007) Diversity and genomics of Antarctic marine micro-organisms. *Phil Trans Royal Soc B* **362:** 2259–2271.

Muto, A., and Osawa, S. (1987) The guanine and cytosine content of genomic DNA and bacterial evolution. *Proc Natl Acad Sci USA* **84:** 166–169.

Neilan, B.A., Burns, B.P., Relman, D.A., and Lowe, D.R. (2002) Molecular identification of cyanobacteria associated with stromatolites from distinct geographical locations. *Astrobiology* **2:** 271–280.

Oliver, J.L., Barber, R.T., Smith, W.O., and Ducklow, H.W. (2004) The heterotrophic bacterial response during the Southern Ocean Iron Experiment (SOFeX). *Limnol Oceanogr* **49:** 2129–2140.

Pakulski, J.D., Coffin, R.B., Kelley, C.A., Holder, S.L., Downer, R., Aas, P., *et al.* (1996) Iron stimularion of Antarctic bacteria. *Nature* **383:** 133–134.

Panzeca, C., Tovar-Sanchez, A., Agusti, S., Reche, I., Duarte, M., Taylor, G.T., and Sanudo-Wilhelmy, S.A. (2006) B vitamins as regulators of phytoplankton dynamics. *EOS* **87:** 593–596.

Panzeca, C., Beck, A., Leblanc, K., Taylor, G.T., Hutchins, D.A., and Sanudo-Wilhelmy, S.A. (2008) Potential cobalt limitation of vitamin B_{12} synthesis in the North Atlantic Ocean. *Global Biogeochem Cycles* **22:** 223–230.

Partensky, F., Hess, W.R., and Vaulot, D. (1999) *Prochlorococcus*, a marine photosynthetic prokaryote of global significance. *Microbial Mol Biol Rev* **63:** 106–127.

Porter, K.G., and Feig, Y.G. (1980) The use of DAPI for identifying and counting aquatic microflora. *Limnol Oceanogr* **25:** 943–948.

Raux, E., Schubert, H.L., Roper, J.M., Wilson, K.S., and Warren, M.J. (1999) Vitamin B_{12}: insight into biosynthesis's mount improbable. *Bioorganic Chem* **27:** 100–118.

Raux, E., Schubert, H.L., and Warren, M.J. (2000) Biosynthesis of cobalamin (vitamin B_{12}): a bacterial conundrum. *Cell Mol Life Sci* **57:** 1880–1893.

Rodionov, D.A., Vitreschak, A.G., Mironov, A.A., and Gelfand, M.S. (2003) Comparative genomics of the vitamin B_{12} metabolism and regulation in prokaryotes. *J Biol Chem* **278:** 41148–41159.

Roth, J.R., Lawrence, J.G., and Bobik, T.A. (1996) Cobalamin (coenzyme B_{12}): synthesis and biological significance. *Annu Rev Microbiol* **50:** 137–181.

Saito, M.A., and Moffett, J.W. (2001) Complexation of cobalt by natural organic ligands in the Sargasso Sea as determined by a new high-sensitivity electrochemical cobalt speciation method suitable for open ocean work. *Mar Chem* **75:** 49–68.

Saito, M.A., and Moffett, J.W. (2002) Temporal and spatial variability of cobalt in the Atlantic Ocean. *Geochim Cosmochim Acta* **66:** 1943–1953.

Saito, M.A., Moffett, J.W., and DiTullio, G. (2004) Cobalt and nickel in the peru upwelling region: a major flux of cobalt utilized as a micronutrient. *Global Biogeochem Cycles* **18:** GB4030.

Saito, M.A., Rocap, G., and Moffett, J.W. (2005) Production of cobalt binding ligands in a *Synechococcus* feature at the Costa Rica Upwelling Dome. *Limnol Oceanogr* **50:** 279–290.

Saito, M.A., Goepfert, T.J., Noble, A.E., Bertrand, E.M.,

Sedwick, P.N., and DiTullio, G.R. (2010) A seasonal study of dissolved cobalt in the Ross Sea, Antarctica: micronutrient behavior, absence of scavenging, and relationships with Zn, Cd, and P. *Biogeosciences* **7:** 4059–4082.

Sañudo-Wilhelmy, S.A., Okbamichael, M., Gobler, C.J., and Taylor, G.T. (2006) Regulation of phytoplankton dynamics by vitamin B12. *Geophys Res Lett* **33:** 4604–4608.

Scanlan, D., and West, N.J. (2002) Molecular ecology of the marine cyanobacterial genera *Prochlorococcus* and *Synechococcus*. *FEMS Microb Ecol* **40:** 1–12.

Sedwick, P.N., DiTullio, G.R., and Mackey, D.J. (2000) Iron and manganese in the Ross Sea, Antarctica: seasonal iron limitation in Antarctic shelf waters. *J Geophys Res* **105:** 11321–11336.

Seshadri, R., Kravitz, S.A., Smarr, L., Gilna, P., and Frazier, M. (2007) CAMERA: a community resource for metagenomics. *PLoS Biol* **5:** 0394–0397.

Smith, W.O.J., and Nelson, D.M. (1985) Phytoplankton bloom produced by a receding ice edge in the Ross Sea: spatial coherence with the density. *Science* **227:** 163–166.

Stemmann, O., Zou, H., Gerber, S.A., Gygi, S.P., and Kirschner, M.W. (2001) Dual inhibition of sister chromatid separation at metaphase. *Cell* **107:** 715–726.

Steward, G.F., Jenkins, B.D., Ward, B.W., and Zehr, J.P. (2005) Development and testing of a DNA macroarray to assess nitrogenase (*nifH*) gene diversity. *Appl Environ Microbiol* **70:** 1455–1465.

Swift, D. (1981) Vitamin levels in the Gulf of Maine and ecological significance of vitamin B12 there. *J Mar Res* **39:** 375–403.

Thompson, J.D., Higgins, D.G., and Gibson, T.J. (1994) CLUSTAL W: improving the sensitivity of progressive multiple sequence alignment through sequence weighting, position-specific gap penalties and and weight matrix choice. *Nucleic Acids Res* **22:** 4673–4680.

Wagner, M., Roger, A.J., Flax, J.L., Brusseau, G.A., and Stahl, D.A. (1998) Phylogeny of dissimilatory sulfite reductases supports an early origin of sulfate respiration. *J Bacteriol* **180:** 2975–2982.

Webster, N.S., Negri, A.P., Munro, M.M., and Battershill, C.N. (2004) Diverse microbial communities inhabit Antarctic sponges. *Environ Microbiol* **6:** 288–300.

Yu, Y., Breitbart, M., McNairnie, P., and Rohwer, F. (2006) FastGroupII: a web-based bioinformatics platform for analyses of large 16S rDNA libraries. *BMC Bioinformatics* **7:** 57.

Supporting information

Additional Supporting Information may be found in the online version of this article:

Fig. S1. Neighbour-joining tree of DNA encoding 16S rRNA gene sequences from 20–100 m depths. The tree is rooted with Methanococcoides and Nitrosopumilus and shown with bootstrap values > 50% (4000 replicates). Reference sequences shown in grey are the closest cultured representatives to each of the environmental sequences displayed. Environmental sequences are labelled in black, as RossSeaNX19100m2 for example, which denotes the 2nd sequence from 100 m depth at station NX19 of the Ross Sea. Major groups are displayed with % of the library classified within that group. Thirty-eight different operational taxonomic units' (97% similarity) were recovered from 41 clone sequences. Alpha- and Gammaproteobacteria and the Bacteroidetes group dominated the 16S rRNA gene sequences recovered from Station NX 19.

Table S1. Identification of representative 16S rRNA gene clone sequences from Station NX19 in the Ross Sea based on percentage identity to sequences in the NCBI nr database.

Please note: Wiley-Blackwell are not responsible for the content or functionality of any supporting materials supplied by the authors. Any queries (other than missing material) should be directed to the corresponding author for the article.

Supplemental Material

For Bertrand et al "A new group of putative polar vitamin B_{12} biosynthesizers"

DNA compliment of 16S rRNA gene sequencing

A neighbor-joining tree based on DNA complements of 16S rRNA gene sequences obtained from station NX 19 in the Ross Sea, is shown in Figure 1. Thirty-eight different OTU's (3% cutoff) were recovered from 41 sequences. The sequenced diversity was dominated by Alpha- and Gammaproteobacteria and the Bacteroidetes group. Table 2 lists the sequences found in the NCBI nr database that were most closely related to the main groups of sequences identified in this study. These results are broadly consistent with a previous study in Terra Nova Bay of the Ross Sea, where DNA complements of 16S rRNA gene sequence library analyses revealed a dominance of eukaryotic plastids, Gammaproteobacteria and Bacteroidetes in samples most representative of open water in the Ross Sea (Gentile et al., 2006). Other studies of the 16S rRNA gene or its DNA complement in clone libraries from Antarctic water column communities have also shown these same broad trends, with Alpha- and Gammaproteobacteria and the Bacteroidetes dominating the diversity (Webster et al., 2004; Murray and Grzymski, 2007).

The Terra Nova Bay study (Gentile et al., 2006) found a smaller percentage of Alphaproteobacteria than this study, perhaps indicative of true community composition differences since the samples analyzed in this study come from the central Ross Sea rather than the coastal area associated with Terra Nova Bay and open ocean regions generally have microbial communities with higher percentages of Alphaproteobacteria (Morris et al., 2002). The

Alphaproteobacterial sequences detected in this study branch closely with the SAR11 clade, consistent with previous Antarctic studies (Murray and Grzymski, 2007). The SAR11 clade comprises a large portion marine microbial communities (Morris et al., 2002), and has been found to comprise ~20% of the bacterial community in waters off the Antarctic Peninsula (Murray and Grzymski, 2007). Notably absent from the Alphaproteobacterial sequences detected in this study are representatives of the Roseobacter clade. This is in contrast to some previous studies where considerable numbers of Roseobacter-like sequences were recovered (Murray and Grzymski, 2007), but consistent with others where few Roseobacter-like sequences were found (Gentile et al. 2006). In addition, the dominance of the Bacteroidetes in this library is notable. This group is becoming increasingly recognized as an important component of marine microbial communities in general (Fuhrman and Hagstrom, 2008) even more-so in marine Antarctic bacterial communities, where many studies have shown this group to be an important portion of the microbial community, particularly during and after substantial phytoplankton blooms (Murray and Grzymski, 2007).

The lack of Cyanobacterial 16S rRNA gene sequences detected in this study using both universal, as well as targeted primers (Jungblut et al., 2005), confirmed other microbiological and molecular studies that have shown Cyanobacteria to be essentially absent from Antarctic marine waters (Marchant et al., 1987; Marchant, 2005; Gentile et al., 2006). This is relevant for vitamin B_{12} dynamics because the genomes of all sequenced representatives of the marine Cyanobacteria indicate that they possess the vitamin B_{12} biosynthesis pathway.

Methods for 16S rRNA gene profiling

The 16S rRNA gene was amplified from DNA extracted from station NX 19 as described in the main text with the universal 27F (5'- AGAGTTTGATCCTGGCTCAG) and 1494R (5' TACGGTTACCTTGTTACGAC) primer set (Neilan et al., 2002), with the following protocol: 94° C for 4 min, 80°C for 2 min (hot start), 25 cycles of 94° C for 20 s, 55° C for 30 s and 72° C for 60 s; and 72° C for 7 min. Samples were cloned into competent *E.coli* DH5 alpha using the pGEM-T-Easy vector (Promega). PCR amplification of the cyanobacterial partial DNA complement of 16S rRNA was also attempted using the cyanobacterial-specific primer set 27F1 (5' AGAGTTTGATCCTGGCTCAG 3') and 809R (5' GCTTCGGCACGGCTCGGGTCGATA 3') (Jungblut et al., 2005). DNA samples from NX19, as well as positive control DNA from *Microcystis aeruginosa* PCC 7806 and negative control DNA from *Escherichia coli*, was used under a range of test conditions, however, amplification was only observed with the *Microcystis* sp. control.

Sequencing was performed as described in the main text for functional genes. Subsequent analyses of partial 16S sequences were conducted on a 400 bp region. These sequence data have been submitted to the GenBank database under accession numbers HQ326536 to HQ326577.

Table S1: Identification of representative 16S rRNA gene clone sequences from Station NX19 in the Ross Sea based on percentage identity to sequences in the NCBI nr database.

Bacterial Division	Representative Clone	Closest relative (Genbank accession no.)	% identity
Alphaproteobacteria	RossSeaNX1960m3	*alpha proteobacterium* IMCC10404 (FJ532499)	98
	RossSeaNX1960m4	*alpha proteobacterium* IMCC10404 (FJ532499)	100
Gammaproteobacteria	RossSeaNX19100m11	Psychrobacter sp. tsz26 (FJ979856)	100
	RossSeaNX1960m4	Uncultured gamma proteobacterium clone 22110149 (AY661623)	98
	RossSeaNX19100m14	Gamma proteobacterium HTCC154 (AY102023)	99
Bacteroidetes	RossSeaNX19100m13	Uncultured bacterium clone EI_40 (AM921069)	99
	RossSeaNX19100m4	Uncultured Flavobacteria bacterium clone NorSea54 (AM279200)	100
	RossSeaNX1940m1	Polaribacter sp. NF3-11 (FJ196052)	99

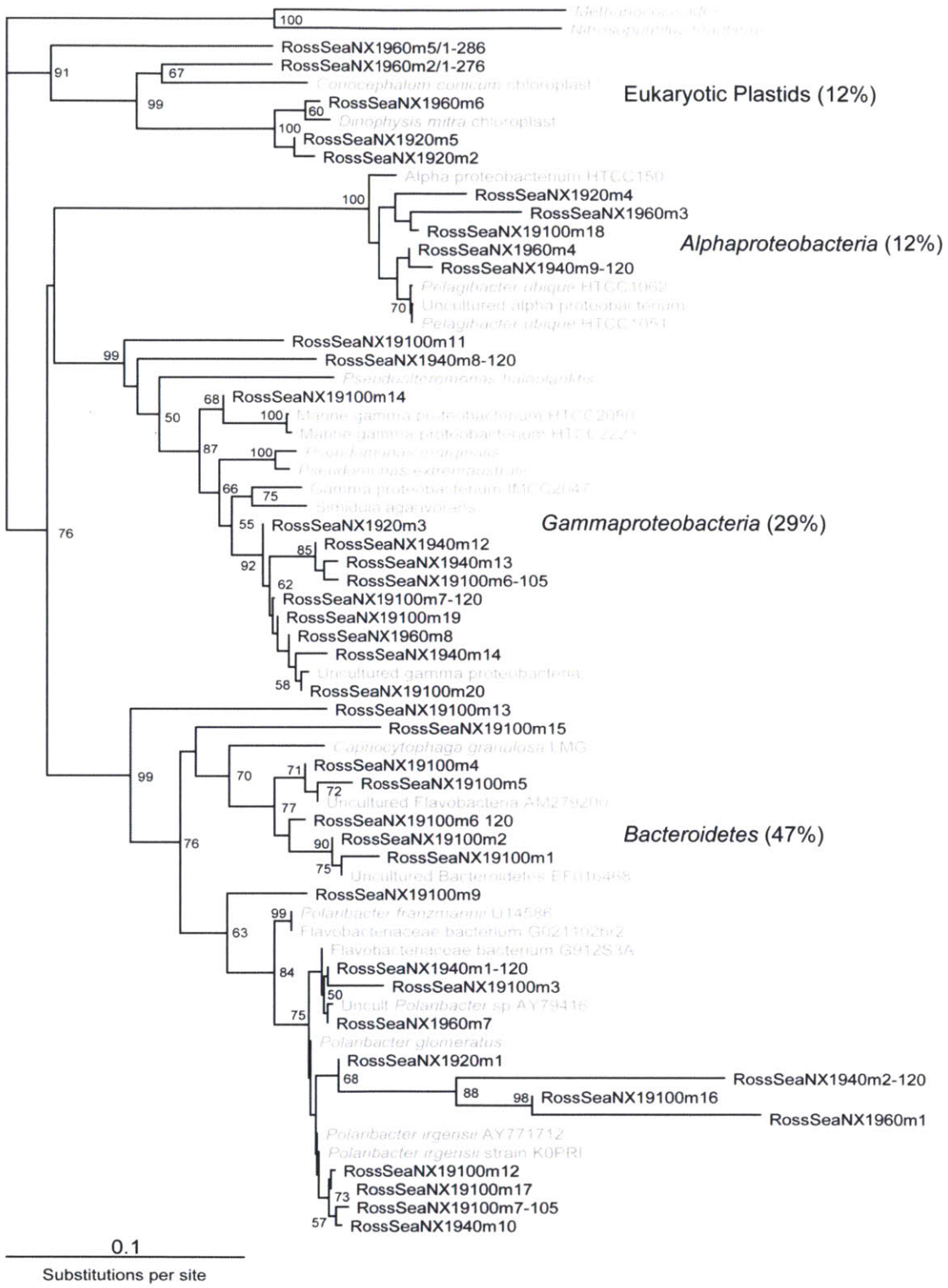
RossSeaNX1960m5/1-286
RossSeaNX1960m2/1-276
RossSeaNX1960m6
RossSeaNX1920m5
RossSeaNX1920m2
Eukaryotic Plastids (12%)
RossSeaNX1920m4
RossSeaNX1960m3
RossSeaNX19100m18
RossSeaNX1960m4
RossSeaNX1940m9-120
Alphaproteobacteria (12%)
RossSeaNX19100m11
RossSeaNX1940m8-120
RossSeaNX19100m14
RossSeaNX1920m3
RossSeaNX1940m12
RossSeaNX1940m13
RossSeaNX19100m6-105
RossSeaNX19100m7-120
RossSeaNX19100m19
RossSeaNX1960m8
RossSeaNX1940m14
RossSeaNX19100m20
Gammaproteobacteria (29%)
RossSeaNX19100m13
RossSeaNX19100m15
RossSeaNX19100m4
RossSeaNX19100m5
RossSeaNX19100m6 120
RossSeaNX19100m2
RossSeaNX19100m1
Bacteroidetes (47%)
RossSeaNX19100m9
RossSeaNX1940m1-120
RossSeaNX19100m3
RossSeaNX1960m7
RossSeaNX1920m1
RossSeaNX1940m2-120
RossSeaNX19100m16
RossSeaNX1960m1
RossSeaNX19100m12
RossSeaNX19100m17
RossSeaNX19100m7-105
RossSeaNX1940m10
0.1
Substitutions per site

Figure S1: Neighbor-joining tree of DNA encoding 16S rRNA gene sequences from 20-100 m depths. The tree is rooted with *Methanococcoides* and *Nitrosopumilus* and shown with bootstrap values >50% (4000 replicates). Reference sequences shown in grey are the closest cultured representatives to each of the environmental sequences displayed. Environmental sequences are labeled in black, as RossSeaNX19100m2 for example, which denotes the 2nd sequence from 100 m depth at station NX19 of the Ross Sea. Major groups are displayed with % of the library classified within that group. Thirty-eight different OTU's (97% similarity) were recovered from 41 clone sequences. *Alpha-* and *Gammaproteobacteria* and the *Bacteroidetes* group dominated the 16S rRNA gene sequences recovered from Station NX 19.

References for Supplemental Information

Fuhrman, J.A., and Hagstrom, A. (2008) Bacterial and archaeal community structure and its pattern. In *Microbial Ecology of the Oceans*. Kirchman, D.L. (ed). Hoboken, NJ: John Wiley and Sons.

Gentile, G., Giuliano, L., D'Auria, G., Smedile, F., Azzaro, M., Domenico, M., and Yakimov, M.M. (2006) Study of bacterial communities in Antarctic coastal waters by a combination of 16S rRNA and 16S rDNA sequencing. *Environ Microbiol* **8**: 2150–2161.

Jungblut, A.D., Hawes, I., Mountfort, D., Hitzfeld, B.C., Dietrich, D.R., Burns, B.P. et al. (2005) Diversity of cyanobacterial mat communities in variable salinity meltwater ponds of McMurdo Ice Shelf. *Environ Microbiol* **7**: 519-529.

Marchant, H.J. (2005) Cyanophytes. In *Antarctic marine protists*. Scott, F.J., and H. J. Marchant. (ed) Australian Biological Resources Study.

Marchant, H.J., Davidson, A.T., and S.W., W. (1987) The distribution and abundance of chroococcoid cyanobacteria in the Southern Ocean. *Proc NIPR Symp Polar Biol* **1**: 1-9.

Morris, R.M., Rappe, M.S., Connon, S.A., Vergin, K.L., Siebold, W.A., Carlson, C.A., and Giovanonni, S.J. (2002) SAR11 clade dominates ocean surface bacterioplankton communities. *Nature* **420**: 806-810.

Murray, A.E., and Grzymski, J.J. (2007) Diversity and genomics of Antarctic marine micro-organisms. *Phil Trans of the Royal Soc B* **362**: 2259-2271.

Neilan, B.A., Burns, B.P., Relman, D.A., and Lowe, D.R. (2002) Molecular identification of cyanobacteria associated with stromatolites from distinct geographical locations. *Astrobiol* **2**: 271-280.

Webster, N.S., Negri, A.P., Munro, M.M., and Battershill, C.N. (2004) Diverse microbial communities inhabit Antarctic sponges. *Environl Microbiol* **6**: 288-300.

Chapter 3

Iron limitation of a springtime bacterial and phytoplankton community in the Ross Sea: implications for vitamin B_{12} nutrition

Iron limitation of a springtime bacterial and phytoplankton community in the Ross Sea: implications for vitamin B_{12} nutrition. *Frontiers in Aquatic Microbiology*. 2011 E.M Bertrand, M.A. Saito, P.A. Lee, R.B. Dunbar, P. N. Sedwick, and G. R. DiTullio. Volume 2, article 160.

frontiers in
MICROBIOLOGY

ORIGINAL RESEARCH ARTICLE
published: xx August 2011
doi: 10.3389/fmicb.2011.00160

Iron limitation of a springtime bacterial and phytoplankton community in the Ross Sea: implications for vitamin B_{12} nutrition

Erin M. Bertrand[1], Mak A. Saito[2]*, Peter A. Lee[3], Robert B. Dunbar[4], Peter N. Sedwick[5] and Giacomo R. DiTullio[6]

[1] *MIT/WHOI Joint Program in Chemical Oceanography and Marine Chemistry and Geochemistry Department, Woods Hole Oceanographic Institution, Woods Hole, MA, USA*
[2] *Marine Chemistry and Geochemistry Department, Woods Hole Oceanographic Institution, Woods Hole, MA, USA*
[3] *Hollings Marine Laboratory, College of Charleston, Charleston, SC, USA*
[4] *Department of Environmental Earth Systems Science, Stanford University, Stanford, CA, USA*
[5] *Department of Ocean, Earth and Atmospheric Science, Old Dominion University, Norfolk, VA, USA*
[6] *Hollings Marine Laboratory, College of Charleston, Charleston, SC, USA*

Edited by:
Karla B. Heidelberg, University of Southern California, USA

Reviewed by:
Chris Gobler, Stony Brook University, USA
Sergio Sanudo-Wilhelmy, University of Southern California, USA

****Correspondence:***
Mak A. Saito, Marine Chemistry and Geochemistry Department, Woods Hole Oceanographic Institution, 360 Woods Hole Road, Woods Hole, MA 02543, USA.
e-mail: msaito@whoi.edu

The Ross Sea is home to some of the largest phytoplankton blooms in the Southern Ocean. Primary production in this system has previously been shown to be iron limited in the summer and periodically iron and vitamin B_{12} colimited. In this study, we examined trace metal limitation of biological activity in the Ross Sea in the austral spring and considered possible implications for vitamin B_{12} nutrition. Bottle incubation experiments demonstrated that iron limited phytoplankton growth in the austral spring while B_{12}, cobalt, and zinc did not. This is the first demonstration of iron limitation in a *Phaeocystis antarctica*-dominated, early season Ross Sea phytoplankton community. The lack of B_{12} limitation in this location is consistent with previous Ross Sea studies in the austral summer, wherein vitamin additions did not stimulate *P. antarctica* growth and B_{12} was limiting only when bacterial abundance was low. Bottle incubation experiments and a bacterial regrowth experiment also revealed that iron addition directly enhanced bacterial growth. B_{12} uptake measurements in natural water samples and in an iron fertilized bottle incubation demonstrated that bacteria serve not only as a source for vitamin B_{12}, but also as a significant sink, and that iron additions enhanced B_{12} uptake rates in phytoplankton but not bacteria. Additionally, vitamin uptake rates did not become saturated upon the addition of up to 95 pM B_{12}. A rapid B_{12} uptake rate was observed after 13 min, which then decreased to a slower constant uptake rate over the next 52 h. Results from this study highlight the importance of iron availability in limiting early season Ross Sea phytoplankton growth and suggest that rates of vitamin B_{12} production and consumption may be impacted by iron availability.

Keywords: iron limitation, vitamin B_{12}, Ross Sea, colimitation, bacteria, phytoplankton, iron fertilization

INTRODUCTION

The Ross Sea of the Southern Ocean (**Figure 1**) hosts massive phytoplankton blooms (Smith and Nelson, 1985) and high rates of dimethylsulfoniopropionate (DMSP) production (DiTullio and Smith, 1995). As a result, this and similar Antarctic coastal ecosystems are considered to have a significant impact on global biogeochemical cycles (Arrigo et al., 1999, 2008). The phytoplankton community in the Ross Sea is typically dominated by the colonial haptophyte *Phaeocystis antarctica* (DiTullio and Smith, 1996) and pennate diatoms such as *Fragilariopsis* and *Pseudonitzschia* spp. (Leventer and Dunbar, 1996; Arrigo et al., 1999; Armand et al., 2005). Because of the significantly higher C:P and N:P ratios of *P. antarctica* compared to diatom communities, the relative abundances of *P. antarctica* and diatoms in the Ross Sea may control carbon uptake and export in the region (Arrigo et al., 1999). These community dynamics are thought to be controlled in part by irradiance, with diatoms dominating when mixed layers are shallow (high irradiance, associated with sea ice meltwater), and *P. antarctica* dominating when mixed layers are deep (low irradiance; DiTullio and Smith, 1996; Arrigo et al., 1999).

Iron has been shown to exert a controlling influence on primary productivity in the Ross Sea, particularly in the austral summer months (Martin et al., 1990; Sedwick and DiTullio, 1997; Sedwick et al., 2000; Bertrand et al., 2007). Iron availability is also thought to impact Ross Sea phytoplankton community composition, as iron additions have in some cases caused substantive diatom blooms (Martin et al., 1990; Sedwick et al., 2000; Rose et al., 2009; Feng et al., 2010). However, other experiments have shown that field populations of *P. antarctica* may also benefit from iron addition (Olson et al., 2000; Coale et al., 2003; Bertrand et al., 2007). It has previously been suggested that elevated dissolved iron concentrations in the springtime, supplied by winter mixing and sea

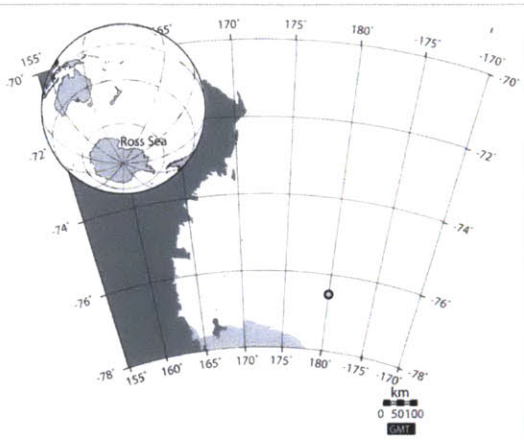

FIGURE 1 | Map of the Ross Sea, with inset globe for orientation, showing the location of the main experiments in this study station SP3, 76.50°S 179.99W. Light gray denotes the approximate location of the ice shelf, while dark gray denotes land.

ice melt, are progressively depleted via phytoplankton uptake, thus resulting in low dissolved iron concentrations and iron limitation of primary productivity during the summer Sedwick et al., 2000; Coale et al., 2005). However, more recent work revealed relatively low dissolved iron concentrations in the Ross Sea polynya during the spring, thus challenging the conceptual model of a gradual progression toward iron limitation of phytoplankton growth (Sedwick et al., in review).

There is increasing evidence that the availability of vitamin B_{12} can also play a role in shaping phytoplankton dynamics in Antarctic coastal ecosystems (Panzeca et al., 2006; Bertrand et al., 2007) as well as other environments including the Gulf of Alaska (Koch et al., 2011), Long Island embayments (Sañudo-Wilhelmy et al., 2006; Gobler et al., 2007), the Sargasso Sea (Menzel and Spaeth, 1962), and the Gulf of Maine (Swift, 1981). Shipboard bottle incubation experiments performed in the Ross Sea during austral summer 2005 demonstrated that vitamin B_{12} became the limiting nutrient once iron was replete, but only in areas with low bacterial abundance (Bertrand et al., 2007). This scenario can be referred to as periodic secondary B_{12} limitation, or vitamin and iron colimitation (Saito et al., 2008). The addition of B_{12} and iron also increased the percentage of diatoms in the bottle incubations relative to iron addition alone, suggesting that vitamin B_{12} may help govern rates of primary production as well as phytoplankton species composition.

Vitamin B_{12} is produced by some bacteria and archaea, while other prokaryotes as well as most eukaryotic phytoplankton require an exogenous supply of B_{12} to sustain growth (Roth et al., 1996; Rodionov et al., 2003; Croft et al., 2005; Tang et al., 2010). Those phytoplankton and bacteria that do not require vitamin B_{12} possess alternative biochemical pathways for accomplishing essential reactions, including use of a di-ferric form of ribonucleotide reductase (type I) rather than the B_{12}-requiring version (type II), and the use of zinc-requiring methionine synthase (MetE) rather than the version that requires vitamin B_{12} and zinc (MetH) (Zhang et al., 2009; Helliwell et al., 2011).

Biosynthesis of vitamin B_{12} requires over 30 enzymatic steps and appreciable amounts of energy, carbon, nitrogen, and transition metals including cobalt, zinc, and in some cases iron (Roth et al., 1996; Raux et al., 2000). Though some B_{12} biosynthesis genes, potentially from an undescribed clade of gamma proteobacteria, have been detected in microbial communities from the Ross Sea (Bertrand et al., 2011), the genetic potential for vitamin B_{12} production remains largely uncharacterized in the Ross Sea or in any other marine environment. This is in part because 16s rRNA profiling, which is commonly used for bacterial community structure analysis, does not provide information about vitamin B_{12} production potential, since the presence of the biosynthesis pathway among bacterial and archaeal lineages is widespread and extremely variable. An exception to this is the marine cyanobacteria, where all available sequenced genomes appear to contain the B_{12} biosynthetic pathway (Rodionov et al., 2003), and a range of strains have been shown to be produce significant amounts of B_{12} (Bonnet et al., 2010). The Ross Sea and other Antarctic marine systems lack appreciable cyanobacterial populations (Caron et al., 2000; Marchant, 2005; Bertrand et al., 2011), leaving Antarctic marine systems potentially deficient in a source of this vitamin, making these regions particularly vulnerable to B_{12} limitation. In addition, genome sequences from representatives of the abundant heterotrophic bacterial clade SAR11 suggest that in addition to not producing vitamin B_{12} (Giovannoni et al., 2005), these microbes do not require the vitamin and do not possess known B_{12} uptake pathways (Zhang et al., 2009), implying that B_{12} independence may be part of the ecological niche of these abundant heterotrophic bacteria.

Either through cycling of the microbial loop (Karl, 2002; Droop, 2007) or through direct symbiotic interaction (Croft et al., 2005), bacteria and archaea must be the ultimate source of vitamin B_{12} to auxotrophic (vitamin-requiring) phytoplankton. Therefore, in areas of the ocean where vitamin B_{12} has been shown to be an important factor in determining phytoplankton growth or community composition, understanding the controls on primary productivity demands consideration of bacterial growth and dynamics. Although bacterial abundance and biomass can reach bloom proportions in the Ross Sea, bacterial production there is relatively low, especially during the austral spring (Ducklow et al., 2000, 2001). Ross Sea bacterial production is thought to be controlled by the availability of dissolved organic matter (DOM), with little direct impact of temperature (Ducklow et al., 2001). However, the role of iron in controlling bacterial production has yet to be fully investigated. Although it is possible for marine bacterial growth rates and efficiency to be limited by iron availability in cultures (Tortell et al., 1996), there has been little study of bacterial iron limitation in the field. Bacterial growth in the Southern Ocean has been observed to be DOM limited (Hall and Safi, 2001; Oliver et al., 2004), iron limited (Pakulski et al., 1996), and iron and DOM colimited (Church et al., 2000). Availability of DOM has been found to be the primary limiting factor for bacterial production in other iron limited HNLC (high nutrient low chlorophyll) areas (Hale et al., 2006), although in some regions

iron quickly becomes limiting when organic carbon limitation is alleviated (Kirchman et al., 2000). In addition, culture-based evidence suggests that low iron availability can induce the production of highly recalcitrant DOM by Antarctic phytoplankton and thus that iron and DOM limitation could be synergistically limiting bacterial growth (Becquevort et al., 2007).

In this study, we sought to investigate several parameters relevant to the cycling of iron and vitamin B_{12} in the southern Ross Sea. The results presented here indicate that availability of iron can regulate phytoplankton growth rates, impact bacterial growth, and influence B_{12} uptake rates during the austral spring.

MATERIALS AND METHODS

STUDY AREA AND WATER COLLECTION

These experiments were conducted in the Ross Sea during the CORSACS 2 cruise in austral spring 2006 (NBP0608). Additional samples were collected during the CORSACS 1 cruise in the austral summer of 2005–2006 (NBP06081). For the bottle incubation experiments, water was collected from ~3 m depth using a trace metal clean (TMC) Teflon diaphragm pumping system (Bruland et al., 2005; Sedwick et al., in review). All sample and incubation bottles used were detergent and acid-cleaned [0.1% citranox for 48 h, 10% HCl (Baker, Instra-analyzed) for 7 days, clean pH 2 water (dilute HCl) rinsed]. Sample bottles were filled and manipulated in a positive-pressure TMC environment constructed with laminar flow hoods and plastic sheeting to avoid trace metal contamination.

SHIPBOARD BOTTLE INCUBATION STUDY

A bottle incubation experiment using whole seawater with additions of 1 nM added iron, 500 pM added cobalt, 1 nM added zinc, and 100 pM added vitamin B_{12} was started in the Ross Sea on December 3, 2006 at 76.50°S 179.99°W, hereafter referred to as Station SP3 (**Figure 1**), and carried out for 6 days. Whole seawater was dispensed into a 50 L TMC mixing carboy and from there into 2.2 L polycarbonate (PC) bottles in triplicate for each treatment (+Co, +Fe, +B_{12}, +Zn, +B_{12}Fe, +CoFe, +ZnFe, and unamended control). The bottles were tightly capped and placed outdoors in deckboard flow-through incubators at ~20% ambient light, shielded with neutral density screening. Ambient temperature (−2 to 1°C) was maintained by a constant flow of surface seawater through the incubators. Approximately every 60 h, nutrients and chlorophyll *a* (Chl *a*) were measured. At the beginning and the end of the experiment, samples were taken for phytoplankton microscopy, pigment analysis, particulate organic carbon (POC) analysis, and bacterial cell counts.

TRACE NUTRIENT SUPPLEMENTATION

In all cases, iron was added as $FeCl_3$ (Fluka), cobalt was added as $CoCl_2$ (Fluka), and zinc was added as $ZnSO_4$ (Fisher), all in weakly acidified (pH 3, SeaStar HCl) Milli-Q water. Vitamin B_{12} (Sigma, Plant-cell culture tested cyanocobalamin, 99%) was added as a solution in Milli-Q water, purified for trace metals by passing through a column of 2–3 mL of prepared Chelex-100 beads (BioRad; Price et al., 1988/1989).

BACTERIAL REGROWTH EXPERIMENT

A TMC bacterial regrowth experiment was conducted at station SP3 (**Figure 1**). Two liters of water, collected in a 2.5 L PC bottle as described above, was filtered using an acid-cleaned 0.2 μm cartridge filter and supplemented with 10% 0.65 μm filtered water, containing a portion of the free-living bacterial community from the same location (syringe filtered with an acid-cleaned PC filter membrane in an acid-cleaned 25 mm Swinnex filter holder). Triplicate aliquots of 250 mL each were removed into acid-cleaned polyethylene bottles as unamended controls. 1 nM Fe (as above) was added to the remaining mixture, and three aliquots of 250 mL each were removed into acid-cleaned polyethylene bottles for iron addition treatments. Sample aliquots (27 mL) were preserved with 10% filtered formalin and retained for bacterial cell enumeration. The experimental treatments were all incubated in the dark at 0°C. After 3 days, 10 mL was removed from each treatment, preserved with 10% filtered formalin, and reserved for bacterial cell enumeration.

NUTRIENT ANALYSIS

Nutrients, including nitrate plus nitrite, nitrite, phosphate, and silicic acid were measured in the incubation experiments approximately every 60 h, in 0.2 μm filtered subsamples from each bottle in the bottle incubation study. Analysis was performed at sea using a Lachat QuickChem Autoanalyzer. Minimum detectable levels were 0.04 μM phosphate, 0.09 μM nitrate plus nitrite, 0.01 μM nitrite, and 0.38 μM silicic acid.

BIOMASS ANALYSIS

Over the course of the bottle incubation experiment, total Chl *a* was measured approximately every 60 h using 90% acetone extracts and the non-acidified fluorometric method (Welschmeyer, 1994), employing a Turner Designs TD700 fluorometer and Whatman GF/F filters. Bacteria were enumerated using a previously published method involving DAPI (4′-6-Diamidino-2-phenylindole) staining (Porter and Feig, 1980). Samples for phytoplankton community composition analysis were preserved with 1% glutaraldehyde, filtered on to 2 μm pore size PC filters, and analyzed by using ~2000 individual counts at 100× magnification via standard epifluorescence microscopy techniques coupled with DAPI staining. Obtaining accurate cell concentration estimates was not possible by our method due to the high abundance and extensive clumping of *Phaeocystis* cells, so these counts can only be used to assess community composition, not abundance. Phytoplankton pigment samples (0.25–1 L) were filtered on to Whatman GF/F filters, flash frozen in liquid nitrogen, and stored at −80°C prior to analysis by HPLC (Zapata et al., 2000; DiTullio and Geesey, 2002). Samples for POC analysis (100–200 mL) were filtered onto pre-combusted (450°C, 2 h) Whatman GF/F glass fiber filters, which were then analyzed using a Carlo Erba NA1500 elemental analyzer/Conflo II device and a Finnigan Delta Plus mass spectrometer at the Stanford University Stable Isotope Biogeochemistry Laboratory. Elemental compositions were measured using the mass 44 beam intensity (V) on the Delta Plus, calibrated against the mass 44 beam intensity of at least five certified reference standards that were analyzed throughout the course of each run

of 40 samples. Relative reproducibility of the acetanilide standard averaged 0.65% for carbon.

VITAMIN B_{12} UPTAKE

Measurement of short-term B_{12} uptake using tracer level additions of the vitamin is difficult given the low picomolar concentrations of B_{12} in natural waters (Menzel and Spaeth, 1962; Panzeca et al., 2009). For this reason, we chose to measure "potential uptake" rates with the addition of ^{57}Co-labeled B_{12} (0.09 pM) and 40 pM unlabeled B_{12}. This measurement is practical in that it can allow for short-term rate assessments and does not require the measurement of water column vitamin concentrations. The measurements reflect rates of uptake at the specific concentration of the vitamin added and not *in situ* rates. As such, they are useful for comparing uptake rates between experimental treatments, but cannot be used to estimate the true rate of removal of B_{12} from the water column by phytoplankton and bacteria.

^{57}Co-labeled cyanocobalamin was used to measure the rate of vitamin B_{12} uptake at the site of the bottle incubation study and in the community present at the end of the bottle incubation experiments, as well as at other sites within the Ross Sea. Uptake by the >2 and >0.2-μm size fractions was measured according to previously published protocols (Bertrand et al., 2007). Briefly, approximately 0.09 pM ^{57}Co B_{12} (360 μCi/g ^{57}Co B_{12}) and 40 pM unlabeled vitamin B_{12} were added to duplicate or triplicate 160 mL PC bottles filled with whole sea water from specific Ross Sea locations or with aliquots of whole incubation experiment water from the different incubation treatments described above. After 24 h, the samples were filtered through 0.2 or 2 μm PC filter membranes and rinsed with 1–2 mL of 0.4 μm- filtered seawater each. The ^{57}Co radioactivity on each filter was determined using a Canberra Germanium Gamma detector. Since natural concentrations of vitamin B_{12} in pristine environments are believed to lie in the low picomolar range (Menzel and Spaeth, 1962; Swift, 1981; Panzeca et al., 2009) and the ^{57}Co-labeled B_{12} was added in sub-picomolar concentrations, the total concentration of B_{12} can be approximated as the amount of unlabeled B_{12} added in these experiments (~40 pM). Using the percent uptake of radiolabeled B_{12} and this total concentration, total vitamin B_{12} uptake per day was calculated for each filter size, as described by the equation B_{12} uptake/L/day = counts of ^{57}Co B_{12} on filter/L/day × 1/counts of ^{57}Co B_{12} added × total B_{12} concentration. The 0.2-μm filter activity was considered indicative of total community uptake. The 2-μm filter represented eukaryotic uptake from the >2-μm size fraction while the 0.2-μm filter minus the 2-μm filter was considered a proxy for the bacterial community uptake rate. Control studies were conducted at several locations during the CORSACS 1 cruise by killing the community with glutaraldehyde (1% final concentration, B_{12} added 3 h after glutaraldehyde added) or with heat (microwaving a 180-mL sample for 5 min, shake, repeat three times; B_{12} added 3 h after heat-killed). Killed controls were incubated at 0°C in the dark. A titration experiment was conducted at station NX 14 (37 m depth, November 18, 2006, 75.93° S, 178.36° E) where varying amounts of non-radiolabeled B_{12} was added to whole seawater and 24 h uptake rate measurements were taken to determine how these added concentrations affected uptake rate by the >2-μm size fraction. In addition, a time course experiment with 40 pM added B_{12} was conducted at station NX 17 (17 m depth, November 26, 2006; 76.50° S, 178.55° E) to examine changes in uptake rate in the >2-μm size fraction between 10 min and 50 h.

STATISTICS

Student's unpaired *t*-test was used to determine the statistical significance of differences between treatments. *T* and *p* values are reported and differences are discussed at the 95% confidence level.

RESULTS AND DISCUSSION

PHYTOPLANKTON AND BACTERIAL GROWTH LIMITATION BY IRON

In the incubation experiment conducted at Station SP3, bottles of unfiltered surface seawater were supplemented in triplicate with iron, cobalt, zinc, and vitamin B_{12} (**Figure 2**). Iron addition increased Chl *a* production as well as nitrate and phosphate drawdown relative to the unamended control treatments, suggesting that primary production in this area was limited by iron availability. Iron limitation of phytoplankton growth in the Ross Sea has previously been observed during summer, but not during spring (Martin et al., 1990; Sedwick et al., 2000; Coale et al., 2003). This finding represents the first evidence of iron limitation in the Ross Sea during the spring, and reflects the low surface dissolved iron concentration measured at station SP3 (0.035 nM), which is considerably lower than previously reported springtime values for this region (Sedwick et al., 2000; Coale et al., 2005; Sedwick et al., in review). These observations require that the conceptual model of seasonal iron limitation in the Ross Sea, where iron becomes gradually depleted from wintertime maxima and phytoplankton populations become iron limited only in summer (e.g., Sedwick et al., 2000), be revised to allow that these waters may become iron limited relatively early in the growing season (Sedwick et al., in review). The observation of springtime iron limitation in this *P. antarctica*-dominated community also demonstrates that *P. antarctica* can be prone to iron limitation in Ross Sea natural communities despite low cellular iron requirements (Garcia et al., 2009; Sedwick et al., in review).

Silicic acid drawdown was negligible in all experimental treatments, suggesting that diatoms comprised only a minor portion of the community. This finding is supported by microscopy-determined phytoplankton community analyses (**Table 1**) and by pigment analyses (**Figure 3**). For all treatments, *P. antarctica*-dominated the community at the beginning and end of the incubation experiment. However, based on the microscopy-determined community composition, both diatom and *Phaeocystis* abundance must have increased their growth rates comparably in response to iron addition since the diatoms remained an approximately constant proportion of the community throughout the experiment (**Table 1**). Likely because of their small initial abundance and thinly silicified nature (e.g., *Pseudonitzschia* spp.), diatom biomass remained relatively low and did not decrease in silicic acid concentrations despite an iron-induced increase in growth.

Figure 3 shows ratios of particulate 19-hexanolyoxyfucoxanthin (Hex), a haptophyte indicator pigment indicative of *P. antarctica* in the Ross Sea, to the pigment fucoxanthin (Fuco), which is primarily indicative of diatoms (DiTullio and Smith, 1996). Hex:Fuco ratios >2 indicate relative dominance of *Phaeocystis*; all samples

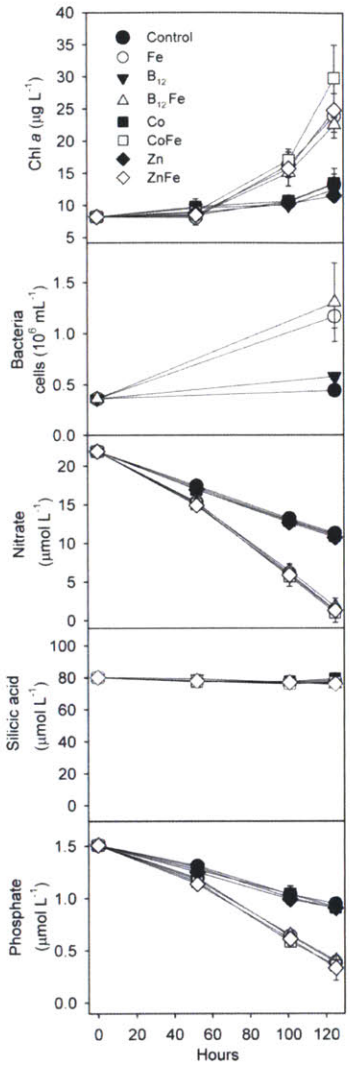

FIGURE 2 | Results of a trace metal clean whole-water bottle incubation experiment demonstrating that both phytoplankton and bacteria were iron limited. This experiment was conducted during the austral spring of 2006 at station SP3 in the Ross Sea; Chl *a*, bacterial cells, and major nutrient concentrations over time are shown. Values shown are means of triplicate treatments with error bars representing one SD. Where error bars are not visible, they fall within the bounds of the symbol. Iron stimulated enhanced Chl *a* production as well as major nutrient drawdown. No significant additional stimulation of Chl *a* production was observed upon the addition vitamin B_{12} and iron, zinc and iron, or cobalt and iron, relative to iron alone, suggesting that neither Co, Zn nor B_{12} was secondarily limiting phytoplankton growth. The addition of iron also, either directly or indirectly through increased availability of fixed organic nutrients, caused increased bacterial growth.

from the incubation experiment had Hex:Fuco ratios >4, indicating strong haptophyte dominance. However, the iron-amended incubation samples had a $35 \pm 7\%$ lower Hex:Fuco ratio than the unamended incubation treatments at the end of the experiment (**Figure 3**). The most likely explanation for this, given the absence of an increase in silicic acid drawdown that should accompany a significant increase in diatom growth, is that *Phaeocystis* increased its fucoxanthin production upon alleviation of iron limitation, as previously observed (Van Leeuwe and Stefels, 1998). The 1-nM iron additions used here have been shown to decrease Hex:Fuco production in *Phaeocystis* approximately 10-fold (DiTullio et al., 2007). It is also possible that the growth of very thinly silicified diatoms were fueled by iron addition, which would not result in a significant silicic acid drawdown (Hutchins et al., 2001). However, the N/P drawdown ratios in both the iron-amended ($N/P = 18.0 \pm 0.4$) and unamended ($N/P = 18.4 \pm 0.4$) treatments were similar (**Figure 2**). Since diatoms display a much lower N:P drawdown ratio than *P. antarctica* populations in the Ross Sea (diatoms: 9.7 ± 0.3; *P. antarctica* 19.2 ± 0.6; Arrigo et al., 1999, 2000), these measured ratios suggests that *P. antarctica*, rather than diatoms, were primarily responsible for nutrient drawdown regardless of iron nutritional status. Taken together, these community analyses suggest that dissolved iron availability was not an important factor in driving community structure in this experiment since *P. antarctica* and diatoms remained in approximately equal proportions throughout. The increase in *Phaeocystis* growth upon iron addition in this experiment is consistent with culture experiments that suggest iron half saturation constants for *P. antarctica* growth are well above the very low concentration of ambient dissolved iron (0.035 nM) that was measured in seawater at station SP3 (Garcia et al., 2009; Saito et al., in preparation).

The paired additions of vitamin B_{12} with iron, zinc with iron, or cobalt with iron did not increase Chl *a* production or nutrient drawdown relative to the addition of iron alone or appreciably change Hex:Fuco ratios beyond those changes induced by iron. While these results initially appear to be in contrast to our previous observations of B_{12} and Fe colimitation of phytoplankton growth in the Ross Sea during summer (Bertrand et al., 2007), we believe that the results of these spring and summer experiments are consistent based on two observations. First, the initial bacterial abundance in this bottle incubation experiment was high ($3.6 \pm 0.05 \times 10^5$ cells mL^{-1}) relative to areas in the Ross Sea where strong vitamin B_{12} and iron colimitation was observed in the summer ($\sim 6 \times 10^4$ cells mL^{-1}), as illustrated in **Figure 4**. If bacteria are indeed the major source of B_{12} in this system, then greater bacterial abundance during spring could result in greater availability of vitamin B_{12}. Second, our previous summer experiments showed that B_{12} addition did not stimulate the growth of *P. antarctica*, the dominant phytoplankter in this experiment. Although it is possible that *P. antarctica* does not require vitamin B_{12} for growth, the lack of a *P. antarctica* response might also reflect the high bacterial abundances associated with *Phaeocystis* colony mucilage (Putt et al., 1994), which may provide a localized source of B_{12}. The lack of evidence for zinc or cobalt limitation or colimitation with iron in this experiment is also comparable with other Ross Sea studies where zinc additions increase Chl *a* production in some but not all locations (Cochlan et al., 2002; Coale et al., 2003)

Table 1 | Phytoplankton community composition during the incubation experiment at station SP3, given as percentage of total individual cells in the community, in the initial community and at the end of the incubation in the control, and iron added treatments. For the initial community and the control treatment, only single counts were conducted. For the final timepoint in the +Fe treatment, single counts on triplicate bottles were performed; ±1 SD is shown.

	Phaeocystis	Chain forming diatoms	Single cell diatoms	Cryptophytes	Dinoflagellates
Initial	80.9	3.2	12.6	2.4	0.9
Final, Cont	86.1	1.4	11.8	0.5	0.3
Final, +Fe	84.0 ± 1.5	1.6 ± 1.2	13.4 ± 0.6	0.7 ± 0.1	0.2 ± 0.1

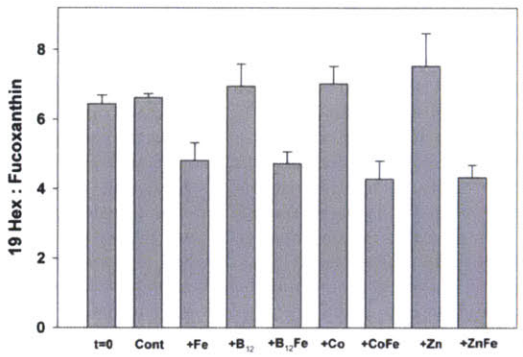

FIGURE 3 | Ratios of particulate 19-hexanolyoxyfucoxanthin (19-Hex) to fucoxanthin (Fuco), measured by HPLC analysis, at the beginning of the incubation experiment and at the end for each treatment. Bars are means of three biological replicates and error bars are one SD. In the Ross Sea 19-Hex predominantly represents *Phaeocystis* and Fuco predominantly represents diatoms. All samples throughout the experiment had ratios in excess of four, illustrating strong *Phaeocystis* dominance.

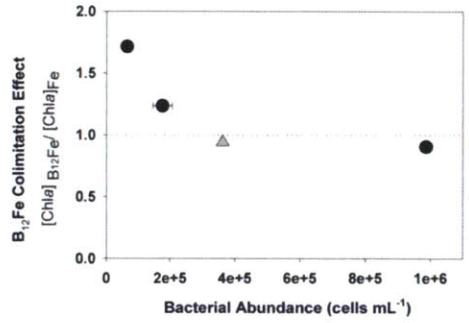

FIGURE 4 | Bacterial abundance at the beginning of an incubation experiment during the austral spring in the Ross Sea (gray diamond, SP3, this study) and three bottle incubations from the austral summer of 2005 in the Ross Sea (Bertrand et al., 2007**, black circles) relative to an index of vitamin B_{12} colimitation (ratio of final Chl *a* concentrations in +B_{12}Fe treatments to final Chl *a* concentrations in the +Fe treatments), where a ratio of one indicates no stimulation of Chl production by B_{12} and a ratio of two means a doubling of Chl production upon the addition of B_{12}.** Stimulation of phytoplankton growth by vitamin addition appears to have an inverse relationship with initial bacterial abundance. This data shows that the lack of vitamin limitation observed at station SP3 is consistent with previous results in that the initial bacterial community was larger than those present in experiments when the vitamin was limiting. Where error bars are not visible, they were smaller than the symbols.

and cobalt additions did not increase Chl *a* production (Bertrand et al., 2007), all consistent with the high concentrations of labile Co in this region (Saito et al., 2010) and the interreplacement of cobalt and zinc in *P. antarctica* (Saito and Goepfert, 2008).

Iron additions also substantially increased bacterial abundance in our bottle incubation experiment (~3-fold greater increase in bacterial abundance over 5 days in the +Fe treatment versus the control; **Figure 2**) indicating that bacterial growth was limited by iron, either directly, or through iron-induced changes in organic matter production by phytoplankton. While iron addition increased phytoplankton abundance and potentially organic matter production, iron additions might also have altered the composition of the organic matter since culture experiments have shown that high iron concentrations (2 nM) substantially increase the lability of *P. antarctica*-derived organic matter (Becquevort et al., 2007).

In order to investigate whether bacterial communities were limited by iron availability directly or by the supply of organic matter from phytoplankton, an additional bacterial regrowth experiment was conducted in which grazers and phytoplankton were excluded by filtration (0.65 μm pore size), and the remaining bacterial community was diluted and allowed to grow with and without 1 nM iron amendments. As shown in **Figure 5**, iron addition increased the cell-specific growth rate to $0.29 \pm 0.01\ day^{-1}$ over a rate of $0.21 \pm 0.03\ day^{-1}$ in the unamended control treatment (error is one SD about the mean of biological triplicate measurements). The filtration employed to remove the grazing and phytoplankton community may have increased DOM concentration and changed DOM composition, but any such changes would have been uniform across the treatments. We thus conclude that dissolved iron addition directly enhanced bacterial growth rates in this assemblage and that bacterial growth rates in these waters may be subject to colimitation by the availability of DOM and iron. While these growth rates are within the range of previously reported values for the Ross Sea ($0.25\ day^{-1}$; Ducklow, 2000), they may deviate from *in situ* rates due to sample manipulation involved in the experiment. These results suggest that iron availability directly impacts bacterial growth rates in the Ross Sea and highlight that bacteria compete with phytoplankton for dissolved iron.

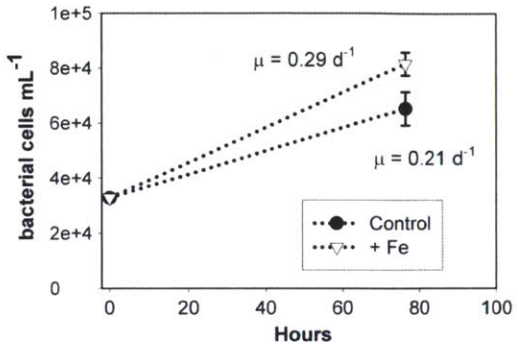

FIGURE 5 | Results from a bacterial regrowth experiment at station SP3, demonstrating that iron directly impacted bacterial growth rates. Bacterial and archaeal abundance (cells per milliliter) over time for the iron added and unamended control are shown, with error bars representing SD of single counts from triplicate incubations. The cell-specific growth rates (shown in figure) in these two treatments are significantly different ($T = 3.8$, $p = 0.03$), suggesting that bacterial growth rate is directly iron limited.

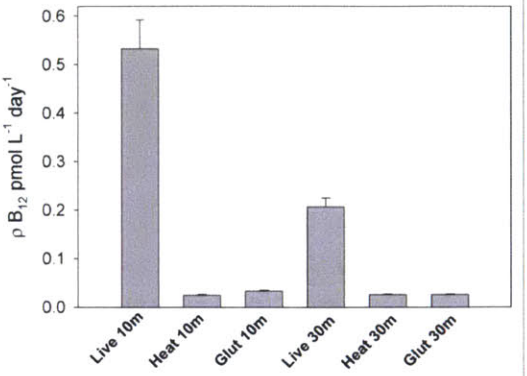

FIGURE 6 | Vitamin B_{12} uptake rates in live samples and killed controls, demonstrating that the method employed here to measure B_{12} uptake is not significantly impacted by non-specific adhesion of B_{12} to particulate matter and primarily measures active uptake. These data demonstrate that a filtered seawater wash is sufficient for removing most non-living particle and surface-associated vitamin B_{12} from filters. This experiment was conducted in the Ross Sea at station NX 8 (77.30°S, 175.44°W) in the austral summer of 2005. Triplicate B_{12} uptake rates were measured in live samples; bars represent means and error bars show one SD. Single killed controls per depth were conducted by killing the community with glutaraldehyde or heat. Error bars on the killed samples represent 5% counting error.

VITAMIN B_{12} UPTAKE: IRON INFLUENCES AND BACTERIAL CONTRIBUTION

Uptake of B_{12} by biota is considered a major sink for the vitamin in natural waters (Karl, 2002). In this study, we used radiotracer additions to examine the effect of iron amendments on vitamin B_{12} uptake rates by microbial communities in the incubation experiment described above and in several proximal locations. Heat and glutaraldehyde-killed treatments verified that this measured B_{12} uptake occurred through active rather than passive mechanisms (**Figure 6**), thus reflecting biological processes rather than adhesion to particulate matter. The technique used to measure these rates involved the addition of large amounts of vitamin B_{12} (~40 pM). This non-tracer level addition was chosen to facilitate a comparison of uptake rates between experimental treatments without the need for measuring ambient vitamin B_{12} concentrations in this small-volume incubation experiment. Since calculated B_{12} uptake = fraction of tracer taken up × total vitamin concentration, these ~40 pM additions significantly increased the calculated uptake rates compared ambient B_{12} concentrations (**Figure 7A**). These calculated rates thus do not represent *in situ* uptake, but rather rates at this relatively high B_{12} concentration.

Typical models for nutrient uptake predict that progressive additions of higher nutrient concentrations increase nutrient uptake rates until the community's uptake machinery is saturated. Interestingly, the ~40 pM B_{12} additions used here did not saturate phytoplankton community uptake rates (**Figure 7A**), and even up to 95 pM of added B_{12} did not appear to saturate these rates. If we assume a Michaelis–Menten type kinetic relationship between uptake rate and added vitamin concentrations, plotting the data in **Figure 7A** in double reciprocal form (data not shown) yields a half saturation constant of 83 pM for B_{12} uptake, which is much higher than typical ambient B_{12} concentrations.

The technique we have applied can be used to compare calculated uptake rates in different experimental treatments assuming that the composition of the community in each experimental treatment does not appreciably change as a result of adding high B_{12} concentrations over the course of the 24-h measurement. This assumption is supported by the observation that the uptake rates measured between 12 and 52 h were the same (**Figure 7B**) since 12 h is not enough time for a community composition change to occur given the typical generation times in polar waters. Interestingly, the uptake rate measured after 13 min was much faster than at the later timepoints, which is consistent with an uptake model whereby cell surface B_{12}-binding proteins are quickly saturated by the high concentrations of added B_{12}, then, in a second slower step, the vitamin is transferred into the cell. This is analogous to experimental results showing that the rate of zinc uptake by diatoms was elevated in the first few minutes after the addition of high Zn concentrations, which was attributed to Zn binding to cell surface sites (Sunda and Huntsman, 1992) and is also consistent with results from B_{12} uptake studies in *Ochromonas* cultures showing that vitamin uptake also occurs sequentially, first rapidly and then a second slower phase (Bradbeer, 1971). The slight depression in B_{12} uptake rate between the 3 and 12-h timepoints (**Figure 7B**) is consistent with cells experiencing minor negative feedback in uptake rates after >3 h of exposure to high B_{12} concentrations, as previously observed for other micro and macronutrients (Sunda and Huntsman, 1992).

There are few studies of B_{12} uptake rates in natural phytoplankton communities to date (Bertrand et al., 2007; Taylor and

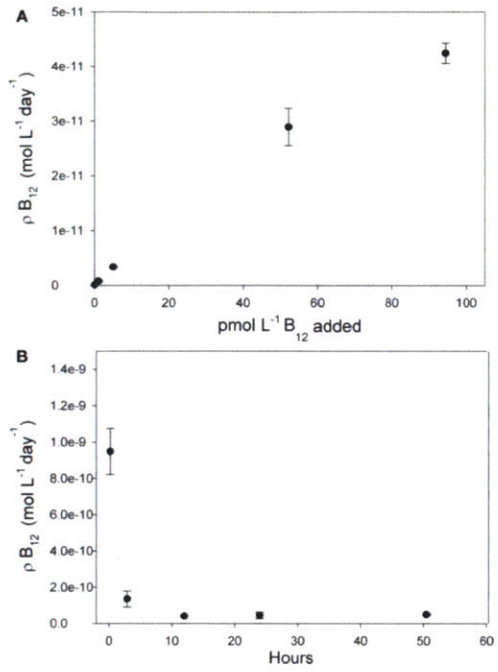

FIGURE 7 | Vitamin B_{12} uptake rate measurements for the >2 μm size fraction of the community in the Ross Sea shown as a function of added vitamin concentration and incubation time. Points denote means of biological triplicate measurements, and error bars are one SD. **(A)** Varying amounts of non-radiolabeled B_{12} were added to 24 h uptake rate measurements at station NX 14 to determine how these added concentrations affected uptake rate. Since calculated B_{12} uptake = fraction of tracer taken up × total vitamin concentration, this uptake rate increased upon increasing vitamin concentrations. The highest concentrations added, 95 pM, did not appear to saturate the community B_{12} uptake rate. **(B)** When 40 pM total B_{12} was added to the community at station NX 17, an elevated uptake rate was measured after the first 13 min of incubation time, and then a lower rate at 2.8 h, decreasing to a constant rate between 12 and 52 h. The consistent rate measured between the 12 h and 52 h timepoints suggests that the 40-pM B_{12} additions and 24 h incubation times used to measure B_{12} uptake rate did not perturb the community uptake rate by stimulation of phytoplankton growth or changing phytoplankton species composition.

Sullivan, 2008; Koch et al., 2011). Such measurements are in early stages of development. Even in laboratory-based culture studies, measurements of B_{12} uptake are complex and have yielded results that are not easy to interpret (Droop, 1968). Measurements presented here offer an initial look at controls on B_{12} uptake in field populations, but further study is required to develop methodology for measuring *in situ* rates and to better constrain factors affecting cellular B_{12} uptake machinery.

Phytoplankton size fraction B_{12} uptake

B_{12} uptake was measured for two separate size fractions of the community, 0.2–2 and >2 μm. The 0.2–2-μm size fraction includes largely non-photosynthetic bacteria and archaea since there are no appreciable cyanobacterial populations in the Ross Sea (Caron et al., 2000; Marchant, 2005) and picoplanktonic phytoplankton were not observed by our microscopy methods. The >2-μm size fraction includes eukaryotic phytoplankton, which comprise the vast majority of photosynthetic biomass in this region (Scott and Marchant, 2005).

At the end of the incubation experiment, the iron-amended treatment exhibited a substantially higher B_{12} uptake rate in the phytoplankton size fraction relative to the control (**Figure 8**). When normalized to Chl *a*, this uptake rate was still higher in the iron-amended treatment than in the control at the final timepoint (significantly different; $T = 7.99$, $p = 0.015$, **Figure 9A**). This normalized value is a measure of how community vitamin uptake rates change relative to Chl *a* changes. It is unlikely that this increase in chlorophyll-normalized B_{12} uptake rate is solely a function of differences in cellular pigment concentration between treatments. This is because cells in the iron-amended treatment might be expected to contain more Chl *a* per cell, since Chl deficiency (chlorosis) is often associated with iron limitation (Zettler et al., 1996). If a Chl-deficient cell (i.e., in the control treatment) had the same cell-specific B_{12} uptake rate as a Chl-replete cell (i.e., in the +Fe treatment), then the Chl *a*-normalized B_{12} uptake rate should be *higher* in the control treatment. In fact, we observed the opposite trend: Chl-normalized B_{12} uptake rate was greater for the Fe-amended treatments, suggesting that this trend reflects an increase in community B_{12} uptake rate rather than changes in pigment composition. This result suggests that vitamin B_{12} uptake by the phytoplankton community increased after iron addition due to (1) a change in species composition, (2) an increase in cellular vitamin transporters, or (3) an increased use of energy allocated to active vitamin transport systems in order to increase vitamin uptake rates in step with growth rates. The first scenario is unlikely, given that the community remained heavily dominated by *P. antarctica* in all treatments (**Table 1**, **Figure 3**), suggesting that the latter two mechanisms may be important.

In addition to revealing an effect of iron on B_{12} uptake, our experiment showed a 4–6 × lower Chl *a*-normalized B_{12} uptake rate at the beginning of the incubation experiment relative to the final timepoint, in both the control and iron-amended treatments (**Figure 9A**). Although both the initial and final uptake measurements were conducted under identical conditions in the deckboard incubator, the initial timepoint measurement was taken immediately upon transfer from *in situ* conditions to the shaded incubator while the final timepoint measurements were taken after a 5-day acclimation inside the bottle incubation experiment. Thus, the large change in uptake rate might partly reflect "bottle effects," or the impact of altered irradiance. If the conditions favored faster growth in the final stages of the experiment, then these enhanced uptake rates could reflect increased growth rate and overall energy available to cells, resulting in an increase in energy allocated to active vitamin transport systems that is unconnected to vitamin nutritional status. However, an increase in available energy at the end of the incubation experiment is unlikely, particularly in the case of the control treatment, since that community was becoming increasingly iron limited. These higher uptake rates may thus in

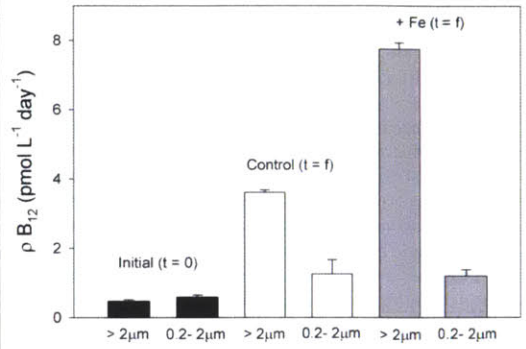

FIGURE 8 | Vitamin B_{12} uptake rates in both the bacterial (0.2–2 μm) and phytoplankton (>2 μm) size fractions at initial and final timepoints in the bottle incubation experiment. While uptake rates increased by the final timepoint in all cases, the uptake rate for the phytoplankton size fraction but not the bacterial size fraction increased more in the iron added treatment. Rates at the final time point were measured from duplicate samples taken from a single replicate of the control (white bars) and Fe added treatments (gray bars). Means of triplicate initial B_{12} uptake measurements are all shown with error bars representing one SD.

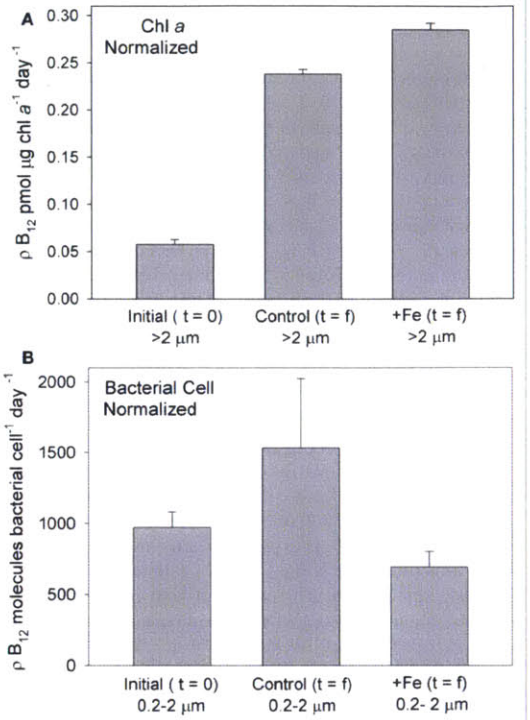

FIGURE 9 | B_{12} uptake rates in the bottle incubation experiment, normalized to biological parameters, demonstrate that B_{12} uptake was significantly enhanced in phytoplankton communities that were supplemented with iron, but not in iron- supplemented bacteria. B_{12} uptake in the greater than 2 μm (phytoplankton) fraction is shown normalized to Chl *a* concentration **(A)** at the initiation of the incubation experiment, and at the end, in both iron added and control treatments. B_{12} uptake in the 0.2- to 2-μm fraction of the community, normalized to bacterial cell number **(B)**, at the initiation of the incubation experiment, and at the end, in both iron added and control treatments is shown. Bacterial abundance at $t = 0$ was $3.6 \pm 0.05 \times 10^5$ cells mL^{-1}, $t = f$ control was $4.4 \pm 0.5 \times 10^5$ cells mL^{-1}, and $t = f$ + Fe was $12 \pm 1.0 \times 10^5$ cells mL^{-1}. POC concentration (GF/F filters, 0.7 μm) at $t = 0$ was 523.5 μg L^{-1}, $t = f$ control was 899.1 μg L^{-1}, and $t = f$ + Fe was 1655.7 μg L^{-1}.

part reflect stress experienced by the phytoplankton due to depletion of available vitamin supplies. Although there is an internal source of vitamin B_{12} in these incubations (bacterial growth), the vitamin sinks due to bacterial and phytoplankton uptake and photochemical degradation (Carlucci et al., 1969) are likely to be considerable. On balance, this may result in progressive depletion of B_{12}, mirroring the nitrate and phosphate drawdown observed in this experiment (**Figure 2**). Such depletion could induce an upregulation of vitamin transporters, which would be reflected in elevated B_{12} uptake rates.

The observed changes in B_{12} uptake rate are consistent with the phytoplankton communities becoming stressed for lack of this vitamin by the end of the incubation experiment, which would result in increased calculated uptake rates. However, the bottle incubation study did not show an increase in phytoplankton biomass upon vitamin B_{12} addition, leading to the conclusion that there was no colimitation by vitamin B_{12} and iron at this time and location. This observation suggests that bottle incubations may not be sensitive to some subtle physiological states of nutrient stress that are nonetheless relevant for biogeochemical cycling and that might indicate susceptibility to nutrient limitation. Nutrient uptake studies like these, as well as the application of protein or transcript-based biomarker assays for gene products that are abundant under defined states of nutrient stress (LaRoche et al., 1996; Webb et al., 2001; Dyhrman et al., 2002), can complement bottle incubation studies and provide more subtle information about the limitation and colimitation experienced by microbial communities. The dramatic increase in vitamin uptake rates from the beginning to end of this incubation experiment and upon increasing B_{12} concentrations (**Figure 7**) suggest that phytoplankton can exert considerable control over the cellular machinery that is used to take up vitamin B_{12}. This implies that future studies to document the cellular response of phytoplankton to vitamin stress and to develop protein or transcript-based biomarkers for vitamin limitation may be feasible.

Bacterial size fraction uptake

The initial B_{12} uptake rates at the beginning of the incubation experiment were slightly greater for the 0.2–2-μm size fraction than for the greater than 2 μm fraction (**Figure 8**, not significantly different; $T = 2.34$, $p = 0.078$). This observation suggests that in addition to being the source of vitamin B_{12}, the bacterial and archaeal community size fraction is also an important sink. This evidence, along with that offered in another study (Koch et al., 2011) favors a departure from the Karl (2002) model of vitamin

B_{12} cycling, which suggests that eukaryotes dominate B_{12} uptake. Our results are also consistent with the fact that, according to currently available genomic sequencing information, many Antarctic marine bacterial strains appear to require an exogenous source of B_{12} (Bertrand et al., 2011).

The rate of B_{12} uptake by the 0.2–2-μm size fraction normalized to the size of the bacterial community at the initial and final timepoints for the iron-amended treatment were not significantly different ($T = 1.19$, $p = 0.41$), while uptake rates in the initial versus final community in the control treatment were significantly different ($T = 3.44$, $p = 0.04$), with a higher B_{12} uptake rate in the final community (**Figure 9B**). Since many bacterial cells, including the abundant SAR11 clade, do not take up vitamin B_{12} (Zhang et al., 2009), these rate measurements that are normalized to total cell abundance should not be taken as reflections of individual cell uptake rates but rather as a measure of the change in vitamin uptake rate relative to the change in bacterial community size. Although our experimental uncertainties are substantial, this trend may suggest a shift in community composition in the control treatment (under iron limitation) toward bacteria that take up exogenous B_{12}, or enhanced cellular B_{12} uptake rate within that community. A similar shift or increase in uptake rate does not seem to have occurred in the iron replete treatments. This suggests that when iron availability is low, vitamin B_{12} uptake by bacteria may increase. This hypothesis is consistent with reports that part of bacterial B_{12} demand arises from use in ribonucleotide reductase (RNR) enzymes, which use either iron or vitamin B_{12} and that, in some bacteria, the transcription of the gene encoding the iron-requiring RNR is only expressed when the B_{12} cell quotas are low (Borovok et al., 2006).

IMPLICATIONS

Iron influences on B_{12} production

The results of our incubation and regrowth experiments suggest that dissolved iron availability can help regulate net bacterial productivity in the Ross Sea. Since vitamin B_{12} production rates are tied to bacterial productivity, our results further suggest that vitamin B_{12} production could be influenced by the availability of dissolved iron. Although there are likely many factors contributing to B_{12} production rates, vitamin availability to phytoplankton appears to scale with bacterial abundance since small bacterial communities were observed where B_{12} limited primary production (**Figure 4**). Constraining the rate of B_{12} production and the factors that regulate it presents challenges similar to those involved constraining the cycling of other trace level nutrients, such as ammonia. Knowing the concentration of vitamin B_{12} may not tell us much about its production rate, given its rapid uptake by the biota and its short photochemical half life in the surface ocean (Carlucci et al., 1969). Since the rate at which individual organisms conduct vitamin biosynthesis may be variable, knowing the number of community members that can produce the vitamin at any one time may also tell us little about the gross B_{12} production rate (Roling, 2007). The rate of vitamin transfer from the particulate to the dissolved pool, and not simply the rate of biosynthesis, must also be considered. This flux will be a function of the production rate within the local microbial communities; the rate of population turnover by grazing, viral lysis, and other factors, as well as the efficiency of the microbial loop. The addition of the vitamin due to mixing with other water masses is likely small (Panzeca et al., 2009), but must also be considered. These issues are beyond the scope of this paper, but are important for understanding the biogeochemistry of vitamin B_{12}.

Persistence and timing of phytoplankton and bacterial blooms in iron fertilization events

The results of this study suggest that DOM consumption rates, insofar as they are related to bacterial growth, may be directly influenced by dissolved iron availability, and that B_{12} production and consumption in the Ross Sea are also likely impacted by iron. When taken together, these results present the possibility that during a natural or engineered iron fertilization event, B_{12} production may increase and bacterial B_{12} demand may decrease, thereby resulting in enhanced availability of B_{12} to phytoplankton. It is possible that this enhanced availability could alleviate B_{12} colimitation of phytoplankton communities, resulting in increased primary production. However, the relative timing of these responses will determine the impact of synergistic vitamin and iron dynamics on iron-induced blooms. If the bacterial response to iron addition lags the phytoplankton response (more likely if the bacterial community is DOM limited), then the phytoplankton community is less likely to receive increased B_{12} supply to meet its enhanced B_{12} demand (**Figure 7**). This is likely to have occurred in the summertime Ross Sea experiments that observed B_{12} stimulation (Bertrand et al., 2007). However, if the bacterial response to dissolved iron addition is concurrent with the phytoplankton response (more likely if bacteria are primarily iron limited), then bacterial vitamin B_{12} production may keep pace with the increasing phytoplankton demand, preventing secondary vitamin B_{12} limitation. The balance between enhanced DOM consumption and altered vitamin B_{12} dynamics should be considered when evaluating the impact of bacterial communities during iron fertilization.

CONCLUSION

This study provides direct evidence of iron limitation of phytoplankton growth in the Ross Sea during spring, thus challenging the idea that this Antarctic shelf ecosystem is iron replete in the early growing season. In addition, bacterial growth in this location was shown to be directly iron limited or colimited by iron and DOM. These results imply that iron availability may limit vitamin B_{12} production, since bacteria and archaea are the only known source of B_{12} production in the water column. The bacterial size fraction of the microbial community also comprised a significant sink of vitamin B_{12} in the water column, with uptake measurements suggesting that this sink may be reduced under iron replete conditions. Despite a lack of enhanced Chl production upon vitamin B_{12} addition to the bottle incubation study here, vitamin B_{12} uptake rate measurements suggest that phytoplankton may have experienced stress due to B_{12} deficiency, particularly when iron limitation was alleviated.

ACKNOWLEDGMENTS

We thank David Hutchins for access to his laboratory van and for helpful discussions. Thanks to Julie Rose for training in phytoplankton identification, bacterial enumeration and helpful discussions, and to Ben Van Mooy for suggestions on bacterial regrowth studies and comments on the manuscript.

We are grateful to Daniel Repeta, Phoebe Lam, Dawn Moran and Abigail Noble for comments on the manuscript. Thanks also to Bettina Sohst and Giulio Catalano for nutrient analyses and to Tyler Goepfert for help in incubation setup and sample processing. Special thanks to the Captain, Crew, and Raytheon Marine and Science Technical Staff of the RVIB N. B. Palmer and the CORSACS science parties. This research was supported by NSF grants OCE-0752291, OPP-0440840, OPP-0338097, OPP-0338164, ANT-0732665, OCE-0452883, and OCE-1031271, the Center for Microbial Oceanography Research and Education (CMORE) and a National Science Foundation (NSF) Graduate Research Fellowship (2007037200) and an Environmental Protection Agency STAR Fellowship to EMB (F6E20324).

REFERENCES

Armand, L. K., Crosta, X., Romero, O., and Pichon, J.-J. (2005). The biogeography of major diatom taxa in Southern Ocean sediments: I. Sea ice related species. *Palaeogeogr. Palaeoclimatol. Palaeoecol.* 223, 93–126.

Arrigo, K. R., DiTullio, G. R., Dunbar, R. B., Robinson, D. H., VanWoert, M., Worthen, D. L., and Lizotte, M. P. (2000). Phytoplankton taxonomic variability in nutrient utilization and primary production in the Ross Sea. *J. Geophys. Res.* 105, 8827–8846.

Arrigo, K. R., Robinson, D. H., Worthen, D. L., Dunbar, R. B., DiTullio, G. R., VanWoert, M., and Lizotte, M. P. (1999). Phytoplankton community structure and the drawdown of nutrients and CO2 in the Southern Ocean. *Science* 283, 365–367.

Arrigo, K. R., van Dijken, G., and Long, M. (2008). Coastal Southern Ocean: a strong anthropogenic CO2 sink. *Geophys. Res. Lett.* 35, 6.

Becquevort, S., Lancelot, C., and Schoemann, V. (2007). The role of iron in the bacterial degradation of organic matter derived from *Phaeocystis antarctica*. *Biogeochemistry* 83, 119–135.

Bertrand, E. M., Saito, M. A., Jeon, Y. J., and Neilan, B. A. (2011). Vitamin B12 biosynthesis gene diversity in the Ross Sea: the identification of a new group of putative polar B12-biosynthesizers. *Environ. Microbiol.* 13, 1285–1298.

Bertrand, E. M., Saito, M. A., Rose, J. M., Riesselman, C. R., Lohan, M. C., and Noble, A. E., Lee Peter, A., and Ditullio Giacomo, R. (2007). Vitamin B12 and iron co-limitation of phytoplankton growth in the Ross Sea. *Limnol. Oceanogr.* 52. 1079–11093.

Bonnet, S., Webb, E. A., Panzeca, C., Karl, D. M., Capone, D. G., and Sanudo-Wilhelmy, S. A. (2010). Vitamin B12 excretion by cultures of the marine cyanobacteria *Crocosphaera* and *Synechococcus*. *Limnol. Oceanogr.* 55, 1959–1964.

Borovok, I., Gorovitz, B., Schreiber, R., Aharonowitz, Y., and Cohen, G. (2006). Coenzyme B12 controls transcription of the *Streptomyces* class Ia ribonucleotide reductase *nrdABS* operon via a riboswitch mechanism. *J. Bacteriol.* 118, 2512–2520.

Bradbeer, C. (1971). Transport of vitamin B12 in *Ochromonas malhamensis*. *Arch. Biochem. Biophys.* 144, 184–192.

Bruland, K. W., Rue, E. L., Smith, G. J., and DiTullio, G. R. (2005). Iron, macronutrients and diatom blooms in the Peru upwelling regime: brown and blue waters of Peru. *Mar. Chem.* 93, 81–103.

Carlucci, A. F., Silbernagel, S. B., and McNally, P. M. (1969). The influence of temperature and solar radiation on persistence of vitamin B12, thiamine, and biotin in seawater. *J. Phycol.* 5, 302–305.

Caron, D. A., Dennett, M. A., Lonsdale, D. J., Moran, D. M., and Shalapyonok, L. (2000). Microzooplankton herbivory in the Ross Sea, Antarctica. *Deep Sea Res. II* 47, 3249–3272.

Church, M. J., Hutchins, D. A., and Ducklow, H. W. (2000). Limitation of bacterial growth by dissolved organic matter and iron in the Southern Ocean. *Appl. Environ. Microbiol.* 66, 455–466.

Coale, K. H., Gordon, R. M., and Wang, X. (2005). The distribution and behavior of dissolved and particulate iron and zinc in the Ross Sea and Antarctic circumpolar current along 170°W. *Deep Sea Res. I* 52, 295–318.

Coale, K. H., Wang, X., Tanner, S. J., and Johnson, K. S. (2003). Phytoplankton growth and biological response to iron and zinc addition in the Ross Sea and Antarctic circumpolar current along 170W. *Deep Sea Res. II* 50, 635–653.

Cochlan, W. P., Bronk, D. A., and Coale, K. H. (2002). Trace metals and nitrogenous nutrition of Antarctic phytoplankton: experimental observations in the Ross Sea. *Deep Sea Res. II* 49, 3365–3390.

Croft, M. T., Lawrence, A. D., Raux-Deery, E., Warren, M. J., and Smith, A. G. (2005). Algae acquire vitamin B12 through a symbiotic relationship with bacteria. *Nature* 438, 90–93.

DiTullio, G. R., Garcia, N., Riseman, S. F., and Sedwick, P. N. (2007). Effects of iron concentration on pigment composition in *Phaeocystis antarctica* grown at low irradiance. *Biogeochemistry* 83, 71–81.

DiTullio, G. R., and Geesey, M. E. (2002). "Photosynthetic pigments in marine algae and bacteria," in *The Encyclopedia of Environmental Microbiology*, ed. G. Bitton (New York, NY: John Wiley and Sons, Inc.), 2453–2470.

DiTullio, G. R., and Smith, W. O. (1995). Relationship between dimethylsulfide and phytoplankton pigment concentrations in the Ross Sea, Antarctic. *Deep Sea Res. II* 42, 873–892.

DiTullio, G. R., and Smith, W. O. (1996). Spatial patterns in phytoplankton biomass and pigment distributions in the Ross Sea. *J. Geophys. Res.* 101, 18467–18478.

Droop, M. R. (1968). Vitamin B12 and marine ecology. IV. The kinetics of uptake, growth and inhibition in *Monochrysis lutheri*. *J. Mar. Biol. Assoc. U.K.* 48, 689–733.

Droop, M. R. (2007). Vitamins, phytoplankton and bacteria: symbiosis or scavenging? *J. Plankton Res.* 29, 107–113.

Ducklow, H. (2000). "Bacterial production and biomass in the oceans," in *Microbial Ecology of the Oceans*, ed. D. Kirchman (New York, NY: Wiley Liss), 85–120.

Ducklow, H. W., Carlson, C. A., Church, M., Kirchman, D. L., Smith, D., and Steward, G. (2001). The seasonal development of the bacterioplankton bloom in the Ross Sea, Antarctica, 1994–1997. *Deep Sea Res. II* 48, 4199–4221.

Ducklow, H. W., Dickson, M.-L., Kirchman, D. L., Steward, G., Orchardo, J., Marra, J., and Azam, F. (2000). Constraining bacterial production, conversion efficiency and respiration in the Ross Sea, Antarctica, January-February, 1997. *Deep Sea Res. II* 47, 3227–3247.

Dyhrman, S. T., Webb, E. A., Anderson, D. M., Moffett, J. W., and Waterbury, J. B. (2002). Cell-specific detection of phosphate stress in *Trichodesmium* from the Western North Atlantic. *Limnol. Oceanogr.* 47, 1832–1836.

Feng, Y., Hare, C. E., Rose, J. M., Handy, S. M., DiTullio, G. R., Lee, P. A., Smith, W. O., Peloquin, J., Tozzi, S., Sun, J., Zhang, Y., Dunbar, R. B., Long, M. C., Sohst, B., Lohan, M., and Hutchins, D. A.(2010). Interactive effects of iron, irradiance and CO2 on Ross Sea phytoplankton. *Deep Sea Res. I* 57, 368–383.

Garcia, N. S., Sedwick, P. N., and DiTullio, G. R. (2009). Influence of irradiance and iron on the growth of colonial *Phaeocystis antarctica*: implications for seasonal bloom dynamics in the Ross Sea, Antarctica Aquat. *Microb. Ecol.* 57, 203–220.

Giovannoni, S. J., Tripp, J., Givan, S., Podar, M., Vergin, K. L., and Baptista, D., Bibbs, L., Eads, J., Richardson, T. H., Noordewier, M., Rappé, M. S., Short, J. M., Carrington, J. C., and Mathur, E. J. (2005). Genome streamlining in a cosmopolitan oceanic bacterium. *Science* 309, 1242–1245.

Gobler, C. J., Norman, C., Panzeca, C., Taylor, G. T., and Sanudo-Wilhelmy, S. A. (2007). Effect of B-vitamins and inorganic nutrients on algal bloom dynamics in a coastal ecosystem. *Aquat. Microb. Ecol.* 49, 181–194.

Hale, M. S., Rivkin, R. B., Matthews, P., Agawin, N. S. R., and Li, W. K. W. (2006). Microbial response to a mesoscale iron enrichment in the NE subarctic pacific: heterotrophic bacterial processes. *Deep Sea Res. II* 53, 2231–2247.

Hall, J. A., and Safi, K. (2001). The impact of in situ Fe fertilization on the microbial food web in the Southern Ocean. *Deep Sea Res. II* 48, 2591–2613.

Helliwell, K. E., Wheeler, G. L., Leptos, K. C., Goldstein, R. E., and Smith, A. G. (2011). Insights into the evolution of vitamin B12 auxotrophy from sequenced algal genomes. *Mol. Biol. Evol.* doi: 10.1093/molbev/msr124. [Epub ahead of print].

Hutchins, D. A., Sedwick, P. N., DiTullio, G. R., Boyd, P. W., Queguiner, B., Griffiths, F. B., and Crossley, C. (2001). Control of phytoplankton growth by iron and silicic acid availablity in the subantarctic Southern Ocean: experimental results from the SAZ project. *J. Geophys. Res.* 106, 31559–31572.

Hutchins, D. A., Sedwick, P. N., DiTullio, G. R., Boyd, P. W., Queguiner, B., Griffiths, F. B., and Crossley, C. (2001). Control of phytoplankton growth by iron and silicic acid availablity in the subantarctic Southern Ocean: experimental results from the SAZ project. *J. Geophys. Res.* 106, 31559–31572.

Karl, D. M. (2002). Nutrient dynamics in the deep blue sea. *Trends Microbiol.* 10, 410–418.

Kirchman, D. L., Meon, B., Cottrell, M. T., Hutchins, D. A., Weeks, D., and Bruland, K. W. (2000). Carbon versus iron limitation of bacterial growth in the California upwelling region. *Limnol. Oceanogr.* 45, 1681–1688.

Koch, F., Marcoval, M. A., Panzeca, C., Bruland, K. W., Sanudo-Wilhelmy, S. A., and Gobler, C. J. (2011). The effect of vitamin B12 on phytoplankton growth and community structure in the Gulf of Alaska. *Limnol. Oceanogr.* 56, 1023–1034.

LaRoche, J., Boyd, P. W., McKay, R. M. L., and Geider, R. J. (1996). Flavodoxin as an in situ marker for iron stress in phytoplankton. *Nature* 382, 802–805.

Leventer, A., and Dunbar, R. B. (1996). Factors influencing the distribution of diatoms and other algae in the Ross Sea. *J. Geophys. Res.* 101, 18489–18500.

Marchant, H. J. (2005). "Cyanophytes," in *Antarctic Marine Protists*, eds F. J. Scott and H. J. Marchant (Canberra: Australian Biological Resources Study), 324–325.

Martin, J. H., Fitzwater, S. E., and Gordon, R. M. (1990). Iron deficiency limits phytoplankton productivity in Antarctic waters. *Global Biogeochem. Cycles* 4, 5–12.

Menzel, D. W., and Spaeth, J. P. (1962). Occurrence of vitamin B12 in the Sargasso Sea. *Limnol. Oceanogr.* 7, 151–154.

Morel, F. M. M. (1987). Kinetics of nutrient uptake and growth in phytoplankton. *J. Phycol.* 23, 137–150.

Oliver, J. L., Barber, R. T., Smith, W. O., and Ducklow, H. W. (2004). The heterotrophic bacterial response during the Southern Ocean iron experiment (SOFeX). *Limnol. Oceanogr.* 49, 2129–2140.

Olson, R. J., Sosik, H. M., Chekalyuk, A. M., and Shalapyonok, A. (2000). Effects of iron enrichment on phytoplankton in the Southern Ocean during late summer: active fluorescence and flow cytometric analyses. *Deep Sea Res. II* 47, 3181–3200.

Pakulski, J. D., Coffin, R. B., Kelley, C. A., Holder, S. L., Downer, R., and Aas, P., Lyons, M. M., and Jeffrey, W. H. (1996). Iron stimulation of Antarctic bacteria. *Nature* 383, 133–134.

Panzeca, C., Beck, A. J., Tovar-Sanchez, A., Segovia-Zavala, J., Taylor, G. T., Gobler, C. J., and Sañudo-Wilhelmy, S. A. (2009). Distributions of dissolved vitamin B12 and Co in coastal and open-ocean environments estuarine, coastal and shelf. *Sciences* 85, 223–230.

Panzeca, C., Tovar-Sanchez, A., Agusti, S., Reche, I., Duarte, M., Taylor, G. T., and Sanudo-Wilhelmy, S. A. (2006). B vitamins as regulators of phytoplankton dynamics. *Eos Trans. AGU* 87, 593–596.

Porter, K. G., and Feig, Y. G. (1980). The use of DAPI for identifying and counting aquatic microflora. *Limnol. Oceanogr.* 25, 943–948.

Price, N. M., Harrison, G. I., Hering, J. G., Hudson, R. J., Nirel, P. M. V., Palenik, B., and Morel, F. M. M. (1988/1989). Preparation and chemistry of the artificial algal culture medium Aquil. *Biol. Oceanogr.* 6, 443–461.

Putt, M., Miceli, G., and Stoecker, D. (1994). Association of bacteria with *Phaeocystis* sp. in McMurdo sound, Antarctica. *Mar. Ecol. Prog. Ser.* 105, 179–189.

Raux, E., Schubert, H. L., and Warren, M. J. (2000). Biosynthesis of cobalamin (vitamin B12): a bacterial conundrum. *Cell. Mol. Life Sci.* 57, 1880–1893.

Rodionov, D. A., Vitreschak, A. G., Mironov, A. A., and Gelfand, M. S. (2003). Comparative genomics of the vitamin B12 metabolism and regulation in prokaryotes. *J. Biol. Chem.* 278, 41148–41159.

Roling, W. F. M. (2007). Do microbial numbers count? Quantifying the regulation of biogeochemical fluxes by population size and cellular activity. *FEMS Microbiol. Ecol.* 62, 202–210.

Rose, J. M., Feng, Y., DiTullio, G. R., Dunbar, R. B., Hare, C. E., and Lee, P. A., Lohan, M., Long, M., Smith, W. O., Sohst, B., Tozzi, S., Zhang, Y., and Hutchins, D. A. (2009). Synergistic effects of iron and temperature on Antarctic phytoplankton and microzooplankton assemblages. *Biogeosciences* 6, 3131–3147.

Roth, J. R., Lawrence, J. G., and Bobik, T. A. (1996). Cobalamin (coenzyme B12): synthesis and biological significance. *Annu. Rev. Microbiol.* 50, 137–181.

Saito, M. A., Goepfert, T. J., Noble, A. E., Bertrand, E. M., Sedwick, P. N., and DiTullio, G. R. (2010). A seasonal study of dissolved cobalt in the Ross Sea, Antarctica: micronutrient behavior, absence of scavenging, and relationships with Zn, Cd, and P. *Biogeosciences* 7, 6387–6439.

Saito, M. A., and Goepfert, T. J. (2008). Zinc-cobalt colimitation of *Phaeocystis antarctica*. *Limnol. Oceanogr.* 53, 266.

Saito, M. A., Goepfert, T. J., and Ritt, J. T. (2008). Some thoughts on the concept of colimitation: three definitions and the importance of bioavailability. *Limnol. Oceanogr.* 53, 276–290.

Sanudo-Wilhelmy, S. A., Okbamichael, M., Gobler, C. J., and Taylor, G. T. (2006). Regulation of phytoplankton dynamics by vitamin B12. *Geophys. Res. Lett.* 33.

Scott, F. J., and Marchant, H. J. (eds), (2005). *Antarctic Marine Protists*. Canberra: Australian Biological Resources Study, 295–307.

Sedwick, P., and DiTullio, G. R. (1997). Regulation of algal blooms in Antarctic shelf waters by the release of iron from melting sea ice. *Geophys. Res. Lett.* 24, 2515–2518.

Sedwick, P. N., DiTullio, G. R., and Mackey, D. J. (2000). Iron and manganese in the Ross Sea, Antarctica: seasonal iron limitation in Antarctic shelf waters. *J. Geophys. Res.* 105, 11321–11336.

Smith, W. O. J., and Nelson, D. M. (1985). Phytoplankton bloom produced by a receding ice edge in the Ross Sea: spatial coherence with the density. *Science* 227, 163–166.

Sunda, W., and Huntsman, S. A. (1992). Feedback interactions between zinc and phytoplankton in seawater. *Limnol. Oceanogr.* 37, 25–40.

Swift, D. (1981). Vitamin levels in the Gulf of Maine and ecological significance of vitamin B12 there. *J. Mar. Res.* 39, 375–403.

Tang, Y. Z., Koch, F., and Gobler, C. J. (2010). Most harmful algal bloom species are vitamin B1 and B12 auxotrophs. *Proc. Natl. Acad. Sci. U.S.A.* 107, 20756–20761.

Taylor, G. T., and Sullivan, C. W. (2008). Vitamin B12 and cobalt cycling among diatoms and bacteria in antarctic sea ice microbial communities. *Limnol. Oceanogr.* 53, 1862–1877.

Tortell, P., Maldonado, M., and Price, N. (1996). The role of heterotrophic bacteria in iron-limited ocean ecosystems. *Nature* 383, 330–332.

Van Leeuwe, M. A., and Stefels, J. (1998). Effects of iron and light stress on the biochemical composition of antarctic *Phaeocystis* sp. (Prymnesiophyceae). II. Pigment composition. *J. Phycol.* 34, 496–503.

Webb, E. A., Moffett, J. W., and Waterbury, J. B. (2001). Iron stress in open ocean cyanobacteria (*Synechococcus*, *Trichodesmium*, and *Crocosphaera*): identification of the IdiA protein. *Appl. Environ. Microbiol.* 67, 5444–5452.

Welschmeyer, N. A. (1994). Fluorometric analysis of chlorophyll a in the presence of chlorophyll b and pheopigments. *Limnol. Oceanogr.* 39, 1985–1992.

Zapata, M., Rodriguez, F., and Garrido, J. L. (2000). Separation of chlorophylls and carotenoids from marine phytoplankton: a new HPLC method using a reversed phase C8 column and pyridine-containing mobile phases. *Mar. Ecol. Prog. Ser.* 195, 29–45.

Zettler, E. R., Olson, R. J., Binder, B. J., Chisholm, S. W., Fitzwater, S. E., and Gordon, M. R. (1996). Iron-enrichment bottle experiments in the equatorial Pacific: responses of individual phytoplankton cells. *Deep Sea Res. II* 43, 1017–1029.

Zhang, Y., Rodionov, D. A., Gelfand, M. S., and Gladyshev, V. N. (2009). Comparative genomics analysis of nickel, cobalt, and vitamin B12 utilization. *BMC Genomics* 10, 78. doi: 10.1186/1471-2164-10-78

Conflict of Interest Statement: The authors declare that the research was conducted in the absence of any commercial or financial relationships that could be construed as a potential conflict of interest.

Received: 07 February 2011; accepted: 13 July 2011; published online: xx August 2011.

Citation: Bertrand EM, Saito MA, Lee PA, Dunbar RB, Sedwick PN and DiTullio GR (2011) Iron limitation of a springtime bacterial and phytoplankton community in the Ross Sea: implications for vitamin B$_{12}$ nutrition. Front. Microbio. 2:160. doi: 10.3389/fmicb.2011.00160

This article was submitted to Frontiers in Aquatic Microbiology, a specialty of Frontiers in Microbiology.

Chapter 4

A novel cobalamin acquisition protein in marine diatoms

Erin M. Bertrand[1,2], Andrew E. Allen[3], Christopher L. Dupont[3], Jing Bai[3], Mak A. Saito[1*]

In preparation for submission to PLoS Biology

[1]Marine Chemistry and Geochemistry Department, Woods Hole Oceanographic Institution, Woods Hole MA 02543 USA

[2]MIT/Woods Hole Oceanographic Institution Joint Program in Chemical Oceanography Woods Hole MA 02543 USA

[3]J. Craig Venter Institute, San Diego CA 92121, USA

Abstract: Diatoms are responsible for approximately 40% of marine primary production and are thus key players in the global carbon cycle. There is mounting evidence that marine phytoplankton growth, particularly that of diatoms, can be influenced by the availability of cobalamin. Cobalamin, also known as vitamin B_{12}, is a cobalt-containing organometallic micronutrient only produced by some bacteria and archaea and required by many diatoms and other eukaryotic phytoplankton. Despite its potential importance, little is known about mechanisms of cobalamin acquisition in diatoms or the impact of cobalamin starvation on diatom molecular physiology. Here, we implicate a previously undescribed diatom protein in cobalamin acquisition and identify genes and transcripts encoding it in natural marine phytoplankton communities. Shotgun proteomic and profiling of cultured diatoms *Thalassiosira pseudonana* (cobalamin-requiring) and *Phaeodactylum tricornutum* (not cobalamin-requiring) revealed a large-scale rearrangement of the *T. pseudonana* proteome in response to cobalamin deprivation and identified a protein detected only under low cobalamin availability in both diatoms. Targeted mass spectrometry showed that this protein was up to 160-fold more abundant when cobalamin is scarce. Autologous overexpression of this protein fused with yellow fluorescent protein revealed outer axis and likely endoplasmic reticulum localization. Cobalamin uptake rates were significantly faster in strains overexpressing this protein, directly implicating it in B_{12} acquisition. To our knowledge, this is the first protein in any marine eukaryotic microbe to be directly linked to cobalamin acquisition. Its sequence is not similar to those of known cobalamin acquisition proteins and, in the ocean, appears to be restricted to larger phytoplankton (>3 μm). The detection of this protein's transcripts in environmental samples supports the

hypothesis that cobalamin is an important nutritional factor for oceanic phytoplankton. We anticipate that the identification of this protein will yield insight into the evolution of cobalamin utilization and facilitate mapping of the distribution of cobalamin starvation in natural diatom communities.

Author Summary: Diatoms are the dominant primary producers in many marine environments. An estimated half of all diatom species require an exogenous source of the cobalt-containing micronutrient vitamin B_{12} (also known as cobalamin), and there is a growing body of evidence that B_{12} availability can influence diatom growth in many natural marine environments. However, little is known about the mechanisms diatoms use to acquire B_{12}. In this study, we used quantitative mass spectrometry-based techniques to detect more than 1,000 diatom proteins and estimate their relative abundances across different growth conditions. This allowed us to identify a previously undescribed protein that was more abundant under low cobalamin availability in two different diatom species. We used genetic manipulation techniques to create diatom cell lines that over-produce this protein, which revealed that it is directly involved in cobalamin acquisition. To our knowledge, this is the first protein to be implicated in cobalamin acquisition by diatoms and we anticipate that it will enable future studies that map gene and protein expression patterns in the ocean to test how vitamin B_{12} availability impacts microbial communities. Future study of this protein will also yield insight into how the use of vitamin B_{12} has evolved over time.

Introduction:

Diatoms are responsible for an estimated 40% of marine primary production and are thus important players in global carbon cycling (Falkowski 2004; Nelson et al. 1995). Though diatom growth in the oceans is thought to be controlled primarily by nitrogen and iron availability (Boyd et al. 2007; Moore et al. 2004), recent studies (Panzeca et al. 2006; Bertrand et al. 2007; Gobler et al. 2007; Koch et al. 2011) support longstanding hypotheses that the availability of cobalamin can impact marine phytoplankton growth and community composition (Cowey 1956; Droop 1957; Menzel and Spaeth 1962). In the open ocean, cobalamin is present in exceedingly low concentrations and is depleted in irradiated surface waters, largely due to biological utilization (Menzel and Spaeth 1962). Since no eukaryotic organism is known to produce cobalamin (Rodionov et al. 2003), marine bacteria and archaea must therefore supply auxotrophic (vitamin-requiring) phytoplankton with the vitamin, either through direct interaction (Croft et al. 2005) or through production and release into the water column upon death and cell lysis (Droop 2007; Karl 2002). This chemical dependency is one of many that underlie interactions between marine microbial groups; assessing the role of these dependencies in oceanic processes is of considerable interest (Azam and Malfatti 2007). Cobalamin availability may play a significant role in the climatically important Southern Ocean where it appears to periodically colimit the growth of diatom-dominated phytoplankton communities (Bertrand et al. 2007) and is likley in short supply relative to other marine environments (Bertrand et al. 2011).

The three available genome sequences of marine diatoms (*P. triconrutum*, *T. pseudonana*, and *F. cylindrus*) lack proteins homologous to known metazoan and bacterial B_{12} acquisition proteins (Croft et al. 2006, Bertrand unpubl. observations). As a result, the mechanisms by which these phytoplankton acquire B_{12} from their environment remain unclear. Cobalamin requirements in eukaryotic algae like diatoms arise primarily from its use in the enzyme methionine synthase (Croft et al. 2005; Helliwell et al. 2011), which is responsible for generating methionine from homocysteine and 5-methyltetrahydrofolate (Banerjee and Matthews 1990). Some eukaryotic algal genomes encode only one version of this enzyme, MetH, which uses cobalamin as an intermediate methyl group carrier (Goulding et al. 1997), while others encode both MetH as well as MetE, an enzyme that accomplishes the same reaction without cobalamin but with much lower efficiency (Gonzalez et al. 1992). Once methionine is produced, it has several known fates within algal cells, including use as a protein-building amino acid. Methionine is the precursor to S-adenosyl methionine (AdoMet, SAM), an important methylating agent and propylamine donor that participates in a wide range of cellular functions. Methionine is also used to produce dimethylsulfonium propionate (DMSP), which is only made by some diatoms, possibly as a cryoprotectant, osmolyte (Stefels 2000) or antioxidant (Sunda et al. 2002), and is the precursor to the climatically important gas dimethylsulfide (DMS) (Lovelock 1972). The potential effects of cobalamin starvation on phytoplankton may thus impact a wide range of cellular and ecological functions.

Here we used quantitative proteomic methods to identify diatom proteins involved in cobalamin metabolism and to assess the overall impact of vitamin starvation on diatom proteomes. We quantified larger changes in the proteome of a cobalamin requiring diatom under cobalamin starvation and successfully identified one protein that is more abundant under low cobalamin availability in two diatoms with different B_{12} requirements. We then showed that this protein is directly involved in cobalamin acquisition through phenotypic characterization of diatom cell lines that were overexpressing this protein. To our knowledge, this represents the first inquiry into the impact of cobalamin starvation on algal proteomes and has yielded the identification of a novel protein involved in cobalamin acquisition.

Results and Discussion:

We used shotgun mass spectrometry-based proteomics to query the response of two distantly related diatoms, *T. pseudonana* (absolute cobalamin requirement, MetH only) and *P. tricornutum* (flexible cobalamin usage, MetE and MetH) to low cobalamin availability, under both high and low iron conditions, in an attempt to identify proteins involved in or impacted by cobalamin metabolism and starvation (Figure 1, A-D). Two major observations arose. First, we measured a large difference in the extent of proteome rearrangement under vitamin starvation that was dependent on the cobalamin-requirements of each diatom (Table 1, Figure 1, C-D). Second, we identified a protein (*P. tricornutum* 48322 and its ortholog in *T. pseudonana* 11697- hereafter referred to as cobalamin acquisition protein 1, CBA1) that was more abundant under low cobalamin availability in both diatoms (Figure 1- C-F).

Verification of nutrient limitation scenarios

Cobalamin and iron re-supply experiments confirmed that these diatom cultures were starved for nutrients as intended, with iron rescuing growth of both low iron cultures, and cobalamin rescuing growth only in the low cobalamin culture of the requiring diatom, *T. pseudonana* (Figure S1). Growth in the low cobalamin and low iron *T. pseudonana* culture was only restored upon the addition of both cobalamin and iron together, demonstrating that this culture was simultaneously limited by the availability of both nutrients. In contrast, growth in low cobalamin and low Fe *P. tricornutum* cultures was rescued by iron addition alone and was further enhanced by the co-addition of cobalamin and iron (Figure S1). These differing responses were expected and are likely due to the different requirements for cobalamin between these diatoms.

Cobalamin- induced proteome rearrangement

In sum, 764 *T. pseudonana* proteins were detected from a total of 4955 unique peptides with a 0.19% peptide false discovery rate. These proteins are listed with their putative function in Table A1 in Appendix F. 859 *P. tricornutum* proteins were detected from 5172 unique peptides with a 0.22% peptide false discovery rate (Table A2, Appendix F).

In the cobalamin-requiring diatom *T. pseudonana,* 19 % of detected proteins were significantly differentially abundant under cobalamin starvation compared to the replete control (Table 1, Figure 1 C). Presuming that this method identified the predominant proteins expressed by this diatom, this suggests that the diatom conducts a significant rearrangement of cellular

function upon growth under cobalamin limitation. Though some of these changing proteins are likely responding to the accompanying growth rate depression, there are many that display different behavior under cobalamin versus iron limitation (Table A1) and have putative functions suggesting they are directly related to B_{12} metabolism (Table 2, S2). Even though iron limitation induced in this study had a much more severe impact on growth rate than cobalamin limitation did, changes induced in the *T. pseudonana* proteome by cobalamin starvation were nearly as large as those induced by iron limitation (Table 1, Figure 1 A,C). In contrast, *P. tricornutum,* which can accomplish methionine synthesis without the use of the vitamin, effected only a slight proteome change in response to cobalamin scarcity (Table 1, Figure 1 B,D). Protein abundance changes under low B_{12} and low iron versus low iron alone showed a similar pattern, where *T. pseudonana,* even under severe iron limitation, rearranged its protein complement significantly to manage cobalamin starvation while *P. tricornutum* changed the abundance of less than 1% of the proteins in its detected proteome. Included in this changing *P. tricornutum* proteome is MetE, which was only detected under low cobalamin or low cobalamin and low iron availability (Figure 1 D, Table 2). This suggests that *P. tricornutum* expresses MetE to replace MetH when cobalamin is scarce, consistent with transcript abundance patterns observed previously in this diatom (Helliwell et al. 2011). MetH was not detected in our study, possibly due to low abundance. Lower concentrations of MetH are expected since this protein has much higher catalytic activity compared to MetE (Gonzalez et al. 1992). A slight growth yield decrease is evident in the low B_{12} *P. tricorutum* cultures versus the replete control (Figure 1 B, Table 1), likely in part as a result of the use of the less efficient MetE protein in this important metabolic reaction.

One particular protein, CBA1, showed high abundance under cobalamin limitation but was not detected under replete conditions or iron limitation in the global proteome analysis in both diatoms (Figure 1 C-E). Absolute quantification via the more sensitive and quantitative technique of selected reaction monitoring (SRM) mass spectrometry revealed that the concentration of this protein was between 10 and 160-fold higher under low B_{12} availability in *P. tricornutum* (Figure 1 F). CBA1 has a clear N-terminal signal peptide sequence for secretion (Cello and SignalP- predicted (Nielsen et al. 1997; Yu et al. 2006)) and no transmembrane domains. It contains a partial conserved domain that is weakly similar to the periplasmic component of a bacterial iron hydroxamate ABC transport system (FepB; N- terminal end is truncated, Pt48322 blastp search E-value 1.33e-4), but the protein is otherwise unlike characterized domains. There appear to be copies of this protein encoded in all sequenced diatom genomes as well as those from other members of the stramenopile lineage, *Ectocarpus siliculosus* and *Aureococcus anophagefferens* (Table S1). However, since these sequences are not tightly conserved and show some similarities to a class of bacterial proteins, rigorous analysis of the functional similarity of these proteins between algal lineages will require the identification of residues essential for this protein's activity.

Overexpression of CBA1, subcellular localization and phenotypic characterization

We examined the sub-cellular localization of CBA1 through overexpression of the Pt48322 isoform in native host *P. tricornutum* as a yellow fluorescent protein (YFP) fusion construct. The protein was localized to the outer axis of the cell, consistent with its predicted

signal peptide sequence, and was also present intracellularly (Figure 2 A,B). The intracellular localization around, but not within, the chloroplast is consistent with the protein being processed within the endoplasmic reticulum (ER), which envelopes the chloroplast in red lineage algae. Since one of the primary pathways for protein export and secretion is through the ER, the likely ER processing detected here for CBA1 is consistent with the predicted signal peptide as well as outer axis localization.

We characterized the phenotypic response of this overexpression in *P. tricornutum* by measuring B_{12} uptake rates in two cell lines overexpressing this protein and comparing them to uptake rates in the wild type and a line overexpressing an unrelated protein, urease. Overexpression of CBA1 enhanced cell specific B_{12} uptake rates in *P. tricornutum* 2 to 3-fold (Figure 2 C), which directly implicates this protein in cobalamin acquisition. This, along with its outer axis localization, suggests that CBA1 may bind cobalamin and aid in shuttling the vitamin into the cell. This finding is significant in that CBA1 is, to our knowledge, the first identified protein in any marine eukaryotic microbe to be directly linked to vitamin B_{12} acquisition.

Single nucleotide polymorphisms in P. tricornutum CBA1 coding sequences:

cDNA sequencing for overexpression efforts revealed eight single nucleotide polymorphisms (SNPs) between the coding sequence (CDS) from the whole genome sequencing project and the PCR-amplified cDNA sequence (Figure 3), likely reflecting different CDS for the protein on each allele of the diatom's diploid genome. These SNPs resulted in three amino acid changes in the protein model, all of which are predicted to be neutral. Both copies of the protein were detected via shotgun mass spectrometry when the PCR-amplified coding sequence model

was added to the reference database. Both were detected only under low cobalamin availability, as shown in Figure 3. Additionally, of the two peptides used to measure CBA1 abundance via SRM, one peptide (Pt48322_1) is present in only one allelic copy of the protein, while the second (Pt48322_2) is present in both. As expected, the abundance of these peptide is linearly correlated across all samples ($r^2 = 0.999$) and Pt48322_2 is consistently more abundant (Figure 1, Figure S4). This is therefore an example of canonical gene expression in a diploid genome where allelic copies display similar expression patterns.

CBA1 and exuded algal vitamin binding complexes:

Previous work revealed that diatoms and other algae exude a protein into their growth media which binds vitamin B_{12} very strongly (Droop 1968; Pintner and Altmeyer 1979). In *T. pseudonana*, this protein was shown to be a distinct, large, multimeric complex (Sahni et al. 2001), but the identity of its components remain unknown. It is possible that CBA1 represents a part of this multimer, though this is unlikely because overexpression of CBA1 without any other components of a complex enhances cobalamin uptake, while the exuded B_{12}-binder is thought to restrict vitamin uptake (Droop 1968; Pintner and Altmeyer 1979). It is also possible that CBA1 interacts with this complex to move cobalamin from the growth media into the cell (Davies and Leftley 1985). Future study will be required to elucidate the relationship between CBA1 and the strong, exuded B_{12} binders produced by algae.

CBA1 in environmental sequencing datasets

We identified nucleic acid sequences that likely encode CBA1 in cDNA libraries generated from natural phytoplankton communities. These communities were from diverse marine locations including sea ice and water column samples from the Ross Sea of the Southern Ocean and water column samples from the North Pacific, Monterey Bay, and Puget Sound. These nucleic acid sequences are displayed as a phylogenetic tree that uses CBA1 sequences from available genomes to construct a reference tree onto which these metatranscriptomic sequences are placed (Matsen et al 2010; Figure 4). cDNA sequences most similar to CBA1 were detected only in large size fraction (>3 μm) samples, suggesting that this protein is restricted to larger phytoplankton. A majority of the detected cDNA sequences from the Ross Sea were most similar to putative CBA1 sequences from *Fragilariopsis cylindrus,* which was expected since *F. cylindrus* is an Antarctic diatom and was in fact present in these locations (data not shown). The detection of CBA1 genes and transcripts in these Antarctic datasets suggests that this protein is of use to field populations and thus that cobalamin acquisition is an important part of the molecular physiology of these phytoplankton communities.

Other uncharacterized cobalamin-responsive proteins:

In addition to CBA1, other proteins displayed abundance patterns suggesting that they may be involved in the cellular response to cobalamin starvation (Figure 5, Tables 2, S2). While some of these proteins have predicted cellular functions, more than half of them play unknown roles (Table 2, S2). Three proteins of unknown function in *T. pseudonana* (24346, 23556, 1896, Table 2) do not have homologs in *P. tricornutum*, were more abundant under low cobalamin alone and low cobalamin with low iron, and did not increase in abundance under low iron alone.

These unknown proteins may be involved in the *T. pseudonana* response to cobalamin starvation and warrant further study, particularly if they are present exclusively in genomes of B_{12}-requiring diatoms. In addition, there are several proteins of unknown function that are more abundant under low cobalamin and low cobalamin with low iron in *T. pseudonana* and were either not detected in *P. tricornutum* or display different abundance patterns (22483, 23657, 24639, 22096,1869- Table 2). These proteins may play a part in the cellular response to severe methionine deprivation in *T. pseudonana* since they do not display the same patterns of abundance in *P. tricornutum,* which would likely not experience such severe methionine deprivation because it can utilize MetE in place of MetH.

Connections between cobalamin, folate and pyridoxal 5' phosphate:

Connections between cobalamin and folate, through their function in methionine cycling, are well-known in metazoans (Selhub 2002), and appear to exist in algae as well, since combined folic acid and methionine addition to B_{12} starved green algal cultures was shown to partially rescue growth (Croft et al. 2005). The mechanism for this is believed be 'methyl folate trapping' whereby methyltetrahydrofolate is produced by an irreversible reaction and then, under conditions of reduced methionine synthase activity, is trapped in this form rather than being recycled for further use in the active folate cycle (Scott and Weir 1981). In our study, a protein involved in folate one carbon metabolism, serine hydroxymethyltransferase (SHMT), is more abundant under both types of vitamin limitation in the two diatoms (Figure 5). SHMT is pyridoxal 5' phosphate (PLP, vitamin B6) dependant and catalyzes the reversible conversion of serine to glycine and tetrahydrofolate (THF) to 5,10-methylene tetrahydrofolate (5,10 MTHF;

Snell et al. 2000). 5,10 MTHF can then be converted irreversibly to 5-methyltetrahydrofolate (MeTHF) by methylenetetrahydrofolate reductase (MTHFR; detected here in low abundance, Table A1). MeTHF, along with homocystine, are then used for methionine production by methionine synthase. It is the buildup of MeTHF at this step that leads to folate trapping. There are two isoforms of SHMT in diatoms, one that appears to be targeted to the mitochondria, and one that is likely cytosolic. In *T. pseudonana*, cytosolic SHMT abundance was lower under Fe limitation versus the replete control (Figure 5), consistent with the trends observed in mammals where the protein is more abundant under faster growth (Fell and Snell 1988). However, low cobalamin also caused a > 2-fold increase in abundance of cytosolic SHMT in both diatoms, consistent with results from *E. coli* showing that SHMT activity increases under B_{12} limitation (Dev and Harvey 1984). This suggests that diatom cells increase the interconversion of THF and 5,10 MTHF under low vitamin conditions, possibly in an effort to prevent folate trapping by reducing the pool of 5,10 MTHF that is irreversibly converted to MeTHF. This is consistent with suggestions that in humans SHMT mediates the partitioning of one carbon units between DNA synthesis and methionine cycling (Herbig et al. 2002).

In humans, low folate, vitamin B_{12}, and PLP (vitamin B6) concentrations are correlated with elevated blood homocysteine levels, suggesting that the use of these four compounds are all linked (Selhub et al. 1993). Here, an enzyme putatively involved in PLP synthesis is much more abundant under both types of vitamin limitation in *T. pseudonana* (Figure 5). This increase is consistent with higher demand for PLP under low B_{12}, potentially for use by the PLP-dependant

SHMT enzymes. Taken together, these data suggest that folate, vitamin B_{12} and PLP metabolism are linked in diatoms, as observed in humans (Selhub et al. 1993).

Evidence for S-adenosyl methionine deprivation:

Another protein that is more abundant under vitamin limitation in both diatoms is S-adenosyl methionine synthase (MetK) (Figure 5). This enzyme is responsible for the conversion of methionine to S-adenosyl methionine (AdoMet, SAM). In addition to many other cellular functions, AdoMet is also responsible, along with flavodoxin, for reductive methylation of cobalamin in methionione synthase when the active cofactor becomes periodically oxidized during its catalytic cycle (Drennan et al. 1994). It is possible that this increase in MetK abundance functions to increase AdoMet production for more efficient repair of oxidized cobalamin in MetH. It is also possible that MetK is more abundant under vitamin limitation to increase encounter rates between methionine and the enzyme in an attempt to meet cellular AdoMet demand despite methionine scarcity. There is no increase in MetK abundance under vitamin and iron colimitation relative to iron limitation; it is possible that the cellular rearrangements diatoms employ to cope with iron limitation alter cellular AdoMet requirements, negating the need for additional MetK. The elevation of MetK under low cobalamin availability suggests that AdoMet starvation may be an important consequence of B_{12} deprivation in these diatoms.

Implications for marine biogeochemistry:

The detection of CBA1 transcripts in environmental datasets suggests that this protein is abundant and utilized by natural phytoplankton populations and thus that cobalamin acquisition is an important component of diatom molecular physiology. This, along with the significant

proteome rearrangement induced by cobalamin starvation in diatoms, supports including cobalamin availability and its production and consumption dynamics in efforts to predict and model marine primary productivity. Future studies mapping the abundance of CBA1 protein or transcripts along with traditional measures of productivity and community composition may prove useful for elucidating the major oceanic controls on B_{12} starvation and utilization in marine phytoplankton communities and could yield insights into the influence of B_{12} availability on marine microbial community composition.

Implications for cobalamin biochemistry:

Our results implicate SHMT abundance changes and altered folate and PLP metabolism in the acclimation of diatom cells to low B_{12} availability and suggest that AdoMet starvation is an important consequence of cobalamin starvation in diatoms. Future metabolomic mapping of the folate, PLP, homocysteine, and methionine-derived compounds involved in these processes will yield important additional insight into these dependencies.

Since CBA1 is a component of a novel cobalamin acquisition pathway that differs from the well-characterized bacterial and metazoan mechanisms, its identification may advance efforts to understand the biochemistry and evolution of cobalamin acquisition. Further analyses are required to elucidate the exact role that CBA1 plays in cobalamin acquisition and to identify the other proteins involved in this process. Studies to test whether CBA1 binds cobalamin directly are underway. Subsequent comparative studies of the different acquisition pathways may then yield valuable insight into cobalamin biochemistry and the evolution of cobalamin utilization through time.

Methods:

Culturing and Experimental Design

Axenic cultures of *Thalassiosira pseudonana* CCMP 1335 *and Phaeodactylum tricornutum* CCMP 632 were obtained from the Provasoli-Guillard National Center for Culture of Marine Phytoplankton and maintained using sterile and trace metal clean technique. All culturing was conducted at 16°C under a constant light level of 150 $\mu E/m^2/sec$. Media was prepared in a 0.2 μm filtered oligotrophic seawater base collected in a trace metal clean manner, microwave sterilized, and supplemented with macronutrients at f/2 concentrations and vitamins with EDTA-buffered trace metals as described by Sunda and Huntsman (Sunda and Huntsman 1995). All culturing was conducted in polycarbonate bottles and manipulations were conducted a class 100 clean room facility. Fe' concentrations were calculated according to Sunda and Huntsman assuming that pH remained constant at 8.2 (Sunda and Huntsman 2003).

***P. tricornutum* colimitation experiment:** Cells were acclimated for the experiment under conditions described above except with 5 nM added total iron (10^{-11} M Fe') and 0.5 pM added vitamin B_{12} for four transfers allowing at least three doublings per transfer. Cells were then inoculated (3.2 %) into twelve 2.2 L bottles containing 1.8 L of media (four treatments, biological triplicates). The media was as described above except for variable iron and vitamin B_{12} concentrations, which were chosen based on previous studies (Allen et al. 2008; Kustka et al. 2007). The low iron treatment had 2.5 nM Fe total ($10^{-11.3}$ M Fe') and 100 pM added vitamin B_{12}; the low B_{12} treatment had no added vitamin B_{12} and 100 nM Fe total ($10^{-9.69}$ M Fe'); the low B_{12} low iron treatment had no added vitamin B_{12} and 2.5 nM Fe total ($10^{-11.3}$ mol L Fe') while the

replete treatment had 100 pM added vitamin B_{12} and 100 nM Fe total ($10^{-9.69}$ M Fe'). Samples were taken daily for fluorescence and cell counts, and harvested for protein after 6 days for the high iron and 9 days for the low iron (Figure 1 A,B arrow locations). Protein samples (200-300 mL) were filtered onto 0.4 μm polyethersulfone filters, flash frozen in liquid nitrogen, and stored at -80C. Just after the protein harvest timepoint, each culture was split in four and re-supplied with either nothing, 100 pM B_{12}, 100 nM Fe total, or both B_{12} and Fe and growth was monitored via fluorescence.

***T. pseudonana* colimitation experiment:** This experiment was conducted as above except with different vitamin B_{12} and iron concentrations due to known differences in B_{12} and iron requirements for these diatoms. Concentrations were chosen based on previous work (Allen et al. 2008; Kustka et al. 2007; Swift and Taylor 1972). Acclimation cultures had 1 pM added vitamin B_{12} and 65 nM added total Fe ($10^{-9.88}$ M Fe'). The low iron treatment had 50 nM Fe total ($10^{-10.0}$ M Fe') and 100 pM added vitamin B_{12}; the low B_{12} treatment had 0.3 pM added vitamin B_{12} and 400 nM Fe total ($10^{-9.09}$ M Fe'); the low B_{12} low iron treatment had 0.3 pM added vitamin B_{12} and 50 nM Fe total ($10^{-10.0}$ M Fe') while the replete treatment had 100 pM added vitamin B_{12} and 400 nM Fe total ($10^{-9.09}$ M Fe'). Just after the protein harvest timepoint, each culture was split in four and re-supplied with either nothing, 100 pM B_{12}, 400 nM Fe, or both B_{12} and Fe and growth was monitored via fluorescence.

Growth monitoring: Cells were counted using a Palmer Maloney nanoplankton counting chamber counting at least 10 fields of view or 200 individuals at 400 x magnification with light

microscopy (Carl Zeiss, Inc., Thornwood, NY). Fluorescence was monitored using a Tuner Designs TD 700 Fluorometer calibrated to a solid standard.

Protein Extraction and Digestion

Cells were scraped from the filters and resuspended in 600 mL B-PER reagent (Thermo Scientific, Rockford, IL) supplemented with 5 mM EDTA and 1 mM phenylmethanesulfonylfluoride (a serine protease inhibitor). Samples were incubated at room temperature for 20 min with occasional gentle vortexing. The cells were then sonicated with a microtip (Branson digital sonifier) on ice, twice for 1 min at constant duty cycle with a 5 min pause on ice between sonication steps. Samples were centrifuged for 30 min at 14,100 RCF and 4°C, and supernatants were precipitated overnight in 50% acetone 50% methanol 0.5 mM HCl at -20 °C. Precipitated protein was collected by centrifugation at 14,100 RCF for 30 min at 4 °C and dried by speed vacuum at room temperature. Protein was resuspended in 100 uL of the extraction buffer for 30 min at room temperature. Aliquots were taken for protein determination by DC assay using bovine serum albumin as a protein standard (BioRad Inc., Hercules CA). Proteins were stored at -80 °C until digestion.

Protein was digested following the tube gel digestion procedure (Lu and Zhu 2005) with minor modifications. Briefly, samples were immobilized in 15% acrylamide in pH 7.5 Tris buffer, fixed with 10% acetic acid and 50% ethanol, washed successively with 10% acetic acid and 50% methanol, then acetonitrile and 25 mM ammonium bicarbonate to remove detergents and protease inhibitors and then cut into 1 mm^2 pieces. Samples were reduced with 10 mM dithiothreitol (DTT) at 56 °C for 1 h, alkyated with 30 mM iodoacetamide for 1 h, and then

washed in 25 mM ammonium bicarbonate and digested with trypsin in 25 mM ammonium bicarbonate for 16 h at 37 °C (1:20 ratio trypsin to total protein, Promega Gold Mass Spectrometry Grade, Promega Inc., Madison WI). The peptides were extracted by successive additions of a peptide extraction buffer containing 50% acetonitrile and 5% formic acid. The extracted peptides were combined and concentrated by speed vacuum for about three hours to less than 20 µL, diluted with 2% acetonitrile and 0.1% formic acid and stored at -80 °C.

Shotgun Mass Spectrometry and Data Processing

The protein digestions were analyzed (4 µg total protein per analysis) using a peptide Cap Trap in-line with a reversed phase Magic C18 AQ column (0.2 x 150 mm, 3 µm particle size, 200 Å pore size, Michrom Bioresources Inc. Auburn CA) on a Paradigm MS4 HPLC system (Michrom Bioresources Inc.). An ADVANCE nanocapillary electrospray source (Michrom Bioresources Inc.) introduced the sample an LTQ (linear ion trap) mass spectrometer (Thermo Scientific Inc. San Jose CA). The chromatography consisted of a hyperbolic gradient from 5% buffer A to 95% buffer B for 300 min, where A was 0.1% formic acid (Michrom Ultra Pure) in water (Fisher Optima) and B was 0.1% formic acid in acetonitrile (Fisher Optima) at a flow rate of 2 µl min^{-1}. The mass spectrometer was set to perform MS/MS on the top 7 ions using data-dependent settings and a dynamic exclusion window of 30 s and parent ions were monitored over the range of 400-2000 m/z. Three technical replicate mass spectrometry experiments were processed for each of 8 biological samples (4 treatments per diatom, 2 diatoms).

The mass spectra were searched using SEQUEST (Bioworks version 3.3, Thermo Inc., San Jose CA) with a fragment tolerance of 1 Da, parent tolerance of 2 Da, +57 on cysteine for

carbamidomethylation by iodoacetamide as a static modification and +16 for methionine oxidation as a dynamic modification, trypsin fully enzymatic peptide cleavage, and a maximum of 2 missed cleavage sites. An amino acid database for *Thalassiosira pseudonana* was compiled by combining data from the Joint Genome Institute (JGI) and the National Center for Biotechnology Information (NCBI) and was comprised of the files Thaps3_chromosomes_geneModels_FilteredModels2_aa.fasta and Thaps3_bd_unmapped_GeneModels_FilteredModels1_aa.fasta from JGI as well as the mitochondrial and plastid genomes from NCBI (Plastid- Project ID: 20561; Mitochondrial- Project ID: 15818), all of which contributed to the complete genome sequencing project (Armbrust et al. 2004). Common contaminants as well as a reversed decoy version of these databases for false positive rate analysis were also included. The *Phaeodactylum tricornutum* database was similarly constructed from files Phatr2_chromosomes_geneModels_FilteredModels2_aa.fasta and Phatr2_bd_unmapped_GeneModels_FilteredModels1_aa.fasta and the plastid genome (Project ID: 18283) all of which contributed to the complete genome sequencing project (Bowler et al. 2008). Database search results were further processed using the PeptideProphet statistical model (Keller et al. 2002) within Scaffold 3.0 (Proteome Software Inc., Portland OR). Proteins were identified if their peptide identification probability was > 95%, protein identification probability was >99%, and two or more peptides from its sequence were detected.

Relative protein abundance was determined via calculating a spectral counting score in Scaffold 3.0. Spectral counts are normalized across all mass spectrometry samples in each

experiment, including three technical replicates or each of four treatments, to allow comparison of relative protein abundance. Proteins discussed as 'differentially expressed' were determined by the Fisher exact test as described by Zhang et al (Zhang et al. 2006). False positive identification rate was estimated as described by Peng et al (Peng et al. 2003).

Targeted Mass spectrometry:

Selected reaction monitoring (SRM) was conducted as previously described (Saito et al. 2011) for peptides unique to CBA1 in *P. tricornutum* (FFSVFFNK, Pt48322_1native; EHTANQVVEAAES, Pt48322_2native) employing isotopically-labeled versions of each peptide (Sigma-Aldrich) (Stemmann et al. 2001) as internal standards (FFS[V_C13N15]FFNK, EHTANQ[V_C13N15]VEAAESR). Standard curves displaying the linear behavior of each peptide are given in Figure S2. Briefly, 20 fmol of heavy isotope labeled versions of each peptide were added to diatom peptide extracts (1 μg total protein) and analyzed via SRM using a Thermo Vantage TSQ Triple Quadrapole Mass Spectrometer with the HPLC and ion source as described above for shotgun mass spectrometry. The reactions monitored for each peptide are given in Table S3.

Overexpression and sub-cellular localization:

Full length *P. tricornutum* 48322 cDNA was PCR amplified and cloned into a TOPO pENTR, subjected to Gateway (Invitrogen) recombination with a diatom C-terminal YFP pDONR vector (Siaut et al. 2007) which was transformed into *P. tricornutum* via particle bombardment (Falciatore et al. 1999). Transformants were screened via PCR and epifluorescence microscopy. Primers used for Pt48322 cDNA amplification were: sense 5' - C

ACC ATG ATG AAG TTT TCG T- 3'and antisense 5'- GAA CAA CAA TAC GTG TAT AAG ACT -3'

B_{12} uptake rate assessments:

Inorganic ^{57}Co was removed from a carrier-free ^{57}Co-B_{12} stock solution (MP Biomedicals) via chelex (Price et al. 1988/1989) and the remaining solution was used as a radiotracer in cultures of *P. triconrutum*. Strains (wild type, two cell lines overexpressing CBA1_48322 and one line overexpressing urease) were grown through three successive transfers into media as described above, with 100 pM B_{12} and 80 μg/mL zeocin added (zeocin not added to wild type). When the cells were in mid-exponential growth in the third transfer, each strain was used to inoculate (3%) three 28 mL polycarbonate tubes containing 20 mL of growth media with 100 pM B_{12} and 80 μg/mL zeocin and allowed to acclimate for 3 h. 0.5 pmol ^{57}Co B_{12} was added to cultures and 24 h later, the samples were each gently filtered onto 1 μm polycarbonate filters and rinsed with 4 mL filtered seawater. B_{12} uptake was measured by assessing the percentage of added tracer that was taken up into the particulate fraction via gamma counting as previously described (Bertrand et al. 2007) and assuming that total B_{12} concentrations were 100 pM for the period of uptake. Cell growth was monitored by fluorescence and then translated to cell number via calibration curves created during growth of the 3rd transfer.

Metatranscriptomic and metagenomic analyses

250-500 L of surface (~3 m) seawater was pumped into a 250 L carboy and then onto 293 mm diameter 3 μm pore size polyethersulfone filters (Versapore, Pall). Sampling locations chosen as part of the J. Craig Venter Institute's Global Ocean Sampling project; established

sampling and filtering protocols were used. Filters were frozen in liquid nitrogen, kept on dry ice for shipping and stored in the laboratory at -80°C and processed as previously described (Rusch et al 2007).

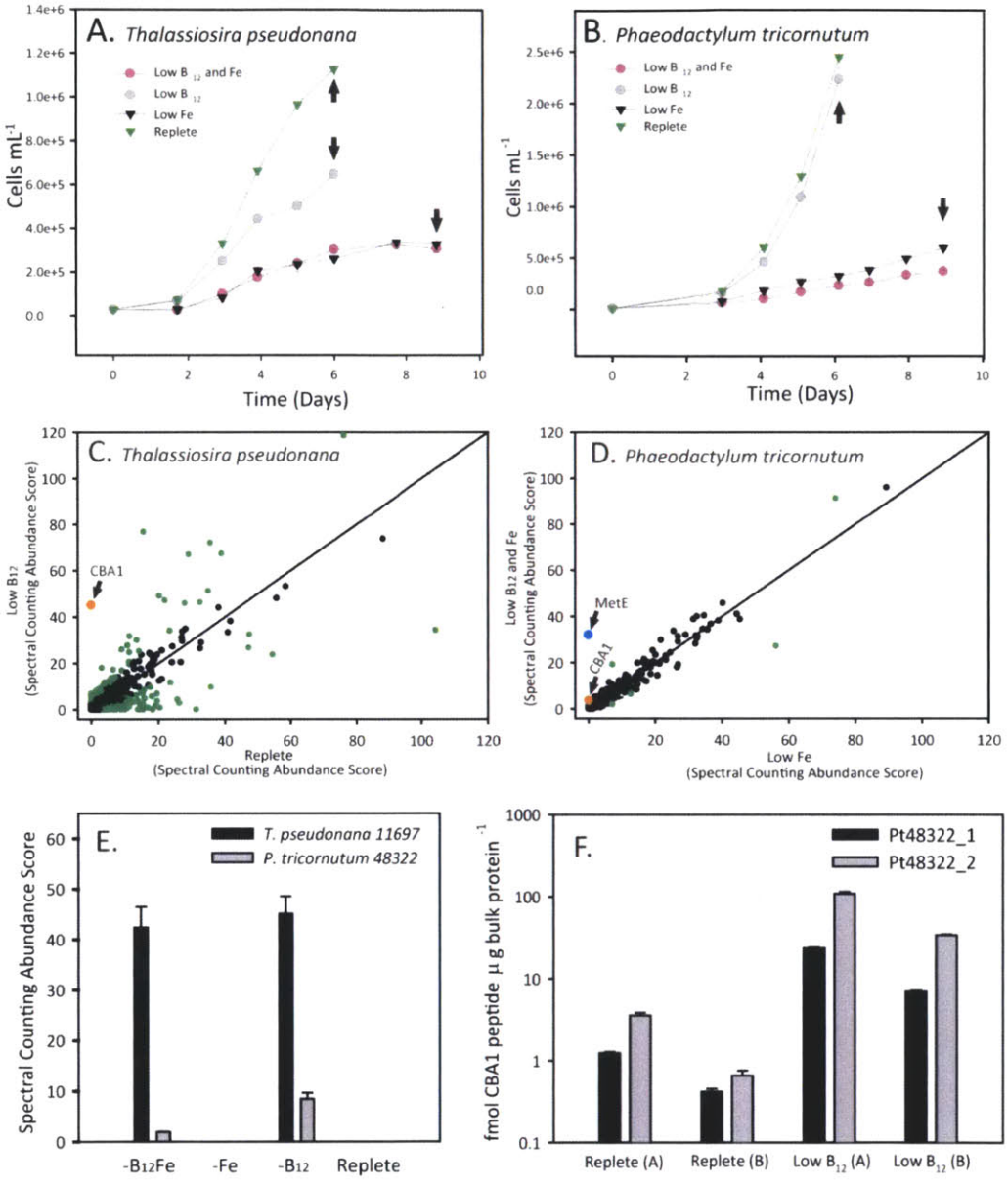

Figure 1: Quantitative assesments of protein abundance under low cobalamin availability in two diatoms. One protein (Pt48322, Tp11697- CBA1) is much more abundant under low cobalamin availability in two diatoms. **Panels A-B:** Cell density over time for *T. pseudonana* **(A)** and *P. tricornutum* **(B)** grown under four different nutrient regimes- low B_{12}, low Fe, low B_{12} with low Fe, and replete. Values shown are means of triplicate cultures and error bars are one standard deviation. Arrows indicate where samples for proteomic analyses were taken (panels C-F). Low

cobalamin availability had a much larger impact on *T. pseudonana* growth than on the growth of *P. tricornutum*, likely due to *P. tricornutum*'s use of MetE as an alternative to the B_{12}-requiring MetH. Low iron had a more severe impact on growth than low B_{12} in both diatoms, as expected given the extreme low iron availability in the experiment. **Panels C-D:** Shotgun mass spectromtry analyses of *T. pseudonana* **(C)** in the low B_{12} versus replete treatment and *P. tricornutum* **(D)** in the low B_{12} with low iron treatment versus the low iron treatment. Each point is an identified protein, with the mean of its technical triplicate abundance scores in one treatment plotted against the mean of abundance scores in another treatment. The solid line is 1:1 abundance. Protein CBA1, Tp11697 and Pt 48322, is highlighted in orange and MetE is highlighted in blue. Protiens in green are considered differentially abundant (Fisher Exact Test $p < 0.01$). **(E)** Bars are means of spectral counting abundance scores for protein CBA1 in four treatments in both diatoms. Error bars represent one standard deviation about the mean of technical triplicate measurements. **(F)** Absolute abundance of two peptides from CBA1 in *P. tricornutum* measured via the highly sensitive and quantitative technique SRM mass spectrometry in low B_{12} and replete cultures. Error bars are one standard deviaton about the mean of technical triplicate measurments.

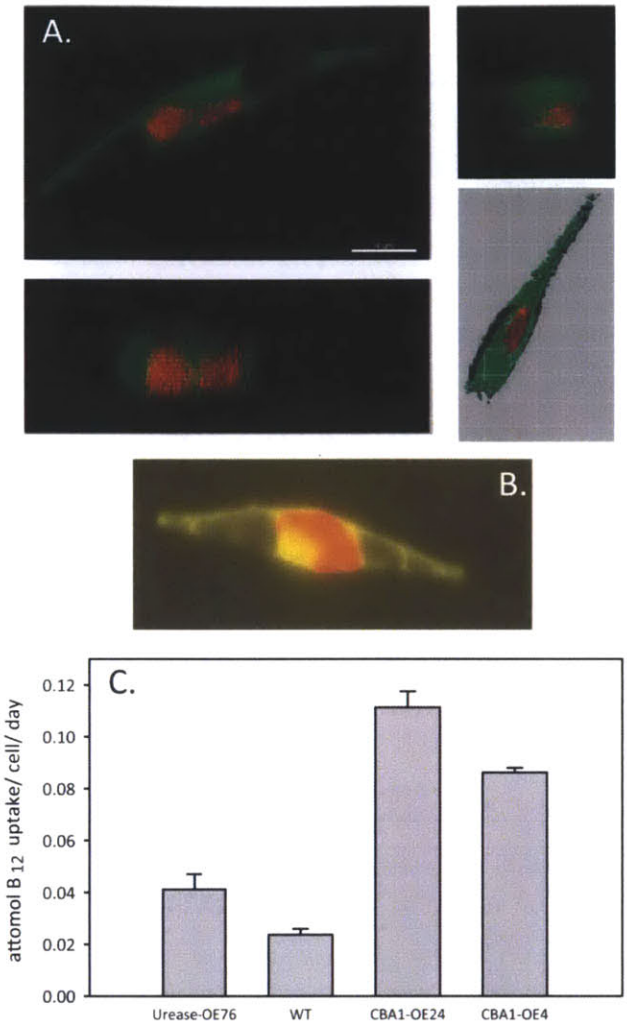

Figure 2: Protein CBA1 appears to be localized to the outer axis of the cell and the endoplasmic reticulum and is directly implicated in cobalamin acquisition. **(A)** Confocal micrographs and an **(B)** epifluorescence micrograph of protein CBA1 fused to yellow fluorescent protein (YFP) and overexpressed in *P. tricornutum*. Yellow and green are YFP and red is chlorophyll autofluorescence. **(C)** Cobalamin uptake rates by wild-type *P. tricornutum* and transgenic *P. tricornutum* cell lines overexpressing CBA1 (CBA1-OE4, CBA1-OE24) or Urease (Urease-OE76) measured over 24h in exponential growth phase under B_{12}-replete conditions. Growth rate over the 24h experiment for the wild type was 0.72+/-0.07, for Urease-OE76: 1.01 +/-0.02, CBA1-OE24: 1.10 +/- 0.03, CBA1-OE4: 1.08 +/- 0.03, given as mean of triplicate cultures +/- one standard deviation.

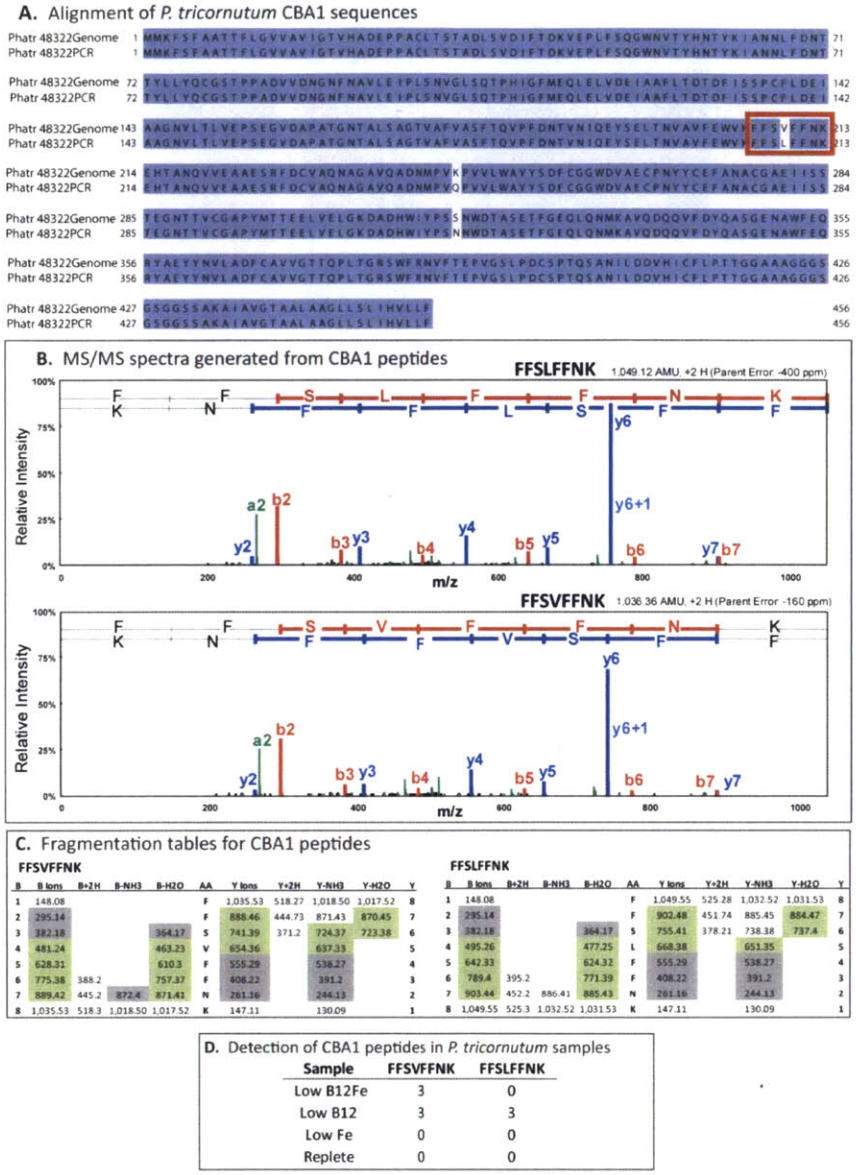

Sample	FFSVFFNK	FFSLFFNK
Low B12Fe	3	0
Low B12	3	3
Low Fe	0	0
Replete	0	0

Figure 3. Two allelic copies of *P. tricornutum* CBA1 protein were expressed. **(A)** The two versions of this protein, one from the genome project CDS and the other from PCR amplification of *P. tricornutum* cDNA aligned, showing three amino acid changes in white, which resulted from eight single nucleotide polymorphisms between these sequences. The peptides highlighted by the orange box have one amino acid difference and were both detected via shotgun LTQ MS in this proteome study, suggesting that both allelic copies of the protein are expressed. **(B)** The product ion (MS/MS) mass spectra generated via LTQ-MS from peptides indicative of each form of CBA1,

with y ions shown in blue, b ions shown in red, and other associated ions shown in green. **(C)** Fragmentation tables for both peptides, showing the masses of the product ions predicted to be generated from these peptides. Product ions highlighted in gray or green were detected via LTQ-MS (spectra shown in B); those in green are different between these two peptides, while those in gray are conserved. **(D)** The number of times these peptides were found in *P. tricornututm* cultures under four culturing conditions.

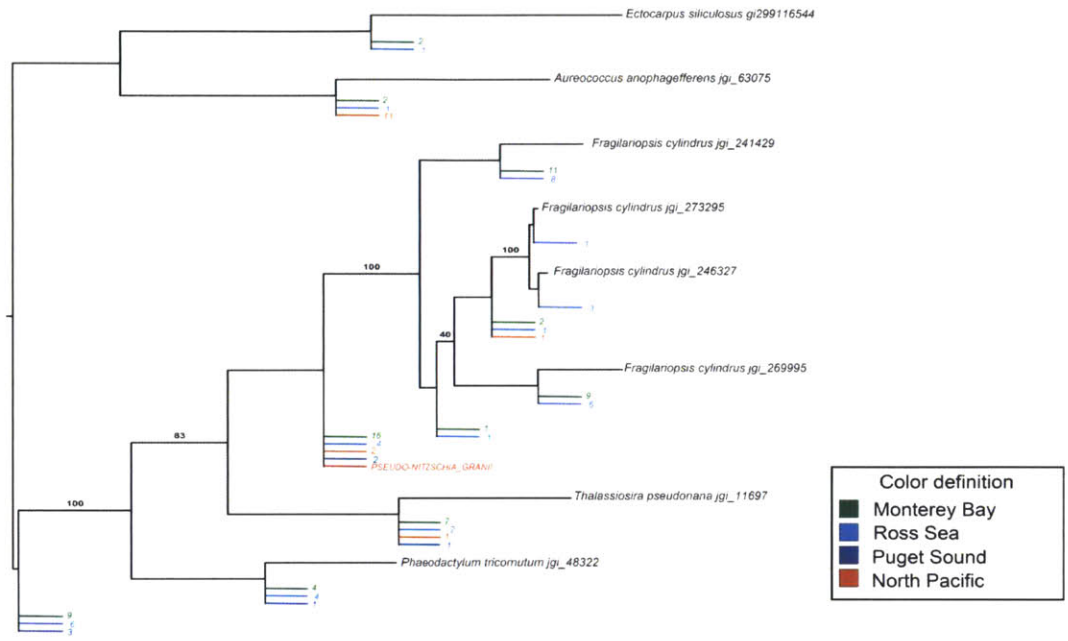

Figure 4: Phylogenetic tree containing CBA1 sequences from metatranscriptomic (cDNA) libraries from the Ross Sea of the Southern Ocean, Monterey Bay, Puget Sound, and the North Pacific. Reference sequences from *Phaeodactylum tricornutum*, *Fragilariopsis cylindrus*, *Thalassiosira pseudonana, Aureococcus anophagefferenas*, and *Ectocarpus siliculosus* genomes were used to construct these trees (Matsen et al 2010) and are shown in black. CBA1-like sequences from environmental samples are shown color, as described in the key.

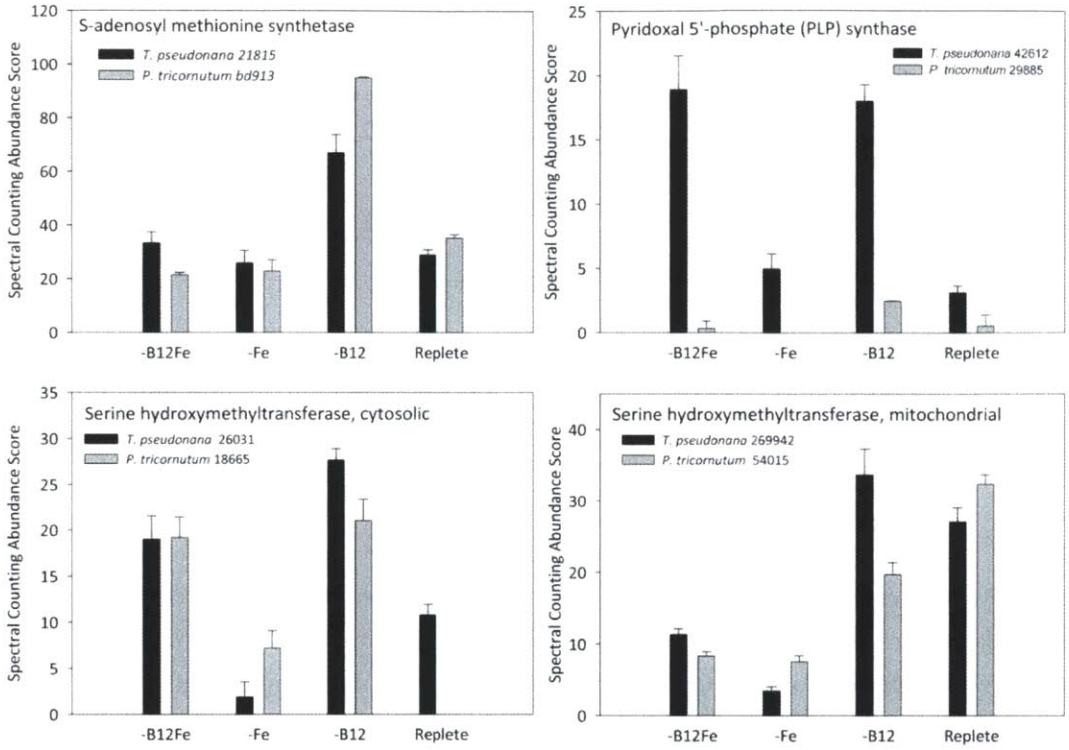

Figure 5: Abundance patterns of select methionine-related proteins in response to cobalamin and iron starvation. Bar graphs of spectral counting abundance scores for proteins of interest in each treatment where bars are means of technical triplicate measurements and error bars are one standard deviation about the mean. S-adenosyl methionine synthase appears to be more abundant in both diatoms under low B_{12} conditions, perhaps in order to increase the efficiency of SAM production when its precursor methionine is in short supply. Cytosolic serine hydroxymethyltransferase (SHMT), which is involved generating active folate for methionine biosynthesis, appears to be more abundant under low B_{12} availability in both diatoms while the mitochondital version of this enzyme appears to be driven more by growth rate in *P. tricornutum*. A putative PLP-synthase appears to be more abundant in *T. pseudonana* under low B_{12} as well as low B_{12} and iron, suggesting that this protein is responding to vitamin scarcity. Since SHMT is a PLP-dependant enzyme, enhanced SHMT activity under low B_{12} may increase the demand for PLP which could be satisfied by an increase in PLP synthase. Overall, these data suggest that folate, cobalamin, and PLP metabolism are linked in diatoms.

Table 1: The impact of cobalamin and iron starvation on diatom growth and proteomes

% proteins differentially abundant	Low B_{12} vs Replete	Low B_{12}Fe vs Low Fe	Low Fe vs Replete
T. pseudonana	19	18	30
P. tricornutum	5	1	20
fold cell yield decrease	**Low B_{12} vs Replete**	**Low B_{12}Fe vs Low Fe**	**Low Fe vs Replete**
T. pseudonana	1.8+/- 0.1	1.0 +/- 0.1	3.4 +/- 0.1
P. tricornutum	1.1 +/- 0.1	1.6 +/- 0.2	4.1 +/- 0.4
fold growth rate decrease	**Low B_{12} vs Replete**	**Low B_{12}Fe vs Low Fe**	**Low Fe vs Replete**
T. pseudonana	1.2+/- 0.1	1.2 +/- 0.1	2.0 +/- 0.1
P. tricornutum	1.0 +/- 0.1	1.3 +/- 0.1	2.8 +/- 0.3

Pairwise comparisons of growth rate, cell yield and protein abundance changes between low cobalamin versus replete growth, low cobalamin with low iron versus low iron growth, and low iron versus replete growth in two diatoms. The percentage of proteins changing in abundance was calculated from the total number of identified proteins and those that had significantly different abundance between the two treatments compared (Fisher Exact test $p < 0.01$) . Fold cell yield and growth rate decreases were calculated by determining the fold change between the maximum cell density or cell-specific growth rate in each treatment and are given as means of biological triplicates ± one standard deviation. Growth rates are cell specific and were calculated from the following time periods: *T. pseudonana* high iron: days 2-4 and low iron: days 3-5. *P. triconrutum* high iron: days 3-6 and low iron: days 5-7.

Table 2: Proteins more abundant under two types of cobalamin limitation

T. pseudonana						Homolog in *P. tricornutum*				
JGI Protein ID	Description	Low B_{12}Fe	Low Fe	Low B_{12}	Rep-lete	JGI Protein ID	Low B_{12}Fe	Low Fe	Low B_{12}	Rep-lete
270138	possible glutamine synthetase	4.0	0.0	118.5	76.1	22357	91.3	74.0	73.5	122.5
269942	serine hydroxymethyltransferase , SHMT2, mitochondrial	29.5	16.1	49.1	20.2	54015	8.3	7.6	19.7	32.4
22483	unknown, conserved protein	31.8	15.2	25.9	9.1	54686	31.0	22.0	0.7	2.0
11697	unknown, conserved protein (like Pt 48322), CBA1	42.4	0.0	45.1	0.0	48322	1.9	0.0	8.5	0.0
24346	unknown protein	22.5	11.4	25.2	14.2	None				
26031	serine hydroxymethyltransferase, SHMT1, cytosolic	19.0	1.9	27.6	10.8	18665	19.2	7.2	21.0	0.0
42612	pyridoxal 5'-phosphate (PLP) synthase	18.9	5.0	18.0	3.1	29885	0.3	0.0	2.5	0.5
23556	unknown protein	12.7	5.8	14.0	7.1	None				
23657	Globin-like protein	6.6	2.2	7.2	1.1	46237	0.0	0.0	0.0	0.0
24639	unknown protein, conserved domains	5.4	1.3	8.0	1.4	42442	1.6	1.6	1.1	0.9
22096	unknown protein with heme binding domain	3.2	0.0	8.0	2.8	bd1699	0.0	0.0	0.0	0.0
1896	unknown protein	5.5	1.3	6.0	1.4	None				
41733	Thiamine biosynthesis protein	3.3	0.0	5.2	0.0	38085	0.0	0.0	5.5	0.4
1738	Clp-like protease	2.2	0.0	2.4	0.0	44382	1.6	1.3	0.0	0.0
P. tricornutum						Homolog in *T. pseudonana*				
18665	serine hydroxymethyltransferase, SHMT1, cytosolic	19.2	7.2	21.0	0.0	26031	19.0	1.9	27.6	10.8
28056	MetE, Methionine synthase, vitamin-B12 independent	32.0	0.0	9.6	0.0	None				
48322	unknown, conserved protein (like Tp11697), CBA1	1.9	0.0	8.5	0.0	11697	42.4	0.0	45.1	0.0

Proteins in higher concentration and significantly differentially abundant ($p < 0.01$) in both low B_{12} compared to replete and low B_{12} with low Fe compared to low Fe alone, shown with a putative functional description and average spectral counting scores for each treatment. The average spectral counting scores for the homologous protein in the other diatom are also given. The two proteins highlighted in bold are driven by B_{12}-availability in both diatoms.

Acknowledgments

We thank Dawn Moran, Abigail Heithoff, Louie Wurch, Matt McIlvin, and Vladimir Bulygin for technical assistance and we acknowledge Cathy Drennan, Sonya Dyhrman, Dianne Newman and Ben Van Mooy for helpful discussions.

Financial Disclosure

This work was supported by NSF awards ANT 0732665 and OCE 0752291, The Gordon and Betty Moore Foundation, a National Science Foundation (NSF) Graduate Research Fellowship (2007037200) and an Environmental Protection Agency STAR Fellowship to EMB (F6E20324). The funders had no role in study design, data collection and analysis, decision to publish, or preparation of the manuscript.

Competing interests: The authors have declared that no competing interests exist.

Abbreviations: Cobalamin acquisition protein 1 (CBA1), methionine synthase, B_{12}-dependant (MetH), methionine synthase, B_{12}-independant (MetE), 5,10-methylene tetrahydrofolate (5,10 MTHF), pyridoxal 5' phosphate synthase (PLP), serine hydroxymethyltransferase (SHMT), S-adenosyl methionine synthase (MetK), S-adenosyl methionine (AdoMet), selected reaction monitoring (SRM)

Author Contributions: EMB, MAS, and AEA conceived the original study. EMB conducted the mass spectrometry and grew the cultures. EMB, AEA, CLD, and MAS designed overexpression studies. EMB, JB and CLD conducted the overexpression experiments. AEA designed metagenomic and metatranscriptomic analyses.

References

Allen, A. E. and others 2008. Whole-cell response of the pennate diatom Phaeodactylum tricornutum to iron starvation. PNAS **105:** 10438-10443.

Armbrust, G. and others 2004. The Genome of the Diatom *Thalassiosira pseudonana*: Ecology, Evolution, and Metabolism. Science **306:** 79-86.

Azam, F., and F. Malfatti. 2007. Microbial structuring of marine ecosystems. *Nat Rev Microbiol.* **5:** 782-791.

Banerjee, R. G., and R. V. Matthews. 1990. Cobalamin- dependent methionine synthase. The FASEB Journal **4:** 1449-1459.

Bertrand, E. M., M. A. Saito, Y. J. Jeon, and B. A. Neilan. 2011. Vitamin B_{12} biosynthesis gene diversity in the Ross Sea: the identification of a new group of putative polar B_{12}-biosynthesizers Environmental Microbiology **13:** 1285-1298.

Bertrand, E. M. and others 2007. Vitamin B_{12} and iron co-limitation of phytoplankton growth in the Ross Sea. Limnology and Oceanography **52**.

Bowler, C. and others 2008. The Phaeodactylum genome reveals the evolutionary history of diatom genomes. Nature **456:** 239-244.

Boyd, P. W. and others 2007. Mesoscale Iron Enrichment Experiments 1993–2005: Synthesis and Future Directions. Science **315:** 612-618.

Cowey, C. B. 1956. A preliminary investigation of the variaton of vitamin B-12 in oceanic and coastal waters. J. Mar. Biol. Ass. U.K. **35:** 609-620.

Croft, M. T., A. D. Lawrence, E. Raux-Deery, M. J. Warren, and A. G. Smith. 2005. Algae acquire vitamin B12 through a symbiotic relationship with bacteria. Nature **438:** 90-93.

Croft, M. T., M. J. Warren, and A. G. Smith. 2006. Algae need their vitamins. Eukaryotic Cell **5:** 1175-1184.

Davies, A. G., and J. W. Leftley. 1985. Vitamin B_{12} binding my microalgal ectocrines: dissociation constant of the vitamin-binder complex using an ultrafiltration technique. Marine Ecology Progress Series **21:** 267-273.

Dev, I. K., and R. J. Harvey. 1984. Regulation of Synthesis of Serine Hydroxymethyltransferase in Chemostat Cultures of *E. coli.* J. Biol. Chem. **259:** 8394-8401.

Drennan, C. L., R. G. Matthews, and M. L. Ludwig. 1994. Cobalamin-dependent methoionine synthase: the structure of a methylcobalamin-binding fragment and implicatiosn for other B_{12}-dependent enzymes. Curr. Op. in Struct. Biol. **4:** 919-929.

Droop, M. R. 1957. Vitamin B_{12} in marine ecology. Nature **180:** 1041-1042.

---. 1968. Vitamin B12 and marine ecology. IV. The kinetics of uptake, growth and inhibition in *Monochrisis lutheri.* J. Mar. Biol. Ass. U.K. **48:** 689-733.

---. 2007. Vitamins, phytoplankton and bacteria: symbiosis or scavenging? Journal of Plankton Research **29:** 107-113.

Falciatore, A., R. Casotti, C. Leblanc, C. Abrescia, and C. Bowler. 1999. Transformation of nonselectable reporter genes in marine diatoms. Marine Biotechnology **1:** 239-251.

Falkowski, P. G., Katz M.E., Knoll, a,H,, Quigg A., Raven J.A., Schofield, O., Taylor, F.J. 2004. The evolution of modern eukaryotic phytoplankton. Science **305:** 354-360.

Fell, D. A., and K. Snell. 1988. Control analysis of serine biosynthesis: feedback inhibition of the final step. Biochemistry Journal **256:** 97-101.

Gobler, C. J., C. Norman, C. Panzeca, G. T. Taylor, and S. A. Sanudo-Wilhelmy. 2007. Effect of B-vitamins and inorganic nutrients on algal bloom dynamics in a coastal ecosystem. Aquat Microb Ecol **49:** 181-194.

Gonzalez, J. C., R. V. Banerjee, S. Huang, J. S. Sumner, and R. G. Matthews. 1992. Comparison of cobalamin- independant and cobalamin-dependant methionine synthases from *E. coli*: two solutions to the same chemical problem,. Biochemistry **31:** 6045-6056.

Goulding, C. W., D. Postigo, and R. G. Matthews. 1997. Cobalamin-dependent methionine synthase is a modular protein with distinct regions for homocysteine, methyltetrahydrofolate, cobalamin and adenosylmethionine. Biochemistry **36:** 8082-8091.

Helliwell, K. E., G. L. Wheeler, K. C. Leptos, R. E. Goldstein, and A. G. Smith. 2011. Insights into the Evolution of Vitamin B_{12} Auxotrophy from Sequenced Algal Genomes. Mol Biol and Evolution.

Herbig, K., E. Chiang, E. Lee, J. Hills, B. Shane, and P. J. Stover. 2002. Cytoplasmic serine hydroxymethyltransferase mediates competition between folate-dependant

deoxyribonucleotide and S-adenosylmethionine biosyntheses. J. Biol. Chem. **277:** 38381-38389.

Karl, D. M. 2002. Nutrient dynamics in the deep blue sea. Trends in Microbiol. **10:** 410-418.

Keller, A., A. I. Nesvizhskii, E. Kolker, and R. Aebersold. 2002. Empirical statistical model to estimate the accuracy of peptide identifications made by MS/MS and database search. Analytical Chemistry **74.**

Koch, F., M. A. Marcoval, C. Panzeca, K. W. Bruland, S. A. Sanudo-Wilhelmy, and C. J. Gobler. 2011. The effect of vitamin B_{12} on phytoplankton growth and community structire in the Gulf of Alaska. Limnol and Oceanog **56:** 1023-1034.

Kustka, A. B., A. E. Allen, and F. M. M. Morel. 2007. Sequence analysis and transcriptional regulation of iron aquisition genes in two marine diatoms. J. Phycol **43:** 715-729.

Lovelock, J. E. 1972. Gaia as seen through the atmosphere. Atmos Environ **6.**

Lu, X., and H. Zhu. 2005. Tube Gel Digestion. Molecular & Cellular Proteomics **4:** 1948-1958.

Matsen, F.A., Kodner, R.B., and Armbrust, E.V. 2010. pplacer: linear time maximum-likelihood and Bayesian phylogenetic placement of sequences onto a fixed reference tree. BMC Bioinformatics.

Menzel, D. W., and J. P. Spaeth. 1962. Occurrence of vitamin B_{12} in the Sargasso Sea. Limnol. Oceanogr. **7:** 151-154.

Moore, J. K., S. C. Doney, and K. Lindsay. 2004. Upper ocean ecosystem dynamics and iron cycling in a global three-dimensional model. Global Biogeochem. Cycles **18:** doi:10.1029/2004GB002220.

Nelson, D. M., P. Treguer, M. A. Brzezinski, A. Leynaert, and B. Queguiner. 1995. Production and dissolution of biogenic silica in the oceans: revised global estimates, comparison with regional data and relationship to biogenic sedimentation. Global Biogeochem Cycles **9:** 359-372.

Nielsen, H., J. Engelbrecht, S. Brunak, and G. Von Heijne. 1997. Identification of prokaryotic and eukaryotic signal peptides and prediction of their cleavage sites. Protein Engineering **10:** 1-6.

Panzeca, C. and others 2006. B vitamins as regulators of phytoplankton dynamics. EOS **87.**

Peng, J., J. E. Elias, C. C. Thoreen, L. J. Licklider, and S. P. Gygi. 2003. Evaluation of Multidimensional Chromatography Coupled with Tandem Mass Spectrometry (LC/LC-MS/MS) for Large-Scale Protein Analysis: The Yeast Proteome. Journal of Proteome Research **2:** 43-50.

Pintner, I. J., and V. L. Altmeyer. 1979. Vitamin B_{12}- binder and Other Algal Inhibitors. J.Phycol **15:** 391-398.

Price, N. M. and others 1988/1989. Preparation and chemistry of the artificial algal culture medium Aquil. Biol. Oceanogr. **6:** 443-461.

Rodionov, D. A., A. G. Vitreschak, A. A. Mironov, and M. S. Gelfand. 2003. Comparative Genomics of the Vitamin B_{12} Metabolism and Regulation in Prokaryotes. J. Biol. Chem. **278:** 41148-41159.

Rusch DB, Halpern AL, Sutton G, Heidelberg KB, Williamson S, et al. 2007 The *Sorcerer II* Global Ocean Sampling Expedition: Northwest Atlantic through Eastern Tropical Pacific. PLoS Biol **5:** e77.

Sahni, M. K., S. Spanos, M. Z. Wahrman, and G. M. Sharma. 2001. Marine Corrinoid- Binding Proteins for the direct Determination of Vitamin B12 by Radioassay. Anal. Biochem **289:** 68-76.

Saito, M. A. and others 2011. Iron Conservation by Reduction of Metalloenzyme Inventories in the Marine Diazotroph *Crocosphaera watsonii.* Proceedings of the National Academies of Sciences **108** 2184-2189.

Scott, J. M., and D. G. Weir. 1981. The Methyl Folate Trap : A physiological response in man to prevent methyl group deficiency in kwashiorkor (methionine deficiency) and an explanation for folic-acid-induced exacerbation of subacute combined degeneration in pernicious anaemia. The Lancet **318:** 337-340.

Selhub, J. 2002. Folate, vitamin B_{12} and vitamin B_6 and one carbon metabolism. *Journal of nutrition, health and aging* **6:** 39-42.

Selhub, J., P. F. Jacques, P. W. Wilson, D. Rush, and I. Rosenberg. 1993. Vitamin status and intake as primary determinants of homocysteinemia in an elderly population. JAMA **270:** 2693-2698.

Siaut, M. and others 2007. Molecular toolbox for studying diatom biology in *Phaeodactlyum tricornutum.* Gene **406:** 23-35.

Snell, K. and others 2000. The genetic organization and protein crystallographic structure of human serine hydroxomethyltransferase. Advances in Enzyme Regulation **40:** 353-403.

Stefels, J. P. 2000. Physiological aspects of the production and conversion of DMSP in marine algae and higher plants. J Sea Res **43:** 183-197.

Stemmann, O., H. Zou, S. A. Gerber, S. P. Gygi, and M. W. Kirschner. 2001. Dual inhibition of sister chromatid separation at metaphase. Cell **107:** 715-726.

Sunda, W., and S. Huntsman. 2003. Effect of pH, light, and temperature on Fe–EDTA chelation and Fe hydrolysis in seawater. Marine Chemistry **84:** 35-47.

Sunda, W., and S. A. Huntsman. 1995. Cobalt and zinc interreplacement in marine phytoplankton: Biological and geochemical implications. Limnol. Oceanogr. **40:** 1404-1417.

Sunda, W., D. J. Kieber, R. P. Kiene, and S. Huntsman. 2002. An antioxidant function for DMSP and DMS in marine algae. Nature **418:** 317-320.

Swift, D. G., and W. R. Taylor. 1972. Growth of vitamin B12 - limited cultures: *Thalassiosira pseudonana, Monochyrsis lutheri,* and *Isochrysis galbana.* J. Phycol. **10:** 385-391.

Yu, C. S., Y. C. Chen, C. H. Lu, and J. K. Hwang. 2006. Prediction of protein subcellular localization. Proteins: Structure, Function and Bioinformatics **64:** 643-651.

Zhang, B., N. C. Verberkmoes, M. A. Langston, E. Uberbacher, R. L. Hettich, and N. F. Samatova. 2006. Detecting Differential and Correlated Protein Expression in Label-Free Shotgun Proteomics. Journal of Proteome Research **5:** 2909-2918.

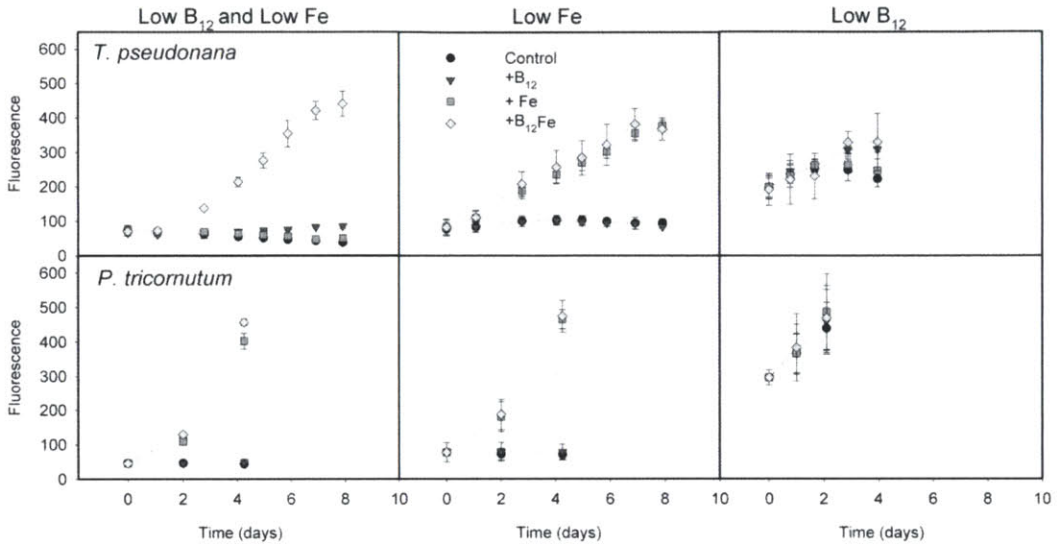

Figure S1: Re-supplying starved diatom cultures with cobalamin and iron verified that these nutrients limited their growth as intended. Fluorescence over time is shown as means of single measurements of triplicate cultures, with error bars representing one standard deviation. Each culture (Figure 1, at arrows) was split in four and re-supplied with nothing (control) B_{12}, iron, or B_{12} and iron together. Growth in low B_{12} with low iron cultures (left) of *T. pseudonana* (top) was only rescued by the addition of both B_{12} and iron together, demonstrating that this culture was simultaneously limited by the availability of both nutrients. Iron addition alone rescued some growth in the low B_{12} and iron *P. tricornutum* (bottom). This difference in the responses of low B_{12} and low iron culture growth was expected because *T. pseudonana* has an absolute requirement for the vitamin while *P. tricornutum* does not. Iron addition rescued growth in low iron cultures of both *T. pseudonana* and *P. tricornutum*, and, as expected, B_{12} additions had no effect (middle panels). Iron additions had no effect on low B_{12} culture growth (right panels), and low B_{12} cultures of *T. pseudonana* saw enhanced growth upon B_{12} re-supply while *P. tricornutum* did not, as expected based on their known vitamin requirements. These results indicate that all cultures used for the proteomic analyses in this study were limited or colimited as expected.

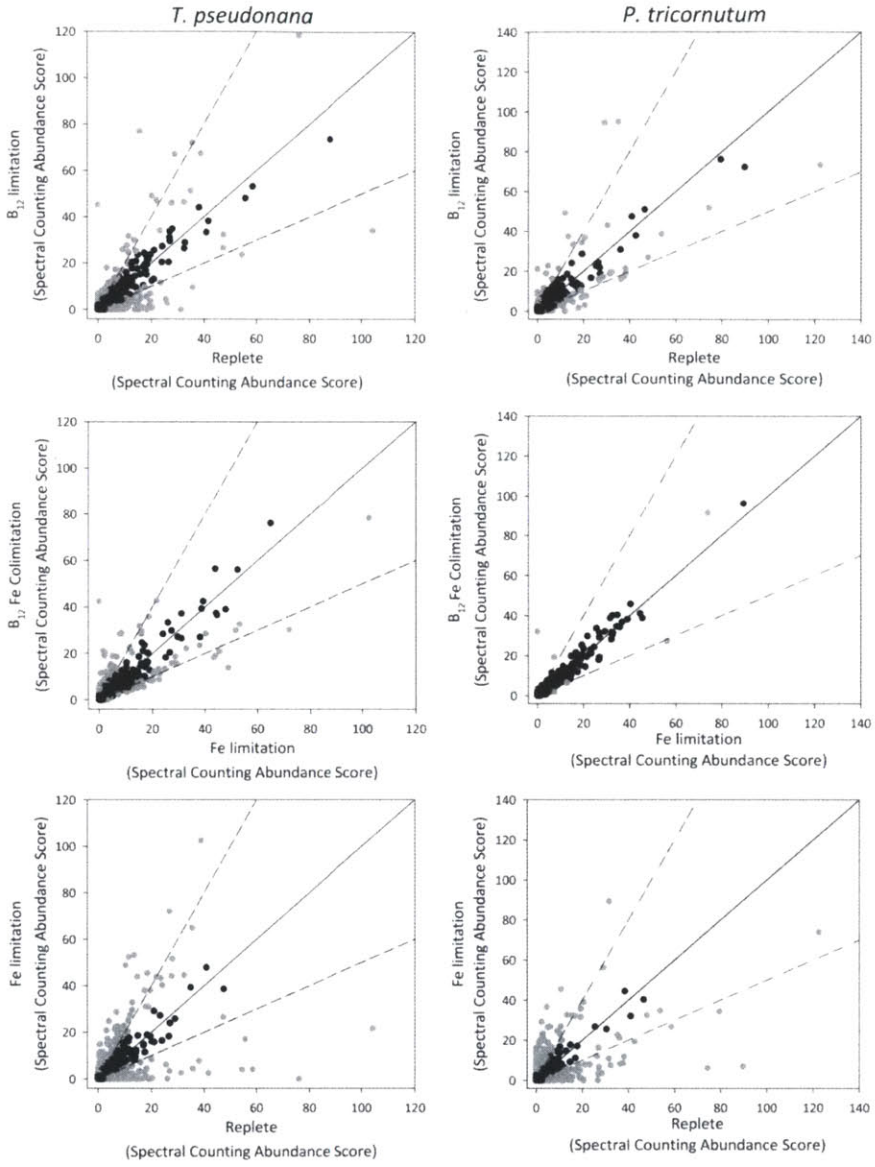

Figure S2: Pairwise comparisons of detected diatom proteomes. Average spectral counting score for each protein in one treatment is plotted against the average spectral counting score in the next treatment. Values are means of technical triplicate measurements. Proteins plotted in black are not significantly differentially abundant (Fisher Exact Test $p < 0.01$) and those plotted in gray are. The solid line is 1:1 protein abundance, and the dashed lines are 2:1.

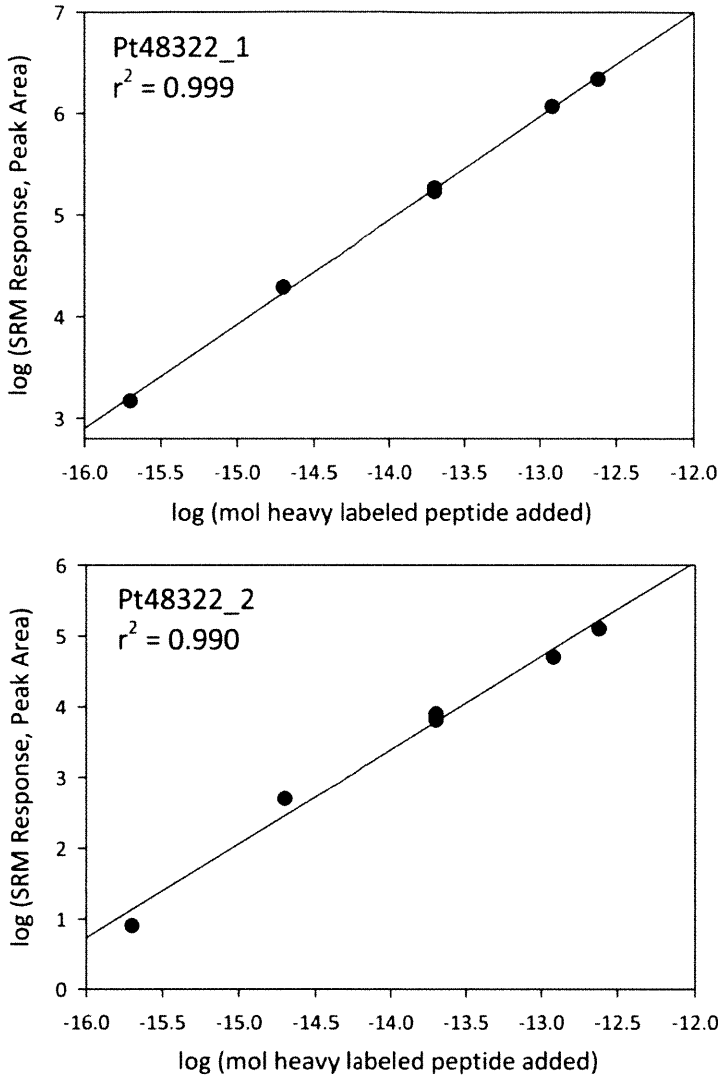

Figure S3: Calibration curves for selected reaction monitoring detection of CBA1 peptides. The SRM response (peak area, sum of product ion intensities) is plotted against moles of stable isotope-labeled (heavy) version of each CBA1 peptide added. Linear regressions are shown in the solid line and the coefficients of variance for each are given. For both peptides, the response is linear over four orders of magnitude, and the lowest concentrations detected were 0.2 fmol.

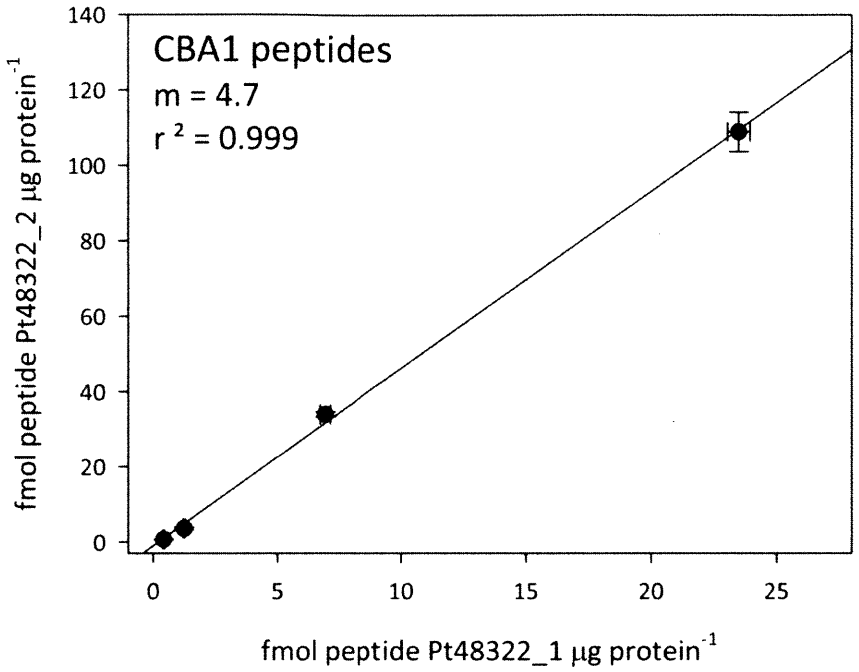

Figure S4: Abundance of peptides diagnostic of CBA1 in *P. tricornutum* plotted against each other as means of technical triplicate measurements, with error bars representing one standard deviation. Linear regression is shown in the solid line and the coefficients of variance (r^2) and the slope (m) is given. The abundance of peptides measuring CBA1 are linearly correlated, as expected, but the slopes of the lines are not. This can be partially explained by the fact that peptide Pt48322_2 is encoded by both allelic copies of the CBA1 while Pt48322_1 is only encoded by one copy.

Table S1: Presence of proteins similar to CBA1 in other algal and eukaryotic genomes from NCBI (National Center for Biotechnology Information) or the Joint Genome Institute (JGI): Blastp vs *P. tricornutum* 48322 with an E-value cutoff of 1e-5

Genome	Protein ID	E-value	% coverage
Thalassiosira pseudonana	11697	4e-57	82
Fragilariopsis cylindrus	241429	5e-47	83
Fragilariopsis cylindrus	246327	9e-37	71
Fragilariopsis cylindrus	273295	8e-27	30
Fragilariopsis cylindrus	269995	3e-24	27
Aureococcus anophagefferens	63075	2e-31	78
Ectocarpus siliculosus	CBN74732	2e-28	80
Chlamydomonas reinhardtii	196738	5e-12	47
Chlorella sp. NC64A	57728	4e-12	25
Volvox carteri f. nagariensis	106040	1e-11	48
Micromonas pusilla CCMP1545	46842	6e-9	51
Micromonas sp. RCC299	NONE		
Ostreococcus lucimarinus	27076	1e-9	50
Ostreococcus sp. RCC809	NONE		
Ostreococcus tauri	NONE		
Emiliania huxleyi	NONE		
Phytophthora capsici	NONE		
Phytophthora ramorum	NONE		
Phytophthora sojae	NONE		

Table S2: Selected reaction monitoring conditions for absolute quantification of CBA1.

The parent to product ion transitions monitored, collision energies applied, the chromatographic retention times over which the peptides were monitored, as well as the S-lens values employed for peptide measurements.

Protein	Peptide	Peptide name	Parent ion + charge	Parent (m/z)	Product (m/z)	Collision Energy	Start time (min)	Stop time (min)	S-lens value
Pt48322	FFS[V_C13N15]FFNK	Pt48322_1heavy	2	521.2686	747.3930	15	16.80	18.80	110
			2	521.2686	660.3610	15	16.80	18.80	110
			2	521.2686	555.2900	16	16.80	18.80	110
Pt48322	FFSVFFNK	Pt48322_1native	2	518.2682	741.3930	15	16.80	18.80	110
			2	518.2682	654.3610	15	16.80	18.80	110
			2	518.2682	555.2900	16	16.80	18.80	110
Pt48322	EHTANQ[V_C13N15]VEA AESR	Pt48322_2heavy	2	773.8712	1280.6335	21	10.10	12.10	136
			2	773.8712	1179.5858	24	10.10	12.10	136
			2	773.8712	866.4472	25	10.10	12.10	136
			2	773.8712	761.3788	25	10.10	12.10	136
Pt48322	EHTANQVVEAAESR	Pt48322_2native	2	770.8712	1274.6335	21	10.10	12.10	136
			2	770.8712	1173.5858	24	10.10	12.10	136
			2	770.8712	860.3788	25	10.10	12.10	136
			2	770.8712	761.3788	25	10.10	12.10	136

Table S3: Proteins more abundant under cobalamin limitation and not iron limitation

Proteins in higher concentration and significantly differentially abundant ($p < 0.01$) in low B_{12} compared to replete and *not* in higher concentration and significantly differentially abundant in low Fe compared to replete are shown with a description and average spectral counting scores for each treatment. The average spectral counting scores for the homologous protein in the other diatom are also given. The proteins highlighted in gray are driven by B_{12}-availability in both diatoms.

T. pseudonana						Homolog in	*P. tricornutum*			
Protein ID	Description	Low B_{12}Fe	Low Fe	Low B_{12}	Replete	JGI Protein ID	Low B_{12}Fe	Low Fe	Low B_{12}	Rep lete
21815	methionine S-adenosyl transferase	33	26	67	29	bd 913	21	23	95	35
YP_874528.1	ATP synthase, beta chain, thylakoid	42	39	51	35	YP_874407.1	34	26	43	30
40771	enolase	30	27	34	23	bd1572	12	11	19	31
27997	dihydroxyacid dehydratase	25	16	20	11	20547	4	5	5	5
39299	ADP-ribosylation factor GTPase	16	18	20	12	43251	11	15	19	13
1093	conserved unknown protein	13	13	25	11	43233	4	3	6	10
37032	ribosomal protein 6, 60S large ribosomal subunit	15	15	17	9	34146	9	9	2	3
4875	Pyruvate kinase	10	9	14	6	22404	2	2	5	2
30193	Urease	10	8	11	5	29702	4	4	2	1
16169	Pyruvate dehydrogenase E1, alpha subunit	10	5	11	4	55035	2	1	0	0
3018	Phosphoserine aminotransferase	10	5	10	4	42458	37	37	23	5
4462	unknown protein	7	5	8	2	46709	1	0	0	2
4439	unknown protein	1	0	13	6	42494	1	2	3	3
21306	conserved unknown protein	5	4	8	1	None				
5026	ATPase, gamma subunit	1	0	12	5	18398	10	7	6	0
21887	unknown protein	5	2	6	2	None				
517	20S proteasome subunit alpha type 1	3	0	6	2	45998	2	1	4	4
9947	conserved unknown protein	4	2	5	1	None				
21965	conserved unknown, similar to disulfide isomerase	5	2	4	1	47306	1	0	2	4
20923	conserved unknown protein	4	1	4	1	6606	0	0	0	0
24738	unknown protein	1	0	6	0	None				
22127	unknown protein	4	1	4	1	None				
24708	unknown protein, multicopy	2	2	3	0	44663	0	0	0	0
21260	unknown protein, multicopy	3	2	2	0	47664	0	0	0	0
11175	conserved unknown protein	1	0	4	0	None				
22442	unknown protein	1	0	2	0	43378	0	0	0	0
23511	unknown protein	1	0	3	0	None				

						Homolog in	*T. pseudonana*			
P. tricornutum		Low B_{12}Fe	Low Fe	Low B_{12}	Replete	JGI Protein ID	Low B_{12}Fe	Low Fe	Low B_{12}	Repl ete
54465	ISIP2A, iron stress induced protein	78	144	268	142	None				
23658	Flavodoxin, plastid targeted	18	27	152	59	19141	3	1	4	2
bd 913	methionine S-adenosyl transferase	21	23	95	35	21815	33	26	67	29

46547	multicopy hypothetical protein	0	0	49	12	None				
51242	adenosine kinase-like protein	8	5	19	4	644	20	2	20	13
44603	ATP synthase	4	4	7	1	29359	11	5	3	7
47395	ascorbate peroxidase	1	2	9	1	262753	15	4	15	18
38085	Thiamin biosynthesis protein	0	0	5	0	41733	3	0	5	0

Chapter 5

Methionine synthase isoform interreplacement in a marine diatom and the development of peptide-based biomarkers of vitamin B_{12} nutrition in Antarctic diatom communities

Abstract:

Availability of vitamin B_{12} has been shown, though bioassays and time series measurements, to influence phytoplankton growth in many marine environments. However, there are currently no tools available to assess the B_{12} nutritional status of marine microbial communities at a molecular level. B_{12} requirements in eukaryotic phytoplankton arise from its use in methionine synthase, MetH, which, in non-requiring phytoplankton, can be replaced by the less efficient but not B_{12}-requiring form MetE. B_{12} acquisition in diatoms has recently been shown to involve a previously undescribed protein CBA1. Here we used selected reaction monitoring mass spectrometry to quantify MetE, MetH, and CBA1 protein abundance in diatom cultures under high and low B_{12} conditions and upon pulsed resupply of the vitamin. We found that MetH abundance was driven by B_{12} availability in some diatoms and that MetE abundance was 50-100 times greater under low B_{12} conditions. CBA1 abundance was 2 to 6-fold higher under low B_{12} conditions and increased another 2 to 4-fold upon pulsed B_{12} resupply to starved cultures. We also measured MetE and MetH abundance in diatom communities from surface seawater in McMurdo Sound of the Southern Ocean, verifying that both these proteins are utilized by natural phytoplankton populations. These data are consistent with previous studies suggesting that B_{12} availability helps control primary productivity in Antarctic regions and also imply that B_{12} supply and phytoplankton biomass are correlated. This study illuminates controls on the expression of B_{12}-related proteins and provides evidence that mass spectrometry-based detection of specific proteins in field populations can yield valuable insight into the functioning of marine microbial communities.

1. Introduction:

Vitamin B_{12}, also known as cobalamin, is a cobalt-containing organometallic complex that is required by an estimated half of all eukaryotic phytoplankton (Croft et al. 2005; Tang et al. 2010). Since no eukaryotic organism is known to produce B_{12} (Rodionov et al. 2003), marine bacteria and archaea must therefore supply auxotrophic (vitamin-requiring) phytoplankton with B_{12} through direct interaction (Croft et al. 2005) or through production and release into the water column upon death and cell lysis (Droop 2007; Karl 2002). In the open ocean, B_{12} is present in femtomolar to low picomolar concentrations and is depleted in irradiated surface waters, largely due to biological utilization (Menzel and Spaeth 1962). It has long been hypothesized that B_{12} availability could influence marine primary production and phytoplankton species composition (Cowey 1956; Droop 1957; Swift and Taylor 1972). More recent field work suggests that vitamin B_{12} availability does in fact impact phytoplankton growth in many areas of the ocean including the Ross Sea (Bertrand et al. 2007), the Antarctic Peninsula sector of the Southern Ocean (Panzeca et al. 2006), the North Pacific (Koch et al. 2011), and Long Island embayments (Gobler et al. 2007; Sañudo-Wilhelmy et al. 2006). B_{12} availability is thought to play a particularly important role in the Southern Ocean where it colimits the growth of some diatom-dominated phytoplankton communities (Bertrand et al. 2007), and may be in short supply compared to other marine environments (Bertrand et al. 2011a).

Bioassay bottle incubation experiments in which bottles filled with unfiltered seawater are supplemented with specific nutrients and monitored for phytoplankton growth have refocused attention on the potentially important role of B_{12} in governing primary productivity (Bertrand et

al. 2007; Panzeca et al. 2006). However, such experiments likely alter *in-situ* community composition and may also impact phytoplankton physiology. Due to the required isolation of communities in bottles, these experiments necessarily separate microbial communities from the physical processes including mixing and changing light conditions that they normally experience in the ocean. Some species may benefit and grow faster in bottles while others may grow more slowly, thereby inducing possible community composition changes that could impact experimental results. In addition, these bottle incubation bioassays may not be sensitive to some subtle physiological states of B_{12} deprivation that are nonetheless relevant for biogeochemical cycling. For instance, in regions of the Ross Sea where bioassays with added B_{12} did not suggest that the community was limited by vitamin availability, B_{12} uptake rates in the bottle incubations increased over time, suggesting that the community may have been becoming starved for the vitamin (Bertrand et al. 2011b, Chapter 3). The application of protein or transcript-based biomarker assays for gene products with abundance patterns that are driven by B_{12} nutritional status would complement bottle incubation bioassays and may provide more subtle information about the potential for vitamin starvation in microbial communities. While such *in-situ* biomarkers have been developed and used for iron and phosphorus (Dyhrman et al. 2002; LaRoche et al. 1996; Webb et al. 2001), there has been no previous inquiry into these kinds of developments for vitamin B_{12}. Such biomarkers have the added benefit of being *in-situ* measurements, requiring no significant perturbation of communities in the process and so offer significant advantage over traditional incubation bioassays for nutrient limitation. These

measurements also have the potential to be high throughput and offer enhanced spatial and temporal resolution at sampling rates that are not feasible using traditional bioassays.

B_{12} demand in eukaryotic algae like diatoms can be attributed to its use in the enzyme methionine synthase (Croft et al. 2005; Helliwell et al. 2011), which is responsible for producing methionine from homocysteine and 5-methyltetrahydrofolate (Banerjee and Matthews 1990). This serves to both produce methionine and regenerate tetrahydrofolate and is thus an essential component of cellular one carbon (C1) metabolism. Some eukaryotic algae only have MetH, the B_{12} and zinc requiring version of this enzyme, encoded in their genomes (e.g. the diatom *Thalassiosira pseudonana*) which uses B_{12} as an intermediate methyl group carrier (Goulding et al. 1997). Other algal genomes encode both MetH and MetE (eg. the diatom *Phaeodactylum tricornutum*), the latter of which is a zinc-only enzyme that accomplishes the same reaction as MetH but with much lower efficiency (Gonzalez et al. 1992). The presence of MetE in marine eukaryotic phytoplankton genomes appears to result in the lack of an absolute B_{12} requirement. Recent work suggests that *metE* is only transcribed by the diatom *P. tricornutum* when B_{12} is unavailable (Helliwell et al. 2011). This is supported by shotgun proteomic results suggesting that MetE protein is much more abundant under low B_{12} conditions (Chapter 4). It is notable that B_{12} requirements, i.e. the lack of B_{12}-independent methionine synthase, does not follow phylogenetic lines in eukaryotic phytoplankton (Croft et al. 2006; Helliwell et al. 2011) and that there are even species-level differences in B_{12} requirements (Tang et al. 2010). This suggests that taxonomically-based analyses of marine microbial community composition are unable to determine the proportion of the community that requires B_{12} and thus does not use MetE.

Methionine has several known functions within algal cells. It is an essential protein-building amino acid and is also the precursor to S-adenosyl methionine (SAM), which is an important metabolite that participates in a range of essential cellular processes. Methionine is also metabolized to form dimethylsulfonium propionate (DMSP) in some diatoms, potentially for use as a cryotprotectant, osmolyte (Stefels 2000), or antioxidant (Sunda et al. 2002). DMSP is the precursor to the important atmospheric gas dimethylsulfide (DMS), which helps form cloud condensation nuclei (Lovelock 1972). In addition, reduced functioning of methionine synthase causes 'methyl folate trapping' in humans whereby folate compounds build up inside the cell in a form only usable by methionine synthase, thus preventing efficient folate recycling for use in its other essential functions such as nucleic acid biosynthesis (Scott and Weir 1981). This phenomenon also likely occurs in algae (Croft et al 2005; Chapter 4). The possible effects of B_{12} starvation and reduced methionine synthase function in phytoplankton thus have the potential impact a host of cellular and ecological functions.

Despite B_{12}'s important role in phytoplankton metabolism, mechanisms for its acquisition are not completely elucidated. One protein, cobalamin acquisition protein 1 (CBA1) was recently identified and shown to be involved in B_{12} uptake into the cell (Chapter 4) and was more abundant in two diatoms when grown under B_{12} limitation. Though its exact role remains uncertain, this protein may function to bind B_{12} outside the cell and participate in its transfer into the cell.

Here we used quantitative selected reaction monitoring mass spectrometry-based methods to measure the abundance of MetE, MetH, and CBA1 proteins in diatoms. Selected

reaction monitoring (SRM) is a mass spectrometry technique that can be extremely sensitive and quantitative, offering potential for measuring low abundance targets, such as specific peptides, in complex samples. In this application of SRM, peptides are first separated by reverse phase liquid chromatography then introduced to a triple quadrupole mass spectrometer via electrospray ionization. These peptides, in a predetermined mass window, are collected in the mass spectrometer's first quadrupole. The isolated ions are then fragmented and the generation of specific, predetermined product ions is monitored. The amount of the product ions detected is proportional to the abundance of the peptide of interest in a sample. This abundance is absolutely calibrated using stable isotope labeled versions of each peptide, added to samples in known quantities as internal standards.

We applied SRM mass spectrometry to measure B_{12}-related proteins in diatom cultures over time, under B_{12} limited conditions and upon pulsed resupply of the vitamin, revealing clear interreplacment (Sunda and Huntsman, 1995) of MetE and MetH proteins as a function of B_{12} availability. We also used this technique to measure MetE and MetH abundance in diatom communities from surface seawater in McMurdo Sound of the Ross Sea in the Southern Ocean, verifying that both these proteins are utilized by natural populations of diatoms and that they may be of utility as biomarkers for evaluating the metabolic status of microbial communities with respect to vitamin B_{12}.

2. Methods

2. 1. Laboratory culturing and sampling

Axenic cultures of *Phaeodactylum tricornutum* CCMP 632 were obtained from the Provasoli-Guillard National Center for Culture of Marine Phytoplankton and maintained using sterile and trace metal clean technique. Axenicity was monitored throughout using marine purity broth tests (Saito et al. 2002). All cultures were grown at 16°C under a constant light level of 150 $\mu E\ m^{-2}\ sec^{-1}$ in polycarbonate bottles. All media preparation and culture manipulation was conducted in a class 100 clean room facility. Media was prepared in a 0.2 μm filtered oligotrophic seawater base collected in a trace metal clean manner, microwave sterilized, and supplemented with macronutrients at f/2 concentrations and with vitamins and EDTA-buffered trace metals at concentrations as previously described by (Sunda and Huntsman 1995), except for modulations of vitamin B_{12} concentrations. Triplicate bottles with 100 pmol L^{-1} added B_{12} or no added B_{12} (1.4 L in 2 L bottles and 2.4 L in 3 L bottles) were inoculated (1.3%) with *P. tricornutum* cells that had been acclimated through three transfers in no added B_{12} media and had gone through at least two doublings per transfer. After 4.5 days of growth, the no B_{12} added cultures were split in two and placed in sterile 2 L polycarbonate bottles. One of each of the bottles was then supplemented with 100 pmol L^{-1} B_{12} and all cultures were returned to the incubator for growth. Culture growth was monitored daily via cell counts, using a Palmer Maloney nanoplankton counting chamber, counting at least 10 fields of view or 200 individuals at 400 x magnification with light microscopy (Carl Zeiss, Inc., Thornwood, NY). Protein samples were taken via gentle filtering (< 15 kPa vacuum) of 135-250 mL of culture onto 47 mm Supor 0.45 μm filters (Pall), flash freezing in

liquid nitrogen, and storing at -80 °C. Protein samples were taken after 3 days of growth, and again 24 h after re-feeding the cultures with B_{12}.

2.2. Protein extraction and digestion from cultures

Cells were scraped from the filters and resuspended in 600 µL B-PER reagent (Thermo Scientific, Rockford, IL) supplemented with 5 mmol L^{-1} EDTA and 1 mmol L^{-1} phenylmethanesulfonylfluoride (PMSF, a serine protease inhibitor). Samples were incubated at room temperature for 20 min with occasional gentle vortexing. The cells were then sonicated with a microtip (Branson digital sonifier) on ice, twice for 1 min at constant duty cycle with a 5 min pause on ice between sonication steps. Samples were centrifuged for 30 min at 14,100 RCF and 4°C, and supernatants were precipitated overnight in 50% acetone 50% methanol 0.5 mmol L^{-1} HCl at -20 °C. Precipitated protein was collected by centrifugation at 14,100 RCF for 30 min at 4 °C and dried by speed vacuum at room temperature. Protein was resuspended in 100 µL of the extraction buffer for 30 min at room temperature. Aliquots were taken for protein concentration determination by DC assay using bovine serum albumin as a protein standard (BioRad Inc., Hercules CA). Proteins were stored at -80 °C until digestion.

2.3. Field sampling

250-500 L of surface (~3 m) seawater was pumped into a 250 L carboy and then onto 293 mm diameter 3 µm pore size polyethersulfone filters (Versapore, Pall) through a hole drilled in sea ice (stations 399, 400, 401) or just over the ice edge (station 402). Station locations were: 402: 77.6442° S, 165.7178° E, 401: 77.6501 ° S, 165.7497° E, 400: 77.6587° S 166.1680° E, 399: 77.6730° S, 166.4238° E. Stations were part of the J. Craig Venter Institute's Global Ocean Sampling

project; established sampling and filtering protocols were used. Filters were frozen in liquid nitrogen, kept on dry ice for shipping and stored in the laboratory at -80°C. Two chlorophyll samples per station were taken from the 250 L carboy and measured according to JGOFS (Joint Global Ocean Flux Study) protocols. A 45 minute net tow sample was taken through an ice hole at station 399. Live light micrographs of the net tow sample were taken at 200x magnification on a Zeiss microscope using a Nikon CoolPix 995 and ambient lighting in the field.

2.4. Field sample protein extraction

Filters were cut in half, half retained for future analysis and half used for protein extraction. For protein extraction, the filter half was cut into strips and incubated on ice for 15 min in 24 mL of extraction buffer (0.1 M Tris HCl, pH 7.5; 5% glycerol, 1% SDS, 10 mmol L^{-1}EDTA) was periodically gently vortexed, then heated to 92-98° C in an Eppendorf Thermomixer for 15 min, gently vortexed for 1 min, then mixed at 20° C for 2 h in a Bambino hybridization oven (Boekel Scientific), with gentle vortexing for 30 s every 30 min. The extraction buffer was then collected and centrifuged at 7,000 rcf at 10° C for 20 min. The supernatant was collected, filtered with a 5 μm polycarbonate filter and concentrated via ultrafilteration in Vivaspin6 5000 Da molecular weight cut-off PES membrane in centrifugal concentrators (Sartorius Stedum) spinning at 2,100 rcf at 12° C until the volume was reduced to ~1200 μL per sample (~3 h). Protein was precipitated overnight at -20° C in 5 volumes of ice cold 50% acetone, 50% methanol with 0.5 mmol L^{-1} HCl. Samples were spun at 13,000 rcf at 4° C for 20 min; pellets were aspirated and then dried at room temperature in a speedvac and resuspended in 100 μL of extraction buffer.

Aliquots were taken for protein concentration determination by DC assay as described for culture samples above.

2.5. Protein digestion

Both culture and field protein samples were digested into peptides following the tube gel procedure (Lu and Zhu 2005) with minor modifications. Briefly, samples (in known amounts of 25-100 μg total protein) were immobilized in 15% acrylamide in pH 7.5 Tris buffer, fixed with 10% acetic acid and 50% ethanol, washed successively with 10% acetic acid and 50% methanol, then acetonitrile and 25 mM ammonium bicarbonate (pH 8) and then cut into 1 mm^2 pieces. Samples were reduced with 10 mmol L^{-1} dithiothreitol (DTT) at 56 °C for 1 h, alkyated with 30 mmol L^{-1} iodoacetamide for 1 h, and then washed in 25 mmol L^{-1} ammonium bicarbonate (pH 8) and digested with trypsin in 25 mmol L^{-1} ammonium bicarbonate at pH 8 for 16 h at 37 °C (1:20 ratio trypsin to total protein, Promega Gold Mass Spectrometry Grade, Promega Inc., Madison WI). The peptides were extracted by successive additions of 50% acetonitrile and 5% formic acid in water. The extracted peptides were combined and concentrated by speed vacuum for about three hours to less than 20 μL, diluted with 2% acetonitrile and 0.1% formic acid and stored at -80 °C.

Additional peptide samples, obtained from experiments with B_{12} and iron-limited cultures of *Thalassiosira pseudonana* harvested in late exponential growth, described elsewhere (Chapter 4), were used for peptide analyses in this study. Once the cells were grown, peptide samples were prepared as describe above for *P. tricornutum.*

Total bulk protein concentrations in the mass spectrometry samples were determined post tryptic digestion via DC assay using a tryptic digest of bovine serum albumin as a protein standard (BioRad Inc., Hercules CA).

2.6. Labeled peptide handling and mass spectrometry

The protein digestions were analyzed by high pressure liquid chromatography coupled to mass spectrometry (HPLC-MS) as follows: a Paradigm MS4 system (Michrom Bioresources Inc.) was employed for HPLC separation. Samples were injected onto a peptide Cap Trap in-line with a reversed phase Magic C18 AQ column (0.2 x 150 mm, 3 μm particle size, 200 Å pore size, Michrom Bioresources Inc. Auburn CA). The chromatography consisted of a hyperbolic gradient from 5% buffer A to 95% buffer B for 40 min, where A was 0.1% formic acid (Michrom Ultra Pure) in water (Fisher Optima) and B was 0.1% formic acid in acetonitrile (Fisher Optima) at a flow rate of 4 μl min^{-1}. An ADVANCE nanocapillary electrospray source (Michrom Bioresources Inc.) was used to introduce the sample into the Thermo Vantage TSQ Triple Quadrapole Mass Spectrometer (TSQ). The TSQ was programmed to perform selected reaction monitoring (SRM) as previously described for cyanobacterial peptides (Saito et al. 2011), this time using peptides relevent to B_{12} metabolism in diatoms (Table 1). Isotopically-labeled versions of each peptide (Sigma-Aldrich) were employed as internal standards (Stemmann et al. 2001). These peptides were handled according to the manufacturer's instructions where 20 μL of one of several solvent mixtures, depending on peptide hydrophobicity and charge, were added to 1 nmol lyophilized vials. The solvent mixtures employed were: 5% acetonitrile 95% water, 90% acetonitrile 1% formic acid 9% water, 95% acetonitrile 0.5% formic acid 5% water, water alone, or 10% formic

acid. These dilutions were then vortexed for 1 min at moderate speed, heated to 45°C for 15 min, vortexed again for 30 s and then placed in a sonication bath for 5 minutes to aid in peptide resuspension. These mixtures were then each diluted by very slowly adding 180 μL of 0.1% formic acid, 2% acetonitrile, 98% water. These 5 pmol μL^{-1} stocks were then stored at 4°C for up to five weeks and used for all subsequent analyses. In some instances, the first initial solvent used for peptide resuspension resulted in poor peptide recovery, as assessed qualitatively through observing the peptide response during direct infusion into the mass spectrometer. In these cases, a different initial solvent was tested; if this did not increase the response, the peptide was not used for subsequent analyses.

The SRM reaction conditions for monitoring each peptide were optimized during direct infusion of each heavy isotope-labeled peptide (48 fmol μL^{-1} in 20% acetonitrile, 80% water, 0.1% formic acid) at 4 μL min^{-1} into the TSQ, optimizing the S-lens value for each parent ion (2+ and 3+) and the collision energy for generating each possible product ion. The most abundant three to five product ions generated from peptide parent ions were chosen for inclusion in the SRM used for quantitative analysis. Q1 operated in 0.2 FWHM resolution and Q3 operated in 0.7 FWHM resolution, with a cycle time of 1.6 seconds. SRM reaction monitoring was scheduled based on peptide pair chromatographic retention times, as shown in Table 1.

Linear behavior of each peptide monitored by these SRMs was validated by creating a standard curve from 0.2 to 240 fmol of each heavy isotope-labeled reference peptide in 2 μg *P. tricornutum* or *T. pseudonana* tryptic peptide sample matrix. For quantitative analyses, 20 fmol

of heavy isotope-labeled versions of each peptide were added to diatom peptide extracts (1-2 μg bulk protein) and the amount of the peptide of interest produced by the diatom (called the native peptide version herein) was calculated as a ratio to the size of the peak produced by 20 fmol of the heavy-labeled version of that peptide. The peptides measured and the reactions monitored for each are given in Table 1. Limits of detection (LOD) are given in Table 1 and were calculated for each peptide as follows: the intensity of the background peak for each reaction monitoring a native peptide was calculated in three blank mass spectrometry runs (no sample injection) and the fmol of native peptide that this background intensity would represent was calculated as a ratio to the intensity of the peak generated by the addition of 20 fmol of heavy peptide in the standard curve analyses; LOD = average fmol native peptide background + 3 x standard deviation about the mean of fmol native peptide background.

3. Results and Discussion

3.1. Peptide abundance through B_{12} starvation and recovery in diatom cultures

Cultures of *P. tricornutum*, first grown through several transfers without added B_{12}, grew to 15 ± 7 % greater cell density and at an 7 ± 3 % faster growth rate when supplemented with 100 pmol L^{-1} B_{12} (Figure 1). This suggests that even though this diatom possesses genes encoding both MetE and MetH and therefore does not require B_{12} absolutely, it receives a growth rate and yield benefit in the presence of the vitamin. In addition, B_{12} resupply to starved cultures resulted in an 11 ± 4 % increase in cell number over 24 hours. These data suggest that access to the vitamin

provides a growth advantage even to strains that do not have an absolute requirement and that overall phytoplankton growth in the environment can still be ultimately limited by B_{12} availability despite the ability of some strains to grow in its absence. Further study using other algal strains is required to understand the range in potential changes in non-B_{12} requiring phytoplankton growth as a result of vitamin scarcity in the ocean. The peptide abundance measurements conducted in this study yield molecular insight into the reasons for these B_{12}-dependant growth differences in *P. tricornutum.*

Peptides chosen for measuring the abundance of MetE, MetH and CBA1 protein are shown in Table 1. The linear response of the heavy-labeled versions of these peptides in the SRM measurements used for their detection is shown in Figure 2. The responses of all seven peptides were linear over four orders of magnitude. The intensity of the mass spectrometry response varied between peptides (Figure 2, y-axis). This supports the use of heavy isotope-labeled versions of *each peptide* of interest as internal standards for proper quantitation.

The abundances of target peptides were measured in *P. tricornutum* samples 3 days after inoculation and again 24 h after B_{12} resupply (Figure 3). The abundance of all three proteins measured was greater at the later timepoint, suggesting that these proteins comprise a larger fraction of total protein at the onset of stationary phase compared to during exponential growth. MetE, B_{12}-independent methionine synthase, was more abundant under low B_{12} at both timepoints. This is consistent with previous shotgun proteomic results showing that MetE was only detectable under conditions of low B_{12}. Similarly, recent work examining *metE* transcript abundance in *P. tricornutum* cultures found that *metE* expression was repressed under high B_{12}

(Helliwell et al. 2011), suggesting that the pattern we observe here in protein abundance is transcriptionally-regulated. Our data (Figure 3) also demonstrates that MetE protein abundance did not decrease within 24 h after B_{12} was resupplied. In contrast, Helliwell et al showed that *metE* transcript abundance decreases rapidly, within 2 h, after resupply. Thus, despite the cessation of MetE production that would result from the lack of transcript presence, this protein did not appear to be actively degraded within 24 h after B_{12} resupply. It is possible that continued presence of MetE protein may be of some benefit to cells as they are accumulating B_{12} from this pulsed addition, or it may be that there is no cellular benefit to degrading the protein during this growth phase.

Peptides from MetH, the B_{12}-dependant methionine synthase isoform, were present in low quantities that were relatively close to our limits of detection (Table 1), consistent with the lack of MetH detection in previous shotgun proteomic studies (Chapter 4). Despite these low concentrations, differences in MetH expression between high and low B_{12} treatments were resolved (Figure 3). MetH was more abundant in the $+B_{12}$ treatments than $-B_{12}$ and increased upon B_{12} resupply to levels measured in the $+B_{12}$ treatment. Mass spectral data supporting this conclusion is shown in Figure 4. These data suggest that MetH protein abundance was repressed by B_{12} scarcity and/or induced by B_{12} availability. Helliwell et al did not observe this response in transcripts encoding MetH, likely because their assays were not quantitative enough to resolve the subtle changes in abundance detected here (Helliwell et al. 2011). As a result, we cannot conclude whether these abundance patterns observed in MetH protein are transcriptionally or translationally regulated. The full recovery of MetH concentrations to replete levels 24 h post-

resupply suggests that the entirety of methionine production and recycling demand could be supported by the more efficient MetH by this time. This recovery supports the notion that the high MetE concentrations post-resupply resulted from a lack of incentive for cells to actively degrade the less efficient MetE rather than the protein being of continued utility. This suggests that MetH expression is more tightly coupled to short-term B_{12} availability than MetE expression.

Maximal MetE concentrations were much higher than maximal MetH concentrations (ratios of peptides bMetE1:dMetH1 = 40:1 to 120:1; peptides defined in Table 1). This is consistent with reports that the catalytic activity (k_{cat}) for MetE is an ~100-fold less than for MetH in *E. coli* (Gonzalez et al. 1992). This difference in efficiency also offers a likely explanation for the growth enhancement seen under high B_{12} concentrations and implies that there are detrimental ramifications of using MetE in place of MetH. The recovery of MetH abundance 24 h post resupply was also consistent with the growth enhancement seen upon B_{12} resupply (Figure 1). This clear advantage of MetH over MetE utilization likely explains how requirements for B_{12} uptake, which include trafficking and transport proteins, are retained in marine microbial genomes and allow for MetH utilization. These data demonstrate that there is a clear switch in metalloenzyme utilization from conditions of high B_{12} (replete growth) to low B_{12}, where MetE is abundant under low B_{12} and MetH is abundant under high B_{12}. The lack of MetE degradation upon B_{12} resupply is notable; since the resupplied treatment was growing at a rate of 0.9 ± 0.4 d^{-1}, this suggests that measurements of MetE reflect the cell's status with respect to B_{12} nutrition over at least one doubling time. However, since the cells in the inoculum used to initiate this experiment were starved for B_{12} and MetE was in lower abundance at day 3 in the $+B_{12}$ treatments

than the $-B_{12}$, this suggests that the approximately three doublings that the culture went through over this time period were enough to make an observable shift in MetE protein abundance and thus the three days was enough time for this strain to satiate B_{12} quotas and begin to use MetH for methionine regeneration. To better constrain what MetE measurements in the environment reflect about phytoplankton nutritional status, further work is needed to determine the range in optimal B_{12} quotas for MetH use as well as the time span in which different species can satiate these quotas.

CBA1 (Pt48322), a protein involved in B_{12} acquisition, was more abundant under low B_{12} conditions compared to replete conditions at each timepoint, consistent with results from previous study (Chapter 4). This reflects an increase in devotion of cellular resources to B_{12} acquisition under low B_{12} conditions, which also may help explain the increase in *P. tricornutum* growth rate under high B_{12}. However, concentrations of CBA1 in the low B_{12} condition during log phase growth are similar to those in replete cells during the onset of stationary phase, suggesting that this protein's abundance is driven by both growth phase and B_{12} availability. In addition, the abundance of CBA1 increases by an average of 2.5-fold post B_{12}-resupply, suggesting that CBA1 production responds not only to sustained low levels of B_{12} availability but also to pulses of high B_{12} availability. This is consistent with CBA1 having a functional role in B_{12} acquisition. Since B_{12} degrades relatively quickly in seawater simply due to photodegradation (Carlucci et al. 1969) and is also rapidly consumed by biota (Bertrand et al. 2011b), phytoplankton cells likely experience selection pressure acquire the vitamin quickly upon sensing a B_{12} pulse and respond efficiently to what is potentially quite periodic availability. In addition, there is likely a

considerable period of time required for cells to effectively up-regulate B_{12} acquisition machinery and then take up enough of the vitamin to satiate B_{12} quotas for growth using MetH. The increase in CBA1 at this 24 h post-resupply timepoint may reflect this process. Increased CBA1 production under pulsed B_{12} addition may also be analogous to the production of iron ligands in surface seawater upon iron addition, which is thought to be a biological response to increase microbial access to the added iron (Rue and Bruland 1997).

The abundance of these B_{12}-related proteins were also measured in the diatom *T. pseudonana*, in cultures grown as previously described (Chapter 4). *T. pseudonana* has only the MetH methionine synthase isoform and thus requires B_{12} absolutely. Abundance of peptides diagnostic of CBA1 and MetH in duplicate replete, low iron, low B_{12}, and low iron and B_{12} cultures of *T. pseudonana* are shown in Figure 5. Unlike in *P. tricornutum*, MetH abundance did not appear to vary as a function of B_{12} availability. This result is expected because there is no MetE available to replace MetH under B_{12} scarcity in this diatom. MetH appeared to be present as a similar proportion of total protein in both these diatoms. As in *P. tricornutum*, CBA1 abundance in *T. pseudonana* was higher under low B_{12} availability. It appears that CBA1 abundance in this diatom was not driven by iron nutritional status, consistent with previous shotgun proteomic results (Chapter 4). CBA1 peptide abundance was quite variable between replicates under low B_{12} conditions. This may reflect differences in timing of B_{12} depletion as a result of batch culture variability between replicates or biological variability in the magnitude of the CBA1 protein abundance changes. Additionally, because of this protein's role in the cell, the

variability may also be a function of small changes in sampling procedure. Previous work showed that CBA1 expression is targeted to the outer membrane and that this protein may help transport B_{12} from the outside to the inside of the cell by functioning as cell surface associated binder and trafficker (Chapter 4). If this is true, small changes in sampling procedures could cause changes in the amount of CBA1 protein retained on the cell versus that which is sheared off into the growth media. However, despite this variability, there is a clear overall trend where cultures grown under low B_{12} produce a much higher concentration of CBA1 protein.

The peptides measured as biomarkers for these proteins (MetE, MetH, and CBA1) all displayed exactly the same trends across treatments (Figure 3), but had somewhat different peptide abundances. This is illustrated in Figure 6 where the abundance of the two peptides diagnostic of each protein were plotted against each other. The abundance of peptides measuring the same protein are strongly linearly correlated, as expected, but the slopes of the lines were not unity, which would be expected if these two peptides were measured in equal concentrations. Since these measurements were so tightly correlated, it is not likely that the changes of slope arose from variability in peptide extraction or digestion efficiency, as one would expect variability induced by these processes to be more random. Here we discuss two possible explanations for the deviation of these slopes from one; the first is biological the second is analytical. Diatom genomes are diploid, meaning there are two copies of each chromosome and thus two copies of each gene per cell. However, when complete genomes are sequenced, the nucleic acid data is reduced to reconstruct only one copy of each chromosome. These peptide biomarkers were all designed

using this reduced dataset. It is therefore possible that there is some sequence variability (typically single nucleotide polymorphisms or SNPs) between two gene copies that can result in amino acid differences in peptides that are being used for these measurements. This has been shown to be the case for protein CBA1 (Chapter 4). One peptide used for this measurement is encoded by the CBA1 gene on only one of the diatom's chromosomes (Pt48322_1), while the other gene copy was determined by PCR amplification and DNA sequencing to encode a peptide that differs by one neutral amino acid change and would thus not be detected in these SRM assays. The second peptide (Pt48322_2), measured as more abundant, is encoded by both copies of the gene, as shown in Figure 6 panel D.

This scenario has not been tested for either the MetE or the MetH peptides, but it is notable that the more abundant bMetE1 peptide is entirely conserved among many organisms and comprises a portion of the tetrahydrofolate binding region of the protein, suggesting that there is pressure to keep this peptide conserved between the two coding sequences. In contrast, the less abundant peptide pMetE1 is not conserved across organisms, suggesting that there is reduced pressure to keep this peptide conserved across *P. tricornutum* chromosomes. It is therefore possible that these two MetE peptides (pMetE1, bMetE1) display the same pattern as the CBA1 peptides, where one is measuring one version of the protein and the other is measuring both. This would entirely explain the slope of two between these two peptide measurements since canonical models of eukaryotic gene expression suggest that the genes on each allele should be equally expressed.

Given this canonical model of eukaryotic gene expression, we would expect that plotting the abundance of both CBA1 peptides (Pt48322_2 abundance against Pt48322_1) would result in a linear regression with a slope of two, as seen for the MetE peptides. This is not the case, as the slope is nearly five, suggesting that there is either unequal expression of these gene copies or that an analytical difference is responsible. One source of analytical error that could explain these trends comes from the use of isotopically labeled internal standard peptides for absolute quantitation. These peptides arrived from the manufacturer lyophilized and in discrete vials containing 1 nmol of the peptide. In order to use them for these measurements, they were resuspended and solubilized. If a peptide was not completely solubilized upon resuspension, this would result in overestimation of the abundance of the corresponding native peptide, but would still allow for linear standard curves, as shown in Figure 2. Despite careful efforts in this study to completely dissolve each peptide, this is a possible partial explanation for some of the variability observed between the two peptide measured for each protein.

3.2. MetE and MetH peptide abundance measurements in McMurdo Sound

Some of the peptides used for measuring these protein abundance levels in diatom cultures may be useful for measuring proteins in field populations. Since the abundance of both MetE and MetH proteins appears to be driven by B_{12} availability to cells, the goal of such field measurements would be to assess the status of marine microbial communities with respect to vitamin B_{12} nutrition. The location chosen for these initial analyses was McMurdo Sound of the

Ross Sea in the Southern Ocean, where B_{12} have previously been shown to impact phytoplankton growth (Bertrand et al 2007; Appendix A).

In order for these peptides to be of use as protein biomarkers in the field, the degree of each peptide's conservation among strains and species must be considered so that the potential origins of each peptide can be constrained. In addition, these peptides must be abundant enough to be detected from within the complex bulk protein pool. This suggests that each peptide biomarker must be produced by some substantial fraction of the community, either by being encoded in the genomes of the more abundant members of the community or by being conserved across the genomes of many different community members. Their N-terminal trypsin cleavage site, a preceding lysine or arginine residue, must also be conserved in order to ensure that the peptide is generated in tryptic digests. In this study, the peptides used to measure CBA1 in diatom cultures are not conserved across species, suggesting that it would be useful to measure these peptides only in regions where the diatom species they were designed for use in comprise a substantial portion of the community. Since both *T. pseudonana* and *P. tricornutum* are temperate species found in coastal systems (Alverson et al. 2011; De Martino et al. 2007), these peptides are not likely to be detectable in McMurdo Sound so were not used for these field sample analyses.

Of the peptides measured in this culture study, only bMetE1 (VIQVDEPALR) and dMetH1 (ISGGISNLSFGFR) are conserved across their respective proteins from several sequenced genomes, as described in Table 2. This suggests that they may be detectable in Antarctic field samples and could be of utility for measuring some subset of MetE and MetH

presence in natural McMurdo Sound communities. As shown in Table 2, dMetH1, ISGGISNLSFGFR, preceded by an N-terminal lysine or arginine residue, is present only in MetH from the three publically available diatom genome sequences. There are single amino acid differences between this peptide in diatoms and the corresponding peptides from other stramenopiles *Ectocarpus* and *Aureococcus,* rendering them not observable using this specific peptide SRM assay. This peptide contains one of the conserved residues for homocysteine binding, but this location is otherwise quite variable amongst other MetH sequences. Based on this information, we can deduce that dMetH1 abundance may be a proxy for diatom MetH protein expression, though this must be re-evaluated as more MetH sequences from different organisms become available. Peptide bMetE1 (VIQVDEPALR) is part of the conserved THF binding region in MetE and is present in many genomes including both diatoms with sequenced genomes that possess *metE* as well as a range of bacteria and fungi (Table 2). This suggests that measurement of bMetE1 abundance can be considered a proxy for some subset of community MetE production, perhaps inclusive of all diatoms, though this should be validated through comparison to a greater number of diatom MetE sequences.

As shown in Figure 7, peptides bMetE1 and dMetH1 were detected and quantified in samples from McMurdo Sound of the Ross Sea, Antarctica. Protein samples were extracted from 3 μm filters containing particulate matter from surface water (~3 m depth) from stations 399-402, as shown (Figure 7 H). Samples 399-401 were collected from underneath first year sea ice and sample 402 was collected at the sea ice edge. Phytoplankton communities in this region were strongly diatom-dominated (Figure 7 F). Given these large filter sizes and the community

composition, peptides detected in this study likely originated predominantly from diatoms with some smaller fraction being from bacteria or archaea associated with larger particles. The identification of these MetE and MetH peptides in field samples is supported by the chromatograms and product ion distributions for these two peptides in samples from station 399, shown in Figure 7 C, D. Since the product ion distributions and retention times are similar for the heavy and native versions of both peptides, both bMetE1 and pMetH1 were positively identified. This is in contrast to the measurement of bMetE1 at station 402, which is problematic and hence marked with an X in Figure 7 B. Despite having a peak at the same retention time as the heavy labeled version of bMetE1, the product ion distribution generated for the SRM designed to monitor the native peptide is quite different from the heavy labeled version at that retention time (Figure 8). This suggests that another parent ion, not generated by peptide VIQVDEPALR but falling into its Q1 mass window, generates a product ion of m/z 927.489 and thus contaminates the SRM measurement of peptide VIQVDEPALR in this sample. As a result, the size of this peak cannot be used to quantify the amount of bMetE1 in this sample. There was little evidence for such contamination in the bMetE1 measurements at other locations since the product ion distributions in the native peak and heavy peak are similar (Figure 7). In order to accurately quantify bMetE in sample 402, the SRM reaction used to detect this peptide could be altered to exclude the contaminating peak m/z 927.489 from the measurement or the chromatography could be modified in order to separate the analyte and contaminant peaks. Alternately, a different peptide that is also diagnostic of MetE in diatoms could be measured. This highlights the importance of carefully examining the product ion distributions generated in

SRM measurements, particularly in complex field samples, and also emphasizes the importance of using stable isotope labeled versions of these peptides as internal standards to verify both the retention times of analyte peptides and their product ion distribution.

The detection of MetH protein, most likely from diatoms, in McMurdo Sound biomass represents molecular level confirmation of the use of vitamin B_{12} for methionine generation by these natural communities (Figure 7 A). It is striking that the concentration of this peptide in bulk protein from this region is several-fold greater than the concentrations measured in this culture study (Figures 3 and 6), suggesting that MetH expression in Antarctic diatoms may be higher relative to these cultured, temperate diatoms. Since Antarctic diatoms such as *Fragilariopsis cylindrus* (observed in these samples, Figure 7) are known to produce relatively large amounts of DMSP (Krell et al. 2007), which is synthesized from methionine, potentially using SAM in subsequent steps (Gage et al. 1997), their metabolism may demand a greater proportion of methionine synthase.

The abundance of the bMetE1 peptide in McMurdo Sound samples (Figure 7 B) likely reflects the concentration of MetE in a subset of organisms. Given the dominance of diatoms here, these measurements likely reflect the abundance of some subset of diatom MetE proteins. It is unclear, however, whether measurements of this peptide as a proxy for MetE are inclusive of all diatom MetE functional diversity. bMetE1 abundance normalized to bulk protein is within the lower range of abundances measured in B_{12}-starved cultures and well above those measured in B_{12} -replete cultures. Presuming that members of the natural community in McMurdo Sound

regulate MetH and MetE abundance similarly to *P. tricornutum*, these data are consistent with a portion of the > 3 μm community being starved for B_{12} within roughly three doubling times of the filtering event. Though this dataset is small, it is intriguing that the abundance of bMetE1 is significantly negatively correlated with chlorophyll *a* concentration ($r^2 = 0.99$). This suggests that high MetE abundance (B_{12} starvation) is found where biomass is low (Figure 9). Though there are many other factors that influence photosynthetic biomass in this region including iron supply, irradiance and seasonal mixing (Ditullio and Smith 1996; Martin et al. 1990; Sedwick and Ditullio 1997), such a correlation is consistent with a lack of B_{12} availability controlling phytoplankton biomass. Since these samples were taken from the water column underneath sea ice, it is likely that light is also limiting phytoplankton growth, perhaps uniformly across these three samples since the trend between our indicator of B_{12} starvation and phytoplankton biomass is so linear. Additional measurements of these proteins, particularly across the large dynamic range of chlorophyll concentrations in the Ross Sea, would be useful for more fully evaluating this trend and its relationship to other factors that impact photosynthetic biomass and vitamin B_{12} supply. Determining constraints on B_{12} production and persistence in the water column are of great import for future studies evaluating the role of phytoplankton B_{12} starvation. For instance, in this region, increased iron availability not only stimulates primary production but may also boost B_{12} supply by enhancing bacterial and archaeal growth (Bertrand et al. 2011b).

Despite the apparent use of MetE by some diatoms in McMurdo Sound, the abundance of MetH suggests that some members of this community must have access to vitamin B_{12} in enough quantity to use the vitamin for methionine generation. This may be a reflection of the range of

B_{12} concentrations or intracellular quotas at which different diatoms become starved for the vitamin or may also suggest that there is a subset of diatoms with localized B_{12} sources, such as closely associated bacterial communities, keeping them supplied with enough B_{12} for MetH utilization, as hypothesized previously for Ross Sea *Phaeocystis* populations (Bertrand et al. 2007). This further emphasizes the potential role of B_{12} in defining niche dimensions in marine microbial communities. Notably, the field location where dMetH1:bMetE1 ratios are highest (station 400) has the greatest Chl *a* concentration (Figure 7 E, G). This is consistent with the community growing to higher densities when B_{12}–dependant MetH is used as the dominant mode of methionine generation, as seen here with *P. tricornutum*. However, as with the negative relationship between MetE abundance and Chl *a*, this observation requires broader contextual information and additional measurements for complete interpretation.

These data represent a first glimpse into the molecular foundation of B_{12} requirements in field populations of diatoms through protein expression patterns and support the use of such measurements in expanded field programs. In order to extract the maximum amount of information from these peptide abundance measurements, future implementation should include timecourse sampling and be coupled with traditional bioassay measurements of vitamin and iron nutritional status as well as B_{12} and iron concentrations; bacterial community composition, growth rates and efficiencies; *metE* and *metH* diversity; and phytoplankton community structure analyses. These enticing initial peptide concentration data suggest that there are complex interactions between B_{12} availability, methionine synthase isoform interreplacment and

phytoplankton abundances and that such future studies may help illuminate the controlling factors in B_{12} use, production, and starvation in marine microbial communities. The negative correlation between MetE and Chl *a* concentration particularly warrants further exploration as a potential indicator of the importance of B_{12} deprivation in Antarctic phytoplankton communities.

Based on the abundance profiles for protein CBA1 in cultured diatoms, this protein represents a promising target to measure, along with MetE and MetH, for assessing community metabolic status with respect to vitamin B_{12}. However, CBA1 amino acid sequences are much more variable than those encoding MetE and MetH, suggesting that multiple peptides would need to be measured via SRM mass spectrometry to assess total community CBA1 abundance. Alternatively, immunochemical approaches may be successful if a single antibody that reacts to a broad range of CBA1 peptides can be developed. However, making multiple mass spectrometry-based measurements of CBA1 peptides may illuminate controls on taxon-specific CBA1 protein expression in microbial communities, which could offer additional insight into the importance of B_{12} in controlling marine microbial community composition. Peptide biomarkers could be designed to target the dominant versions of CBA1 in specific seasonal and geographic locations of interest via nucleic acid sequencing at those locations.

The data presented here suggest that the development of SRM-based peptide measurements for a range of proteins in environmental samples may prove useful for asking questions of particular biogeochemical relevance in a manner that is independent of the "bottle effects" that likely impact rate measurements and bioassays. One of the major benefits of SRM-

based peptide analyses like those described here is their ability to directly measure the abundance of multiple proteins simultaneously in field populations. This may eventually allow for estimation of rates of biochemical reactions that could aid in the evaluation of roles of specific functional groups in key processes.

3.3 Summary

Here we have used culture studies and newly designed peptide biomarkers to track the expression of three proteins related to vitamin B_{12} nutrition in diatoms. These results demonstrate that even amongst phytoplankton without an absolute B_{12} requirement, access to the vitamin may provide a growth advantage in the environment and that community-wide phytoplankton growth can still be ultimately limited by B_{12} availability. On a molecular level, this is likely explained by (1) the much higher efficiency of MetH compared to its non-B_{12} requiring replacement MetE and (2) the increased cellular resources expended to acquire B_{12} under starved conditions, as shown in CBA1 abundance patterns. In *P. tricornutum,* interreplacement between MetE and MetH was clearly demonstrated to be a function of B_{12} availability. High MetE protein abundance indicated that *P. tricornutum* was starved for vitamin B_{12} or has been within several doubling times. In diatoms that can replace MetH when starved for B_{12}, MetH abundance appeared to be a function of B_{12} availability. The abundance of B_{12} acquisition protein CBA1 increased under low vitamin availability and upon pulsed B_{12} resupply to starved cultures, likely in an effort by cells to take full advantage of episodic vitamin availability and satiate B_{12} quotas over time. This culture work lays a foundation for interpreting the abundance patterns of these

proteins in natural communities. We show here that MetE and MetH were detectable via peptide SRM mass spectrometry in natural diatom assemblages, that their abundance patterns may reflect B_{12} metabolic status of the community, and that B_{12} supply may correlate with phytoplankton biomass in this region. However, these data also highlight the importance of careful design and evaluation of SRM measurements to avoid possible contaminating reactions and determination of the conservation of each peptide and their potential environmental sources. Despite these considerations, the data presented here suggest that the development of SRM-based peptide measurements for a range of proteins may prove useful in environmental samples and enable evaluation of the role of specific functional groups in biogeochemical processes.

Acknowledgments: We thank Dawn Moran and Matt McIlvin for excellent technical assistance. We thank Andy Allen, Dawn Moran, Jeff Hoffman, Jeff McQuaid and Abigail Noble for field sampling efforts, and we acknowledge Andy Allen, Chris Dupont, Cathy Drennan, Sonya Dyhrman, Dianne Newman and Ben Van Mooy for helpful discussions. This work was supported by NSF awards ANT 0732665, OCE 0752291, and OCE 1031271, The Gordon and Betty Moore Foundation, a National Science Foundation (NSF) Graduate Research Fellowship (2007037200) and an Environmental Protection Agency STAR Fellowship to EMB (F6E20324).

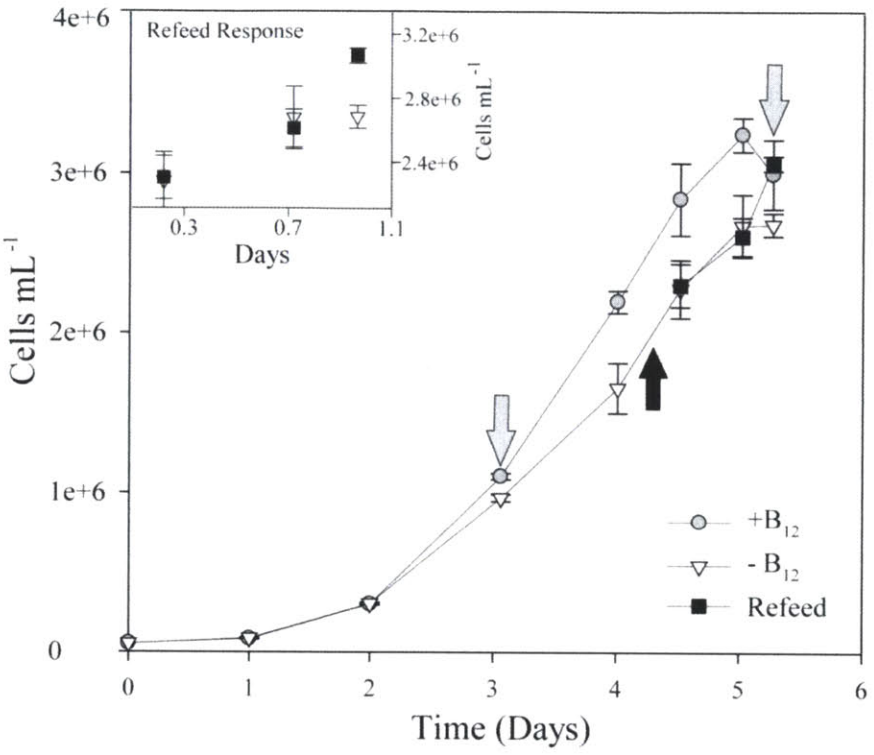

Figure 1: Growth of *P. tricornutum*, with and without added B_{12} and upon resupply of B_{12} to starved cultures, shown as cells per mL over time. Symbols are means of single counts from triplicate cultures, with error bars representing one standard deviation. The results of the resupply are repeated as an inset, with the x-axis as time in days since B_{12} was resupplied. Gray arrows indicate locations where protein samples were taken, and the black arrow indicates where the low B_{12} culture was split and half was resupplied with the vitamin. The growth rate of cultures during exponential growth (days 1-3) was 1.26 ± 0.01 d^{-1} for the $+B_{12}$ culture and 1.17 ± 0.02 d^{-1} for the $-B_{12}$ culture, showing that despite the fact that *P. tricornutum* grows well in the absence of B_{12}, it receives a growth rate enhancment when it utilizes the vitamin. This is supported by results from the resupply of 100 pmol L^{-1} B_{12} to $-B_{12}$ cultures which showed an increase in cell number as a result of the vitamin addition.

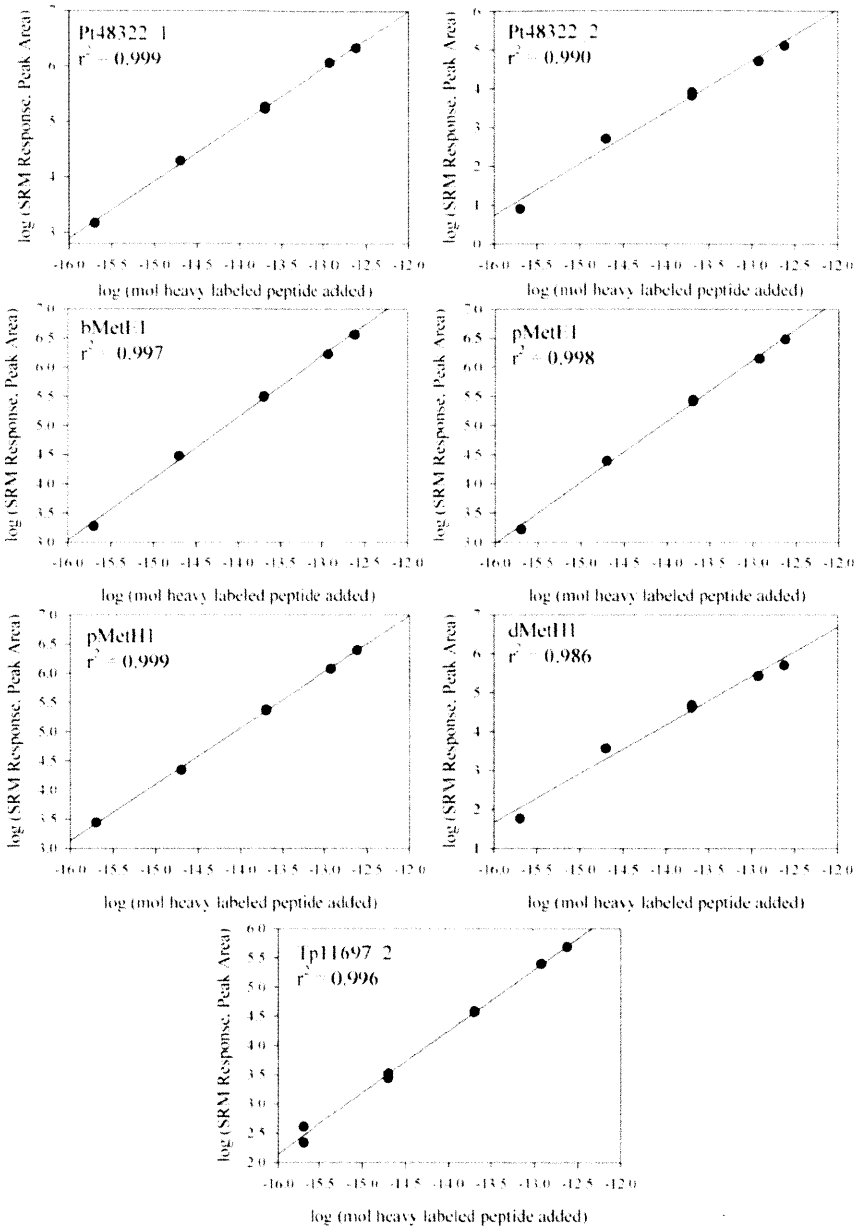

Figure 2: Standard curves for selected reaction monitoring detection of diatom peptides. The log of the intensity of the SRM response (peak area, sum of product ion intensities) is plotted against the log of moles of stable isotope-labeled (heavy) version of each peptide added (Table 1). Linear regressions are shown in the solid line and the coefficients of variance for each are given. For each peptide, the response is linear over four orders of magnitude, and the lowest concentrations detected were 0.2 fmol. These data verify the linear behavior of each peptide employed here for measurement of diatom proteins.

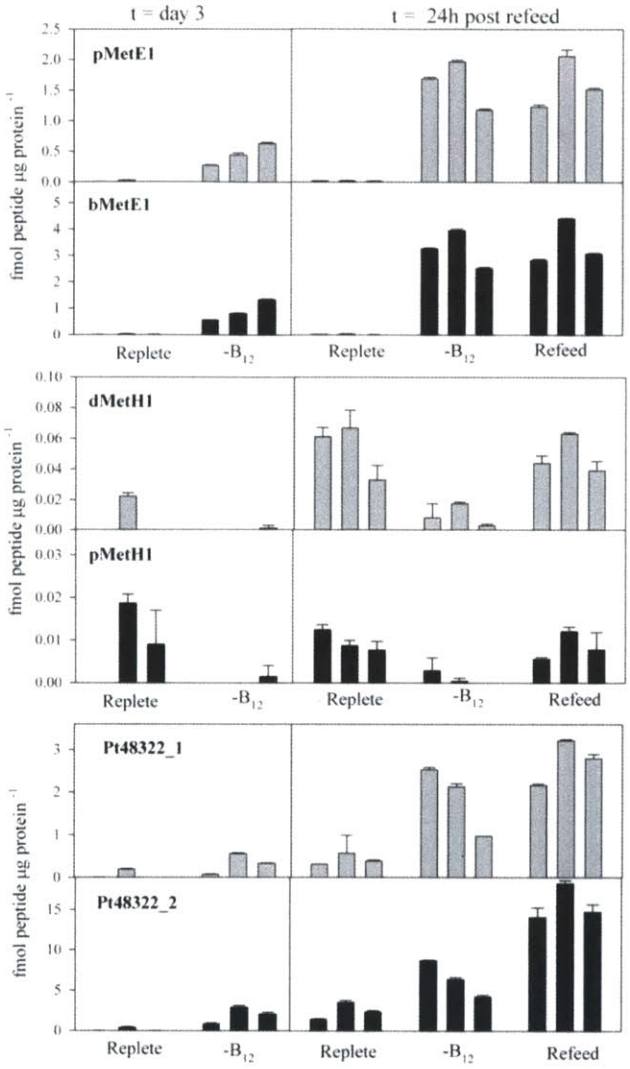

Figure 3: Abundance of B_{12}-related peptides in cultures of *P. tricornutum*. Concentrations of two peptides diagnostic of each protein of interest, CBA1, MetH, and MetE, are given normalized to total protein for triplicate cultures of $+B_{12}$ and $-B_{12}$ treatments after 3 days, and $+B_{12}$, $-B_{12}$, and refeed treatments 24 h after the refeed. Bars are means of technical triplicate measurements with error bars as one standard deviation. MetE, B_{12}-independent methionine synthase, was much more abundant under low B_{12} at both timepoints and did not decrease in abundance 24 h after B_{12} was resupplied. MetH, B_{12}-dependant methionine synthase, was present in low quantities that were close to our detection limit, was more abundant in the + B_{12} treatments and increased upon B_{12} resupply. Pt48322 (CBA1), a B_{12} acquisition protein (Chapter 4), was more abundant under - B_{12} conditions and increased further upon B_{12} resupply.

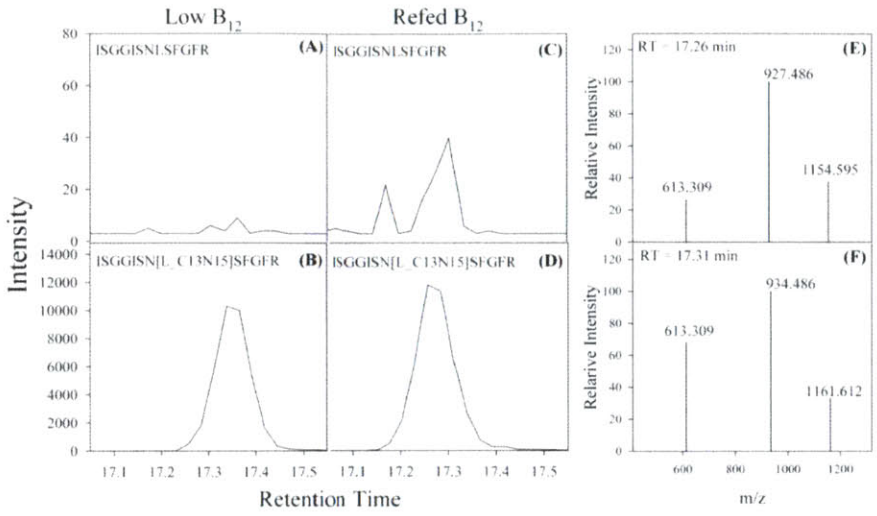

Figure 4: Chromatograms showing the intensity of the SRM response for the native and heavy-labeled version of peptide dMetH1 (ISGGISNLSFGFR), diagnostic of MetH, from *P. tricornutum* cultures. Chromatograms from a low B_{12} culture and a culture resupplied with B_{12}, both 24h after the resupply, are shown. Intensity (A-D) is the sum of the abundance of specific product ion peaks generated from the parent ion for each peptide. For ISGGISNLSFGFR, the SRM monitored is parent 677.859 to products 613.308-613.310, 927.467-927.469, 1154.594-1154.596 and for ISGGISN[L_C13N15]SFGFR the SRM monitored is parent 681.368 to products 613.308-613.310, 934.485-934.487, 1161.611-1161.613. Shown in panels E and F are the product ion distributions for native dMetH1 and heavy-labeled dMetH1peaks in the resupplied culture (chromatograms shown in C, D). The product ion distributions and retention times are similar between the heavy and native versions of this peptide in this sample, which support the positive identification and quantification of dMetH1 in the resupplied culture.

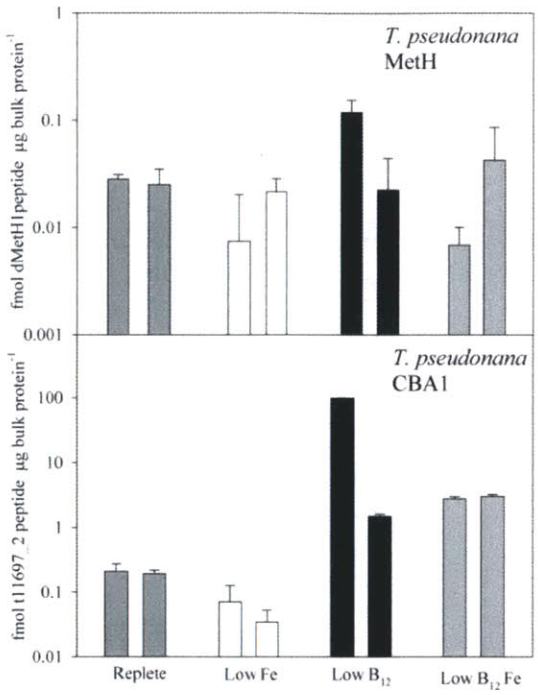

Figure 5: Abundance of peptides diagnostic of CBA1 (peptide Tp11697_2) and MetH (peptide dMetH1) in cultures of *T. pseudonana*. Peptide concentrations are given normalized to total protein for duplicate replete, low iron, low B_{12}, and low iron and B_{12} cultures as described elsewhere (Chapter 4). Bars are means of technical triplicate measurements with error bars as one standard deviation. Unlike in *P. tricornutum*, MetH abundance did not appear to be a function of B_{12} availability. As in *P. tricornutum*, CBA1 abundance was higher under low B_{12} availability regardless of iron nutritional status.

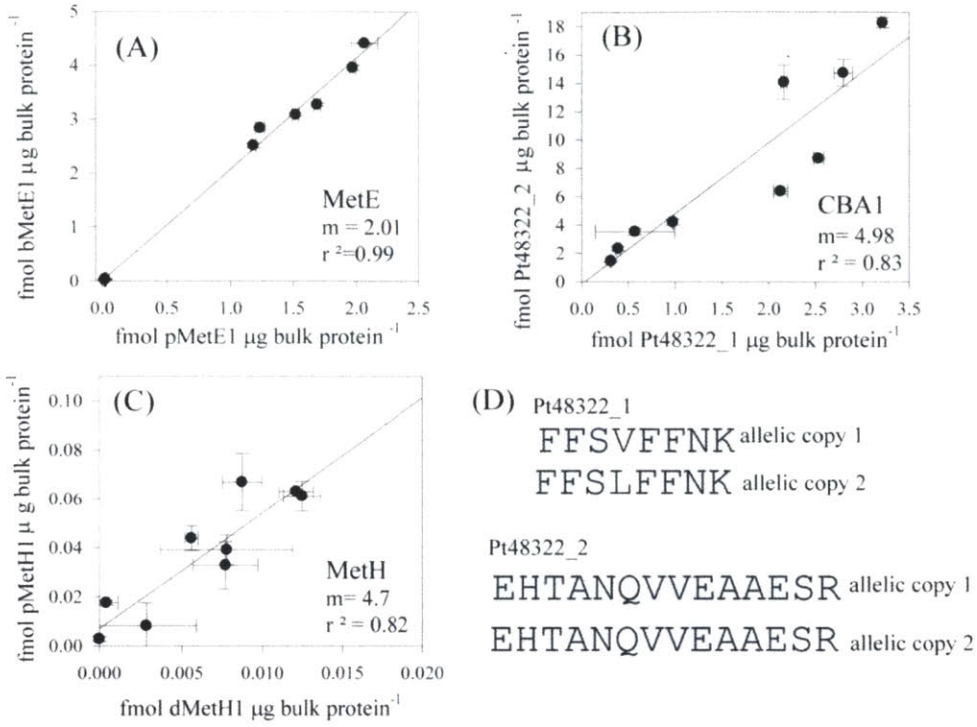

Figure 6. Comparison of the abundance of peptides diagnostic of the same proteins. The abundance of each peptide (means of technical triplicate measurements with error bars representing one standard deviation) is given versus the abundance of a different peptide from the same protein in each *P. tricornutum* culture sample (A-C). Linear regressions are shown in the solid line and the coefficients of variance (r^2) and the slope (m) for each are given. The abundance of peptides measuring the same protein were linearly correlated, as expected. There are several possible explanations for the deviation of the slope from unity, some analytical and some biological. One biological explanation for part of this slope variability is described in panel D, where one peptide used for these measurements is encoded by the CBA1 gene on only one of the diatom's chromosome copies while the gene copy on the second copy of the chromosome encodes a peptide that differs by one neutral amino acid change (Chapter 4). The second peptide is encoded by the genes on both chromosomes (allelic copies). Conserved amino acids are shaded in gray, and the differing amino acid is highlighted in white.

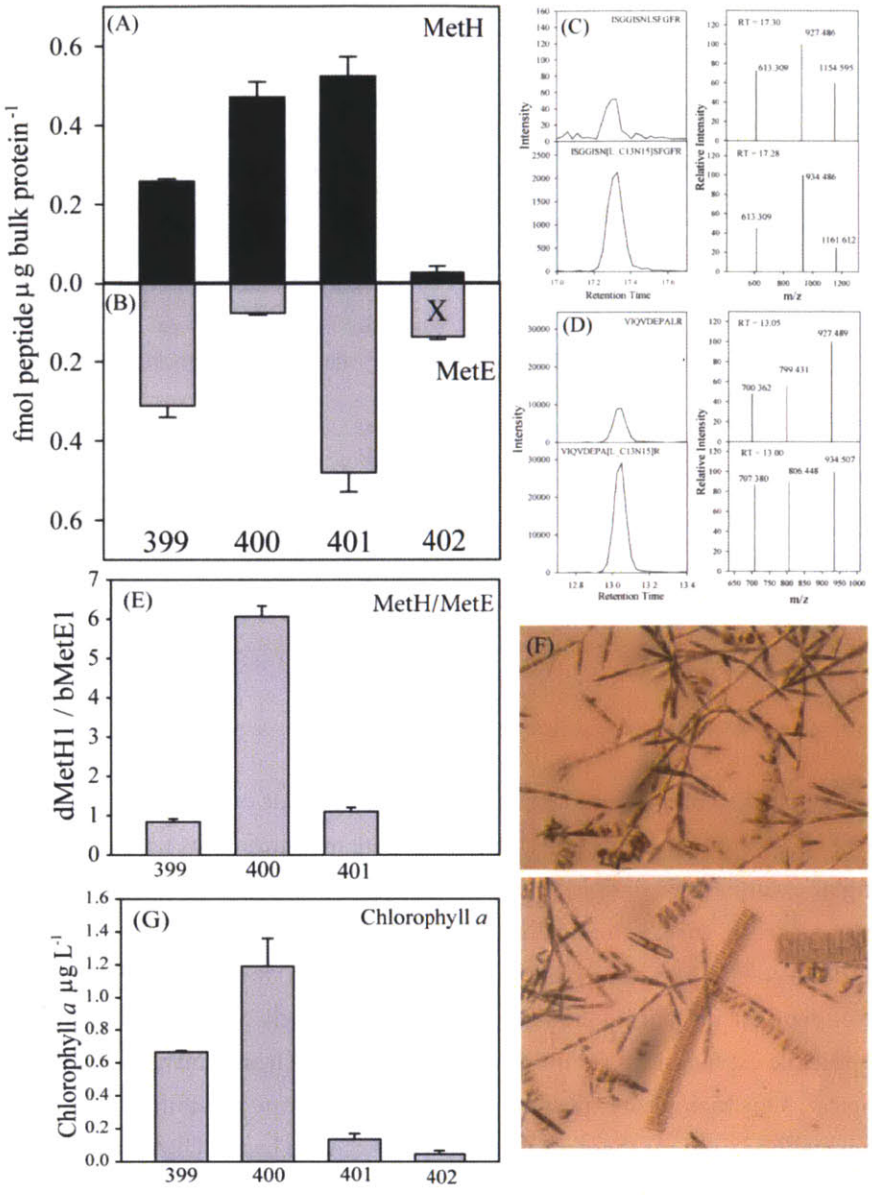

Figure 7: Peptides diagnostic of MetE and MetH were detected and quantified in phytoplankton samples from McMurdo Sound of the Ross Sea, Antarctica. Protein extracted from 3 μm filters containing particulate matter from surface water from stations 399-402 had detectable MetH (A) and MetE (B) peptide present. Bars are means of technical triplicate measurements, with error bars representing one standard deviation. Chromatograms showing the intensity of the SRM response for the native and heavy-labeled versions of peptide dMetH1 ISGGISNLSFGFR (C) and

peptide bMetE1 VIQVDEPALR (D) in the sample from station 399 are given, along with product ion distributions generated by the peptides. The product ion distributions and retention times were similar for the heavy and native versions of both peptides, leading to the positive identification and quantification of dMetH1 and bMetE1 in these field samples. The measurement for bMetE1 at station 402 appear contaminated (Figure 8) so it is marked with an X to denote analytical difficulties (B). The ratio of dMetH1 to bMetE1 abundance at the three stations without bMetE contamination1 are given in panel E. Means of duplicate chlorophyll a measurements at each location are given in panel G, with error bars as one standard deviation. All samples were dominated by diatoms, as shown in the light micrograph (F) from a net tow sample taken at station 399, and supported by the fact that all filters were brown in color. Diatoms observed in this net tow were *Nitzschia stellata, Fragilariopsis cylindrus* and *Amphiprora kufferathii.*

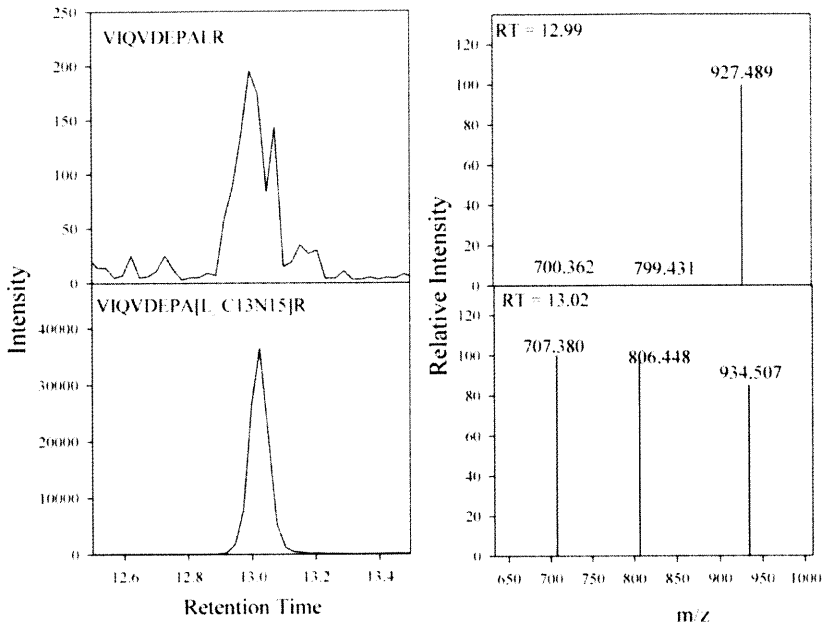

Figure 8: The bMetE1 measurement at station 402 was contaminated. Chromatograms on the left show the intensity of the SRM response measured as the native (top) and heavy-labeled version (bottom) of peptide bMetE1 (VIQVDEPALR) at station 402. The product ion distributions for the native and heavy-labeled peaks are shown to the right of their corresponding chromatograms. Note that the product ion distribution for the native peptide was vastly different than the heavy labeled version at the same retention time, suggesting that another parent ion, not generated by peptide VIQVDEPALR but falling into its Q1 mass window, generates a product ion of mass 927.489, thus contaminating the SRM measurement of peptide VIQVDEPALR in this sample. There was little evidence for such contamination in the bMetE1 measurements at other locations.

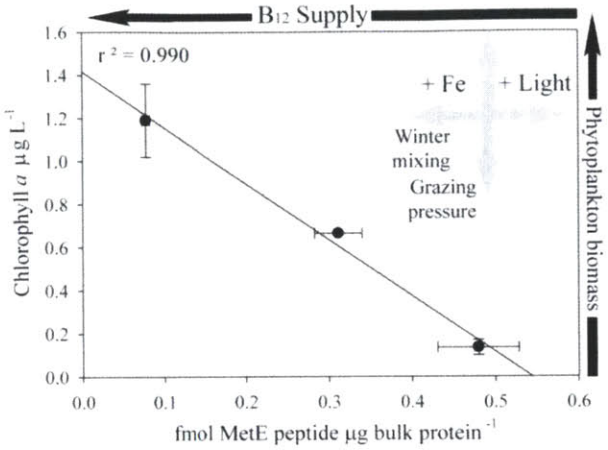

Figure 9: There is a significant negative relationship between bMetE1 peptide abundance and chlorophyll concentrations across these three stations, the potential import of which is described by the schematic diagram in the upper right hand corner. This trend is consistent with the suggestion that B_{12}-starvation helps control photosynthetic biomass in this region since, in cultures, MetE appears to be abundant only when diatoms are starved for B_{12}. Chlorophyll *a* concentrations are a proxy for phytoplankton biomass, and MetE concentrations may be inversely related to B_{12} supply to phytoplankton. Other factors controlling phytoplankton growth in this region are known to include Fe supply, light and mixed layer depth, and grazing pressure. These processes may also impact B_{12} supply since enhanced iron availability to bacteria may increase the pool of B_{12} available to phytoplankton (Bertrand et al. 2011b), increased light may increase B_{12} photodegradation (Carlucci et al. 1969), winter mixing could bring higher B_{12} concentrations to the surface (Menzel and Spaeth 1962), and increased grazing pressure may release more B_{12} to the water column.

Table 1 Peptide sequences, names, selected reaction monitoring parameters, and limits of detection.

Protein	Peptide	Peptide name	Parent ion (+z)	Parent (m/z)	Product (m/z)	Collision Energy	Start time (min)	Stop time (min)	S-lens value	LOD (fmol)
Tp11697 CBA1	VIISD[V_C13N15]GESPEEALDQNR	Tp11697_2heavy	3	657.6604	532.2470	17	14.15	16.15	118	
			3	657.6604	645.3320	16	14.15	16.15	118	
			3	657.6604	716.3690	27	14.15	16.15	118	
			3	657.6604	1071.5070	22	14.15	16.15	118	
	VIISDVGESPEEALDQNR	Tp11697_2native	3	659.6604	532.2470	17	14.15	16.15	118	0.0079
			3	659.6604	645.3320	16	14.15	16.15	118	
			3	659.6604	716.3690	27	14.15	16.15	118	
			3	659.6604	1071.5070	22	14.15	16.15	118	
Pt48322 CBA1	FFS[V_C13N15]FFNK	Pt48322_1heavy	2	521.2686	747.3930	15	16.80	18.80	110	
			2	521.2686	660.3610	15	16.80	18.80	110	
			2	521.2686	555.2900	16	16.80	18.80	110	
	FFSVFFNK	Pt48322_1native	2	518.2682	741.3930	15	16.80	18.80	110	0.0011
			2	518.2682	654.3610	15	16.80	18.80	110	
			2	518.2682	555.2900	16	16.80	18.80	110	
Pt48322 CBA1	EHTANQ[V_C13N15]VEAAESR	Pt48322_2heavy	2	773.8712	1280.6335	21	10.10	12.10	136	
			2	773.8712	1179.5858	24	10.10	12.10	136	
			2	773.8712	866.4472	25	10.10	12.10	136	
			2	773.8712	761.3788	25	10.10	12.10	136	
	EHTANQVVEAAESR	Pt48322_2native	2	770.8712	1274.6335	21	10.10	12.10	136	0.0240
			2	770.8712	1173.5858	24	10.10	12.10	136	
			2	770.8712	860.3788	25	10.10	12.10	136	
			2	770.8712	761.3788	25	10.10	12.10	136	
MetE, Pt	GS[L_C13N15]SEVDLIK	pMetE_1heavy	2	534.3065	803.4509	14	13.2	15.2	124	
			2	534.3065	716.4189	13	13.2	15.2	124	
			2	534.3065	587.3763	21	13.2	15.2	124	
	GSLSEVDLIK	pMetE_1native	2	530.7979	803.4509	14	13.2	15.2	124	0.0008
			2	530.7979	716.4189	13	13.2	15.2	124	
			2	530.7979	587.3763	21	13.2	15.2	124	
MetE, broad	VIQVDEPA[L_C13N15]R	bMetE_1heavy	2	573.8332	934.5066	16	11.9	13.9	135	
			2	573.8332	806.448	21	11.9	13.9	135	
			2	573.8332	707.3796	20	11.9	13.9	135	
	VIQVDEPALR	bMetE_1native	2	570.3246	927.4894	16	11.9	13.9	135	0.0008
			2	570.3246	799.4308	21	11.9	13.9	135	
			2	570.3246	700.3624	20	11.9	13.9	135	
MetH, Pt	IGIT[V_C13N15]IDTVK	pMetH_1heavy	2	532.8264	951.5615	18	13.6	15.6	116	
			2	532.8264	781.456	18	13.6	15.6	116	
			2	532.8264	575.3399	16	13.6	15.6	116	
			2	532.8264	894.5401	17	13.6	15.6	116	
			2	532.8264	680.4083	18	13.6	15.6	116	
	IGITVIDTVK	pMetH_1native	2	529.8264	945.5615	18	13.6	15.6	116	0.0010
			2	529.8264	775.456	18	13.6	15.6	116	
			2	529.8264	575.3399	16	13.6	15.6	116	
			2	529.8264	888.5401	17	13.6	15.6	116	
			2	529.8264	674.4083	18	13.6	15.6	116	
MetH, diatoms	ISGGISN[L_C13N15]SFGFR	dMetH_1heavy	2	681.3679	1161.6124	21	16.15	18.15	149	
			2	681.3679	934.4855	20	16.15	18.15	149	
			2	681.3679	613.3093	24	16.15	18.15	149	
	ISGGISNLSFGFR	dMetH_1native	2	677.8593	1154.5953	21	16.15	18.15	149	0.0057
			2	677.8593	927.4683	20	16.15	18.15	149	
			2	677.8593	613.3093	24	16.15	18.15	149	

Table 2: Known origins of peptides pMetH and bMetE from sequence databases including NCBI (National Center for Biotechnology Information) and JGI (Joint Genome Institute) obtained by blastP searching the peptide sequences against these databases with an E-value threshold of 10. Single amino acid changes are highlighted in gray and bold.

	dMetH1 **(K/R)ISGGISNLSFGFR**	bMetE1 **(K/R)VIQVDEPALR**
genomes, proteins with exact match	*Phaeodactylum tricornutum*, MetH 23399 (K)ISGGISNLSFGFR	*Phaeodactylum tricornutum*, MetE, 28056 (K)VIQVDEPALR
	Thalassiosira pseudonana, MetH 693 (K)ISGGISNLSFGFR	*Fragilariospis cylindrus*, MetE, 228154 (R)VIQVDEPALR
	Fragilariospis cylindrus, MetH 207237 (K)ISGGISNLSFGFR	> 125 genomes including fungi and bacteria, with many from *Clostridium* and *Bacillus* groups
genomes, proteins with one mutation	*Ectocarpus siliculosus*, MetH 0279_0006 (K)ISGG**V**SNLSFGFR	
	Aureococcus anophagefferens, MetH 15101 (K)ISGG**V**SNLSFGFR	
	Plesiocystis pacifica SIR-1 MetH (R)ISGGISNLSF**S**FR	
	Frankia alni ACN14a MetH (R)ISGGISNLSF**S**FR	
	Frankia sp. EUN1f MetH (R)ISGGISNLSF**S**FR	

References

Alverson, A. J., B. Beszteri, M. L. Julius, and E. C. Theriot. 2011. The model marine diatom *Thalassiosira pseudonana* likely descended from a freshwater ancestor in the genus *Cyclotella*. BMC Evolutionary Biology **11**.

Banerjee, R. G., and R. V. Matthews. 1990. Cobalamin- dependent methionine synthase. The FASEB Journal **4:** 1449-1459.

Bertrand, E. M., M. A. Saito, Y. J. Jeon, and B. A. Neilan. 2011a. Vitamin B_{12} biosynthesis gene diversity in the Ross Sea: the identification of a new group of putative polar B_{12}-biosynthesizers Environmental Microbiology **13:** 1285-1298.

Bertrand, E. M., M. A. Saito, P. A. Lee, R. B. Dunbar, P. N. Sedwick, and G. R. Ditullio. 2011b. Iron limitation of a springtime bacterial and phytoplankton community in the Ross Sea: implications for vitamin B_{12} nutrition. Frontiers in Aquatic Microbiology **Accepted**.

Bertrand, E. M. and others 2007. Vitamin B_{12} and iron co-limitation of phytoplankton growth in the Ross Sea. Limnology and Oceanography **52**.

Carlucci, A. F., S. B. Silbernagel, and P. M. Mcnally. 1969. The influence of temperature and solar radiation on persistence of vitamin B_{12}, thiamine, and biotin in seawater. Journal of Phycology **5:** 302-305.

Cowey, C. B. 1956. A preliminary investigation of the variaton of vitamin B-12 in oceanic and coastal waters. J. Mar. Biol. Ass. U.K. **35:** 609-620.

Croft, M. T., A. D. Lawrence, E. Raux-Deery, M. J. Warren, and A. G. Smith. 2005. Algae acquire vitamin B12 through a symbiotic relationship with bacteria. Nature **438:** 90-93.

Croft, M. T., M. J. Warren, and A. G. Smith. 2006. Algae need their vitamins. Eukaryotic Cell **5:** 1175-1184.

De Martino, A., A. Meichenin, J. Shi, K. H. Pan, and C. Bowler. 2007. Genetic and phenotypic characterization of *Phaeodactylum tricornutum* (Bacillariophyceae) accessions. J. Phycol **43:** 992-1009.

Ditullio, G. R., and W. O. Smith. 1996. Spatial patterns in phytoplankton biomass and pigment distributions in the Ross Sea. J. Geophys. Res **101:** 18467-18478.

Droop, M. R. 1957. Vitamin B_{12} in marine ecology. Nature **180:** 1041-1042.

---. 2007. Vitamins, phytoplankton and bacteria: symbiosis or scavenging? Journal of Plankton Research **29:** 107-113.

Dyhrman, S. T., E. A. Webb, D. M. Anderson, J. W. Moffett, and J. B. Waterbury. 2002. Cell-specific detection of phosphate stress in *Trichodesmium* from the Western North Atlantic. Limnol. Oceanogr. **47:** 1832-1836.

Gage, D. A. and others 1997. A new route for synthesis of dimethylsulphoniopropionate in marine algae. Nature **387:** 891:894.

Gobler, C. J., C. Norman, C. Panzeca, G. T. Taylor, and S. A. Sanudo-Wilhelmy. 2007. Effect of B-vitamins and inorganic nutrients on algal bloom dynamics in a coastal ecosystem. Aquat Microb Ecol **49:** 181-194.

Gonzalez, J. C., R. V. Banerjee, S. Huang, J. S. Sumner, and R. G. Matthews. 1992. Comparison of cobalamin- independant and cobalamin-dependant methionine synthases from *E. coli*: two solutions to the same chemical problem,. Biochemistry **31:** 6045-6056.

Goulding, C. W., D. Postigo, and R. G. Matthews. 1997. Cobalamin-dependent methionine synthase is a modular protein with distinct regions for homocysteine, methyltetrahydrofolate, cobalamin and adenosylmethionine. Biochemistry **36:** 8082-8091.

Helliwell, K. E., G. L. Wheeler, K. C. Leptos, R. E. Goldstein, and A. G. Smith. 2011. Insights into the Evolution of Vitamin B_{12} Auxotrophy from Sequenced Algal Genomes. Mol Biol and Evolution.

Karl, D. M. 2002. Nutrient dynamics in the deep blue sea. Trends in Microbiol. **10:** 410-418.

Koch, F., M. A. Marcoval, C. Panzeca, K. W. Bruland, S. A. Sanudo-Wilhelmy, and C. J. Gobler. 2011. The effect of vitamin B_{12} on phytoplankton growth and community structire in the Gulf of Alaska. Limnol and Oceanog **56:** 1023-1034.

Krell, A., D. Funck, I. Plettner, U. John, and G. Dieckmann. 2007. Regulation of proline metabolism under salt stress in the psychrophilic diatom *Fragilariopsis cylindrus*. Journal Of Phycology **43:** 753-762.

Laroche, J., P. W. Boyd, R. M. L. Mckay, and R. J. Geider. 1996. Flavodoxin as an in situ marker for iron stress in phytoplankton. Nature **382:** 802-805.

Lovelock, J. E. 1972. Gaia as seen through the atmosphere. Atmos Environ **6.**

Lu, X., and H. Zhu. 2005. Tube Gel Digestion. Molecular & Cellular Proteomics **4:** 1948-1958.

Martin, J. H., S. E. Fitzwater, and R. M. Gordon. 1990. Fe in Antarctic waters. Nature **345:** 156-158.

Menzel, D. W., and J. P. Spaeth. 1962. Occurrence of vitamin B_{12} in the Sargasso Sea. Limnol. Oceanogr. **7:** 151-154.

Panzeca, C. and others 2006. B vitamins as regulators of phytoplankton dynamics. EOS **87**.

Rodionov, D. A., A. G. Vitreschak, A. A. Mironov, and M. S. Gelfand. 2003. Comparative Genomics of the Vitamin B_{12} Metabolism and Regulation in Prokaryotes. J. Biol. Chem. **278:** 41148-41159.

Rue, E. L., and K. W. Bruland. 1997. The role of organic complexation on ambient iron chemistry in the equatorial Pacific Ocean and the response of a mesocale iron addition experiment. Limnol. Oceanogr. **42:** 901-910.

Saito, M. A. and others 2011. Iron Conservation by Reduction of Metalloenzyme Inventories in the Marine Diazotroph Crocosphaera watsonii Proceedings of the National Academies of Sciences **108** 2184-2189.

Saito, M. A., J. W. Moffett, S. W. Chisholm, and J. B. Waterbury. 2002. Cobalt limitation and uptake in *Prochlorococcus*. Limnol. Oceanogr. **47:** 1629-1636.

Sañudo-Wilhelmy, S. A., M. Okbamichael, C. J. Gobler, and G. T. Taylor. 2006. Regulation of phytoplankton dynamics by vitamin B12. Geophysical Research Letters **33**.

Scott, J. M., and D. G. Weir. 1981. The Methyl Folate Trap : A physiological response in man to prevent methyl group deficiency in kwashiorkor (methionine deficiency) and an explanation for folic-acid-induced exacerbation of subacute combined degeneration in pernicious anaemia The Lancet **318:** 337-340.

Sedwick, P., and G. R. Ditullio. 1997. Regulation of algal blooms in Antarctic shelf waters by the release of iron from melting sea ice. Geophys. Res. Lett. **24:** 2515-2518.

Stefels, J. P. 2000. Physiological aspects of the production and conversion of DMSP in marine algae and higher plants. J Sea Res **43:** 183-197.

Stemmann, O., H. Zou, S. A. Gerber, S. P. Gygi, and M. W. Kirschner. 2001. Dual inhibition of sister chromatid separation at metaphase. Cell **107:** 715-726.

Sunda, W., and S. A. Huntsman. 1995. Cobalt and zinc interreplacement in marine phytoplankton: Biological and geochemical implications. Limnol. Oceanogr. **40:** 1404-1417.

Sunda, W., D. J. Kieber, R. P. Kiene, and S. Huntsman. 2002. An antioxidant function for DMSP and DMS in marine algae. Nature **418:** 317-320.

Swift, D. G., and W. R. Taylor. 1972. Growth of vitamin B12 - limited cultures: *Thalassiosira pseudonana, Monochyrsis lutheri,* and *Isochrysis galbana.* J. Phycol. **10:** 385-391.

Tang, Y. Z., F. Koch, and C. J. Gobler. 2010. Most harmful algal bloom species are vitamin B1 and B_{12} auxotrophs. Proceedings of the National Academies of Sciences **107:** 20756-20761.

Webb, E. A., J. W. Moffett, and J. B. Waterbury. 2001. Iron Stress in Open Ocean Cyanobacteria (*Synechococcus, Trichodesmium* , and *Crocosphaera*): Identification of the IdiA protein. Appl. Environ. Microbiol. **67:** 5444-5452.

6. Conclusions

6.1. Summary of major findings

Two major and interrelated questions in marine biogeochemistry are (1) what controls the distribution and magnitude of primary production and (2) what are the niche dimensions that lead to the vast functional and phylogenetic diversity in marine planktonic organisms. This thesis takes steps towards developing tools to examine the possible roles of vitamin B_{12} in these questions and implements them for the study of B_{12} production, use, and starvation in an Antarctic shelf ecosystem. Results from this thesis support the inclusion of vitamin B_{12} in studies to constrain primary production and species dynamics in marine environments and make steps towards the design of molecular tools to enable this inclusion.

In this thesis, nucleic acid probes for B_{12} biosynthesis genes were designed and used to identify a potentially dominant group of B_{12} producers in the Ross Sea. The activity of this group was then verified by mass spectrometry-based peptide measurements (Chapter 2). Then, using

field-based bottle incubation experiments and vitamin uptake measurements, possible interconnections between iron and B_{12} dynamics in this region were identified, showing that iron availability may impact both B_{12} production and consumption (Chapter 3). Large scale changes in diatom proteomes were induced by low B_{12} availability were documented in Chapter 4. One previously unknown protein, CBA1, was much more abundant under low B_{12} in two diatoms. This protein was then shown to be directly involved in B_{12} uptake in diatoms and thus represents the first identification of a B_{12} acquisition protein in eukaryotic phytoplankton. The detection of CBA1 transcripts in environmental datasets suggests that this protein is abundant and utilized by natural phytoplankton populations and thus that B_{12} acquisition is an important component of diatom molecular physiology (Chapter 4). Selected reaction monitoring mass spectrometry was used to measure the abundance of this and other B_{12}-related proteins in diatoms cultures, revealing distinct protein abundance patterns as a function of B_{12} availability. These peptide measurements were then implemented to measure the abundance B_{12}-related proteins in McMurdo Sound, revealing that there is both B_{12} utilization and starvation in natural diatom communities and that these peptide measurements hold promise for revealing the metabolic status of phytoplankton communities with respect to vitamin B_{12} (Chapter 5). All these data support the inclusion of B_{12} production and consumption dynamics in studies to constrain marine primary production, particularly in Antarctic shelf ecosystems.

6.2. Future directions

6.2.1. Development of field programs implementing peptide biomarkers of B_{12} use and starvation

The detection of MetH and MetE via peptide SRM mass spectrometry in natural diatom communities and the inverse relationship between Chl *a* and MetE abundance supports the use of these peptide measurements in expanded field campaigns. In order to use CBA1 abundance as a biomarker for B_{12} deprivation in diatom communities, additional work is required. Additional nucleic acid sequencing information to determine the diversity of CBA1 sequences in particular environments can be used to design specific SRM peptide biomarkers for each location of interest. Studies that couple MetE, MetH, and CBA1 protein measurements with traditional assessments of biomass, primary production, species composition, cobalt and iron concentrations, bacterial growth rates and efficiency, B_{12} concentrations, traditional bottle incubation bioassay experiments, and improved versions of B_{12} biosynthesis peptide biomarkers (Chapter 2) have the potential to elucidate controls on B_{12} use, production, and consumption. A first location to attempt a broad study such as this would be Antarctic shelf ecosystems. Not only are these regions disproportionally important for biogeochemical cycling (Arrigo et al. 1999), but they are best suited for the application of these newly developed tools since they are predictably diatom-dominated and may also be lacking in the major source of B_{12} available in temperate and tropical seas- cyanobacteria (Marchant 2005, Bonnet et al. 2010), making inquiries into B_{12} dynamics particularly relevant. The North Pacific HNLC (high nutrient low chlorophyll) region is also a priority, as it is also frequently diatom dominated, can be an important region for carbon export

out of the surface ocean (Charette et al. 1999), and has different potential B_{12} production and consumption dynamics than the Ross Sea (Koch et al. 2011) making it a possibly useful region for comparison.

6.2.2. Further characterization of CBA1

The functional role of protein CBA1 should be verified through confirming that the protein binds B_{12} and measuring its binding and dissociation constants. This can be done through studies using ^{57}Co-B_{12}, ultrafiltration and dialysis membranes and dextran-coated charcoal to adsorb non-protein bound B_{12} (Marchaj et al. 1995). Working towards crystal structure characterization for CBA1 bound to B_{12} would yield insight into its similarities and differences with other B_{12} binding proteins and hopefully lend new perspectives to studies of B_{12} binding sites and the evolution of B_{12} use. Characterizing the interaction of CBA1 with other diatom proteins is of considerable interest, particularly for elucidating the complete B_{12} uptake pathway. Determining the relationship between CBA1 and the strong, exuded B_{12} binding protein complexes described in a range of phytoplankton species (Pintner & Altmeyer 1979) is also an important consideration in order to evaluate the potential roles of these proteins as growth inhibitors and agents of 'chemical warfare' in resource competition.

If the B_{12} binding role of CBA1 is verified, this protein will represent a new class of B_{12}, and therefore cobalt, utilizing protein. It may then be useful to revisit past studies that analyzed cobalt use through time as a function of the presence of known cobalt -utilizing protein families in modern genomes (Dupont et al. 2006). This study concluded that Co use is concentrated in prokaryotic genomes and reduced in eukaryotic ones which reflects enhanced Co availability in

early Earth environments. Including CBA1 in these analyses will likely increase the amount of cobalt use documented in eukaryotic genomes though without detailed analysis it is difficult to determine if this will skew the conclusion that cobalt use is predominantly found in prokaryotic lineages.

6.2.3. Evaluating the impact of reduced methionine synthase activity on phytoplankton metabolism

The downstream effects of reduced methionine synthase activity as a result of B_{12} starvation may have significant ramifications for a range of metabolic processes in phytoplankton. Since methionine synthase catalyzes the conversion of 5-methyltetrahydrofolate and homocysteine to methionine and tetrahydrofolate (THF), reduced activity could potentially decrease cellular supplies of methionine for protein synthesis as well as for the production of DMSP and S-adenosylmethionine (SAM), which is an important methyl and propylamine group donor. In plants, only 20% of methionine produced appears to be used in protein; the other 80% is converted to SAM to be used in a range of metabolic processes (Giovanelli et al. 1985). This suggests that SAM pools may be dramatically affected by a reduction in methionine synthase activity in phytoplankton as well, but this requires experimental confirmation. Additionally, by causing a buildup in 5-methyltetrahydrofolate, reduced methionine synthesis activity deprives cells of THF for recycling and reuse in other cellular functions such as nucleotide biosynthesis (Scott & Weir 1981). This reduced THF availability for nucleic acid synthesis has the potential to slow the process of DNA repair, potentially leaving cells in a vulnerable state, more open to unfavorable mutations.

Notably, the majority of SAM metabolites within cells are methylated molecules which are formed through methyltransferase-mediated reactions (Sufrin et al. 2009). Methylation increases steric bulk and changes binding properties of substrates. These changes are exploited for a range of biological purposes. An important example is DNA methylation, which typically involves the addition of a methyl group to CpG sites in DNA. These sites are concentrated in regulatory regions of genes, with increased methylation usually leading to reduced activity. Methylation patterns and the resulting changes in activity can be replicated during cell division, thus offering a mechanism for epigenetic inheritance (Bossdorf et al. 2008). This epigenetic inheritance may be extremely important for explaining phenotypic variability in marine microbes, as it is a direct mechanism by which environmental variability can to lead to heritable changes (Bossdorf et al. 2008), and it is becoming increasingly recognized that epigenetic variation greatly exceeds genetic variation in many organisms (Keyte et al. 2006, Vaughn et al. 2007). Reduced cellular methylation potential is a possible consequence of B_{12} deprivation in phytoplankton. This could lead to decreased DNA methylation and thus potentially loss of important, environmentally induced changes in epigenetics which may have the potential to reduce fitness. This remains unexplored, however, and may warrant investigation if phytoplankton cellular SAM pools are found to decrease substantially in response to B_{12} deprivation.

The potential effects of reduced methionine synthase activity may also leave B_{12}-starved phytoplankton more vulnerable to other types of nutrient stress. Some of these synergistic

vulnerabilities are described in detail in the following section. Determination of intracellular concentrations of SAM, homocystine, and 5-methyl THF, methionine in protein, and DMSP as well as the rates of change of each metabolite under varying degrees of B_{12} limitation would enable evaluation of the potential for each specific effect of decreased methionine synthase activity to be important for phytoplankton cell physiology. This determination would highlight potential effects of B_{12} starvation that may be important to consider in marine biogeochemical studies.

6.2.4. Possible interactive effects between B_{12} and Fe, P, and Si

Traditional notions of nutrient limitation have recently been expanded to include the recognition that colimitation, growth limitation by the availability of more than one nutrient simultaneously, may be an important environmental phenomenon. There are three general types of colimitation that have been described; independent colimitation (type I) occurs when the bioavailable concentrations of two or more nutrients are close to limiting concentrations. Biochemical substitution (type II) colimitation occurs if two nutrients can substitute for one another in biochemical roles, and dependant colimitation (type III) is possible if one nutrient is required for the acquisition, utilization or biosynthesis of another (Saito et al. 2008).

Limitation by B_{12} was documented in this thesis in Ross Sea phytoplankton communities, though this was only observed after the community was supplemented with additional iron, suggesting that iron and B_{12} were both limiting nutrients (Appendix 1, Bertrand et al 2007). Both independent and dependant colimitation between iron and vitamin B_{12} are potential scenarios consistent with this instance of Fe and B_{12} limitation. Primary vitamin limitation has been

documented in other areas of the Southern Ocean (Panzeca et al. 2006), which is inconsistent with dependant colimitation. However, since the full vitamin uptake pathway in eukaryotic phytoplankton remains uncharacterized, the possibility for dependant co-limitation is difficult to evaluate. Since methionine synthase (MetH) is likely responsible for the main B_{12} requirement in eukaryotic phytoplankton (Croft et al. 2005, Helliwell et al. 2011) and the only non-B_{12} requiring isoform (MetE) does not require iron, this precludes iron and B_{12} biochemical substitution. If biochemical substitution occurred between iron and vitamin B_{12} in eukaryotic phytoplankton via another set of enzymes, one might expect the iron replete communities to decrease B_{12} uptake rate due to decreased vitamin requirements under high iron. This is counter to a trend observed in this thesis (Chapter 3, Figure 9, panel A), where iron supplementation increased B_{12} uptake rates. These field data suggest that eukaryotic phytoplankton experience independent (type I) colimitation by B_{12} and iron. However, a culture-based study with a subarctic diatom found higher iron quotas and less efficient iron use under B_{12} starvation; this trend was amplified under high CO_2 conditions (King et al. 2011). The authors propose that this may be explained by the S-adenosyl methionine (SAM) deprivation that could result from B_{12} starvation leading to decreased methylation of phylloquinone, a molecule which functions as part of the photosystem I electron transport chain. The authors suggest that reduction in active, methylated phylloquinone could then lead to increased demand for iron-containing electron transporters such as cytochromes and ferredoxin. However, this has yet to be verified biochemically and may be unlikely since phylloquinone plays a very different role in electron transport than do cytochromes and ferredoxins (Lohmann et al. 2006).

The requirements for B_{12} in bacteria differ from those of eukaryotic phytoplankton and thus so do the possibilities for colimitation. In addition to many other uses, some bacteria require the vitamin in the enzyme ribonucleotide reductase, which is important for nucleic acid synthesis. They can have an iron-requiring or a B_{12}-requiring form of this enzyme or both, suggesting that there may be biochemical substitution between these nutrients. Indeed, in some bacteria the transcription of the gene encoding the iron-requiring ribonucleotide reductase has been shown to be controlled by vitamin B_{12} availability such that the iron-requiring form is only expressed when the B_{12} concentration inside the cell is low (Borovok et al. 2006). Iron stress, as would be experienced by the control treatments in Chapter 3 (Figure 9), could thus be partially alleviated by enhanced intracellular availability of the vitamin, achievable through enhanced B_{12} uptake, consistent with observations in Chapter 3. In addition, iron is required for B_{12} biosynthesis in some bacteria, particularly for the enzymes CobG (Schroeder et al. 2009) and CobZ (McGoldrick et al. 2005). Bacteria employing these enzymes, when iron starved, could conceivably respond by increasing B_{12} uptake from the environment rather than enhancing *de novo* biosynthesis, though this has not been investigated. The bacterial vitamin uptake data in Chapter 3, considered in light of known vitamin and iron biochemistries, are consistent with type II (biochemical substitution) and/or type III (dependant) colimitation.

Though the only interactive effect of B_{12} starvation with another nutrient assessed in this study was with iron, results from this thesis suggest that other possibly important interactive effects may be worth evaluating, specifically with phosphorus (P) and silica (Si) metabolism. One

of the strategies used by phytoplankton to cope with P scarcity is the replacement of phospholipids in the membrane with alternative lipids, thus leaving P available for other metabolic functions (Van Mooy et al. 2009). Some of the important alternative lipids are a series of betaine lipids. Under low P availability, *Thalassiosira pseudonana* substitutes the phospholipid phosphatidylcholine (PC) with the betaine lipid diacylglycerylcarboxyhydroxymethylcholine (DGCC) within one cell division or less (Martin et al. 2011). This same substitution has been observed in a number of additional phytoplankton species (Van Mooy et al 2009). Betaine lipid biosynthesis pathways, though not totally elucidated in phytoplankton, typically use SAM as a methyl and propylamine group donor (Kato et al. 2006). Thus, B_{12} starvation could potentially impair the ability of phytoplankton cells to cope with phosphorus limitation by reducing the efficiency of betaine lipid production through reduced SAM availability. Tests for this synergistic impact would entail measuring P quotas and intact polar lipid composition in cultures under a range of B_{12} and P concentrations, specifically looking for reduced fitness and impaired lipid switching availability of P-limited cultures under low B_{12} conditions. If B_{12} starvation is found to synergistically reduce the fitness of phytoplankton in low P environments, this may have significant ramifications for conceptual models of controls on primary production in low P oceanic regions such as the Western North Atlantic (Wu et al. 2000) and the Mediterranean (Thingstad et al. 1998).

There are also possible connections between silica metabolism and B_{12} use in diatoms. The major organic constituent of diatom silica frustules are a series of long chain polyamines

(LCPAs). Different diatoms synthesize different suites of LCPAs (Kroger et al. 2000). These molecules, along with silica deposition proteins called silafins, induce biomineralization and are responsible to for the differences in frustule morphology between diatom groups. LCPAs vary in chain length and degree of methylation, but appear to all be synthesized from putricine, spermidine or spermine precursors. These precursors are synthesized sequentially from ornithine, with spermidine and spermine production both requiring SAM as a propylamine donor. Subsequent steps in LCPA formation likely require SAM as well (Kroger & Poulsen 2008). Conceivably, reduced SAM production through B_{12} starvation could induce changes in silica frustule formation by decreasing the pool of available LCPAs. Indeed, reduction of LCPA production as a result of synthetic inhibitor addition dramatically reduced biogenic silica formation in *T. pseudonana* (Frigeri et al. 2006). Experiments measuring biogenic silica formation as well as LCPA composition as a function of B_{12} availability would help determine whether B_{12} metabolic status should be considered if efforts to predict silica demand by diatoms and rates of biogenic silica formation in the ocean. If LCPA composition is found to change predictably as a result of B_{12} nutritional status, LCPA composition in surface water diatom samples as well as those preserved in sediments (Bridoux & Ingalls 2010) may be of use for tracing B_{12} metabolic status in current communities as well as through recent geologic history.

References

Arrigo KR, Robinson DH, Worthen DL, Dunbar RB, DiTullio GR, VanWoert M, Lizotte MP (1999) Phytoplankton community structure and the drawdown of nutrients and CO_2 in the Southern Ocean. *Science* 283:365-367

Bonnet S, Webb EA, Panzeca C, Karl DM, Capone DG, Sanudo-Wilhelmy SA (2010) Vitamin b_{12} excretion by cultures of the marine cyanobacteria *Crocosphaera* and *Synechococcus*. *Limnol and Oceanog* 55:1959-1964

Borovok I, Gorovitz B, Schreiber R, Aharonowitz Y, Cohen G (2006) Coenzyme b_{12} controls transcription of the *Streptomyces* class ia ribonucleotide reductase *Nrdabs* operon via a riboswitch mechanism. *J Bacteriol* 118:2512-2520

Bossdorf O, Richards CL, Pigliucci M (2008) Epigenetics for ecologists. *Ecology Letters* 11:106-115

Bridoux MC, Ingalls AE (2010) Structural identification of long-chain polyamines associated with diatom biosilica in a southern ocean sediment core. *Geochimica et Cosmochimica Acta* 74:4044-4057

Charette MA, Moran BS, Bishop JK (1999) 234th as a tracer of particulate organic carbon export in the subarctic northeast pacific ocean. *Deep-Sea Res* II 46:2833-2961

Croft MT, Lawrence AD, Raux-Deery E, Warren MJ, Smith AG (2005) Algae acquire vitamin B_{12} through a symbiotic relationship with bacteria. *Nature* 438:90-93

Dupont CL, Yang S, Palenik B, Bourne PE (2006) Modern proteomes contain putative imprints of ancient shifts in trace metal geochemistry. *Proc Natl Acad Sci* 103:17822-17827

Frigeri LG, Radabaugh TR, Haynes PA, Hildebrand M (2006) Identification of proteins from a cell wall fraction of the diatom *Thalassiosira pseudonana*. *Molecular & Cellular Proteomics* 5:182-193

Giovanelli J, Mudd SH, Datko AH (1985) Quantitative analysis of pathways of methionine metabolism and their regulation in *Lemna*. *Plant Physiology* 78:555-560

Helliwell KE, Wheeler GL, Leptos KC, Goldstein RE, Smith AG (2011) Insights into the evolution of vitamin B_{12} auxotrophy from sequenced algal genomes. *Mol Biol and Evolution*

Kato M, Kobayashi Y, Torii A, Yamada M (2006) Betaine lipids in marine algae. In: Murata N (ed) Advanced research on plant lipids: Proceedings of the 15th international symposium on plant lipids. Dordrecht, Kluwer, p 19-22

Keyte AL, Percifield R, Liu B, Wendel JF (2006) Intraspecific DNA methylation polymorphism in cotton (*Gossypium hirsutum* l.). *J Hered* 97:444-450

King AL, Sanudo-Wilhelmy SA, Leblanc K, Hutchins DA (2011) CO2 and vitamin B12 interactions determine bioactive trace metal requirements of a subarctic pacific diatom. *ISME Journal* 5:1388-1396

Koch F, Marcoval MA, Panzeca C, Bruland KW, Sanudo-Wilhelmy SA, Gobler CJ (2011) The effect of vitamin B_{12} on phytoplankton growth and community structire in the gulf of alaska. *Limnol and Oceanog* 56:1023-1034

Kroger N, Deutzmann R, Bergsdorf C, Sumper M (2000) Species-specific polyamines from diatoms control silica morphology. *Proc Natl Acad Sci* 97:14133-14138

Kroger N, Poulsen N (2008) Diatoms- from cell wall biogeneisis to nanotechnology. *Annu Rev Genet* 42:83-107

Lohmann A, Schöttler MA, Bréhélin C, Kessler F, Bock B, Cahoon EB, Dörmann P (2006) Deficiency in phylloquinone (vitamin k1) methylation affects prenyl quinone distribution, photosystem i abundance, and anthocyanin accumulation in the *Arabidopsis* atmeng mutan. *J Biol Chem* 281:40461-40472

Marchaj A, Jacobsen DW, Savon SR, Brown KL (1995) Kinetics and thermodynamics of the interaction of vitamin B12 with haptocorrin: Measurments of the highest protein ligand binding constant yet reported. *J Am Chem Soc* 117:11640-11646

Marchant HJ (2005) Cyanophytes. In: Scott FJ, and H. J. Marchant. (ed) Antarctic marine protists. Australian Biological Resources Study, Hobart

Martin P, Van Mooy BAS, Heithoff A, Dyhrman ST (2011) Phosphorus supply drives rapid turnover of membrane phospholipids in the diatom *Thalassiosira pseudonana. ISME Journal* 5:1057-1060

McGoldrick HM, Roessner CA, Raux E, Lawrence ADand others (2005) Identification and characterization of a novel vitamin B12 (cobalamin) biosynthetic enzyme (Cobz) from *Rhodobacter capsulatus*, containing flavin, heme, and Fe-s cofactors. *J Biol Chem* 280:1086-1094

Panzeca C, Tovar-Sanchez A, Agusti S, Reche I, Duarte M, Taylor GT, Sanudo-Wilhelmy SA (2006) B vitamins as regulators of phytoplankton dynamics. *EOS* 87

Pintner IJ, Altmeyer VL (1979) Vitamin B_{12}- binder and other algal inhibitors. *JPhycol* 15:391-398

Saito MA, Goepfert TJ, Ritt JT (2008) Some thoughts on the concept of colimitation: Three definitions and the importance of bioavailability. *Limnol and Oceanogr* 53:276-290

Schroeder S, Lawrence AD, Biedendieck R, Rose RS and others (2009) Demonstration that CobG, the monooxygenase associated with the ring contraction process of the aerobic cobalamin (vitamin B12) biosynthetic pathway, contains a Fe-s center and a mononuclear non-heme iron center. *J Biol Chem* 284:4796-4805

Scott JM, Weir DG (1981) The methyl folate trap : A physiological response in man to prevent methyl group deficiency in kwashiorkor (methionine deficiency) and an explanation for folic-acid-induced exacerbation of subacute combined degeneration in pernicious anaemia. *The Lancet* 318:337-340

Sufrin JR, Finckbeiner S, Oliver CM (2009) Marine-derived metabolites of s-adenosylmethionine as templates for new anti-infectives. *Marine Drugs* 7:401-434

Thingstad TF, Zweifel UL, Rassoulzadegan F (1998) P limitation of heterotrophic bacteria and phytoplankton in the northwest mediterranean. *Limnol and Oceanog* 43:99-94

Van Mooy BAS, Fredricks HF, Pedler BE, Dyhrman STand others (2009) Phytoplankton in the ocean use non-phosphorus lipids in response to phosphorus scarcity. *Nature* 458:69-72

Vaughn MW, Tanurdzic M, Lippman Z, Jiang H, Carrasquillo R, Rabinowicz PD (2007) Epigenetic natural variation in *Arabidopsis thaliana. PLoS Biol* 5:e174

Wu J, Sunda W, Boyle E (2000) Phosphate depletion linked to nitrogen fixation and iron suppy in the western north atlantic ocean. *Science* 289:759-762

Appendix A:

Vitamin B_{12} and iron colimitation of phytoplankton growth in the Ross Sea

Vitamin B_{12} and iron colimitation of phytoplankton growth in the Ross Sea. *Limnology and Oceanography.* 2007. E.M Bertrand, M.A. Saito, J. M. Rose,C. R. Riesselman, M. C. Lohan, A.E. Noble, P.A. Lee, and G. R. DiTullio. 52(3) 1079–1093

Limnol. Oceanogr., 52(3), 2007, 1079–1093

Vitamin B_{12} and iron colimitation of phytoplankton growth in the Ross Sea

Erin M. Bertrand[2] *and Mak A. Saito*[1,2]
Marine Chemistry and Geochemistry Department, Woods Hole Oceanographic Institution, Woods Hole, Massachusetts 02543

Julie M. Rose
Department of Biological Sciences, University of Southern California, Los Angeles, California 90089

Christina R. Riesselman
Department of Geological and Environmental Sciences, Stanford University, Stanford, California 94305

Maeve C. Lohan
School of Earth, Ocean and Environmental Sciences, University of Plymouth, Drake Circus, Plymouth PL4 8AA, United Kingdom

Abigail E. Noble
Marine Chemistry and Geochemistry Department, Woods Hole Oceanographic Institution, Woods Hole, Massachusetts 02543

Peter A. Lee and Giacomo R. DiTullio
Grice Marine Laboratory, College of Charleston, Charleston, South Carolina 29412

Abstract

Primary production in the Ross Sea, one of the most productive areas in the Southern Ocean, has previously been shown to be seasonally limited by iron. In two of three bottle incubation experiments conducted in the austral summer, significantly higher chlorophyll *a* (Chl *a*) concentrations were measured upon the addition of iron and B_{12}, relative to iron additions alone. Initial bacterial abundances were significantly lower in the two experiments that showed phytoplankton stimulation upon addition of B_{12} and iron relative to the experiment that did not show this stimulation. This is consistent with the hypothesis that the bacteria and archaea in the upper water column are an important source of B_{12} to marine phytoplankton. The addition of iron alone increased the growth of *Phaeocystis antarctica* relative to diatoms, whereas in an experiment where iron and B_{12} stimulated total phytoplankton growth, the diatom *Pseudonitzschia subcurvata* went from comprising approximately 70% of the phytoplankton community to over 90%. Cobalt additions, with and without iron, did not alter Chl *a* biomass relative to controls and iron additions alone in the Ross Sea. Iron and vitamin B_{12} plus iron treatments caused reductions in the DMSP (dimethyl sulfoniopropionate):Chl *a* ratio relative to the control and B_{12} treatments, consistent with the notion of an antioxidant function for DMSP. These results demonstrate the importance of a vitamin to phytoplankton growth and community composition in the marine environment.

[1] Corresponding author (mak@whoi.edu).
[2] Coauthors.

Acknowledgments

We thank Peter Sedwick for allowing us to utilize his trace-metal-clean fish sampling system and David Hutchins for allowing us to work in his laboratory van and for helpful discussions. We also thank Bettina Sohst and Carol Pollard for nutrient analyses and Tyler Goepfert for help in *Phaeocystis antarctica* culture studies, and Sheila Clifford for comments on the manuscript. Special thanks to the captain, crew, and Raytheon marine and scientific technical staff of the RV *N. B. Palmer*. Thanks also to two anonymous reviewers for helpful comments and suggestions.

This research was supported by NSF grants OPP-0440840, OPP-0338097, OCE-0327225, OCE-0452883, The Carl and Pancha Peterson Endowed Fund for Support of Summer Student Fellows, and the Center for Environmental Bioinorganic Chemistry at Princeton.

The nutritional controls on marine phytoplankton growth have important implications for the regulation of the global carbon cycle. Nitrogen and iron are thought to be the dominant controllers of phytoplankton growth in the oceans, and hence the discovery of a vitamin such as B_{12} having an influence on marine primary productivity would be a finding of significance. The limited information about the biogeochemical cycle of this vitamin suggests that it may be in limiting quantities in seawater. B_{12} is a biologically produced cobalt-containing organometallic molecule, and only select bacteria and archaea possess the capability for B_{12} biosynthesis. As a result, all eukaryotic organisms, from eukaryotic phytoplankton to humans, must either acquire B_{12} from the environment or possess an alternate biochemistry that does not require the vitamin. Removal of B_{12} from the water column has never been directly quantified but likely includes photodegradation

(Carlucci et al. 1969; Saito and Noble unpubl. data), phytoplankton and bacterial uptake, export in sinking biogenic material, and physical transport (Karl 2002). The biogeochemical cycle of vitamin B_{12} must also be inextricably tied to that of cobalt, given the cobalt metal center inside the corrin ring of B_{12}. Both of these substances (B_{12} and cobalt) are found in vanishingly low concentrations in seawater. The few measurements of vitamin B_{12} in seawater reveal extremely low concentrations, in the subpicomolar range, in oceanic regions and higher concentrations in a heavily populated coastal region (Menzel and Spaeth 1962; Okbamichael and Sañudo-Wilhelmy 2004; Sañudo-Wilhelmy et al. 2006). Moreover, B_{12} concentrations have been found to vary seasonally, with a maximum in winter followed by a decline during the spring bloom in the Gulf of Maine and the Sargasso Sea (Menzel and Spaeth 1962; Swift 1981).

Early workers demonstrated a B_{12} requirement in many marine algae and hypothesized that B_{12} could influence marine primary production and phytoplankton species composition (Droop 1957; Guillard and Cassie 1963; Swift 1981). A recent literature review of 326 algal species found more than half to be B_{12} auxotrophs (Croft et al. 2005), similar to earlier estimates that 70% of phytoplankton species require the vitamin (Swift 1981). The enzyme methionine synthase is believed to be responsible for this B_{12} requirement in phytoplankton, where B_{12}-requiring phytoplankton have the B_{12}-dependent methionine synthase (MetH), while nonrequirers have a B_{12}-independent methionine synthase (MetE) (Rodionov et al. 2003; Croft et al. 2005). This enzyme catalyzes the last step in the synthesis of the amino acid methionine. The variation in methionine synthase isoforms is a likely mechanism for the hypothesized influence of vitamin B_{12} concentrations on phytoplankton species composition in the ocean.

The sources of vitamin B_{12} to marine phytoplankton in the natural environment are only beginning to be understood. The arrival of whole genome sequencing suggests distinct niches in the surface ocean. For example, the need for an exogenous source of B_{12} in eukaryotic phytoplankton is evident in the first marine eukaryotic phytoplankton genome, *Thalassiosira pseudonana*: it lacks the vast majority of the B_{12} biosynthesis pathway (Armbrust et al. 2004) and contains the B_{12}-requiring metH for methionine synthesis (Croft et al. 2005), consistent with the culture studies described above. In contrast, the B_{12} biosynthesis pathway is found in many, though not all, bacteria and archaea (Rodionov et al. 2003 and references therein), including all of the currently available genomes of marine cyanobacteria (oxygenic photoautotrophs) such as the globally abundant *Prochlorococcus* and *Synechococcus* (Partensky et al. 1999; Palenik et al. 2003). Interestingly, the genome of the marine heterotrophic bacterium *Pelagibacter ubique* (a cultured isolate from the highly abundant SAR11 clade) lacks the B_{12} biosynthetic pathway as well as that of several other vitamins (Giovannoni et al. 2005), suggesting that this microbe is dependent on an external dissolved supply of vitamins. Early work suggested that marine heterotrophic bacteria could supply phytoplankton with enough B_{12} for growth in culture experiments (Haines and Guillard 1974). More recently, a laboratory study has shown that a eukaryotic phytoplankter (*Porphyridium purpureum*) can acquire vitamin B_{12} through a close bitrophic symbiotic relationship with cell-surface-associated heterotrophic bacterial populations (Croft et al. 2005). Together this information suggests at least two possible sources of B_{12} to eukaryotic marine phytoplankton in the natural environment: uptake of dissolved B_{12} and acquisition of B_{12} through cell-surface symbioses. We hypothesize that in the former scenario, dissolved B_{12} is released through grazing and viral lysis of bacteria and archaea as part of the microbial loop (Azam 1998 and references therein), and this flux may be important in regions where the cyanobacteria are a major component of the ecosystem.

It has been hypothesized that methionine biosynthesis could be involved in controlling the rate of dimethyl sulfoniopropionate (DMSP) production by some phytoplankton (Gröne and Kirst 1992). Because of the role of vitamin B_{12} in methionine synthesis, it is possible that there may be a connection between B_{12} and the cycling of the DMSP in the surface ocean. DMSP serves as the precursor to dimethyl sulfoxide and other atmospherically and climatically important chemical species (Charlson et al. 1987). DMSP is believed to be produced by phytoplankton for several biochemical roles, including as an osmolyte, a cryoprotectant (Stefels 2000), and as an antioxidant (Sunda et al. 2002).

In this study we present experimental data from the Ross Sea, which harbors one of the most extensive phytoplankton blooms in the Southern Ocean (Smith and Nelson 1985) and hence is believed to play a significant role in the global carbon cycle (Arrigo et al. 1999). The phytoplankton community in the Ross Sea is dominated by the colonial haptophyte *Phaeocystis antarctica* and a variety of diatoms such as *Pseudonitzschia subcurvata* (Arrigo et al. 1999). The phytoplankton population varies seasonally (Smith et al. 2000), with *P. antarctica* typically blooming in the spring and early summer, followed by an increase in diatom growth in the later summer (Arrigo et al. 1999 and references therein; Leventer and Dunbar 1996; Smith et al. 2000). Primary production in the Ross Sea has been shown to be controlled by the availability of iron as a micronutrient as well as physical factors such as irradiance (Martin et al. 1990 and references therein; Sedwick et al. 2000; Coale et al. 2003). Alternative micronutrients, such as zinc, have not demonstrated any influence on phytoplankton growth in the Ross Sea (Coale et al. 2003), likely due to relatively high concentrations of these metals near the photic zone. The Ross Sea is a region of biogeochemical significance because of its particularly efficient carbon export (Buesseler et al. 2001), and the high rate of biological production of DMSP by phytoplankton, notably *P. antarctica*. The efficient export of biogenic material in this region (DiTullio et al. 2000; Buesseler et al. 2001) also suggests that incorporated micronutrients such as vitamin B_{12} are being exported rather than recycled within the ecosystem.

The low heterotrophic bacterial production rates (Ducklow and Carlson 1992; Ducklow 2000; Ducklow et al. 2001 and references therein), low grazing rates (Caron et al.

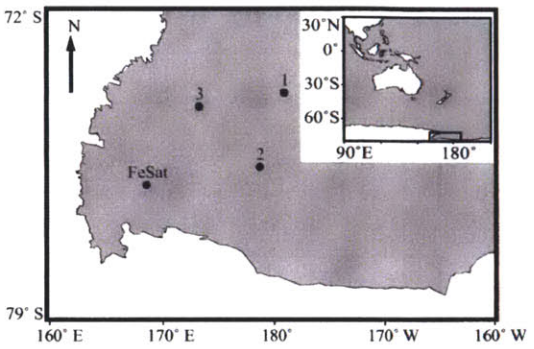

Fig. 1. Location of incubation experiments in the Ross Sea on the Antarctic continental shelf. Incubation 1 was carried out at 74 26′S, 179 23′W; incubation 2 at 76 00′S, 178 66′E; incubation 3 at 74 60′S, 173 20′E; and the iron saturation curve experiment (FeSat) at 076 39′S, 168 58′E.

2000), and absence of cyanobacterial populations in the Ross Sea (Walker and Marchant 1989; Caron et al. 2000; Marchant 2005 and references therein) suggest that this region may lack the potential sources of B_{12} to the marine environment that are common in subtropical and tropical oceanic environments. In addition, the higher intensity of ultraviolet irradiation in the Southern Ocean due to the ozone hole in the austral spring (Cruzen 1992) could conceivably increase photodegradation of the vitamin relative to other areas of the ocean. Hence, the Ross Sea is an ideal location to study the influence of vitamin B_{12} on primary productivity and phytoplankton community structure. In this manuscript, we present experiments demonstrating the colimitation of the Ross Sea by iron and vitamin B_{12} during the austral summer.

Materials and methods

Study area and water collection—All experiments were conducted in the Ross Sea on the CORSACS 1 (Controls on Ross Sea Algal Community Structure) cruise, in the austral summer of 2005 (NBP0601). Experiment 1 was started on 27 December 2005 at 74 26′S, 179 23′W. Experiment 2 was started on 08 January 2006 at 76 00′S, 178 67′E. Experiment 3 was started 16 January 2006 at 74 60′S 173 20′E (Fig. 1). For all experiments, water was collected from 5–8 m depth using a trace-metal-clean Teflon pumping system. Water was dispensed into a 50-liter trace-metal-clean mixing carboy and then into detergent- and acid-washed (0.1% citranox for 48 h, 10% HCl for 7 d, clean pH 2 water rinsed) 1.1- or 4.5-liter polycarbonate bottles. Incubation bottles were filled in a positive-pressure trace-metal-clean environment constructed with laminar flow hoods and plastic sheeting to avoid trace metal contamination.

Shipboard incubations—In general, bottle incubations with additions of 1 or 2 nmol L^{-1} iron, 500 pmol L^{-1} added cobalt, and 100 pmol L^{-1} added vitamin B_{12} were started from three locations within the Ross Sea and carried out for 7–9 d. The length of the experiments was determined by the extent of nutrient depletion in each experiment using shipboard analyses in near-real time. Treatment concentrations were later corrected to account for exact bottle volume. Experiment 1 consisted of six treatments (control, Fe, B_{12}, B_{12}Fe, Co, and CoFe). Duplicate treatments were prepared in 1.1-liter bottles and single treatments were prepared in 4.5-liter bottles at concentrations of 0.9 nmol L^{-1} added iron (Fe), 90 pmol L^{-1} added vitamin B_{12} (B_{12}), 450 pmol L^{-1} added cobalt (Co), 450 pmol L^{-1} added cobalt and 0.9 nmol L^{-1} added iron (CoFe), or 90 pmol L^{-1} B_{12} and 0.9 nmol L^{-1} iron (B_{12}Fe). Experiment 2 consisted of six treatments (control, Fe, B_{12}, B_{12}Fe, Co, and CoFe). Triplicate treatments were prepared in 1.1-liter bottles and single treatments were prepared in 4.5-liter bottles at concentrations of 1.8 nmol L^{-1} added iron (Fe), 90 pmol L^{-1} added vitamin B_{12} (B_{12}), 450 pmol L^{-1} added cobalt (Co), 450 pmol L^{-1} added cobalt and 1.8 nmol L^{-1} added iron (CoFe), or 90 pmol L^{-1} B_{12} and 1.8 nmol L^{-1} iron (B_{12}Fe). Experiment 3 consisted of four treatments (control, Fe, B_{12}, and B_{12}Fe). Triplicate treatments in 1.1-liter bottles were prepared in concentrations of 1.8 nmol L^{-1} added iron (Fe), 90 pmol L^{-1} added vitamin B_{12} (B_{12}), or 90 pmol L^{-1} B_{12} and 1.8 nmol L^{-1} iron (B_{12}Fe). When nitrate levels in any of the treatments dropped below approximately 5 μmol L^{-1}, the experiment was ended.

All three experiments were tightly capped and placed in deckboard flow-through incubators at ~20% ambient light, shielded with neutral density screening. Ambient temperature was maintained by a constant flow of surface seawater through the incubators. In all cases, iron was added as $FeCl_3$ (Fluka) in pH 2 (SeaStar HCl) MilliQ water. Cobalt was added as $CoCl_2$ (Fluka) in pH 2 (SeaStar HCl) MilliQ water. Vitamin B_{12} (Sigma, plant cell culture tested cyanocobalamin, 99%) was added as a solution in Milli-Q water, cleaned for trace metals by running through a column with 2–3 mL of prepared Chelex-100 beads (BioRad) (Price et al. 1988/1989). Student's unpaired *t*-tests were used to establish significant difference between treatments; degrees of freedom = 4 in all analyses and *p* values are presented with each data set.

Nutrient analysis—Nutrients, including N+N, nitrite, phosphate, and silicic acid, were measured in the incubation experiments approximately every 60 h on 0.2-μm-filtered samples from each bottle. Analysis was performed at sea using a Lachat QuickChem Autoanalyzer. Minimum detectable levels were 0.02 μmol L^{-1} for phosphate, 0.16 μmol L^{-1} for N+N, 0.03 μmol L^{-1} for nitrite, and 0.18 μmol L^{-1} for silicic acid.

Biomass analysis—Total chlorophyll *a* (Chl *a*) was measured approximately every 60 h using the nonacidified fluorometric method of JGOFS (Joint Global Ocean Flux Study), with a Turner Designs TD700 fluorometer (Whatman GF/F filtered). Bacteria and archaea were enumerated using a previously published method involving DAPI (4′-6-diamidino-2-phenylindole) staining (Porter and Feig,

1980). Diatoms were identified by transmitted light microscopy at ×400 and ×1000 magnification on gridded mixed cellulose ester membrane filters with a 0.45 μm pore size. Phytoplankton were enumerated by 400-individual counts, using standard epifluoresence microscope techniques at ×1000 magnification on 0.2 μm pore size polycarbonate membrane filters. All epifluorescence slides were filtered from 10-mL samples to facilitate visual comparison.

In the iron treatments in incubation 1, atypically high *P. antarctica* populations combined with generally high phytoplankton populations made phytoplankton cell enumeration by our method problematic. These atypical samples were found to have heterogeneous cell distribution across the slide, with diatoms adhering to numerous irregularly dispersed *Phaeocystis* colonies, resulting in large standard deviations for cell counts, but low standard deviations for community composition. In addition, the extremely dense cell concentrations in incubation 1 reduced the count area necessary for enumeration and identification of 400 cells. Given that the *P. antarctica* component increases relative to diatoms only in the Fe addition treatment, that *P. antarctica* colonies greatly increased sample heterogeneity, and that high cellular densities resulted in fewer fields being counted to obtain species composition, we infer that our random field counting method underestimated true cell concentrations in these samples.

Total iron measurements—Total dissolved Fe concentrations were measured using adsorptive cathodic stripping voltammetry (ACSV) based on the method described by Rue and Bruland (1995). Reagents were prepared as follows: A 5 mmol L^{-1} salicylaldoxime (SA: Aldrich, ≥98%) solution was prepared in quartz-distilled methanol (Q-MeOH) and stored in the refrigerator. A final concentration of 25 μmol L^{-1} SA was used for total dissolved Fe measurements. A 1.5 mol L^{-1} borate buffer was prepared as previously described (Ellwood and Van Den Berg 2000). Fe standards were prepared from dilution of a 1,000 parts per million atomic adsorption standard with pH 1.7 quartz-distilled hydrochloric acid (Q-HCl).

The voltammetric system consisted of Princeton Applied Research (PAR) 303A interfaced with a computer-controlled μAutolabII potentiostat/galvanostat (Eco Chemie). The working electrode was a "large" mercury drop (2.8 mm^2), the reference electrode was Ag : saturated AgCl, saturated KCl, and the counterelectrode was a platinum wire. During ACSV analyses, all samples were contained in fluorinated ethylene propylene–Teflon voltammetric cell cups, and stirred with a PTFE (polytetraflrethylane) – Teflon-coated stirring bar driven by a PAR magnetic stirrer (model 305).

Filtered samples were acidified to pH 1.7 with 4 mL L^{-1} Q-HCl. Samples were microwaved 2 × 15 s at 1,100 W to release dissolved Fe from ambient organic ligands (Bruland et al. 2005), neutralized once with cool 1 mol L^{-1} Q-NH_4OH, and buffered to pH 8.2 with the borate buffer. Once buffered, Fe and SA additions were made and following ACSV analysis Fe concentrations were determined from a linear regression of the standard addition curve. The detection limit for the ACSV method is 0.02 nmol L^{-1}, calculated from three times the standard deviation of a 0.05 nmol L^{-1} Fe addition, as no peak is observed in either Milli-Q or ultraviolet (UV)-oxidized seawater (from which trace metals and metal-chelating organic ligands are removed from seawater [Donat and Bruland 1988]) at deposition times of up to 600 s. Deposition times for sample analyses here were between 10 and 300 s, depending on ambient Fe and ligand concentrations.

Cobalt total concentration and speciation measurements—Total cobalt and cobalt speciation analyses were performed by ACSV using a Metrohm 663 hanging mercury drop electrode and Eco-Chemie μAutolab III as described previously (Saito and Moffett 2002; Saito et al. 2005). Briefly, cobalt total measurements were made by first UV-irradiating the seawater for 1 h to destroy the strong organic ligands that bind cobalt. The seawater (9.25 mL) was then analyzed with 0.2 mmol L^{-1} dimethylglyoxime, 0.113 mol L^{-1} sodium nitrite, and 2.5 mmol L^{-1} *N*-(2-hydroxyethy)piperazine-*N*-(3-propanesulfonic acid), as cobalt ligand, catalyst, and buffer respectively. Cobalt speciation was measured similarly but without UV irradiation and with overnight equilibration with the dimethylglyoxime ligand. Cobalt was then measured using 25 pmol L^{-1} standard additions, deposition for 90 s at −0.6 V, and linear sweep stripping from −0.6 V to −1.4 V at 10 V s^{-1}.

Iron blank in vitamin stock—Total iron in the vitamin B_{12} stock was measured using the above technique through dilution into seawater with a known total iron concentration 7 d after it was first used to prepare incubation 1. After use in incubation 1, the B_{12} stock had been used outside a clean area for experiments not described here. At that time, it was found to contain 76 pmol L^{-1} total iron for every 100 pmol L^{-1} vitamin B_{12}. The vitamin stock was then treated with Chelex-100 and the iron concentration was subsequently found to be 29 pmol L^{-1} for every 100 pmol L^{-1} vitamin B_{12}. This stock was then used in incubations 2 and 3. Since the stock had been carefully treated with Chelex-100 and not used outside a clean area before its use with incubation 1, we assume the initial B_{12} solution had an iron concentration of 29 pmol L^{-1} for every 100 pmol L^{-1} vitamin B_{12} when used in all three incubations, although the 76 pmol L^{-1} concentration would not alter the interpretation of experiments presented here. The small amounts of iron added with the B_{12} solution only increased the iron in the iron-B_{12} treatments marginally (from 0.89 nmol L^{-1} to 0.92 nmol L^{-1} iron (Fe) and (B_{12}Fe) iron concentrations in experiment 1, and from 1.81 nmol L^{-1} to 1.84 nmol L^{-1} (Fe) and (B_{12}Fe) iron concentrations in experiments 2 and 3).

Iron saturation curve experiment—An iron saturation curve was constructed (after Hutchins et al. 2002) to demonstrate that this small iron addition with the B_{12} stock could not account for additional phytoplankton growth.

Chl *a* net specific growth rate as a function of total dissolved iron concentration (nmol L^{-1}) was calculated at 76 39′S, 168 58′E on 18 January 2006 where total ambient dissolved iron concentration was 0.09 nmol L^{-1}. This experiment was performed at similar geographical location to the incubation studies (Fig. 1) and with similar initial nutrient profile and Chl *a* concentrations (Table 1). Water was collected with a 10-liter Go-Flo bottle (General Oceanics) from 10 m depth. This water was dispensed, using trace-metal-clean techniques, into 60-mL polycarbonate bottles, trace-metal-cleaned as described above. Duplicate unamended controls and duplicates of 0.2 nmol L^{-1}, 0.45 nmol L^{-1}, 0.9 nmol L^{-1}, and 2.5 nmol L^{-1} added iron were placed in a sealed plastic bag in deckboard flow-through incubators for 7 d at ~20% ambient light, shielded with neutral density screening. At the end of the 7-d incubation period, 50 mL of each bottle were used to measure total Chl *a*. Chl *a* net specific growth rate (μ) was calculated using standard growth rate equations. The relation between iron concentration and Chl *a* net specific growth rate was assumed to follow the Michaelis–Menten equation and the data were fit to this equation using a nonlinear regression.

DMSP measurements—Samples for DMSP were collected following the small-volume gravity filtration procedure of Kiene and Slezak (2006). In a cold room held at 0°C, a small aliquot (≤20 mL) of each sample was gravity-filtered through a Whatman GF/F filter, recollected, and acidified with 100 μL of 50% sulfuric acid for the determination of dissolved DMSP. A second unfiltered aliquot of sample was acidified with 100 μL of 50% sulfuric acid for the measurement of total DMSP. Particulate DMSP was calculated as the difference between the total and dissolved DMSP fractions. All DMSP samples were base-hydrolyzed in strong alkali (>1 mol L^{-1} sodium hydroxide; [White 1982]) and analyzed for dimethyl sulfide (DMS) using a cryogenic purge and trap system coupled to either a Hewlett-Packard 6890 or 5890 Series II gas chromatograph fitted with flame photometric detector (DiTullio and Smith 1995).

Vitamin B_{12} uptake—^{57}Co-labeled cyanocobalamin was used to measure the rate of vitamin B_{12} uptake by the community at 30 m depth at 74 40′S, 168 52′E on 20 January 2006. Uptake by the greater-than-2-μm-size fraction and greater-than-0.2-μm-size fraction was measured.

Radiolabeled vitamin B_{12} (^{57}Co B_{12}) was isolated from Rubratope57 pills (Radiopharmacy). The gelatin capsule coating was removed from the pill and the remaining sponge, laden with ^{57}Co B_{12}, was placed in 5 mL of pH 2.5 Milli-Q water (HCl) and mixed until the sponge was pulverized. The mixture was left to stand protected from light at 4°C for 24 h. The liquid was decanted to remove any large remaining pieces of sponge. The pH of the solution was raised to 7 with NaOH and was cleaned for inorganic ^{57}Co and other trace metals by running through a column with 2–3 mL of Chelex-100 beads (BioRad) and

Table 1. Initial physical, chemical, and biological conditions at each location where an experiment was started. <MDL is less than minimum detectable limit. N.M. is parameter not measured. Where applicable, ±1 SD is indicated.

	Latitude	Longitude	NO_3 (μmol L^{-1})	PO_4 (μmol L^{-1})	SiO_2 (μmol L^{-1})	NH_4 (μmol L^{-1})	Total Fe (nmol L^{-1})	Total Co (pmol L^{-1})	Labile Co (pmol L^{-1})	Chl *a* (μg L^{-1})	Bacteria and archaea (cells mL^{-1})	Phytoplankton (cells mL^{-1})
Incubation 1	074°26′S	179°23′W	19.89	1.36	63.64	0.17	0.31	31.0	30.1	4.319	$6.47\times10^4\pm7.2\times10^3$	1.4×10^4
Incubation 2	076°00′S	178°67′E	20.00	1.33	62.00	0.12	0.11	38.8	8.4	1.489	$9.86\times10^5\pm1.2\times10^4$	$0.4\times10^4\pm0.1\times10^4$
Incubation 3	074°60′S	173°20′E	22.98	1.63	62.00	0.49	0.13	51.0	21.0	0.886	$1.76\times10^5\pm3.0\times10^4$	0.2×10^4
Saturation experiment	076°39′S	168°58′E	13.37	1.49	74.75	<MDL	0.09	N.M.	N.M.	1.470	N.M.	N.M.

filtered through a 0.2-μm sterile filter to remove any remaining sponge particles. The concentration of ^{57}Co B_{12} in this stock was measured by gamma detection and normalized to $^{57}CoCl_2$ standards using Canberra Germanium Gamma detector.

Six identical unfiltered seawater samples were taken from 30 m depth using a trace-metal-clean Go-Flo bottle (General Oceanics) and dispensed into six acid- and detergent-cleaned 125-mL polycarbonate bottles. Immediately after dispensing the water (within 1 h of collection), approximately 0.09 pmol L^{-1} ^{57}Co B_{12} and 43 pmol L^{-1} unlabeled vitamin B_{12} were added to each and the bottles were placed in a deckboard incubator. Exact concentrations were later calculated for individual replicates on the basis of slight variations in volume associated with each bottle. After 24 h, the bottle incubations were measured for volume and filtered at 48 kPa, three replicates through a 2-μm polycarbonate filter membrane and three through 0.2-μm polycarbonate filter membrane. The filters were rinsed with 1–2 mL of 0.4-μm-filtered seawater each. The filter was centered and placed in a tight-lid petri dish (Fisher Scientific) and sealed with Parafilm.

^{57}Co radioactivity on each filter was determined using a Canberra Germanium Gamma detector. Counts per minute at 122 keV were corrected for decay and normalized to percentage uptake per day, calculated by dividing the activity on each filter by the total activity added. Since natural concentrations of vitamin B_{12} in pristine environments are believed to be subpicomolar (Menzel and Spaeth 1962; Swift 1981; Okbamichael and Sañudo-Wilhelmy 2004) and ^{57}Co-labeled B_{12} was also added in subpicomolar concentrations, the total concentration of B_{12} should be equivalent to the amount of unlabeled B_{12} added in these experiments, approximately 43 pmol L^{-1}. Using the percentage uptake of labeled B_{12} and this total concentration, total vitamin B_{12} uptake per day was calculated for each filter size. The 0.2-μm filter was considered total community uptake. The 2-μm filter represented uptake from the >2-μm-size fraction, whereas the 0.2-μm filter minus the 2-μm filter represented the 0.2-μm- to 2-μm-size fraction of the community.

Results

Three bottle incubation experiments were conducted examining the influence of iron, vitamin B_{12}, and cobalt in the Ross Sea (locations shown in Fig. 1, with initial conditions described in Table 1). Nutrients, including N+N, nitrite, phosphate, and silicic acid, as well as the micronutrients cobalt and iron, were measured over the course of these incubations. Phytoplankton growth and community composition was measured by Chl *a* fluorescence and epifluorescence microscopy. Bacterial and archaeal abundance was analyzed by microscopy, and DMSP was measured over the course of the experiments. In all cases, iron addition yielded increased phytoplankton growth. In two of three cases, vitamin B_{12} addition along with iron resulted in greater stimulation of phytoplankton growth than iron alone, and in no case did vitamin B_{12} alone result in significant stimulation. Where bacterial and archaeal abundance was highest, the least stimulation upon B_{12} addition with iron was seen; where it was lowest, the greatest stimulation was seen.

B_{12} enrichment bottle incubation results—In all three bottle incubation experiments, iron additions caused a significant ($p < 0.01$) increase in phytoplankton growth relative to unamended controls, shown by maximum Chl *a* concentration and nutrient consumption, as is consistent with previous studies in the Ross Sea (Martin et al. 1990; Sedwick and DiTullio 1997; Sedwick et al. 2000). Trends in phytoplankton cell concentrations agreed with those in Chl *a* concentration except in incubation 1, where enumeration of cells in the iron treatment was complicated by significant *Phaeocystis* colony formation (see Methods, Biomass analysis, and Table 2).

In two of the three incubation experiments (experiments 1 and 3), combined B_{12} and iron amendments, hereafter referred to as B_{12}Fe, resulted in a significant increase in phytoplankton growth above that seen in the iron treatments, as evidenced by maximum Chl *a* concentration ($p < 0.01$; final time point results summarized in Fig. 2), macronutrient consumption (Fig. 3A–H), and phytoplankton cell concentration (Table 2). This B_{12}Fe stimulation was not observed in one of the three experiments (experiment 2; Figs. 2, 3; Table 2). Additions of vitamin B_{12} alone did not result in a significant ($p > 0.05$) stimulation of Chl *a* relative to the unamended control in all three experiments. These results suggest that the Ross Sea polynya in late austral summer is limited by iron, and variably colimited by iron and the B_{12} vitamin.

Changes in community composition, nutrient depletion, and DMSP production—The Fe-B_{12} colimitation effect observed in the Ross Sea is evident in all of the relevant biological measurements from experiments 1 and 3. There were statistically significant increases in Chl *a* concentrations, nearly doubling in experiment 1 and over 20% higher in experiment 3 relative to iron treatments (Figs. 2, 3A–D, I–L). This increase is associated primarily with an increase in the diatom species *P. subcurvata*, which increased from 73% of the population to over 92% in experiment 1, and from 59% to 74% in experiment 3 (Table 3). In contrast, in these experiments (1 and 3) the *P. antarctica* component of the community decreased in all treatments except the iron-only addition where it increased from 14% to 34% in incubation 3 and remained at 28% in incubation 1 (Table 2). These results indicate that combined B_{12}Fe additions can influence the growth rates of phytoplankton as well as alter the phytoplankton species composition relative to iron-only additions and unamended controls.

The diatom community in incubation experiment 2, where no B_{12}Fe stimulation was observed, was substantially different from that in incubations 1 and 3. Notably, *Fragilariopsis cylindrus* and *Chaetoceros* spp. comprised a much greater fraction of the diatom community than in incubations 1 and 3 (Table 3). This may have been due to variable inputs from pack ice, as these diatoms are known to form a large component of Antarctic pack ice

Table 2. Community composition (shown in relative abundance of diatoms and *Phaeocystis* with 1 SD where applicable) displayed with bacterial and phytoplankton abundances in the initial conditions (t_0) and at the final time points (t_f) (160, 223, and 180 h respectively) in the unamended (Control) treatment, added vitamin B_{12} (B_{12}), added cobalt (Co), added iron (Fe), added iron and cobalt (CoFe), and added iron and vitamin B_{12} (B_{12}Fe) from incubation experiments 1, 2, and 3. N.M. is parameter not measured.

	Phaeocystis antarctica: Percentage of total community	Total diatoms: Percentage of total community	Phytoplankton cells mL^{-1}	Bacterial and archaeal cells mL^{-1}
Incubation 1				
t_0	27.8±5.2%	72.3±5.5%	1.4×10^4	$6.47\times10^4\pm7.2\times10^3$
Control (t_f)	18.2±3.2%	81.8±4.2%	$7.45\times10^4\pm2.5\times10^4$*	$1.44\times10^5\pm1.6\times10^4$
B_{12} (t_f)	15.6±4.9%	84.4±4.3%	$5.86\times10^4\pm4.0\times10^4$*	$1.76\times10^5\pm1.3\times10^4$
Co (t_f)	N.M.	N.M.	N.M.	$1.36\times10^5\pm1.3\times10^4$
Fe (t_f)	28.7±4.8%	71.2±6.1%	$7.08\times10^4\pm1.3\times10^4$*	$3.47\times10^5\pm3.5\times10^4$
CoFe (t_f)	N.M.	N.M.	N.M.	$3.78\times10^5\pm3.2\times10^4$
B_{12}Fe (t_f)	5.48±1.3%	94.5±1.5%	$18.0\times10^4\pm2.9\times10^4$	$2.64\times10^5\pm4.7\times10^4$
Incubation 2				
t_0	35.9±4.3%	64.1±8.2%	$0.4\times10^4\pm0.1\times10^4$	$9.86\times10^5\pm1.2\times10^4$
Control (t_f)	16.1±4.4%	84.3±7.9%	$1.30\times10^4\pm0.2\times10^4$	$1.17\times10^6\pm1.5\times10^5$
B_{12} (t_f)	17.9±3.2%	82.1±5.8%	$1.39\times10^4\pm0.1\times10^4$	$1.21\times10^6\pm1.7\times10^5$
Co (t_f)	N.M.	N.M.	N.M.	$1.41\times10^6\pm1.6\times10^5$
Fe (t_f)	13.0±2.5%	87.0±7.9%	$3.45\times10^4\pm0.9\times10^4$	$1.17\times10^6\pm8.8\times10^4$
CoFe (t_f)	N.M.	N.M.	N.M.	$1.09\times10^6\pm9.0\times10^4$
B_{12}Fe (t_f)	17.9±0.7%	82.1±3.6%	$3.35\times10^4\pm0.05\times10^4$	$1.11\times10^6\pm1.5\times10^5$
Incubation 3				
t_0	13.6%	86.4%	0.2×10^4	$1.76\times10^5\pm3.0\times10^4$
Control (t_f)	14.13±6.1%	85.9±9.6%	$3.31\times10^4\pm0.1\times10^4$	$2.90\times10^5\pm2.4\times10^4$
B_{12} (t_f)	12.7±1.9%	87.2±3.0%	$3.50\times10^4\pm0.5\times10^4$	$3.02\times10^5\pm1.0\times10^4$
Fe (t_f)	24.3±4.6%	75.7±3.8%	$7.32\times10^4\pm0.6\times10^4$	$3.09\times10^5\pm3.3\times10^4$
B_{12}Fe (t_f)	13.3±5.0%	86.7±5.4%	$8.94\times10^4\pm1.1\times10^4$	$3.96\times10^5\pm1.2\times10^4$

* Approximate representation only; high *Phaeocystis* abundance prevented accurate cell counts by our method (see Methods, Biomass analysis).

communities (Leventer and Dunbar 1996 and references therein; Arrigo et al. 2003). Communities in open water near melting sea ice have been shown to mirror the assemblages in sea ice (Leventer and Dunbar 1996). This substantially different community yielded a very different response to the incubation amendments. Iron addition alone did not yield a relative increase in *Phaeocystis* populations as seen in incubations 1 and 3, but rather favored an increase in *P. subcurvata* and *F. cylindrus* populations relative to the control. Most strikingly, there was no increase in phytoplankton growth in the iron and B_{12} treatment relative to the iron treatment alone. This result cannot likely be explained by a difference in community structure only, as the species that responded to B_{12}Fe supplementation most (*P. subcurvata*) in incubations 1 and 3 were still present in the incubation 2 community, but did not yield the same response. An alternative explanation for the geographical variability in B_{12} effects is the relative abundances of bacteria and archaea as a source of the vitamin (see Bacterial section below).

The depletion of seawater nutrients is also indicative of phytoplankton species composition changes and changes in growth parameters. In the B_{12}Fe-supplemented incubations in experiments 1 and 3, nutrient drawdown was enhanced over the control and B_{12}-alone additions (Fig. 3). Notably, the silicic acid drawdown by B_{12} and iron treatments was significantly more ($p < 0.01$) in incubations 1 and 3 relative to iron treatments. Diatoms are the major users of silicic acid in the Ross Sea, and hence this result is consistent with the measurements of increasing *P. subcurvata* described above. The consumption of the micronutrients cobalt and iron were strongly influenced by iron additions but did not show differences between the B_{12}Fe additions and iron-only treatments (Table 4). Iron drawdown in all three incubation experiments was substantial; for example, in experiment 1 iron-supplemented treatments were depleted to 0.09 and 0.08 nmol L^{-1}, whereas the control and B_{12} additions were depleted to 0.13 and 0.18 nmol L^{-1}. Cobalt drawdown was also substantial in the treatments where iron was added, with an undetectable level (close to the 3 pmol L^{-1} detection limit) of labile cobalt present in the Fe and B_{12}Fe treatments (Table 4).

DMSP is produced by phytoplankton such as *Phaeocystis* for several biochemical roles including as an osmolyte, a cryoprotectant (Stefels 2000), and as an antioxidant (Sunda et al. 2002). Our incubation experiments are consistent with previous observations of DMSP cycling where nutrient stress by iron and carbon dioxide have been shown to induce DMSP production against the resulting oxidative stress experienced by the cell (Sunda et al. 2002), and iron stress has been shown to result in increased DMSP production in *P. antarctica* (Stefels and Leeuwe 1998). In our experiments, total DMSP (dissolved and particulate) increased as a result of iron additions (both Fe and B_{12}Fe, Fig. 4 and Table 5). When normalized to Chl *a* $DMSP_P$ (particulate DMSP) decreased, likely indicating alleviation of micronutrient (iron) limitation-induced oxidative stress.

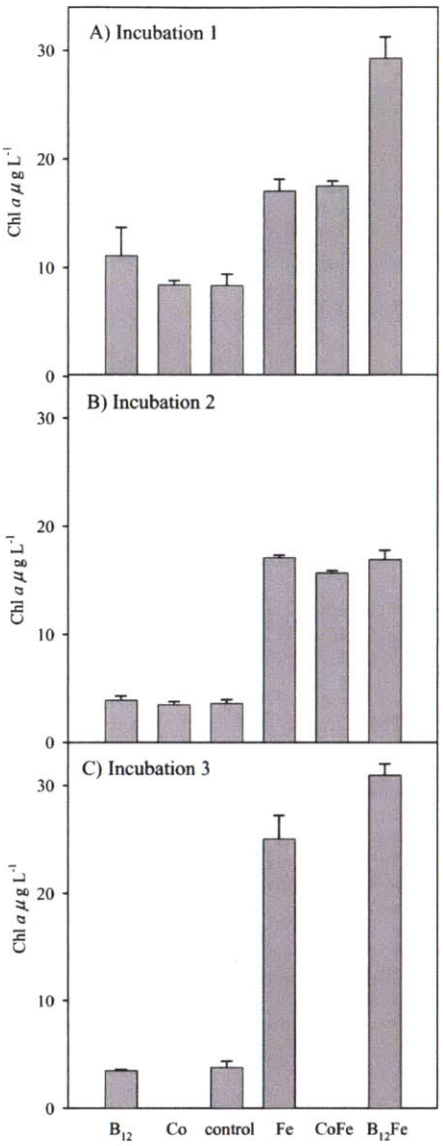

Fig. 2. Total Chl *a* concentrations in the unamended (control) treatment, added vitamin B_{12} (B_{12}), added cobalt (Co), added iron (Fe), added iron and cobalt (CoFe), and added iron and vitamin B_{12} (B_{12}Fe) from (A) incubation experiment 1 after 137 h of incubation, (B) incubation experiment 2 after 223 h, and (C) incubation experiment 3 after 180 h. Different incubation times were adopted to maximize the length of each experiment while preventing major nutrients (nitrate, phosphate, silicic acid) from becoming limiting. Values shown are means of triplicate treatments in 1.1- or 4.5-liter bottles (experiment 1) or triplicate treatments in 1.1-liter bottles (experiments 2 and 3) with error bars representing 1 SD. In all incubations, the addition of iron resulted in significantly more Chl *a* (t = 9.9, 54, 16; $p = 6 \times 10^{-4}$, 7×10^{-7}, 8×10^{-5} respectively, t-test). In incubations 1 and 3, there is a significant difference between Chl *a* in the B_{12}Fe treatment versus the Fe treatment: t = 9.3, 4 .2; $p = 7 \times 10^{-4}$, 0.01. B_{12} treatments did not show any significant stimulation relative to the control in any of the three incubation experiments: t = 1.7, 0.9, 0.8; p = 0.2, 0.4, 0.5.

Of the major phytoplankton species in the Ross Sea, *Phaeocystis* is believed to be an important producer of DMSP (DiTullio and Smith 1995). Methionine is hypothesized to control the rate of DMSP production by some phytoplankton (Gröne and Kirst 1992), and as described above, vitamin B_{12} has been implicated in methionine production and utilization. When $DMSP_P$ production is normalized to estimated *Phaeocystis* cellular densities, it tends to be higher in B_{12} additions (with and without added iron) than in Fe-only treatments in all incubation experiments (data not shown), despite no obvious influence of B_{12} when $DMSP_P$ is normalized to Chl *a*, with the possible exception of incubation 2 (Fig. 4). One possible explanation for these observations is that B_{12} is influencing methionine biosynthesis in *Phaeocystis*, and methionine availability is in turn influencing DMSP production rates (Gröne and Kirst 1992). As a result, higher B_{12} abundances in seawater could potentially lead to increased DMSP production. This creates an interesting dichotomy of competing mechanisms where iron additions decrease DMSP production via a supposed reduction of oxidative stress, but alleviation from B_{12} limitation would result in subsequent recovery of methionine biosynthesis and allow increases in DMSP production. The possibility of these competing mechanisms in DMSP production should be investigated through future laboratory experiments.

Bacterial and archaeal abundances—Variation in bacterial and archaeal abundance (hereafter referred to as bacterial abundance for simplicity) is consistent with the geographical variability we observe in Fe-B_{12} colimitation in the Ross Sea where the degree of B_{12} stimulation is negatively related to bacterial abundance. Initial bacterial abundances were much higher in experiment 2 (986,000 ± 12,300 cells mL^{-1}) where no stimulatory B_{12} effect was observed, relative to initial abundances in experiments 1 and 3 (64,700 ± 7,180 and 176,000 ± 29,900 cells mL^{-1} respectively) where B_{12} stimulation of growth was observed (see Fig. 5, Tables 1, 2). In addition, B_{12}Fe treatment stimulated more growth in experiment 1, where bacterial numbers were lowest, than in experiment 3, where numbers were slightly higher (Fig. 5). This is consistent with the idea that bacteria provide vitamin B_{12} to phytoplankton: in experiment 2 there seemed to be enough bacteria to supply an abundance of the vitamin, whereas in experiments 1 and 3, the increase in phytoplankton biomass upon iron addition likely exhausted the vitamin B_{12} naturally available until it became limiting. In fact, the initial abundance

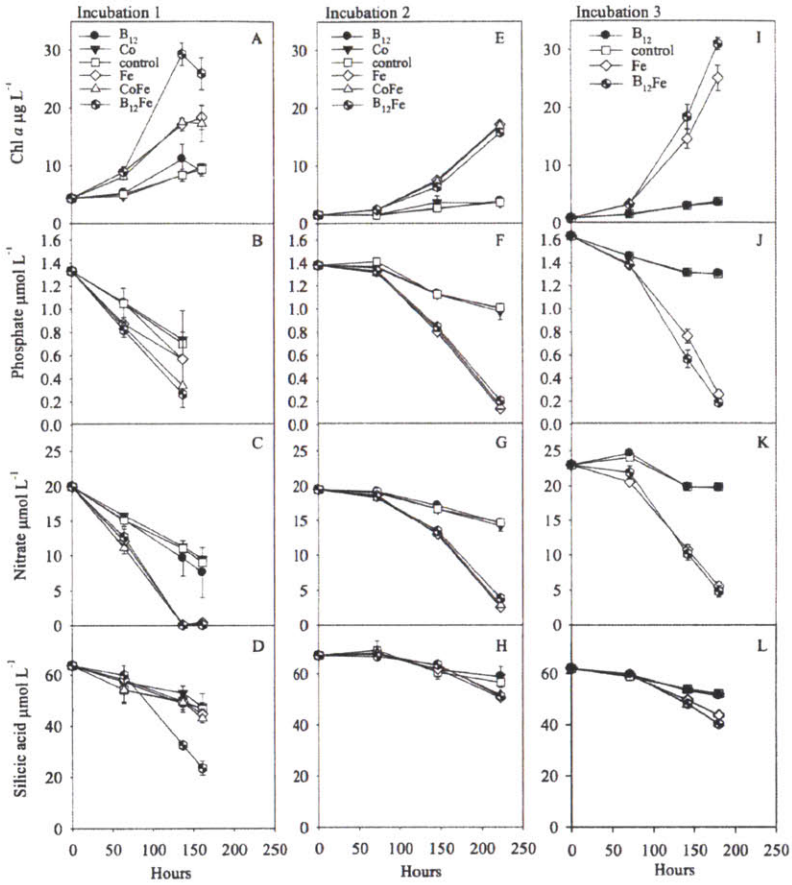

Fig. 3. (A–D): Total chloropyll *a* (Chl *a*), phosphate, dissolved nitrate, and silicic acid over time for incubation 1. Concentrations of these variables are shown for the unamended (control) treatment, 90 pmol L^{-1} added vitamin B_{12} (B_{12}), 450 pmol L^{-1} added cobalt (Co), 0.9 nmol L^{-1} added iron (Fe), 450 pmol L^{-1} added cobalt and 0.9 nmol L^{-1} added iron (CoFe), and 0.90 nmol L^{-1} added iron and 90 pmol L^{-1} vitamin B_{12} ($B_{12}Fe$) from incubation 1. Values shown are means of triplicate treatments (1.1- and 4.5-liter bottles) with error bars representing standard deviations. Values for phosphate at 161 h were omitted because of an observed systematic error in this analysis on the day these values were measured. (E–H) Total Chl *a*, phosphate, dissolved nitrate, and silicic acid over time for incubation 2. Concentrations of these variables are shown for the unamended (control) treatment, 90 pmol L^{-1} added vitamin B_{12} (B_{12}), 450 pmol L^{-1} added cobalt (Co), 1.8 nmol L^{-1} added iron (Fe), 450 pmol L^{-1} added cobalt and 1.8 nmol L^{-1} added iron (CoFe), and 1.8 nmol L^{-1} added iron and 90 pmol L^{-1} vitamin B_{12} ($B_{12}Fe$). Values shown are means of triplicate treatments (1.1-liter bottles) with error bars representing standard deviations. (I–L) Total Chl *a*, phosphate, dissolved nitrate, and silicic acid over time for incubation 3. Concentrations of these variables are shown for the Fe, B_{12}, control, and $B_{12}Fe$ treatments in the same concentrations as incubation 2. Values shown are means of triplicate treatments (1.1-liter bottles) with error bars representing 1 SD.

in incubation 2 was in line with the highest values observed in the Ross Sea (Ducklow et al. 2001 and references therein). Bacterial production of B_{12} has been shown to be an effective source of vitamin B_{12} to phytoplankton cultures (Haines and Guillard 1974; Croft et al. 2005).

Size-fractionated uptake experiments from the Ross Sea—Experiments were performed to discern what size fraction of the community in the Ross Sea was responsible for the majority of the vitamin B_{12} uptake in this study area and confirm the ability of phytoplankton to take up dissolved vitamin B_{12}. Size-fractionated vitamin B_{12} uptake in the surface waters as measured by addition of 43 pmol L^{-1} cyanocobalamin and trace amounts of ^{57}Co-labeled cyanocobalamin showed that 2.08 ± 0.05 pmol L^{-1} d^{-1} B_{12} was utilized by the >2-µm-size fraction, while the smaller (0.2–2 µm) size fraction utilized 0.88 ± 0.27 pmol L^{-1} d^{-1} B_{12}. Since this smaller-size fraction is comprised mostly of

Table 3. Relative abundance of diatoms in total community in the initial conditions (t_0) and at the final time point (t_F) (160, 223, and 180 h respectively) in the unamended (Control) treatment, added vitamin B_{12} (B_{12}), added iron (Fe), and added iron and vitamin B_{12} (B_{12}Fe) from incubation experiments 1, 2, and 3. Rare indicates where the indicated diatom comprised <0.5% of the total community. N.M. is parameter not measured.

	Pseudonitzchia subcurvata	*Fragilariopsis cylindrus*	*F. curta*	*Chaetoceros* spp.*	*Pseudonitzschia* sp.	*Fragiliaropsis* sp.	*Corethron pennatum*
Incubation 1							
t_0	Dominated	N.M.	N.M.	N.M.	N.M.	N.M.	N.M.
Control (t_F)	77.2%±3.2%	3.86%±2.7%	Rare	0.62%±0.7%	0	0	Rare
B_{12} (t_F)	79.9%±4.1%	3.95%±1.2%	0	Rare	Rare	0	0
Fe (t_F)	66.3%±5.6%	3.34%±1.1%	0	1.57%±1.9%	0	0	Rare
B_{12}Fe (t_F)	92.7%±1.1%	1.10%±0.8%	0	0.72%±0.7%	0	0	0
Incubation 2							
t_0	15.6%±2.5%	11.3%±0.5%	1.1%±1.1%	34.2%±7.7%	0.60%±0.5%	0	Rare
Control (t_F)	14.9%±2.3%	35.3%±3.2%	0.67%±0.7%	29.4%±6.7%	0.95%±0.7%	0.89%±1.3%	Rare
B_{12} (t_F)	14.1%±2.1%	30.9%±2.7%	0.56%±0.5%	33.3%±4.5%	0.88%±0.9%	0	Rare
Fe (t_F)	26.5%±3.3%	36.4%±1.1%	1.01%±0.5%	21.0%±6.9%	Rare	0	Rare
B_{12}Fe (t_F)	18.7%±2.3%	43.7%±0.6%	0.85%±0.3%	16.1%±2.2%	2.17%±1.4%	0	0
Incubation 3							
t_0	58.90%	12.70%	1.15%	10.37%	Rare	0	0.92%
Control (t_F)	76.9%±9.2 %	6.63%±2.3%	0.73%±0.9%	0.81%±0.4%	Rare	0	Rare
B_{12} (t_F)	79.0%±0.8%	7.37%±2.8%	0	Rare	Rare	0	Rare
Fe (t_F)	62.4%±3.2%	9.7%±1.6%	0	2.61%±1.1%	Rare	0	0
B_{12}Fe (t_F)	73.8%±4.7%	10.2%±2.2%	Rare	2.12%±1.6%	0	0	Rare

	Nitzschia stellata	*Plagiotropis gaussii*	*Trichotoxon reinboldii*	*Eucampia antarctica*	*Asteromphalus parvulus*	Other centrics	Other pennates
Incubation 1							
t_0	N.M.	N.M.	N.M.	N.M.	N.M.	N.M.	N.M.
Control (t_F)	0	0	0	0	0	0	0
B_{12} (t_F)	0	0	0	0	0	0	0
Fe (t_F)	0	0	0	0	0	0	0
B_{12}Fe (t_F)	0	0	0	0	0	0	0
Incubation 2							
t_0	Rare	0	Rare	0	Rare	Rare	Rare
Control (t_F)	Rare	Rare	Rare	Rare	Rare	0	0.62%±0.7%
B_{12} (t_F)	Rare	0.80%±0.1%	Rare	0	Rare	Rare	0.87%±0.8%
Fe (t_F)	Rare	Rare	Rare	0	0	Rare	Rare
B_{12}Fe (t_F)	Rare	Rare	Rare	Rare	Rare	0	Rare
Incubation 3							
t_0	Rare	0	0	0	0	0.69%	0.92%
Control (t_F)	0	0	0	0	0	0	Rare
B_{12} (t_F)	0	0	0	0	Rare	0	Rare
Fe (t_F)	0	0	0	0	Rare	Rare	Rare
B_{12}Fe (t_F)	Rare	0	0	0	0	0	0

* Identified under light microscopy as *C. criophilum*, *C. dichaeta*, and small specimens similar to *C. neglectus*.

Table 4. Metal (cobalt and iron) concentrations at final time points of incubation experiments 1, 2, and 3 (160, 223, and 180 h respectively) in the unamended (Control) treatment, added vitamin B_{12} (B_{12}), added cobalt (Co), added iron (Fe), added iron and cobalt (CoFe), and added iron and vitamin B_{12} (B_{12}Fe). N.M. indicates no measurement made; ND indicates none detected. Measurements were made on one replicate bottle only except the incubation 3 cobalt determinations, which were measured in all three replicates. Values presented are averages ± 1 SD (where available).

	Total Fe (nmol L^{-1})	Total Co (pmol L^{-1})	Labile Co (pmol L^{-1})
Incubation 1			
Cont.	0.13	26	6
B_{12}	0.18	88	7
Co	N.M.	104	50
Fe	0.08	35	ND
CoFe	0.08	97	34
B_{12}Fe	0.09	99	ND
Incubation 2			
Cont.	N.M.	35	11
B_{12}	N.M.	95	8
Co	N.M.	530	186
Fe	N.M.	30	5
CoFe	N.M.	203	50
B_{12}Fe	N.M.	101	7
Incubation 3			
Cont.	0.08	32±3	3±2
B_{12}	0.08	101±22	2±2
Fe	N.M.	31± 9	ND
B_{12}Fe	0.03	58±12	2±1

bacteria and archaea along with some picoeukaryotes, and on the basis of the microscopically determined phytoplankton community profiles in this study, picoeukaryotes are not abundant; these data indicate that approximately one-third of the vitamin B_{12} uptake under these conditions can be attributed to bacteria and archaea, which are believed to be responsible for vitamin B_{12} production in the ecosystem as well. The larger-size fraction, comprised of eukaryotic phytoplankton including diatoms and *Phaeocystis* (colonial and free-living cells), takes up about two-thirds of the B_{12} consumed. These data suggest that the microbial community of the Ross Sea can take up dissolved vitamin B_{12}, implying a vitamin cycling pattern within the microbial loop there, with recycling of dissolved B_{12} and export by sinking eukaryotic phytoplankton.

Consideration of alternative explanations for phytoplankton stimulation—The possibility that a vitamin could substantially influence phytoplankton growth and community composition in the marine environment is a novel and exciting finding. To confirm these results, we analytically and experimentally verified that the B_{12} stimulation effects described above were not due to iron contamination (see Materials and methods for complete description). Quantifying the small iron blank associated with the added B_{12}, and then comparing it to an iron saturation growth curve (Fig. 6) demonstrates that the marginal increase in iron

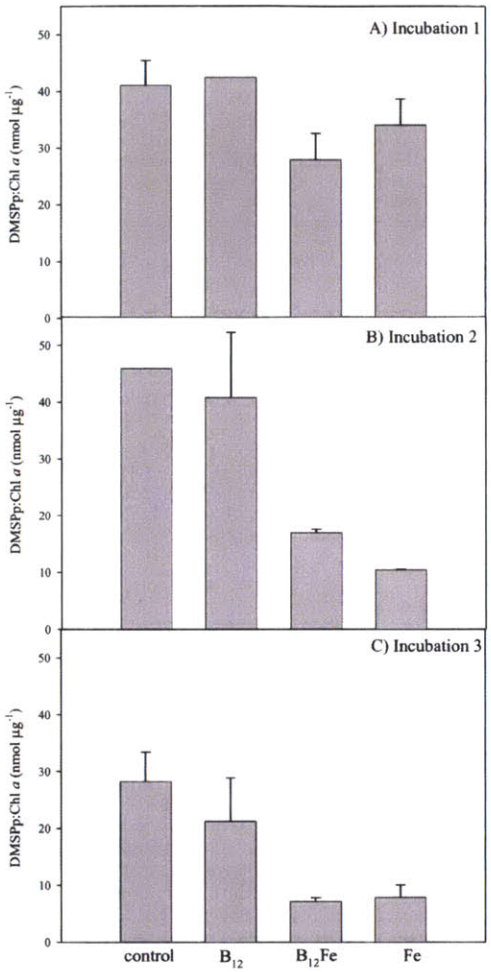

Fig. 4. Particulate DMSP production (nmol μg^{-1} Chl *a*) in the unamended (control) treatment, added vitamin B_{12} (B_{12}), added iron and vitamin B_{12} (B_{12}Fe), and added iron (Fe), from (A) incubation experiment 1 after 160 h of incubation, from (B) incubation experiment 2 after 223 h, and (C) incubation experiment 3 after 180 h. Values shown are means of single to triplicate treatments in 1.1- or 4.5-liter bottles (experiment 1) or single to triplicate treatments in 1.1-liter bottles (experiments 2 and 3) with error bars representing 1 SD. Particulate DMSP production at the start of incubation 2 was 52.7 ± 4.1 nmol μg^{-1} Chl *a* and was 68.8 ± 9.6 nmol μg^{-1} Chl *a* in incubation 3.

in the B_{12}Fe treatments relative to Fe-only treatments cannot account for the stimulation observed in the B_{12}Fe treatments of experiments 1 and 3: the small iron increase associated with the blank in the B_{12} solution would have resulted in changes to total iron concentrations only in the saturating portion of the apparent growth curve, where

Table 5. DMS (dimethyl sulfide) and DMSP (β-dimethyl sulfoniopropionate) in the initial conditions (t_0) and at the final time points (t_f) (160, 223, and 180 h respectively) in the unamended (Control) treatment, added vitamin B_{12} (B_{12}), added iron (Fe), and added iron and vitamin B_{12} (B_{12}Fe) from incubation experiments 1, 2, and 3. $DMSP_t$ is total DMSP; $DMSP_p$ is particulate (>0.2 μm) DMSP, and $DMSP_d$ is dissolved (<0.2 μmol L^{-1}) DMSP. Values are averages of single to triplicate treatments shown with 1 SD. N.M. indicates not measured.

	DMS (nmol L^{-1})	$DMSP_t$ (nmol L^{-1})	$DMSP_d$ (nmol L^{-1})	$DMSP_p$ (nmol L^{-1})
Incubation 1				
t_0	N.M.	77.1±3.1	N.M.	N.M.
t_f Control	N.M.	427.2±14	45.2±43	382±39
t_f B_{12}	N.M.	540±130	36.1±13	445±130
t_f Fe	N.M.	641±71	22.3±6.4	618±68
t_f B_{12}Fe	N.M.	747±144	23.7±4.1	722±140
Incubation 2				
t_0	10.7±6.5	98.9±1.7	20.6±1.8	78.2±0.1
t_f Control	5.08±3.0	198±9.0	5.37	182
t_f B_{12}	3.57±0.6	165±27	8.75±1.3	156±25
t_f Fe	6.22±2.6	189±1.0	12.2±6.0	177±5.1
t_f B_{12}Fe	4.45±0.7	264±18	9.27±2.9	255±16
Incubation 3				
t_0	14.7±2.1	95.9±1.0	35.1±5.4	60.8±6.4
t_f Control	17.2±7.6	120±8.5	16.7±7.6	104±12
t_f B_{12}	15.4±3.8	111±9.6	38.0±13	73.3±22.5
t_f Fe	14.6±3.9	223±24	30.0±20	193±40
t_f B_{12}Fe	9.23±6.1	240±21	19.3±2.1	220±19

increases in iron are not expected to significantly improve growth rates. By this logic, the iron blank in the B_{12} stock cannot account for any increase in phytoplankton growth.

The increase in phytoplankton growth in the B_{12} and iron addition also does not appear to be the result of B_{12} being used as a source of nitrogen. Vitamin B_{12} contains 14 atoms of nitrogen, thus the 90 pmol L^{-1} addition of B_{12} to these incubations translated into a 1.3 nmol L^{-1} addition of B_{12}-associated nitrogen. This was between 0.005% and 0.01% of the nitrogen found as nitrate at the start of each of these experiments and thus an insignificant addition.

Discussion

Our bottle incubation experiments demonstrate that vitamin B_{12} and iron colimit phytoplankton growth in the Ross Sea during the austral summer. Given that neither iron contamination nor the contribution of nitrogen from within the B_{12} molecule explain the results shown here, we hypothesize that the B_{12}Fe colimitation observed resulted from depletion of naturally present levels of dissolved vitamin B_{12} upon Fe fertilization. When vitamin B_{12} was added with iron, concentrations of the vitamin were sufficient to prevent vitamin limitation in the iron-caused phytoplankton bloom. This Fe-B_{12} colimitation effect was not seen in our second of three incubation experiments, suggesting that there was a difference in the chemistry or biology of this site relative to the other two experimental

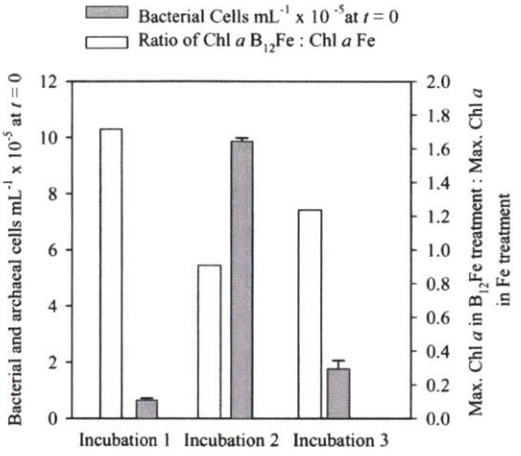

Fig. 5. Bacterial and archaeal counts at initiation of each experiment (gray) shown with the ratio of the maximum Chl a concentration in the vitamin B_{12} and iron addition to the maximum Chl a concentration in the iron-only addition (white). A ratio of 1 would mean that vitamin B_{12} added with iron yielded no change from the iron addition alone. A ratio of 2 would mean that the addition of B_{12} with iron doubled the Chl a yield above iron alone. This demonstrates that when bacterial and archaeal abundances were lowest in the initial conditions, vitamin B_{12} additions made the greatest difference in Chl a yield.

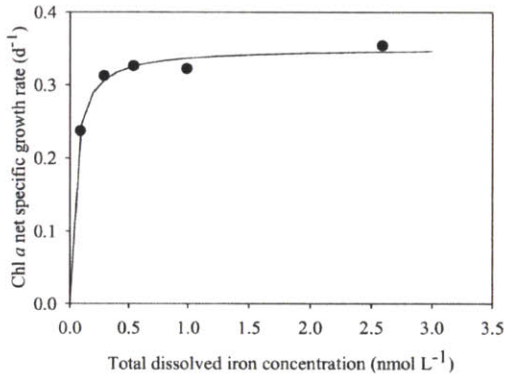

Fig. 6. Chl a net specific growth rate as a function of total dissolved iron concentration (iron added plus naturally occurring). The curve was fit with an r^2 value of 0.95 using the Droop equation. μ_m corresponded to a net specific growth rate of 0.35 per day and K_m corresponded to an iron concentration of 42 pmol L^{-1}. Duplicate measurements of total Chl a used to create this graph varied by less than 10%. Concentrations of 0.89 and 0.92 nmol L^{-1} iron ([Fe] and [B_{12}Fe] iron concentrations in experiment 1) and 1.81 and 1.84 ([Fe] and [B_{12}Fe] iron concentrations in experiments 2 and 3) occur only in the saturating portion of the curve. This suggests that the small iron blank associated with the B_{12} additions in the (B_{12}Fe) treatments could not account for the increase in Chl a observed.

stations. We hypothesize that this difference was caused by variation in the bacteria and archaeoplankton community within the three study sites.

Colimitation versus secondary limitation—We should note that this colimitation may also be described by the term "secondary limitation" where B_{12} is limiting once iron is replete. Moreover, since iron and B_{12} are micronutrients with independent biological functions, this would be a type I colimitation scenario, relative to type II colimitation in which biochemical substitution occurs (e.g., cobalt–zinc substitution), and type III colimitation between two interdependent nutrients (e.g., zinc-dependent carbon acquisition) as recently described (Saito, Goepfert, and Ritt unpubl.).

Potential sources of vitamin B_{12} in the Ross Sea—Although the sources of B_{12} to the Ross Sea have yet to be characterized, we can describe the potential components of a B_{12} biogeochemical cycle on the basis of phytoplankton culture studies, genomic information, and results presented here. As mentioned above, only the members of bacterial and archaeal domains are known to be capable of biosynthesizing vitamin B_{12}, and hence eukaryotic phytoplankton with a B_{12} requirement must acquire this vitamin from external sources. We hypothesize that given their abundance in tropical and subtropical marine environments (Partensky et al. 1999), the marine cyanobacteria are likely a major source of B_{12} to the marine environment, yet these microbes are virtually nonexistent in the Southern Ocean and Ross Sea (Caron et al. 2000; Marchant 2005). As a result, the remaining possible sources of B_{12} to the Ross Sea are either the bacteria and archaea living in the water column, or physical advection of B_{12} from other water masses or sedimentary environments. The bacterial production rates in the Ross Sea are among the lowest measured anywhere in the oceans, contributing only 5.5 mg m^{-2} d^{-1} C, or only 4% of phytoplankton production (Carlson et al. 1998)—much lower than the 25–30% found in other marine environments (Ducklow 2000; Ducklow and Carlson 1992). The specific reasons for these lower bacterial production rates are unknown, but are likely related to organic matter limitation (Ducklow 2000). Given these lower bacterial production rates in the Ross Sea and Southern Ocean, phytoplankton growth in this region could be especially prone to vitamin B_{12} limitation.

There is limited information about the bacterial diversity of the Ross Sea and the vitamin B_{12} production capabilities of that diversity. If bacteria in the water column of the Ross Sea are the major source of vitamin B_{12} (and other vitamins), they would have to be significantly different from *Pelagibacter ubique*, which is known to be lacking the B_{12} biosynthetic pathway and is representative of the SAR11 clade that numerically dominates clone libraries from the tropical and subtropical regions. 16S rDNA sequence analysis has revealed members of the *Pseudoalteromonas, Phychrobacter, Roseobacter, Paracoccus, Arthrobacter, Rhodococcus, Janibacter,* and *Planococcus* genera in McMurdo Sound of the Ross Sea (Michaud et al. 2004), at least some of which have members with vitamin B_{12} biosynthesis capabilities (Rodionov et al. 2003). The sequenced genome (Medigue et al. 2005) of the Antarctic marine bacterium *Pseudoalteromonas haloplanktis* TAC125 reveals that it has the genetic machinery to take up B_{12} and possible B_{12} degradation products, as it has the gene *btuB*, which can take up the vitamin as well as cobinamides and other corrinoids (Rodionov et al 2003). It also possesses the genes needed to complete the last few steps in vitamin B_{12} synthesis only (*cobS, cobU*) but cannot make the molecule outright. We hypothesize that without a cyanobacterial foundation to the high-latitude microbial food web, a number of bacteria and archaea would have retained their B_{12} biosynthesis capabilities in contrast to *P. ubique* of the SAR11 clade.

B_{12} requirements of phytoplankton from the Ross Sea—Cultivated phytoplankton strains related to those found in the Ross Sea have been shown to have a vitamin B_{12} requirement. Of the 55 diatoms reviewed by Croft et al. (2005), 35 (65%) required vitamin B_{12} for growth, including 5 of the 13 *Nitzschia* (closely related to *Pseudonitzschia*) strains surveyed. There is currently no direct evidence for a B_{12} requirement for *P. subcurvata* (the strain shown to comprise a very large portion of the community upon B_{12}Fe addition, Table 3). When cultured in the laboratory, its culture media contains added B_{12}. Our incubation results suggest that *P. subcurvata* likely requires vitamin B_{12} in the Ross Sea.

A vitamin B_{12} requirement for *Phaeocystis globosa* has been reported (Peperzak et al. 2000), and our experiments demonstrate slightly improved growth rates and yields of *P. antarctica* when grown in culture with B_{12} amendments (data not shown), although these experiments were conducted with nonaxenic cultures that may have B_{12} contributions from the co-occurring heterotrophic bacteria. If *P. antarctica* does require vitamin B_{12} in the field, the fact that diatom growth increased more than *Phaeocystis* growth upon vitamin and iron addition in our Ross Sea experiments indicates that *P. antarctica* likely has an alternative source of vitamin B_{12} that diatoms cannot access. This source could possibly be a close association with heterotrophic bacteria, similar to the symbiosis observed in the laboratory experiments using *Porphyridium purpureum* and heterotrophic bacteria (Croft et al. 2005). Putt et al. (1994) observed 2–11-fold increase in concentration of bacteria around *Phaeocystis* sp. colonies over ambient bacterial concentrations in McMurdo Sound of the Ross Sea. This close bacterial association could provide *Phaeocystis* with sufficient concentrations of the B_{12} and explain how the vitamin addition spurred diatom growth over *Phaeocystis* growth. This scenario also suggests that diatoms rely on dissolved vitamin B_{12} released through the microbial loop while *Phaeocystis* may acquire their vitamins through direct interaction with heterotrophic bacteria. These two distinct means of acquiring B_{12}, uptake of dissolved B_{12} or symbiosis with heterotrophic bacteria, could result in unique niches for phytoplankton species.

In the Ross Sea, *P. antarctica* dominates in the spring and early summer; a bacterioplankton bloom follows (Ducklow et al. 2001), perhaps due to the decay of the *Phaeocystis* bloom. Diatom species such as *P. subcurvata* (Arrigo et al. 1999) and *Fragilariopsis curta* (Leventer and

Dunbar 1996) dominate after the *Phaeocystis* bloom. Our results suggest that this bacterioplankton bloom could supply the vitamin B_{12} needed by diatoms and may be involved in the phytoplankton community shift observed seasonally in the Ross Sea.

Implications for the biogeochemical cycling of B_{12}, cobalt, and carbon—Our observations that iron and the B_{12} vitamin colimit phytoplankton growth in the Ross Sea suggest that B_{12} sources are limited in this region. In the Ross Sea, the microbial food web is lacking in cyanobacteria and has low bacterial production rates, two presumed major sources of B_{12} in the ocean. The combination of this microbial profile, a high export rate of biologically produced material, and the increased UV irradiation found seasonally in this region could together cause this region to become B_{12} limited. This is a significantly different picture of B_{12} cycling from what must exist in most of the world's oceans, where cyanobacteria are often a significant or major component of the phytoplankton community and where heterotrophic bacteria are more abundant and productive. A large fraction of the dissolved cobalt in the Ross Sea was found to be in a labile form, meaning it was not bound to strong organic ligands (Table 1). This labile cobalt is operationally defined as exchangeable with added strong competitor ligands and is believed to be the more bioavailable fraction (Saito and Moffett 2001; Saito et al. 2005 and references therein). These findings are consistent with results from incubation experiments 1 and 2 in which the cobalt addition did not yield any significant phytoplankton growth over the unamended control, and the combined cobalt and iron addition yielded no significant phytoplankton growth over the iron treatment alone. Because B_{12} contains a cobalt atom, this indicates that the stimulatory effect of B_{12} is not attributable to the cobalt atom being extracted and used for other metabolic functions.

These results form a picture of cobalt and vitamin B_{12} cocycling within the Ross Sea. It appears that here, cobalt is abundant in a bioavailable form, and that the amount of available cobalt does not limit the amount of B_{12} produced and cycled within the microbial food web. It is also possible that vitamin B_{12} or its degradation products comprise a significant if not numerically dominant portion of the organically bound cobalt in this study area as suggested for some tropical regions (Saito et al. 2005), particularly since in some areas of the Ross Sea (Table 1) less than 1 pmol L^{-1} of cobalt was found to be organically complexed.

The colimitation of phytoplankton growth by iron and B_{12} in the Ross Sea illustrates the potential importance of this vitamin to marine primary productivity and carbon cycling. We have shown that the addition of B_{12} and iron together can both increase phytoplankton growth and modulate phytoplankton community composition, compared to the addition of iron alone. Community composition in the Ross Sea was previously shown to be an important factor in determining the rate of carbon export (Arrigo et al. 1999). This study also suggests an important mechanism by which bacterial and archaeal populations within the microbial loop can affect carbon fixation and export. Our results also suggest that different modes of vitamin B_{12} acquisition, whether through uptake of dissolved B_{12} or through a symbiosis with cell-surface-associated bacteria, could have significant effects for phytoplankton and confer ecological advantages. This study highlights vitamin B_{12} as a biogeochemically relevant micronutrient and suggests that it can influence the cycling of carbon in the marine environment.

References

ARMBRUST, G., AND OTHERS. 2004. The genome of the diatom *Thalassiosira pseudonana*: Ecology, evolution, and metabolism. Science **306:** 79–86.

ARRIGO, K. R., D. H. ROBINSON, R. B. DUNBAR, A. R. LEVENTER, AND M. P. LIZOTTE. 2003. Physical control of chlorophyll a, POC, and TPN distributions in the pack ice of the Ross Sea, Antarctica. J. Geophys. Res. **108:** 3316–3338.

———, ———, D. L. WORTHEN, R. B. DUNBAR, G. R. DITULLIO, M. VANWOERT, AND M. P. LIZOTTE. 1999. Phytoplankton community structure and the drawdown of nutrients and CO_2 in the Southern Ocean. Science **283:** 365–367.

AZAM, F. 1998. Microbial control of oceanic carbon flux: The plot thickens. Science **280:** 694–696.

BRULAND, K. W., E. L. RUE, G. SMITH, AND G. R. DITULLIO. 2005. Iron, macronutrients and diatom blooms in the Peru upwelling regime: Brown waters of Peru versus blue waters. Mar. Chem. **93:** 81–103.

BUESSELER, K., AND OTHERS. 2001. Upper ocean export of particulate organic carbon and biogenic silica in the Southern ocean along 107.1W. Deep-Sea Res. II **48:** 4275–4297.

CARLSON, C. A., H. W. DUCKLOW, D. A. HANSELL, AND W. O. SMITH. 1998. Organic carbon partitioning during spring phytoplankton blooms Ross Sea polynya and the Sargasso Sea. Limnol. Oceanogr. **43:** 375–386.

CARLUCCI, A. F., S. B. SILBERNAGEL, AND P. M. MCNALLY. 1969. The influence of temperature and solar radiation on persistence of vitamin B_{12}, thiamine, and biotin in seawater. J. Phycol. **5:** 302–305.

CARON, D. A., M. A. DENNETT, D. J. LONSDALE, D. M. MORAN, AND L. SHALAPYONOK. 2000. Microzooplankton herbivory in the Ross Sea, Antarctica. Deep-Sea Res. II **47:** 3249–3272.

CHARLSON, R. J., J. E. LOVELOCK, M. O. ANDREAE, AND S. G. WARREN. 1987. Oceanic phytoplankton, atmospheric sulphur, cloud albedo, and climate. Nature **326:** 655–661.

COALE, K. H., X. WANG, S. J. TANNER, AND K. S. JOHNSON. 2003. Phytoplankton growth and biological response to iron and zinc addition in the Ross Sea and Antarctic Circumpolar Current along 170W. Deep-Sea Res II **50:** 635–653.

CROFT, M. T., A. D. LAWRENCE, E. RAUX-DEERY, M. J. WARREN, AND A. G. SMITH. 2005. Algae acquire vitamin B_{12} through a symbiotic relationship with bacteria. Nature **438:** 90–93.

CRUZEN, P. J. 1992. Ultraviolet on the increase. Nature **356:** 104–105.

DITULLIO, G. R., AND OTHERS. 2000. Rapid and early export of *Phaeocystis antarctica* blooms in the Ross Sea, Antarctica. Nature **404:** 595–598.

———, AND W. O. SMITH. 1995. Relationship between dimethylsulfide and phytoplankton pigment concentrations in the Ross Sea, Antarctic. Deep-Sea Res. II **42:** 873–892.

DONAT, J. R., AND K. W. BRULAND. 1988. Direct determination of dissolved cobalt and nickel in seawater by differential pulse cathodic stripping voltammetry preceded by adsorptive collection of cyclohexane-1,2,-dione dioxime complexes. Anal. Chem. **60:** 240–244.

DROOP, M. R. 1957. Vitamin B_{12} in marine ecology. Nature **180:** 1041–1042.

DUCKLOW, H. 2000. Bacterial production and biomass in the oceans. Wiley-Liss.

———, AND C. A. CARLSON. 1992. Oceanic bacterial productivity. Adv. Microb. Ecol. **12:** 113–118.

———, M. CHURCH, D. L. KIRCHMAN, D. SMITH, AND G. STEWARD. 2001. The seasonal development of the bacterioplankton bloom in the Ross Sea, Antarctica, 1994–1997. Deep-Sea Res. II **48:** 4199–4221.

ELLWOOD, M. J., AND C. M. G. VAN DEN BERG. 2000. Zinc speciation in the Northeastern Atlantic Ocean. Mar. Chem. **68:** 295–306.

GIOVANNONI, S. J., AND OTHERS. 2005. Genome streamlining in a cosmopolitan oceanic bacterium. Science **309:** 1242–1245.

GRÖNE, T., AND G. O. KIRST. 1992. The effect of nitrogen deficiency, methionine and inhibitors of methionine metabolism on the DMSP contents of *Tetraselmis subcordiformis* (Stein). Mar. Biol. **112:** 497–503.

GUILLARD, R., AND V. CASSIE. 1963. Minimum cyanocobalamin requirements of some marine centric diatoms. Limnol. Oceanogr. **8:** 161–165.

HAINES, K. C., AND R. R. L. GUILLARD. 1974. Growth of vitamin B_{12} requiring marine diatoms in mixed laboratory cultures with vitamin B_{12}-producing marine bacteria. J. Phycol. **10:** 245–252.

HUTCHINS, D. A., AND OTHERS. Phytoplankton iron limitation in the Humboldt Current and Peru Upwelling. Limnol Oceanogr **47:** 997–1011.

KARL, D. M. 2002. Nutrient dynamics in the deep blue sea. Trends Microbiol. **10:** 410–418.

KIENE, R. P., AND D. SLEZAK. 2006. Low dissolved DMSP concentrations in seawater revealed by small-volume gravity filtration and dialysis sampling. Limnol. Oceanogr. Methods **4:** 80–95.

LEVENTER, A., AND R. B. DUNBAR. 1996. Factors influencing the distribution of diatoms and other algae in the Ross Sea. J. Geophys. Res. **101:** 18489–18500.

MARCHANT, H. J. 2005. Cyanophytes, p. 324–325. *In* F. J. Scott and H. J. Marchant [eds.]. Antarctic marine protists. Australian Biological Resources Study.

MARTIN, J. H., S. E. FITZWATER, AND R. M. GORDON. 1990. Iron deficiency limits phytoplankton productivity in Antarctic waters. Glob. Biogeochem. Cycles **4**.

MEDIGUE, C., AND OTHERS. 2005. Coping with cold: The genome of the versatile marine Antarctica bacterium *Pseudoalteromonas haloplanktis* TAC125. Genome Res. **15:** 1325–1335.

MENZEL, D. W., AND J. P. SPAETH. 1962. Occurrence of vitamin B_{12} in the Sargasso Sea. Limnol. Oceanogr. **7:** 151–154.

MICHAUD, L., F. D. CELLO, M. BRILLI, R. FANI, A. L. GIUDICE, AND V. BRUNI. 2004. Biodiversity of cultivable psychrotrophic marine bacteria isolated from Terra Nova Bay (Ross Sea, Antarctica). FEBS Microbiol. Lett. **230:** 63–71.

OKBAMICHAEL, M., AND S. A. SAÑUDO-WILHELMY. 2004. A new method for the determination of vitamin B_{12} in seawater. Anal. Chim. Acta **517:** 33–38.

PALENIK, B., AND OTHERS. 2003. The genome of a motile marine *Synechococcus*. Nature **424:** 1037–1042.

PARTENSKY, F., W. R. HESS, AND D. VAULOT. 1999. *Prochlorococcus*, a marine photosynthetic prokaryote of global significance. Microbiol. Mol. Biol. Rev. **63:** 106–127.

PEPERZAK, L., W. W. C. GIESKES, R. DUIN, AND F. COLIJN. 2000. The vitamin B requirement of *Phaeocystis globosa*. J. Plankton. Res. **22:** 11529–11537.

PORTER, K. G., AND Y. S. FEIG. 1980. The use of DAPI for identifying and counting aquatic microflora. Limnol. Oceanogr. **25:** 943–948.

PRICE, N. M., G. I. HARRISON, J. G. HERING, R. J. HUDSON, P. M. V. NIREL, B. PALENIK, AND F. M. M. MOREL. 1988/1989. Preparation and chemistry of the artificial algal culture medium Aquil. Biol. Oceanogr. **6:** 443–461.

PUTT, M., G. MICELI, AND D. STOECKER. 1994. Association of bacteria with *Phaeocystis* sp. in McMurdo Sound, Antarctica. Mar. Ecol. Prog. Ser. **105:** 179–189.

RODIONOV, D. A., A. G. VITRESCHAK, A. A. MIRONOV, AND M. S. GELFAND. 2003. Comparative genomics of the vitamin B_{12} metabolism and regulation in prokaryotes. J. Biol. Chem. **278:** 41148–41159.

RUE, E. L., AND K. W. BRULAND. 1995. Complexation of iron (III) by natural ligands in the Central North Pacific as determined by a new competitive ligand equilibration/adsorptive cathodic stripping voltammetric method. Mar. Chem. **50:** 117–138.

SAITO, M. A., AND J. W. MOFFETT. 2001. Complexation of cobalt by natural organic ligands in the Sargasso Sea as determined by a new high-sensitivity electrochemical cobalt speciation method suitable for open ocean work. Mar. Chem. **75:** 49–68.

———, AND ———. 2002. Temporal and spatial variability of cobalt in the Atlantic Ocean. Geochim. Cosmochim. Acta **66:** 1943–1953.

———, G. ROCAP, AND J. W. MOFFETT. 2005. Production of cobalt binding ligands in a *Synechococcus* feature at the Costa Rica Upwelling Dome. Limnol. Oceanogr. **50:** 279–290.

SAÑUDO-WILHELMY, S., M. OKBAMICHAEL, C. GOBLER, AND G. TAYLOR. 2006. Regulation of phytoplankton dynamics by vitamin B_{12}. Geophys. Res. Lett. **33:** doi:10.1029/2005gl025046.

SEDWICK, P., AND G. DITULLIO. 1997. Regulation of algal blooms in Antarctic shelf waters by the release of iron from melting sea ice. Geophys. Res. Lett. **24:** 2515–2518.

———, ———, AND D. J. MACKEY. 2000. Iron and manganese in the Ross Sea, Antarctica: Seasonal iron limitation in Antarctic shelf waters. J. Geophys. Res **105:** 11321–11336.

SMITH, W. O., J. MARRA, M. R. HISCOCK, AND R. T. BARBER. 2000. The seasonal cycle of phytoplankton biomass and primary productivity in the Ross Sea, Antarctica. Deep-Sea Res. II **47:** 3119–3140.

———, AND D. M. NELSON. 1985. Phytoplankton bloom produced by a receding ice edge in the Ross Sea: Spatial coherence with the density. Science **227:** 163–166.

STEFELS, J. P. 2000. Physiological aspects of the production and conversion of DMSP in marine algae and higher plants. J. Sea Res. **43:** 183–197.

———, AND M. A. V. LEEUWE. 1998. Effects of iron and light stress on the biochemical composition of antarctic *Phaeocystis* sp. (Prymnesiophyceae). I. Intracellular DMSP concentrations. J. Phycol **34:** 486–495.

SUNDA, W., D. J. KIEBER, R. P. KIENE, AND S. HUNTSMAN. 2002. An antioxidant function for DMSP and DMS in marine algae. Nature **418:** 317–320.

SWIFT, D. 1981. Vitamin levels in the Gulf of Maine and ecological significance of vitamin B_{12} there. J. Marine Res. **39:** 375–403.

WALKER, T. D., AND H. J. MARCHANT. 1989. Seasonal occurrence of chroococcoid cyanobacteria at an Antarctic coastal site. Polar Biol. **9:** 193–199.

WHITE, R. H. 1982. Analysis of dimethyl sulfonium compounds in marine algae. J. Mar. Res. **40:** 529–536.

Received: 11 September 2006
Accepted: 20 November 2006
Amended: 3 January 2007

Appendix B:

Iron conservation by reduction of metalloenzyme inventories in the marine diazotroph *Crocosphaera watsonii*

Iron conservation by reduction of metalloenzyme inventories in the marine diazotroph *Crocosphaera watsonii. Proceedings of the National Academy of Sciences.* M. A. Saito, E. M. Bertrand, S. Dutkiewicz, V. V. Bulygin, D. M. Moran, F.M. Monteiro, M. J. Follows, F. W. Valois, J. B. Waterbury. 2011. 108 (6) 2184-2189.

Additional supplemental information available at:
http://www.pnas.org/content/suppl/2011/01/19/1006943108.DCSupplemental

Iron conservation by reduction of metalloenzyme inventories in the marine diazotroph *Crocosphaera watsonii*

Mak A. Saito[a,1], Erin M. Bertrand[a], Stephanie Dutkiewicz[b], Vladimir V. Bulygin[a,2], Dawn M. Moran[a], Fanny M. Monteiro[b], Michael J. Follows[b], Frederica W. Valois[c], and John B. Waterbury[c]

[a]Marine Chemistry and Geochemistry Department and [c]Biology Department, Woods Hole Oceanographic Institution, Woods Hole, MA 02543; and [b]Earth Atmospheric and Planetary Sciences Department, Massachusetts Institute of Technology (MIT), 77 Massachusetts Avenue, Cambridge, MA 02139

Edited* by Paul G. Falkowski, Rutgers, State University of New Jersey, Brunswick, NJ, and approved November 19, 2010 (received for review May 31, 2010)

The marine nitrogen fixing microorganisms (diazotrophs) are a major source of nitrogen to open ocean ecosystems and are predicted to be limited by iron in most marine environments. Here we use global and targeted proteomic analyses on a key unicellular marine diazotroph *Crocosphaera watsonii* to reveal large scale diel changes in its proteome, including substantial variations in concentrations of iron metalloproteins involved in nitrogen fixation and photosynthesis, as well as nocturnal flavodoxin production. The daily synthesis and degradation of enzymes in coordination with their utilization results in a lowered cellular metalloenzyme inventory that requires ~40% less iron than if these enzymes were maintained throughout the diel cycle. This strategy is energetically expensive, but appears to serve as an important adaptation for confronting the iron scarcity of the open oceans. A global numerical model of ocean circulation, biogeochemistry and ecosystems suggests that *Crocosphaera's* ability to reduce its iron-metalloenzyme inventory provides two advantages: It allows *Crocosphaera* to inhabit regions lower in iron and allows the same iron supply to support higher *Crocosphaera* biomass and nitrogen fixation than if they did not have this reduced iron requirement.

cyanobacteria | marine iron cycle | nitrogen cycle

The biological fixation of atmospheric dinitrogen into ammonia has a major impact on the extent of marine primary production (1, 2). Only a small number of bacteria are known to contribute to nitrogen fixation in open ocean environments, and they typically comprise a tiny fraction (<0.1%) of the overall microbial community (3, 4). Among these, the unicellular diazotroph *Crocosphaera watsonii* is estimated to be a significant contributor to oceanic nitrogen fixation (4–6). Whereas much of the primary productivity in the tropical and subtropical regions of the oceans is predicted to be nitrogen limited, the diazotrophs' nitrogen source, resupplied from the large atmospheric reservoir, is essentially limitless. Instead, iron is considered the critical micronutrient for marine diazotrophs due to their use of the iron-nitrogenase protein complex containing a homodimeric iron protein with a 4Fe:4S metallocluster (NifH) and a heterotetrameric molybdenum-iron protein with an 8Fe:7S P cluster and a 7 Fe and 1 Mo MoFe cofactor (NifDK, α and β subunits) (7, 8) (Table S1). Field experiments and models both predict the distribution of oceanic nitrogen fixation to be primarily constrained by the availability of iron (2, 9–11). Despite this importance of iron on marine nitrogen fixation, there is a limited understanding of how marine diazotrophs have adapted to this low iron environment (12–17).

The coexistence of oxygenic photosynthesis and nitrogen fixation metabolisms presents a unique challenge for diazotrophs due to their high iron demands and the chemical incompatibility of molecular oxygen and the nitrogenase protein complex. Previous elemental studies measuring whole cell iron content in *Crocosphaera* found increased iron during the dark period when nitrogen fixation is occurring (15). Whereas this finding was consistent with theoretical studies predicting a large iron requirement in marine diazotrophs (13, 18), it has been somewhat controversial due to the implication of a dynamic yet poorly understood diel cycle for intracellular iron. Several unicellular diazotrophs, including *Crocosphaera watsonii*, have been observed to fix nitrogen during the dark period (Fig. 1*A*), and this is widely viewed as an adaption for temporal separation of photosynthesis and nitrogen fixation to avoid the oxygen disruption of the nitrogenase complex (6, 19, 20). Global transcriptional studies have also observed large scale changes in the transcriptomes of the unicellular diazotrophs *Crocosphaera watsonii* (21), *Cyanothece* (22), *Gloeothece* (23), and a hot-spring *Synechococcus* (24) during the diel cycle, consistent with a temporal separation of photosynthesis and nitrogen fixation. Yet the possibility that diel cycling of the transcriptome or proteome might affect the iron requirement has not been previously discussed, likely because transcriptional studies provide information about gene expression rather than actual enzyme inventories, and immunological protein studies thus far, while having detected diel oscillations of the NifH subunit in *Crocosphaera* and *Gloeothece* (23, 25), are limited to a few select proteins with no global or absolute quantitative proteome studies of diazotrophs published as of yet. As a result, it has remained uncertain whether the observed diel transcriptome cycling was needed for the maintenance of a relatively consistent proteome or was in fact causing large changes in the global proteome composition during each diel cycle.

Recent advances in proteomic technologies hold promise for elucidating mechanistic connections between the biochemistry of important microbes and global biogeochemical cycles. There are two broad approaches to mass spectrometry based proteomics: global shotgun proteomic approaches that can semiquantitatively survey the relative abundance of hundreds of proteins simultaneously using spectral counting (26), and targeted approaches that use selected reaction monitoring (SRM) mass spectrometry with isotopically labeled peptide standards for absolute quantification of proteins of interest (27). Though there are several culture-based studies of marine microbes (26, 28) and field assessments of abundant proteins (29, 30), the combined application of global and targeted proteomic approaches to problems of

Author contributions: M.A.S., E.M.B., S.D., and J.B.W. designed research; M.A.S., E.M.B., S.D., V.V.B., D.M.M., F.M.M., M.J.F., F.W.V., and J.B.W. performed research; M.A.S., E.M.B., S.D., V.V.B., and D.M.M. analyzed data; and M.A.S., E.M.B., and S.D. wrote the paper.

The authors declare no conflict of interest.

*This Direct Submission article had a prearranged editor.

Freely available online through the PNAS open access option.

To whom correspondence should be addressed. E-mail: msaito@whoi.edu.

[2]Deceased June 28, 2009.

This article contains supporting information online at www.pnas.org/lookup/suppl/doi:10.1073/pnas.1006943108/-/DCSupplemental.

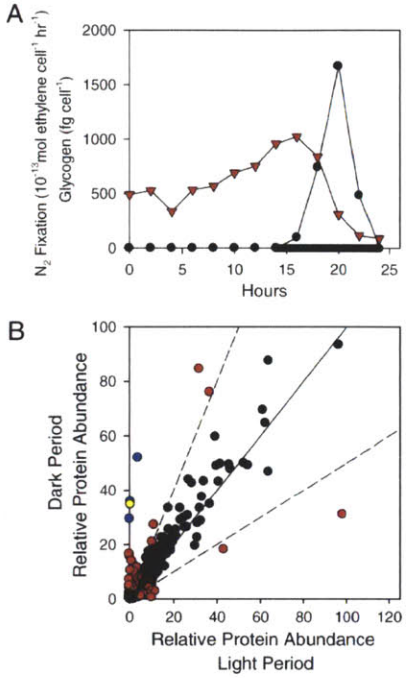

Fig. 1. Variations in the *Crocosphaera* proteome between the light and dark photoperiod. (*A*) Dark period nitrogen fixation (black) and glycogen storage (red) during a diel cycle (dark, black bar). (*B*) Relative protein abundance during light and dark periods, where similar expression (solid line, black circles; also see Fig. S1*A* for comparison of technical replicates) is contrasted by a number of proteins (colors), including the nitrogenase complex metalloenzymes (blue) and flavodoxin (yellow), with greater than 2-fold change in relative abundance (dashed lines) above a threshold of 5 normalized spectral counts in at least one treatment. Data are mean of six technical replicates.

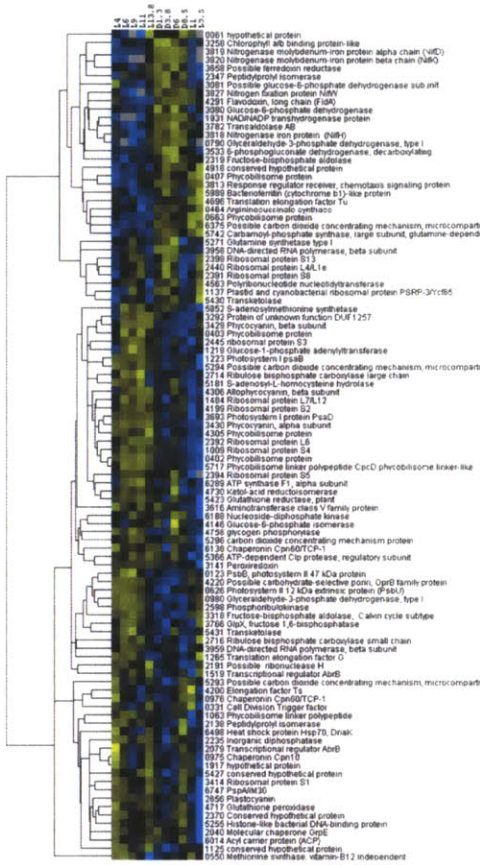

Fig. 2. Cluster analysis of global proteome during the diel cycle. Color indicates higher (yellow) or lower (blue) relative abundance relative to the centered mean value (black). Horizontal axis is hours from onset of light (L) or dark (D) period. Proteome data was filtered for proteins with at least three time points having greater than 10 spectral counts and a difference between maximum and minimum signals ≥14 spectral counts, prior to log transformation and normalization. Two major clusters were observed corresponding to the light and dark photoperiods.

marine biogeochemical relevance, such as the iron limitation of marine diazotrophy, has not yet been reported.

Results and Discussion

The diel cycle and inventory of iron metalloenzymes in *Crocosphaera watsonii* were investigated using global and targeted liquid chromatography mass spectrometry (LC-MS) proteomic techniques from three distinct culture experiments all grown on a 14:10 light:dark cycle: a day-night experiment sampled during the light and dark photoperiod (sampled 10 h from lights on and 7 h from lights off) analyzed for global proteome using both 1D and 2D LC-MS approaches, a time course study (diel hereon) sampled every 2–3 h for 30 h (beginning 4 h from lights on) and analyzed for global proteome using 1D LC-MS and for absolute quantities of targeted proteins, and a set of biological triplicate cultures (sampled 6.5 h into light period, and 3 and 6 h into the dark period) analyzed for targeted protein abundances by mass spectrometry.

Of the 477 unique proteins identified in the global proteomic 1D analysis of the day-night experiment [0.65% false positive rate (FPR) (31)], 37 proteins were found to have a 2-fold or greater change in abundance between the day and night (Fig. 1*B*). These results were confirmed in the deeper 2D chromatography proteome where 160 of the 1,108 identified proteins (0.11% FPR) showed a greater than 2-fold change (Fig. S1*B*). A time course of the diel cycle clearly showed a cycling of protein abundance (Fig. 2), where 100 proteins were found to be above a threshold spectral count signal (≥10) and displayed a diel variation in amplitude (max - min ≥ 14). Cluster analysis revealed two major groups that include key photosystem or nitrogen fixation proteins with increased abundances during the day and night respectively. These experiments demonstrate that the diel cycling observed in the transcriptome of unicellular diazotrophs (21, 22, 32) manifests itself in large scale changes in the global proteome, where more than 20% of the measured proteins in the diel experiment showed diel variation. In both the day-night and diel experiments, the metalloenzymes involved in nitrogen fixation in *Crocosphaera watsonii* were among those with the most pronounced changes in abundance, being largely absent during the day and present at night (Figs 1*B* and 2, Fig. S2, and Dataset S1).

Based on these global experiments, the absolute abundances of nine protein targets in the diel experiment were determined by triple quadrapole SRM mass spectrometry using isotopically labeled internal standards (Table S2). The abundance of the three nitrogenase metalloproteins ranged from nondetectable levels during the photoperiod to being among the most abundant pro-

teins in the proteome in the dark period (Fig. 3 *A–C*). At their peak abundances, the ratio of the iron protein to molybdenum-iron protein subunits (α used here) was 3.5:1, consistent with previous observations of a 3:1 cellular ratio (23) and a 2:1 stoichiometry within the nitrogenase protein complex (33). Together these global and targeted proteome measurements provide evidence for the nocturnal synthesis of the metalloenzymes in the nitrogenase complex followed by their complete diurnal degradation.

Flavodoxin was observed to increase in abundance during the dark period (Fig. 3*D*), similar to the nitrogenase metalloenzymes and in contrast with the increased flavodoxin abundances observed in most phytoplankton under iron deprivation (34). This suggests the ferredoxin-flavodoxin substitution for electron transport in photosynthesis does not occur appreciably in *Crocosphaera*. The global proteome of a short-term iron deprivation experiment was sampled during the light photoperiod to allow differentiation of iron effects from the dark expression. No increase in flavodoxin in response to iron stress was observed 24 h after the addition of an exogenous siderophore (Fig. S1 *C–F*), consistent with the hypothesis that flavodoxin could be functioning as an electron carrier for nitrogenase instead of ferredoxin (35). The use of flavodoxin at night even under iron replete conditions appears to be an adaptation for the overall minimization of the cellular iron demand in this microbe.

In a mirror image of the nitrogenase metalloenzymes and flavodoxin, numerous proteins were more abundant during the photoperiod (Figs. 1*B* and 2). In particular, several proteins from iron-rich photosystem I decreased during the dark period and increased during light period, including PsaA, PsaB, PsaD, and PsaF (PsaA and PsaB shown in Fig. 3 *E* and *F*). The iron-containing cytochromes b6 and c550 were among the most abundant cytochromes detected by spectral counting (f, P450, and b559 and c oxidase were also detected) and showed large decreases in abundance during the dark period as measured by targeted mass spectrometry (Fig. 3 *G* and *H*; 2- and 15-fold respectively). The degradation of substantial quantities of cytochrome b6 and c550 should release a number of iron-containing hemes during the dark period. Two heme oxygenases, which are capable of liberating iron from heme, were identified in the proteome, showed diel variations, and may be important in iron recycling (Fig. S2). Iron storage bacterioferritin proteins were also identified in the proteome, one of which showed some diel periodicity (Fig. S2). Diel cycling is not necessarily expected for bacterioferritin given that iron is thought to be added and removed from the ferritin cage without its degradation.

These results portray a *Crocosphaera* proteome that is dynamic, shifting its metalloenzyme inventory to suit the alternating temporal needs of nitrogen fixation and photosynthetic biochemical activity. Whereas *Crocosphaera*'s distinct nocturnal nitrogenase activity is one of its defining characteristics in both laboratory

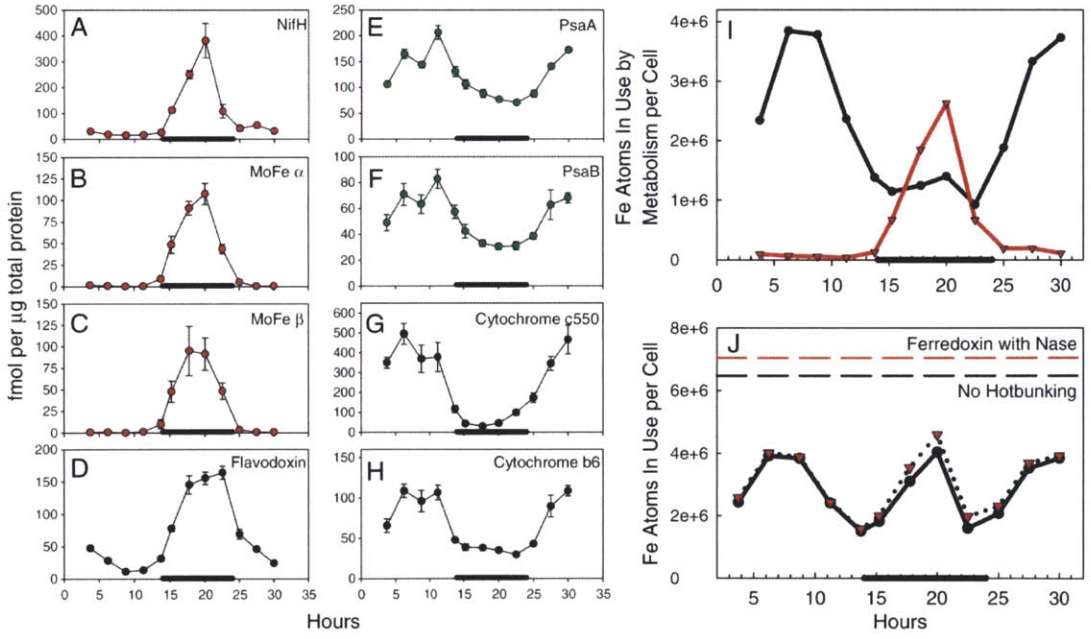

Fig. 3. Absolute quantitation of nitrogenase metalloproteins and selected photosynthesis and electron transport proteins during the diel cycle, and estimates of cellular iron stoichiometry based on absolute protein concentrations. (*A–H*) Targeted proteomic analysis of iron-nitrogenase (NifH), molybdenum-iron protein subunits (NifDK, MoFe α, MoFe β), and flavodoxin, photosystem I proteins PsaA and PsaB, and cytochromes b6 and c550 during the diel cycle (darkness, black bar) as measured using SRM triple quadrapole liquid chromatography mass spectrometry employing isotopically labeled standards. Data are mean and one standard deviation of technical triplicates. (*I*) Iron demand associated with nitrogen fixation or photosynthesis estimated from protein abundances in *A–H*, total protein and cell concentrations, and metal enyzme stoichiometries (Fig. S3 and Table S1) assuming metalloenzymes were populated with iron (darkness, black bar). (*J*) Sum of photosynthesis and nitrogenase iron estimates in two scenarios (darkness, black bar): (*i*) the *Crocosphaera* hotbunking scenario summing the calculated values in panel *I* (black circles), and (*ii*) a hypothetical nonhotbunking scenario (dashed black line), where the maximum iron required for each process [the peak of each line in panel (*I*) is summed]. Two additional scenarios are shown, where measured flavodoxin is replaced by ferredoxin, assuming a conservative 1:1 substitution (hotbunking, red triangles; nonhotbunking, dashed red line). The hotbunking scenario represents an estimated 40% savings in iron through a reduction of the iron-metalloenzyme inventory involved with nitrogenase and photosynthesis.

and field studies (6, 36), the fate of the nitrogenase protein complex during the light period has remained controversial due to the technical limitations of transcriptional and immunological methods, where transcripts do not measure protein abundance and immunological methods may not detect posttranslationally modified proteins (6, 15, 21, 36, 37). Using mass spectrometry-based analysis of multiple tryptic peptides from each protein, this study demonstrates the near complete degradation of the metalloenzymes from the nitrogenase complex and the partial degradation of certain iron-containing components of photosynthesis. The extent of proteome cycling we observed in *Crocosphaera watsonii* was surprising given the potentially significant energetic cost. This proteome cycling likely serves the dual functions of preventing oxygen disruption to the nitrogenase complex as discussed previously (6, 19), as well as providing a mechanism for a significant reduction in metabolic iron demand. We argue that the latter is true based on stoichiometric calculations from the quantitative metalloenzyme data in Fig. 3 *A–H* and the associated iron stoichiometry for each metalloenzyme (Table S1). By summing the iron associated with major metalloenzymes, we calculated the amount of iron involved in nitrogen fixation and photosynthesis throughout the diel cycle (Fig. 3*I*). By degrading these metalloenzymes when they are not in use, *Crocosphaera* reduces its iron-metalloenzyme inventory for these metabolic functions at any given time by 38%, 40%, and 75% for peak night, peak day, and minimum, respectively, compared to a hypothetical situation where these metalloenzymes are not degraded (Fig. 3*J*). An additional experiment with targeted protein analyses on biological triplicates was consistent with these estimates of iron conservation from the diel experiment, using 45 ± 19% less iron during the photoperiod (6.5 h from lights on, $n = 3$), and 38 ± 14% and 38 ± 22% less iron during the dark period (sampled at 3 h and 6 h from lights off, $n = 3$ for each). These savings in iron use would be even larger if the iron-free flavodoxin observed during the dark period (Fig. 3*D*) was replaced by iron-requiring ferredoxin (Fig. 3*J*). Iron released by the degradation of these metalloenzymes could have several fates including storage in bacterioferritin or chaperones, loss from the cell, and reuse in other metalloenzymes. Given the severe iron limiting conditions of the upper oceans (2, 9), it seems likely that a fraction of this liberated iron inventory is participating in both nitrogen fixation and photosynthesis metabolic processes. This iron conservation strategy is analogous to the maritime practice of hotbunking, referring to ships that sail with more sailors (metalloenzyme requirements) than bunks (iron atoms), where sailors on opposing shifts share the same bunk—keeping the bunks continually hot (or iron atoms in use). Whereas it is methodologically difficult to document the sharing of individual iron atoms between metabolisms, our data clearly demonstrates the reduction in iron-metalloenzyme inventory and concurrent reduction in metabolic iron demand through diel proteome cycling (Fig. 3*J*).

Iron conservation by reducing the metalloenzyme inventory likely serves as a key component of a low iron marine niche for *Crocosphaera*. *Trichodesmium* sp. is another dominant oxygenic marine diazotroph that differs from *Crocosphaera* in that it fixes both nitrogen and carbon during the photoperiod (38, 39). As a result *Trichodesmium* sp. likely does not employ this iron conservation strategy to the extent used by *Crocosphaera*. This is consistent with reports of an approximately double cellular iron to carbon stoichiometry in *Trichodesmium* compared to *Crocosphaera* (>35 and 16 ± 11 μmol Fe mol C^{-1}, respectively) (14–16), as well as estimates of a large fraction of cellular iron being necessary for nitrogen fixation (22–50%) in *Trichodesmium* (13). A previous study of cellular iron in *Crocosphaera watsonii* observed an increase in iron concentrations per cell during the dark period (15). Our calculated iron per cell attributed to nitrogen fixation and photosynthesis are roughly consistent with measured values (15), and the higher iron content at night likely results from diel proteome cycling with the added contributions of daytime uptake and accumulation of ferrous iron (21) produced by photochemical reduction (40) and photoperiod cell division (Fig. S4).

By reducing the nitrogen fixation and photosynthetic metalloenzyme inventory when each is not in use, *Crocosphaera watsonii* has evolved to require ~40% less iron than if these enzymes where maintained throughout the diel cycle (Fig. 3*J*). Though difficult to quantify, this process of resynthesizing enzymes every day must have an energetic expense. Based on our quantitative measurements, diel cycling of the three nitrogenase metalloproteins alone contributes ~2.3% of the total protein and all eight targeted proteins in Fig. 3 contribute 5.0% (using the difference between the maximum and minimum expression levels during the diel cycle). With many lower abundance proteins also undergoing diel cycling (Fig. 2), and with protein contributing roughly 40% of cellular biomass (41), these calculations provide some rough sense of the energetic cost for the increased protein synthesis required for this reduction in iron metabolic demand ("hotbunking" hereon). If *Crocosphaera watsonii* had evolved hotbunking from an ancestor that maintained its metalloenzymes through the diel, how would the trade-off between lower iron requirement and higher energetic cost affect where *Crocosphaera* would be competitive relative to its progenitor and other diazotrophs? A numerical global ocean circulation and ecosystem model (10, 42) is a useful tool to explore the implications of hotbunking on *Crocosphera's* habitat and nitrogen fixation rates in the global ocean. Our model resolves several phytoplankton types competing for resources, including analogs of several nondiazotrophs types, and unicellular and colonial marine diazotrophs, analogous to *Crocosphaera* and *Trichodesmium*, respectively. The modeled unicellular diazotrophs consist of two groups: a hypothetical control group that could not share cellular iron between photosynthesis and nitrogen fixation machinery (analogous to potential *Crocosphaera* ancestors that maintained their metalloenzyme inventory), and a hotbunking group (analogs of *Crocosphaera*, as suggested by this study) that are conferred with a lower cellular iron demand (R) at a cost to their growth rate (μ):

$$\mu_H = \alpha\mu_C, \qquad R_H = \gamma R_C \quad \text{where } \alpha,\gamma < 1.$$

The subscript H refers to hotbunkers and C refers to the non-hotbunking control group. We conducted a suite of simulations with different assumptions of the trade-off between reduced growth and iron requirement, the respective values of α and γ. A larger value of α indicates less energetic cost, and a larger value of γ indicates iron requirements closer to the control group.

Iron conservation strategies in *Crocosphaera* provided an ecological advantage in the low iron environments of the open ocean (Fig. 4 and Fig. S5). The geographical habitat of the hotbunking-analogs extended further into iron-depleted water than both the hypothetical control group and the *Trichodesmium*-analogs. In simulations with favorable combinations of trade-offs (e.g., Fig. 4), the distribution of *Crocosphaera*-analogs is broadly consistent with those suggested by observations (4, 10). These simulation results are consistent with observations suggesting that *Trichodesmium* outcompetes *Crocosphaera* in areas with high iron (43). The extent of the hotbunking unicellular diazotoph habitat is strongly regulated by the trade-off assumed (Fig. 5 and Fig. S5). Predictably, if the energetic cost is too high, hotbunking is not a desirable trait. For large cost to growth (small α) hotbunking diazotrophs do not survive (Fig. 5 *A* and *C*). On the other hand, for very little cost to growth (large α) and a high reduction in iron requirement (low γ), the hotbunking diazotrophs outcompeted the control group and expand into even more oligotrophic regions (Figs. 4*C* and 5*B* and Fig. S5 *E* and *F*). Simulations with lower requirements for iron (γ smaller) lead to a larger biomass of unicellular diazotrophs at any location than in a simulation

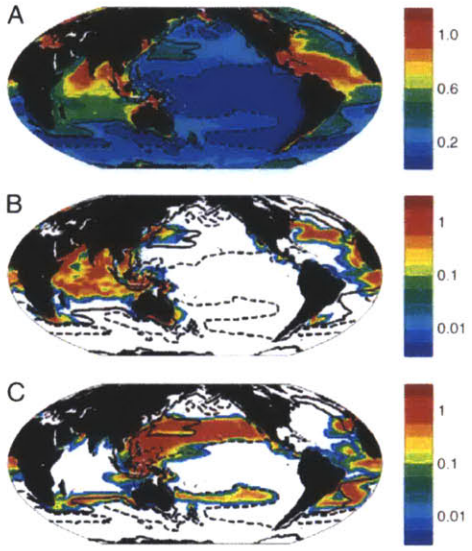

Fig. 4. Hotbunking unicellular diazotrophs inhabit waters with lower iron than the *Trichodesmium*-analogs and the unicellular control group (see Fig. S5) in the numerical simulations. Results are shown here for simulation where the hotbunking group have 90% of the growth rate and 60% the iron requirement of the control group ($\alpha = 0.9$, $\gamma = 0.6$, circle in Fig. 5). In this simulation the hotbunking diazotrophs outcompete the hypothetical control group everywhere. Annual mean model results for 0–50 m: (*A*) iron concentration (nM); (*B*) *Trichodesmium*-analogs (mgC m^{-3}); (*C*) hotbunking unicellular diazotrophs (mgC m^{-3}), analogs of *Crocosphaera watsonii*. Dashed and solid contours indicate 0.1 nM and 0.3 nM Fe respectively, and no shading (in *B* and *C*) indicates areas devoid of diazotrophs. The distribution of the diazotrophs is broadly consistent with those suggested by observations (4, 10). The model also includes analogs of several types of nondiazotrophic phytoplankton (diatoms, other large eukaryotes, *Prochlorococcus*, and other small phytoplankton). For less advantageous combinations of α and γ, the hotbunking group outcompete the control group only in the most iron-depleted regions (see Fig. 5 and Fig. S5).

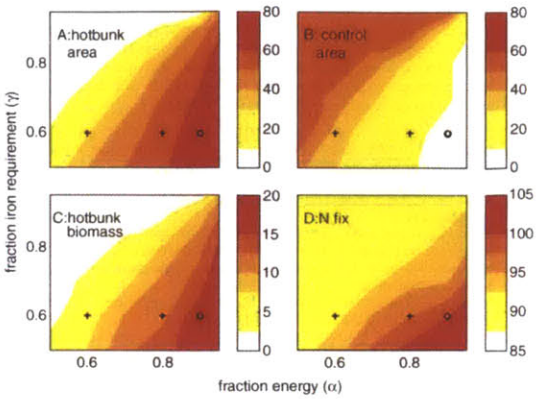

Fig. 5. Results from a series of global circulation/ecosystem model numerical simulations with different assumptions on the trade-off between reduced growth and iron requirement (values of α and γ). (*A*) Area (10^6 km^2) inhabited by hotbunking unicellular diazotrophs. (*B*) Area (10^6 km^2) inhabited by the control nonhotbunking unicellular diazotrophs. (*C*) Global abundance of hotbunking unicellular diazotrophs (TgC). (*D*) Changes in global total nitrogen fixation (TgN/y). With increased α (a smaller cost to growth) and a decreased γ (a lower requirement for iron) there are more regions where diazotrophy is supported, there is higher biomass of unicellular diazotrophs, and consequently higher total global autotrophic nitrogen fixation rates. If the energetic cost is low enough the hotbunking diazotrophs outcompete the control group everywhere (white regions of *B*). "Area" is calculated as the ocean surface area where the respective unicellular diazotrophs biomass is greater than 10^{-3} mgC m^{-3}. Nitrogen fixation rate is calculated from all three types of diazotrophs included in the simulation (hotbunking unicellular diazotrophs, control group, and *Trichodesmium*-analogs). The circle denotes parameter values used for results shown in Fig. 4 and crosses for those in Fig. S5.

with higher γ; the same iron supply could support a higher biomass. Sharing cellular iron between photosynthesis and nitrogen fixation machinery allowed the model hotbunking diazotrophs to not only expand their habitat, but also to have higher biomass per mole of available iron. These two benefits of hotbunking lead to increased global unicellular diazotroph biomass than simulations that did not include this adaptation (Fig. 5*C*). As a consequence, total global nitrogen fixation increases between simulations with α and γ combinations that shifted the population of unicellular diazotrophs from only control types to only hotbunking types (Fig. 5*D*). For the simulation shown in Fig. 4 (circles in Fig. 5) there was a 10% increase in global autotrophic nitrogen fixation relative to simulation with no hotbunkers (e.g., the white area of Fig. 5*A*). The overall affect of hotbunking on total global nitrogen fixation would be less than this value, because recent evidence demonstrates that heterotrophic nitrogen fixers also contribute significantly to marine nitrogen fixation (44).

Enzymes are agents for chemical transformations in the cycling of elements on Earth. Whereas genomic and transcriptional techniques can monitor the potential for enzyme synthesis, proteomic methods are now capable of their direct quantitation. Many require metals and hence reside at the intersection of coupled biogeochemical cycles. Our study demonstrates an application of proteomic technologies to study iron conservation in marine nitrogen fixation, where the important diazotroph *Crocosphaera* appears to have evolved a complex diel proteome cycle that results in a reduction of iron-metalloenzyme inventory. The process elucidated by the molecular-level measurements described here appears to be of global importance. With rising atmospheric CO_2 suggested to cause increases in marine nitrogen fixation (45), as well as a potential decrease in iron availability to marine phytoplankton in general (46), understanding the biochemical adaptations for iron scarcity in diazotrophs and their implications for marine primary productivity will be of increasing importance.

Methods

Axenic cultures of *Crocosphaera watsonii* were grown in SO medium (15) on a 14:10 light dark cycle. Frozen pellets were resuspended, sonicated, and centrifuged, and supernatants were solvent precipitated at −20 °C. Precipitated protein was resuspended, reduced, alkylated, and trypsin-digested. The whole cell lysate digests were analyzed using by liquid chromatography mass spectrometry (LC-MS) using a Paradigm MS4 HPLC system with reverse phase chromatography, a Michrom ADVANCE source, and a Thermo LTQ ion trap mass spectrometer. Two-dimensional chromatography involved adding an offline strong cation exchange separation using a salt gradient prior to reverse phase separation. Nine specific peptides were selected for quantitative analyses via selected reaction monitoring (SRM). Known amounts of heavy labeled versions of each peptide of interest (AQUA peptides; Sigma) were added as internal standards to *Crocosphaera* peptide extracts and analyzed using a Thermo Vantage TSQ Triple Quadrapole Mass Spectrometer with the LC and source as described for the LTQ. Peptide standard sequences and transition information are listed in Table S2. Linear Ion Trap mass spectra were processed using SEQUEST and PeptideProphet, and spectral counts were tabulated in Scaffold 2.0, with a false positive rate of less than 1% (31). Numerical simulations used the MIT general circulation model (MITgcm). The physical circulation flow fields and diffusion, constrained by observations (47), transport the organic and inorganic components of the ecosystem model. The ecosystem model was adapted from Monteiro et al. (10) and includes several types of autotrophs including several nondiazotrophs (analogs of diatoms, other large eukaryotes, *Prochlorococcus*, and other small

phytoplankton) and three types of diazotrophs (analogs of *Trichodesmium*, *Crocosphaera*, and a hypothetic control group of unicellulars that could not share cellular iron between photosynthesis and nitrogen fixation machinery). Other abundant groups of marine diazotroph groups (3) such as *Richelia* sp. symbionts found inside the diatom *Rhizosolenia* spp. and the uncultivated unicellular group A (UCYN-A) are not represented in this study due to lack of information on their iron requirements (4, 44).

ACKNOWLEDGMENTS. We acknowledge funding from US National Science Foundation Chemical and Biological Oceanography and Polar Programs (OCE-0452883, OCE-0752291, OCE-0723667, OCE-0928414, and ANT-0732665), an Environmental Protection Agency (EPA) Star Fellowship, the Woods Hole Oceanographic Institution Ocean Life Institute, the Center for Microbial Research and Education, and the Center for Environmental Bioinorganic Chemistry. This manuscript is dedicated to the memory of Vladimir Bulygin.

1. Falkowski PG (1997) Evolution of the nitrogen cycle and its influence on the biological sequestration of CO_2 in the ocean. *Nature* 387:272–274.
2. Moore JK, Doney SC, Lindsay K (2004) Upper ocean ecosystem dynamics and iron cycling in a global three-dimensional model. *Global Biogeochem Cy* 18:10.1029/2004GB002220.
3. Church MJ, Björkman KM, Karl DM, Saito MA, Zehr JP (2008) Regional distributions of nitrogen fixing bacteria in the Pacific Ocean. *Limnol Oceanogr* 53:63–77.
4. Moisander PH, et al. (2010) Unicellular cyanobacterial distributions broaded the oceanic N_2 fixation domain. *Science* 327:1512–1514.
5. Montoya JP, et al. (2004) High rates of N_2 fixation by unicellular diazotrophs in the oligotrophic Pacific Ocean. *Nature* 430:1027–1032.
6. Zehr JP, et al. (2001) Unicellular cyanobacteria fix N_2 in the subtropical North Pacific Ocean. *Nature* 412:635–638.
7. Howard JB, Rees DC (1996) Structural basis of biological nitrogen fixation. *Chem Rev* 96:2965–2982.
8. Rubio LM, Ludden PW (2008) Biosynthesis of the iron molybdenum cofactor of nitrogenase. *Annu Rev Microbiol* 62:93–111.
9. Moore CM, et al. (2009) Large-scale distribution of Atlantic nitrogen fixation controlled by iron availability. *Nat Geosci* 2:867–871.
10. Monteiro F, Follows MJ, Dutkiewicz S (2010) Distribution of diverse diverse nitrogen fixers in the global ocean. *Global Biogeochem Cy* 24:10.1029/2009GB003731.
11. Mills MM, Ridame C, Davey M, Roche JL, Geider RJ (2004) Iron and phosphorus co-limit nitrogen fixation in the eastern Tropical Atlantic. *Nature* 429:292–294.
12. Castruita M, et al. (2006) Overexpression and characterization of an iron storage and DNA-binding Dps protein from *Trichodesmium erythraeum*. *Appl Environ Microbiol* 72:2918–2924.
13. Kustka A, Sanudo-Wilhelmy S, Carpenter EJ, Capone DG, Raven JA (2003) A revised estimate of the iron use efficiency of nitrogen fixation, with special reference to the marine cyanobacterium *Trichodesmium* spp. (Cyanophyta). *J Phycol* 39:12–25.
14. Kustka A, Sanudo-Wilhelmy SA, Carpenter EJ (2003) Iron requirements for dinitrogen- and ammonium-supported growth in cultures of *Trichodesium (IMS 101)*: Comparison with nitrogen fixation rates and iron:carbon ratios of field populations. *Limnol Oceanogr* 48:1869–1884.
15. Tuit C, Waterbury J, Ravizza G (2004) Diel variation of molybdenum and iron in marine diazotrophic cyanobacteria. *Limnol Oceanogr* 49:978–990.
16. Berman-Frank I, Cullen JT, Shaked Y, Sherrell RM, Falkowski PG (2001) Iron availability, cellular iron quotas, and nitrogen fixation in *Trichodesmium*. *Limnol Oceanogr* 46:1249–1260.
17. Shi T, Sun Y, Falkowski PG (2007) Effects of iron limitation on the expression of metabolic genes in the marine cyanobacterium *Trichodesmium erythraeum* IMS101. *Environ Microbiol* 9:2945–2956.
18. Raven JA (1988) The iron and molybdenum use efficiencies of plant growth with different energy, carbon, and nitrogen sources. *Plant Phytol* 109:279–287.
19. Compaore J, Stal LJ (2009) Oxygen and the light-dark cycle of nitrogenase activity in two unicellular cyanobacteria. *Environ Microbiol* 12:54–62.
20. Schneegurt MA, Sherman DM, Nayar S, Sherman LA (1994) Oscillating behavior of carbohydrate granule formation and dinitrogen fixation in the cyanobacterium *Cyanothece* sp. strain ATCC 51142. *J Bacteriol* 176:1586–1597.
21. Shi T, Ilikchyan I, Rabouille S, Zehr JP (2010) Genome-wide analysis of diel gene expression in the unicellular N_2-fixing cyanobacterium *Crocosphaera watsonii* WH 8501. *ISME J* 4:621–632.
22. Stockel J, et al. (2008) Global transcriptomic analysis of *Cyanothece* 51142 reveals robust diurnal oscillation of central metabolic processes. *Proc Natl Acad Sci USA* 105:6156–6161.
23. Reade JPH, Dougherty LJ, Rogers LJ, Gallon JR (1999) Synthesis and proteolytic degradation of nitrogenase in cultures of the unicellular cyanobacterium *Gloeothece* strain ATCC 27152. *Microbiology* 145:1749–1758.
24. Steunou A-S, et al. (2006) In situ analysis of nitrogen fixation and metabolic switching in unicellular thermophilic cyanobacteria inhabiting hot spring microbial mats. *Proc Nat Acad Sci USA* 103:2398–2403.
25. Mohr W, Intermaggio MP, LaRoche J (2009) Diel rhythm of nitrogen and carbon metabolism in the unicellular, diazotrophic cyanobacterium *Crocosphaera watsonii* WH8501. *Environ Microbiol* 12:412–421.
26. Xia Q, et al. (2006) Quantitative proteomics of the archaeon *Methanococcus maripaludis* validated by microarray analysis and real time PCR. *Mol Cell Proteomics* 5:868–881.
27. Malmstrom J, et al. (2009) Proteome-wide cellular protein concentrations of the human pathogen *Leptospira interrogans*. *Nature* 460:762–765.
28. Sowell SM, et al. (2008) Proteomic analysis of stationary phase in the marine bacterium *Candidatus Pelagibacter ubique*. *Appl Environ Microbiol* 74:4091–4100.
29. Ram RJ, et al. (2005) Community proteomics of a natural microbial biofilm. *Science* 308:1915–1920.
30. Sowell SM, et al. (2008) Transport functions dominate the SAR11 metaproteome at low-nutrient extremes in the Sargasso Sea. *ISME J* 3:93–105.
31. Peng J, Elias JE, Thoreen CC, Licklider LJ, Gygi SP (2003) Evaluation of multidimensional chromatography coupled with tandem mass spectrometry (LC/LC-MS/MS) for large-scale protein analysis: The yeast proteome. *J Proteome Res* 2:43–50.
32. Toepel J, Welsh E, Summerfield TC, Pakrasi HB, Sherman LA (2008) Differential transcriptional analysis of the cyanobacterium *Cyanothece* sp. strain ATCC 51142 during light-dark and continuous-light Growth. *J Bacteriol* 190:3904–3913.
33. Schindelin H, Kisker C, Schlessman JL, Howard JB, Rees DC (1997) Structure of ADP x AlF4(-)-stabilized nitrogenase complex and its implications for signal transduction. *Nature* 387:370–376.
34. Erdner DL, Anderson DM (1999) Ferredoxin and flavodoxin as biochemical indicators of iron limitation during open-ocean iron enrichment. *Limnol Oceanogr* 44:1609–1615.
35. Fillat MF, Sandmann G, Gomez-Moreno C (1988) Flavodoxin from the nitrogen-fixingcyanobacterium *Anabaena* PCC 7119. *Arch Microbiol* 150:160–164.
36. Webb EA, Ehrenreich IM, Brown SL, Valois FW, Waterbury JB (2009) Phenotypic and genotypic characterization of multiple strains of the diazotrophic cyanobacterium, *Crocosphaera watsonii*, isolated from the open ocean. *Environ Microbiol* 11:338–348.
37. Church MJ, Short CM, Jenkins BD, Karl DM, Zehr JP (2005) Temporal patterns of nitrogenase gene (nifH) expression in the oligotrophic North Pacific ocean. *Appl Environ Microbiol* 71:5362–5370.
38. Finzi-Hart JA, et al. (2009) Fixation and fate of C and N in the cyanobacterium *Trichodesmium* using nanometer-scale secondary ion mass spectrometry. *Proc Natl Acad Sci USA* 106:6345–6350.
39. Capone D, Zehr J, Paerl H, Bergman B, Carpenter E (1997) *Trichodesmium*, a globally significant marine cyanobacterium. *Science* 276:1221–1229.
40. Weber L, Volker C, Oschlies A, Burchard H (2007) Iron profiles and speciation of the upper water column at the Bermuda Atlantic time-series study site: A model based sensitivity study. *Biogeosciences* 4:689–706.
41. Rhee G-Y (1978) Effects of N:P atomic ratios and nitrate limitation on algal growth, cell composition, and nitrate uptake. *Limnol Oceanogr* 23:10–25.
42. Follows MJ, Dutkiewicz S, Grant S, Chisholm SW (2007) Emergent biogeography of microbial communities in a model ocean. *Science* 315:1843–1846.
43. Campbell J, Carpenter EJ, Montoya JP, Kustka AB, Capone DG (2005) Picoplankton community structure within and outside a *Trichodesmium* bloom in the southwestern Pacific Ocean. *Vie Milieu* 55:185–195.
44. Zehr JP, et al. (2008) Globally distributed uncultivated oceanic N_2-fixing cyanobacteria lack oxygenic photosystem II. *Science* 322:1110–1112.
45. Fu F-X, et al. (2008) Interactions between changing pCO_2, N_2 fixation, and Fe limitation in the marine unicellular cyanobacterium *Crocosphaera*. *Limnol Oceanogr* 53:2472–2484.
46. Shi D, Xu Y, Hopkinson BM, Morel FMM (2010) Effect of ocean acidification on iron availability to marine phytoplankton. *Science* 327:676–679.
47. Wunsch C, Heimbach P (2006) Estimated decadal changes in the North Atlantic meridional overturning circulation and heat flux 1993–2004. *J Phys Oceanogr* 36:2012–2024.

Supporting Information

Saito et al. 10.1073/pnas.1006943108

SI Methods

Culture Technique and Treatment. Axenic cultures of *Crocosphaera watsonii* strain WH8501 from the Waterbury laboratory culture collection were grown in nitrogen-free iron-replete SO medium (1) at 28 °C under a 14:10 light-dark cycle at 150 $\mu E\,m^{-2}\,sec^{-1}$ in polycarbonate vessels, unless otherwise noted. All cultures were verified as axenic prior to each experiment by marine purity broth test (2) and during the experiment by examination of DNA staining microscopy slides used for cell counts (see *Microscopy and Flow Cytometry* below). Three distinct diel experiments were conducted to obtain proteome samples. The day-night experiment consisted of discrete day and night samples collected from a 1 L culture at 10 h into the light period and 7 h into the dark period during exponential growth and analyzed for relative abundance of major proteins (1D chromatography; Fig. 1*B*) and deeper proteome comparison (2D chromatography; Fig. S1*B*). The diel experiment consisted of a 1.5 L culture grown to late log phase in a gently stirred magnetic culture vessel (Nalgene) sampled every 2–3 h over a diel cycle (under dim red light at night) for protein, microscopy (Fig. S3*A*), and flow cytometry (Fig. S3 *D–F*) analyses. Protein samples were analyzed for relative abundance of major proteins (1D chromatography; Fig. 2) and absolute protein abundances of selected targets (Fig. 3*A–H*). A biological triplicate experiment was also conducted using 3 1 L cultures in glass furnbach flasks in midlog growth phase. Protein samples were taken 6.5 h into the light cycle and again at 3 and 6 h from onset of darkness. Two night sampling times were used to capture the transient nature of the nitrogenase expression peak. The triplicate cultures were analyzed for absolute protein abundances of selected targets, and used for an additional estimate of the overall reduction in iron-metalloenzyme inventories at each time point (see main text). An iron stress experiment was conducted with two 250 mL cultures, one with replete iron and one transferred into media with no added iron (Fig. S1 *C–E*). In late log phase, each culture was split into two flasks and 500 nM of the iron binding ligand desferrioxamine B (DFB, Sigma) was added to one high and one low-iron replicate. This resulted in four treatments: high iron with and without DFB and low-iron with and without DFB. In all experiments, biomass was harvested 24 h after the addition of DFB during the light period, and centrifuged at 12,400 rcf for 20 min at 4 °C, decanted and microcentrifuged at 6,700 rcf for 8 min, decanted and frozen at −80 °C.

Nitrogenase Activity and Glycogen Content. Nitrogenase activity and glycogen content were measured as previously described (3) on a separate culture experiment in 14:10 light-dark cycle. Briefly, nitrogen fixation was measured using acetylene-reduction assay on a Shimadzu gas chromatograph. Glycogen abundance was measured by digestion of amyloglucosidase and amylase followed by a hexokinase/glucose-6-phosphate dehydrogenase assay coupled to $NADP^+$ reduction.

Microscopy and Flow Cytometry. Cells were preserved in 0.125% final concentration ultrapure transmission electron microscopy (TEM) grade gluteraldehyde (Tousimis Research Corporation), incubated at room temperature in the dark for 15 min, flash frozen in liquid nitrogen and stored at −80 °C. 200 μL of thawed cells were collected on 0.22 μm Poretics polycarbonate filters (Osmonics Inc.) and mounted on glass slides using Vectashield hard set mounting media with DAPI (Vector Laboratories, Inc.). *Crocosphaera* cells were counted by epifluorescence microscopy and cultures were examined for bacterial contamination on a Zeiss Axioplan 2 microscope (Carl Zeiss, Inc.). For flow cytometry preserved cells were thawed, diluted with 0.22 μm filtered sterile seawater and stained with SYBR Green I fluorescent dye (Invitrogen) at a final concentration of 10×. Sodium citrate was added to the mixture at a final concentration of 10^{-5} M. A FACSCalibur flow cytometer (Becton Dickinson) was used with filtered seawater for the sheath fluid and 2.5 μm fluorescent beads for standardization (Calibrite, Becton Dickinson). Data was analyzed with WinMDI 2.8 software (J. Trotter, the Scripps Institute).

Protein Extraction and Digestion. Pellets were resupsended in cold 100 mM ammonium bicarbonate (pH 8.0, ambic hereon) and sonicated on ice with a microtip twice for 4 min on 70% duty cycle with a 5 min pause between sonication steps. Samples were centrifuged for 30 min at 6,700 rcf and 4 °C, and supernatants were precipitated overnight in 100% acetone at −20 °C, with the exception of the diel and iron experiments that were precipitated overnight in 50% acetone-50% methanol and 0.5 mM HCl at −20 °C. Precipitated protein was collected by centrifugation at 6,700 rcf for 30 min at 4 °C and dried by speed vacuum. Protein was resuspended in 0.1 mL of 6 M urea 0.1 M ambic and shaken at 400 rpm for 20 min at room temperature, then at 95 °C for 15 min. Aliquots were taken for protein determination by DC assay using bovine serum albumin as a protein standard (BioRad Inc.). Samples were reduced with 10 mM dithiothreitol (DTT) at 56 °C for 1 h, alkyated with 30 mM iodoacetamide for 1 h, and incubated with 40 mM of DTT for 1 h, prior to dilution in 1 mL ambic and digestion with trypsin for 16 h at 37 °C (1:50 ratio with total protein, Promega Gold Mass Spectrometry Grade, Promega Inc.). The sample was concentrated by speed vacuum for 3 h and stored at −80 °C. Aliquots for liquid chromatography mass spectrometry (LC-MS) were mixed 2:1 with ambic and injection volumes were adjusted to achieve equal protein loading in each experiment.

Shotgun Mass Spectrometry. The whole cell lysate digests were analyzed using a peptide Cap Trap in-line with a reversed phase Magic C18 AQ column (0.2 × 50 mm, 3 μm particle size, 200 Å pore size, Michrom Bioresources Inc.) on a Paradigm MS4 HPLC system (Michrom Bioresources Inc.) at a flow rate of 4 $\mu L\ min^{-1}$. A LTQ linear ion trap mass spectrometer (Thermo Scientific Inc.) was used with an ADVANCE nano-capillary electrospray source (Michrom Bioresources Inc.). The chromatography consisted of a hyperbolic gradient from 5% buffer A to 95% buffer B for 300 min, where A was 0.1% formic acid (Michrom) in water (Fisher Optima) and B was 0.1% formic acid in acetonitrile (Fisher Optima). The mass spectrometer was set to perform MS/MS on the top 7 ions using data-dependent settings and a dynamic exclusion window of 30 s. Ions were monitored over the range of 400–2000 m/z. 2D chromatography consisted of strong cation exchange (SCX) chromatography offline, followed by reverse phase chromatography of the fractions. Strong cation exchange was run on a 1 × 150 mm 5 μm particle size 200 Å pore size strong cation exchange column (Michrom Bioresources Inc.). A gradient was run from Buffer C (95% water, 5% acetonitrile, 0.1% formic acid), to filtered Buffer D (80% water, 20% acetonitrile, 0.1% formic acid, 1M NaCl) at 50 $\mu L\ min^{-1}$, 5 min at 2% D, ramping hyperbolically to 90% by 64 min, followed by 10 min of reequilibration at 2% D. 19–21 fractions were collected and analyzed by reverse phase chromatography using the 1D protocol described above except with a shorter 140 min gradient.

Shotgun Mass Spectra Data Processing. The 1,404,663 LTQ mass spectra collected in this study were searched using SEQUEST (Bioworks version 3.3, Thermo Inc.). An amino acid database for *Crocosphaera watsoniii* from the Joint Genome Institute Integrated Microbial Genomics server (downloaded in November 2008) was combined with a reverse sequence genome for false positive analysis for all subsequent analyses (labels with prefix CwatDraft are shortened to Cwat). The genome has not been manually annotated or closed; as a result we manually annotated the 100 most abundant proteins with diel periodicity found in Fig. 2, whereas JGI-IMG annotations were used otherwise. Database search results were further processed using the PeptideProphet statistical model (4) within Scaffold 2.0 (Proteome Software Inc.). Relative protein abundance was determined using Scaffold 2.0 for normalized spectral counting software operating on a 64-bit Ubuntu Linux workstation. Spectral counts are normalized across samples in each experiment in Scaffold, including technical replicates, to allow comparison of relative protein abundance. For the 2D experiment the spectral counts in each treatment (19 and 21 fractions each) were summed prior to normalization across samples. For the 2D day-night dataset protein identifications results from SEQUEST used filters of $\Delta CN > 0.1$, >30% ions, Xcorr vs charge state of 1.9, 2.4, and 2.9 for +1, +2, +3 charges respectively, and peptide probability $<1e{-}3$ for protein identification (Dataset S1). For all other datasets (Dataset S1), Scaffold was used for protein identifications with protein and peptide probability settings of 99.9 and 95%, respectively, with one tryptic peptide required for identification. Both approaches (SEQUEST and Scaffold) resulted in false positive rates of less than 1% (5). For cluster analysis data were log transformed, centered around the mean, and normalized with the sum of the squares equaling 1, in Cluster 3.0 (6). Analysis was performed using Kendall's tau nonparametric distance metric cluster and the dendogram was displayed using self-organizing mapping with Pearson's correlation metric (6, 7).

Targeted Mass Spectrometry. Peptides were designed as internal standards for quantitative analyses by selected reaction monitoring (SRM) using the global shotgun mass spectrometry results. Peptides were in the mass range of 800–2400 Da and lacked methionine or cysteine. SRM reactions for monitoring each peptide were selected based on successful peptide identification in the global proteomic analyses as well as those theoretically predicted by Protein Prospector MS Digest (http://prospector.ucsf.edu/prospector). Heavy isotope-labeled versions of the specific peptides (8) were obtained from Sigma-Aldrich in defined concentrations calibrated by amino acid analysis (AQUA Peptides) and handled according to the manufacturer's instructions. Heavy and native sequences of peptides, their SRMs, and collision energies are shown in Table S2. SRM analyses were performed on a Thermo Vantage TSQ Triple Quadrapole Mass Spectrometer with a Michrom Advance ion source. The SRM reactions were validated through tuning the mass spectrometer on heavy labeled reference peptides, introduced by direct infusion, to select the most abundant transitions for monitoring and to optimize the collision energies. Reverse phase chromatographic separation consisted of a peptide Cap Trap in-line with a reversed phase Magic C18 AQ column (0.2 × 50 mm, 3 mm particle size, 200 Å pore size) on a Paradigm MS4 HPLC system at a flow rate of 4 μL min^{-1} with a gradient from 5% buffer A then to 45% buffer B over 25 min and to 95% buffer B in 10 min. Buffer A and B are the same as Shotgun LC-MS analysis above. Q1 operated in 0.2 FWHM resolution and Q3 operated in 0.7 FWHM resolution. SRM reaction monitoring was scheduled based on individual peptide pair chromatographic retention times and the cycle time was 1.6 s (Table S2). Linear behavior of each peptide was validated by creating a standard curve from 1.5 to 1,650 fmol of the heavy labeled reference peptides in 1 μg *Crocosphaera* tryptic peptide sample matrix. For quantitative analysis, 150 fmols of each heavy labeled peptide was added as an internal standard to *Crocosphaera* peptide samples (1 μg protein per injection on the mass spectrometer). The amount of each target peptide of interest was calculated by ratio to the corresponding internal standard peptide abundance measured via SRM. Each biological sample was analyzed by mass spectrometry in triplicate.

Metabolic Iron Use Estimates. Absolute protein abundances were measured by targeted mass spectrometry (Fig. 3 *A–H*) and normalized to total protein extracted (Fig. S3*B*). These values were used to estimate the iron use by metabolism (Fig. 3*I*) using quantities of iron nitrogenase, molybdenum-iron β subunit, PsaA, cytochrome b6, and cytochrome c550 proteins to estimate iron involved in nitrogen fixation (former 2) and photosynthesis (latter 3) using the stoichiometries for each protein complex (Table S1). Assumptions of a 1:1:1 ratio of photosystems I, II, and ferredoxin were used here as in previous studies (9, 10), with the modification that only two iron atoms were attributed to PSII in our study (for 1 nonheme iron in PSII and 1 heme iron in cytochrome b-559), because we have direct measurements of the abundant cytochrome c550 [Fig. 3*G*; c550 can be found as part of the PSII complex and in soluble form (11)]. Because photosystem I, which we measure directly, contains far more iron that photosystem II and ferredoxin (Table S1), these assumptions should have a small effect on the calculations. Due to a potential inability to detect the dominant photosynthesis-associated ferredoxin (see *SI Results and Discussion*), the 4Fe4S stoichiometry was conservatively used. For the hypothetical situation, calculated in Fig. 3*J*, where nitrogenase substitutes ferredoxin for flavodoxin as its primary electron carrier, we used the 2Fe2S stoichiometry based on observations that a 2Fe2S ferredoxin increased slightly in abundance at night, and a conservative 1:1 stoichiometric substitution (ferredoxins are known to be more efficient than flavodoxins). Protein abundances were converted to per cell concentrations by multiplying by the measured total protein from extracted cells and dividing by the cell concentration at each time point. Whereas the measured peptide signals associated with targeted peptides appeared to be robust during the diel experiment (Fig. 3) suggesting reproducible results, we interpret these as lower estimates due to the potential for inefficiencies associated with the protein extraction. The extraction protocol was chosen for minimal processing to improve quantitative reproducibility, yet some proteins such as membrane associated proteins were likely not completely extracted. These calculations assume that the metalloproteins are populated with iron. These iron use by metabolism estimates should be lower than total cellular iron due to use in other unconstrained iron reservoirs such as other metalloenzymes (e.g., aconitase), bacterioferritin storage, and chaperones. As a result, we use the terminology "iron-metalloenzyme inventory" to describe the total number of iron atoms that could be associated with each metabolism based on our measurements of peptide abundance.

Global Circulation Ecosystem Modeling. We used the global three-dimensional physical-biogeochemical-ecosystem model of Follows et al. (12) to investigate the potential global importance of hotbunking trophs. The model used here had various adaptations discussed in Dutkiewicz et al. (13) and Monteiro et al. (14), in particular to explicitly include nitrogen-fixing phytoplankton (diazotrophs) and a representation of denitrification. We use the Massachusetts Institute of Technology (MIT) general circulation model (MITgcm) and the physical circulation flow fields and diffusion are state estimates as produced by ECCO-GODAE and have been constrained by observations (15). The biogeochemical cycling of nitrogen, phosphorus, silicon and iron is represented and the ecosystem model includes several types of autotrophs consisting of nondiazotrophs and diazotrophs. The model re-

solves a diatom-analog, an analog of other large eukaryotes, high and low light *Prochlorococcus*-analogs, an analog of other small phytoplankton, *Trichodesmium*-analog, hotbunking unicellular diazotrophs (analogs of *Crocosphaera watsonii*) and nonhotbunking unicellular diazotrophs (a hypothetical control group). Nondiazotrophs' growth could be limited by phosphorus, silica (for diatoms), iron or nitrogen; diazotrophs growth is limited by phosphorus or iron. Growth rates are parameterized as a function of light, temperature and nutrient concentration. Simple allometric trade-offs are imposed (see refs. 12 and 13 for more discussion), in particular smaller phytoplankton have lower nutrient half-saturations (more efficient at acquiring nutrients) than large phytoplankton. The model also resolves explicit grazing and sinking and all organic and inorganic components were advected and diffused by the physical fields. Parameter values for the different phytoplankton analogs are taken from those found most fit in a previous simulation representing 10s of phytoplankton types (14). Here, given the number of simulations required, we only resolve the above 8 functional types. Additional modifications over (14) are to use the aeolian iron source fields as modeled by (16) that includes estimation of the variable solubility of the iron in seawater, as well as to include a sedimentary source of iron [following Elrod et al. (17)]. These modifications to the iron cycling parameterization used in Monterio et al. (14) provided more iron in some regions of the ocean (e.g., Equatorial Pacific) that had been potentially too low in Monterio et al., though this also leads to concentrations too high relative to observations in other regions (e.g., North Atlantic).

The hotbunking diazotrophs were modeled with a lower cellular iron to nitrogen ratio (R) relative to the control group as a consequence of their ability to share iron between photosynthesis and nitrogen fixation processes. But because this is an energetically expensive process, we also assumed that the hotbunking diazotrophs had a lower growth rate (μ) than the control group:

$$\mu_H = \alpha\mu_C, \qquad R_H = \gamma R_C \quad \text{where } \alpha,\gamma < 1.$$

The subscript H refers to the hotbunking group and C refers to the control nonhotbunking group. The trade-off between reduced growth and iron requirement is therefore represented by the values of α and γ. A larger value of α indicates less energetic cost, and a larger value of γ indicates iron requirements closer to the control group. We conduct several simulations with different combinations of α and γ. The laboratory studies described here suggest a decrease of iron requirement by as much as 40% ($\gamma = 0.6$), thus we consider a range of $\gamma = [0.5, 0.6, 0.7, 0.8, 0.9, 0.95]$. Crude back of the envelope calculations on the energetic cost suggest that it is at least 5%, but potentially several fold higher. Thus we consider the cost to growth $\alpha = [0.5, 0.6, 0.7, 0.8, 0.9, 0.95]$. Fig. 5 is constructed from results from the 36 simulations with the combinations of these values of α and γ. The simulations were run for 10 years and results from the annual mean for the tenth year are shown in Fig. 4 and Fig. S5. In all the experiments we set $\mu_C = 0.7\ d^{-1}$, $K_{FeC} = 0.36$ nM, and $R_C = 7.5 \times 10^{-4}$ mol Fe/mol N. We relate the change in the iron cellular demand (R) to the half saturation coefficient of growth (K_{Fe}) following Verdy et al. (18).

SI Results and Discussion

Global Proteome Results. Relative quantitation results obtained using 1D chromatography LC-MS analysis of the day-night experiment resulted in 477 unique protein and 3,800 unique tryptic peptides identifications with a false positive rate (FPR) of 0.65% (5), based on 20,506 total peptide identifications from 12 LC-MS injections (6 technical replicates per sample) and a total of 380,015 mass spectra (Dataset S1). Additional 2D chromatography analyses of the day-night experiment identified 1,108 unique proteins and 3,540 unique tryptic peptides (Dataset S1) for 18% coverage of the genome open reading frames and a 0.11% FPR, based on 21,620 total peptide identifications over 40 LC-MS fraction injections (~20 fractions per sample) for a total of 388,076 mass spectra. The diel experiment and iron stress experiments also identified 552 and 589 proteins, respectively, for a combined total of 724 proteins identified from the 1D global proteome experiments (day-night, diel, and iron stress experiments, see Dataset S1 for complete list of protein identifications, spectral count values of technical replicates, and fold change calculations). As is typical of proteomic experiments, each individual injection provided a large number of protein identifications, whereas repeat injections and 2D chromatographic separation provided confidence in the robustness of the results and increased proteome coverage incrementally with discovery of lower abundance tryptic peptides.

Examination of Flavodoxin and Ferredoxin Expression by Iron Stress Experiment. Whereas ferredoxin and flavodoxin are typically involved in electron transport in photosynthesis, an electron donor is also needed for the nitrogenase enzyme in the diazotrophic cyanobacterial species. Ferredoxins contain iron-sulfur centers and have a higher catalytic efficiency than the iron-free flavodoxin (19). In marine phytoplankton flavodoxin is generally considered a low-iron alternative to ferredoxin that is upregulated under iron stress in eukaryotic algae. Based on this expression behavior, flavodoxin has been applied as an iron nutrition diagnostic (20). Yet, as described in the main text, the expression of flavodoxin in *Crocosphaera* diverged from this behavior and was clearly present and abundant at night in *Crocosphaera* under iron-replete conditions (Fig. 3*D*).

The effect of reduced iron availability on the flavodoxin expression in the *Crocosphaera* proteome was examined through the growth of cultures under high and low total iron concentration, as well as with and without the addition of the strong iron chelator desferrioxamine B (DFB; Fig. S1 *C–F*). Cell counts showed a cessation of growth with the addition of DFB in both iron conditions, whereas the no iron added treatment did not show a physiological effect, as evidenced by growth similar to that of the standard (+Fe) media. This similar growth was expected based on the lack of multiple transfers in low-iron media, and allowed a low-iron treatment under similar growth rates for comparison with the replete iron. DFB is an exogenous siderophore and is known to greatly reduce the iron available to phytoplankton by depressing the abundances of the free ionic form and inorganic chemical species of the metal (21, 22). Flavodoxin protein expression under iron stress was examined during the light period because the influence of iron stress would potentially be difficult to differentiate from the high dark period expression observed (Fig. 3*D*). Flavodoxin (Cwat4291) was more abundant under high iron relative to no iron added (Fig. S1*D*), although both of these light period treatments were >5-fold less than the large peak in flavodoxin observed during the dark period in the day-night experiment (Fig. S2 and Fig. 1*B* in spectral count units; also Fig. 3*D*). Flavodoxin during the day period did not appear affected by DFB. Additionally, ferredoxin (Cwat3830) was 3-fold more abundant under high iron conditions relative to low-iron conditions (Fig. S1*D*), regardless of whether DFB was added. The absence of a light period increase in flavodoxin abundance under these two iron stress treatments (−Fe, and +DFB) suggests that flavodoxin's primary role is as the major electron donor protein for nitrogen fixation, rather than as a low-iron substitute for ferredoxin associated with photosynthesis as observed in other phytoplankton (19, 20, 23). The dark period expression of flavodoxin even under iron-replete conditions may be an adaptation for the minimization of *Crocosphaera*'s cellular iron demand.

Analysis of other putative ferredoxins in the genome revealed that three ferredoxin-like proteins lack more than one suitable

tryptic peptide for shotgun mass spectrometry detection. Because confidence in protein identification increases greatly with the identification of more than one tryptic peptide for a given protein, some of these small putative ferredoxin proteins may have been present but were not detected. Many open reading frames are annotated as ferredoxin in the current *Crocosphaera watsonii* genome, but of these only four were identified in our proteome samples. Cwat3830 is a 2Fe-2S ferredoxin, whereas Cwat5974 is misannotated and is actually *psaC*. Cwat5441 and Cwat1598 are barely detected and are likely too large to be real ferredoxins. We suspect that due to the small size of this protein, the major cellular ferredoxin has gone undetected in our study due to the lack of a suitable tryptic peptide within the sequence. Cwat1273, Cwat1274, and Cwat0916 are possible candidates for the major ferredoxin because all are lacking more than one suitable internal tryptic peptide needed for the shotgun proteomic techniques applied here.

Several other notable changes in global protein expression under iron stress were observed as shown in Fig. S1 *E* and *F* and Dataset S1, including a tripling in relative abundance of a possible carbon concentrating mechanism/microcompartments protein (Cwat5294) under low-iron without the addition of DFB. Ribulose-bisphosphate carboxylase (Cwat2714) was two to three-fold more highly expressed under low-iron, and fructose-bisphosphate aldolase (Cwat1319), which is involved in carbohydrate synthesis, was 20-fold higher under iron stress. The upregulation of these proteins suggests that reduced iron availability results in cellular demand for more efficient inorganic carbon fixation. *Crocosphaera* strains have been observed to secrete significant amounts of extracellular organic material (24). The increases in carbon fixation proteins under iron stress observed here may be connected to these organic secretions, perhaps to promote bacterial associations that produce siderophores and aid iron scavenging and acquisition (25).

Other Proteins of Interest. Cytochrome c550 is a monoheme cytochrome containing 1 Fe atom present as a component of the PSII complex of cyanobacteria and involved in the stabilization of the PSII Mn cluster (26). It has also been isolated as a soluble protein with a possible additional role in anaerobic carbon and hydrogen metabolism (11). This protein had a particularly strong diel pattern decreasing 15-fold during the dark from the daytime maximum as measured by targeted proteomic analysis (Fig. 3*G*). This decreased abundance during the dark period should reduce the oxygen production capability of PS II, which would be beneficial to the preventing damage to the nitrogenase complex. Cytochrome b6 also decreases in abundance by more than 2-fold during the dark period in our targeted proteomic analyses (Fig. 3*H*). This protein is a component of the b6f complex, which contains four iron containing heme groups and an Fe_2S_2 cluster (27) and is reported to have a dual function in photosynthesis and respiration in cyanobacteria (28).

Two heme oxygenases (Cwat4859, Cwat2459) were identified in the proteome, one with a dark period maxima (Cwat2459) and the other with a day period maxima (Cwat4859) in relative abundance (Fig. S2). Heme oxygenases are capable of releasing iron from hemes, for example by pathogenic bacteria to gain nutritional iron from host cells (29). This enzyme has also been shown to be involved in phycobilin synthesis in cyanobacteria through the conversion of hemin to ferric-biliverdin IX_α (29). We hypothesize that one of these heme oxygenases (Cwat2459) is involved in releasing the iron from cytochrome heme groups at night for use in the nitrogenase complex, whereas the other (Cwat4859) is involved in the conversion of hemin to ferric biliberdin IX_α phycobilin. Peptidase S41A also showed strong diel cycling with a presence during the photoperiod (Fig. S2), suggestive of its involvement in the changing proteome composition throughout the diel cycle (e.g., Fig. 2). Measurements of the ribosomal protein L3 (Cwat2439) are consistent with two more highly active periods of protein synthesis per diel cycle (Fig. S3*C*), and is consistent with the two peaks of ribosomal protein activity observed in the diel global proteome in Fig. 2. Plastocyanin, the copper containing water soluble electron carrier, was identified in the *Crocosphaera* proteome (Dataset S1). In addition, the iron-manganese superoxide dismutase present in the genome (Cwat6299) was not found in any of the proteome analyses here, whereas a nickel superoxide dismutase was detected in the 2D proteome (Cwat2983; Dataset S1), consistent with the theme of iron conservation in *Crocosphaera*.

Connecting Cellular Iron Estimates with Iron Biogeochemistry, Uptake, and Cell Division. Cellular iron was estimated during a diel cycle by combining light period ferrous iron uptake (30), our proteomic measurements, and allowing cell division after dawn. As mentioned in the main text, the motivation for this effort was to reconcile our diel protein cycling observations with the observation of increased cellular iron during the dark period in Tuit et al's study (31) by overlaying the two processes of cell division and ferrous iron uptake (and their temporal variability) onto our iron-metalloenzyme inventories. Before describing the results of this calculation below, we describe what is known about each of these processes with respect to *Crocosphaera*.

Cell division is known to occur solely during the photoperiod in *Crocosphaera* (e.g., Fig. S3*A*), and division must divide the cellular iron between two daughter cells, perhaps also involving some cellular leakage in the process. With growth rates of ~0.5 d^{-1} observed in Tuit et al. (31), 65% of cells are dividing daily, contributing to a 40% decrease in iron per cell when averaged across the population. Hence, cell division alone can account for a significant amount of the lower photoperiod cellular iron content observed by Tuit et al. In addition, a potential iron uptake pathway for *Crocosphaera* involves a combination of photochemical reduction of the natural iron ligands that dominate seawater iron chemistry or Fe–EDTA complexes in laboratory media and uptake of the resultant ferrous iron (30, 32, 33). This scenario would cause production of Fe(II) during the light period followed by rapid reoxidation and complexation by strong ligands in darkness at tropical and subtropical temperatures as modeled by Weber et al. (30) (Fig. S4*A*). In addition, the *Crocosphaera watsonii* genome contains genes for the ferrous iron transporter, which a recent microarray transcriptional study showed are greatly upregulated during the photoperiod (34), consistent with light period photochemical ferrous iron source. Ferrous iron is very rapidly oxidized to ferric iron in seawater (35), and hence only exists in appreciable amounts during the photoperiod under the tropical temperature conditions of *Crocosphaera*'s niche (30). *Crocosphaera*'s genome does not appear to contain genes for other important iron acquisition mechanisms such as an iron reductase system, siderophore biosynthesis, or siderophore transport (36). These facts taken together suggest a scenario where *Crocosphaera* acquires ferrous iron during the light period, resulting in iron accumulating through the light period as shown in the schematic in Figs. S4 *A* and *B*.

Combining the influence of the temporal processes of cell division and ferrous iron uptake, with our diel iron-metalloenzyme inventory calculations allows a schematic of diel cellular iron budget to be estimated that might be expected in natural environments. Ferrous iron uptake was calculated to be proportional to the light period ferrous iron availability from Weber et al. (30) (Fig. S4*A*), where the timing of iron uptake was inferred from chemical modeling of ferrous iron abundance (30), whereas the magnitude of uptake was tuned to minimize storage category (see below) to emphasize the extent of intracellular trafficking and to allow a steady-state cellular iron abundance. The iron estimated to be involved in nitrogen fixation and photosynthesis (Fig. 3 *I* and *J*) was then subtracted to make a rough estimate of

the remaining cellular iron that might be found in storage (bacterioferritin), other enzymes (e.g., aconitase), and chaperones (storage category from hereon). This storage/other reservoir is estimated to be quite dynamic during the diel cycle as shown in red in Fig. S4*B*. No efflux term is needed in these calculations to approximate steady-state growth. Increasing the ferrous iron production and resultant uptake rate in this calculation increases this reservoir as well as cellular iron in subsequent generations, as might be expected during transient pulses caused by dust input or increased light fluxes, presumably with iron storage in bacterioferritin. Our estimates of cellular iron associated with iron metalloenzymes involved in photosynthesis and nitrogen fixation are consistent with previous quota studies (10, 31, 37) differing by a factor of less than 2, which is within the error observed in those cellular iron measurements. This schematic also highlights the possibility of apo forms of nitrogen fixation and photosynthetic metalloenzymes existing, a likely scenario given the challenge of coordinating the movement of iron between intracellular reservoirs as estimated here. Future research on how chaperones and metal trafficking are involved in the diel metalloenzyme cycling we have observed would be particularly interesting in *Crocosphaera watsonii*.

Global Circulation Ecosystem Modeling. The simulations produced nutrient and biomass fields that compare well with observations. Total global primary production was between 38.2 and 38.8 GtC/y and total global nitrogen fixation rates were between 90 and 107 TgN/y (depending on the values of α and γ). The distribution of the different phytoplankton types compare well to observations, as shown in Follows et al. (12), Dutkiewicz et al. (13) and Monteiro et al. (14). Though never dominant in the model, diazotrophs could coexist with nondiazotrophs in regions where nitrate concentrations are low and there is sufficient iron and phosphorus for the diazotrophs to exist (38). Unicellular diazotrophs, due to their small size, can out-compete the *Trichodesmium*-analogs in more oligotrophic regions and their distribution and abundance are broadly consistent with those suggested by observations (14, 39). Observations of *Crocosphaera* as summarized in ref. 14 suggest higher abundances in the tropical North Atlantic (40, 41), eastern subtropical North Pacific (42, 43) and Arabian Sea (44). *Crocosphaera* have also been detected in the eastern subtropical North Atlantic (40) and eastern tropical South Atlantic (41), eastern subtropical and tropical North Pacific (42) and western South Pacific (45). They were however not detected in the western subtropical North Atlantic (40), eastern subarctic North Pacific, and eastern subtropical South Pacific (46). The pattern of presence and absence of *Crocosphaera*-analogs is in general captured by the numerical model (Fig. 4), with concentration levels consistent in most regions with the observations (see ref. 14 for details). The iron concentrations in the Caribbean and eastern tropical North Atlantic are too high in this version of the model, leading to strong phosphorous limitation there. This discrepancy leads to less than ideal conditions for diazotrophs, and concentrations there do not compare as well as in other parts of the oceans. A similar problem was found by Moore et al. (47). Presence, absence and abundances of *Trichodesmium*-analogs are also, in general, captured by the model. In particular the geographic patterns of *Trichodesmium* limited to regions with higher iron and *Crocosphaera* existing in regions with lower iron matches patterns suggested by the observations of Campbell et al. (45), who found that in the southwest Pacific *Trichodesmium* appeared constrained to coastal areas with high iron, whereas *Crocosphaera* dominated in offshore waters where Fe was low.

A series of experiments were conducted with varying degrees of trade-off between cellular iron to nitrogen reduction (γ) and cost to growth rate (α). These results (Fig. 5) indicate that the cost to growth cannot be too high (small α) or the hotbunkers do not survive. However, for lower cost to growth, hotbunking can confer an advantage in low-iron regions (Fig. 4 and Fig. S5). With the right combinations of α and γ the hotbunking diazotrophs could inhabit some model regions that would not support the control group (Fig. S5 *B* and *D*): The maximum area covered by unicellular diazotrophs increases by over 30% (from 59×10^6 km^2 to more than 79×10^6 km^2; Fig. 5 *A* and *B*) from simulations where only the control group survived to ones where hotbunkers are the only unicellular group surviving. However, the region of parameter space (α, γ) where hotbunkers completely out-compete the control group (white area of Fig. 5*B*) is quite small, suggesting that the energetic cost cannot be too high and there must be a significant reduction in iron needs. With more advantageous values of α and γ, the hotbunking diazotrophs could even outcompete *Trichodesmium* in some specific areas of the model ocean, leading to a reduced global biomass of *Trichodesmium* in those simulations (compare Fig. 4*A* and Fig. S5 *A* and *B*).

The value of γ also affected the local concentration of hotbunking diazotrophs. Simulations with lower requirement for iron (γ smaller) leads to a larger biomass of unicellular diazotrophs at any location compared to simulations with higher γ: the same iron supply could support a higher biomass. This leads to a globally increased biomass of hotbunking unicellular diazotrophs (Fig. 5*C*) with lower γ, and consequently an increase in total global nitrogen fixation (Fig. 5*D*) by as much as 20% (from 90 GtN/y for simulations with no hotbunkers to 107 GtN/y for most extreme case of α and γ, bottom right Fig. 5*D*). We note that more reasonable values of the trade-off would suggest a 5 to 10% increase. Because over many regions of the ocean the nondiazotrophic phytoplankton are nitrogen limited, this increased source of fixed nitrogen led to increased primary production. Globally this increase was as much as 1.5% between a simulation with no hotbunking unicellular diazotrophs (poor combination of α and γ) and one where hotbunkers outcompeted the control group everywhere (advantageous α and γ).

Other Supporting Information Files

Dataset S1 (XLSX)

1. Waterbury JB, Willey JM (1988) Isolation and growth of marine planktonic cyanobacteria. *Methods of Enzymology* eds Packer L, Glazer AN (Academic, San Diego), pp 100–105.
2. Saito MA, Moffett JW, Chisholm SW, Waterbury JB (2002) Cobalt limitation and uptake in *Prochlorococcus*. *Limnol Oceanogr* 47:1629–1636.
3. Ernst A, Kirschenlohr H, Diez J, Boger P (1984) Glycogen content and nitrogenase activity in *Anabaena variabilis*. *Arch Microbiol* 140:120–125.
4. Keller A, Nesvizhskii AI, Kolker E, Aebersold R (2002) Empirical statistical model to estimate the accuracy of peptide identifications made by MS/MS and database search. *Anal Chem* 74:5383–5392.
5. Peng J, Elias JE, Thoreen CC, Licklider LJ, Gygi SP (2003) Evaluation of multidimensional chromatography coupled with tandem mass spectrometry (LC/LC-MS/MS) for large-scale protein analysis: The yeast proteome. *J Proteome Res* 2:43–50.
6. de Hoon MJL, Imoto S, Nolan J, Miyano S (2004) Open source clustering software. *Bioinformatics* 20:1453–1454.
7. Eisen MB, Spellman PT, Brown PO, Botstein D (1998) Cluster analysis and display of genome-wide expression patterns. *Proc Natl Acad Sci USA* 95:14863–14868.
8. Stemmann O, Zou H, Gerber SA, Gygi SP, Kirschner MW (2001) Dual inhibition of sister chromatid separation at metaphase. *Cell* 107:715–726.
9. Raven JA (1988) The iron and molybdenum use efficiencies of plant growth with different energy, carbon and nitrogen sources. *Plant Phytol* 109:279–287.
10. Kustka A, Sanudo-Wilhelmy S, Carpenter EJ, Capone DG, Raven JA (2003) A revised estimate of the iron use efficiency of nitrogen fixation, with special reference to the marine cyanobacterium *Trichodesmium* spp. (Cyanophyta). *J Phycol* 39:12–25.
11. Krogmann DW (1991) The low-potential cytochrome c of cyanobacteria and algae. *Biochim Biophys Acta* 1058:35–37.
12. Follows MJ, Dutkiewicz S, Grant S, Chisholm SW (2007) Emergent biogeography of microbial communities in a model ocean. *Science* 315:1843–1846.
13. Dutkiewicz S, Follows MJ, Bragg J (2009) Modelling the coupling of ocean ecology and biogeochemistry. *Global Biogeochem Cy* 23:GB4017.
14. Monteiro F, M.J. Follows, & Dutkiewicz S (2010) Distribution of diverse diverse nitrogen fixers in the global ocean. *Global Biogeochemical Cycles* 24:10.1029/2009GB003731.

15. Wunsch C, Heimbach P (2006) Estimated decadal changes in the North Atlantic meridional overturning circulation and heat flux 1993–2004. *J Phys Oceanogr* 36:2012–2024.
16. Luo C, et al. (2008) Combustion iron distribution and deposition. *Global Biogeochemical Cycles* 22:10.1029/2007GB002964
17. Elrod VA, Berelson WM, Coale KH, Johnson K (2004) The flux of iron from continental shelf sediments: A missing source for global budgets. *Geophys Res Lett* 31:10.1029/2004GL020216.
18. Verdy A, Follows M, Flierl G (2009) Evolution of phytoplankton cell size in an allometric model. *Mar Ecol-Prog Ser* 379:1–12.
19. Raven JA, Evans MCW, Korb RE (1999) The role of trace metals in photosynthetic electron tranpsort in O_2-evolving organisms. *Photosynth Res* 60:111–149.
20. LaRoche J, Boyd PW, McKay RML, Geider RJ (1996) Flavodoxin as an in situ marker for iron stress in phytoplankton. *Nature* 382:802–805.
21. Wells ML (1999) Manipulating iron availability in nearshore waters. *Limnol Oceanogr* 44:1002–1008.
22. Hutchins DA, Franck M, Brezezinski MA, Bruland KW (1999) Inducing phytoplankton iron limitation in iron-replete coastal waters witha a strong chelating ligand. *Limnol Oceanogr* 44:1009–1018.
23. Erdner DL, Anderson DM (1999) Ferredoxin and flavodoxin as biochemical indicators of iron limitation during open-ocean iron enrichment *Limnol Oceanogr* 44:1609–1615.
24. Webb EA, Ehrenreich IM, Brown SL, Valois FW, Waterbury JB (2009) Phenotypic and genotypic characterization of multiple strains of the diazotrophic cyanobacterium, *Crocosphaera watsonii*, isolated from the open ocean. *Environ Microbiol* 11:338–348.
25. Amin SA, et al. (2009) Photolysis of iron siderophore chelates promotes bacterial algal mutualism. *Proc Natl Acad Sci USA* 106:17071–17076.
26. Kerfeld CA, et al. (2003) Structural and EPR characterization of the soluble form of cytochrome c-550 and of the psbV2 gene product from the cyanobacterium *Thermosynechococcus elongatus*. *Plant Cell Physiol* 44:697–706.
27. Kurisu G, Zhang H, Smith JL, Cramer WA (2003) Structure of the cytochrome b6f complex of oxygenic photosynthesis: Tuning the cavity. *Science* 302:1009–1014.
28. Peschek GA, Schmetterer G (1982) Evidence for plastoquinol-cytochrome f/b-563 reductase as a common electron donor to P700 and cytochrome oxidase in cyanobacteria. *Biochem Bioph Res Co* 108:1188–1195.
29. Migita CT, Zhang X, Yoshida T (2003) Expression and characterization of cyanobacterium heme oxygenase, a key enzyme in the phycobilin synthesis. *Eur J Biochem* 270:687–698.
30. Weber L, C.Volker, Oschlies A, Burchard H (2007) Iron profiles and speciation of the upper water column at the Bermuda Atlantic time-series study site: a model based sensitivity study. *Biogeosciences* 4:689–706.
31. Tuit C, Waterbury J, Ravizza G (2004) Diel variation of molybdenum and iron in marine diazotrophic cyanobacteria. *Limnol Oceanogr* 49:978–990.
32. Voelker B, Morel FMM, Sulzberger B (1997) Iron redox cycling in surface waters: Effects of humic substances and light. *Environ Sci Technol* 31:1004–1011.
33. Shaked Y, Kustka AB, Morel FMM (2005) A general kinetic model for iron acquisition by eukaryotic phytoplankton. *Limnol Oceanogr* 50:872–882.
34. Shi T, Ilikchyan I, Rabouille S, Zehr JP (2010) Genome-wide analysis of diel gene expression in the unicellular N_2-fixing cyanobacterium *Crocosphaera watsonii* WH 8501. *ISME J* 4:621–632.
35. Millero FJ, Sotolongo S, Izaguirre M (1987) The oxidation kinetics of Fe(II) in seawater. *Mar Chem* 51:793–801.
36. Hopkinson B, Morel FMM (2009) The role of siderophores in iron acquisition by photosynthetic marine microorganisms. *Biometals* 22:659–669.
37. Fu F-X, et al. (2008) Interactions between changing pCO_2, N_2 fixation, and Fe limitation in the marine unicellular cyanobacterium *Crocosphaera*. *Limnol Oceanogr* 53:2472–2484.
38. Monteiro F, Dutkiewicz S, Follows MJ (2010) Biogeographical controls on marine nitrogen fixers. *Global Biogeochemical Cycles* 10.1029/2010GB003902.
39. Moisander PH, et al. (2010) Unicellular cyanobacterial distributions broaded the oceanic N_2 fixation domain. *Science* 327:1512–1514.
40. Langlois RJ, Hummer D, LaRoche J (2008) Abundances and distributions of the dominant nifH phylotypes in the northern Atlantic ocean. *Appl Environ Microb* 74:1922–1931.
41. Foster RA, Subramaniam A, Zehr JP (2009) Distribution and activity of diazotrophs in the eastern equatorial Atlantic. *Environ Microbiol* 11:741–750.
42. Church MJ, Björkman KM, Karl DM, Saito MA, Zehr JP (2008) Regional distributions of nitrogen-fixing bacteria in the Pacific Ocean. *Limnol Oceanogr* 53:63–77.
43. Church MJ, Short CM, Jenkins BD, Karl DM, Zehr JP (2005) Temporal patterns of nitrogenase gene (nifH) expression in the oligotrophic north Pacific ocean. *Appl Environ Microbiol* 71:5362–5370.
44. Mazard SL, Fuller NJ, Orcutt KM, Bridle O, Scanlan DJ (2004) PCR analysis of the distribution of unicellular cyanobacterial diazotrophs in the Arabian Sea. *Appl Environ Microbiol* 70:7355–7364.
45. Campbell L, Carpenter EJ, Montoya JP, Kustka AB, Capone DG (2005) Picoplankton community structure within and outside a *Trichodesmium* bloom in the southwestern Pacific Ocean. *Vie Milieu* 55:185–195.
46. Bonnet S, et al. (2008) Nutrient limitation of primary production in the Southeast Pacific (BIOSOPE cruise). *Biogeosciences* 5:215–225.
47. Moore JK, Doney SC, Lindsay K (2004) Upper ocean ecosystem dynamics and iron cycling in a global three-dimensional model. *Global Biogeochem Cy* 18:10.1029/2004GB002220.

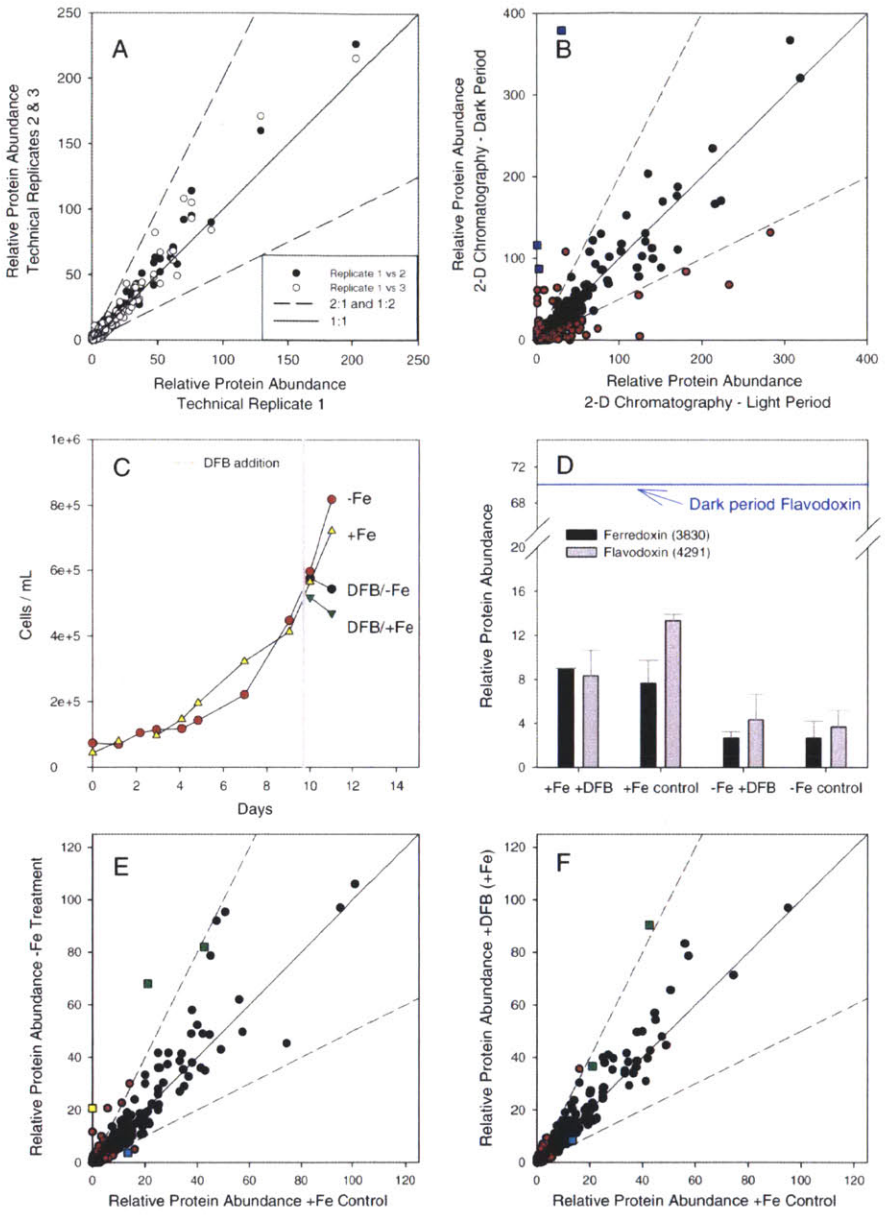

Fig. S1. Supplementary global proteome results. Relative protein abundance determined by spectral counting. (*A*) Comparison of three technical replicates from the light period from the light-dark experiment (Fig. 1*B*) showed good reproducibility; 1:1 and 2-fold change lines are shown for comparison. (*B*) Comparative global proteomes of the light-dark experiment *Crocosphaera watsonii* samples as analyzed by 2D-chromatography. Proteins with greater than two-fold change in relative abundance are in red (≥5 spectral counts), with the exception of the nitrogenase metalloenzymes in blue squares; and trends are consistent with the 1D chromatography analyses in Fig. 1*B*. (*C*) Cell abundances during the iron stress experiment, where high and low abundance iron cultures were both split and one bottle of each was treated with 500 nM of the iron chelator DFB. Both DFB treatments showed cessation of growth within 24 h. (*D*) Relative abundance of ferredoxin and flavodoxin proteins in the iron stress experiment showed no increase in flavodoxin during the light period either under DFB addition or no iron added treatment, in contrast to the large dark period flavodoxin relative and absolute abundances observed in all dark period analyses (Figs. 1*B*, 2, and 3*D*; and Fig. S2). A decrease in ferredoxin (Cwat3830) was observed in treatments without added iron. Data and error bars are the average and standard deviation of technical triplicate analyses. (*E* and *F*) Comparative global proteomes of iron stress in *Crocosphaera* samples, with relative protein abun-

dance given by average of technical triplicate spectral counts from samples taken during growth in the light period under high and low-iron (*E*) and under high iron with and without the addition of iron chelator desferrioxamine B (*F*). Proteins with greater than 2-fold change (dashed lines) in relative abundance are in red (≥5 spectral counts). The carbon concentrating mechanism/microcompartments protein (Cwat5294) and ribulose-biphosphate carboxylase (Cwat2714), shown in green squares, appear modestly more abundant in iron limited treatments. Fructose-bisphosphate aldolase shown in yellow squares (panel *E*; Cwat2319) is involved in carbohydrate synthesis and was more abundant in low-iron. Flavodoxin shown in cyan squares (panels *E* and *F*; Cwat4291).

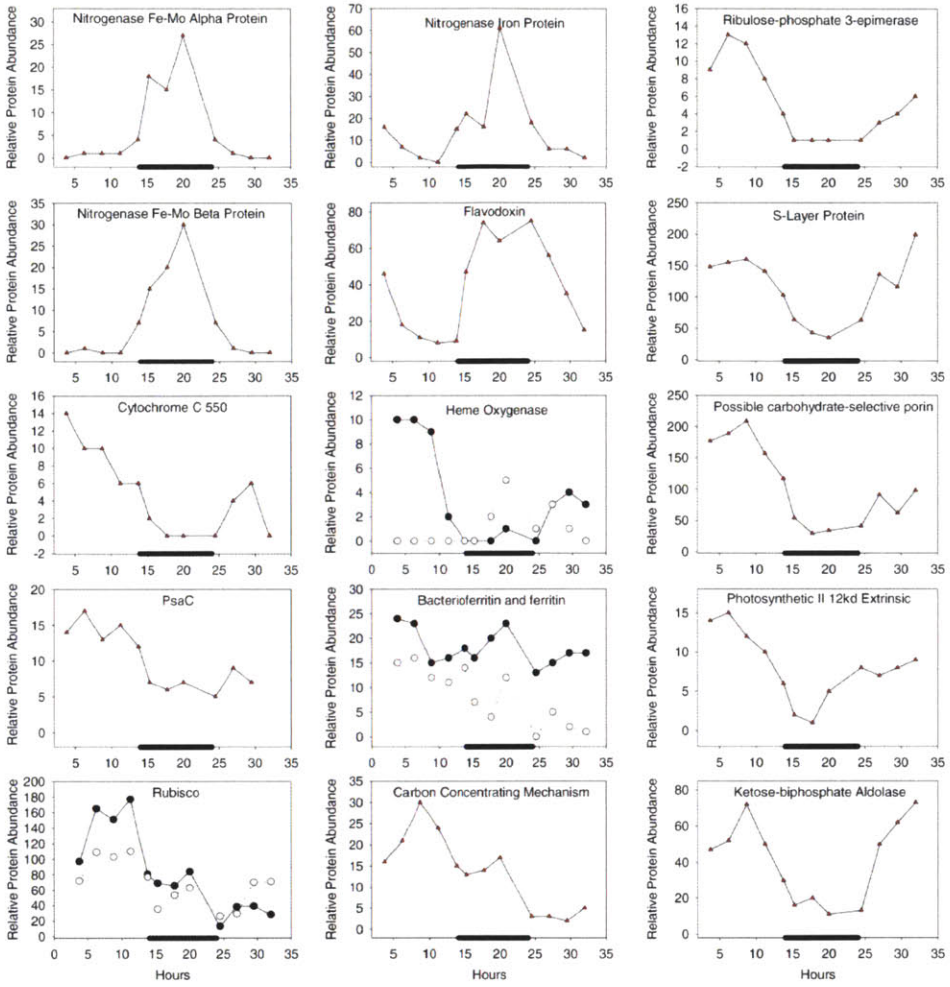

Fig. S2. Relative abundance of proteins of interest as determined using spectral counting. Relative abundance as determined by spectral counting on a linear trap mass spectrometer during the diel cycle (dark, black bar) showed good agreement with trends observed using targeted proteomic analysis on a triple quadrapole mass spectrometer for iron metalloproteins (Fig. 3). For the heme oxygenases, the empty circles are Cwat2459 whereas the filled circles are Cwat4859. The nitrogenase iron protein is Cwat3818, molybdenum-iron protein subunits MoFe α, MoFe β are Cwat3819 and 3120, flavodoxin is Cwat4291, and c550 is Cwat5304. PsaC is Cwat5975, bacterioferritin (closed) and ferritin (open) are Cwat5989 and Cwat4924, Rubisco refers to ribulose-bisphosphate carboxylase long (Cwat2714, closed) and short (Cwat2716, open) chain. Carbon concentrating mechanism is Cwat5296, ribulose-phosphate 3-epimerase is Cwat4803, and possible carbohydrate-selective porin is Cwat6588. S-layer protein is Cwat4220, photosynthetic II 12 kD extrinsic is Cwat0626, and ketose-biphosphate aldolase is Cwat3318.

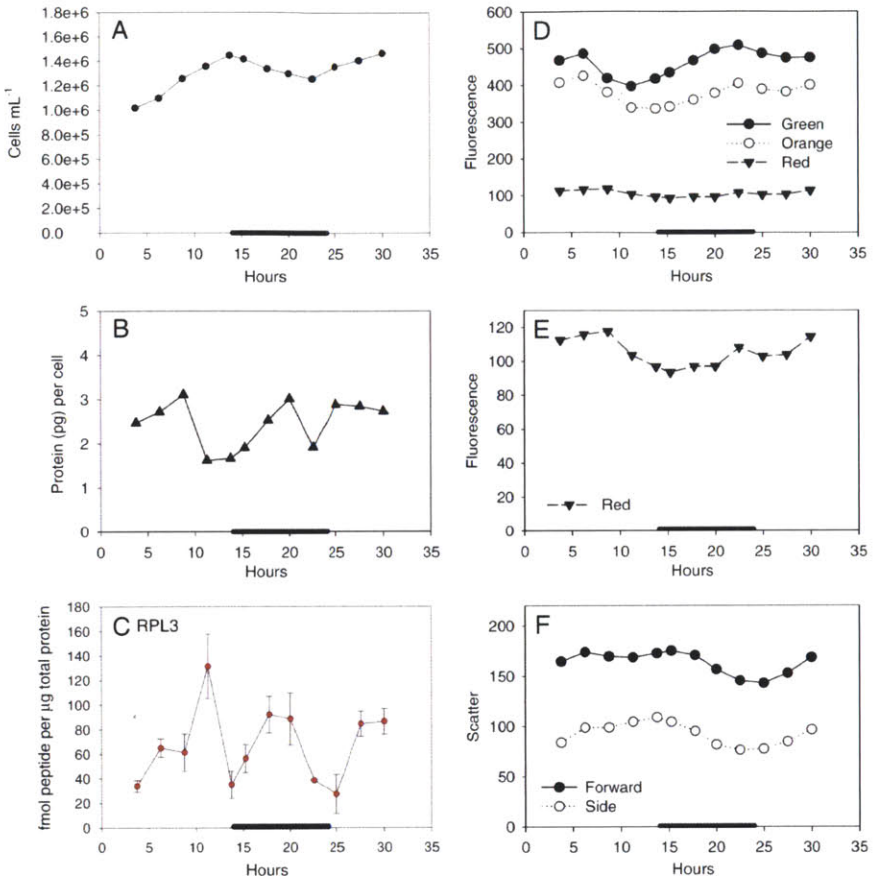

Fig. S3. Ancillary data for the diel *Crocosphaera* experiment. (*A*) Cell density at each time point, as measured by microscopy. (*B*) Total protein concentration in cellular extracts. (*C*) Targeted protein abundance of the ribosomal protein (RP) L3 (Cwat2439, see Table S2), displaying a triple peak consistent with two active periods of protein synthesis per diel cycle. (*D*) Fluorescence per cell as measured by flow cytometry, where green corresponds to a SYBR Green I DNA stain, orange for phycoerthyrin, and red for chlorophyll. (*E*) Expanded scale of red fluorescence per cell. (*F*) Forward and side scatter by flow cytometry with decreasing cell size at night as glycogen stores are consumed (see Fig. 1*A*).

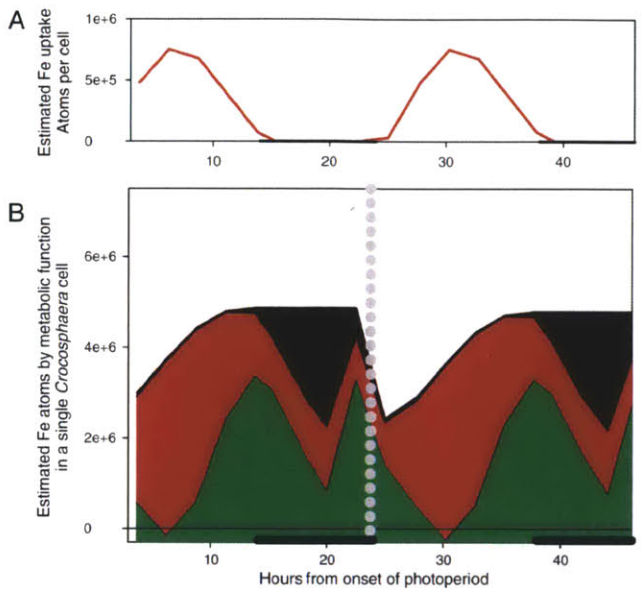

Fig. S4. Schematic of iron uptake and intracellular iron reservoirs in *Crocosphaera* during the diel cycle. (*A*) Idealized iron uptake during the light period (dark, black bar), where ferrous iron abundance has a midphotoperiod maximum due to photochemical reduction of abundant natural Fe(III)-ligand complexes and rapid abiotic reoxidation, consistent with chemical modeling (30), and ferrous iron is considered the accessible form of iron based on the presence of ferrous iron transporters (*feoA* and *feoB*) in the *Crocosphaera* genome. The magnitude of uptake was tuned to minimize the "other" category in steady-state (see below). (*B*) Estimated iron atoms used for nitrogen fixation (black), photosynthesis (red), and the aggregate of storage molecules (bacterioferritin), chaperones, and other metabolic functions (green; estimated by difference of total iron from uptake in (*A*) with the measured nitrogen fixation and photosynthesis reservoirs in Fig. 3), with the assumption of no iron loss or efflux. Cell division (dashed gray) halves the total iron inventory and each individual reservoir. This schematic shows that our measurements of iron metalloprotein inventories over the diel cycle, when combined with estimates of iron uptake and cell division, are consistent with observations of increases in iron quota in the dark relative to the light period (31).

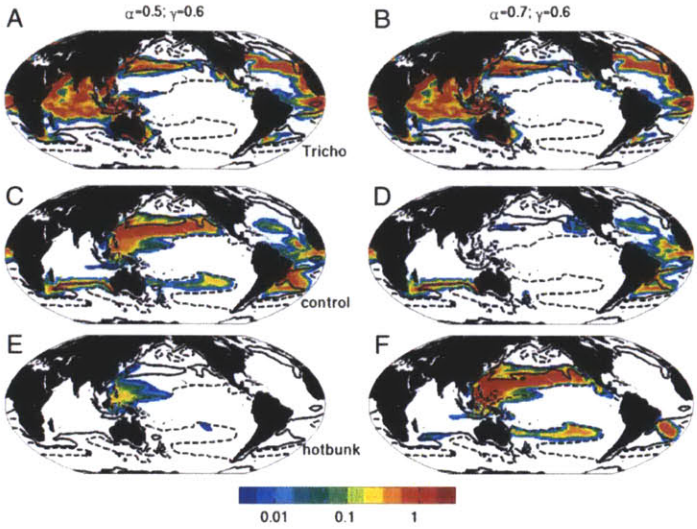

Fig. S5. Hotbunking unicellular diazotrophs habitat is determined by the assumption of the trade-off between lower iron requirement and energetic expense (values of γ and α). Left panels shows results from simulation where the energetic cost is assumed to be high ($\alpha = 0.5$, $\gamma = 0.6$, left cross in Fig. 5) and right panels where the energetic cost is lower ($\alpha = 0.7$, $\gamma = 0.6$, middle cross in Fig. 5). (*A*, *B*) Model analogs of *Trichodesmium*, (*C*, *D*) nonhotbunking unicellular diazotrophs (mgC m^{-3}), the control group; (*E*, *F*) hotbunking unicellular diazotrophs (mgC m^{-3}), analogs of *Crocosphaera watsonii*. Dashed and solid contours indicate 0.1 nM and 0.3 nM Fe respectively (see Fig. 4*A*), and no shading indicates areas devoid of unicellular diazotrophs. These results can be compared to a simulation with a lower energetic cost ($\alpha = 0.9$) shown in Fig. 4. With high cost (*Left*), hotbunking is not advantageous and the *Crocosphaera*-analogs are only competitive in regions where iron is very low (just enough to support diazotrophy). For more advantageous combination of α and γ (right panel), the hotbunking group will out-compete the control group in more regions, and with even higher α (Fig. 4), the hotbunking group will completely out-compete the control and their habitat will include waters with even lower iron supply (Fig. 4), and spread into regions inhabited by *Trichodesmium* simulations where the energetic cost was higher.

Table S1. Iron stoichiometry of photosynthesis and diazotrophy in cyanobacteria

Complex/protein	Iron content (reference)	Fe/complex or Fe/protein
Photosynthesis		
Photosystem I	3 Fe_4S_4 clusters (1)	12
Photosystem II	1 nonheme iron (1)	1
Cytochrome b-559	1 heme iron (1)	1
Cytochrome c-550	1 heme iron (2)	1
b_6f complex	4 heme, 1 Fe_2S_2 per monomer (3)	12 per dimer
Ferredoxin	2Fe-2S bacterial type (1)	2
Ferredoxin	4Fe-4S plant type (1)	4
Nitrogen fixation		
Nitrogenase	Fe protein (NifH) (4)	4 per homodimer
	MoFe protein (NifDK, α and β) (4)	15 per heterodimer
Flavodoxin	None (5)	0

1 Raven JA, Evans MCW, Korb RE (1999) The role of trace metals in photosynthetic electron transport in O_2-evolving organisms. *Photosynth Res* 60:111–149.
2 Kerfeld CA, et al. (2003) Structural and EPR characterization of the soluble form of cytochrome c-550 and of the psbV2 gene product from the cyanobacterium *Thermosynechococcus elongatus*. *Plant Cell Physiol* 44:697–706.
3 Kurisu G, Zhang H, Smith JL, Cramer WA (2003) Structure of the cytochrome b6f complex of oxygenic photosynthesis: Tuning the cavity. *Science* 302:1009–1014.
4 Rubio LM, Ludden PW (2008) Biosynthesis of the iron molybdenum cofactor of nitrogenase. *Annu Rev Microbiol* 62:93–111.
5 LaRoche J, Boyd PW, McKay RML, Geider RJ (1996) Flavodoxin as an in situ marker for iron stress in phytoplankton. *Nature* 382:802–805.

Table S2. Heavy and native sequences of peptides, their SRMs, and collision energies

Protein description	Peptide name	Peptide sequence	Parent m/z	Product m/z	Collision energy	Start time (min)	Stop time (min)
Photosystem 1 protein PsaB (Cwat 1223)	psaB L	TPLANLVR	442.272	501.314	18	12.9	15.1
				572.351	21	12.9	15.1
				685.436	21	12.9	15.1
	psaB H	TPLAN[L_C13N15]VR	445.78	508.331	18	12.9	15.1
				579.368	21	12.9	15.1
				692.452	21	12.9	15.1
Nitrogenase molybdenum-iron protein alpha subunit (Cwat3819)	MoFeA2 L	ILLEEIGLR	528.327	345.22	18	18	21
				716.39	19	18	21
				829.48	17	18	21
	MoFeA2 H	I[L_C13N15]LEEIGLR	531.84	345.22	18	18	21
				716.39	19	18	21
				829.48	17	18	21
Nitrogenase NifH protein (Cwat 3818)	nifH2 L	LNTQMIHFVPR	678.37	655.368	27	15.5	19
				768.452	23	15.5	19
				899.492	22	15.5	19
	nifH2 H	[L_C13N15]NTQMIHFVPR	681.88	655.37	27	15.5	19
				768.45	23	15.5	19
				899.49	22	15.5	19
Nitrogenase molybdenum-iron protein alpha subunit (Cwat 3819)	MoFeA1 L	LIADVLSTYPEK	674.872	373.208	29	15.2	17.6
				724.351	17	15.2	17.6
				837.435	20	15.2	17.6
				1122.567	21	15.2	17.6
	MoFeA1 H	[L_C13N15]IADVLSTYPEK	678.38	373.208	29	15.2	17.6
				724.351	17	15.2	17.6
				837.435	20	15.2	17.6
				1122.567	21	15.2	17.6
Cytochrome b6 of the b6f complex; PetB (Cwat 4239)	petB1 L	LEIQAISDDITTK	723.888	779.378	26	15.4	17.9
				892.462	28	15.4	17.9
				963.499	28	15.4	17.9
	petB1 H	[L_C13N15]EIQAISDDITTK	727.397	779.378	26	15.4	17.9
				892.462	28	15.4	17.9
				963.499	28	15.4	17.9
Photosystem 1 protein PsaA (Cwat 1222)	psaA1 L	VAVDVDPVPTSFEK	751.89	708.356	33	14.9	17.1
				904.477	27	14.9	17.1
				1019.504	24	14.9	17.1
	psaA1 H	VA[V_C13N15]DVDPVPTSFEK	754.897	708.356	33	14.9	17.1
				904.477	27	14.9	17.1
				1019.504	24	14.9	17.1
Flavodoxin, long chain, PetE (Cwat 4291)	petE1 L	FVGLPIDEINQSDK	787.907	591.273	32	16.7	19
				948.426	31	16.7	19
				1158.563	22	16.7	19
	petE1 H	FVG[L_C13N15]PIDEINQSDK	791.415	591.273	32	16.7	19
				948.426	31	16.7	19
				1158.563	22	16.7	19
Nitrogenase molybdenum-iron protein beta subunit (Cwat 3829)	MoFeB1 L	INFIPGFETYIGNLR	877.467	402.246	11	22.5	25.5
				459.267	20	22.5	25.5
				572.351	20	22.5	25.5
				836.462	8	22.5	25.5
				1266.648	30	22.5	25.5
				1379.732	20	22.5	25.5
	MoFeB1 H	INFIPGFETYIGN[L_C13N15]R	880.976	409.263	11	22.5	25.5
				466.285	20	22.5	25.5
				579.369	20	22.5	25.5
				843.479	8	22.5	25.5
				1273.664	30	22.5	25.5
				1386.749	20	22.5	25.5

Protein description	Peptide name	Peptide sequence	Parent m/z	Product m/z	Collision energy	Start time (min)	Stop time (min)
Photosystem II stabilizing cytochrome c550 (Cwat 5304)	c550 L	TNNNVSLGLEDLAGAEPR	935.469	529.272	35	16.6	19
				600.309	25	16.6	19
				1127.569	31	16.6	19
	c550 H	TNNNVS[L_C13N15] GLEDLAGAEPR	938.977	529.272	35	16.6	19
				600.309	25	16.6	19
				1127.569	31	16.6	19
Ribosomal protein L3 (Cwat 2439)	RPL3 L	TTETDGYSAVQLGYLEVK	987.489	708.392	31	16.8	19.2
				949.535	37	16.8	19.2
				1206.673	33	16.8	19.2
	RPL3 H	TTETDGYSAVQ[L C13N15] GYLEVK	990.997	708.392	31	16.8	19.2
				956.552	37	16.8	19.2
				1213.689	33	16.8	19.2

List includes the proteins (description and Cwat number) selected for quantitative monitoring, the peptides, and their heavy labeled versions used as internal standards and the SRM transitions (parent and product ions), collision energies, and scheduled monitoring for triple quadropole mass spectrometery.

Appendix C

Putative cobalt uptake proteins and B_{12} riboswitches in twelve strains of *Prochlorococcus*

Strain	Description	HupE	Switch	Riboswitch Locus Tag, location	CbiQ
Med4-CCMP1986	HL, Med Sea	X			X
AS9601	HL, Arabian Sea				X
MIT 9211	LL, Eq Pac	X			X
MIT 9215	HL, Eq Pac				X
MIT 9301	HL, Sar Sea	X			X
MIT 9303	LL Sar Sea	X	X	1842638-1902782	X
MIT 9312	HL, Gulf Stream				X
MIT 9313	LL, Gulf Stream	X	X	PMT_R0057	X
MIT 9515	HL, Eq Pac				X
NATL1A	LL, NAtl	X			X
NATL2A	LL, NAtl	X			X
CCMP1375, SS120	LL Sar Sea	X	X	Pro_R0047	X

HupE and CbiQ are putative Co uptake proteins (Rodionov et al. 2003). Of 12 sequenced *Prochlorococcus* genomes, all appear to have CbiQ, 8 have HupE, 3 have HupE preceded by a putative B_{12} riboswitch. Strains are described with their location of isolation and light level preference. HL is high light adapted, and LL is low light adapted. Patterns in Co uptake protein and B_{12} riboswitch presence do not show obvious patterns with isolation location or phylogenetic relationship, as observed previously for other transporters (Kettler et al 2007). B_{12} riboswitches preceding some genes encoding Co uptake machinery suggest that in some cases, *Prochlorococcus* strains regulate Co uptake as a function of intracellular B_{12} availability.

References

Rodionov DA, Vitreschak AG, Mironov AA, Gelfand MS (2003) Comparative genomics of the vitamin b_{12} metabolism and regulation in prokaryotes. J Biol Chem 278:41148-41159

Kettler GC, Martiny AC, Huang K, Zucker Jand others (2007) Patterns and implications of gene gain and loss in the evolution of *Prochlorococcus*. PLoS Genetics 10.1371/journal.pgen.0030231

Appendix D:

B_{12} uptake by three cultured phytoplankton strains

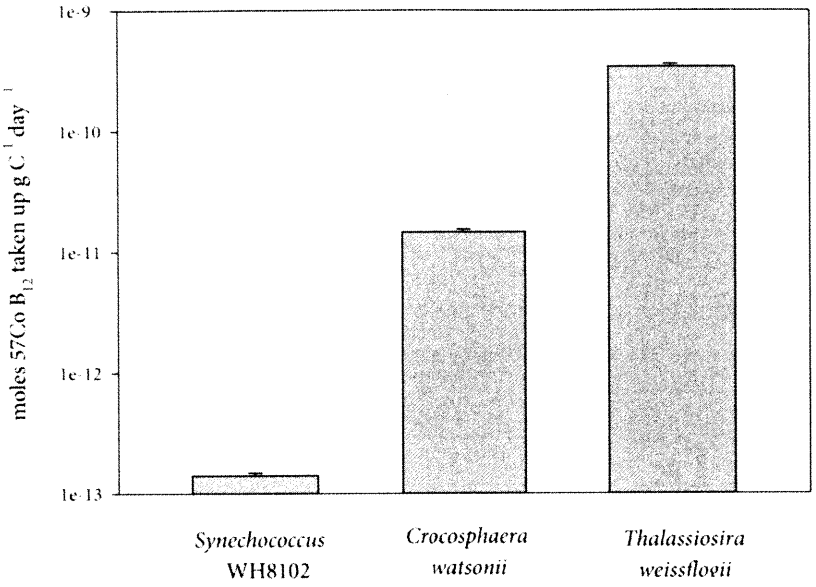

^{57}Co labeled B_{12} uptake, normalized to cellular carbon content, in cultures of the marine diatom *Thalasiosira weissflogii*, the diazatroph *Crocosphaera watsonii* and the abundant unicellular cyanobacterium *Synechococcus* WH8102. Measurements were obtained using ^{57}Co cobalamin extracted from Rubratope 57 (Radiopharmacy, Evansville, Indiana) and purified for inorganic metal contaminants (including inorganic ^{57}Co) using Chelex-100 (BioRad). The ^{57}Co labeled cobalamin was introduced to 50 mL of culture in mid to late log growth phase without added vitamins in the media, or to 50 mL of heat shocked culture as a killed control. After 24h of incubation, the samples were filtered onto 0.2 μm polycarbonate filter membranes and ^{57}Co activity was assayed using a Canberra Germanium Gamma detector. The data displayed represent live minus killed control 'uptake,' shown with error bars representing 5% counting error. These data demonstrate significant uptake in the marine diatom culture, but nearly undetectable uptake in by *Synechococcus*, consistent with genomic analysis and implying *Synechococcus* synthesizes its entire B_{12} requirement (Rodionov et al 2003). *Crocosphaera* appears to be able to satisfy at least a portion of its vitamin requirement through uptake from the environment, despite its proven ability to take up the vitamin and the absence of a known B_{12} uptake system in its sequenced genome (Bonnet et al 2010).

References

Bonnet S, Webb EA, Panzeca C, Karl DM, Capone DG, Sanudo-Wilhelmy SA (2010) Vitamin B_{12} excretion by cultures of the marine cyanobacteria *Crocosphaera* and *Synechococcus*. Limnol and Oceanog 55:1959-1964

Rodionov DA, Vitreschak AG, Mironov AA, Gelfand MS (2003) Comparative genomics of the vitamin b_{12} metabolism and regulation in prokaryotes. J Biol Chem 278:41148-41159

Appendix E:

Thalassiosira pseudonana CBA1 (Tp11697) coding sequence analyses

Attempts were made to amplify the coding sequence (CDS) for *T. pseudonana* protein 11697 (CBA1) from cDNA synthesized from mRNA extracted from B_{12}- starved *T. pseudonana* cultures for overexpression, as described in Chapter 4 for *P. tricornutum*. Four separate primer sets used to amplify this CDS are listed below:

(1) ThapsB12B_pENTR_noSP_s1: 5′ C ACC GAG TAC ACC CCT CCA ACC ACA 3′
ThapsB12B_pENTR_SP_s2: 5′ C ACC ATG AAG CTA TCC AAC AGC TGG 3′

(2) ThapsB12B_pENTR_stop_a1: 5′ TCA CCT CCA ATG CCC ATG CTC TTC 3′
ThapsB12B_pENTR_nostop_a2: 5′ CCT CCA ATG CCC ATG CTC TTC TAT 3′

(3) ThapsB12B_pENTR_noSP_s3: 5′ C ACC GAG TAC ACC CCT CCA 3′
ThapsB12B_pENTR_stop_a3: 5′ TCA CCT CCA ATG CCC ATG CT 3′

(4) ThapsB12B_pENTR_SP_s4: 5′ C ACC ATG AAG CTA TCC AAC 3′
ThapsB12B_pENTR_nostop_a4: 5′ CCT CCA ATG CCC ATG CTC 3′

In all cases, the amplified product appeared much larger than the coding sequence predicted by the genome project (~4500 bp versus 1815bp) via gel electrophoresis (Figure 1). Sequencing this product end to end revealed that it is 2158 bp, is not exactly as predicted from the whole genome and includes considerable amounts of sequence that was predicted to be intron in the genome project (Figure 2). This amplification and sequencing was repeated four times using separate primer sets, all yielding the same result. Control PCR reactions performed on products from cDNA synthesis reactions without added reverse transcriptase were all negative, suggesting that this result is not a product of genomic DNA contamination. The resulting intron splice sites, inferred from this model and the genome project Tp11697 gene sequence, are not canonical (are not GT at the beginning of the intron and AG at the end) as expected in diatoms. There is also a new stop codon in the PCR amplified CDS that truncates the predicted protein and excludes

peptides that were identified from the genome CDS in the proteomic study in Chapter 4 (Figure 2, 3). These data suggest that the CDS predicted from the PCR amplification of cDNA is not correct. Additionally, an alignment of four CBA1 amino acid sequences predicted in whole genome sequencing projects from three diatoms reveals that the C-terminal end of the *T. pseudonana* protein is extended, calling the genome project CDS model into question as well (Figure 4). These data are difficult to explain and warrant further attention. These efforts should consider the role of atypical post-transcriptional processing.

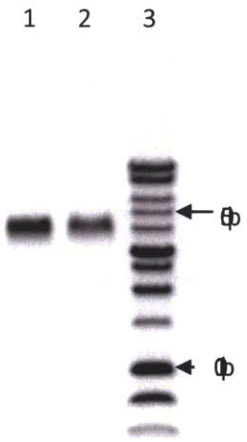

Figure 1: Amplifying Tp 11697 from cDNA prepared from *T. pseudonana* cells as described for *P. tricornutum* in Chapter 4 yielded a product much larger than the coding sequence predicted by the genome project (~4500 bp versus 1815bp). Lanes 1 and 2 are PCR products amplified from cDNA using primer sets 1 and 2. Lane 3 is a molecular weight marker.

(A)

ATGAAGCTATCCAACAGCTGGTCCTCCCTCCTACTTCTCCTCGCAGCGGCAGCCTCCACCACATCGGCAGAGTACACCC
CTCCAACCACAAACTACGACCGATGCCTCACCGCCGACGAAGCAGCCGACATCACCACCGCCCTCTCCAACGGTGTCGA
GGTTGATCTCTTCCCTGAGAAGGTATCCAGCGATCAATCCGTTTACTGGGAGATTGACTATCGTTCCACCTACAAGATC
CTCAAGAATACACAAGATACAGTCAACACCACCTACCTTTTGTACCAATGTGGTCTCCCCGAACCTACTCCCGAGACAC
ACCCTGAACTCGAAGGAATCACATTTGATAGCGTCTTTAGTGTCCCTCACACTGGAGGACTGCTTGTTACTGCTACTAC
TCAGATCCCAAACATCGAGATACTTAACCGTCGTAGTCAAGTTGTTGCGTTTGCAGTATCTGAGAACTTGGTTTCCAGT
CCTTGTTTGTCTCAGCAGATCATCCCTGCCGGGAAAGAAGATGGGAGTATCACCTTCTTGCCATTGTATAATGATACAG
TGATTGAGGACTACGTAACGGAACACCCTGACACTTTAGTGTTGGGTGGAGCGTGGGATACCGATCTCAAGATGAAGAA
CAAGGTCATCATCTCGGACGTGGGTGAGTCGCCCGAAGAGGCACTGGACCAAAATCGTGATGTGAACGAAGCCATCTTT
GAATGGTTGGAAGTGTATGGGTCTTTGTTTAACGAGGAGGGATTGGCGGGAGGAGTTGTGAGTGATACGAAGGGGAGGT
ATAATTGTCATACTGATAATGCTGCAATGATTGCTGAGTCGAGGAGGGAGTTGAGGGATGTCGAGGAGAGGAGGCTGGA
AGAGGGTAGTCGTGTGAGTACTTGTCGATGTTTCATTGCAAACCTCTTGAACAGCTCATGTCTTCTCTCAAATCAAAGT
ACTAATCTTCATCACCTGCACTCCTTCTTTGCAATCCTCAACTACAAACGAACAACAGCCCGTGGTACTTTGGGCATAC
CACAACCAGGACTT**TGA**AGGAAACGACGTTGGATGGGACGTTGGTGAATGTCCCAACTACTACTGCACCTATGCCAAGC
ATTGCCATGTTGAGATGTTGAACTCTACGGAAGGAAGTATTGATTATTGGGGATATCCTCGCATGACGGATGAGGAGTT
TTTGGAGTTTGGAAAGAAGTGAGTTCATATGTATTGATCTTGATGTATCTTGATTTCTCCAGCGGCGGGTAGCTCACAA
TGTGCTTCATTCCTTTCACATAGTGCCGATGTATGGGTTTACCCCTCTTCTGATTGGAACAGGGTATCAACCCAAAAGA
TGTTCTACCTCAGTCAGTTCAAGGCTGTTCAGGATGAGAAGGTCTATGACTACCAGATGAGTGGAGAGAGTGCTTGGTT
TGAGCAGCGTTGATACACTTCTTATCCAACCACACAACAGATACTGTCCTCCTTGACCTCTGTCACATCGTTGATCGTG
CCGTATCCACCGACCCACCCCACATTCGTAAGTGGTTTCGCAACGTCTACACCGAAGGAGTAGGAACGTTGGGAATGTG
TGAAGACCCTGAAGAGCCATACACCTCTCGTGCTACTGAGTGTGTAAGGCTTGATGATGTTGTTGGCGGTGGTGATGTT
GAGGGGGGAGGTGATACTGCTACTGAAGTTCCCGCTGCTTCTTCTGGAAGTCGTTTGGCCGTTGTGTTGGGAGCTGTCT
CTATCTTGTCCGTGGTTGCGAATGTGGCGTTTACTCTTTGAATAATTGGAGGCGGTATTTAGATTTGACCCTTTAATCC
CGATCTATTTCTTTCTAGAGTAACTAAGATTGCGCTGGTGTTATGAAGGAGGTGTTTACCAGCGCCCGAGAGCTTAGCT
TCACGAAAGAAATGTCCATCGATGATGTAGCGAATGTTCTGAGCGACTGCAGAGTTATCTTTGGGATACACGGAGCTGG
ACATATGAATGCCTTGTTTGCAAGACCTGATGTTGCCGTCATTGAAATCATTGGAAAAGATCCTTCTTATCACAGCTCT
GATGAAGATCAGAAAGGATATCCTGCATACTTTCGGAATATAAACATGTTGCTTGGACAGTACTATCAAAGCATCGCTG
GAGATTCAACACGTGGGATGTATGACGATGGGTATGTTATTGATTTGGAAGAGGCAAGAGAGGCGCTTGTACGAGCTAG
ACATCATTCTACTTCGTGGATAGAAGAGCATGGGCATTGGAGGTGA

(B)

MKLSNSWSSLLLLLAAAASTTSAEYTPPTTNYDRCLTADEAADITTALSNGVEVDLFPEKVSSDQSVYWEIDYRSTYKI
LKNTQDTVNTTYLLYQCGLPEPTPETHPELEGITFDSVFSVPHTGGLLVTATTQIPNIEILNRRSQVVAFAVSENLVSS
PCLSQQIIPAGKEDGSITFLPLYNDTVIEDYVTEHPDTLVLGGAWDTDLKMKNKVIISDVGESPEEALDQNRDVNEAIF
EWLEVYGSLFNEEGLAGGVVSDTKGRYNCHTDNAAMIAESRRELRDVEERRLEEGSRVSTCRCFIANLLNSSCLLSNQS
TNLHHLHSFFAILNYKRTTARGTLGIPQPGL*RKRRWMGRW*MSQLLLHLCQALPC*DVELYGRKY*LLGISSHDG*GV
FGVWKEVSSYVLILMYLDFSSGG*LTMCFIPFT*CRCMGLPLF*LEQGINPKDVLPQSVQGCSG*EGL*LPDEWRECLV
*AALIHFLSNHTTDTVLLDLCHIVDRAVSTDPPHIRKWFRNVYTEGVGTLGMCEDPEEPYTSRATECVRLDDVVGGGDV
EGGGDTATEVPAASSGSRLAVVLGAVSILSVVANVAFTL*IIGGGI*I*PFNPDLFLSRVTKIALVL*RRCLPAPESLA
SRKKCPSMM*RMF*ATAELSLGYTELDI*MPCLQDLMLPSLKSLEKILLITALMKIRKDILHTFGI*TCCLDSTIKASL
EIQHVGCMTMGMLLIWKRQERRLYELDIILLRG*KSMGIGG

Figure 2: (A) The sequence amplified from *T. pseudonana* cDNA, retrieved several times using four separate sets of primers and two different polymerase enzymes for the PCR reaction. Nucleotides colored in black were deemed exons while red were deemed introns in the genome sequencing project. The first stop codon is shown in bold. (B) The amino acid sequence encoded by the CDS above, with * denoting stop codons.

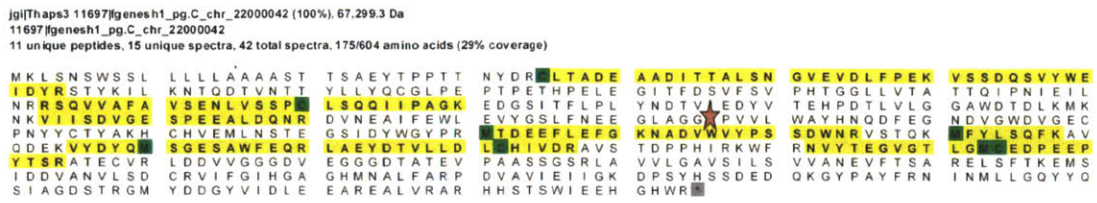

Figure 3: Several peptides predicted in the genome CDS for Tp11697, very reproducibly and clearly detected in the proteome study, are not included in the PCR amplified CDS because of the inclusion of sequence that was predicted in the genome project to be intron. The genome project predicted CDS is shown above, with peptides identified in Chapter 4 highlighted in green and yellow- green denotes chemical modifications of cysteine and methionine residues. The location at which the PCR amplified CDS changes the predicted protein sequence is denoted with a star. Since there are many peptides clearly detected that were C-terminal to this change, it suggests that the PCR-amplified CDS is not correct. Notably, there were no peptides identified C-terminal to peptide NVYTEGVGTLGMCEDPEEPYTSR, supporting the suggestion based on the CBA1 sequence alignment (Figure 4), that the C-terminal end of the genome project CDS is not correct either.

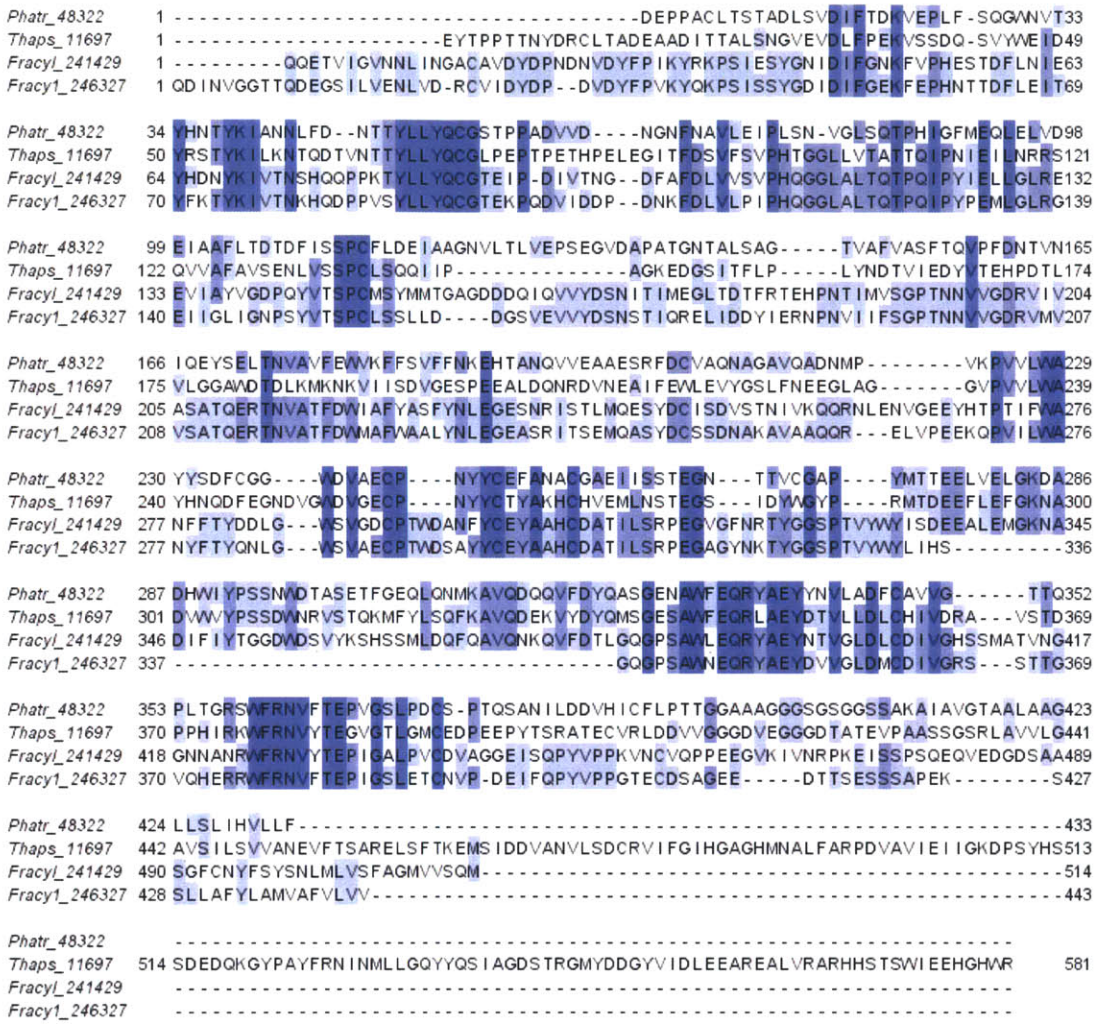

Figure 4: Alignment of four predicted amino acid sequences for protein CBA1 from three diatoms with signal peptides removed. Darker shading indicates higher percent identity. The C-terminal end of the *T. pseudonana* protein is extended, calling this protein model into question.

Appendix F

Proteins identified in Chapter 4 via shotgun proteomic analyses of *T. pseudonana* and *P. tricornutum*

Tables include protein identification numbers from the genome project; either the JGI assigned number or NCBI assigned number if a JGI number is unavailable; a putative functional assignment compiled from JGI and NCBI annotations and manual inspection; spectral counting abundance scores for technical triplicate analyses of each treatment- low B_{12} with low Fe, low B_{12}, low Fe and replete, and Fisher Exact Test scores for pairwise comparisons between treatment.

Table A1: *T. pseudonana* protein identifications and spectral counting abundance scores. 764 proteins were identified with a 0.19% peptide false discovery rate.

Protein Id, Description		Spectral Counting Abundance Scores												Fisher Exact Test P values					
		Colim			B12 lim			Fe lim			Replete			Colim vs B12 lim	Colim vs Fe lim	Colim vs replete	B12 lim vs Fe lim	B12 lim vs replete	Fe lim vs replete
		a	b	c	a	b	c	a	b	c	a	b	c						
bd 573	cytochrome f	105	120	142	69	79	74	146	143	163	96	85	84	5.2E-09	0.0017	0.00001	9.9E-19	0.029	1.4E-14
23813	putative protease inhibitor	109	118	122	77	75	79	127	124	140	17	16	13	0.000002	0.066	0	1.9E-10	2.2E-31	0
31383	GAPD1	76	69	66	27	25	26	170	163	173	33	37	28	1.9E-13	2E-29	2.2E-11	0	0.096	0
bd 2088	RuBisco	21	24	18	54	61	63	1	2	2	190	203	213	2.1E-12	7.9E-15	0	0	0	0
38191	HSP	78	83	73	62	73	68	96	105	107	40	38	39	0.072	0.00099	3.7E-11	2.5E-06	1.1E-06	3E-24
36716	lipoamide dehydrogenase	69	71	88	75	64	76	65	66	63	38	41	28	0.3	0.055	4.1E-12	0.17	6.3E-10	4E-08
34830	PSBO	48	35	41	25	28	34	122	125	136	32	30	37	0.0098	5.1E-32	0.044	8E-43	0.22	0
38494	Chlorophyll A-B binding protein	43	45	40	41	30	31	22	24	19	102	108	103	0.073	3.1E-06	9E-20	0.0024	4.6E-25	2.8E-45
270138	possible Glutamine synthetase	4	3	5	113	126	116	0	0	0	84	71	74	0	0.00019	0	0	7E-08	0
20812	uncharacterized, conserved algal protein	53	59	57	54	41	46	43	42	47	25	20	21	0.077	0.017	1E-12	0.3	6.2E-08	2.8E-07
4914	NADP/FAD dependent oxidoreductase	39	41	38	31	28	41	44	46	53	44	32	47	0.15	0.056	0.41	0.0036	0.081	0.083
40391	Enolase	29	34	27	34	34	25	71	74	71	30	27	23	0.45	4.1E-13	0.24	6.9E-12	0.19	9.8E-18
28334	GAPD4	29	43	38	51	40	48	46	46	42	34	30	34	0.051	0.079	0.19	0.39	0.0037	0.006
7881	uncharacterized, conserved algal protein	46	35	37	32	35	30	37	41	38	47	53	43	0.12	0.5	0.058	0.12	0.0022	0.042
41829	putative translation elongation factor alpha	21	27	23	43	58	43	17	17	17	57	59	51	1.7E-06	0.042	1.2E-10	2E-11	0.1	8.5E-18
10417	uncharacterized, conserved algal protein	41	34	37	49	47	41	45	51	37	24	30	30	0.066	0.1	0.023	0.4	0.00015	0.00021
21815	methionine adenosyltransferase	37	33	29	59	73	69	20	29	28	27	30	31	2.2E-08	0.061	0.19	1.6E-13	6.8E-12	0.25
26041	copper-induced, girdle assoc	63	50	55	31	29	35	58	50	50	12	11	11	0.000016	0.3	4.5E-24	0.000093	3.5E-08	5.2E-23
YP_874528.1	ATP synthase, beta chain, thylakoid	47	40	41	53	48	53	41	46	31	31	37	37	0.076	0.3	0.077	0.02	0.0014	0.19
1287	ATP synthase alpha chain, thylakoid ATPase	30	32	27	35	33	36	53	47	55	28	31	25	0.18	0.00002	0.36	0.0014	0.083	6.2E-07

Table A1 cont.

Protein Id, Description		Spectral Counting Abundance Scores												Fisher Exact Test P values					
		Colim			B12 lim			Fe lim			Replete			Colim vs B12 lim	Colim vs Fe lim	Colim vs replete	B12 lim vs Fe lim	B12 lim vs replete	Fe lim vs replete
		a	b	c	a	b	c	a	b	c	a	b	c						
24932	thioredoxin related	37	29	31	32	28	30	54	49	57	14	15	12	0.34	0.00007	4.4E-07	0.00001	0.00001	2E-20
260953	ornithine cyclodeaminase	20	20	22	34	21	25	25	27	27	47	50	46	0.078	0.071	5.1E-09	0.51	0.00003	5.1E-06
41256	F-type H-ATPase beta subunit	14	13	10	53	58	49	5	5	3	59	56	60	6.1E-18	0.00034	1.4E-23	6.2E-34	0.21	7.1E-43
22610	RL4e, ribosomal protein	30	25	30	26	27	29	42	41	38	22	25	26	0.43	0.0086	0.16	0.0048	0.25	0.00013
39799	glycine decarboxylase P-protein	27	26	32	46	38	49	7	10	6	37	37	40	0.0018	6.3E-10	0.023	1.4E-19	0.14	1.3E-17
40771	enolase	28	30	31	34	35	33	29	24	28	24	22	23	0.22	0.29	0.063	0.082	0.0087	0.17
269942	Glycine/serine hydroxymethyltransferase, mitochondria targeted	30	31	27	53	48	46	17	15	16	20	20	21	0.00019	0.00034	0.011	7.5E-13	5.7E-10	0.13
269900	Glutamate synthase	27	29	29	31	30	28	30	21	21	29	25	27	0.43	0.15	0.39	0.1	0.3	0.23
1039	Cytochrome c550, PsbV. Located in thylakoid	22	20	20	23	19	23	45	47	44	20	18	17	0.46	1E-07	0.28	6.3E-07	0.22	1.7E-10
20804	unknown, possibly plastid targetted	28	28	25	26	23	24	39	38	37	19	17	16	0.31	0.011	0.0062	0.0024	0.035	1.4E-07
27892	ornithine aminotransferase	36	40	36	22	21	23	34	28	31	20	17	20	0.00062	0.11	6.9E-06	0.019	0.25	0.00087
997	ornithine transcarbamylase	25	27	28	23	22	26	34	30	29	17	19	17	0.27	0.18	0.012	0.057	0.074	0.00035
35712	Phosphoglycerate kinase precursor	13	13	18	23	21	28	4	4	5	54	54	56	0.011	0.00001	6.6E-18	2.5E-11	1.4E-09	2.9E-39
29842	Possible oxidoreductase activity, Rieske [2Fe-2S] center	19	18	18	11	11	13	44	43	43	26	22	22	0.032	2E-08	0.088	2.2E-13	0.00041	4.8E-06
21175	transketolase, glycolaldehydetransferase	12	13	12	34	34	46	4	1	3	42	42	40	8.2E-10	5.9E-06	4.1E-13	1.2E-25	0.26	4.1E-32
32874	MnSOD	18	22	17	18	17	18	42	45	44	15	16	13	0.4	3.3E-08	0.12	1E-08	0.22	5.3E-13
269240	HSP70	36	35	36	22	27	23	20	19	16	16	18	11	0.0066	0.00003	1.3E-07	0.11	0.011	0.15
24512	unknown, conserved algal protein	25	20	26	6	6	9	35	43	36	21	19	19	5.7E-07	0.00076	0.18	6.1E-16	0.000016	4.2E-06
24864	ATP synthase-like	32	27	23	18	22	21	27	32	30	15	12	12	0.072	0.29	0.000039	0.017	0.014	9.1E-07
31829	probable cysteine synthase	28	28	29	27	27	23	18	16	14	23	20	20	0.29	0.0006	0.036	0.0061	0.14	0.068
24769	unknown, conserved protein	16	14	12	9	8	9	49	51	47	10	10	11	0.056	6E-15	0.12	5.3E-20	0.34	3.2E-22
25840	possible CdCA	13	17	19	18	24	19	19	18	18	26	29	25	0.17	0.33	0.0039	0.31	0.07	0.013
20726	malate dehydrogenase	20	24	23	15	21	18	37	29	33	12	13	13	0.14	0.0088	0.0029	0.00022	0.079	2.1E-08

Table A1 cont.

Protein Id, Description		Spectral Counting Abundance Scores												Fisher Exact Test P values					
		Colim			B12 lim			Fe lim			Replete			Colim vs B12 lim	Colim vs Fe lim	Colim vs replete	B12 lim vs Fe lim	B12 lim vs replete	Fe lim vs replete
		a	b	c	a	b	c	a	b	c	a	b	c						
26146	14-3-3-like protein	18	23	23	22	17	23	18	16	15	25	20	27	0.46	0.11	0.27	0.15	0.21	0.019
28842	Thioredoxin/protein disulfide isomerase	20	19	16	16	19	26	23	26	25	13	13	8	0.32	0.045	0.016	0.14	0.0035	0.000017
bd 1766	unknown, conserved protein	23	20	17	23	21	28	19	19	17	22	19	18	0.22	0.34	0.48	0.095	0.17	0.38
22483	unknown, conserved protein	33	30	32	31	22	25	16	15	15	9	10	8	0.13	0.00002	7.6E-11	0.0027	3.3E-07	0.015
35934	cytochrome c	13	13	13	23	19	16	21	16	19	17	20	18	0.032	0.039	0.047	0.46	0.41	0.48
25892	putative ferredoxin-NADP reductase	15	16	16	15	13	11	31	28	28	19	22	22	0.26	0.00037	0.075	0.00003	0.015	0.021
11697	unknown, conserved protein (like Pt 48322), CBA1	46	44	38	48	46	41	0	0	0	0	0	0	0.33	4.2E-40	1.7E-42	1.3E-41	4.9E-44	1
269322	mitochondreial ATPase	12	10	12	33	30	38	4	3	4	28	25	28	2.7E-08	0.00022	0.000006	7.2E-20	0.081	1.2E-16
5293	Possible 3-isopropylmalate dehydrogenase	22	23	22	22	21	16	15	11	9	18	18	16	0.29	0.00081	0.11	0.0085	0.32	0.023
24346	unknown	21	26	20	24	25	26	10	14	11	15	14	14	0.3	0.00058	0.0088	0.000071	0.0015	0.19
27997	dihydroxyacid dehydratase	29	21	24	19	22	18	17	15	16	11	13	10	0.14	0.014	0.000065	0.18	0.0067	0.059
32459	conserved unknown protein	20	18	18	9	13	14	28	29	29	7	6	8	0.034	0.0069	0.000019	7.1E-06	0.026	1.8E-12
1810	FAD linked oxidase	19	23	19	19	21	23	10	14	14	15	13	15	0.5	0.0095	0.037	0.0085	0.033	0.29
20613	Diaminopimelate decarboxylase	18	14	16	16	10	10	29	26	26	14	10	13	0.16	0.0016	0.12	0.000031	0.53	3.7E-06
11411	Probable citrate synthase, mitochondrial precursor	9	11	15	9	8	11	4	5	4	40	34	32	0.24	0.00064	8.9E-10	0.012	1.5E-11	4.8E-22
39299	ADP-ribosylation factor (ARF1), GTPase	18	17	15	21	18	20	20	16	17	12	12	11	0.22	0.4	0.068	0.33	0.0088	0.026
1765	conserved unknown protein	13	10	13	17	18	20	14	14	16	16	18	18	0.039	0.24	0.065	0.15	0.38	0.24
1093	conserved unknown protein	16	11	11	26	28	20	14	13	12	9	12	13	0.00092	0.53	0.35	0.00051	0.000065	0.35
25387	unknown protein	16	11	12	16	17	19	25	24	18	6	6	7	0.14	0.0053	0.0056	0.1	0.00009	2.4E-08
22792	Rab-type small G protein, similar to Ypt1 (Rab1)	13	16	14	15	17	10	14	18	20	9	13	12	0.52	0.2	0.16	0.19	0.18	0.019
269961	Ribosomal protein L7A	13	10	11	10	10	13	17	27	24	9	10	10	0.48	0.00044	0.3	0.00034	0.38	0.000011
802	RL5, ribosomal protein 5, 60S large ribosomal subunit	9	15	10	13	15	15	19	24	19	10	13	10	0.23	0.0036	0.51	0.042	0.18	0.0014

Table A1 cont.

Protein Id, Description		Spectral Counting Abundance Scores												Fisher Exact Test P values					
		Colim			B12 lim			Fe lim			Replete			Colim vs B12 lim	Colim vs Fe lim	Colim vs replete	B12 lim vs Fe lim	B12 lim vs replete	Fe lim vs replete
		a	b	c	a	b	c	a	b	c	a	b	c						
26031	serine hydroxymethyltransferase, SHMT	21	20	16	26	28	29	3	0	3	9	11	12	0.024	2.7E-12	0.0051	8.4E-19	1.3E-06	1.8E-06
1247	Putative cysteine synthase	18	18	13	19	21	19	10	12	9	12	13	13	0.19	0.031	0.14	0.0023	0.019	0.22
37032	RL6, ribosomal protein 6, 60S large ribosomal subunit	16	13	15	15	17	19	17	11	19	9	8	11	0.3	0.43	0.029	0.38	0.0057	0.011
672	conserved, predicted protein	13	10	9	10	10	11	18	13	15	20	16	15	0.53	0.09	0.021	0.087	0.021	0.27
25040	conserved unknown protein	13	16	12	11	12	11	24	24	25	3	6	3	0.31	0.0011	0.000029	0.00018	0.00052	5.1E-14
21081	unknown protein	11	9	8	18	15	15	16	15	19	12	8	12	0.017	0.0069	0.34	0.46	0.041	0.018
262753	Putative ascorbate peroxidase, stroma located	14	16	16	18	15	13	5	4	5	20	17	18	0.53	8.9E-06	0.22	0.00002	0.22	3.4E-08
644	Adenosine kinase (AK2) (Adenosine 5'-phosphotransferase 2)	22	20	19	19	21	21	1	3	3	13	12	13	0.54	9E-13	0.012	2.4E-12	0.014	1.7E-07
27187	Transaldolase	13	18	16	15	13	11	16	19	19	7	6	8	0.26	0.29	0.00094	0.095	0.013	0.000039
1882	unknown protein	7	14	16	7	7	8	22	19	21	9	8	5	0.039	0.0084	0.04	0.00001	0.48	3.4E-06
38608	putative reductase, conserved	14	10	11	11	11	10	22	22	20	6	7	5	0.43	0.0025	0.016	0.0013	0.038	4.6E-08
1821	unknown protein	15	15	17	13	13	11	17	16	15	6	4	9	0.19	0.53	0.00022	0.17	0.0093	0.00011
270136	N-acetylornithine aminotransferase (ACOAT, argD)	8	14	13	16	15	20	0	2	0	19	18	16	0.074	2.5E-09	0.029	2.2E-13	0.42	7.2E-16
2343	conserved unknown protein	8	9	9	8	10	9	22	21	24	7	8	7	0.55	0.00001	0.32	0.00003	0.32	1.4E-07
YP_874490.1	photosystem I p700 chlorophyll A apoprotein A	4	6	4	13	12	13	11	6	8	22	18	21	0.0019	0.06	3E-08	0.084	0.014	0.000031
27167	RL7, ribosomal protein 7, 60S large ribosomal subunit	7	9	10	11	12	11	16	19	20	9	8	9	0.19	0.0011	0.55	0.027	0.17	0.00052
3817	Uncharacterized conserved protein	14	13	11	14	8	13	10	15	15	8	9	9	0.45	0.43	0.083	0.33	0.14	0.038
27656	heat shock protein/chaperone	27	29	30	16	15	13	12	8	5	16	14	11	0.00025	1.8E-09	0.000032	0.021	0.48	0.02
26678	transketolase, glycolaldehydetransferase	18	21	17	13	13	13	6	8	5	9	8	13	0.059	0.000016	0.0019	0.01	0.15	0.096
29506	Chaperonin Cpn10	12	11	14	9	12	10	12	14	15	7	7	7	0.29	0.39	0.022	0.17	0.11	0.0056
28049	Ribosomal protein S3	7	8	9	8	12	13	12	13	14	9	11	12	0.18	0.051	0.16	0.3	0.54	0.27
428	Fructose 1,6-bisphosphate aldolase	4	4	3	3	6	4	5	7	6	26	25	26	0.42	0.11	1.5E-13	0.23	1.2E-11	7.6E-11

Table A1 cont.

Protein Id, Description		Spectral Counting Abundance Scores												Fisher Exact Test P values					
		Colim			B12 lim			Fe lim			Replete			Colim vs B12 lim	Colim vs Fe lim	Colim vs replete	B12 lim vs Fe lim	B12 lim vs replete	Fe lim vs replete
		a	b	c	a	b	c	a	b	c	a	b	c						
26063	guanine nucleotide binding protein beta subunit-like protein	14	13	16	14	12	10	4	5	7	15	14	10	0.28	0.00049	0.35	0.0064	0.44	0.0014
40156	putative ATP synthase gamma chain (chloroplast precursor)	9	9	12	16	11	11	15	11	14	8	12	10	0.23	0.19	0.5	0.52	0.18	0.14
41319	RL18, ribosomal protein 18, 60S large ribosomal subunit	8	9	11	11	12	13	18	15	16	8	6	6	0.23	0.013	0.15	0.1	0.026	0.00016
37338	conserved protein with thioredoxin dmain	14	11	9	10	10	10	13	17	13	8	6	8	0.37	0.19	0.069	0.095	0.17	0.0044
2848	similar to extrinsic protein in photosystem II	9	7	8	9	10	5	20	19	21	7	8	6	0.56	0.000083	0.39	0.00013	0.4	3.4E-06
34125	carbonic anhydrase	4	1	2	16	15	15	7	7	7	16	17	15	9.9E-08	0.0045	4.8E-09	0.0025	0.46	0.00053
26131	probable cytochrome b6-f complex iron sulfer subunit, (Rieske iron-sulfer protein)	8	8	9	1	2	1	20	20	21	9	10	10	0.00037	0.00011	0.31	2.2E-12	0.00002	0.0004
269235	RL3, ribosomal protein 3, 60S large ribosomal subunit	14	8	10	14	13	15	7	9	9	8	7	9	0.16	0.23	0.17	0.028	0.017	0.48
42612	conserved protein, similar to pyridoxal 5'-phosphate (PLP) synthase	18	22	17	19	17	18	6	5	4	3	3	4	0.44	2.6E-07	2.7E-10	1.7E-06	3.1E-09	0.16
269258	protein of unknown function containing an aspartic protease domain	12	13	11	6	7	6	22	22	18	3	5	2	0.031	0.0041	0.000044	2.6E-06	0.048	2.4E-12
21161	protein of unknown function, distant similarity to proteins involved in cholesterol metabolism	12	10	11	9	8	11	4	3	3	18	19	15	0.37	0.00017	0.019	0.0013	0.0062	1.2E-09
1339	PSI PsaD	11	8	11	3	5	3	10	11	8	13	15	13	0.0045	0.51	0.09	0.0046	0.00002	0.064
40713	manganese superoxide dismutase precursor (putative mitochnodrial)	8	17	17	10	6	11	10	8	13	7	7	5	0.06	0.098	0.0018	0.4	0.15	0.063
40329	RL18a, ribosomal protein 18a, 60S large ribosomal subunit	9	8	12	10	12	9	11	11	13	9	9	9	0.47	0.32	0.38	0.4	0.31	0.17
2073	photosystem II chlorophyll A core antenna apoprotein	0	0	0	0	0	0	5	1	2	31	31	31	1	0.0073	2.7E-28	0.01	2.1E-26	1.5E-22
24710	conserved unknown protein	11	10	10	10	10	10	18	16	17	3	3	4	0.53	0.016	0.00071	0.016	0.0012	7.2E-09
22476	RL13e, ribosomal protein 13e, 60S large ribosomal subunit,	8	13	8	9	10	8	13	16	14	6	6	9	0.46	0.06	0.15	0.039	0.23	0.0019

Table A1 cont.

Protein Id, Description		Spectral Counting Abundance Scores												Fisher Exact Test P values					
		Colim			B12 lim			Fe lim			Replete			Colim vs B12 lim	Colim vs Fe lim	Colim vs replete	B12 lim vs Fe lim	B12 lim vs replete	Fe lim vs replete
		a	b	c	a	b	c	a	b	c	a	b	c						
38807	conserved unknown protein, methyltransferase/aldolase domains	11	11	9	10	11	13	9	10	11	9	9	10	0.42	0.5	0.37	0.36	0.25	0.41
37509	putative Vacuolar proton pump D subunit	8	13	11	7	7	9	12	11	8	12	7	9	0.16	0.49	0.36	0.19	0.28	0.41
39735	RL17A, ribosomal protein 27A, 60S large ribosomal subunit	6	5	5	6	8	8	18	16	16	6	5	8	0.27	0.000027	0.41	0.00082	0.38	0.000034
1048	photosystem I iron-sulfur center PsaC	9	7	8	10	8	8	18	16	14	8	6	5	0.44	0.0043	0.29	0.013	0.2	0.0002
31424	putative aspartate aminotransferase	8	10	11	10	11	10	8	8	8	9	11	12	0.47	0.27	0.41	0.21	0.5	0.15
24571_1	conserved unknown, copper responsive	11	14	14	9	5	11	9	9	7	7	6	10	0.081	0.062	0.03	0.55	0.43	0.43
40728	putative V-type H-ATPase	7	9	10	7	8	10	13	11	13	8	9	11	0.51	0.13	0.5	0.11	0.45	0.14
23556	unknown hypothetical	11	15	13	15	15	13	4	5	8	9	6	6	0.39	0.0039	0.016	0.0014	0.0062	0.32
20786	unknown protein	19	17	20	5	5	3	17	15	13	2	0	0	3E-07	0.15	2.1E-16	0.00002	0.0039	1.4E-13
4875	Pyruvate kinase	11	9	11	15	15	11	7	10	9	8	5	5	0.16	0.31	0.041	0.049	0.0019	0.12
30193	Urease	9	10	11	11	11	11	9	9	7	6	4	5	0.42	0.27	0.014	0.17	0.0062	0.069
28241	Glyceraldehyde 3-phosphate dehydrogenase	6	10	12	9	11	8	11	9	7	8	8	7	0.52	0.47	0.26	0.52	0.31	0.32
39499	RL14, ribosomal protein 14, 60S large ribosomal subunit	6	9	6	9	6	5	11	17	14	8	7	7	0.48	0.0093	0.55	0.0064	0.46	0.006
40669	Ubiquitin/ribosomal protein fusion	11	11	8	10	12	11	10	9	10	5	6	5	0.37	0.51	0.03	0.32	0.0094	0.031
24887	possible phosphoadenosine-phosphosulphate reductase	2	3	3	2	2	4	0	0	0	27	26	26	0.57	0.002	2.6E-15	0.003	1.2E-14	8.6E-27
17214	acetylglutamate kinase (arginine biosynthesis)	7	5	5	5	6	8	10	7	7	15	13	13	0.54	0.2	0.002	0.23	0.0034	0.023
268009	Ftr1_plasma membrane iron permease	12	15	11	7	7	6	5	5	4	9	8	11	0.027	0.00075	0.15	0.18	0.18	0.015
YP_874583.1	heat shock protein 70	7	6	6	7	10	9	3	4	4	18	14	15	0.27	0.059	0.00056	0.0099	0.0086	1.1E-07
20603	possible oxygen-evolving enhancer protein 3	5	6	4	5	2	4	14	16	14	11	7	10	0.27	0.00018	0.035	0.000011	0.0052	0.033
467	Cytochrome B6	6	6	6	2	4	4	10	14	13	13	10	14	0.084	0.013	0.0078	0.00011	0.00005	0.48

Table A1 cont.

Protein Id, Description		Spectral Counting Abundance Scores												Fisher Exact Test P values					
		Colim			B12 lim			Fe lim			Replete			Colim vs B12 lim	Colim vs Fe lim	Colim vs replete	B12 lim vs Fe lim	B12 lim vs replete	Fe lim vs replete
		a	b	c	a	b	c	a	b	c	a	b	c						
39282	RL15, ribosomal protein 15, 60S large ribosomal subunit	7	6	8	7	10	6	16	10	10	7	7	9	0.45	0.037	0.43	0.075	0.55	0.056
8028	unknown protein	7	7	8	6	8	8	18	16	15	3	5	5	0.55	0.0012	0.077	0.0015	0.09	5.8E-07
268965	aconitase hydratase 2 (B) (Fe-containing)	6	7	4	5	5	8	2	0	1	16	22	16	0.53	0.00069	6.9E-06	0.0013	0.000008	4.2E-15
1757	predicted protein, iron starvation induced in Phatr (47674)	7	7	9	5	8	6	13	14	10	8	7	6	0.35	0.058	0.45	0.019	0.44	0.024
10234	geranylgeranyl hydrogenase/ reductase	8	8	6	9	12	8	0	2	2	16	14	13	0.27	0.000099	0.01	5.2E-06	0.07	1.3E-10
3393	putative formate/nitrite transporter family member	8	7	6	7	7	5	17	15	14	3	4	4	0.41	0.003	0.025	0.0012	0.069	1.8E-07
21517	conserved unknown. Pt 44651 homol.	9	14	13	11	5	8	8	5	5	5	6	5	0.094	0.0081	0.0021	0.21	0.11	0.4
24711	conserved unknown, multicopy	12	10	12	9	11	8	10	9	12	3	3	3	0.27	0.39	0.000034	0.4	0.00098	0.0001
36208	glycine decarboxylase T-protein	5	6	6	0	0	0	16	13	13	9	10	11	0.000031	0.0018	0.049	1.1E-11	7E-09	0.099
21748	Fructose-bisphosphate aldolase (putative)	6	8	10	5	4	5	5	4	5	11	8	12	0.069	0.068	0.22	0.53	0.0074	0.0057
1350	PSAF, Photosystem I reaction centre subunit III	4	6	5	2	4	4	11	12	12	10	10	10	0.2	0.0054	0.016	0.00024	0.0009	0.36
38879	Fucoxanthin chlorophyll a/c protein, LI818 clade	11	9	9	7	7	11	5	5	3	12	8	11	0.4	0.0072	0.44	0.025	0.28	0.0019
1611	Photosystem I psaB	4	3	3	7	7	8	4	4	2	16	14	15	0.037	0.54	5.4E-07	0.022	0.0026	6.2E-08
268304	putative unknown protein with no similarities	2	6	8	8	7	6	15	14	15	3	4	5	0.27	0.00035	0.25	0.006	0.066	2.9E-06
38724	putative ascorbate peroxidase	7	4	8	10	11	11	2	2	3	10	12	7	0.048	0.012	0.069	0.000022	0.42	0.000024
260835	putative Alkaline Phosphatase (Mak annotated)	7	5	6	6	7	9	8	8	5	5	7	11	0.39	0.39	0.3	0.54	0.48	0.45
976	putative unknown protein with no similarities	7	7	6	3	5	8	9	10	11	6	8	5	0.27	0.14	0.43	0.031	0.37	0.061
21290	N-acetyl-gamma-glutamyl-phosphate reductase (urea cycle)	7	9	10	6	7	6	3	2	2	11	14	10	0.21	0.00035	0.14	0.011	0.02	7.8E-07
267987	Putative cysteine synthase	6	3	6	10	8	5	10	8	10	9	6	9	0.13	0.041	0.14	0.36	0.5	0.28
28521	glycine decarboxylase H-protein	6	6	5	7	8	13	12	11	6	7	5	4	0.11	0.068	0.41	0.5	0.042	0.022
3353	L-lactate dehydrogenase (fe-containing)	5	3	4	13	16	13	1	1	1	11	12	13	0.00013	0.014	0.00039	8.1E-10	0.32	2.2E-09

Table A1 cont.

Protein Id, Description		Spectral Counting Abundance Scores												Fisher Exact Test P values					
		Colim			B12 lim			Fe lim			Replete			Colim vs B12 lim	Colim vs Fe lim	Colim vs replete	B12 lim vs Fe lim	B12 lim vs replete	Fe lim vs replete
		a	b	c	a	b	c	a	b	c	a	b	c						
24399	Probable dihydrolipoamide dehydrogenase	6	9	10	8	7	8	11	7	8	7	5	5	0.44	0.51	0.1	0.39	0.18	0.071
46	RL13A, ribosomal protein 13A, 60S large ribosomal subunit	7	7	9	9	10	9	5	5	7	6	6	8	0.32	0.2	0.4	0.073	0.19	0.31
598	ATP synthase CF0 B' chain subunit II	12	9	8	5	4	4	10	11	8	6	7	5	0.012	0.54	0.096	0.0086	0.16	0.079
28239	triosephosphate isomerase/glyceraldehyde-3-phosphate dehydrogenase precursor	8	7	8	7	6	8	6	6	8	9	8	10	0.42	0.41	0.32	0.56	0.21	0.18
34810	putative calreticulin-like protein (calcium storage)	5	14	9	5	10	8	3	2	2	9	11	11	0.27	0.0002	0.34	0.0038	0.12	9.3E-06
2779	Arginine biosynthesis protein ArgJ	7	13	11	5	5	4	9	4	8	6	8	6	0.01	0.098	0.093	0.16	0.15	0.56
269120	Heat shock protein 70	7	8	6	10	6	9	5	5	4	9	7	8	0.38	0.12	0.4	0.054	0.53	0.046
6363	RL23a, ribosomal protein 23a, 60S large ribosomal subunit	5	6	6	7	7	1	6	7	9	4	6	5	0.45	0.28	0.41	0.19	0.55	0.15
6817	unknown, possible methyltrasferase	12	11	12	0	2	4	8	13	11	3	5	6	0.000012	0.38	0.0011	0.000038	0.074	0.0032
16169	Pyruvate dehydrogenase E1, alpha subunit	16	6	8	10	12	10	5	6	5	5	4	3	0.42	0.028	0.0036	0.013	0.0014	0.27
24060	Putative protein of unknown function	5	5	4	7	6	9	0	0	0	14	14	17	0.16	0.00004	0.00005	3.2E-07	0.0044	1.9E-15
12594	possible chitin binding, copper-induced girdle band-associated	12	9	10	5	4	3	6	5	6	7	7	7	0.0031	0.041	0.12	0.15	0.052	0.32
27292	RS4, ribosomal protein 4, 40S small ribosomal subunit	7	8	3	8	5	4	7	7	9	7	6	10	0.46	0.29	0.35	0.21	0.25	0.49
5240	Porphobilinogen synthase (ALA dehydratase)	5	8	9	7	4	9	4	5	4	10	8	9	0.41	0.064	0.27	0.14	0.16	0.0075
23024	conserved unknown (Pt 44484)	11	8	9	8	6	8	8	9	6	4	6	5	0.27	0.33	0.041	0.47	0.19	0.12
29117	puttive V-type H-ATPase subunit E	4	7	9	3	5	4	3	5	6	10	10	13	0.14	0.26	0.051	0.37	0.0021	0.0049
25507	unknown protein	12	10	9	3	2	5	11	12	12	2	2	1	0.0031	0.37	4.4E-06	0.00055	0.12	2E-07
25022	ong-chain acyl-CoA synthetase-like protein	0	0	0	3	4	4	0	0	0	18	19	22	0.0013	1	5.3E-18	0.00057	6.7E-09	2.9E-20
4700	unknown protein	5	9	10	9	10	8	9	6	6	5	5	5	0.44	0.4	0.1	0.28	0.059	0.18

Table A1 cont.

Protein Id, Description		Spectral Counting Abundance Scores												Fisher Exact Test P values					
		Colim			B12 lim			Fe lim			Replete			Colim vs B12 lim	Colim vs Fe lim	Colim vs replete	B12 lim vs Fe lim	B12 lim vs replete	Fe lim vs replete
		a	b	c	a	b	c	a	b	c	a	b	c						
23191	unknown protein	6	8	4	7	6	6	9	8	8	6	5	5	0.53	0.21	0.34	0.25	0.31	0.069
3018	Phosphoserine aminotransferase	12	8	9	9	8	11	4	5	5	3	4	4	0.54	0.018	0.0033	0.018	0.0035	0.34
21371	putative spermidine synthase	1	1	2	7	11	13	0	1	0	13	16	10	0.000019	0.14	2.9E-08	1.4E-08	0.17	2.2E-12
1863	conserved unknown protein	4	5	4	3	5	5	13	12	13	5	6	5	0.58	0.00057	0.41	0.00085	0.42	0.00092
6285	HSP90 family member (HSP82, HSP81-2)	4	1	1	1	1	0	1	0	0	21	22	19	0.27	0.075	3.3E-13	0.4	7.8E-15	1.4E-19
42962	Fucoxanthin chlorophyll a/c protein 5 (FCP5)	7	8	8	9	10	9	2	3	4	7	9	9	0.32	0.0066	0.46	0.0011	0.39	0.0019
24262	RS2, ribosomal protein 2, 40S small ribosomal subunit	6	6	3	6	6	5	10	5	3	6	8	7	0.48	0.41	0.2	0.52	0.29	0.32
39424	RL12, ribosomal protein 11, 60S large ribosomal subunit	6	7	8	5	7	8	8	8	6	4	6	6	0.48	0.47	0.27	0.38	0.37	0.19
9394	unknown protein, no similarities	8	7	11	10	8	8	10	5	6	2	2	4	0.55	0.24	0.00033	0.24	0.00041	0.0041
29359	putative ATP synthase, H+ transporting, mitochondrial F1 complex, O subunit	9	11	11	3	2	4	3	6	5	7	6	7	0.00098	0.0059	0.071	0.26	0.04	0.16
26137	RL9, ribosomal protein 9, 60S large ribosomal subunit, nuclear	5	4	4	6	4	3	8	8	11	7	6	7	0.5	0.022	0.14	0.016	0.1	0.19
264670	putative peroxiredoxin, thioredoxin peroxidase	14	9	8	6	6	4	5	6	7	5	6	5	0.028	0.056	0.014	0.38	0.55	0.33
25281	conserved unknown, Pt 42835	7	10	5	6	6	5	7	5	5	4	3	5	0.23	0.25	0.039	0.52	0.23	0.17
YP_874497.1	ribulose-1,5-bisphosphate carboxylase/oxygenase small subunit	4	5	2	8	8	13	2	4	2	9	11	12	0.0058	0.28	0.00077	0.00031	0.38	0.000016
40312	RS16, ribosomal protein 16, 40S small ribosomal subunit	2	4	4	6	6	5	4	6	6	8	10	5	0.2	0.19	0.028	0.56	0.21	0.18
269779	RS6, ribosomal protein 6, 40S small ribosomal subunit	4	6	5	3	4	5	7	7	11	7	6	6	0.35	0.087	0.29	0.029	0.13	0.23
YP_874584.1	50S ribosomal protein L3, chloropolast	9	6	8	7	5	5	12	13	10	2	2	2	0.23	0.088	0.00034	0.013	0.0095	2E-07
33241	RL17, ribosomal protein 17-like, 60S large ribosomal subunit,	8	6	5	8	5	4	8	5	5	7	6	5	0.4	0.43	0.5	0.52	0.44	0.49
2705	unknown protein	8	11	10	2	4	3	12	12	11	1	2	0	0.001	0.32	1.6E-07	0.000092	0.067	2.1E-09

Table A1 cont.

Protein Id, Description		Spectral Counting Abundance Scores												Fisher Exact Test P values					
		Colim			B12 lim			Fe lim			Replete			Colim vs B12 lim	Colim vs Fe lim	Colim vs replete	B12 lim vs Fe lim	B12 lim vs replete	Fe lim vs replete
		a	b	c	a	b	c	a	b	c	a	b	c						
269908	Pyruvate carboxylase	0	1	0	1	2	1	0	0	0	19	18	21	0.16	0.46	5.1E-16	0.036	7.5E-12	1.1E-19
4270	phospholipid scramblase	7	9	6	7	7	8	7	5	7	4	2	4	0.49	0.35	0.017	0.43	0.031	0.05
29007	RL21, ribosomal protein 21, 60S large ribosomal subunit	4	6	6	8	5	6	4	7	5	8	6	7	0.4	0.52	0.31	0.35	0.49	0.25
23918	conserved unknown protein	6	8	8	3	7	8	3	4	4	9	8	9	0.34	0.029	0.35	0.11	0.17	0.0049
26383	Ribosomal L37ae protein	1	6	9	7	4	4	3	1	5	10	6	7	0.44	0.077	0.19	0.15	0.11	0.0043
34104	putatuive peptidylprolyl isomerase, FKBP-type	6	6	5	6	5	5	10	11	11	2	2	3	0.45	0.032	0.02	0.018	0.048	0.00001
35816	Glyceraldehyde-3-phosphate dehydrogenase	11	5	5	8	8	8	6	2	3	6	4	5	0.39	0.041	0.22	0.015	0.11	0.19
38672	GTP-binding Ras small GTPase, Rab type	6	8	8	5	4	6	3	4	5	6	4	5	0.16	0.064	0.17	0.4	0.51	0.32
269148	putative translation factor Tu	0	0	0	0	0	0	0	1	1	18	17	20	1	0.29	9.5E-17	0.32	1.2E-15	3.9E-16
40107	translation initiation factor 5A	6	5	5	5	6	6	5	7	6	6	5	6	0.55	0.43	0.53	0.46	0.56	0.45
40630	Putative protein of unknown function similar to hypersensitive response-induced protein	0	0	0	6	2	6	0	0	0	14	17	17	0.00014	1	9.6E-15	0.00005	0.00002	1.4E-16
269348	putative inorganic pyrophosphatase protein (PPase)	4	4	3	6	7	9	4	4	3	12	8	6	0.058	0.52	0.0082	0.035	0.3	0.0034
39520	Putative vacuolar membrane proton pump	2	2	0	10	12	10	1	1	0	10	13	9	5.5E-06	0.27	1.5E-06	2.5E-08	0.54	3.3E-09
4462	unknown protein	8	7	5	8	8	9	5	5	5	2	2	3	0.33	0.25	0.0047	0.1	0.00074	0.034
22869	possible DNA repair endonuclease XPF	8	11	8	5	5	5	7	5	6	3	2	1	0.044	0.12	0.00003	0.3	0.028	0.0024
308	PSAE, Photosystem I reaction center subunit IV	5	5	6	2	4	1	6	8	5	6	9	6	0.061	0.43	0.26	0.025	0.0081	0.38
1326	similar to sulfate adenylytransferase	4	3	3	7	6	4	1	0	0	11	10	13	0.15	0.0053	0.00016	0.00008	0.013	9.7E-11
37123	putative Vacuolar proton pump alpha subunit	0	1	0	1	0	1	0	1	0	16	16	19	0.47	0.71	4.6E-14	0.4	5.8E-12	5.8E-16
19298	putative F-type H-ATPase (d)	7	7	5	7	5	4	8	6	5	3	4	5	0.32	0.49	0.11	0.38	0.3	0.13
1387	photosystem II protein V	4	2	4	1	2	3	7	13	12	4	4	3	0.27	0.00061	0.48	0.000038	0.17	0.00057
24248	Carbamyl phosphate synthetase III (urea cycle)	0	0	0	0	0	4	0	0	0	16	17	13	0.11	1	5.4E-14	0.083	9.5E-10	9.9E-16

Table A1 cont.

Protein Id, Description		Spectral Counting Abundance Scores												Fisher Exact Test P values					
		Colim			B12 lim			Fe lim			Replete			Colim vs B12 lim	Colim vs Fe lim	Colim vs replete	B12 lim vs Fe lim	B12 lim vs replete	Fe lim vs replete
		a	b	c	a	b	c	a	b	c	a	b	c						
22763	unknown protein	2	3	4	8	8	10	1	2	2	8	9	6	0.0074	0.13	0.016	0.000064	0.36	0.00014
29244	putative peptidyl-prolyl cis-trans isomerase	6	5	5	5	2	4	0	0	0	13	12	10	0.21	8.4E-06	0.0066	0.00057	0.00036	2.5E-12
31394	hypothetical aspartate aminotransferase,	2	2	3	1	2	3	0	0	0	16	13	15	0.45	0.0043	1.9E-07	0.016	7E-08	3.7E-15
38769	photosystem II stability/assembly factor HCF136	11	7	13	1	0	0	10	10	9	0	1	1	1.9E-07	0.45	1.3E-08	2.8E-07	0.63	1.8E-08
25772	similar to actin	0	2	1	1	2	4	0	0	0	15	15	16	0.21	0.097	8.1E-11	0.0069	7.8E-08	5.2E-16
26046	RS3A, ribosomal protein 3A, 40S small ribosomal subunit	5	4	4	6	2	5	6	8	9	3	2	5	0.58	0.068	0.41	0.077	0.41	0.02
20810	Ftr1_plasma membrane iron permease (multi-copy)	6	4	8	2	4	5	9	8	9	2	2	2	0.17	0.13	0.011	0.012	0.17	0.000096
6979	putative protein of unknown function	4	5	4	9	5	6	4	4	2	8	6	6	0.16	0.27	0.17	0.034	0.51	0.031
21177	Dihydrolipoamide S-acetyltransferase	5	4	9	7	7	5	6	5	6	4	2	4	0.47	0.51	0.11	0.41	0.069	0.12
6672	unknown protein, similar to Pt 32219, 49651	7	7	9	6	4	5	6	6	6	3	3	2	0.13	0.3	0.0061	0.3	0.15	0.029
31785	conserved unknown, GATase domain, similar to Pt 32791	7	7	6	7	6	8	6	3	5	4	4	2	0.54	0.12	0.037	0.14	0.047	0.34
21595	unknown protein, protein binding sites	5	4	2	1	4	4	3	3	4	9	10	8	0.39	0.44	0.0082	0.52	0.0023	0.0018
4439	unknown protein, simialr to Pt 42494	0	2	2	14	12	13	0	1	0	7	7	5	2.5E-07	0.14	0.0014	5.4E-11	0.0092	3.7E-06
5785	unknown protein	5	3	4	5	5	5	9	8	8	3	2	4	0.41	0.025	0.28	0.071	0.15	0.0017
25949	RL11A, ribosomal protein 11A, 60S large ribosomal subunit	4	4	4	5	5	4	9	11	10	2	2	2	0.5	0.005	0.11	0.011	0.075	0.000011
34487	cation transporting ATPase	5	6	4	3	2	4	1	1	1	8	8	12	0.2	0.0023	0.045	0.05	0.0035	7E-07
39470	Ran-type small G protein	6	5	5	6	4	9	1	1	1	9	7	6	0.47	0.0013	0.22	0.00066	0.32	0.00002
39622	conserved unknown protein, like Pt 48728	6	6	4	7	4	4	9	10	9	1	1	2	0.44	0.06	0.002	0.033	0.007	9.5E-07
21600	conserved unknown protein, like Pt 32237	7	6	6	5	5	5	8	7	8	2	2	0	0.26	0.35	0.0003	0.11	0.007	0.00002
27850	Phosphoglycerate mutase	4	5	6	2	2	4	1	3	0	10	11	9	0.14	0.0061	0.016	0.15	0.00038	3.5E-07
22301	Phosphomannomutase	5	7	5	3	2	4	5	6	4	4	6	6	0.11	0.38	0.47	0.21	0.14	0.47

Table A1 cont.

Protein Id, Description		Spectral Counting Abundance Scores												Fisher Exact Test P values					
		Colim			B12 lim			Fe lim			Replete			Colim vs B12 lim	Colim vs Fe lim	Colim vs replete	B12 lim vs Fe lim	B12 lim vs replete	Fe lim vs replete
		a	b	c	a	b	c	a	b	c	a	b	c						
26893	RS18, ribosomal protein 18, 40S small ribosomal subunit	5	5	4	6	7	4	3	3	4	6	7	6	0.4	0.21	0.23	0.11	0.39	0.031
38964	putative chorismate synthase (aromatic amino acid biosynthesis	9	7	8	3	2	3	4	4	4	7	5	5	0.0081	0.021	0.13	0.36	0.093	0.2
35409	Cytochrome C peroxidase (CCP), mitochondrial	5	7	5	7	10	9	2	1	2	5	6	3	0.17	0.0047	0.3	0.00012	0.044	0.022
30976	unknown protein, similar to Pt 8045	1	6	6	3	2	3	5	5	10	3	4	4	0.18	0.19	0.26	0.025	0.43	0.036
31084	40S ribosomal protein S14	5	6	4	6	7	5	7	6	5	3	2	4	0.4	0.41	0.11	0.54	0.048	0.042
262506	conserved unknown, like Pt 44639, Aureo 71644(Low under - P, recovers in refeed)	4	7	8	6	8	8	3	3	5	3	3	4	0.39	0.083	0.053	0.035	0.02	0.5
41005	Pyruvate dehydrogenase E1, beta subunit	7	7	6	9	5	5	3	1	4	2	2	4	0.48	0.0089	0.0087	0.019	0.019	0.57
28443	RL10, ribosomal protein 10, 60S large ribosomal subunit	5	5	5	6	6	8	6	5	6	2	3	2	0.33	0.48	0.048	0.41	0.011	0.023
32577	Aspartate-semialdehyde dehydrogenase	2	2	2	7	4	3	0	0	0	12	11	12	0.12	0.0093	5.1E-06	0.00011	0.0016	2.5E-12
YP_874611.1	30S ribosomal protein S7, chloroplast	5	5	5	7	5	5	5	5	5	3	3	5	0.48	0.54	0.26	0.5	0.18	0.22
38925	40S ribosomal protein S28	6	5	6	5	5	6	5	6	5	3	4	2	0.45	0.45	0.077	0.56	0.15	0.12
22293	ferredoxin-sulfite reductase	0	0	0	0	0	0	0	1	0	10	15	17	1	0.54	3.1E-13	0.56	2.2E-12	1.8E-13
40522	Putative Vacuolar ATPase beta subunit, transporting ATPase	0	0	0	0	0	0	0	0	0	17	14	15	1	1	3.1E-14	1	2.6E-13	5.2E-16
24423	Protein 23 of the large ribosomal subunit	4	6	4	6	5	4	5	7	6	1	2	3	0.57	0.28	0.046	0.3	0.047	0.0051
38266	Glucose-6-phosphate isomerase	4	5	4	7	6	8	3	1	4	3	5	3	0.16	0.15	0.41	0.012	0.068	0.25
37628	40S ribosomal protein S12	4	4	3	5	4	5	5	5	5	3	4	5	0.42	0.29	0.5	0.46	0.48	0.34
28425	40S ribosomal protein S19	4	4	6	3	4	3	0	4	2	5	8	5	0.26	0.041	0.27	0.23	0.069	0.0037
9021	Porphobilinogen deaminase,	6	5	5	7	6	5	2	2	0	7	5	6	0.47	0.0035	0.47	0.0019	0.56	0.00094
7906	conserved unknown, similar to Pt 46347	5	6	4	5	7	4	5	5	5	3	2	3	0.56	0.47	0.075	0.45	0.073	0.11
33855	peptidylpropyl isomerse	5	5	5	5	2	1	5	5	7	3	3	5	0.14	0.41	0.2	0.062	0.43	0.093
20223	unknown protein, RRM domain	4	3	8	3	5	4	5	5	5	3	4	5	0.42	0.53	0.39	0.37	0.57	0.34

Table A1 cont.

Protein Id, Description		Spectral Counting Abundance Scores												Fisher Exact Test P values					
		Colim			B12 lim			Fe lim			Replete			Colim vs B12 lim	Colim vs Fe lim	Colim vs replete	B12 lim vs Fe lim	B12 lim vs replete	Fe lim vs replete
		a	b	c	a	b	c	a	b	c	a	b	c						
21749	cytochrome c oxidase like, Pt36600	6	4	4	5	5	5	5	5	5	4	3	3	0.57	0.53	0.26	0.55	0.26	0.21
36081	Chlorophyll A-B binding/light harvesting protein	5	4	4	3	4	4	8	4	6	3	3	4	0.41	0.27	0.34	0.15	0.53	0.093
21306	conserved unknown protein	5	5	6	8	7	8	4	4	4	3	2	0	0.22	0.21	0.0046	0.036	0.00019	0.05
21871	similar to 40S ribosomal protein (laminin receptor-like protein)	4	4	4	1	5	3	3	3	3	5	6	7	0.31	0.28	0.15	0.59	0.041	0.026
10741	conserved unknown protein	8	4	8	7	7	8	0	0	1	3	6	4	0.46	8.7E-06	0.14	3.6E-06	0.09	0.00047
YP_874517.1	50S ribosomal protein L11	6	5	5	1	2	1	11	9	13	0	1	0	0.016	0.016	0.000039	6.7E-06	0.099	1.2E-10
42545	conserved unknown, with protease domain	6	5	4	6	7	5	3	2	2	3	5	3	0.4	0.045	0.2	0.018	0.1	0.23
30659	conserved unknown, possible beta lactamase domain	7	5	4	6	1	3	1	0	0	6	7	5	0.15	0.000076	0.41	0.0072	0.069	6.9E-06
4820	conserved unknown protein	0	0	0	0	0	0	0	0	0	14	14	14	1	1	5.5E-13	1	3.8E-12	1.4E-14
8968	conserved unknown with Proteasome activator domain	2	4	3	5	2	4	7	6	5	3	2	3	0.51	0.076	0.3	0.12	0.24	0.0099
26221	RS13, ribosomal protein 13, 40S small ribosomal subunit	2	4	3	5	5	5	4	2	1	4	5	5	0.26	0.28	0.23	0.069	0.57	0.05
5026	H+-transporting two-sector ATPase, gamma subunit	1	0	1	11	11	14	0	0	0	3	6	6	3.2E-08	0.21	0.0013	1.5E-11	0.0027	8.1E-06
267922	20S proteasome, regulatory subunit beta type	6	3	4	6	8	5	2	1	2	4	3	5	0.21	0.035	0.48	0.0025	0.13	0.048
23657	Globin-like protein	8	5	6	8	7	6	2	3	2	1	2	1	0.46	0.0075	0.0003	0.0038	0.00013	0.23
42577	Phosphoglycerate kinase	0	0	1	6	4	5	0	0	0	9	12	10	0.001	0.46	9.5E-09	0.000047	0.0099	3.4E-11
9795	conserved unknown protein	7	4	4	3	5	5	3	5	5	2	2	2	0.43	0.4	0.029	0.56	0.075	0.065
31912	putative cyclophilin-type peptidyl-prolyl cis-trans isomerase	5	7	8	6	2	9	0	1	1	5	3	4	0.4	0.000049	0.11	0.00038	0.23	0.0035
13393	2-isopropylmalate synthase A	7	7	5	1	0	1	8	3	5	3	3	3	0.00041	0.31	0.023	0.0022	0.069	0.084
10527	possible clathrin	6	4	3	5	4	5	4	6	4	3	2	3	0.58	0.52	0.15	0.53	0.16	0.11
22535	RS11, ribosomal protein 11, 40S small ribosomal subunit,	4	3	4	3	1	4	6	5	7	4	2	2	0.39	0.15	0.37	0.062	0.59	0.042
26250	RL26, ribosomal protein 26, 60S large ribosomal subunit,	1	2	2	3	5	5	5	5	5	2	2	3	0.075	0.033	0.56	0.46	0.075	0.03

Table A1 cont.

Protein Id, Description		Spectral Counting Abundance Scores												Fisher Exact Test P values					
		Colim			B12 lim			Fe lim			Replete			Colim vs B12 lim	Colim vs Fe lim	Colim vs replete	B12 lim vs Fe lim	B12 lim vs replete	Fe lim vs replete
		a	b	c	a	b	c	a	b	c	a	b	c						
264201	RL8, ribosomal protein 8, 60S large ribosomal subunit	4	6	4	5	5	4	1	2	2	3	2	4	0.51	0.022	0.15	0.038	0.21	0.19
11068	20S proteasome subunit alpha	4	4	4	6	4	5	3	2	1	4	3	4	0.41	0.094	0.5	0.042	0.32	0.12
9830	Putative cystathionine beta-lyase *Methionine metabolism*	5	4	2	3	6	5	1	1	2	7	5	5	0.33	0.049	0.17	0.011	0.39	0.0015
263081	unknown protein containing leucine-rich repeats	6	4	3	2	1	3	8	8	6	2	2	1	0.1	0.088	0.024	0.0026	0.4	0.00011
YP_874612.1	translation elongation factor Tu	0	1	1	1	1	1	1	0	0	13	13	8	0.46	0.44	1.7E-08	0.22	4.7E-07	9.7E-11
35710	Acyl-CoA dehydrogenase	7	4	6	2	1	3	4	5	2	3	6	4	0.022	0.11	0.19	0.23	0.13	0.43
38460	Putative protein similar to SKP1 in ubiquitin protein degradation pathway	2	3	3	6	4	4	8	3	5	1	2	3	0.25	0.12	0.31	0.4	0.075	0.019
37976	peptidyl prolyl cis-trans isomerase A	4	2	2	2	1	3	1	1	3	5	10	6	0.45	0.28	0.006	0.46	0.0024	0.00023
20194	unknown pprotein, short model, with Zn finger	5	5	4	3	4	5	5	5	4	2	2	2	0.42	0.48	0.046	0.51	0.11	0.065
24639	unknown protein, conserved domains, like Pt42442	5	6	5	7	8	9	2	2	0	2	2	1	0.17	0.0035	0.0046	0.000077	0.00009 9	0.55
30154	60S subunit (cytoplasmic) ribosomal protein L27	5	3	2	3	4	5	2	2	3	4	4	5	0.42	0.28	0.34	0.15	0.52	0.097
29955	RS5, ribosomal protein 5, 40S small ribosomal subunit	2	3	4	2	5	3	2	2	2	3	6	6	0.58	0.2	0.15	0.23	0.14	0.013
8031	conserved unknown protein	2	3	3	3	4	4	4	2	4	3	3	4	0.42	0.55	0.46	0.46	0.53	0.5
34210	Histone H2B	6	6	6	3	5	4	1	1	2	2	5	3	0.18	0.0011	0.053	0.034	0.36	0.082
21887	unknown protein	8	4	3	8	6	5	3	1	1	1	2	2	0.33	0.013	0.016	0.0025	0.003	0.56
32860	Enoyl-[acyl-carrier protein] reductase	2	2	2	0	1	0	4	6	4	5	6	3	0.079	0.083	0.088	0.0014	0.0014	0.55
29314	aminopeptidase	1	2	2	2	1	3	4	5	4	3	4	4	0.57	0.094	0.17	0.13	0.22	0.41
23509	unknown protein	4	5	5	6	6	5	3	1	3	3	2	3	0.4	0.068	0.073	0.028	0.03	0.57
39550	RS7, ribosomal protein 7, 40S small ribosomal subunit	1	2	2	5	2	1	5	3	4	6	3	5	0.33	0.13	0.049	0.36	0.19	0.37
264111	hypothetical protein with thioredoxin type domains	5	3	4	3	5	1	6	5	5	1	2	3	0.4	0.31	0.068	0.17	0.18	0.01
268958	unknown protein	8	5	3	1	4	3	3	6	5	1	1	0	0.061	0.46	0.00019	0.09	0.06	0.00035

Table A1 cont.

Protein Id, Description		Spectral Counting Abundance Scores												Fisher Exact Test P values					
		Colim			B12 lim			Fe lim			Replete			Colim vs B12 lim	Colim vs Fe lim	Colim vs replete	B12 lim vs Fe lim	B12 lim vs replete	Fe lim vs replete
		a	b	c	a	b	c	a	b	c	a	b	c						
31091	Nucleoside diphosphate kinase	4	2	5	5	5	4	0	0	0	4	6	5	0.42	0.00041	0.21	0.00011	0.37	4.2E-06
3463	conserved unknown protein	2	3	4	3	6	4	5	3	4	2	2	3	0.33	0.48	0.3	0.42	0.11	0.19
24250	urea active transport protein	6	5	4	1	0	1	4	4	4	4	4	2	0.0036	0.27	0.2	0.022	0.031	0.5
34592	conserved protein with ferredoxin domain, like Pt 15777	6	3	2	3	2	0	0	0	0	11	12	11	0.2	0.00041	0.00038	0.016	8.6E-06	4.8E-12
24318	probable 20S proteasome beta type subunit	4	2	3	3	5	4	4	4	2	3	4	3	0.33	0.55	0.46	0.36	0.43	0.5
32845	Predicted dehydrogenase	4	5	2	5	2	3	3	2	4	3	3	2	0.49	0.36	0.37	0.48	0.49	0.58
6809	conserved unknown with Clp protease domain	4	5	2	3	6	4	5	3	3	2	1	1	0.42	0.52	0.035	0.35	0.013	0.042
21651	unknown protein	8	7	3	1	2	4	0	2	2	3	2	4	0.029	0.0011	0.022	0.23	0.56	0.17
36788	similar to myo-inositol-1-phosphate synthase	1	2	2	1	1	3	0	0	1	4	9	8	0.56	0.075	0.0017	0.12	0.0013	1.1E-06
1786	possible chitinase	0	1	2	5	5	4	1	1	0	6	6	7	0.019	0.42	0.00072	0.003	0.22	0.000042
1512	unknown protein	7	7	6	2	2	1	5	5	5	0	0	0	0.0063	0.2	1.5E-07	0.051	0.012	7.5E-06
22096	unknown protein with heme binding domain	0	4	5	9	7	8	0	0	0	2	3	4	0.017	0.0009	0.46	6.1E-08	0.0047	0.0015
25629	putative protein similar to elongation factor G	0	0	0	0	1	0	0	0	0	10	10	11	0.48	1	5.5E-10	0.44	3.9E-08	3.4E-11
24571_2	Copper induced cell-surface protein	4	4	3	3	5	3	2	4	3	2	2	2	0.58	0.36	0.16	0.38	0.17	0.34
26991	putative glutaredoxin	4	3	5	2	6	3	1	4	3	3	2	1	0.49	0.21	0.068	0.3	0.12	0.33
29825	RS8, ribosomal protein 8, 40S small ribosomal subunit	4	4	3	1	4	3	2	2	2	4	3	5	0.29	0.14	0.43	0.43	0.16	0.059
1896	unknown protein	6	5	5	5	6	8	2	1	1	2	2	1	0.47	0.0035	0.0046	0.0019	0.0025	0.55
8713	conserved unknown, similar to Pt46395	2	3	2	3	4	3	3	6	6	2	2	1	0.43	0.073	0.32	0.17	0.18	0.01
39941	Possible branched-chain amino acid aminotransferase	5	5	3	5	5	4	2	1	2	2	2	0	0.58	0.035	0.012	0.038	0.013	0.45
30380	Triose-phosphate isomerase	2	2	2	2	1	4	0	0	0	9	5	7	0.55	0.0093	0.0058	0.0069	0.011	1.6E-07
5174	Fucoxanthin chlorophyll a/c protein 8	4	3	2	5	4	4	0	0	0	9	9	9	0.33	0.002	0.0021	0.00025	0.017	1.7E-09
30075	Proteasome subunit alpha type 5	2	2	2	2	4	3	4	3	4	3	3	5	0.43	0.27	0.26	0.44	0.43	0.58

Table A1 cont.

Protein Id, Description		Spectral Counting Abundance Scores												Fisher Exact Test P values					
		Colim			B12 lim			Fe lim			Replete			Colim vs B12 lim	Colim vs Fe lim	Colim vs replete	B12 lim vs Fe lim	B12 lim vs replete	Fe lim vs replete
		a	b	c	a	b	c	a	b	c	a	b	c						
23510	unknown protein	5	5	5	1	2	3	2	5	3	1	1	2	0.049	0.15	0.0036	0.3	0.3	0.066
32321	possible thioredoxin	4	2	2	2	2	3	8	7	6	1	1	0	0.57	0.0094	0.042	0.0088	0.06	3.8E-06
25206	unknown protein, multicopy	6	5	4	6	6	5	3	3	1	0	0	0	0.48	0.045	9.4E-06	0.028	4.5E-06	0.0057
34809	3-ketoacyl-CoA thiolase	4	5	8	3	2	3	2	1	2	2	2	4	0.1	0.008	0.031	0.23	0.44	0.35
269316	similar to acyl-CoA dehydrogenase; oxidoreductase	2	4	4	2	4	3	1	1	1	3	2	5	0.39	0.024	0.44	0.087	0.51	0.041
29075	argininosuccinate	2	4	3	5	1	3	1	1	3	3	2	5	0.48	0.13	0.56	0.23	0.43	0.099
22547	unknown protein, symilar to Pt 43658	4	3	3	2	5	4	4	3	5	2	2	2	0.51	0.48	0.16	0.56	0.12	0.086
24963	unknown proteins	5	5	5	3	1	3	4	5	3	1	1	0	0.086	0.27	0.0004	0.26	0.06	0.0041
42457	RS25, ribosomal protein 25, 40S small ribosomal subuni	2	2	2	5	4	4	0	0	2	3	3	6	0.17	0.097	0.12	0.006	0.52	0.002
24591	unknown protein	1	3	4	7	6	8	3	2	4	0	0	0	0.033	0.56	0.0013	0.021	3.2E-07	0.0013
24056	Myosin light chain kinase	0	0	0	1	1	0	1	0	0	8	10	7	0.23	0.54	3.1E-08	0.4	9.6E-06	5E-08
4819	conserved unknown, multiple copies	0	0	1	0	1	0	0	0	0	9	11	9	0.73	0.46	5E-08	0.44	1.8E-07	2.4E-10
7607	putative methyltransferase, has S-adenosylmethionine binding site, like Pt 39627	2	3	3	3	4	5	1	2	3	2	1	4	0.33	0.28	0.31	0.1	0.11	0.56
29217	cytosolic ribosomal protein L30	4	2	2	3	2	3	3	2	3	4	4	4	0.54	0.58	0.23	0.5	0.3	0.19
261381	Rab-type small G protein, similar to canine Rab5	4	2	1	1	2	1	3	1	4	3	2	3	0.43	0.52	0.49	0.34	0.31	0.57
23215	unknown protein	2	3	2	1	1	1	3	3	2	2	1	1	0.21	0.58	0.15	0.22	0.61	0.15
YP_874529.1	ATP synthase CF1 epsilon chain	4	5	3	1	1	0	4	3	4	3	3	3	0.017	0.43	0.35	0.034	0.046	0.5
5954	adenosylhomocysteinase	1	2	3	5	5	4	1	0	0	3	3	5	0.12	0.04	0.2	0.00078	0.41	0.0015
37277	trigger factor-like, as Pt bd1648	4	1	1	5	4	4	0	0	0	4	4	3	0.11	0.02	0.13	0.00025	0.5	0.00021
261499	putative Tha4/Hcf106 protein	1	3	2	2	4	4	4	4	3	1	2	2	0.33	0.27	0.34	0.54	0.12	0.077
33018	Fucoxanthin chlorophyll a/c protein 6	6	6	4	1	1	1	1	1	1	3	3	4	0.0065	0.0013	0.11	0.53	0.1	0.041
23814	Probable serine protease inhibitor	2	3	2	3	2	3	4	5	4	1	2	2	0.54	0.18	0.23	0.23	0.19	0.021

Table A1 cont.

Protein Id, Description		Spectral Counting Abundance Scores												Fisher Exact Test P values					
		Colim			B12 lim			Fe lim			Replete			Colim vs B12 lim	Colim vs Fe lim	Colim vs replete	B12 lim vs Fe lim	B12 lim vs replete	Fe lim vs replete
		a	b	c	a	b	c	a	b	c	a	b	c						
38066	aldehyde dehydrogenase	0	2	4	3	2	4	1	1	2	3	3	4	0.33	0.28	0.26	0.094	0.54	0.055
517	20S proteasome subunit alpha type 1	2	4	2	8	5	4	0	0	1	2	3	0	0.099	0.01	0.23	0.00008	0.0095	0.078
23528	rab-type small GTPase, similar to mouse Rab11	5	2	2	3	4	4	0	0	0	5	5	4	0.42	0.002	0.21	0.00057	0.37	0.00003
33024	isochorismatase, putative	4	3	3	3	1	4	1	1	4	2	2	4	0.48	0.2	0.38	0.32	0.52	0.37
30683	Proteasome subunit alpha type 2	4	1	1	6	4	5	1	1	2	2	2	4	0.049	0.4	0.37	0.011	0.11	0.17
262032	unknown protein	4	3	4	1	2	1	3	0	3	3	2	3	0.12	0.14	0.29	0.54	0.31	0.37
9947	conserved unknown protein	6	5	1	6	5	5	0	3	2	0	1	1	0.33	0.056	0.0032	0.013	0.00043	0.19
37443	conserved unknown, with dioxygenase domain, like Pt25000	1	1	2	1	1	1	0	2	1	6	6	6	0.55	0.41	0.0022	0.53	0.0015	0.00017
1049	putative NAD(P) dependant oxidoreductase	1	2	1	7	2	5	0	0	0	5	4	4	0.025	0.044	0.036	0.000047	0.45	0.000057
23668	uknown protein	5	5	4	2	2	3	1	2	1	2	1	2	0.12	0.01	0.014	0.23	0.28	0.55
39813	Fucoxanthin chlorophyll a/c protein 7 (FCP7)	4	3	3	1	1	1	1	2	2	3	5	4	0.098	0.13	0.41	0.51	0.036	0.048
33649	20S Proteasome subunit beta type 6 precursor	1	1	2	1	2	4	3	5	5	2	3	4	0.32	0.051	0.19	0.21	0.48	0.27
1095	possible ATP-dependent protease hslV	4	3	3	2	5	3	4	2	5	2	1	1	0.58	0.56	0.058	0.54	0.071	0.042
985	unknwon protein, like Pt42891	7	5	5	0	0	1	2	1	4	2	1	2	0.00027	0.019	0.0026	0.074	0.21	0.33
31362	Probable succinyl-CoA synthetase beta chain	0	0	0	0	0	0	0	0	0	7	10	10	1	1	1.8E-08	1	6E-08	1.7E-09
3621	unknown protein	2	5	4	5	4	4	1	1	1	3	2	2	0.58	0.014	0.16	0.016	0.17	0.14
22596	possible siderophore binding protein homolog, also similar to gamma CA??	2	3	4	1	1	3	3	3	2	1	2	5	0.17	0.37	0.38	0.34	0.31	0.57
34551	conserved unknown protein, like Pt 43657	1	2	2	2	2	1	5	5	5	1	2	2	0.57	0.033	0.46	0.051	0.4	0.0079
225	possible ribosome recycling factor	4	2	3	2	4	1	3	3	3	3	3	1	0.46	0.56	0.4	0.5	0.56	0.43
41697	thioredoxin, TRX	1	2	1	5	4	4	1	2	1	3	3	1	0.065	0.54	0.34	0.034	0.17	0.24
21965	conserved unknown, similar to disulfide isomerase, like Pt47306	5	3	6	5	4	5	3	1	1	2	1	0	0.51	0.022	0.0025	0.038	0.0055	0.32

Table A1 cont.

Protein Id, Description		Spectral Counting Abundance Scores												Fisher Exact Test P values					
		Colim			B12 lim			Fe lim			Replete			Colim vs B12 lim	Colim vs Fe lim	Colim vs replete	B12 lim vs Fe lim	B12 lim vs replete	Fe lim vs replete
		a	b	c	a	b	c	a	b	c	a	b	c						
YP_874519.1	50S ribosomal protein L12, chloroplast	2	1	2	1	1	0	4	5	5	1	2	1	0.27	0.047	0.35	0.0056	0.51	0.0057
36037	serine protease	5	4	5	5	4	4	2	2	0	3	1	0	0.42	0.01	0.0065	0.034	0.023	0.59
23025	60S ribosomal protein L10A	2	1	0	0	0	0	2	1	1	5	7	5	0.14	0.59	0.0018	0.1	0.000022	0.0015
28330	Probable bifunctional purine synthesis protein (Phosphoribosylaminoimidazolecarboxamide formyltransferase	0	0	0	1	2	0	0	0	0	7	7	9	0.11	1	1.8E-07	0.083	0.00017	2.3E-08
19141	bacterial-like flavodoxin	5	2	3	5	4	5	1	1	2	1	2	3	0.33	0.079	0.16	0.02	0.046	0.43
26457	glutathione reductase	2	3	3	2	5	1	0	2	2	3	3	2	0.57	0.12	0.48	0.15	0.52	0.17
1758	similar to Ftr1, plasma membrane iron permease	2	1	2	1	1	3	2	2	2	3	2	2	0.56	0.61	0.46	0.54	0.4	0.46
21414	unknown protein, multiple copies	2	2	3	1	4	3	5	4	4	1	1	1	0.57	0.23	0.088	0.21	0.12	0.0067
6071	RL22, ribosomal protein 22, 60S large ribosomal subunit,	0	0	2	3	1	3	2	2	2	4	4	3	0.12	0.21	0.014	0.43	0.26	0.12
21916	unknown protein, multiple copies	1	1	1	0	1	3	2	0	2	5	5	5	0.61	0.59	0.0067	0.64	0.011	0.0063
269459	unknown protein, multiple copies, like Tp 24060, Pt 49287	1	1	1	0	2	0	0	0	0	6	6	7	0.54	0.097	0.00046	0.19	0.00026	3.1E-07
9776	unknown protein, like Pt46690	5	3	2	2	2	1	1	2	2	2	2	3	0.27	0.13	0.22	0.46	0.6	0.45
8461	unknown protein	2	2	3	2	1	3	1	2	1	2	2	3	0.45	0.19	0.51	0.35	0.53	0.24
33574	acyl carrier protein	5	2	3	2	1	1	1	1	0	2	1	2	0.17	0.017	0.1	0.23	0.55	0.26
261226	Thylakoid lumenal 17.4 kDa protein	2	2	2	3	1	1	4	5	4	1	1	1	0.56	0.15	0.15	0.13	0.2	0.0067
23855	possible 60S acidic ribosomal protein P2	2	2	2	1	1	1	4	3	4	2	1	3	0.3	0.27	0.44	0.077	0.45	0.13
264891	putative glucosylceramidase	5	4	2	3	4	3	1	2	4	0	1	1	0.49	0.2	0.0062	0.31	0.016	0.07
4888	unknown protein	2	1	1	1	1	1	6	4	5	1	1	2	0.55	0.016	0.49	0.011	0.61	0.0034
27273	probable Methylenetetrahydrofolate reductase *methionine metabolism*	4	2	1	1	5	3	0	1	0	3	2	5	0.43	0.04	0.26	0.015	0.43	0.0027
262242	similar to long-chain fatty-acid-CoA ligase	5	4	5	3	4	4	2	1	0	2	1	1	0.34	0.0043	0.0065	0.028	0.041	0.55

Table A1 cont.

Protein Id, Description		Spectral Counting Abundance Scores												Fisher Exact Test P values					
		Colim			B12 lim			Fe lim			Replete			Colim vs B12 lim	Colim vs Fe lim	Colim vs replete	B12 lim vs Fe lim	B12 lim vs replete	Fe lim vs replete
		a	b	c	a	b	c	a	b	c	a	b	c						
264807	Possible V-ATPase subunit	4	2	2	2	4	1	3	4	4	1	2	1	0.57	0.36	0.23	0.33	0.28	0.077
268316	putative Ca2+-dependent membrane-binding protein annexin	2	2	2	3	4	4	0	1	0	3	3	4	0.24	0.04	0.33	0.0035	0.46	0.0049
25295	glutathione S-transferase domain, weird model	1	2	1	2	4	4	0	0	0	3	4	3	0.15	0.044	0.1	0.0013	0.54	0.0004
27101	60S ribosomal protein L31	1	1	1	3	1	1	1	1	2	3	3	5	0.31	0.59	0.035	0.35	0.17	0.037
YP_874598.1	30S ribosomal protein S8, chloroplast	5	3	3	5	2	4	2	3	1	1	1	1	0.58	0.14	0.016	0.15	0.02	0.21
262056	RS20, ribosomal protein 20, 40S small ribosomal subunit	5	2	2	5	4	0	0	1	0	1	4	3	0.57	0.01	0.48	0.015	0.52	0.015
20923	conserved unknown protein	2	6	2	2	5	5	0	2	1	0	1	1	0.51	0.024	0.0062	0.016	0.0039	0.46
264688	glutathione peroxidase (GPX)	2	3	3	0	0	0	1	0	1	3	6	5	0.0056	0.031	0.26	0.32	0.00032	0.002
3184	Histone H4	2	0	3	2	2	1	0	0	0	5	4	5	0.57	0.02	0.049	0.016	0.074	0.00003
267952	putative cell division cycle protein similar to CDC48 in SOTBN	1	0	1	5	5	6	0	0	0	3	3	5	0.0022	0.21	0.014	0.000021	0.25	0.00021
23111	unknown protein with peptidase domain	0	0	0	0	0	0	1	1	0	7	8	6	1	0.29	5.6E-07	0.32	1.5E-06	7.4E-06
262674	Hypothetical protein with some similarity to putative short-chain dehydrogenase/reductase	0	0	1	0	0	0	0	0	0	4	8	7	0.52	0.46	0.00002	1	4.4E-06	3.1E-07
25812	60S acidic ribosomal protein P0	0	0	0	0	0	0	0	0	0	5	9	8	1	1	3.1E-07	1	8.8E-07	4.4E-08
4718	epimerase/dehydrogenase	2	1	2	3	4	3	2	2	2	2	2	2	0.24	0.61	0.57	0.23	0.18	0.55
29782	putative eukaryotic translation initiation factor 6	4	4	1	1	1	1	1	1	2	4	2	4	0.15	0.12	0.54	0.64	0.1	0.082
25544	putative phosphoglycolate phosphatase	0	1	2	1	1	1	2	6	3	1	1	1	0.61	0.037	0.53	0.053	0.49	0.012
6290	Nucleoside diphosphate kinase	6	0	2	2	2	1	1	1	0	4	2	2	0.45	0.056	0.52	0.14	0.36	0.027
268713	conserved unknown protein, like Pt42543	1	2	1	3	2	4	0	0	0	4	3	5	0.15	0.044	0.036	0.0013	0.33	0.000057
28544	possible dihydrodipicolinate reductas	2	2	5	3	0	0	0	0	0	3	2	3	0.098	0.0009	0.38	0.083	0.19	0.0029
26706	Proteasome subunit alpha type 7-1 (20S proteasome a subunit D1	0	0	1	5	4	5	0	0	1	3	2	4	0.002	0.71	0.017	0.00078	0.21	0.0086

Table A1 cont.

Protein Id, Description		Spectral Counting Abundance Scores												Fisher Exact Test P values					
		Colim			B12 lim			Fe lim			Replete			Colim vs B12 lim	Colim vs Fe lim	Colim vs replete	B12 lim vs Fe lim	B12 lim vs replete	Fe lim vs replete
		a	b	c	a	b	c	a	b	c	a	b	c						
269866	glutathione S-transferase (GST)	0	0	0	0	0	0	0	1	0	6	6	7	1	0.54	3.2E-06	0.56	7.5E-06	6.9E-06
20866	unknown protein, like Pt 32031	4	2	2	1	2	3	3	1	3	1	0	2	0.45	0.48	0.088	0.57	0.2	0.14
40233	protein containing a cold-shock DNA-binding domain	1	1	2	2	4	4	4	2	2	2	2	1	0.15	0.28	0.61	0.39	0.12	0.24
268160	Putative protein of unknown function, similar to hypersensitive response-induced protein	0	0	0	1	1	1	0	0	0	5	6	7	0.11	1	3.2E-06	0.083	0.0015	6E-07
22213	Phosphofructokinase	0	0	0	0	1	0	0	0	0	5	7	8	0.48	1	0.000001	0.44	0.000028	1.6E-07
YP_874579.1	30S ribosomal protein S4, chloroplast	2	2	5	2	5	3	1	2	1	1	2	1	0.58	0.079	0.058	0.094	0.071	0.59
23249	unknown protein, NADH dehydrogenase domain	1	3	2	3	4	0	1	2	2	2	1	2	0.55	0.39	0.34	0.33	0.28	0.57
19991	thioredoxin	2	3	4	1	4	3	2	2	1	0	2	2	0.37	0.13	0.058	0.33	0.19	0.45
24564_1	unknown protein, multicopy	4	1	4	1	4	4	3	0	1	2	1	2	0.57	0.12	0.16	0.15	0.19	0.55
1219	conserved unknown protein, like Pt32261	2	1	3	0	1	3	0	0	1	1	3	5	0.3	0.04	0.4	0.22	0.14	0.0086
2107	unknown protein	5	2	3	3	2	5	4	1	2	0	0	0	0.51	0.28	0.00059	0.22	0.00036	0.0057
1820	conserved unknown, not in Pt	1	1	1	2	2	4	0	0	0	3	3	5	0.14	0.097	0.052	0.003	0.43	0.0004
28350	Phosphoglycerate mutase	2	3	2	2	1	1	0	0	0	4	2	2	0.33	0.0043	0.52	0.036	0.24	0.0015
23205	unknown protein, like Pt 47403	2	3	3	2	5	3	0	0	0	0	3	1	0.52	0.002	0.16	0.0013	0.12	0.039
24738	unknown protein, not in Pt	1	2	1	6	6	8	0	0	0	0	1	0	0.0032	0.044	0.12	1.7E-06	0.000008	0.52
21348	unknown protein, like Pt 38175	1	3	3	1	1	1	2	4	4	1	2	1	0.21	0.44	0.15	0.11	0.61	0.066
35523	Isocitrate lyase	2	2	3	2	4	1	1	1	3	1	0	3	0.57	0.28	0.15	0.33	0.19	0.45
25062	conserved unknown, multicopy, like Pt 48084	2	3	3	1	1	1	2	1	0	2	2	1	0.15	0.069	0.23	0.53	0.45	0.3
22127	unknown protein	5	3	3	3	4	4	1	1	1	1	1	0	0.58	0.024	0.0062	0.028	0.0079	0.46
10647	unknown protein	0	3	3	1	6	3	0	1	0	2	2	1	0.33	0.04	0.44	0.0072	0.18	0.078
27365	putative serine threonine protein phosphatase	1	0	1	1	2	3	0	1	1	3	4	4	0.19	0.62	0.021	0.14	0.22	0.0099

Table A1 cont.

Protein Id, Description		Spectral Counting Abundance Scores												Fisher Exact Test P values					
		Colim			B12 lim			Fe lim			Replete			Colim vs B12 lim	Colim vs Fe lim	Colim vs replete	B12 lim vs Fe lim	B12 lim vs replete	Fe lim vs replete
		a	b	c	a	b	c	a	b	c	a	b	c						
2078	unknown protein, not in Pt	0	0	0	5	4	3	1	0	1	3	3	3	0.0013	0.29	0.0018	0.012	0.46	0.017
41733	Thiamine biosynthesis protein	5	2	3	5	5	6	0	0	0	0	0	0	0.2	0.0009	0.00059	0.000021	0.000011	1
40323	carbamoyl-phosphate synthetase *urea cycle*	0	0	0	0	0	1	0	0	0	3	6	6	0.48	1	0.000056	0.44	0.00088	0.000016
40387	RL34, ribosomal protein 34, 60S large ribosomal subunit	2	2	2	2	1	1	1	2	1	2	3	2	0.43	0.28	0.58	0.49	0.4	0.24
268372	RL19, ribosomal protein 19, 60S large ribosomal subunit,	0	2	1	2	2	3	3	2	1	3	2	2	0.21	0.34	0.29	0.43	0.47	0.56
9073	predicted protein, like Pt 34270	2	1	2	2	2	3	3	2	4	1	0	1	0.44	0.31	0.14	0.5	0.06	0.024
263461	Putative methyltransferase, possible biotin synthesis role	4	1	2	3	1	4	0	2	1	1	2	2	0.43	0.18	0.44	0.087	0.26	0.3
5456	unknown protein, multicopy	2	2	5	3	2	3	0	1	1	0	1	1	0.48	0.017	0.012	0.041	0.031	0.65
37911	conserved unknown, like Pt 9400	1	3	3	2	2	3	1	0	0	2	2	1	0.57	0.02	0.32	0.03	0.38	0.078
2892	translation elongation factor Ts	1	3	2	2	2	1	0	0	0	3	2	4	0.56	0.0093	0.4	0.016	0.36	0.0015
5362	unknown protein, conserved domain	4	2	3	5	2	4	0	0	0	2	1	1	0.42	0.002	0.096	0.00057	0.041	0.074
YP_874586.1	50S ribosomal protein L23, chloroplast	2	2	3	2	2	3	2	2	3	0	0	1	0.57	0.48	0.015	0.53	0.023	0.027
268840	conserved unknown with CBS domain, like Pt 47178	2	1	0	3	5	4	0	0	0	3	2	3	0.032	0.097	0.21	0.00025	0.17	0.0055
8044	unknown protein with conserved pentapeptide repeat domain	1	1	0	1	1	0	4	5	4	0	2	0	0.65	0.0089	0.59	0.014	0.55	0.0022
26192	glutamate dehydrogenase	0	1	0	2	4	4	0	0	0	2	3	3	0.014	0.46	0.028	0.0013	0.41	0.0029
15093	Putative serine carboxypeptidase	1	3	3	1	1	1	1	1	2	3	2	2	0.21	0.19	0.42	0.64	0.35	0.32
20069	60S acidic ribosomal protein P2	2	2	1	1	1	1	2	2	2	3	2	2	0.41	0.61	0.56	0.39	0.35	0.56
19311	6,7-dimethyl-8-ribityllumazine synthase	4	1	4	1	4	3	0	0	0	2	1	2	0.46	0.002	0.16	0.0069	0.28	0.039
YP_316615.1	NADH dehydrogenase subunit 11, mitochondrian	1	1	3	5	2	4	2	0	0	3	1	0	0.16	0.16	0.35	0.012	0.041	0.38
39754	Thioredoxin reductase	5	2	0	3	4	1	0	0	0	3	2	2	0.43	0.0093	0.54	0.003	0.35	0.01
22315	conserved unknown	4	3	5	3	2	1	0	0	1	0	1	0	0.22	0.0013	0.00081	0.03	0.023	0.73

Table A1 cont.

Protein Id, Description		Spectral Counting Abundance Scores												Fisher Exact Test P values					
		Colim			B12 lim			Fe lim			Replete			Colim vs B12 lim	Colim vs Fe lim	Colim vs replete	B12 lim vs Fe lim	B12 lim vs replete	Fe lim vs replete
		a	b	c	a	b	c	a	b	c	a	b	c						
7883	conserved unknown, multicopy	0	0	0	0	0	0	0	0	0	6	5	5	1	1	0.000018	1	0.000038	4.2E-06
22497	conserved unknown, multicopy	2	2	3	1	2	1	1	1	2	3	1	1	0.33	0.19	0.23	0.49	0.55	0.55
29531	RL35A, ribosomal protein 35A, 60S large ribosomal subunit	1	2	2	2	1	1	0	2	0	2	2	1	0.56	0.16	0.57	0.23	0.6	0.17
33353	Thioredoxin, maybe bad model	2	1	1	1	1	1	2	4	4	1	2	1	0.55	0.15	0.49	0.11	0.61	0.066
36592	unknown protein, HMG-box containing	4	1	2	2	2	3	3	1	1	2	1	1	0.55	0.39	0.24	0.33	0.19	0.45
24572	protein with heme peroxidase domain, like Pt 48286, 48278	7	2	3	3	1	1	1	0	0	1	1	2	0.14	0.0013	0.02	0.06	0.3	0.22
5434	unknown protein	1	1	4	1	0	0	1	4	2	1	1	1	0.079	0.6	0.15	0.074	0.45	0.14
36614	putative diaminopimelate epimerase	4	4	2	1	1	3	0	0	0	3	2	1	0.17	0.0009	0.16	0.036	0.6	0.02
41530	possible cytochrome C	5	4	4	1	1	1	2	2	2	0	0	0	0.027	0.063	0.000049	0.39	0.071	0.012
270017	unknown protein, like Pt 42426 , with Fe(II) oxygenase domain	0	2	3	2	1	4	1	0	0	2	1	1	0.44	0.075	0.35	0.03	0.19	0.22
23960	unknown protein, like Pt 46187 with cytochrome c oxygenase domain	4	3	5	1	1	3	2	1	0	0	1	0	0.083	0.014	0.00081	0.36	0.099	0.28
261275	similar to PSB29	2	2	2	2	1	1	2	1	2	2	1	2	0.43	0.39	0.34	0.61	0.55	0.57
264007	hypothetical protein with some similarity to flavin reductase	1	3	1	1	1	1	3	2	3	1	1	1	0.41	0.4	0.24	0.22	0.49	0.088
YP_874578.1	30S ribosomal protein S16, chloroplast	4	4	2	2	1	3	1	1	0	2	1	1	0.27	0.017	0.058	0.14	0.3	0.38
24708	unknown protein, multicopy	2	1	2	3	4	3	2	2	1	0	1	0	0.24	0.52	0.061	0.15	0.005	0.09
26523	Zn- alcohol dehydrogenase	2	1	1	1	0	3	4	4	2	1	0	1	0.55	0.15	0.24	0.11	0.34	0.013
3258	possible PSII protein	4	2	3	0	0	0	3	1	4	1	2	1	0.0056	0.47	0.096	0.01	0.12	0.15
22734	unknown protein, multicopy	1	3	2	1	0	1	2	4	3	0	0	0	0.18	0.42	0.007	0.078	0.17	0.0013
264184	CTPA, Carboxyl-terminal processing protease	1	3	3	0	0	0	2	4	3	1	1	1	0.011	0.53	0.088	0.0058	0.2	0.054
38715	Fucoxanthin chlorophyll a/c protein 3 (FCP3)	5	4	3	0	5	0	0	0	0	3	3	5	0.083	0.00019	0.5	0.036	0.1	0.00021
261904	Ubiquinol-cytochrome-c reductase-like protein	2	4	4	0	0	0	4	1	3	0	0	0	0.0015	0.28	0.00026	0.01	1	0.0027

Table A1 cont.

Protein Id, Description		Spectral Counting Abundance Scores												Fisher Exact Test P values					
		Colim			B12 lim			Fe lim			Replete			Colim vs B12 lim	Colim vs Fe lim	Colim vs replete	B12 lim vs Fe lim	B12 lim vs replete	Fe lim vs replete
		a	b	c	a	b	c	a	b	c	a	b	c						
2770	conserved unknown, like Pt 43945	0	0	1	0	0	0	0	2	1	4	5	4	0.52	0.38	0.0013	0.18	0.00032	0.0063
937	conserved unknown, like Pt 48449	0	0	2	0	0	0	1	0	0	4	3	5	0.27	0.44	0.0054	0.56	0.00032	0.00047
4376	ribulose-5-phosphate kinase	0	0	0	0	0	0	0	0	0	5	6	5	1	1	0.000018	1	0.000038	4.2E-06
22820	conserved unknown, multicopy	1	2	2	2	2	3	2	3	1	1	0	1	0.44	0.61	0.14	0.43	0.06	0.12
1880	unknown protein, multicopy	2	2	1	1	2	4	1	0	1	1	2	1	0.44	0.16	0.46	0.076	0.28	0.26
30385	Fucoxanthin chlorophyll a/c protein -LI818 clade	2	1	2	1	0	1	0	2	0	2	2	3	0.27	0.16	0.56	0.59	0.2	0.11
718	glutaredoxin-like protein	2	1	1	2	2	4	0	1	0	3	1	1	0.22	0.14	0.61	0.015	0.19	0.13
20641	unknown protein, like Pt 42672	1	0	1	1	1	3	2	0	1	3	1	3	0.3	0.58	0.17	0.36	0.49	0.21
25409	unknown protein	2	1	2	2	1	3	2	0	1	3	1	0	0.57	0.28	0.35	0.23	0.3	0.55
298	weird model, similar to bacterial autoinducer 2-degrading protein lsrG	1	1	1	0	2	1	1	4	3	2	1	2	0.61	0.18	0.51	0.22	0.56	0.24
24564_2	unknown protein, multicopy	2	3	3	1	2	3	2	2	0	1	1	0	0.35	0.12	0.023	0.35	0.11	0.3
YP_874568.1	50S ribosomal protein L21, chloroplast	2	0	3	1	1	1	2	3	1	1	1	1	0.41	0.61	0.24	0.39	0.49	0.21
2209	unknown protein, like Pt 43181	1	3	1	3	2	3	0	1	1	0	2	0	0.33	0.16	0.14	0.041	0.031	0.65
21260	unknown protein	4	2	2	2	2	3	1	2	2	0	0	0	0.57	0.28	0.0031	0.33	0.0051	0.025
YP_874585.1	50S ribosomal protein L4, chloroplast	4	3	3	0	2	1	1	3	2	0	0	0	0.098	0.2	0.00059	0.39	0.071	0.012
4946	unknown protein	1	1	1	2	1	1	2	2	2	1	1	1	0.45	0.34	0.53	0.54	0.32	0.21
262414	protein containing a cold-shock DNA-binding domain	1	1	2	2	1	3	0	1	1	2	2	2	0.44	0.27	0.43	0.14	0.6	0.11
263178	3-hydroxyacyl-CoA dehydrogenase type II	1	1	1	1	1	3	2	3	1	2	1	2	0.45	0.34	0.51	0.54	0.55	0.44
31862	possible protein phosphatase 2C	1	1	2	1	1	1	1	0	2	3	2	2	0.55	0.41	0.43	0.53	0.35	0.21
37198	possible aureochrome	1	2	1	2	1	3	0	1	1	2	1	2	0.44	0.27	0.61	0.14	0.4	0.26
1360	hypothetical conserved plastid protein, probable ABC transporter membrane protein	1	1	2	2	2	3	1	1	2	1	0	0	0.32	0.54	0.12	0.23	0.023	0.16

Table A1 cont.

Protein Id, Description		Spectral Counting Abundance Scores												Fisher Exact Test P values					
		Colim			B12 lim			Fe lim			Replete			Colim vs B12 lim	Colim vs Fe lim	Colim vs replete	B12 lim vs Fe lim	B12 lim vs replete	Fe lim vs replete
		a	b	c	a	b	c	a	b	c	a	b	c						
25011	unknown protein, like Pt _49774	0	1	4	2	1	1	2	1	2	0	1	1	0.56	0.52	0.14	0.61	0.2	0.19
24931	disulfide-isomerase-like protein	1	2	2	1	2	3	3	1	3	0	0	0	0.57	0.5	0.016	0.57	0.012	0.0057
17193	phosphoglycerate/bisphosphoglycerate mutase family protein	1	1	2	1	1	3	2	0	0	1	2	0	0.59	0.27	0.37	0.23	0.32	0.54
37809	40S ribosomal protein S17	1	1	1	2	1	1	0	0	0	3	4	3	0.45	0.097	0.075	0.036	0.18	0.00077
261102	Putative carboxyl-terminal protease	2	1	2	5	4	0	1	0	0	1	2	0	0.33	0.075	0.24	0.015	0.067	0.35
24669	serine hydroxymethyltransferase-like domain, like Pt 43939	4	2	2	2	1	4	0	0	0	3	0	2	0.57	0.0043	0.23	0.0069	0.28	0.039
31113	partial cytochrome c oxidase	2	4	3	2	1	0	0	0	0	1	2	1	0.098	0.0009	0.058	0.083	0.61	0.074
21114	unknown protein, VAC14 domain	5	1	1	3	2	1	0	0	0	2	0	0	0.55	0.0093	0.077	0.0069	0.06	0.27
261635	putative pcna-like protein	0	0	1	5	5	4	0	0	0	3	1	2	0.002	0.46	0.11	0.00011	0.046	0.02
23393	unknown protein	6	4	3	0	0	0	1	0	0	0	1	0	0.00042	0.00065	0.00038	0.56	0.59	0.73
39143	Adenine Nucleotide translocator	2	2	0	0	0	0	1	0	0	4	2	4	0.075	0.14	0.1	0.56	0.0016	0.0027
36462	Triose-phosphate isomerase	0	1	1	1	0	0	0	0	0	3	3	5	0.53	0.21	0.0086	0.44	0.0037	0.00011
42475	Succinate dehydrogenase flavoprotein subunit	0	0	3	0	0	1	0	0	0	5	3	3	0.35	0.097	0.035	0.44	0.006	0.00021
35048	Fructose-bisphosphate aldolase	0	0	0	0	0	0	0	0	0	4	5	6	1	1	0.000032	1	0.000064	8.1E-06
21972	unknown with oxidoreductase domain, like Pt 44510	0	0	0	0	0	0	0	0	0	5	6	5	1	1	0.000032	1	0.000064	8.1E-06
33270	Histone H2A	1	1	3	1	1	1	1	1	1	2	2	1	0.41	0.28	0.46	0.53	0.56	0.41
22208	alanine glyoxylate aminotransferase	2	2	1	1	1	3	0	1	1	1	1	2	0.56	0.16	0.35	0.23	0.44	0.38
21060	unknown protein	1	1	2	1	1	1	1	0	1	2	2	3	0.55	0.27	0.43	0.38	0.35	0.11
4382	conserved unknown, like Pt 48524	2	1	1	0	2	1	0	2	0	2	1	1	0.55	0.27	0.49	0.38	0.61	0.38
25439	unknown protein, multicopy	1	1	1	0	1	1	1	2	0	3	2	2	0.54	0.58	0.21	0.62	0.14	0.14
YP_874587.1	50S ribosomal protein L2, chloroplast	4	4	2	2	1	1	1	0	0	1	1	1	0.17	0.0053	0.029	0.12	0.32	0.35
32332	ribose-5-phosphate isomerase	1	1	0	2	1	3	0	1	0	3	2	1	0.19	0.44	0.24	0.06	0.51	0.078

Table A1 cont.

Protein Id, Description		Spectral Counting Abundance Scores												Fisher Exact Test P values					
		Colim			B12 lim			Fe lim			Replete			Colim vs B12 lim	Colim vs Fe lim	Colim vs replete	B12 lim vs Fe lim	B12 lim vs replete	Fe lim vs replete
		a	b	c	a	b	c	a	b	c	a	b	c						
22899	unknown protein	2	2	3	2	1	1	0	1	0	0	2	1	0.33	0.02	0.088	0.12	0.32	0.35
2669	conserved unknown oxidoreductase	0	0	1	1	1	1	0	0	0	4	4	3	0.28	0.46	0.0038	0.083	0.051	0.00021
4225	unknown protein	1	0	3	0	2	0	0	1	0	0	2	0	0.39	0.14	0.24	0.4	0.55	0.53
23228	possible Ketol-acid reductoisomerase	0	0	0	1	0	1	0	0	0	3	6	4	0.23	1	0.00018	0.19	0.009	0.000057
269718	2-oxoglutarate dehydrogenase E1 component	0	0	0	1	0	0	0	0	0	3	4	5	0.48	1	0.00032	0.44	0.0037	0.00011
268621	Phosphoglucomutase	0	0	0	0	0	0	0	0	0	5	4	5	1	1	0.000056	1	0.00011	0.000016
21295	conserved unknown, like Pt 47865	1	1	1	1	1	1	3	2	1	1	1	1	0.61	0.34	0.53	0.39	0.49	0.21
22180	unknown protein, no homology	2	2	2	2	1	1	1	1	1	1	2	0	0.43	0.18	0.15	0.36	0.32	0.62
4516	conserved unknown, like Pt 49286	2	1	1	1	1	1	2	3	2	0	1	0	0.55	0.37	0.12	0.3	0.2	0.027
20577	unknown protein	4	2	2	2	1	0	2	1	1	0	1	1	0.21	0.19	0.042	0.64	0.34	0.3
263878	Acyl-CoA Oxidase	2	2	1	1	1	1	0	0	1	2	2	0	0.41	0.075	0.46	0.22	0.56	0.13
6807	unknown protein	0	2	0	2	1	3	1	0	1	1	0	1	0.19	0.62	0.59	0.14	0.11	0.65
3229	possible ubiquinol cytochrome c reductase subunit	2	4	1	0	0	1	0	2	0	2	1	1	0.046	0.056	0.15	0.6	0.31	0.38
22599	unknown protein	4	3	1	1	2	4	0	0	0	0	1	0	0.57	0.0043	0.015	0.0069	0.023	0.52
866	possible chloroplast clp protease P	5	1	2	0	2	1	0	0	0	2	1	1	0.21	0.0043	0.15	0.083	0.61	0.074
23126	unknown protein, like Pt 43309	1	2	0	0	0	1	1	0	1	3	2	2	0.35	0.42	0.21	0.6	0.059	0.071
41178	ATP phosphoribosyltransferase	1	1	1	1	1	0	0	0	0	3	3	4	0.54	0.097	0.075	0.19	0.046	0.00077
11175	conserved unknown protein	1	1	1	2	4	5	0	0	1	0	0	0	0.053	0.25	0.084	0.0035	0.00036	0.48
31451	possible Chloroplast 50S ribosomal protein L15	5	3	3	2	0	0	0	0	0	1	1	1	0.028	0.00041	0.016	0.19	0.66	0.14
2845	fucoxanthin-chlorophyll a-c binding protein	0	0	0	1	1	1	0	0	0	3	3	5	0.11	1	0.001	0.083	0.073	0.0004
269393	Sulfolipid (UDP-sulfoquinovose) biosynthesis protein	0	0	0	0	0	1	0	0	0	3	3	3	0.48	1	0.0032	0.44	0.024	0.0015
34030	putative NAD dependent malic enzyme (oxidoreductase)	0	0	0	3	2	4	0	0	0	0	2	1	0.0027	1	0.1	0.0013	0.071	0.074

Table A1 cont.

Protein Id, Description		Spectral Counting Abundance Scores												Fisher Exact Test P values					
		Colim			B12 lim			Fe lim			Replete			Colim vs B12 lim	Colim vs Fe lim	Colim vs replete	B12 lim vs Fe lim	B12 lim vs replete	Fe lim vs replete
		a	b	c	a	b	c	a	b	c	a	b	c						
6770	Acetyl-CoA Carboxylase (Biotin Carboxylase)	0	0	0	0	0	0	0	0	0	3	3	5	1	1	0.00056	1	0.00094	0.00021
24491	conserved unknown, multicopy like Pt 44152	1	2	1	2	1	0	1	2	1	1	1	2	0.55	0.54	0.49	0.64	0.61	0.59
23278	heat shock protein GrpE	1	1	1	1	2	1	1	2	2	0	2	1	0.45	0.46	0.53	0.61	0.32	0.32
25918	porin	2	2	1	0	1	1	0	1	1	2	2	1	0.27	0.16	0.46	0.59	0.39	0.26
23857	conserved unknown, like Pt 46652 , with zinc finger	0	1	1	1	2	3	0	0	1	1	1	1	0.19	0.44	0.62	0.06	0.2	0.35
20008	RS26, ribosomal protein 26, 40S small ribosomal subunit	1	2	1	1	1	3	0	0	1	1	2	1	0.59	0.14	0.49	0.12	0.44	0.22
1666	unknown protein, Tic22 - like domain	2	2	2	0	2	1	1	1	1	1	0	0	0.3	0.18	0.031	0.53	0.2	0.28
5186	Phosphoenolpyruvate carboxykinase (PEPCK)	1	1	2	0	1	1	1	0	0	1	2	4	0.39	0.14	0.43	0.4	0.2	0.046
269935	hisD, histidinol dehydrogenase	1	1	1	1	1	0	0	0	0	3	2	3	0.54	0.097	0.21	0.19	0.14	0.0055
28317	Probable dUTP pyrophosphatase	0	1	1	2	2	3	3	2	2	0	0	0	0.12	0.14	0.19	0.53	0.0051	0.0057
24123	fumarate hydratase	1	2	1	0	0	0	1	0	1	1	2	2	0.075	0.27	0.54	0.32	0.04	0.17
29850	NADH-ubiquinone oxidoreductase	1	2	0	1	4	4	0	0	0	1	0	2	0.14	0.097	0.53	0.003	0.067	0.14
21235	unknown with binding S1 domain protein	1	1	0	1	1	0	0	0	0	3	2	2	0.65	0.21	0.11	0.19	0.14	0.0055
42719	Argininosuccinate synthase (urea cycle)	1	1	0	0	0	0	1	0	1	3	2	2	0.27	0.62	0.11	0.32	0.014	0.071
21213	unknown protein	4	3	3	1	0	0	2	2	1	0	0	0	0.016	0.13	0.00059	0.18	0.41	0.025
26868	Proteasome subunit alpha type 3	1	0	0	1	2	1	0	0	0	3	3	2	0.16	0.46	0.028	0.036	0.31	0.0029
22442	unknown protein, like Pt 43378	1	0	1	2	2	3	0	0	1	0	0	0	0.12	0.44	0.19	0.03	0.0051	0.48
23329	heat shock protein 60, chaperone GroEL	0	0	0	1	1	3	0	0	0	3	2	3	0.052	1	0.0032	0.036	0.24	0.0015
411	Probable succinyl-CoA synthetase, citric acid cycle	0	0	0	0	0	0	0	0	1	2	4	5	1	0.54	0.001	0.56	0.0016	0.0027
262083	ABC cassette containing protein, possible elongation factor	1	1	0	2	2	3	1	1	1	1	1	1	0.12	0.58	0.62	0.15	0.12	0.62
32252	ribose-5-phosphate isomerase	2	2	2	1	2	1	1	0	0	1	0	1	0.43	0.04	0.077	0.12	0.2	0.53

Table A1 cont.

Protein Id, Description		Spectral Counting Abundance Scores												Fisher Exact Test P values					
		Colim			B12 lim			Fe lim			Replete			Colim vs B12 lim	Colim vs Fe lim	Colim vs replete	B12 lim vs Fe lim	B12 lim vs replete	Fe lim vs replete
		a	b	c	a	b	c	a	b	c	a	b	c						
31809	possible adenylate kinase protein	4	1	2	1	1	1	0	0	0	1	2	2	0.3	0.0093	0.34	0.083	0.56	0.039
41433	glutathione reductase	0	1	0	2	2	1	1	1	0	2	0	1	0.089	0.56	0.41	0.14	0.2	0.54
10997	unknown protein	2	2	2	2	2	1	2	0	1	0	0	0	0.56	0.18	0.007	0.23	0.012	0.11
25130	D-3-phosphoglycerate dehydrogenase	1	1	0	0	0	0	2	2	1	1	2	2	0.27	0.3	0.34	0.057	0.069	0.57
10661	unknown protein	2	1	1	1	0	1	0	3	3	0	0	0	0.39	0.48	0.037	0.24	0.17	0.012
22473	aliphatic amidase, carbon nitrogen hydrolase, nitrogen metabolism	0	1	2	1	1	1	0	0	0	3	1	3	0.61	0.097	0.21	0.083	0.26	0.0055
4830	similar to the actin binding protein cofilin	0	2	1	0	1	3	0	0	0	3	0	2	0.61	0.097	0.51	0.083	0.56	0.039
36099	iron-sulphur assembly protein isc	1	1	3	1	5	3	0	0	0	0	2	0	0.33	0.02	0.14	0.003	0.031	0.27
8409	unknown protein not in Pt	2	1	3	0	0	0	1	3	2	1	0	0	0.02	0.5	0.031	0.032	0.59	0.05
2325	methyltransferase	4	4	1	0	0	0	0	0	2	1	1	1	0.0056	0.031	0.051	0.32	0.2	0.54
41548	Putative dual function enzyme: UDP-glucose 4-epimerase and dTDP-glucose 4,6-dehydratase	0	0	0	0	0	1	1	0	1	2	5	0	0.48	0.29	0.01	0.6	0.059	0.071
263742	putative synaptobrevin	1	2	2	1	1	0	1	2	0	1	2	0	0.27	0.28	0.24	0.62	0.66	0.62
23416	protein of unknown function that contains a SCP/Tpx-1/Ag5/PR-1/Sc7 domain	1	3	1	1	2	1	1	1	1	0	0	0	0.56	0.28	0.016	0.36	0.03	0.11
17443	putative myo-inositol monophosphatase (IMPase)	1	1	0	2	1	0	0	1	1	1	0	1	0.46	0.62	0.59	0.38	0.34	0.65
1911	RK1, ribosomal protein 1, 50S large ribosomal subunit, chloroplast,	1	3	3	1	1	1	0	0	0	1	1	1	0.21	0.0043	0.088	0.083	0.49	0.14
7474	conserved unknown protein like Pt 14294	1	0	1	0	2	0	2	1	1	0	1	2	0.65	0.42	0.62	0.47	0.66	0.45
5576	unknown protein, like Pt 48250	0	0	2	2	1	1	0	0	0	1	2	1	0.3	0.21	0.47	0.036	0.44	0.074
31810	Pyruvate kinase	2	1	2	1	2	3	0	0	0	2	1	0	0.57	0.02	0.24	0.016	0.2	0.14
21590	unknown protein	1	2	1	1	4	3	0	0	0	1	0	0	0.32	0.044	0.12	0.0069	0.023	0.52

Table A1 cont.

Protein Id, Description		Spectral Counting Abundance Scores												Fisher Exact Test P values					
		Colim			B12 lim			Fe lim			Replete			Colim vs B12 lim	Colim vs Fe lim	Colim vs replete	B12 lim vs Fe lim	B12 lim vs replete	Fe lim vs replete
		a	b	c	a	b	c	a	b	c	a	b	c						
262125	Nitrite Reductase - Ferredoxin Dependent (nitrate uptake)	0	0	0	0	0	1	1	1	1	0	3	1	0.48	0.16	0.056	0.41	0.21	0.41
3186	unknown protein, conserved domain, not in Pt	5	0	1	1	1	1	1	2	0	0	0	0	0.41	0.28	0.016	0.53	0.071	0.11
37047	putative RanGAP	1	0	2	1	0	4	0	0	0	2	2	1	0.45	0.097	0.51	0.036	0.55	0.039
39946	S-adenosylmethionine synthetase (methionine metabolism)	2	0	1	3	4	1	0	0	0	1	1	0	0.14	0.097	0.38	0.003	0.031	0.27
15259	RS1, ribosomal protein 1, 40S small ribosomal subunit	1	0	0	0	0	1	0	0	0	1	2	2	0.73	0.46	0.11	0.44	0.14	0.02
32955	conserved protein, oxidoreductase/dehydrogenase domain, Zn binding	0	0	0	0	0	0	0	0	0	3	2	2	1	1	0.0056	1	0.008	0.0029
5335	cytochrome b-561-like protein	1	0	1	1	2	1	1	2	1	1	0	1	0.3	0.42	0.59	0.49	0.2	0.3
37409	regulatory proteasome non-atpase subunit 10	2	1	1	3	0	1	0	1	1	1	1	0	0.59	0.27	0.24	0.23	0.2	0.65
40483	20S proteasome subunit PAC1	0	0	1	1	0	0	1	2	1	2	1	2	0.73	0.24	0.18	0.28	0.21	0.55
20585	unknown protein	2	2	0	2	1	3	1	1	0	0	1	0	0.44	0.27	0.12	0.14	0.048	0.47
42508	putative chromatin assembly factor	1	1	1	2	2	3	0	0	0	1	0	1	0.21	0.097	0.38	0.0069	0.06	0.27
25396	unknown protein with conserved unknown domain	0	0	2	1	1	1	2	2	2	0	1	0	0.46	0.21	0.41	0.39	0.2	0.05
25492	unknown protien, like Pt 49248	2	0	1	0	1	0	1	2	3	0	1	0	0.35	0.34	0.23	0.12	0.66	0.05
10571	unknown protein, like Pt50545	2	1	0	3	1	4	0	1	0	0	1	0	0.14	0.25	0.23	0.015	0.011	0.73
1738	ClpP protease	1	1	4	2	2	3	0	0	0	0	0	0	0.55	0.0093	0.007	0.0069	0.0051	1
39255	putative glycyl tRNA synthetase	0	0	0	1	2	1	0	0	0	1	2	3	0.052	1	0.018	0.036	0.49	0.01
YP_316601.1	ATPase subunit 8, mitochondrial	2	2	2	0	0	0	3	2	0	0	0	0	0.02	0.39	0.007	0.057	1	0.025
22771	unknown protein, RING zinc finger domain	0	1	2	3	1	0	0	0	0	0	0	1	0.45	0.097	0.23	0.036	0.099	0.52
261882	Putative protein of unknown function, similar to glutaredoxins	2	3	2	1	0	0	0	0	0	1	0	0	0.046	0.0043	0.015	0.44	0.66	0.52
15398	FtsZ protein; plastid division	0	0	0	3	2	3	0	0	0	1	1	3	0.0056	1	0.056	0.003	0.19	0.039
269616	putative translation factor elongation factor EF-Tu	0	0	0	3	0	1	0	0	0	3	1	1	0.052	1	0.032	0.036	0.6	0.02

Table A1 cont.

Protein Id, Description		Spectral Counting Abundance Scores												Fisher Exact Test P values					
		Colim			B12 lim			Fe lim			Replete			Colim vs B12 lim	Colim vs Fe lim	Colim vs replete	B12 lim vs Fe lim	B12 lim vs replete	Fe lim vs replete
		a	b	c	a	b	c	a	b	c	a	b	c						
22863	Predicted Zn-dependent peptidase	0	0	0	0	0	0	0	0	0	3	1	4	1	1	0.01	1	0.014	0.0055
268280	Dihydrolipoamide S-acetyltransferase	0	0	0	0	0	0	0	0	0	3	3	5	1	1	0.001	1	0.0016	0.0004
25042	Long-chain acyl-CoA synthetases (AMP-forming)	0	0	0	0	0	0	0	0	0	3	3	5	1	1	0.001	1	0.0016	0.0004
33606	ucoxanthin Chl a/c protein, Lhca4	0	0	0	0	0	0	0	0	0	3	2	4	1	1	0.0018	1	0.0027	0.00077
24034	unknown protein	1	1	2	1	1	1	0	1	0	1	1	1	0.55	0.14	0.37	0.22	0.49	0.35
7964	Proteasome subunit beta type 4	1	1	1	1	2	1	0	0	0	1	2	1	0.45	0.097	0.63	0.036	0.44	0.074
21757	unknown protein with phospholipase domain	2	1	2	1	2	1	1	1	0	0	0	0	0.56	0.16	0.016	0.23	0.03	0.23
22714	unknown protein	1	2	1	2	1	3	1	0	0	0	0	0	0.44	0.14	0.037	0.06	0.012	0.48
25262	unknown protein with possible chromosome segregation domain	2	1	1	1	1	0	0	1	0	2	0	2	0.39	0.14	0.49	0.4	0.51	0.22
20602	unknown protien, similar to ribosomal protein L22	1	1	2	0	1	3	0	1	1	0	1	0	0.55	0.27	0.12	0.38	0.2	0.47
28570	L7Ae, ribosomal protein 7Ae, 60S large ribosomal subunit	1	2	2	0	1	0	1	1	0	0	1	1	0.13	0.16	0.14	0.6	0.63	0.65
13308	putative phosphoribosylaminoimidazole carboxylase (AIR carboxylase)	1	2	1	0	0	1	0	0	0	2	1	1	0.22	0.044	0.49	0.44	0.31	0.074
2386	conserved unknown protein	0	1	0	2	1	1	0	0	0	2	1	1	0.16	0.46	0.28	0.036	0.44	0.074
23492	unknown protien, like Pt50384	2	1	2	1	0	0	0	0	0	2	1	0	0.13	0.02	0.24	0.44	0.45	0.14
40958	Triose-phosphate isomerase	2	2	2	2	1	0	0	0	0	1	0	0	0.3	0.0093	0.031	0.083	0.2	0.52
40586	GDP-D-mannose 4,6-dehydratase	1	1	2	0	0	0	2	3	1	0	0	0	0.075	0.48	0.037	0.032	1	0.012
729	unknown protein	2	2	1	0	2	1	3	0	0	0	0	0	0.41	0.28	0.016	0.53	0.071	0.11
264674	Prolyl 4-hydroxylase alpha subunit, Fe(II) oxygenase domain	0	0	0	2	1	3	0	0	0	1	2	2	0.025	1	0.032	0.016	0.51	0.02
23511	unknown protein	1	1	1	1	5	3	0	0	0	0	0	0	0.14	0.097	0.084	0.003	0.0021	1
264583	Putative Pyruvate Kinase	2	2	2	1	1	1	0	0	0	0	0	0	0.3	0.0093	0.007	0.083	0.071	1
6974	unknown protein, snare domain	2	2	1	0	0	0	2	2	0	0	0	0	0.039	0.4	0.016	0.1	1	0.052
7679	unknown protein	2	3	2	0	0	3	0	0	0	1	0	0	0.11	0.0043	0.015	0.19	0.37	0.52

Table A1 cont.

Protein Id, Description		Spectral Counting Abundance Scores												Fisher Exact Test P values					
		Colim			B12 lim			Fe lim			Replete			Colim vs B12 lim	Colim vs Fe lim	Colim vs replete	B12 lim vs Fe lim	B12 lim vs replete	Fe lim vs replete
		a	b	c	a	b	c	a	b	c	a	b	c						
6089	unknown protein	0	1	1	0	0	0	3	3	2	0	0	0	0.27	0.09	0.19	0.01	1	0.0027
10059	unknown protein	1	1	1	1	0	1	0	0	1	1	2	1	0.54	0.25	0.63	0.4	0.51	0.22
2919	unknown protein	1	2	2	1	1	1	0	1	1	0	0	0	0.41	0.16	0.016	0.38	0.071	0.23
262575	Putative protein, similar to dihydroorate oxidase	1	0	1	0	0	0	1	1	1	1	1	3	0.27	0.58	0.34	0.18	0.069	0.41
1857	unknown protein with p23_like domain	1	0	0	1	0	0	1	1	0	2	2	1	0.73	0.56	0.18	0.6	0.21	0.26
34595	Aspartate carbamoyltransferase	0	0	0	2	1	0	0	2	1	1	1	1	0.11	0.16	0.18	0.53	0.49	0.62
33126	Rab-type small G protein	5	4	0	0	0	0	3	5	5	3	3	0	0.0056	0.25	0.31	0.00033	0.023	0.065
39901	Phosphoglycerate kinase	0	0	2	2	2	1	0	1	0	0	0	1	0.19	0.44	0.41	0.06	0.048	0.73
22388	unknown protein, like Pt 33952	4	2	1	2	1	1	0	0	0	0	0	0	0.43	0.0093	0.007	0.036	0.03	1
269968	Putative protein of unknown function containing a rhodanese domain	2	0	0	1	2	1	0	0	0	1	0	0	0.3	0.21	0.41	0.036	0.099	0.52
22890	unknown ERO1-lik	2	1	0	1	0	1	0	0	0	1	0	0	0.54	0.097	0.23	0.19	0.37	0.52
6802	unknown protein like Pt47708	0	0	0	2	0	1	2	0	2	0	1	0	0.11	0.086	0.56	0.64	0.2	0.16
5108	unknown protien with conserved domain	0	0	0	0	0	1	0	0	0	1	2	1	0.48	1	0.056	0.44	0.21	0.039
24220	unknown protein like Pt 44054	0	0	0	0	0	1	0	0	0	2	3	2	0.48	1	0.01	0.44	0.059	0.0055
23988	unknown multicopy protein	1	0	0	1	2	1	0	0	0	0	1	0	0.16	0.46	0.68	0.036	0.099	0.52
20843	unknown protein	0	1	0	2	2	0	0	0	0	0	0	0	0.16	0.46	0.44	0.036	0.03	1
1545	PSBC, Photosystem II 44 kDa reaction center protein	0	0	0	0	0	1	0	0	0	3	2	3	0.48	1	0.01	0.44	0.059	0.0055
21640	isocitrate dehydrogenase	0	0	0	0	0	0	0	0	0	3	2	4	1	1	0.0056	1	0.008	0.0029
268970	putative D-3-phosphoglycerate dehydrogenase	0	0	0	0	0	0	2	2	5	0	0	0	1	0.004	1	0.0058	1	0.0013
YP_874601.1	30S ribosomal protein S5	1	1	1	1	0	1	0	0	0	1	1	2	0.54	0.097	0.63	0.19	0.51	0.074
26889	RL38, ribosomal protein 38, 60S large ribosomal subunit	0	1	1	1	0	0	0	0	0	1	1	2	0.53	0.21	0.47	0.44	0.31	0.074

Table A1 cont.

Protein Id, Description		Spectral Counting Abundance Scores												Fisher Exact Test P values					
		Colim			B12 lim			Fe lim			Replete			Colim vs B12 lim	Colim vs Fe lim	Colim vs replete	B12 lim vs Fe lim	B12 lim vs replete	Fe lim vs replete
		a	b	c	a	b	c	a	b	c	a	b	c						
25054	unknown protein	1	2	1	2	1	1	0	0	1	0	0	0	0.59	0.14	0.037	0.12	0.03	0.48
36431	Peptidyl-prolyl cis-trans isomerase	1	0	1	0	0	0	1	1	2	2	0	1	0.27	0.42	0.62	0.1	0.2	0.45
18220	Rab2 GTPase	1	2	1	1	0	0	0	0	0	2	1	1	0.22	0.044	0.49	0.44	0.31	0.074
24506	unknown protein	2	1	1	0	1	3	0	0	0	1	1	0	0.55	0.044	0.24	0.083	0.34	0.27
5021	3-oxoacyl-(acyl-carrier protein) synthase	0	0	1	1	1	3	0	0	0	2	1	1	0.16	0.46	0.28	0.036	0.44	0.074
22424	unknown protein with FKBP domain	1	2	2	0	1	0	0	0	0	1	1	1	0.13	0.02	0.24	0.44	0.45	0.14
36078	putative peroxiredoxin, thioredoxin peroxidase	1	0	0	0	1	1	0	0	0	2	2	2	0.47	0.46	0.11	0.19	0.28	0.02
21327	unknown protein	0	1	0	2	1	3	0	0	0	1	1	0	0.089	0.46	0.59	0.016	0.11	0.27
4331	fructose-6-phosphate-aldolase	2	1	1	0	2	3	0	0	0	0	0	1	0.59	0.044	0.12	0.036	0.099	0.52
33653	possible mitochondrial protein translocase	0	1	2	0	0	0	1	2	1	0	1	0	0.14	0.59	0.23	0.1	0.59	0.16
22464	Fumarate hydratase class I	0	0	1	0	0	0	0	0	0	2	1	2	0.52	0.46	0.18	1	0.069	0.039
25692	unknown protein	0	0	0	2	2	1	0	0	0	2	1	0	0.025	1	0.18	0.016	0.2	0.14
24325	unknown protein with CnaB domain	0	1	2	2	0	4	0	0	0	1	0	0	0.31	0.097	0.23	0.016	0.048	0.52
22844	Choline transporter-like protein	1	1	0	2	0	0	0	2	2	0	0	0	0.65	0.42	0.19	0.47	0.17	0.052
268552	Pentafunctional AROM protein	0	0	0	0	0	0	0	0	1	3	2	2	1	0.54	0.018	0.56	0.023	0.046
32752	RL24, ribosomal protein 24, 60S large ribosomal subunit	0	0	0	0	0	1	0	0	0	2	2	3	0.48	1	0.01	0.44	0.059	0.0055
42971	valine--tRNA ligase-like protein	0	0	0	0	0	0	0	0	0	3	2	1	1	1	0.018	1	0.023	0.01
33343	6-Phosphogluconate dehydrogenase	0	0	0	0	0	0	0	0	0	1	2	3	1	1	0.032	1	0.04	0.02
16303	calcium/calmodulin-dependent protein kinase	0	0	0	0	0	0	0	0	0	2	2	4	1	1	0.01	1	0.014	0.0055
1515	adenylosuccinate lyase	0	0	0	0	0	0	0	0	0	1	3	3	1	1	0.01	1	0.014	0.0055
2702	conserved unknown with cyclophilin domain	1	1	0	1	0	0	1	1	1	0	0	2	0.53	0.58	0.59	0.41	0.63	0.46

Table A1 cont.

Protein Id, Description		Spectral Counting Abundance Scores												Fisher Exact Test P values					
		Colim			B12 lim			Fe lim			Replete			Colim vs B12 lim	Colim vs Fe lim	Colim vs replete	B12 lim vs Fe lim	B12 lim vs replete	Fe lim vs replete
		a	b	c	a	b	c	a	b	c	a	b	c						
41216	Electron transfer flavoprotein	1	1	2	1	0	1	1	0	0	0	1	0	0.39	0.14	0.12	0.4	0.37	0.73
YP_874595.1	50S ribosomal protein L14	1	1	0	1	1	3	0	1	0	0	0	1	0.3	0.44	0.41	0.12	0.099	0.73
7043	unknown protein	1	1	1	1	2	1	0	0	0	1	0	0	0.45	0.097	0.23	0.036	0.099	0.52
268651	RS9, ribosomal protein 9, 40S small ribosomal subunit	0	0	1	1	1	1	0	0	0	0	1	2	0.28	0.46	0.41	0.083	0.49	0.14
21033	uknown protein with lipoase domain	2	1	1	0	1	3	0	1	0	0	0	0	0.55	0.14	0.037	0.22	0.071	0.48
264532	cyanate lyase	1	2	1	2	1	1	0	0	0	0	0	0	0.59	0.044	0.037	0.036	0.03	1
268062	putative DnaJ protein	2	1	2	1	1	0	0	0	0	0	1	0	0.27	0.02	0.061	0.19	0.37	0.52
9135	putative protein with Esterase/lipase/thioesterase domain	0	1	1	3	1	1	1	0	0	0	0	0	0.19	0.44	0.19	0.06	0.012	0.48
YP_874608.1	30S ribosomal protein S9	1	0	2	0	0	0	0	0	0	1	2	1	0.14	0.097	0.63	1	0.12	0.074
23606	unknown, multicopy protein	0	1	0	1	4	1	0	0	0	0	1	1	0.089	0.46	0.59	0.016	0.11	0.27
923	unknown protein with conserved domain	1	2	2	0	0	0	1	0	1	0	0	0	0.039	0.16	0.016	0.32	1	0.23
25796	unknown protein	0	1	0	2	1	0	0	0	0	0	1	0	0.28	0.46	0.68	0.083	0.2	0.52
1954	unknown protein	2	1	0	2	1	1	0	0	0	0	0	0	0.45	0.097	0.084	0.036	0.03	1
29861	ferredoxin-dependent glutamate synthase	0	1	0	0	0	3	0	0	0	1	1	1	0.47	0.46	0.41	0.19	0.66	0.14
23494	unknown protein	0	0	0	2	1	0	1	0	0	0	0	0	0.11	0.54	1	0.22	0.071	0.48
11331	ACT domain protein	1	1	0	0	1	0	0	0	0	0	1	2	0.53	0.21	0.62	0.44	0.45	0.14
22860	conserved unknown protien like Pt43725	0	0	0	1	1	4	0	0	0	1	0	0	0.025	1	0.56	0.016	0.048	0.52
25861	conserved unknown, like Ptbd1626	1	1	0	0	4	0	0	0	0	0	2	1	0.46	0.21	0.62	0.083	0.49	0.14
24231	unknown protein, similar to Pt44084	0	0	0	2	0	0	0	0	0	1	0	0	0.23	1	0.56	0.19	0.37	0.52
25573	unknown multicopy protein	2	0	1	0	0	0	0	0	1	0	0	0	0.14	0.25	0.084	0.56	1	0.48
18503	putative thioredoxin	0	0	0	0	1	0	0	0	0	3	2	1	0.48	1	0.018	0.44	0.092	0.01

Table A1 cont.

Protein Id, Description		Spectral Counting Abundance Scores												Fisher Exact Test P values					
		Colim			B12 lim			Fe lim			Replete			Colim vs B12 lim	Colim vs Fe lim	Colim vs replete	B12 lim vs Fe lim	B12 lim vs replete	Fe lim vs replete
		a	b	c	a	b	c	a	b	c	a	b	c						
268480	Geranylgeranyl pyrophosphate synthetase	0	0	0	0	0	0	0	0	0	2	2	2	1	1	0.018	1	0.023	0.01
1736	photosystem II D1 protein	0	0	0	0	0	0	0	0	0	2	2	3	1	1	0.01	1	0.014	0.0055
34187	Acetyl-coenzyme A synthetase	0	0	0	0	0	0	0	0	0	2	2	2	1	1	0.032	1	0.04	0.02
264181	conserved unknown protein	0	0	0	0	0	0	0	0	0	2	2	3	1	1	0.01	1	0.014	0.0055
21837	possible heat shock protein 33	0	0	0	2	0	0	0	0	0	3	1	0	0.23	1	0.1	0.19	0.51	0.074
3020	unknown protein	1	0	0	1	0	0	1	1	2	0	0	1	0.73	0.24	0.68	0.28	0.66	0.16
7060	unknown protein with myosin-3-like domain	1	1	1	1	2	1	0	0	0	0	0	0	0.45	0.097	0.084	0.036	0.03	1
25024	unknown protein with ubiquitin reg domain	2	0	1	1	1	1	0	0	0	0	1	0	0.61	0.097	0.23	0.083	0.2	0.52
3438	unknown protein with FtsZ domain (cell division)	2	1	1	1	0	1	0	0	0	1	0	0	0.39	0.044	0.12	0.19	0.37	0.52
1584	possible cyclophilin	1	0	1	0	0	0	0	1	0	1	1	2	0.27	0.44	0.47	0.56	0.12	0.22
9513	possible cyclophilin	1	1	2	0	0	0	0	0	1	0	1	1	0.075	0.14	0.24	0.56	0.34	0.53
9679	possible mannose-6-phosphate isomerase	0	0	0	2	1	1	0	0	0	1	1	1	0.052	1	0.18	0.036	0.32	0.14
24761	unknown protein	1	0	1	2	1	0	0	0	0	0	1	0	0.46	0.21	0.41	0.083	0.2	0.52
7256	unknown multicopy protein	1	1	0	0	0	0	1	0	1	2	0	0	0.27	0.62	0.59	0.32	0.34	0.65
36641	Transaldolase	1	2	1	1	1	0	0	0	0	0	0	0	0.39	0.044	0.037	0.19	0.17	1
22521	unknown protein	0	0	0	1	2	1	0	0	0	2	0	1	0.052	1	0.18	0.036	0.32	0.14
32140	Hypothetical protein with similarity to dihydrodipicolinate synthase	1	0	0	0	0	0	0	0	1	1	1	3	0.52	0.71	0.18	0.56	0.069	0.13
269764	Pseudouridine synthase	1	0	0	1	0	0	0	0	0	3	1	1	0.73	0.46	0.18	0.44	0.21	0.039
843	Rab-type small G protein	5	4	5	0	4	0	0	0	0	0	0	3	0.017	0.00004	0.0025	0.083	0.49	0.14
21821	unknown protein, like Pt32316	2	1	0	1	0	0	0	0	0	0	1	0	0.35	0.097	0.23	0.44	0.66	0.52
264377	26S proteasome beta type 7 subunit	0	0	2	1	0	0	0	0	0	0	1	1	0.53	0.21	0.59	0.44	0.63	0.27

Table A1 cont.

Protein Id, Description		Spectral Counting Abundance Scores												Fisher Exact Test P values					
		Colim			B12 lim			Fe lim			Replete			Colim vs B12 lim	Colim vs Fe lim	Colim vs replete	B12 lim vs Fe lim	B12 lim vs replete	Fe lim vs replete
		a	b	c	a	b	c	a	b	c	a	b	c						
32924	Ribulose-phosphate 3-epimerase	0	0	0	2	1	0	0	1	0	0	0	2	0.11	0.54	0.32	0.22	0.34	0.53
20986	unknwon protein	0	0	0	0	0	0	0	0	0	1	0	2	1	1	0.18	1	0.2	0.14
33008	similar to 5-enolpyruvylshikimate-3-phosphate (EPSP) synthase	0	0	0	0	0	0	1	0	1	3	2	0	1	0.29	0.056	0.32	0.069	0.26
19501	RS10, ribosomal protein 10, 40S small ribosomal subunit	0	0	1	0	0	1	0	0	0	0	2	2	0.73	0.46	0.18	0.44	0.21	0.039
21538	5-oxoprolinase	0	0	0	0	0	1	0	0	0	0	1	3	0.48	1	0.1	0.44	0.31	0.074
7217	unknown protein, like Pt47936	0	0	1	0	1	0	2	0	0	0	0	0	0.73	0.56	0.44	0.6	0.41	0.23
21282	unknown protein like Pt4413	0	0	0	0	0	0	0	0	0	1	2	0	1	1	0.1	1	0.12	0.074
26367	RS15A, ribosomal protein 15	0	0	0	0	0	0	0	0	0	2	2	2	1	1	0.032	1	0.04	0.02
7805	possible aldo/keto reductase activity	0	0	0	0	0	0	0	0	0	2	1	1	1	1	0.1	1	0.12	0.074
22527	Ferredoxin reductase-like protein	0	0	2	0	1	1	1	1	0	0	0	0	0.65	0.62	0.19	0.59	0.17	0.23
9049	unknown protein	1	2	1	0	0	0	0	1	1	0	0	0	0.075	0.27	0.037	0.32	1	0.23
30301	putative phosphoribosylformylglycinamidine synthase	1	1	0	0	0	0	2	1	1	0	0	0	0.27	0.42	0.19	0.1	1	0.052
7806	unknown protein	1	0	0	1	1	1	0	0	2	0	0	0	0.28	0.56	0.44	0.38	0.071	0.23
1396	RK19, ribosomal protein 19, 50S large ribosomal subunit	0	1	2	0	0	0	0	1	1	0	0	0	0.14	0.42	0.084	0.32	1	0.23
21594	unknown protein	1	0	2	1	1	0	0	0	0	0	0	0	0.54	0.097	0.084	0.19	0.17	1
989	RR20, ribosomal protein 20, 30S small ribosomal subunit	0	2	2	0	1	0	0	1	0	0	0	0	0.22	0.14	0.037	0.68	0.41	0.48
4142	Ran GTPase-activating protein	0	0	0	1	1	3	0	0	0	0	0	1	0.052	1	0.56	0.036	0.099	0.52
20909	unknown protein	2	0	0	0	0	0	1	0	0	0	0	0	0.27	0.44	0.19	0.56	1	0.48
261711	Hypothetical protein with a sulfotransferase domain	0	0	0	0	0	0	0	0	0	1	2	1	1	1	0.1	1	0.12	0.074
41632	aspartyl protease	0	0	0	0	0	0	1	2	1	0	1	0	1	0.086	0.56	0.1	0.59	0.16
21868	unknown protein	0	0	0	2	1	0	0	0	1	0	0	0	0.11	0.54	1	0.22	0.071	0.48

Table A1 cont.

Protein Id, Description		Spectral Counting Abundance Scores												Fisher Exact Test P values					
		Colim			B12 lim			Fe lim			Replete			Colim vs B12 lim	Colim vs Fe lim	Colim vs replete	B12 lim vs Fe lim	B12 lim vs replete	Fe lim vs replete
		a	b	c	a	b	c	a	b	c	a	b	c						
31930	plastid division protein, metalloprotease	0	0	1	0	0	0	0	0	0	2	1	0	0.52	0.46	0.41	1	0.2	0.14
31636	Putative aldose-1-epimerase	0	0	0	0	0	0	0	0	0	2	2	2	1	1	0.032	1	0.04	0.02
35878	Phosphoglucomutase	0	0	0	0	0	0	0	0	0	2	2	2	1	1	0.032	1	0.04	0.02
22246	unknown protein	0	0	0	0	0	0	0	0	0	2	1	2	1	1	0.056	1	0.069	0.039
263240	putative ATP-dependent helicase	0	0	1	0	1	0	2	0	0	0	0	0	0.73	0.56	0.44	0.6	0.41	0.23
23275	pyrroline-5-carboxylate reductase	0	0	0	0	0	0	1	0	1	0	0	3	1	0.29	0.18	0.32	0.2	0.54
37359	catalytic subunit of clp protein superfamily	0	0	2	0	0	0	0	0	0	0	0	2	0.27	0.21	0.59	1	0.34	0.27
269160	Glutamate synthase small subunit	0	0	0	0	0	0	0	0	0	0	2	1	1	1	0.1	1	0.12	0.074
21419	unknown protein, like Pt47215	1	0	0	2	1	1	0	0	0	0	0	0	0.16	0.46	0.44	0.036	0.03	1
268835	3,2-TRANS-ENOYL-COA ISOMERASE	1	1	2	0	0	1	0	0	0	0	0	0	0.22	0.044	0.037	0.44	0.41	1
37596	putative GTP pyrophosphokinase	2	0	0	0	0	0	1	0	0	0	0	1	0.27	0.44	0.41	0.56	0.59	0.73
3379	unknown protein like Pt41244	0	1	2	0	0	0	0	1	0	1	0	0	0.14	0.25	0.23	0.56	0.59	0.73
5957	unknown protein	1	1	0	0	0	3	0	0	0	0	0	1	0.65	0.21	0.41	0.19	0.37	0.52
262858	homolog to yeast IKI3; confers sensitivity to killer toxin	1	1	0	0	0	3	0	0	0	0	0	0	0.65	0.21	0.19	0.19	0.17	1
3418	unknown protein like Pt 48909	0	0	0	0	0	3	0	0	1	0	1	0	0.23	0.54	0.56	0.4	0.37	0.73
1456	Putative partial isocitrate dehydrogenase	0	0	0	0	0	0	0	0	0	1	2	1	1	1	0.1	1	0.12	0.074
31226	Putative transporter	2	0	2	0	0	0	0	0	1	0	0	0	0.075	0.14	0.037	0.56	1	0.48
264361	putative aminopeptidase	0	0	0	0	1	0	0	0	0	2	1	0	0.48	1	0.18	0.44	0.45	0.14
264717	hypothetical aspartoacylase	0	2	0	0	0	0	0	0	0	0	1	0	0.27	0.21	0.41	1	0.59	0.52
1806	unknown protein	0	1	0	0	0	0	0	0	0	0	1	3	0.52	0.46	0.28	1	0.12	0.074
31762	carnitine acetyl transferase	0	0	0	0	0	0	0	0	0	1	2	1	1	1	0.1	1	0.12	0.074
1676	unknown protein	0	0	0	0	0	0	0	0	0	1	2	1	1	1	0.1	1	0.12	0.074
31851	unknown protein	0	0	2	1	1	0	0	0	0	0	0	0	0.65	0.21	0.19	0.19	0.17	1

Table A1 cont.

Protein Id, Description		Spectral Counting Abundance Scores												Fisher Exact Test P values					
		Colim			B12 lim			Fe lim			Replete			Colim vs B12 lim	Colim vs Fe lim	Colim vs replete	B12 lim vs Fe lim	B12 lim vs replete	Fe lim vs replete
		a	b	c	a	b	c	a	b	c	a	b	c						
37988	ADP-ribosylation factor 1	0	0	0	2	1	0	0	0	0	1	0	0	0.11	1	0.56	0.083	0.2	0.52
19977	Thioredoxin like protein	0	0	1	0	0	3	0	0	0	0	1	0	0.47	0.46	0.68	0.19	0.37	0.52
20933	unknown protein like Pt48094	0	0	0	1	0	0	0	0	0	0	2	1	0.48	1	0.18	0.44	0.45	0.14
23778	unknown protein	0	0	0	0	0	0	0	0	0	1	1	2	1	1	0.1	1	0.12	0.074
261823	sedoheptulose-bisphosphatase	0	0	2	0	0	0	0	0	0	1	0	1	0.27	0.21	0.59	1	0.34	0.27
33131	fucoxanthin chlorophyll a/c protein, Lhca clade	0	0	0	0	0	0	0	0	0	1	2	1	1	1	0.1	1	0.12	0.074
35871	D-isomer specific 2-hydroxyacid dehydrogenase	0	0	0	0	0	0	0	0	0	1	2	1	1	1	0.1	1	0.12	0.074
40393	putative Pyruvate kinase	0	0	0	0	0	0	0	0	0	2	1	1	1	1	0.1	1	0.12	0.074
1927	unknown protein	0	0	0	0	1	3	0	0	0	0	0	0	0.11	1	1	0.083	0.071	1
23620	unknown protein	2	0	1	0	0	0	0	0	0	0	0	0	0.14	0.097	0.084	1	1	1
29375	fucoxanthin Chl a/c protein, Lhca1 clade	0	0	0	0	1	0	0	0	0	0	2	0	0.48	1	0.32	0.44	0.63	0.27
1160	Peptidylprolyl isomerase domain-containing	0	0	2	0	0	0	0	0	0	1	0	0	0.27	0.21	0.41	1	0.59	0.52
21806	unknown protein	0	0	0	2	0	1	0	0	0	0	0	0	0.11	1	1	0.083	0.071	1
26941	NADPH Nitrite Reductase	0	0	0	0	0	0	0	0	0	1	2	0	1	1	0.18	1	0.2	0.14
YP_874542.1	photosystem II reaction center protein D2	0	0	0	0	0	0	0	0	0	0	2	2	1	1	0.1	1	0.12	0.074
36494	possible carbohydrate kinase	0	0	0	0	0	0	0	0	0	2	0	1	1	1	0.18	1	0.2	0.14
8732	unknwon protein, like Pt 45927	0	0	0	0	0	0	0	0	0	0	2	0	1	1	0.32	1	0.34	0.27
11460	unknown protein, like Pt 49015	2	0	0	0	1	0	0	0	0	0	0	0	0.53	0.21	0.19	0.44	0.41	1
21058	Ankyn repeat containing, like Pt 49011	0	0	0	2	1	0	0	0	0	0	0	0	0.11	1	1	0.083	0.071	1
27377	possible peptidase S9 prolyl oligopeptidase	0	0	0	0	0	0	0	0	0	1	0	2	1	1	0.18	1	0.2	0.14
41425	cytosolic malate dehydrogenase	0	0	0	0	0	0	0	0	0	1	0	2	1	1	0.18	1	0.2	0.14
240	cysteine desulfurase	0	0	0	0	0	0	0	0	0	0	1	2	1	1	0.18	1	0.2	0.14

Table A1 cont.

Protein Id, Description		Spectral Counting Abundance Scores												Fisher Exact Test P values					
		Colim			B12 lim			Fe lim			Replete			Colim vs B12 lim	Colim vs Fe lim	Colim vs replete	B12 lim vs Fe lim	B12 lim vs replete	Fe lim vs replete
		a	b	c	a	b	c	a	b	c	a	b	c						
31907	putative 4-diphosphocytidyl-2C-methyl-D-erythritol kinase	0	0	0	0	0	0	0	0	0	0	1	2	1	1	0.18	1	0.2	0.14
1879	unknown multicopy protein with Zn peptidase domains	0	0	0	0	0	3	0	0	0	0	0	0	0.23	1	1	0.19	0.17	1
YP_874597.1	50S ribosomal protein L5	0	0	0	0	0	0	0	0	0	2	0	0	1	1	0.32	1	0.34	0.27
1692	unknown protein	0	0	2	0	0	0	0	0	0	0	0	0	0.27	0.21	0.19	1	1	1
21469	unknown protein, cossible chromasome binding domain	0	0	0	0	0	0	2	0	0	0	0	0	1	0.29	1	0.32	1	0.23
21673	Vigilin-like protein	0	0	0	0	0	0	0	0	0	2	0	0	1	1	0.32	1	0.34	0.27
21811	Putative ubiquitin conjugating enzyme	0	0	0	0	0	0	0	0	0	0	2	0	1	1	0.32	1	0.34	0.27
22488	unknown protein, like Pt 46277	0	2	0	0	0	0	0	0	0	0	0	0	0.27	0.21	0.19	1	1	1
24035	unknown protein with peptidase domain	0	2	0	0	0	0	0	0	0	0	0	0	0.27	0.21	0.19	1	1	1
31006	light-repressed protein a	0	0	0	0	0	0	0	0	0	2	0	0	1	1	0.32	1	0.34	0.27

Table A2: *P. tricornutum* protein identifications and spectral counting abundance scores. 859 proteins were identified with a 0.22% peptide false discovery rate.

Protein ID, Description		Spectral Counting Abundance Scores												Fisher Exact Test P value					
		Colim			B12 lim			Fe lim			Replete			Colim vs B12 lim	Colim vs Fe lim	Colim vs replete	B12 lim vs Felim	B12 lim vs replete	Fe lim vs replete
		a	b	c	a	b	c	a	b	c	a	b	c						
54465	ISIP2A, iron stress induced protein	76	75	84	262	265	276	162	137	134	160	145	121	0	7.4E-16	1.2E-12	3.4E-30	5.1E-26	0.39
22357	GLNA, Glutamine Synthase III	90	89	96	68	77	75	75	74	73	125	129	114	0.0056	0.0096	0.00034	0.48	2.3E-09	1.4E-08
23658	Flavodoxin	21	18	16	150	154	153	36	27	17	55	65	55	0	0.015	1.6E-14	0	2.1E-27	1.8E-08
YP_874418.1	ribulose-1,5-bisphosphate carboxylase/oxygenase large subunit	101	86	102	18	21	20	91	94	83	27	35	33	6.3E-44	0.2	1.3E-20	2E-38	0.0029	1.5E-17
24820	Mitochondria-targeted chaperonin, groL homolog	36	35	34	73	87	68	41	35	27	77	81	81	1.4E-13	0.51	2.7E-12	1.4E-13	0.34	2.7E-12
25168	Fucoxanthin chlorophyll a/c protein, Lhcf type (multiple gene copies)	29	30	23	103	91	89	62	56	50	30	29	29	1E-30	9.4E-09	0.37	6.4E-09	1.1E-22	1.8E-06
bd913	methionine S-adenosyl transferase	22	21	21	95	95	95	27	19	22	34	37	35	1.6E-38	0.38	0.002	5.5E-36	2.4E-18	0.0061
54086	Ftype ATPase	47	46	44	55	49	48	39	38	44	39	46	55	0.18	0.16	0.46	0.022	0.25	0.15
45443	plastid carbonic anhydrase	5	6	8	68	75	74	8	7	6	89	93	87	0	0.41	0	0	0.013	0
54987	ISIP2B unknown protein; highly expressed under iron starvation; secretory pathway	39	40	42	40	31	45	36	27	41	62	55	44	0.4	0.14	0.015	0.21	0.0057	0.00071
44488	unknown protein, signal peptide	29	26	30	47	49	46	33	28	35	42	47	34	0.00003	0.21	0.0089	0.00094	0.13	0.061
54065	Fucoxanthin chlorophyll a/c protein, LI818 type	39	38	43	28	26	26	30	32	35	49	47	48	0.002	0.065	0.093	0.11	0.00003	0.003
55031	ISIP1, unknown protein highly expressed under iron starvation	35	38	42	37	39	35	37	39	41	19	17	26	0.42	0.46	0.00022	0.35	0.00035	0.00013
54019	heat shock protein Hsp70, small	38	40	44	17	21	20	45	45	43	35	40	40	1.4E-07	0.27	0.35	3.2E-09	0.00002	0.16
41856	transketolase, thiamine diphosphate-dependent	24	28	24	42	35	37	21	24	13	41	46	42	0.0021	0.068	0.00043	4.3E-06	0.22	1E-06
41423	Fructose-bisphosphate aldolase, class-I	31	32	32	41	31	40	36	32	30	16	12	12	0.1	0.41	0.00001	0.17	2.3E-08	4.3E-06
51305	Putative beta carbonic anhydrase (located in the plastid) (CA-IV)	7	3	5	45	54	57	8	4	7	84	82	57	9.9E-34	0.34	1.7E-44	8.7E-31	0.00056	2.4E-41
14618	ATP synthase F1, alpha subunit	35	40	41	25	31	30	29	30	35	20	18	20	0.014	0.07	0.00004	0.28	0.018	0.0048

Table A2 cont.

Protein Id, Description		Spectral Counting Abundance Scores												Fisher Exact Test P values					
		Colim			B12 lim			Fe lim			Replete			Colim vs B12 lim	Colim vs Fe lim	Colim vs replete	B12 lim vs Fe lim	B12 lim vs replete	Fe lim vs replete
		a	b	c	a	b	c	a	b	c	a	b	c						
50214	unknown, multicopy protein	31	33	28	32	33	35	30	34	33	14	15	18	0.28	0.35	0.00039	0.45	0.00003	0.00009
YP_874407.1	ATP synthase CF1 beta chain	31	33	37	44	43	43	26	27	23	31	29	31	0.026	0.037	0.3	0.000064	0.0095	0.16
42458	phosphoserine transaminase	39	40	32	24	23	20	36	39	35	4	5	5	0.00042	0.51	1.2E-16	0.00051	8.8E-09	1.8E-16
YP_874417.1	ribulose-1,5-bisphosphate carboxylase/oxygenase small subunit	33	29	33	20	23	25	28	25	27	24	26	26	0.017	0.17	0.12	0.16	0.28	0.41
42566	Thioredoxin domain containing	21	18	19	32	31	30	20	23	21	34	37	38	0.0021	0.35	0.0002	0.0094	0.16	0.001
55230	HSP90 family member	39	36	41	7	6	5	48	43	45	9	14	9	8.5E-22	0.11	8.4E-11	2.5E-27	0.038	4E-14
54246	ER luminal binding protein precursor	32	33	31	14	12	11	30	34	32	14	20	17	4.9E-08	0.49	0.00038	3.5E-08	0.12	0.0003
51157	Actin	23	26	24	19	21	25	25	25	24	9	8	10	0.23	0.51	0.00002	0.21	0.00027	0.00002
35766	Translation elongation factor 2	20	21	20	22	20	24	18	14	17	30	29	22	0.35	0.16	0.07	0.063	0.13	0.0067
49287	hypothetical protein with oxidoreductase domain, like Tp 24060	27	35	26	11	12	9	27	26	27	8	12	12	1.4E-08	0.32	2E-06	3.4E-07	0.51	0.00002
40880	putative agmatinase	18	11	14	23	21	21	12	11	12	38	43	34	0.013	0.25	3.5E-08	0.0013	0.00023	6.3E-10
5651	14-3-3-like protein, used in intracellular signaling	23	23	24	18	17	14	15	24	21	11	11	12	0.025	0.21	0.00062	0.16	0.063	0.008
28694	guanine nucleotide binding protein beta subunit-like protein	15	12	12	27	21	25	12	13	11	28	26	25	0.00035	0.45	0.00029	0.00015	0.34	0.00013
bd1572	enolase, phosphopyruvate hydratase complex	10	14	11	17	20	20	9	12	11	31	32	31	0.013	0.4	6.6E-07	0.0047	0.0018	1.3E-07
YP_874426.1	ATP synthase CF1 alpha chain [Phaeodactylum tricornutum]	19	23	19	24	24	25	16	19	18	12	18	14	0.16	0.27	0.09	0.044	0.01	0.25
54015	serine/glycine hydroxymethyltransferase, mitochontrial, Tp homolog is 269942	8	8	9	18	20	21	7	8	8	34	32	31	0.00006	0.42	1.9E-10	0.000015	0.002	3.3E-11
46547	multicopy hypothetical protein	0	0	0	46	52	50	0	0	0	14	14	9	0	1	7.9E-11	0	2.4E-15	1.1E-10
17633	Heat shock protein 70, DNAk	31	32	34	1	2	3	28	28	31	4	2	1	6.1E-26	0.28	1.4E-17	5.4E-23	0.48	1.3E-15
45465	multicopy hypothetical, has signal peptide, like Tp7881	32	38	34	37	32	34	35	36	36	20	18	20	0.51	0.41	0.00082	0.41	0.00054	0.00033
YP_874387.1	photosystem II chlorophyll A core antenna apoprotein	6	10	8	19	16	17	8	8	9	34	44	35	0.00023	0.41	3.9E-14	0.00093	3.3E-06	5.6E-13

Table A2 cont.

Protein Id, Description		Spectral Counting Abundance Scores												Fisher Exact Test P values					
		Colim			B12 lim			Fe lim			Replete			Colim vs B12 lim	Colim vs Fe lim	Colim vs replete	B12 lim vs Fe lim	B12 lim vs replete	Fe lim vs replete
		a	b	c	a	b	c	a	b	c	a	b	c						
18319	S-adenosyl-L-homocysteine hydrolase	25	18	26	11	12	11	25	22	23	3	3	3	0.00017	0.51	4.5E-11	0.00015	0.00014	3.9E-11
23924	glucose-6-phosphate isomerase, cytosolic	10	7	10	15	16	16	8	8	8	37	33	39	0.0059	0.42	4.5E-12	0.0023	1.2E-06	7.8E-13
50236	possible porin, voltage dependent anion channel	21	22	20	9	9	8	25	22	23	9	12	9	0.00002	0.32	0.0013	1.2E-06	0.34	0.00024
25308	triosephosphate isomerase/glyceraldehyde-3-phosphate dehydrogenase precursor	21	19	24	9	9	8	17	16	17	8	14	9	0.00001	0.1	0.001	0.0025	0.34	0.031
43251	Arf-type small GTPase, probable Arf1, ortholog of T. pseudonana TPS_121381	10	10	12	19	19	18	17	12	15	12	14	13	0.0043	0.089	0.25	0.13	0.064	0.34
54686	Highly expressed in ESTs, unknown function	29	31	30	0	1	1	19	25	21	3	5	1	5E-29	0.027	2.9E-15	1.6E-20	0.034	3.9E-10
bd542	cysteine synthase, PLP dependant	7	11	8	17	21	19	7	6	7	26	26	30	0.00024	0.21	1.9E-07	5.5E-06	0.023	2E-09
11823	Histone H2B isoform 1a, putative	14	16	13	17	16	15	13	17	13	7	11	9	0.35	0.54	0.043	0.35	0.014	0.043
27838	Unknown with duplicated ABC cassette domains	21	21	16	3	4	5	27	30	23	7	5	7	1.6E-09	0.029	0.00002	1.6E-15	0.2	3.8E-09
51230	Fucoxanthin chlorophyll a/c protein, Lhcf type	16	12	10	15	18	15	19	15	16	5	8	7	0.13	0.1	0.02	0.46	0.00071	0.00058
18665	serine hydroxymethyltransferase (glycine hydroxymethyltransferase)	20	21	17	24	19	20	8	8	5	0	0	0	0.33	0.00002	1.8E-14	1.3E-06	2.8E-16	7.6E-06
54801	clathrin heavy chain, vesicle coat protein	16	18	20	2	4	1	25	26	28	7	5	4	4.6E-12	0.014	0.00002	1E-19	0.053	5.6E-10
49202	unknown, multicopy protein	8	10	10	17	16	17	8	6	10	24	26	20	0.0053	0.32	0.00005	0.00083	0.052	5E-06
22122	glyceraldehyde-3-phosphate dehydrogenase, calvin cycle	16	14	16	11	9	8	18	18	20	7	5	4	0.02	0.16	0.00032	0.00072	0.051	7E-06
44651	methyltransferase 6 family protein like Tp 21517	10	14	11	14	12	17	12	11	10	16	17	18	0.2	0.49	0.058	0.16	0.22	0.045
15393	flavoxoxin-like oxidoreductase	19	18	22	8	8	7	19	19	19	8	3	4	0.00003	0.48	2.4E-06	0.000053	0.14	4.8E-06
30514	possible ornithine transcarbamoylase, like Tp 997	11	14	12	16	16	16	8	8	11	16	14	14	0.1	0.15	0.24	0.0079	0.39	0.042
22006	Fucoxanthin chlorophyll a/c protein, Lhcf10	14	13	16	11	12	8	18	13	12	9	12	8	0.083	0.5	0.098	0.068	0.5	0.084
48882	Fucoxanthin chlorophyll a/c protein, Lhcf15	18	17	18	3	1	1	15	18	18	14	15	25	4.2E-13	0.47	0.49	1.8E-12	8.7E-12	0.43

Table A2 cont.

Protein Id, Description		Spectral Counting Abundance Scores												Fisher Exact Test P values					
		Colim			B12 lim			Fe lim			Replete			Colim vs B12 lim	Colim vs Fe lim	Colim vs replete	B12 lim vs Fe lim	B12 lim vs replete	Fe lim vs replete
		a	b	c	a	b	c	a	b	c	a	b	c						
1884	metallopeptidase	3	2	3	17	14	20	4	3	4	30	24	31	3.2E-10	0.31	1.2E-16	2.2E-08	0.0029	2E-14
28737	translation elongation factor, EF-1	16	18	15	8	8	11	16	16	15	5	8	5	0.0047	0.46	0.00039	0.0087	0.14	0.00074
50445	UDP-Glucose-Pyrophosphorylase/Phosphoglucomutase	7	8	8	13	14	12	8	7	8	19	18	18	0.014	0.47	0.00024	0.024	0.067	0.00054
30145	Citrate synthase mitochondrial trageting sequence	17	21	22	1	2	2	18	22	20	4	3	3	5.6E-16	0.52	1.6E-08	5.7E-16	0.11	1.5E-08
41172	putative calreticulin	18	17	19	5	3	2	22	15	19	1	2	1	2E-09	0.45	3.7E-10	6.5E-10	0.1	1.4E-10
23717	ferredoxin-nadp reductase-like	5	2	2	13	16	16	4	3	3	23	30	27	3.5E-08	0.48	1.2E-14	1.7E-07	0.0018	9.4E-14
28056	MetE, Methionine synthase, vitamin-B12 independent	34	29	34	10	10	9	0	0	0	0	0	0	3E-11	1.9E-30	1.2E-23	5.9E-10	8.7E-08	1
42398	Malate dehydrogenase mitochondrial precursor	12	13	12	9	8	7	13	13	15	8	12	10	0.066	0.33	0.3	0.019	0.26	0.15
20331	PsbO oxygen-evolving enhancer protein 1	11	12	12	15	15	11	11	10	9	9	5	8	0.28	0.35	0.087	0.14	0.023	0.19
26921	Succinyl-CoA synthetase, beta chain, mitochondrial	12	13	18	7	9	6	11	17	14	5	6	9	0.0049	0.54	0.0096	0.0052	0.49	0.0099
30660	Ribosomal protien-like	15	15	17	7	7	4	14	17	14	1	6	5	0.00008	0.46	0.000028	0.00018	0.23	0.000061
41417	heat shock protein Hsp70	12	15	16	6	5	6	15	22	25	3	2	3	0.00013	0.039	1.5E-06	1.5E-08	0.054	3E-10
29157	Phosphoglycerate kinase, glycolysis	16	12	7	15	16	9	7	6	6	7	8	12	0.28	0.018	0.21	0.0023	0.072	0.18
27923	vacuolar proton pump alpha subunit	19	22	21	0	1	2	15	22	21	1	0	3	2E-18	0.41	7.8E-12	3.8E-17	0.4	5.3E-11
51018	probable ribosomal protein L4	20	20	20	3	2	2	16	17	11	3	3	5	3.9E-13	0.075	5.9E-08	1E-08	0.27	0.000034
31906	Aldehyde dehydrogenase	6	7	5	14	12	12	5	7	6	19	18	17	0.0026	0.54	0.000024	0.0033	0.061	0.000035
51797	Frustulin 3, cell wall associated	10	8	11	9	5	9	8	7	9	23	21	20	0.23	0.27	0.00043	0.51	0.000011	0.000035
46721	NrmA family protein	10	15	14	7	8	7	13	17	16	3	3	4	0.013	0.26	0.000077	0.0013	0.031	5.4E-06
47667	possible sodium phosphate cotransporter, Na/Pi cotransport system protein	0	0	0	16	15	17	0	0	0	28	26	26	1.5E-16	1	2.7E-23	2.7E-16	0.0039	5.9E-23
33839	Phosphoglyceromutase (glycolosis)	6	7	8	16	10	13	5	5	4	15	20	18	0.006	0.17	0.00022	0.00016	0.11	3.7E-06
54708	unknown function, 1 transmem. domain.	5	7	5	14	11	13	4	5	6	20	20	17	0.0015	0.46	4.2E-06	0.00062	0.035	1.4E-06

Table A2 cont.

Protein Id, Description		Spectral Counting Abundance Scores												Fisher Exact Test P values					
		Colim			B12 lim			Fe lim			Replete			Colim vs B12 lim	Colim vs Fe lim	Colim vs replete	B12 lim vs Fe lim	B12 lim vs replete	Fe lim vs replete
		a	b	c	a	b	c	a	b	c	a	b	c						
YP_874481.1	translation elongation factor Tu [Phaeodactylum tricornutum]	14	14	11	8	7	7	13	13	15	5	0	3	0.017	0.42	0.000039	0.0072	0.016	0.000013
20657	ATPase gamma subunit, plastid precursor	10	9	11	12	12	11	8	8	10	7	8	10	0.28	0.33	0.33	0.12	0.13	0.54
51242	adenosine kinase-like protein	8	8	7	18	22	16	6	4	5	4	5	3	0.00005	0.11	0.046	9.3E-08	1.1E-07	0.33
42018	ferredoxin--NADP+ reductase	4	6	6	11	12	15	7	4	5	15	20	16	0.00085	0.54	0.000034	0.0011	0.12	0.000047
45510	putative long chain acyl-CoA synthetase	6	7	9	9	10	10	9	14	9	9	8	12	0.16	0.076	0.18	0.35	0.53	0.41
42612	conserved unknown protein	8	11	11	11	12	14	8	9	9	5	5	9	0.24	0.33	0.12	0.099	0.025	0.25
42543	conserved unknown protein	11	10	9	7	9	7	16	14	13	4	6	5	0.23	0.069	0.035	0.0077	0.14	0.00064
27877	ammonium trasnporter	4	6	5	10	13	9	6	6	7	22	17	16	0.0046	0.28	3.1E-06	0.034	0.014	0.00006
50804	FMN-dependent alpha-hydroxy acid oxidase	7	7	9	10	12	15	7	9	6	12	11	9	0.048	0.47	0.17	0.03	0.37	0.12
26896	Histone H4 isoform 1b	8	12	10	8	9	8	11	12	12	4	6	8	0.31	0.28	0.082	0.11	0.19	0.022
12583	SOD1 Superoxide dismutase [Fe/Mn], mitochondrial	3	5	7	12	15	14	7	4	6	16	15	14	0.00011	0.41	0.00009	0.00055	0.35	0.00039
30139	Rab-type small GTPase, ortholog of T. pseudonana TPS_98341	13	10	6	9	7	8	11	12	12	5	5	8	0.27	0.24	0.1	0.069	0.25	0.022
27278	Fucoxanthin chlorophyll a/c protein, LI818 type	7	8	8	11	11	11	9	12	13	8	5	7	0.081	0.063	0.42	0.46	0.056	0.044
26432	dihydrolipoamide dehydrogenase (glycine/serine hmt coupled)	8	9	7	6	10	10	5	6	5	8	15	16	0.47	0.12	0.053	0.075	0.067	0.0024
YP_874452.1	Hsp70-type chaperone	9	9	12	3	5	5	9	12	10	9	6	10	0.0046	0.46	0.39	0.0025	0.029	0.32
28222	Transaldolase	13	14	12	8	7	6	11	12	9	4	0	3	0.0089	0.24	7.9E-06	0.069	0.0096	0.00016
22713	Rab-type small GTPase, ortholog of T. pseudonana TPS_98467	6	9	10	10	11	9	10	5	9	7	3	9	0.25	0.52	0.32	0.28	0.12	0.3
31433	predicted protein with ABC trans domain and walker motif	16	16	14	0	0	0	14	16	18	0	0	0	6.3E-17	0.46	1E-11	1.6E-17	1	3.9E-12
30031	Fucoxanthin chlorophyll a/c protein, Lhcf6	7	7	6	10	9	7	7	9	9	12	9	12	0.17	0.25	0.047	0.46	0.23	0.18
24978	possible vacular ATPase	16	14	14	1	4	2	10	11	12	7	3	4	2.7E-09	0.13	0.0002	2.6E-06	0.086	0.0074
50577	Acetylornithine aminotransferase, N-starve upregulated	3	5	5	17	16	12	3	5	3	8	9	9	3.2E-06	0.44	0.027	7.6E-07	0.025	0.013

Table A2 cont.

Protein Id, Description		Spectral Counting Abundance Scores												Fisher Exact Test P values					
		Colim			B12 lim			Fe lim			Replete			Colim vs B12 lim	Colim vs Fe lim	Colim vs replete	B12 lim vs Fe lim	B12 lim vs replete	Fe lim vs replete
		a	b	c	a	b	c	a	b	c	a	b	c						
11673	band 7 family protein	8	11	9	8	9	9	7	10	9	3	6	7	0.46	0.43	0.056	0.51	0.077	0.098
54499	Oxygen-evolving enhancer protein 3	3	2	3	15	11	12	2	4	3	11	11	10	7.6E-07	0.48	0.00018	3.3E-06	0.27	0.00048
51128	Glyceraldehyde-3-phosphate dehydrogenase (phosphorylating) activity in mitochondria	14	11	10	2	3	5	12	12	10	5	5	7	0.00004	0.54	0.016	0.000051	0.14	0.017
21122	tubulin	12	12	12	0	0	0	17	18	17	1	2	1	3.3E-13	0.045	2.6E-06	6.8E-19	0.051	9.8E-10
22873	putative mitochondrial ADP/ATP translocase	11	12	10	2	2	2	12	13	11	3	2	4	1.2E-06	0.37	0.0004	1.4E-07	0.34	0.00009 7
YP_874359.1	photosystem I P700 apoprotein A1	2	0	1	11	10	10	1	3	1	20	17	20	7.4E-08	0.35	3.3E-13	2.1E-06	0.0051	2E-11
34536	Fucoxanthin chlorophyll a/c protein, Lhcf type 16	5	6	5	10	7	7	6	4	9	11	14	13	0.082	0.34	0.0031	0.21	0.073	0.014
41515	plastidic enolase	4	3	2	9	12	12	3	5	2	9	9	9	0.00005	0.48	0.0021	0.00015	0.32	0.0046
16798	synaptobrevin-like protein	8	6	9	4	6	7	11	14	10	3	2	5	0.16	0.065	0.026	0.0035	0.16	0.00038
33660	ribosomal protein-like	11	13	12	2	2	2	10	12	11	4	6	4	6.3E-07	0.44	0.0037	2.6E-06	0.086	0.0074
50964	putative O-acetylhomoserine (Thiol)-lyase (O-acetylhomoserine sulfhydrylase)(OAH sulfhydrylase) (Homocysteine synthase)	5	4	5	7	7	9	3	8	4	14	12	12	0.051	0.48	0.0011	0.085	0.058	0.0023
54869	unknown protein, similarity to RAN GTPase activating protein	7	7	6	11	9	9	4	2	6	9	9	8	0.13	0.091	0.24	0.0039	0.44	0.02
29260	Transketolase	9	10	9	9	7	7	6	6	9	3	0	4	0.27	0.18	0.00097	0.41	0.0052	0.015
43841	unknown protein	7	7	8	10	8	7	8	6	9	3	5	3	0.3	0.47	0.046	0.39	0.01	0.031
54892	unknown protein, contains von Willebrand factor, type A; similarity to zinc finger proteins	4	6	5	7	7	7	6	7	4	12	14	14	0.18	0.41	0.0007	0.31	0.0095	0.0025
19030	mitochondrial phosphate carrier-like protein	9	14	11	2	2	1	9	15	13	3	3	4	2.8E-08	0.42	0.00049	5E-09	0.11	0.00018
32747	glyceraldehyde-3-phosphate dehydrogenase	7	5	4	7	8	7	5	7	9	8	12	5	0.13	0.23	0.11	0.41	0.44	0.33
49286	conserved unknown, like Tp4516	7	9	9	7	4	5	8	7	6	8	9	9	0.076	0.31	0.49	0.23	0.072	0.27
24886	unknown protein with DNA binding site	11	13	12	2	1	2	13	10	12	3	2	4	1.5E-08	0.54	0.00013	1.9E-08	0.19	0.00014

Table A2 cont.

Protein Id, Description		Spectral Counting Abundance Scores												Fisher Exact Test P values					
		Colim			B12 lim			Fe lim			Replete			Colim vs B12 lim	Colim vs Fe lim	Colim vs replete	B12 lim vs Fe lim	B12 lim vs replete	Fe lim vs replete
		a	b	c	a	b	c	a	b	c	a	b	c						
42282	possible ATP-sulfurylase	8	8	7	9	7	5	10	9	9	3	0	5	0.39	0.26	0.013	0.14	0.027	0.002
25172	Fucoxanthin chlorophyll a/c protein, Lhcf type2	7	5	6	11	11	7	6	5	6	7	5	8	0.051	0.53	0.44	0.042	0.14	0.4
54642	putative cell cycle control protein cdc48, NEM-sensitive factor (NSF), SNAP receptor (SNARE) complex component	8	13	10	2	1	2	8	14	13	5	3	3	3.7E-07	0.37	0.0043	3.7E-08	0.065	0.0013
27118	Ubiquitin extension protein 3	6	6	6	6	6	7	6	4	6	12	9	8	0.51	0.46	0.07	0.4	0.077	0.043
13073	3-oxoacyl-[acyl-carrier protein] reductase	9	6	10	3	5	6	6	8	6	5	6	7	0.04	0.25	0.21	0.19	0.3	0.48
22395	Fucoxanthin chlorophyll a/c protein, Lhcf8	5	8	6	7	8	5	8	8	10	4	3	5	0.47	0.17	0.23	0.22	0.16	0.04
46098	conserved unknown protein	13	9	10	2	1	1	13	11	9	1	5	3	1.9E-07	0.46	0.00057	7.1E-08	0.19	0.00031
44526	carbonic anhydrase with signal peptide	3	4	3	6	7	9	6	4	4	11	14	10	0.014	0.25	0.00025	0.096	0.069	0.0036
11014	acyl-CoA dehydrogenase-like protein	7	8	8	4	5	3	8	7	7	5	6	7	0.037	0.53	0.29	0.045	0.2	0.32
50191	unknown protein	6	6	6	3	5	7	5	5	8	7	11	9	0.44	0.54	0.13	0.41	0.072	0.15
17954	eucarytic translation initiation factor 5A	6	6	4	10	8	9	5	5	5	5	8	7	0.04	0.52	0.32	0.032	0.19	0.29
26293	possible Photosystem II 12 kDa extrinsic protein (PsbU)	1	1	1	8	8	7	0	1	0	20	20	21	0.000016	0.32	2.8E-14	5.7E-07	0.00003	3.7E-16
18398	ATP synthase subunit gamma putative	11	12	8	6	6	6	6	8	8	0	0	1	0.025	0.13	6.8E-07	0.27	0.00051	0.000077
31160	Rab-type small GTPAse, ortholog of T. pseudonana TPS_106973	6	4	4	6	5	7	8	8	6	4	5	3	0.25	0.083	0.42	0.27	0.16	0.054
34933	cyclophilin-type peptidyl-prolyl cis-trans isomerase	5	4	4	7	8	9	2	2	1	14	11	9	0.026	0.053	0.0028	0.000096	0.16	6.2E-06
28794	vacuolar proton translocating ATPase A subunit, putative	7	5	8	6	4	4	5	5	6	9	11	8	0.21	0.33	0.16	0.43	0.026	0.062
21030	vacuolar proton pump D subunit	6	4	5	7	7	6	0	4	2	12	12	10	0.18	0.044	0.0047	0.0023	0.043	9.5E-06
22819	peroxisomal membrane protein-related	9	9	8	4	2	3	9	8	10	1	3	3	0.0029	0.47	0.002	0.0015	0.35	0.0012
42104	Nucleoside Diphosphate Kinase 2	2	2	2	7	8	10	2	1	2	18	14	16	0.00014	0.52	1.1E-08	0.00006	0.0088	4.2E-09
51066	RS19, ribosomal protein 19 40S small ribosomal subunit	11	11	13	2	2	0	11	12	9	0	0	0	6.1E-09	0.44	5.8E-09	3.2E-08	0.16	2.1E-08

Table A2 cont.

Protein Id, Description		Spectral Counting Abundance Scores												Fisher Exact Test P values					
		Colim			B12 lim			Fe lim			Replete			Colim vs B12 lim	Colim vs Fe lim	Colim vs replete	B12 lim vs Fe lim	B12 lim vs replete	Fe lim vs replete
		a	b	c	a	b	c	a	b	c	a	b	c						
29097	RS5, ribosomal protein 5	8	8	11	2	2	2	10	7	12	4	3	4	0.00004	0.41	0.015	9.6E-06	0.15	0.0068
YP_874404.1	cytochrome f	1	1	3	11	10	8	1	1	2	15	11	10	4.1E-06	0.51	1.1E-06	1.4E-06	0.25	4E-07
34146	RL6, ribosomal protein 6	9	9	8	3	3	1	7	11	9	1	3	4	0.00039	0.52	0.0049	0.00031	0.51	0.0041
45679	unknown protein	1	2	0	7	7	7	0	1	2	23	17	18	0.000073	0.65	1.5E-13	0.000092	0.00002	2.5E-13
54926	Acetyl-CoA carboxylase (biotin carboxylase)	3	3	4	2	3	5	4	3	5	11	5	7	0.57	0.4	0.027	0.4	0.025	0.069
23079	onserved unknown protein	13	8	9	2	2	3	8	10	11	0	0	0	0.00002	0.53	8.1E-08	0.000026	0.024	1E-07
29014	fructose bishosphate aldolase class II, cytosolic	10	8	7	0	2	1	15	17	11	0	0	0	4.5E-06	0.016	1.1E-06	1.6E-11	0.16	5.7E-11
41409	unknown protein, similar to glutaredoxin	8	10	8	0	1	0	10	13	16	0	0	0	1.2E-08	0.059	6.7E-07	4.5E-13	0.63	4.9E-10
34120	possible aldolase, unknown function	2	5	5	8	9	7	8	3	6	5	6	8	0.021	0.16	0.13	0.2	0.33	0.46
51183	small flavoprotein with acylphosphatase activity	4	3	3	11	7	9	2	3	5	8	9	9	0.0025	0.57	0.0065	0.0031	0.55	0.0076
45813	conserved unknown with signal peptide	7	7	10	5	6	6	5	5	7	1	5	5	0.16	0.19	0.046	0.54	0.23	0.23
48983	Phosphoglycerate kinase possibly targeted to the mitochondria	7	6	4	11	8	7	3	4	3	4	6	7	0.091	0.14	0.55	0.0044	0.14	0.15
54381	Histone linker H1	9	10	9	4	4	5	8	9	9	0	2	0	0.0098	0.43	3E-06	0.024	0.0041	0.000011
47905	cold-shock DNA-binding domain-containing protein	3	6	4	7	7	8	4	2	3	9	5	8	0.045	0.28	0.086	0.0066	0.53	0.019
9046	conserved unknown with Reiske center	5	3	4	6	6	6	3	4	3	12	15	13	0.17	0.44	0.00011	0.096	0.0021	0.00003
36347	glutamate-1-semialdehyde aminotransferase (heme biosynth)	7	6	5	7	7	6	7	6	6	0	3	4	0.41	0.54	0.033	0.44	0.013	0.029
22774	RL7, ribosomal protein 7	11	13	11	0	2	0	10	11	10	0	0	1	1.5E-10	0.39	9.2E-08	1.9E-09	0.69	5.1E-07
YP_874423.1	ATP synthase CF0 B' chain subunit II	6	5	5	7	6	6	4	5	6	8	6	7	0.38	0.52	0.25	0.33	0.39	0.22
18893	possible quinone oxidoreductase/alcohol dehydrogenase	5	4	2	11	8	11	3	2	2	5	3	9	0.0012	0.26	0.13	0.000054	0.08	0.029
23629	cation transporting ATP-ase, E1/E2 type	1	2	1	7	7	7	4	6	3	9	11	14	0.00016	0.022	6.3E-07	0.085	0.055	0.0021

Table A2 cont.

Protein Id, Description		Spectral Counting Abundance Scores												Fisher Exact Test P values					
		Colim			B12 lim			Fe lim			Replete			Colim vs B12 lim	Colim vs Fe lim	Colim vs replete	B12 lim vs Fe lim	B12 lim vs replete	Fe lim vs replete
		a	b	c	a	b	c	a	b	c	a	b	c						
24195	CPS III, Carbamoyl-phosphate synthase (urea cycle)	12	11	9	0	1	1	10	10	9	0	0	3	1.4E-09	0.44	3.1E-06	8.3E-09	0.47	9.8E-06
50645	serine/threonineprotein phosphatase PP1gamma catalytic subunit putative	5	3	5	7	7	6	5	4	4	4	6	7	0.096	0.55	0.3	0.11	0.34	0.32
31683	possible geranylgeranyl reductase, chl modification	2	1	4	8	11	6	2	2	2	8	12	12	0.00055	0.52	0.00007	0.00027	0.21	0.000036
YP_874424.1	ATP synthase CF0 B chain subunit I	3	4	5	7	6	8	5	5	6	8	5	7	0.066	0.27	0.13	0.25	0.51	0.34
44639	possible phosphate ABC transporter, periplasmic phosphate-binding protein	3	3	4	9	7	7	2	4	4	8	8	8	0.0073	0.57	0.017	0.0088	0.56	0.02
49053	conserved hypothetical with possible sulfotransferase domain	7	6	6	6	5	3	7	6	5	4	2	4	0.26	0.53	0.1	0.29	0.28	0.12
21548	ABC transporter compnant, ATP binding, MDR-like	6	7	7	0	0	0	13	13	12	0	0	1	1.8E-07	0.0072	0.00025	4.3E-14	0.37	1.4E-08
43233	conserved multicopy hypothetial	6	4	4	7	3	7	4	2	2	11	11	9	0.29	0.16	0.011	0.038	0.042	0.0004
20424	Membrane targted urea transporter, plant-like, DUR3	7	4	5	6	6	7	6	4	7	3	5	3	0.32	0.47	0.21	0.42	0.081	0.15
22187	Glycine decarboxylase P-protein, glycine cleavage system P-protein,	8	10	9	2	2	3	4	9	7	1	2	1	0.00024	0.18	0.00014	0.0091	0.29	0.0035
17545	RS3A, ribosomal protein 3A 40S small ribosomal subunit	10	11	8	1	1	0	7	7	12	1	2	4	1.2E-08	0.38	0.00066	1.5E-07	0.071	0.0025
43152	possible peptidyl prolyl cis-trans isomerase	4	4	3	10	11	11	2	2	2	4	5	5	0.00055	0.18	0.34	7.3E-06	0.012	0.074
20934	3--isopropylmalate dehydrogenase	3	4	3	8	11	7	0	0	0	7	9	9	0.0025	0.0011	0.011	3.7E-09	0.5	1.3E-07
44091	unknown multicopy protein, similar to Tp 24322	4	3	3	4	7	6	1	3	2	14	14	10	0.11	0.24	0.00008	0.016	0.0036	2.4E-06
36226	predicted RL18a, ribosomal protein 18a 60S large ribosomal subunit	10	10	11	0	0	0	9	9	10	0	0	0	1.6E-11	0.43	4.8E-08	1.2E-10	1	1.8E-07
8091	thioredoxin f	4	5	4	3	6	7	4	4	4	8	8	9	0.33	0.52	0.04	0.28	0.1	0.031
20547	probable dihydroxyacid dehydratase	4	6	4	3	7	4	6	4	4	8	2	7	0.54	0.55	0.36	0.56	0.38	0.38
54971	Putative lipoprotein, type 6	4	9	7	4	2	3	6	4	7	4	5	4	0.045	0.4	0.19	0.11	0.37	0.31
24610	Triose phosphate/phosphate translocator	8	8	8	0	0	0	9	10	11	0	2	0	3.7E-09	0.23	0.000022	2.4E-11	0.37	8.5E-07
YP_874427.1	cell division protein FtsH-like protein	7	3	5	3	4	4	7	5	6	5	5	4	0.27	0.41	0.48	0.15	0.4	0.34

Table A2 cont.

Protein Id, Description		Spectral Counting Abundance Scores												Fisher Exact Test P values					
		Colim			B12 lim			Fe lim			Replete			Colim vs B12 lim	Colim vs Fe lim	Colim vs replete	B12 lim vs Fe lim	B12 lim vs replete	Fe lim vs replete
		a	b	c	a	b	c	a	b	c	a	b	c						
52498	putative cell surface protein	4	4	4	4	5	8	2	3	6	12	8	7	0.17	0.52	0.018	0.14	0.12	0.013
31073	predicted RS7, ribosomal protein 7	8	5	6	3	7	5	6	7	7	0	0	1	0.26	0.53	0.00025	0.23	0.0018	0.00021
21183	possible inorganic pyrophosphatase	7	9	9	4	3	5	7	4	6	0	0	0	0.019	0.13	1.1E-06	0.24	0.00095	0.00011
14760	frustulin-like protein	3	5	4	4	6	6	4	3	4	5	11	9	0.26	0.52	0.027	0.22	0.1	0.02
43245	unknown protein	7	6	6	6	3	3	6	6	6	0	0	1	0.16	0.53	0.0004	0.19	0.0062	0.00055
47612	alkaline phosphatase-like protein	0	0	0	2	4	2	0	0	0	22	18	22	0.0011	1	3.2E-18	0.0013	4.3E-11	5.7E-18
26176	possible elongation factor protein	8	8	6	2	2	2	9	6	10	0	2	4	0.0014	0.36	0.0035	0.00023	0.52	0.0009
54251	possible carbonic anhydrase	1	0	0	7	7	7	1	0	0	16	12	14	4.5E-06	0.74	1.7E-11	5.6E-06	0.0028	2.6E-11
YP_874401.1	PsbV	4	6	3	6	4	5	3	4	4	8	6	8	0.39	0.44	0.086	0.27	0.15	0.047
49897	possible proteasome subunit alph	3	3	4	8	5	6	4	4	3	5	6	7	0.049	0.48	0.096	0.085	0.52	0.15
54738	Triosephosphate isomerase, cytosolic	3	3	4	5	7	6	3	2	2	9	9	7	0.086	0.33	0.011	0.021	0.16	0.002
30113	Lipoamide dehydrogenase	3	3	4	4	6	5	2	3	3	12	12	7	0.18	0.43	0.0013	0.094	0.016	0.0004
33928	unknown protein	5	5	4	6	3	7	4	3	5	5	5	5	0.35	0.45	0.45	0.23	0.51	0.34
46126	conserved hypothetical, possibly involved in membrane trafficking	3	2	2	5	7	7	4	2	2	3	3	3	0.009	0.48	0.45	0.02	0.046	0.56
48822	perdicted protein, possible elongation factor-1 B beta	6	7	8	2	1	1	10	5	7	3	2	4	0.00031	0.41	0.034	0.000076	0.19	0.016
16481	light harvesting complex protein	7	5	6	7	3	6	5	5	6	1	2	1	0.44	0.46	0.0088	0.55	0.015	0.017
14386	light harvesting complex protein	4	3	2	6	4	6	3	4	4	8	8	9	0.098	0.39	0.0061	0.22	0.1	0.02
13682	40S ribosomal protein-like protein	6	7	6	3	3	2	8	6	7	1	3	1	0.027	0.41	0.015	0.01	0.36	0.0064
49037	NiSOD with ubiquitin fusion	2	5	2	6	7	5	4	4	1	7	8	8	0.056	0.57	0.017	0.063	0.27	0.019
19025	RL9, ribosomal protein	7	7	5	3	2	2	7	6	7	1	3	0	0.018	0.53	0.004	0.016	0.23	0.0035
51811	hydroxymethylbilane synthase, HemC (heme synthesis)	2	1	1	6	5	6	0	2	0	12	12	14	0.0026	0.35	6.4E-08	0.00029	0.0023	3E-09
YP_874365.1	Rubisco expression protein	7	6	5	3	2	2	11	7	5	1	2	4	0.025	0.2	0.045	0.0014	0.58	0.0052
44659	unknown protein	3	4	3	5	4	5	3	3	3	9	11	5	0.23	0.52	0.011	0.18	0.059	0.0072

Table A2 cont.

Protein Id, Description		Spectral Counting Abundance Scores												Fisher Exact Test P values					
		Colim			B12 lim			Fe lim			Replete			Colim vs B12 lim	Colim vs Fe lim	Colim vs replete	B12 lim vs Fe lim	B12 lim vs replete	Fe lim vs replete
		a	b	c	a	b	c	a	b	c	a	b	c						
9400	possible peptidyl-prolyl cis-trans isomerase	5	3	4	4	4	5	4	4	3	4	6	5	0.44	0.52	0.32	0.38	0.42	0.27
25127	Nucleoside Diphosphate Kinase 3	2	2	3	7	7	4	2	0	2	7	6	9	0.013	0.29	0.0052	0.0013	0.32	0.00051
YP_874358.1	photosystem I P700 apoprotein A2	1	0	1	7	8	10	2	1	0	7	12	7	5.9E-07	0.49	7.3E-06	4.3E-06	0.54	0.00004
YP_874394.1	photosystem I ferredoxin-binding protein	1	0	0	4	5	5	0	0	0	14	17	16	0.00025	0.51	3.1E-12	0.000033	0.000032	2.3E-13
49522	unknown with 5-hydroxyisourate hydrolase and OHCU decarboxylase domains	5	5	6	2	3	2	4	5	4	9	6	5	0.054	0.38	0.25	0.14	0.01	0.13
29266	Fucoxanthin chlorophyll a/c protein, Lhcf6	6	5	5	2	3	2	6	6	5	5	3	5	0.082	0.47	0.48	0.051	0.17	0.4
53939	Proteasome alpha 1 subunit (20S)	3	1	1	8	10	8	1	1	0	5	6	7	0.000029	0.24	0.0072	4.6E-07	0.16	0.00042
54986	putative cell surface protein	3	4	3	7	5	7	2	2	2	5	5	4	0.065	0.24	0.27	0.0075	0.31	0.074
bd1626	conserved unknown protein, like Tp 25861	6	8	10	3	2	2	4	4	5	3	2	1	0.0017	0.057	0.0024	0.14	0.44	0.1
27976	phosphoenolpyruvate carboxylase with a mitochondrial precursor sequence	5	5	5	0	1	2	6	7	9	1	2	3	0.0036	0.15	0.06	0.000045	0.34	0.0044
44603	ATP synthase	4	3	4	8	7	6	4	4	3	1	0	1	0.032	0.56	0.051	0.038	0.00034	0.047
17519	RS16, ribosomal protein 16 40S small ribosomal subunit	8	7	8	1	0	1	5	7	9	1	0	1	8.2E-07	0.41	0.0002	5.2E-06	0.47	0.00064
13361	RL3, ribosomal protein 3, 60S large ribosomal subunit	6	7	7	1	0	1	8	7	10	0	2	0	0.000013	0.25	0.00025	3.1E-07	0.69	0.00002
6847	RS9, ribosomal protein 9	7	7	9	1	0	0	8	5	10	0	0	0	2.4E-07	0.47	5.5E-06	8.5E-08	0.63	2.6E-06
47999	alanine-trna ligase	4	3	5	5	4	4	4	4	5	8	2	3	0.44	0.48	0.51	0.55	0.54	0.57
39687	RL22, ribosomal protein 22 60S large ribosomal subunit	7	7	7	0	2	2	6	6	6	3	3	3	0.00006	0.34	0.025	0.00053	0.12	0.074
14792	Phosphoglycerate kinase. Probably mitochondrial targeted	5	9	9	1	0	1	8	5	4	1	3	3	1.6E-06	0.24	0.0086	0.000084	0.071	0.055
25375	possible RL13A, ribosomal protein 13A 60S large ribosomal subunit	8	9	7	0	0	0	8	8	6	0	0	0	3.7E-09	0.41	1.9E-06	2.9E-08	1	7.6E-06
47103	unknown protein	3	4	5	5	7	5	2	1	3	3	5	5	0.17	0.13	0.51	0.011	0.27	0.12
47657	unknown protein	5	5	4	6	4	5	5	5	3	1	2	1	0.47	0.52	0.04	0.42	0.021	0.052

Table A2 cont.

Protein Id, Description		Spectral Counting Abundance Scores												Fisher Exact Test P values					
		Colim			B12 lim			Fe lim			Replete			Colim vs B12 lim	Colim vs Fe lim	Colim vs replete	B12 lim vs Fe lim	B12 lim vs replete	Fe lim vs replete
		a	b	c	a	b	c	a	b	c	a	b	c						
21116	ASSY (Argininosuccinate synthase)-urea cycle	8	9	6	0	0	1	7	8	8	0	0	1	1.1E-07	0.53	0.000035	1.8E-07	0.6	0.00005
bd1649	unknown multicopy protein, similar to Tp 24569	1	1	1	6	6	6	1	2	1	8	9	8	0.00055	0.49	0.00003	0.002	0.16	0.00013
28359	60S ribosomal protein L10A	7	6	9	0	0	0	7	7	6	0	3	0	1.8E-08	0.41	0.00031	1.4E-07	0.14	0.001
10757	aspartate-semialdehyde dehydrogenase	0	0	0	9	7	6	0	0	0	9	8	8	5.8E-08	1	1E-07	7.6E-08	0.4	1.3E-07
45068	unknown protein	0	0	0	9	7	9	0	0	0	9	6	5	9.1E-09	1	1.5E-06	1.2E-08	0.36	1.8E-06
42426	unknown protein, ER target, oxygenase domain	4	1	4	7	6	6	1	1	3	5	5	5	0.041	0.22	0.15	0.0033	0.4	0.026
54534	Alpha tubulin	7	6	4	1	1	0	11	7	7	0	0	1	0.0001	0.098	0.001	1.5E-07	0.69	0.00001
38015	DnaJ -like protein	7	7	4	1	0	0	8	5	9	0	0	0	4.4E-06	0.3	0.000045	1.8E-07	0.63	4.5E-06
46529	predicted protein, similar to extrinsic PS II protein in Chaetoceros	4	3	2	5	6	6	2	2	1	4	3	5	0.074	0.22	0.29	0.0075	0.32	0.073
16786	possible heat shock protein	6	4	6	2	2	1	4	6	8	4	2	3	0.0049	0.41	0.14	0.0014	0.19	0.074
12732	possible adenylate kinase	7	6	4	2	2	2	5	4	5	1	5	3	0.022	0.38	0.11	0.067	0.42	0.21
55192	Enyol-CoA hydratase, mitochondrial	1	1	1	2	5	5	1	0	0	11	9	9	0.0096	0.32	3.2E-06	0.00087	0.0078	1.2E-07
24474	proteasome alpha subunit	3	3	2	5	3	5	2	4	2	4	5	5	0.15	0.58	0.15	0.16	0.52	0.16
30003	proteosome beta subunit	2	3	3	4	6	5	4	4	2	4	3	4	0.085	0.39	0.31	0.2	0.33	0.49
19004	proteasome subunit alpha type 7	4	2	4	5	6	5	3	3	2	1	5	4	0.14	0.43	0.58	0.07	0.19	0.44
47395	ascorbate peroxidase	1	1	2	9	9	9	1	2	2	1	2	0	4.9E-06	0.49	0.53	0.000024	0.00002	0.39
27726	possible ornithine amodotransferase	6	5	6	2	1	3	8	6	6	1	0	0	0.022	0.35	0.001	0.0049	0.097	0.00021
12004	possible chaperonin	6	6	8	2	2	2	7	7	5	0	0	0	0.0029	0.53	0.00003	0.0041	0.039	0.000038
44056	PetJ, cytochrome c6 PS1	1	1	2	6	6	4	2	1	1	5	6	7	0.0041	0.62	0.0032	0.0048	0.4	0.0037
25743	possible translation initiation factor 4A	7	5	6	1	0	0	7	7	6	0	0	0	9.2E-06	0.41	0.000077	1.7E-06	0.63	0.00002
17504	possible peptidase, FtsH domain	3	5	4	3	3	3	2	2	3	5	5	5	0.42	0.19	0.32	0.3	0.2	0.074
25577	RL14, ribosomal protein 14 60S large ribosomal subunit	4	5	5	1	2	1	4	5	5	3	2	4	0.0063	0.55	0.22	0.0055	0.12	0.21

Table A2 cont.

Protein Id, Description		Spectral Counting Abundance Scores												Fisher Exact Test P values					
		Colim			B12 lim			Fe lim			Replete			Colim vs B12 lim	Colim vs Fe lim	Colim vs replete	B12 lim vs Fe lim	B12 lim vs replete	Fe lim vs replete
		a	b	c	a	b	c	a	b	c	a	b	c						
51058	possible v-type h-atpase subunit	6	3	6	4	3	3	4	3	4	1	2	0	0.27	0.3	0.01	0.56	0.044	0.047
43162	RL17A, ribosomal protein 27A	4	4	7	2	2	1	8	6	4	3	0	3	0.0083	0.34	0.06	0.0014	0.44	0.019
48728	conserved unknown	2	3	4	3	2	4	3	2	3	5	6	4	0.47	0.52	0.15	0.4	0.2	0.11
28202	Proteasome subunit alpha	4	3	2	4	5	4	4	2	4	3	2	3	0.21	0.48	0.46	0.3	0.15	0.36
51691	Proteasome beta subunit	2	1	2	4	7	7	1	3	2	3	5	5	0.0043	0.48	0.067	0.011	0.27	0.12
51169	Ran-family small GTPase, ortholog of T. pseudonana TPS_164980	5	6	5	2	2	2	5	6	5	1	0	1	0.02	0.54	0.0067	0.017	0.29	0.0059
45935	unknown protein like Tp 23216	2	3	2	2	1	2	0	0	1	0	0	1	0.28	0.038	0.097	0.16	0.28	0.66
50886	possible ribosomal protein	5	7	6	2	0	2	6	4	4	0	2	0	0.0017	0.32	0.00064	0.012	0.28	0.0038
14529	pyrophosphatase-like protein	6	4	5	2	4	3	4	5	4	0	0	0	0.21	0.45	0.00037	0.32	0.0038	0.00095
30486	ribosomal protein 18 40S	7	6	8	1	0	0	7	6	5	0	0	1	0.000001	0.4	0.00015	7.4E-06	0.6	0.00055
31919	RL5, ribosomal protein 5	7	5	5	0	0	0	8	11	7	0	0	0	1.9E-06	0.098	0.00013	1.2E-09	1	8.9E-07
40430	Dihydrolipoamide succinyltransferase	2	4	4	4	2	3	4	4	5	1	3	3	0.57	0.32	0.38	0.32	0.35	0.17
46188	thioredoxin h	2	2	3	6	4	3	2	1	2	5	5	7	0.097	0.4	0.042	0.035	0.33	0.015
35396	unknown protein, like Tp8417	2	2	4	3	4	5	2	3	3	3	5	3	0.19	0.58	0.42	0.21	0.39	0.44
55086	delta l-pyrroline-5-carboxylate synthetase	4	3	4	1	0	2	8	6	7	1	2	1	0.014	0.048	0.11	0.000024	0.4	0.0023
43037	unknown protein	2	0	2	4	5	5	0	2	2	5	9	7	0.0099	0.62	0.00085	0.011	0.17	0.001
27696	conserved unknown protein, like isochorismatase	2	0	1	5	6	4	0	1	0	8	9	9	0.0024	0.32	0.000015	0.00017	0.054	6.5E-07
45811	unknown protein with Sec14p-like lipid-binding domain, like Tp 24725	5	4	4	2	2	2	4	3	4	3	3	3	0.11	0.44	0.28	0.2	0.42	0.4
23871	aspartate aminotransferase	4	3	3	5	3	3	3	4	3	3	3	3	0.41	0.57	0.5	0.44	0.34	0.48
32237	unknown protein with Armet domain	2	2	2	6	2	6	1	2	2	7	5	7	0.041	0.52	0.014	0.024	0.3	0.0082
49098	pyruvate kinase 2, cytosolic	1	2	1	6	8	6	1	3	1	3	2	3	0.00041	0.49	0.29	0.0014	0.018	0.4
17276	possible SCF ubiquitin ligase, SKP1 component	6	4	3	5	4	4	2	2	3	3	3	0	0.52	0.14	0.11	0.11	0.084	0.49

Table A2 cont.

Protein Id, Description		Spectral Counting Abundance Scores												Fisher Exact Test P values					
		Colim			B12 lim			Fe lim			Replete			Colim vs B12 lim	Colim vs Fe lim	Colim vs replete	B12 lim vs Fe lim	B12 lim vs replete	Fe lim vs replete
		a	b	c	a	b	c	a	b	c	a	b	c						
15613	possible actin binding protein cofilin-like protein	3	3	4	5	4	4	3	2	2	4	3	3	0.28	0.33	0.58	0.11	0.33	0.35
46522	unknown protein with nuclear transport factor domain	3	3	3	4	2	5	2	1	3	5	5	3	0.33	0.32	0.29	0.12	0.5	0.12
29736	urate oxidase-like protein	4	2	3	2	5	3	1	1	1	7	3	9	0.47	0.078	0.042	0.039	0.061	0.00069
45335	unknown protein, Ca binding site	6	6	3	2	2	1	5	4	6	0	2	0	0.017	0.55	0.0027	0.015	0.2	0.0023
YP_874483.1	ATP-dependent clp protease ATP-binding subunit	3	8	4	0	1	0	7	5	5	1	3	4	0.00008	0.41	0.18	0.000016	0.012	0.097
29711	putative v-type h-ATPase subunit	7	7	3	2	2	1	4	3	4	1	0	0	0.0029	0.19	0.001	0.053	0.28	0.015
41746	HemB, porphobilinogen synthase	2	1	1	3	3	2	2	0	0	11	5	9	0.11	0.35	0.00011	0.025	0.0055	9.1E-06
41686	aminotransferase, PLP dependant	0	0	0	6	4	7	0	0	0	9	8	7	2.4E-06	1	2.5E-07	2.9E-06	0.21	3.1E-07
27821	possible DEAD box helicase	6	4	5	0	0	0	8	8	7	0	0	0	8.8E-06	0.088	0.00037	6E-09	1	2.6E-06
32531	unknown protein with guanine nucleotide exchange domain	3	3	3	2	2	2	4	2	5	3	5	5	0.37	0.39	0.29	0.2	0.14	0.46
12578	small ubiquitin-like modifier	3	3	3	4	2	2	3	3	3	4	6	4	0.55	0.57	0.21	0.57	0.22	0.22
55111	putative phospholipid scramblase	3	3	3	4	3	4	2	3	3	1	3	1	0.33	0.52	0.33	0.26	0.14	0.4
17401	Dihydrolipoamide acetyltransferase	4	4	2	2	5	3	2	4	1	3	3	7	0.57	0.33	0.36	0.3	0.37	0.17
21519	putative HSP70, BiP	5	5	4	2	2	1	6	4	3	3	2	1	0.014	0.52	0.082	0.02	0.44	0.1
19341	possible proteasome subunit beta type 4	2	1	2	3	4	5	1	1	2	5	5	4	0.046	0.51	0.04	0.025	0.46	0.023
42501	unknown protein	4	4	3	2	2	3	1	0	1	5	8	7	0.36	0.012	0.092	0.039	0.028	0.0002
43671	unknown protein, possible membrane trafficking domain	1	2	1	7	5	2	4	3	2	1	0	0	0.0099	0.12	0.32	0.18	0.0027	0.038
22909	possible aspartate aminotransferase, PLP binding domain	5	4	3	4	2	3	3	4	4	0	3	0	0.35	0.52	0.034	0.41	0.086	0.047
23497	ATP-binding Cassette protein	3	6	4	0	0	0	6	5	3	1	2	1	0.000041	0.48	0.056	0.000016	0.051	0.036
17324	RS4, ribosomal protein 4	4	8	4	0	0	0	8	6	5	0	0	0	0.000004	0.29	0.00022	1.4E-07	1	0.000022
54197	possible Tic22 family protein	3	3	3	2	2	3	2	1	4	5	5	5	0.37	0.42	0.15	0.56	0.053	0.074
54998	pyruvate kinase	2	2	2	4	3	2	3	1	1	4	3	4	0.2	0.52	0.17	0.14	0.48	0.12

Table A2 cont.

Protein Id, Description		Spectral Counting Abundance Scores												Fisher Exact Test P values					
		Colim			B12 lim			Fe lim			Replete			Colim vs B12 lim	Colim vs Fe lim	Colim vs replete	B12 lim vs Fe lim	B12 lim vs replete	Fe lim vs replete
		a	b	c	a	b	c	a	b	c	a	b	c						
13358	possib;e cytochrome b6-f complex iron-sulfur subunit	1	1	2	6	4	3	2	2	3	4	3	4	0.015	0.26	0.065	0.11	0.44	0.25
48449	unknown protein with possible Chalcone Isomerase domain	1	1	0	4	5	4	2	1	3	3	6	9	0.0019	0.14	0.00036	0.065	0.25	0.016
49167	glutathione-disulfide reductase.	4	3	4	2	2	3	4	5	1	0	3	1	0.21	0.52	0.11	0.27	0.37	0.14
23281	unknown protein with NAD dependent epimerase/dehydratase domain	3	2	2	3	3	4	6	5	7	0	0	0	0.22	0.019	0.025	0.11	0.0024	0.000065
22388	Peroxiredoxin, putative	1	1	0	7	6	6	2	0	0	3	5	7	0.000082	0.68	0.0034	0.0001	0.31	0.0038
48322	unknown, conserved protein (like Tp11697), CBA1	2	2	2	10	7	8	0	0	0	0	0	0	0.00014	0.017	0.043	6.7E-09	5.6E-07	1
35819	glutathione reductase	2	2	1	4	4	5	2	2	1	3	5	5	0.032	0.61	0.067	0.035	0.54	0.073
54958	glutathione reductase	5	4	4	2	2	2	5	3	4	1	2	1	0.07	0.52	0.056	0.094	0.46	0.073
10774	possible 50S ribosomal protein L15	5	3	3	2	1	2	5	4	6	1	2	3	0.058	0.26	0.2	0.0072	0.44	0.054
15632	60S ribosomal protein-like	1	4	2	5	5	5	1	2	2	1	2	3	0.052	0.4	0.51	0.017	0.048	0.55
13587	copine-like with meta-ion dependant adhesion site	4	5	8	3	3	2	6	5	6	5	3	4	0.085	0.54	0.33	0.077	0.3	0.31
29702	urease	4	3	4	2	1	2	4	4	4	0	2	0	0.096	0.48	0.017	0.058	0.2	0.0097
38534	unknown protein with thioredoxin domain	1	0	0	5	4	5	0	1	0	8	8	9	0.00025	0.74	1.2E-06	0.00029	0.059	1.5E-06
232	unknown protein with zinc protease domain	7	4	4	0	0	0	5	6	5	0	0	0	0.000004	0.54	0.00022	3.3E-06	1	0.00019
28562	possible 40S ribosomal protein S11	5	5	7	0	0	0	6	5	5	0	0	0	1.9E-06	0.53	0.00013	3.3E-06	1	0.00019
YP_874487.1	photosystem I iron-sulfur center	0	0	0	3	4	2	0	0	0	11	15	8	0.00061	1	4.7E-10	0.00069	0.00031	6.5E-10
50240	unknown protein with HMGB-UBF_HMG-box domain	2	3	3	2	3	2	2	2	2	5	6	5	0.56	0.41	0.067	0.44	0.049	0.027
49272	putative cell surface protein	4	4	3	2	1	3	5	3	4	3	3	3	0.15	0.48	0.42	0.094	0.34	0.33
22404	pyruvate kinase	2	1	2	4	6	5	3	1	2	3	0	3	0.015	0.48	0.54	0.033	0.048	0.6
54476	FMDA Formidase, like Tp 21465	2	0	0	5	4	5	1	2	2	5	3	5	0.0012	0.22	0.0034	0.024	0.58	0.044
19761	glycyl tRNA synthetase	3	2	2	5	3	6	0	2	3	1	0	0	0.071	0.4	0.097	0.024	0.0027	0.21

Table A2 cont.

Protein Id, Description		Spectral Counting Abundance Scores												Fisher Exact Test P values					
		Colim			B12 lim			Fe lim			Replete			Colim vs B12 lim	Colim vs Fe lim	Colim vs replete	B12 lim vs Fe lim	B12 lim vs replete	Fe lim vs replete
		a	b	c	a	b	c	a	b	c	a	b	c						
9199	RS13, ribosomal protein 13	5	6	5	0	0	0	5	6	4	0	2	0	0.000004	0.52	0.0017	7.3E-06	0.37	0.0023
18745	UDP-glucose 6-dehydrogenase	4	5	4	0	0	0	5	8	6	0	0	0	0.000041	0.17	0.0011	3.1E-07	1	0.000038
bd1645	Hypothetical protein with peroxidase domain	0	0	0	5	5	4	0	0	0	9	8	8	0.000028	1	1E-07	0.000033	0.059	1.3E-07
49151	possible NmrA family protein	2	3	2	2	2	2	2	2	3	4	6	8	0.58	0.59	0.026	0.56	0.018	0.029
32847	Glycine decarboxylase, glycine cleavage system, H-protein	3	3	4	2	4	2	3	2	1	3	3	3	0.53	0.24	0.5	0.28	0.55	0.37
YP_874395.1	50S ribosomal protein L12	2	1	2	2	4	3	3	2	2	4	2	4	0.13	0.37	0.17	0.3	0.59	0.35
YP_874444.1	photosystem II reaction center protein D1	5	4	4	1	1	2	5	4	5	1	2	1	0.011	0.48	0.056	0.0055	0.52	0.036
53935	Plastidic Ribulose-phosphate 3-epimerase	1	1	2	2	2	2	1	1	1	5	5	4	0.28	0.51	0.021	0.18	0.086	0.01
55079	pyruvate kinase	4	2	3	3	4	2	4	2	5	1	0	1	0.55	0.39	0.11	0.41	0.086	0.047
YP_874377.1	photosystem II reaction center protein D2	4	3	6	0	1	1	5	5	6	1	3	1	0.0014	0.33	0.11	0.00017	0.14	0.039
42949	unknown protein	5	5	5	2	1	2	4	2	7	1	0	0	0.0083	0.45	0.0027	0.02	0.28	0.0061
18274	cyclophilin-like protein	2	2	1	5	3	5	0	0	0	4	6	7	0.032	0.033	0.013	0.000061	0.33	0.000026
12799	Prohibitin-like protein	6	6	5	0	0	0	5	6	4	0	0	0	1.9E-06	0.46	0.00013	7.3E-06	1	0.00032
28979	RL12, ribosomal protein 11 60S large ribosomal subunit	6	4	2	2	1	1	3	4	5	1	3	3	0.018	0.56	0.24	0.016	0.21	0.23
45017	possible isocitrate dehydrogenase, NADP-dependent, with signal peptide	3	7	2	0	0	0	6	6	4	0	0	0	0.00009	0.27	0.0018	3.3E-06	1	0.00019
33342	possible glutathione s-transferase	2	2	2	2	2	2	2	3	2	4	5	7	0.51	0.48	0.041	0.56	0.053	0.074
17766	Fucoxanthin chlorophyll a/c protein, Lhcr type	2	1	2	2	2	2	2	1	2	5	5	8	0.4	0.61	0.0072	0.41	0.018	0.0082
23324	RL11A, ribosomal protein 11A 60S	4	3	4	1	2	2	3	3	4	3	3	1	0.096	0.52	0.3	0.13	0.39	0.36
39304	regulator of chromosome condensation (RCC1)-like protein	1	2	2	5	3	2	1	1	1	3	3	4	0.092	0.38	0.17	0.026	0.52	0.066
45998	20S proteasome subunit alpha type 1	3	1	3	5	4	2	1	1	1	4	5	3	0.22	0.18	0.24	0.026	0.55	0.037
42712	unknown protein with ran-binding	3	1	2	3	4	2	3	2	4	0	2	1	0.2	0.29	0.3	0.49	0.062	0.1

Table A2 cont.

Protein Id, Description		Spectral Counting Abundance Scores												Fisher Exact Test P values					
		Colim			B12 lim			Fe lim			Replete			Colim vs B12 lim	Colim vs Fe lim	Colim vs replete	B12 lim vs Fe lim	B12 lim vs replete	Fe lim vs replete
		a	b	c	a	b	c	a	b	c	a	b	c						
10847	RS1, ribosomal protein 1	4	3	5	1	2	3	5	2	5	0	0	1	0.15	0.56	0.011	0.14	0.097	0.0097
54954	unknown function; Calcium-binding EF-hand	5	5	3	1	1	2	5	6	5	0	0	0	0.011	0.33	0.0011	0.0017	0.16	0.00019
16322	fucoxanthin chlorophyll a/c protein	0	1	1	4	4	5	3	5	3	1	0	0	0.0019	0.01	0.63	0.38	0.0041	0.015
bd1186	2-phosphoglycolate phosphatase	0	1	0	4	5	4	0	0	1	4	6	8	0.00043	0.74	0.000078	0.0005	0.25	0.000091
48411	RS2, ribosomal protein 2	5	6	3	0	0	0	6	5	6	0	0	1	0.000019	0.34	0.0042	1.5E-06	0.37	0.00089
44694	putative metalloprotease; secretory pathway	0	0	0	2	2	2	0	0	0	12	9	12	0.0039	1	4.7E-10	0.0043	0.000035	6.5E-10
48084	unknown protein with protease-like domain	1	2	2	3	2	4	2	1	0	3	8	4	0.13	0.38	0.04	0.039	0.27	0.01
YP_874396.1	50S ribosomal protein L1	5	5	3	2	1	1	2	4	3	0	2	1	0.023	0.28	0.023	0.13	0.48	0.1
47152	possible dTDP-D-glucose 4,6-dehydratase	5	4	5	0	0	0	5	4	5	0	0	0	0.00002	0.55	0.00063	0.000016	1	0.00055
42494	predicted protein with possible cathepsin propeptide inhibitor domain	2	1	1	2	3	2	1	2	2	3	2	4	0.15	0.49	0.18	0.25	0.58	0.28
YP_874376.2	photosystem II chlorophyll A core antenna apoprotein CP43	4	3	3	1	2	1	2	5	3	1	3	4	0.05	0.57	0.5	0.046	0.12	0.48
5685	proteasome subunit alpha type 3	1	1	1	4	4	5	1	2	1	3	2	4	0.006	0.49	0.11	0.017	0.23	0.19
26802	Histone H2A isoform 3b, putative	3	3	3	2	2	2	3	2	5	1	3	1	0.28	0.48	0.33	0.19	0.61	0.24
20677	Short-chain dehydrogenase/reductase SDR	3	5	5	1	0	1	3	3	5	3	2	3	0.0014	0.44	0.19	0.0046	0.071	0.29
44109	Putative Annexin	4	3	3	1	0	0	8	4	4	0	0	0	0.0027	0.11	0.0052	0.000016	0.63	0.00011
46612	possible mitochondrial carrier protein	5	6	3	0	1	0	5	6	3	0	0	0	0.00016	0.55	0.00063	0.00014	0.63	0.00055
50500	NAD-dependent epimerase/dehydratase	2	3	3	0	0	0	5	6	8	0	0	0	0.002	0.023	0.015	3.1E-07	1	0.00004
54681	Endo-1,3-beta-glucosidase (glycosyl hydrolase family 16), putative	0	0	0	5	2	3	0	0	0	7	11	8	0.00061	1	1E-07	0.00069	0.0091	1.3E-07
47403	unknown protien, like Tp23205	2	1	3	2	1	2	3	2	2	4	2	3	0.39	0.48	0.36	0.27	0.19	0.47
42015	Succinate-CoA ligase, mitochondrial putative	6	3	3	2	1	2	2	2	2	1	3	1	0.064	0.13	0.15	0.49	0.54	0.6

Table A2 cont.

Protein Id, Description		Spectral Counting Abundance Scores												Fisher Exact Test P values					
		Colim			B12 lim			Fe lim			Replete			Colim vs B12 lim	Colim vs Fe lim	Colim vs replete	B12 lim vs Fe lim	B12 lim vs replete	Fe lim vs replete
		a	b	c	a	b	c	a	b	c	a	b	c						
18458	possible peptidyl-prolyl cis-trans isomerase, cyclophyllin	3	1	2	4	3	2	1	3	1	1	0	4	0.2	0.52	0.61	0.14	0.23	0.55
50006	unknown protein with possible phytochelatin synthase-like domain	0	1	2	4	2	4	1	1	1	1	5	5	0.023	0.65	0.034	0.026	0.55	0.037
45797	Gene of unknown function with EST support	1	0	1	2	2	4	1	2	0	5	5	5	0.023	0.49	0.0016	0.059	0.15	0.0054
YP_874416.1	elongation factor Ts	2	3	3	2	2	2	3	2	3	0	0	1	0.47	0.58	0.063	0.45	0.097	0.06
19089	gelosin/severin like protein	1	2	2	5	4	4	1	1	2	0	0	1	0.032	0.51	0.22	0.017	0.0041	0.31
36913	n-acetyl-gamma-glutamyl-phosphate reductase, urea cycle	1	0	1	4	3	5	0	1	0	5	6	4	0.0032	0.51	0.0016	0.00087	0.36	0.00046
42129	possible thioredoxin reductase (Selenoprotein)	0	0	0	3	6	4	2	1	0	3	3	4	0.000052	0.12	0.0019	0.0069	0.33	0.066
27125	conserved unknown protein, similar to ribosomal	3	4	4	0	2	0	4	4	5	0	0	0	0.0051	0.4	0.0031	0.0012	0.4	0.00095
26934	Phosphogluconate dehydrogenase (decarboxylating)	3	6	3	0	0	0	5	4	7	0	0	0	0.00009	0.27	0.0018	3.3E-06	1	0.00019
23850	Dihydrolipoamide acetyl transferase	0	0	0	2	2	4	0	0	0	8	11	7	0.0021	1	1E-07	0.0023	0.0032	1.3E-07
YP_874393.1	cytochrome b6	4	3	3	1	1	1	4	4	3	3	2	1	0.024	0.48	0.26	0.013	0.24	0.19
3311	cysteine synthase, O-acetylserine(thiol)lyase	1	1	1	3	3	2	1	0	1	5	6	5	0.081	0.51	0.0024	0.039	0.073	0.00089
42434	unknown protien with AAA ATPase domain	4	6	5	0	1	1	2	3	3	1	3	1	0.00039	0.11	0.06	0.029	0.14	0.4
44821	unknown protein	2	2	2	2	2	2	2	2	0	4	5	5	0.51	0.39	0.068	0.29	0.086	0.023
51092	Glutamine synthetase II	4	2	3	2	2	2	4	3	4	0	2	0	0.2	0.39	0.041	0.089	0.2	0.015
19690	unknwon protein with peptidyl-prolyl cis-trans isomerase domain	0	1	1	3	3	3	0	0	0	7	3	5	0.014	0.26	0.0016	0.00069	0.2	0.00006
25417	GDP-mannose 4,6-dehydratase	4	4	5	0	0	0	4	5	4	0	0	0	0.00004	0.55	0.0011	0.000035	1	0.00095
bd1735	Beta adaptin, large invariable subunit of AP1 and AP2 complexes, ortholog of TPS_101301	3	2	1	0	0	0	9	6	6	0	0	0	0.0095	0.0015	0.043	2.9E-08	1	7.6E-06
54940	putative ferric reductase	5	3	5	2	2	1	2	2	1	1	2	3	0.023	0.053	0.11	0.51	0.44	0.55
50440	unknown protien with TUDOR and SNase domains, like Tp20637	4	1	1	2	2	3	1	1	1	0	2	1	0.42	0.26	0.3	0.13	0.16	0.66

Table A2 cont.

Protein Id, Description		Spectral Counting Abundance Scores												Fisher Exact Test P values					
		Colim			B12 lim			Fe lim			Replete			Colim vs B12 lim	Colim vs Fe lim	Colim vs replete	B12 lim vs Fe lim	B12 lim vs replete	Fe lim vs replete
		a	b	c	a	b	c	a	b	c	a	b	c						
46599	Putative clathrin light chain, clathrin vesicle coat component	5	3	2	2	1	3	2	2	4	1	0	0	0.21	0.43	0.026	0.36	0.14	0.06
50026	possible Solute:Sodium symporter family protein	1	0	0	4	3	3	1	2	1	1	2	3	0.0023	0.18	0.094	0.055	0.18	0.44
50259	Ribosomal protein L14	4	3	4	2	2	0	3	3	2	1	0	0	0.096	0.34	0.017	0.27	0.2	0.06
9816	Copine 1, putative	3	4	3	1	0	0	4	2	3	3	0	1	0.0027	0.52	0.15	0.0049	0.15	0.2
41676	Nucleoside Diphosphate Kinase 1	1	0	0	2	3	3	0	0	0	8	9	4	0.012	0.51	0.000015	0.0023	0.017	1.8E-06
48699	RL10, ribosomal protein 10	6	4	1	0	0	0	4	5	6	0	0	0	0.0002	0.26	0.0031	7.3E-06	1	0.00032
55018	Phosphoenolpyruvate carboxykinase (ATP), mitochondrial precursor	5	4	6	0	0	0	3	2	3	0	0	0	8.8E-06	0.11	0.00037	0.0018	1	0.014
44347	unknown protein	0	0	0	0	0	0	0	0	0	12	11	13	1	1	7.9E-11	1	6.3E-12	1.1E-10
36600	possible cytochrome c oxidase subunit	0	4	2	2	2	2	3	3	1	1	2	0	0.51	0.48	0.3	0.56	0.22	0.21
25714	RL15, ribosomal protein 15 60S large ribosomal subunit	3	3	3	1	2	2	4	5	3	0	2	0	0.14	0.31	0.041	0.033	0.28	0.0097
YP_874397.1	50S ribosomal protein L11	2	4	2	2	3	3	3	1	4	0	2	0	0.54	0.58	0.063	0.56	0.045	0.06
46454	putative Mucin-associated surface protein	3	3	3	2	2	2	4	4	2	0	0	0	0.28	0.48	0.0088	0.19	0.039	0.0047
54222	putative ornithine cyclodeaminase	1	0	0	3	2	5	0	0	0	4	6	5	0.0023	0.51	0.0004	0.00038	0.25	0.000062
50047	unknown protein	3	1	1	2	2	3	1	1	2	3	2	1	0.24	0.51	0.54	0.16	0.36	0.44
bd611	possible proteosome beta subunit	2	2	3	2	3	4	1	2	2	1	0	1	0.36	0.4	0.21	0.19	0.086	0.39
48735	multicopy predicted protein	2	2	2	2	2	2	1	1	2	5	3	3	0.51	0.39	0.17	0.29	0.21	0.07
21135	possible ATP-dependant protease	2	2	2	3	2	2	2	3	2	1	0	0	0.42	0.48	0.15	0.55	0.067	0.092
51291	RS20, ribosomal protein 20 40S small ribosomal subunit	4	4	1	1	2	0	4	2	5	0	0	1	0.042	0.39	0.041	0.013	0.53	0.015
21592	putative Diaminopimelate decarboxylase (DAP decarboxylase)	2	2	2	1	2	1	3	6	5	0	0	0	0.28	0.052	0.043	0.0055	0.16	0.00055
29016	2-oxoglutarate dehydrogenase (succinyl-transferring) E1 componen	5	6	4	0	1	0	3	1	4	0	0	0	0.00008	0.11	0.00037	0.0098	0.63	0.014
13076	possible nitrite transporter NAR1	3	2	2	4	3	2	1	1	1	1	2	1	0.36	0.18	0.36	0.059	0.17	0.49
47006	unknown protein	1	1	1	2	2	2	1	1	1	4	3	5	0.12	0.65	0.018	0.13	0.19	0.02

Table A2 cont.

Protein Id, Description		Spectral Counting Abundance Scores												Fisher Exact Test P values					
		Colim			B12 lim			Fe lim			Replete			Colim vs B12 lim	Colim vs Fe lim	Colim vs replete	B12 lim vs Fe lim	B12 lim vs replete	Fe lim vs replete
		a	b	c	a	b	c	a	b	c	a	b	c						
	T.pseudonana TPS_98354																		
44724	unknown protein	1	2	0	4	2	2	1	2	1	1	3	4	0.081	0.49	0.11	0.16	0.58	0.19
9462	unknown protein with Tetratricopeptide repeat domain	0	2	1	3	1	2	1	2	3	4	2	1	0.17	0.24	0.19	0.53	0.56	0.51
46917	unknown protein	5	2	2	2	2	2	3	2	2	0	0	1	0.28	0.42	0.041	0.47	0.14	0.092
bd420	glutathione S-transferase like protein	2	2	4	1	2	2	4	3	3	0	0	0	0.28	0.39	0.015	0.13	0.062	0.0047
36139	fumarate hydratase	0	1	0	4	5	4	2	1	0	1	2	4	0.00043	0.3	0.045	0.0069	0.15	0.2
23247	Fructose-1,6-bisphosphatase, cytosolic	0	1	0	4	3	2	0	1	0	3	5	4	0.004	0.74	0.0045	0.0045	0.48	0.0049
45997	pyruvate kinase 4a, cytosolic	0	1	0	3	5	5	0	2	0	1	2	3	0.00043	0.49	0.094	0.0022	0.084	0.2
35158	heat shock protein Hsp20	3	5	0	1	0	1	3	2	3	0	0	0	0.032	0.58	0.015	0.029	0.4	0.014
25893	Fucoxanthin chlorophyll a/c protein, Lhcf14	3	2	3	0	1	0	5	5	5	0	0	0	0.011	0.095	0.015	0.000067	0.63	0.00032
49764	possible mitochondrial carrier protein	2	3	4	0	0	0	5	3	4	0	0	0	0.00093	0.31	0.0088	0.000078	1	0.0016
42307	translation initiation factor eIF-2, gamma subunit	1	2	2	2	2	2	2	1	1	3	2	1	0.61	0.51	0.54	0.49	0.54	0.44
8670	possible M3 dipeptidyl carboxypeptidase	2	2	1	2	1	2	1	3	1	4	2	1	0.52	0.61	0.39	0.51	0.3	0.4
41721	Nuclear-encoded homolog of chloroplast groEL	0	2	2	2	2	3	2	2	2	4	0	1	0.21	0.36	0.43	0.44	0.44	0.6
24119	Fucoxanthin chlorophyll a/c protein, deviant	0	2	2	2	2	2	3	1	3	3	0	4	0.37	0.26	0.29	0.47	0.48	0.6
26290	aconitase hydratase	2	2	3	0	2	0	3	0	2	1	3	3	0.057	0.4	0.59	0.16	0.071	0.4
43840	similar to 60S ribosomal protein L30	2	5	3	3	1	1	4	2	2	0	0	0	0.14	0.43	0.0052	0.27	0.062	0.014
17414	RS8, ribosomal protein 8	3	3	3	1	0	0	4	3	4	0	2	0	0.0054	0.39	0.041	0.0012	0.6	0.015
14827	putative Rab GTPase:GTP Dissociation Inhibitor	3	5	8	1	0	0	1	1	4	1	0	0	0.000039	0.03	0.0017	0.038	0.6	0.14
48085	unknown protein	1	0	0	3	3	5	0	0	0	4	3	4	0.0013	0.51	0.0045	0.0002	0.57	0.00087
49881	unknown protien with Kelch domain	0	0	0	6	6	5	0	0	0	1	0	1	4.4E-06	1	0.17	5.4E-06	0.0035	0.17
51933	unknown protein with PAS domain and heme binding pocket	3	1	1	2	3	2	1	1	1	3	2	1	0.24	0.38	0.54	0.087	0.36	0.32

Table A2 cont.

Protein Id, Description		Spectral Counting Abundance Scores												Fisher Exact Test P values					
		Colim			B12 lim			Fe lim			Replete			Colim vs B12 lim	Colim vs Fe lim	Colim vs replete	B12 lim vs Fe lim	B12 lim vs replete	Fe lim vs replete
		a	b	c	a	b	c	a	b	c	a	b	c						
45653	unknown protein	2	2	2	2	2	2	2	3	1	1	2	1	0.6	0.6	0.46	0.59	0.46	0.45
48795	unknown protein	2	2	1	2	2	2	2	3	0	3	2	1	0.5	0.61	0.54	0.51	0.61	0.55
YP_874369.1	cytochrome b559 alpha chain	2	1	1	2	2	2	1	1	0	4	2	1	0.48	0.35	0.29	0.21	0.39	0.11
23794	putative Calmoduline	1	1	0	3	2	2	1	1	0	0	3	3	0.057	0.68	0.19	0.061	0.44	0.2
29658	possible Cytochrome b5 reductase	1	3	3	2	2	2	1	1	1	0	0	0	0.58	0.18	0.025	0.18	0.024	0.2
25433	cysteine protease	1	4	2	3	3	2	1	1	1	0	0	0	0.44	0.18	0.025	0.087	0.0096	0.2
YP_874480.1	30S ribosomal protein S7	5	2	5	0	0	1	4	2	3	0	0	1	0.00067	0.35	0.011	0.0049	0.6	0.038
48901	unknown protein	0	1	1	3	2	0	0	1	0	5	5	5	0.14	0.51	0.0016	0.06	0.033	0.00046
39627	SAM-binding methyltranferase	1	0	1	4	6	4	0	0	0	3	2	1	0.0012	0.26	0.19	0.000033	0.064	0.03
46347	unknown protein, CreA-like domain	0	0	0	2	3	3	0	0	0	4	6	7	0.0021	1	0.00002	0.0023	0.073	0.00003
5311	26S proteasome beta type 7 subunit	0	0	0	5	5	5	0	0	0	1	0	0	0.00002	1	0.41	0.000018	0.0018	0.41
25932	short chain acyl-coenzyme A dehydrogenase	2	4	1	2	2	2	2	1	2	1	2	1	0.38	0.4	0.36	0.62	0.56	0.56
6062	chl a/c binding protein	3	2	2	1	1	1	2	3	3	3	2	1	0.11	0.48	0.51	0.065	0.24	0.4
17846	60S subunit ribosomal protein L27	2	3	3	1	1	1	3	2	3	1	2	1	0.07	0.58	0.28	0.065	0.4	0.26
42487	unknown protien like Tp 3481	2	2	2	2	2	2	2	2	0	1	3	3	0.5	0.39	0.49	0.49	0.39	0.3
YP_874425.1	ATP synthase CF1 delta chain	3	2	2	2	1	2	3	2	2	1	0	3	0.28	0.59	0.36	0.27	0.62	0.35
11174	putative X-prolyl aminopeptidase	2	3	2	2	1	1	3	1	4	1	2	0	0.19	0.48	0.21	0.12	0.6	0.14
10208	phosphoribulokinase	1	0	1	4	2	2	3	1	1	3	2	3	0.036	0.22	0.11	0.25	0.49	0.4
30648	Fucoxanthin chl a/c protein, Lhcf5	2	1	1	3	3	2	1	1	1	0	2	1	0.11	0.51	0.53	0.059	0.086	0.66
42442	unknown protein with EF loop	1	3	1	1	2	1	5	0	0	1	0	1	0.4	0.61	0.4	0.39	0.6	0.39
19901	APS kinase/ATP sulfurlyase/pyrophosphatase fusion	1	2	2	1	2	1	0	0	2	4	0	1	0.4	0.24	0.54	0.43	0.34	0.2
20143	putative long chain acyl-CoA synthetase/ligase	1	1	0	0	1	0	1	2	2	5	5	4	0.44	0.22	0.0034	0.072	0.00036	0.044
28234	Ribosomal protein L2	3	3	2	2	1	0	3	4	2	0	2	0	0.07	0.48	0.063	0.038	0.53	0.038

Table A2 cont.

Protein Id, Description		Spectral Counting Abundance Scores												Fisher Exact Test P values					
		Colim			B12 lim			Fe lim			Replete			Colim vs B12 lim	Colim vs Fe lim	Colim vs replete	B12 lim vs Fe lim	B12 lim vs replete	Fe lim vs replete
		a	b	c	a	b	c	a	b	c	a	b	c						
17332	stomatin-like protein	3	2	1	2	1	1	2	1	3	0	0	0	0.28	0.6	0.043	0.27	0.16	0.04
49189	unknown protein, similar to glutathione S-transferase	3	6	3	1	0	1	2	2	3	0	0	0	0.0027	0.19	0.0018	0.053	0.4	0.024
54535	Putative methylmalonate semialdhyde dehydrogenase	0	1	0	2	2	1	1	0	0	5	5	5	0.093	0.74	0.0004	0.098	0.019	0.00046
30466	possible NAD-dependent epimerase/dehydratase	0	0	1	2	4	1	0	0	0	4	3	5	0.02	0.51	0.002	0.0043	0.19	0.00036
49957	unknown protein	3	2	3	0	0	0	3	3	2	0	0	0	0.002	0.58	0.015	0.0018	1	0.014
55215	Heat shock protein Hsp90	3	4	3	0	0	0	3	3	3	0	0	0	0.00043	0.52	0.0052	0.00083	1	0.0081
42574	possible carbonic anhydrase	0	0	0	2	2	2	0	0	0	5	6	7	0.0072	1	0.000009	0.0078	0.018	0.000011
47648	unknown protein	1	1	1	2	2	2	1	1	1	4	2	4	0.17	0.65	0.062	0.18	0.3	0.066
42786	unknown protein	1	2	1	1	1	2	1	1	1	4	5	4	0.55	0.51	0.037	0.6	0.019	0.02
44643	unknown protein	1	1	1	2	2	1	0	1	1	4	3	4	0.45	0.51	0.034	0.31	0.065	0.016
4413	conserved unknown, like Tp21282	1	1	1	2	2	2	0	1	1	1	5	4	0.24	0.51	0.062	0.14	0.23	0.031
4936	possible cathepsin Z-like proteinase	0	2	2	3	2	3	2	1	1	1	0	0	0.11	0.62	0.32	0.11	0.031	0.31
30967	possible Ketol-acid reductoisomerase	4	3	4	0	0	1	3	3	1	0	0	3	0.0014	0.26	0.051	0.019	0.31	0.21
21929	possible coatomer protein subunit alpha	3	1	2	0	0	0	5	3	3	0	0	0	0.0095	0.15	0.043	0.00017	1	0.0028
9538	possible ferredoxin-sulfite reductase	0	1	0	0	1	0	1	0	2	5	9	4	0.71	0.3	0.000078	0.25	0.000023	0.0014
YP_874409.1	30S ribosomal protein S18	4	3	4	0	0	0	4	3	3	0	0	0	0.0002	0.52	0.0031	0.00038	1	0.0047
21323	RS24, ribosomal protein 24 40S small ribosomal subunit	4	3	3	0	0	0	4	3	4	0	0	0	0.00043	0.48	0.0052	0.00017	1	0.0028
38085	possible ThiC thiamin biosynthesis protein	0	0	0	6	6	5	0	0	0	0	0	1	4.4E-06	1	0.41	5.4E-06	0.00078	0.41
45053	unknown protein	1	2	2	2	1	2	1	1	1	3	3	4	0.52	0.38	0.17	0.47	0.11	0.066
8686	Ribosomal protein S12	2	1	1	2	2	2	2	1	1	3	2	1	0.37	0.62	0.43	0.38	0.61	0.44
9697	unknown protein	1	1	1	2	2	1	1	1	1	4	2	4	0.34	0.65	0.062	0.35	0.17	0.066
46281	unknown protein	3	1	2	2	2	0	3	2	2	1	2	1	0.28	0.48	0.46	0.18	0.52	0.35

Table A2 cont.

Protein Id, Description		Spectral Counting Abundance Scores												Fisher Exact Test P values					
		Colim			B12 lim			Fe lim			Replete			Colim vs B12 lim	Colim vs Fe lim	Colim vs replete	B12 lim vs Fe lim	B12 lim vs replete	Fe lim vs replete
		a	b	c	a	b	c	a	b	c	a	b	c						
52304	unknown multicopy protein with tryptophan rich domain	1	2	1	2	2	2	0	1	1	1	3	1	0.21	0.35	0.43	0.061	0.44	0.2
bd866	probable 20S proteasome beta type subunit	1	0	1	3	2	2	1	0	1	1	3	3	0.057	0.68	0.11	0.061	0.58	0.11
13174	L-ascorbate peroxidase, putative	1	0	1	2	4	2	1	1	1	1	2	1	0.036	0.49	0.33	0.087	0.23	0.49
46364	uncharacterized conserved protein	2	2	2	2	2	2	3	1	2	0	0	1	0.6	0.6	0.15	0.59	0.14	0.14
14442	protein fucoxanthin chlorophyll a/c protein	0	0	1	2	2	2	1	2	1	3	3	5	0.093	0.18	0.0045	0.49	0.1	0.07
44618	putative 2-isopropylmalate synthase	3	3	3	1	0	1	1	4	2	0	0	0	0.018	0.42	0.0088	0.053	0.4	0.024
47192	unknown protein	1	4	0	0	0	0	0	0	1	1	2	0	0.021	0.11	0.4	0.45	0.14	0.37
44420	unknown, possible helicase	1	0	0	2	3	2	0	0	0	3	5	1	0.012	0.51	0.021	0.0023	0.58	0.0051
49218	unknown protein	0	0	0	2	2	1	0	0	0	7	3	8	0.025	1	0.000009	0.026	0.0056	0.000011
18559	similar to RS6, ribosomal protein 6	2	4	2	0	0	0	3	2	5	0	0	0	0.002	0.39	0.015	0.00038	1	0.0047
37671	unknown protein with NADPH-dependent FMN reductase domain	2	5	2	0	0	0	4	3	3	0	0	0	0.00093	0.48	0.0088	0.00038	1	0.0047
41601	unknown protien with RNA/RNA binding domain	2	1	0	2	2	2	1	1	1	3	3	3	0.34	0.65	0.11	0.35	0.26	0.12
19093	epsilon coatomer, subunit of the Coat Protein complex COP I	3	1	1	0	2	1	2	1	1	3	2	3	0.28	0.51	0.39	0.4	0.13	0.3
23257	Fucoxanthin chl a/c protein, Lhcr11	1	0	2	2	2	2	1	3	1	1	2	3	0.34	0.35	0.31	0.62	0.54	0.55
17487	3--hydroxybutyrate dehydrogenase	1	1	2	1	2	2	0	1	0	1	2	3	0.37	0.19	0.43	0.06	0.61	0.099
13895	possible photosystem II stability factor	4	2	3	1	1	2	2	1	1	0	2	0	0.081	0.14	0.041	0.53	0.39	0.31
46131	unknown protein with protease-like domain	1	2	1	0	0	2	1	2	2	3	2	4	0.41	0.49	0.18	0.27	0.071	0.28
44050	possible V-type proton ATPase subunit G 2	1	2	2	2	1	1	4	4	2	0	0	0	0.4	0.14	0.072	0.046	0.16	0.0047
16018	LepA-like GTPase	1	1	3	0	0	0	1	1	1	1	3	0	0.021	0.38	0.57	0.094	0.051	0.49
43716	unknown protein	1	1	0	2	2	2	0	0	0	4	2	4	0.14	0.26	0.029	0.014	0.23	0.0021
44510	unknown protein with oxidoreductase domain	4	2	3	1	0	1	3	3	1	0	0	0	0.018	0.42	0.0088	0.053	0.4	0.024
48533	unknown protein	1	0	1	2	4	2	1	2	0	0	0	1	0.023	0.49	0.63	0.059	0.031	0.45

Table A2 cont.

Protein Id, Description		Spectral Counting Abundance Scores												Fisher Exact Test P values					
		Colim			B12 lim			Fe lim			Replete			Colim vs B12 lim	Colim vs Fe lim	Colim vs replete	B12 lim vs Fe lim	B12 lim vs replete	Fe lim vs replete
		a	b	c	a	b	c	a	b	c	a	b	c						
26029	Membrane associated nitrate transporter	2	3	2	0	1	0	4	2	3	0	0	0	0.021	0.38	0.025	0.0049	0.63	0.0081
23748	similar to 40S ribosomal protein	4	2	2	0	1	0	3	3	3	0	0	0	0.011	0.48	0.015	0.0049	0.63	0.0081
15089	thioredoxin h	0	0	0	2	2	0	1	0	1	5	5	4	0.046	0.24	0.00013	0.31	0.019	0.0038
54190	annexin	1	2	4	1	0	0	4	3	4	0	0	0	0.021	0.23	0.025	0.0012	0.63	0.0028
39827	multicopy unknown protein	0	0	0	2	2	1	0	0	0	5	6	4	0.025	1	0.000054	0.026	0.019	0.000062
23552	Nicotinamide nucleotide transhydrogenase	3	2	3	0	0	0	2	3	5	0	0	0	0.002	0.39	0.015	0.00038	1	0.0047
19314	40S ribosomal protein 17	2	2	4	0	0	0	3	4	2	0	0	0	0.002	0.48	0.015	0.00083	1	0.0081
12762	arginine biosynthesis bifunctional protein argJ	1	2	1	0	2	0	3	2	1	1	2	1	0.27	0.36	0.6	0.093	0.27	0.45
46513	unknown protein	1	1	0	2	1	1	1	1	0	3	3	5	0.42	0.68	0.014	0.43	0.037	0.016
19805	conserved unknown protein	2	2	2	0	1	0	2	1	2	0	0	3	0.04	0.52	0.3	0.072	0.31	0.39
17344	Xanthine/uracil permease	3	3	1	1	1	1	3	1	2	0	0	0	0.11	0.52	0.025	0.17	0.25	0.04
38891	histidinol-phosphate aminotransferase, PLP dependant	1	1	0	3	2	2	0	0	2	1	2	3	0.057	0.68	0.19	0.061	0.44	0.2
YP_874468.1	50S ribosomal protein L6	2	2	1	2	1	1	3	4	2	0	0	0	0.4	0.2	0.072	0.075	0.16	0.0081
22896	anion-transporting ATPase	3	3	2	2	0	0	3	1	2	0	0	0	0.032	0.41	0.015	0.093	0.4	0.04
8950	possible cbbx rubisco expression protein, AAA-type protein	3	2	1	1	1	0	3	2	4	0	0	0	0.098	0.29	0.043	0.016	0.4	0.0081
47306	protein disulfide isomerase-like	1	1	0	2	1	2	0	0	0	3	6	4	0.14	0.26	0.0071	0.014	0.094	0.00036
5512	alanine racemase family protein	0	0	0	2	2	2	0	0	0	3	3	5	0.013	1	0.00078	0.014	0.15	0.00087
27518	beta prime (beta', beta2) coatomer, subunit of the Coat Protein complex	2	2	2	0	0	0	5	2	4	0	0	0	0.0095	0.15	0.043	0.00017	1	0.0028
15619	RL13e, ribosomal protein 13e 60S	4	4	3	0	0	0	3	1	1	0	0	0	0.0002	0.11	0.0031	0.019	1	0.069
YP_874361.1	photosystem I protein F	0	0	0	0	2	3	0	0	0	7	5	4	0.025	1	0.00005	0.026	0.019	0.00006
49172	unknown protein with Putative zinc binding domain	1	1	1	2	2	0	1	1	1	3	3	1	0.59	0.65	0.19	0.6	0.21	0.2
48921	unknown protein	2	2	1	1	2	2	2	2	2	0	0	1	0.52	0.48	0.22	0.38	0.28	0.14

Table A2 cont.

Protein Id, Description		Spectral Counting Abundance Scores												Fisher Exact Test P values					
		Colim			B12 lim			Fe lim			Replete			Colim vs B12 lim	Colim vs Fe lim	Colim vs replete	B12 lim vs Fe lim	B12 lim vs replete	Fe lim vs replete
		a	b	c	a	b	c	a	b	c	a	b	c						
45623	conserved hypothetical protein	1	2	2	2	2	1	2	1	2	0	0	1	0.52	0.61	0.22	0.51	0.28	0.21
43058	Calcyclin-Binding protein, putative	2	3	3	1	1	1	1	2	2	0	0	1	0.07	0.3	0.063	0.27	0.53	0.21
48094	conserved unknown protein	1	2	2	1	1	1	3	3	0	1	0	0	0.28	0.48	0.22	0.17	0.53	0.14
48879	conserved unknown, like Tp269759	3	2	2	2	0	1	0	1	2	1	0	1	0.11	0.18	0.21	0.57	0.61	0.66
45921	predicted protein with thioredoxin domain	1	2	2	1	1	2	0	0	1	0	0	0	0.52	0.11	0.072	0.16	0.098	0.59
49523	predicted protein with Fe(II) oxygenase domain	3	1	1	1	0	2	4	2	1	0	0	1	0.28	0.37	0.22	0.11	0.53	0.092
49056	Threonine synthase, PLP-dependant	4	2	2	0	0	0	2	2	2	1	2	0	0.002	0.41	0.15	0.0088	0.14	0.29
50245	predicted protein with possible ATP-dependent protease La (LON) domain	2	2	2	1	1	2	1	1	2	0	0	0	0.39	0.39	0.043	0.61	0.098	0.12
48946	2-hydroxyacid dehydrogenase, putative	2	2	2	0	1	0	2	3	3	0	0	0	0.04	0.38	0.043	0.0098	0.63	0.014
YP_874453.1	50S ribosomal protein L3	2	1	3	0	0	1	2	2	5	0	0	0	0.04	0.29	0.043	0.0049	0.63	0.0081
22095	Rab-type small GTPase, ortholog of T. pseudonana TPS_125766	2	3	3	0	0	0	3	3	2	0	0	0	0.002	0.58	0.015	0.0018	1	0.014
10824	sterol 24-C-methyltransferase (AdoMet-dependant)	2	3	2	0	0	0	3	4	3	0	0	0	0.0044	0.3	0.025	0.00038	1	0.0047
29177	RL17, ribosomal protein 17-like	3	2	3	0	0	0	3	2	4	0	0	0	0.002	0.48	0.015	0.00083	1	0.0081
27851	unknown protein	2	3	3	0	0	0	3	3	3	0	0	0	0.002	0.48	0.015	0.00083	1	0.0081
44297	unknwon protein	0	0	0	3	3	4	0	0	0	0	2	0	0.00033	1	0.41	0.00038	0.014	0.41
11006	fucoxanthin chl a/c light-harvesting protein, lhcr typ	0	0	1	0	0	1	0	0	0	7	8	5	0.71	0.51	0.000034	0.55	9.2E-06	4.4E-06
3639	Myo-inositol 2-dehydrogenase putative	2	2	1	1	1	2	1	1	2	1	2	1	0.4	0.51	0.57	0.53	0.52	0.61
43429	Chorismate synthase	1	1	1	2	2	1	0	1	1	3	2	3	0.45	0.51	0.19	0.31	0.3	0.11
44873	possible glycoside hydrolase	1	1	1	2	1	2	1	1	1	3	2	1	0.34	0.65	0.31	0.35	0.54	0.32
19244	phosphoserine phosphatase	1	2	1	2	2	0	1	0	1	3	2	3	0.55	0.35	0.29	0.43	0.21	0.11

Table A2 cont.

Protein Id, Description		Spectral Counting Abundance Scores												Fisher Exact Test P values					
		Colim			B12 lim			Fe lim			Replete			Colim vs B12 lim	Colim vs Fe lim	Colim vs replete	B12 lim vs Fe lim	B12 lim vs replete	Fe lim vs replete
		a	b	c	a	b	c	a	b	c	a	b	c						
12713	Peroxiredoxin family protein, like cyanobacteria bacterioferratin comigratory protein	2	1	2	0	1	1	0	1	2	1	2	1	0.17	0.38	0.57	0.42	0.27	0.49
17895	possible aldose-1-epimerase	2	2	2	2	1	0	1	2	1	1	0	1	0.18	0.39	0.3	0.4	0.61	0.51
23059	Aspartate transaminase	2	1	0	1	0	1	1	1	2	1	2	4	0.43	0.49	0.19	0.26	0.071	0.3
49160	unknown protein with Armadillo/beta-catenin-like repeats	1	2	2	1	1	1	3	2	2	0	0	0	0.28	0.37	0.072	0.11	0.25	0.024
26382	epimerase/dehydrogenase	0	0	1	2	2	2	0	0	1	1	2	1	0.093	0.74	0.19	0.098	0.56	0.2
18899	possible Metallophosphoesterase	0	1	1	2	2	0	1	1	1	0	3	7	0.42	0.49	0.029	0.6	0.068	0.066
54969	putative Aliphatic amidase (Acylamide amidohydrolase)	2	1	2	1	3	0	1	2	1	0	2	0	0.52	0.51	0.22	0.61	0.28	0.31
47178	uknown protein with CbS domain	2	0	1	2	1	2	1	0	0	3	0	1	0.24	0.32	0.47	0.06	0.46	0.2
8269	unknown protien with RNA binding domain	3	4	2	1	0	0	2	0	2	1	2	0	0.0054	0.14	0.11	0.14	0.31	0.51
18585	RL28, ribosomal protein 28-like protein	2	3	3	0	1	0	2	1	3	0	2	0	0.011	0.41	0.063	0.038	0.6	0.14
11151	dihydrodipicolinate synthase, lysine biosynthesis	0	1	0	2	2	2	0	0	0	4	5	3	0.056	0.51	0.0045	0.014	0.15	0.00087
bd521	Glycine decarboxylase T-protein	2	3	2	0	2	0	2	2	0	0	0	0	0.057	0.29	0.025	0.26	0.4	0.12
45701	aminotransferase with PLP binding domain	0	0	1	4	2	2	0	0	0	3	2	1	0.0069	0.51	0.094	0.0013	0.29	0.03
YP_874415.1	30S ribosomal protein S2	3	1	1	0	1	0	1	4	2	0	0	0	0.076	0.37	0.072	0.019	0.63	0.024
19661	PspA-like protein	0	0	0	2	1	2	0	0	0	5	5	5	0.046	1	0.000054	0.048	0.01	0.000062
42545	predicted protien with possible Mg transporter domain	1	1	1	1	1	2	1	1	1	3	2	1	0.59	0.65	0.31	0.6	0.34	0.32
9171	unknown protein with thioredoxin domain	1	2	1	1	1	2	1	1	1	1	2	3	0.55	0.51	0.43	0.6	0.34	0.32
13424	DnaJ-like protein	1	1	1	1	0	2	1	1	1	1	2	1	0.58	0.65	0.47	0.57	0.4	0.49
47573	unknown multicopy protein	0	1	1	1	1	1	1	1	1	3	5	3	0.57	0.49	0.029	0.57	0.036	0.066
17326	light harvesting like, red elip protein	2	1	0	1	0	1	2	1	1	1	2	1	0.43	0.49	0.47	0.26	0.27	0.61

Table A2 cont.

Protein Id, Description		Spectral Counting Abundance Scores												Fisher Exact Test P values					
		Colim			B12 lim			Fe lim			Replete			Colim vs B12 lim	Colim vs Fe lim	Colim vs replete	B12 lim vs Fe lim	B12 lim vs replete	Fe lim vs replete
		a	b	c	a	b	c	a	b	c	a	b	c						
51511	Rab-family small GTPase, ortholog of T. pseudonana TPS_7642	0	2	1	1	1	2	1	1	0	3	2	1	0.59	0.51	0.31	0.43	0.34	0.2
44054	conserved unknown like Tp 24220	0	0	1	2	2	2	1	1	1	1	2	1	0.034	0.3	0.19	0.18	0.37	0.49
14995	ftsZ-like protein	2	2	2	0	1	0	2	1	1	1	0	0	0.04	0.39	0.15	0.14	0.6	0.31
25379	pyrroline-5-carboxylate reductase	2	2	1	0	1	0	2	2	2	0	0	1	0.076	0.48	0.22	0.038	0.6	0.14
bd998	Rab-type small GTPase, ortholog of T. pseudonana TPS_105101	3	2	0	2	3	2	2	0	0	4	3	3	0.31	0.24	0.17	0.061	0.38	0.031
23083	Possible TufA-like protein	1	2	1	0	1	0	2	2	2	0	0	1	0.14	0.36	0.32	0.038	0.6	0.14
18036	possible DnaJ-like, like Tp 268157	1	0	0	2	2	2	0	0	0	3	2	3	0.093	0.51	0.045	0.026	0.39	0.012
30262	RL19, ribosomal protein 19 60S large ribosomal subunit	1	3	2	1	0	1	2	2	2	0	0	0	0.098	0.6	0.043	0.093	0.4	0.04
14898	Peroxiredoxin-like protein	0	1	0	1	2	2	0	1	0	3	0	3	0.093	0.74	0.094	0.098	0.54	0.099
44804	predicted protein with SNARE domain	1	0	1	2	1	2	0	1	1	0	0	0	0.3	0.68	0.35	0.31	0.098	0.34
43657	unknown protein with 60Kd inner membrane protein-like domain	0	1	1	0	2	3	0	0	0	3	3	3	0.2	0.26	0.056	0.026	0.26	0.0051
21659	RL32, ribosomal protein 32 60S large ribosomal subunit	2	2	1	2	0	1	2	2	2	0	0	0	0.28	0.48	0.072	0.17	0.25	0.04
20007	proteasome subunit beta type 5 precursor-like	0	0	2	2	3	2	0	0	0	1	2	1	0.057	0.26	0.33	0.0043	0.29	0.071
32326	possible phosphoribosylpyrophosphate synthetase	4	2	3	1	0	0	2	1	1	0	0	0	0.0054	0.14	0.0088	0.14	0.63	0.12
29885	possible pyridoxal biosynthesis lyase pdxS	0	0	1	2	2	2	0	0	0	0	2	0	0.02	0.51	0.65	0.0043	0.067	0.41
48573	unknown protien with DNA binding domain	2	2	4	0	0	0	1	2	1	0	0	0	0.002	0.2	0.015	0.043	1	0.12
48827	unknown multicopy protein	0	0	0	2	2	2	0	0	0	3	3	4	0.013	1	0.0019	0.014	0.23	0.0021
11189	plastid translation elongation factor EF-G-like protein	2	3	3	0	0	0	1	2	3	0	0	0	0.002	0.41	0.015	0.0088	1	0.04
12902	ferredoxin nitrite reductase	0	0	0	4	2	2	0	0	0	3	2	1	0.0021	1	0.028	0.0023	0.36	0.03
bd1725	GrpE protein, HSP90 cofactor, chloroplast targeted	1	1	0	2	1	1	0	1	2	1	2	1	0.42	0.49	0.33	0.6	0.52	0.49
23429	probable purine synthesis protein	1	1	1	1	2	2	1	0	1	0	3	1	0.34	0.51	0.47	0.21	0.56	0.34

Table A2 cont.

Protein Id, Description		Spectral Counting Abundance Scores												Fisher Exact Test P values					
		Colim			B12 lim			Fe lim			Replete			Colim vs B12 lim	Colim vs Fe lim	Colim vs replete	B12 lim vs Fe lim	B12 lim vs replete	Fe lim vs replete
		a	b	c	a	b	c	a	b	c	a	b	c						
20183	Pyruvate dehydrogenase E1 beta subunit, mitochondrial precursor	1	2	2	1	1	2	1	2	2	0	0	0	0.4	0.61	0.072	0.39	0.16	0.069
43746	unknown protein, like Tp 5308	1	2	1	1	1	1	2	1	2	0	0	0	0.41	0.49	0.12	0.27	0.25	0.069
40017	putative tyrosinase	0	1	1	2	2	2	0	1	1	1	2	0	0.2	0.68	0.54	0.21	0.38	0.55
34526	argininosuccinate lyase	3	0	1	1	1	1	2	1	1	0	0	0	0.41	0.62	0.12	0.4	0.25	0.12
49215	unknown protein with possible calcium channel-like domain	1	1	0	1	2	2	0	0	0	3	3	3	0.3	0.26	0.056	0.048	0.19	0.0051
YP_874451.1	60 kDa chaperonin	1	2	2	1	1	1	1	3	0	0	0	0	0.28	0.51	0.072	0.4	0.25	0.12
48680	conserved unknown, like Tpbd1658, with metallophosphoprotease domain	2	4	2	0	1	0	0	2	1	0	2	0	0.011	0.12	0.063	0.25	0.6	0.45
28882	Phosphomannose mutase	2	2	3	0	1	2	1	1	0	0	0	0	0.11	0.095	0.025	0.58	0.25	0.34
41790	heat shock protein HslVU, ATPase	2	3	2	0	0	1	2	2	1	0	0	0	0.021	0.4	0.025	0.072	0.63	0.069
bd1648	Trigger factor-like protein	2	2	1	1	0	0	2	2	2	0	0	0	0.076	0.48	0.072	0.038	0.63	0.04
10438	Phytoene desaturase-like	1	2	1	0	0	0	2	3	1	1	0	0	0.045	0.36	0.32	0.0088	0.37	0.14
47887	conserved hypothetical protein	1	0	1	3	1	2	1	0	0	0	0	1	0.089	0.51	0.63	0.036	0.097	0.66
47843	Mitochondrial Carrier (MC) Family protein	4	3	2	0	0	0	0	1	1	0	2	0	0.00093	0.035	0.041	0.21	0.37	0.63
19413	ribosomal protein	2	2	2	0	0	0	2	2	2	0	0	0	0.0095	0.6	0.043	0.0088	1	0.04
25752	membrane spanning protein of the nonaspanin family	3	1	1	0	0	0	2	3	3	0	0	0	0.021	0.28	0.072	0.0018	1	0.014
42788	unknown protein with spermidine synthase domain	2	3	2	0	0	0	3	0	2	0	0	0	0.0044	0.4	0.025	0.019	1	0.069
46735	RL21, ribosomal protein 21, 60S large ribosomal subunit	2	1	1	0	0	0	5	3	1	0	0	0	0.045	0.12	0.12	0.00083	1	0.0081
20787	possible mitochondrial-processing peptidase subunit beta	1	1	2	1	0	1	1	2	1	1	2	1	0.27	0.62	0.6	0.26	0.27	0.61
49306	unknown protein	1	1	0	1	1	2	0	1	0	3	3	3	0.42	0.51	0.056	0.25	0.12	0.023
50499	conserved unknown protein	1	2	1	0	0	0	2	2	2	1	2	0	0.045	0.36	0.53	0.0088	0.14	0.29
39529	unknown protein with ATP synthase epsilon chain domain	1	0	2	1	1	1	2	2	2	1	0	0	0.58	0.24	0.46	0.17	0.53	0.14
30436	coatomer protein subunit delta	1	2	1	1	0	0	0	0	1	1	2	0	0.14	0.19	0.53	0.7	0.31	0.37

Table A2 cont.

Protein Id, Description		Spectral Counting Abundance Scores												Fisher Exact Test P values					
		Colim			B12 lim			Fe lim			Replete			Colim vs B12 lim	Colim vs Fe lim	Colim vs replete	B12 lim vs Fe lim	B12 lim vs replete	Fe lim vs replete
		a	b	c	a	b	c	a	b	c	a	b	c						
15472	possible mannosyltransferase	0	0	0	2	2	2	0	1	1	3	3	1	0.025	0.24	0.011	0.21	0.39	0.11
8230	Chaperonin Cpn10	1	0	0	2	2	2	0	0	1	0	2	1	0.056	0.74	0.37	0.06	0.29	0.37
35304	conserved unknown with gamma CA domain	1	1	0	2	2	2	1	0	2	0	0	0	0.14	0.49	0.35	0.26	0.039	0.2
54754	Ubiquitin-Activating enzyme E1	1	1	1	0	0	1	2	3	1	0	0	0	0.26	0.24	0.21	0.038	0.63	0.04
47918	possible Mitochondrial glycoprotein	2	2	2	0	1	0	2	2	2	0	0	0	0.04	0.6	0.043	0.038	0.63	0.04
54151	putative long chain acyl-CoA synthetase	0	2	2	0	1	0	0	1	1	3	2	4	0.14	0.35	0.18	0.43	0.012	0.059
11032	RL26, ribosomal protein 26 60S large ribosomal subunit	1	1	1	1	0	0	1	3	2	0	0	0	0.26	0.24	0.21	0.038	0.63	0.04
42774	unknown protein with SET domain, like Tp 21263	0	0	0	2	2	2	1	0	0	3	2	1	0.0072	0.49	0.028	0.036	0.52	0.099
46710	unknown protein	1	2	2	0	0	0	3	1	2	0	2	0	0.021	0.48	0.22	0.0088	0.37	0.14
15211	cold-shock DNA-binding domain-containing protein	2	1	1	2	2	2	0	0	0	1	0	0	0.28	0.065	0.32	0.0078	0.097	0.41
19949	mercuric reductase-like protein	0	0	0	2	0	1	0	0	0	3	3	4	0.16	1	0.0019	0.16	0.036	0.0021
30810	LMBR1-like conserved region-containing protein	3	0	3	0	1	0	0	2	1	1	0	0	0.04	0.26	0.15	0.25	0.6	0.45
22993	Fructose-1,6-bisphosphate aldolase	2	2	1	0	0	0	2	2	2	0	0	0	0.021	0.48	0.072	0.0088	1	0.04
13396	coatomer COPII	3	1	2	0	0	0	1	3	3	0	0	0	0.0095	0.48	0.043	0.004	1	0.024
55035	Pyruvate dehydrogenase E1 component alpha subunit	3	2	2	0	0	0	0	1	2	0	0	0	0.0044	0.18	0.025	0.094	1	0.2
29217	possible methionine aminopeptidase, perhaps Co requiring	0	4	0	0	0	0	3	2	3	0	0	0	0.045	0.18	0.12	0.0018	1	0.014
12663	lactyolglutathione lyase	0	0	0	2	4	3	1	0	0	0	0	0	0.00061	0.49	1	0.0045	0.0038	0.59
30394	receptor mediated endocytosis protein-like protein	2	1	2	0	1	0	1	1	1	1	2	1	0.076	0.38	0.57	0.25	0.15	0.49
3851	conserved unknown protein like Tp7953	2	1	1	0	1	0	1	2	1	0	2	1	0.14	0.62	0.53	0.14	0.31	0.51
43658	unknown protein	0	1	1	1	1	2	1	0	1	3	2	1	0.42	0.68	0.19	0.43	0.34	0.2
45624	unknown protein	1	1	1	1	2	1	1	0	1	0	0	1	0.59	0.51	0.46	0.43	0.39	0.63
48918	conserved unknown, like Tp21060	0	1	1	2	2	2	1	1	0	1	0	1	0.2	0.68	0.54	0.21	0.38	0.55

Table A2 cont.

Protein Id, Description		Spectral Counting Abundance Scores												Fisher Exact Test P values					
		Colim			B12 lim			Fe lim			Replete			Colim vs B12 lim	Colim vs Fe lim	Colim vs replete	B12 lim vs Fe lim	B12 lim vs replete	Fe lim vs replete
		a	b	c	a	b	c	a	b	c	a	b	c						
22974	Acetate-CoA, ligase putative	1	2	2	0	0	0	1	0	1	1	2	1	0.021	0.24	0.57	0.21	0.051	0.34
45582	unknown protein	2	1	2	1	2	0	1	1	0	0	0	0	0.28	0.24	0.072	0.58	0.25	0.34
46321	unknown protein with Prenylated rab acceptor domain	0	0	1	2	2	2	1	0	0	0	2	1	0.056	0.74	0.37	0.06	0.29	0.37
49120	unknown protein	1	2	1	1	1	1	0	1	2	0	0	0	0.41	0.51	0.12	0.57	0.25	0.2
33463	possible Short-chain alcohol dehydrogenase	1	2	1	1	1	0	1	1	0	0	0	0	0.27	0.35	0.12	0.62	0.4	0.34
48103	putative soluble NSF attachment protein ortholog	1	1	1	1	1	0	2	3	1	0	0	0	0.43	0.24	0.21	0.093	0.4	0.04
23687	Ribosomal protein L35Ae	2	2	2	0	0	0	2	2	1	0	0	0	0.0095	0.52	0.043	0.019	1	0.069
49313	unknown protein, possible dehydrogenase domain	0	0	0	1	1	1	0	0	0	3	2	4	0.16	1	0.0047	0.16	0.071	0.0051
21201	UDP-sulfoquinovose synthase	2	2	2	0	0	0	3	2	1	0	0	0	0.0095	0.6	0.043	0.0088	1	0.04
39681	possible 3-hydroxyacyl-Coenzyme A dehydrogenase	2	1	3	0	0	0	1	0	2	0	0	0	0.0095	0.26	0.043	0.094	1	0.2
45580	coronin like protein	2	3	1	0	0	0	2	1	1	0	0	0	0.0095	0.39	0.043	0.043	1	0.12
50464	unknown protein with C-term rubredoxin domain	1	3	1	0	0	0	3	2	1	0	0	0	0.021	0.48	0.072	0.0088	1	0.04
YP_874467.1	30S ribosomal protein S8	3	2	1	0	0	0	1	3	1	0	0	0	0.0095	0.52	0.043	0.019	1	0.069
38413	tryptophan rich domain protein	0	0	0	1	1	2	0	0	0	4	3	4	0.085	1	0.00078	0.088	0.037	0.00087
29758	Zn binding aminopeptidase	3	1	1	0	0	0	2	4	1	0	0	0	0.021	0.37	0.072	0.004	1	0.024
27166	D-3-phosphoglycerate dehydrogenase [T	1	0	2	0	0	0	4	1	1	0	0	0	0.097	0.24	0.21	0.0088	1	0.04
42990	conserved unknown protein	0	0	0	1	0	2	0	0	0	4	5	1	0.16	1	0.0019	0.16	0.036	0.0021
46929	unknown protein, not in other algae, like bacterial periplasmic Fe binders	0	1	2	0	0	0	1	3	1	0	0	0	0.097	0.35	0.21	0.019	1	0.069
46770	possible SAM-dependant methyltransferase	1	2	0	0	0	0	2	2	0	0	0	0	0.097	0.49	0.21	0.043	1	0.12
16944	possible histidyl tRNA synthetase	1	2	0	0	0	0	3	2	1	0	0	0	0.097	0.24	0.21	0.0088	1	0.04
43564	RAD23, putative	1	1	1	2	1	1	0	1	0	1	2	1	0.59	0.32	0.47	0.25	0.52	0.2
48293	unknown protein	1	1	1	0	2	1	1	1	0	1	2	1	0.58	0.51	0.47	0.58	0.4	0.34

Table A2 cont.

Protein Id, Description		Spectral Counting Abundance Scores												Fisher Exact Test P values					
		Colim			B12 lim			Fe lim			Replete			Colim vs B12 lim	Colim vs Fe lim	Colim vs replete	B12 lim vs Fe lim	B12 lim vs replete	Fe lim vs replete
		a	b	c	a	b	c	a	b	c	a	b	c						
13047	cyclase-associated protein, putative	0	1	1	1	1	1	1	1	0	1	3	1	0.57	0.68	0.19	0.58	0.24	0.2
35590	unknown protein	0	1	0	1	1	1	2	1	0	1	2	1	0.37	0.3	0.19	0.57	0.4	0.49
44725	unknown protein	1	0	2	1	1	1	1	0	1	0	2	1	0.58	0.51	0.67	0.58	0.61	0.55
16243	ApaG protein	1	0	0	1	1	1	1	0	1	3	2	1	0.37	0.49	0.094	0.58	0.24	0.2
17259	Regulatory Proteasome Non-ATPase subunit 8	2	1	2	0	0	0	1	1	2	0	2	1	0.021	0.51	0.4	0.043	0.14	0.51
43181	unknwon protein	1	0	0	1	2	2	0	1	1	0	2	1	0.15	0.49	0.37	0.31	0.48	0.55
YP_874455.1	50S ribosomal protein L23	1	3	1	1	0	0	1	1	1	0	0	1	0.076	0.38	0.22	0.25	0.6	0.45
48054	frustulin 2	0	0	1	2	2	2	0	0	0	3	2	1	0.093	0.51	0.094	0.026	0.54	0.03
39528	Carbamoyl-phosphate synthase II	2	2	1	0	0	1	2	1	0	0	0	0	0.076	0.38	0.072	0.25	0.63	0.2
22418	catalase	0	1	0	1	1	2	0	0	0	1	2	3	0.24	0.51	0.094	0.088	0.34	0.03
19324	Histidine biosynthesis protein HisF	2	2	2	1	1	0	1	0	0	0	2	0	0.098	0.066	0.15	0.57	0.69	0.66
20434	Regulatory Proteasome Non-ATPase subunit 12	0	1	1	2	2	2	0	1	1	0	0	0	0.14	0.68	0.35	0.14	0.039	0.34
25521	unknown protein, oxidoreductase	1	1	1	1	0	0	3	2	2	0	0	0	0.26	0.16	0.21	0.019	0.63	0.024
42590	multicopy unknown protein	1	1	0	1	1	0	2	0	1	0	0	0	0.63	0.49	0.35	0.42	0.4	0.2
15689	Mitochondrial processing peptidase, alpha subunit	0	0	0	1	0	1	0	0	1	3	2	3	0.29	0.49	0.011	0.57	0.071	0.048
12411	Peptidylprolyl isomerase	0	0	0	1	1	2	0	0	0	1	2	4	0.085	1	0.011	0.088	0.21	0.012
21897	G protein beta subunit, putative	0	1	0	1	1	2	0	0	0	1	2	4	0.15	0.51	0.045	0.048	0.3	0.012
48909	unknown protein	0	0	0	2	2	2	0	0	0	3	2	1	0.025	1	0.028	0.026	0.54	0.03
YP_874466.1	50S ribosomal protein L5	2	2	1	0	0	0	2	1	2	0	0	0	0.021	0.61	0.072	0.019	1	0.069
54466	unknown protein, similar to ISIP	0	1	0	0	2	2	0	0	0	4	2	3	0.24	0.51	0.021	0.088	0.12	0.0051
2097	possible RNA helicase, DEAD box	1	1	1	0	0	0	1	2	1	0	0	0	0.097	0.49	0.21	0.043	1	0.12
18337	asparagine synthetase	2	1	2	0	0	0	1	2	1	0	0	0	0.021	0.51	0.072	0.043	1	0.12
17772	phosphoribosylformylglycinamidine synthase	1	1	2	0	0	0	1	2	2	0	0	0	0.045	0.49	0.12	0.019	1	0.069

Table A2 cont.

Protein Id, Description		Spectral Counting Abundance Scores												Fisher Exact Test P values					
		Colim			B12 lim			Fe lim			Replete			Colim vs B12 lim	Colim vs Fe lim	Colim vs replete	B12 lim vs Fe lim	B12 lim vs replete	Fe lim vs replete
		a	b	c	a	b	c	a	b	c	a	b	c						
28730	peptidyl-prolyl cis-trans isomerase	0	0	0	1	2	2	0	0	0	1	2	4	0.046	1	0.011	0.048	0.3	0.012
31447	conserved unknown protein	1	2	2	0	0	0	1	2	1	0	0	0	0.021	0.51	0.072	0.043	1	0.12
42289	lysyl-trna synthetase	1	1	0	0	1	0	3	2	0	0	0	0	0.44	0.22	0.35	0.072	0.63	0.069
48086	unknown protein	0	0	0	1	2	1	0	0	0	3	3	4	0.085	1	0.0019	0.088	0.068	0.0021
47461	unknown protein	0	1	1	0	0	1	3	1	3	0	0	0	0.44	0.084	0.35	0.019	0.63	0.024
30160	40S ribosomal protein	1	1	3	0	0	0	2	2	2	0	0	0	0.021	0.48	0.072	0.0088	1	0.04
48704	SAM dependent methyltransferase	0	1	0	2	2	3	0	1	0	0	0	0	0.034	0.74	0.59	0.036	0.024	0.59
YP_87 4454.1	50S ribosomal protein L4	1	1	3	0	0	0	3	1	0	0	0	0	0.021	0.51	0.072	0.043	1	0.12
15068	Coproporphyrinogen III oxidase	0	0	0	2	1	0	0	0	0	3	3	5	0.16	1	0.00078	0.16	0.018	0.00087
51214	Ferredoxin-dependent glutamate synthase	1	0	2	0	0	0	0	2	1	0	0	0	0.097	0.65	0.21	0.094	1	0.2
42051	aspartate-trna ligase	0	1	0	0	0	0	1	2	0	0	0	0	0.46	0.3	0.59	0.094	1	0.2
10068	enoyl-ACP reductase	1	0	0	1	1	2	0	1	1	1	2	1	0.24	0.49	0.19	0.43	0.52	0.34
18524	threonyl-tRNA synthetase	2	1	1	0	0	0	2	1	1	1	0	1	0.045	0.62	0.53	0.043	0.14	0.51
49054	unknown protein ankyrin repeat and possible ion itransport domain	1	1	2	1	1	2	0	0	1	1	0	0	0.55	0.19	0.32	0.25	0.39	0.66
47473	unknown protein with cytochrome c oxidase-like domain	1	1	1	1	1	1	2	0	1	0	0	0	0.58	0.65	0.21	0.57	0.25	0.2
44547	unknown protein witn ankyrin repeat and possible Pho88 domain	1	2	1	1	0	1	1	1	1	0	0	0	0.27	0.51	0.12	0.42	0.4	0.2
31440	Acyl Carrier Protein	0	1	0	2	2	1	0	0	0	1	2	1	0.15	0.51	0.19	0.048	0.62	0.071
46336	conserved unknown protein	0	0	1	0	0	2	1	0	1	1	3	1	0.56	0.49	0.094	0.62	0.14	0.2
46395	unknown protein	0	0	0	2	2	1	1	0	0	1	3	1	0.046	0.49	0.028	0.16	0.44	0.099
30246	zn dependant dehydrogenase	2	2	1	0	0	2	1	0	1	1	0	0	0.17	0.24	0.22	0.62	0.69	0.63
30670	possible ribosomal protein 21	1	0	2	2	1	1	1	0	2	0	0	0	0.59	0.65	0.21	0.6	0.16	0.2
7173	6,7-dimethyl-8-ribityllumazine synthase	1	0	0	2	1	2	0	1	1	1	0	0	0.15	0.49	0.65	0.31	0.28	0.63
42794	unknown protein, cytochrome c-like domains	1	1	0	0	0	2	0	0	2	3	2	0	0.63	0.68	0.33	0.62	0.27	0.34

Table A2 cont.

Protein Id, Description		Spectral Counting Abundance Scores												Fisher Exact Test P values					
		Colim			B12 lim			Fe lim			Replete			Colim vs B12 lim	Colim vs Fe lim	Colim vs replete	B12 lim vs Fe lim	B12 lim vs replete	Fe lim vs replete
		a	b	c	a	b	c	a	b	c	a	b	c						
43945	unknown protein, possible peptidase domain	1	0	1	2	0	1	3	1	1	0	0	0	0.57	0.22	0.35	0.27	0.25	0.069
55122	HSP70 family protein	0	2	1	0	0	1	1	1	0	0	0	1	0.26	0.51	0.46	0.43	0.6	0.63
46709	unknown protein	1	0	1	0	0	0	0	1	0	1	2	3	0.21	0.51	0.19	0.45	0.019	0.099
29824	possible isoleucine-trna synthetase	0	0	1	0	0	1	2	2	1	1	0	0	0.71	0.1	0.65	0.072	0.6	0.21
45947	3-ketoacyl-coa thiolase	0	0	0	2	0	0	1	1	1	4	0	3	0.29	0.12	0.011	0.42	0.071	0.2
44382	possible Clp peptidase	2	1	2	0	0	0	1	1	2	0	0	0	0.021	0.51	0.072	0.043	1	0.12
42911	unknown protein	0	0	2	0	1	2	0	0	1	0	0	1	0.57	0.51	0.63	0.38	0.53	0.66
43532	conserved unknown with peptidase dimerization domain, like Tp6045	0	0	0	1	1	2	0	0	0	4	2	1	0.046	1	0.011	0.048	0.3	0.012
50796	possible Peptide chain release factor eRF/aRF subunit	0	0	0	0	0	0	0	2	1	0	0	0	1	0.12	1	0.094	1	0.2
49879	unknown protein	0	0	0	2	1	1	0	0	0	1	3	0	0.046	1	0.068	0.048	0.62	0.071
YP_874390.1	magnesium-chelatase subunit I	2	3	0	1	0	0	0	0	1	0	0	1	0.076	0.11	0.22	0.7	0.6	0.66
23164	Peptidyl-prolyl cis-trans isomerase	0	1	3	0	0	0	2	0	2	0	0	0	0.045	0.62	0.12	0.043	1	0.12
50738	possible triosephosphate isomerase	1	0	0	2	2	1	1	0	0	1	0	1	0.15	0.74	0.37	0.16	0.48	0.37
43097	prolyl-tRNA synthetase, Zn binding	0	0	0	1	1	2	1	0	0	1	3	1	0.085	0.49	0.028	0.25	0.34	0.099
43817	unknown protein, conserved domain	2	1	1	0	0	0	1	2	1	0	2	0	0.045	0.62	0.32	0.043	0.37	0.31
9799	fucoxanthin chlorophyll a/c protein	0	0	0	1	2	1	0	0	0	1	2	3	0.085	1	0.028	0.088	0.34	0.03
45204	unknown protein, like Tp20808	2	1	0	0	1	1	2	1	0	0	2	0	0.43	0.65	0.46	0.42	0.69	0.45
13877	Chlorophyll A-B binding protein	0	0	0	1	1	1	0	1	1	1	0	3	0.16	0.24	0.068	0.58	0.4	0.34
44484	unknown protein	1	0	1	1	1	0	2	2	1	0	0	0	0.63	0.22	0.35	0.16	0.4	0.069
9612	pyrophosphokinase-like protein	0	0	0	1	1	1	0	0	1	3	0	3	0.16	0.49	0.028	0.38	0.24	0.099
42659	possible flavin reductase	0	0	1	1	1	2	0	0	1	1	3	0	0.24	0.74	0.19	0.25	0.52	0.2
16854	Glutaredoxin, probably cytosolic	1	1	1	0	0	1	2	2	1	0	0	0	0.26	0.35	0.21	0.072	0.63	0.069
52648	3-oxoacyl-[acyl-carrier-protein] synthase	2	1	0	1	1	0	0	2	1	0	0	0	0.43	0.65	0.21	0.42	0.4	0.2

Table A2 cont.

Protein Id, Description		Spectral Counting Abundance Scores												Fisher Exact Test P values					
		Colim			B12 lim			Fe lim			Replete			Colim vs B12 lim	Colim vs Fe lim	Colim vs replete	B12 lim vs Fe lim	B12 lim vs replete	Fe lim vs replete
		a	b	c	a	b	c	a	b	c	a	b	c						
YP_874460.1	30S ribosomal protein S3	0	0	1	2	0	1	2	1	2	0	0	0	0.37	0.1	0.59	0.27	0.25	0.069
54026	unknown proetin	1	1	2	1	0	0	2	2	0	0	0	0	0.14	0.62	0.12	0.14	0.63	0.12
44216	Rab-family small GTPase	0	0	1	2	2	2	1	0	0	0	0	0	0.093	0.74	0.59	0.098	0.062	0.59
47027	unknown protein, possible protosome domain	1	0	1	0	0	0	3	2	2	0	0	0	0.21	0.084	0.35	0.004	1	0.024
21988	PEP utilizing plastid enzyme	0	0	1	0	2	0	0	1	0	0	0	1	0.56	0.74	0.65	0.57	0.69	0.66
11204	carboxypeptidase	3	1	2	0	0	0	0	2	0	0	0	0	0.0095	0.15	0.043	0.21	1	0.34
bd645	Acetyl-coenzyme A synthetase, putative	0	0	0	2	0	0	1	0	0	0	2	3	0.29	0.49	0.068	0.57	0.27	0.2
46210	Calcium/calmodulin dependent protein kinase domain protein	0	0	0	1	1	1	0	0	1	1	2	3	0.16	0.49	0.028	0.38	0.24	0.099
51810	Rab-type small GTPase, ortholog of T. pseudonana TPS_100340	1	2	1	0	0	2	2	2	2	0	0	0	0.27	0.36	0.12	0.093	0.4	0.04
45953	ras-related GTP-ase protein	1	1	0	0	0	1	1	2	1	0	0	0	0.44	0.33	0.35	0.14	0.63	0.12
13078	unknown protein with Sulfate permease-like domain	1	1	0	1	1	0	1	0	2	0	0	0	0.63	0.49	0.35	0.42	0.4	0.2
32031	unknown protein	0	0	0	2	1	1	1	1	1	0	0	0	0.085	0.12	1	0.6	0.16	0.2
34010	Alanine aminotransferase	1	2	1	0	0	0	1	1	2	0	0	0	0.045	0.62	0.12	0.043	1	0.12
42989	unknown protein	1	0	1	0	1	0	2	1	1	0	0	0	0.44	0.33	0.35	0.14	0.63	0.12
1372	unknown protein with hydrolase domain	0	0	1	1	1	1	0	0	0	1	0	3	0.37	0.51	0.19	0.16	0.4	0.071
27719	Aminopeptidase, Zn dependant	0	0	0	2	2	1	0	0	1	0	2	0	0.046	0.49	0.41	0.16	0.28	0.66
41812	Succinate dehydrogenase (ubiquinone) flavoprotein	0	1	2	0	0	0	1	0	1	1	0	0	0.097	0.51	0.46	0.21	0.37	0.63
54863	Tryptophan rich domain protein	0	0	0	0	2	1	0	0	0	3	2	1	0.16	1	0.028	0.16	0.24	0.03
3137	possible sorting nexin	1	0	0	0	0	0	1	2	1	0	0	1	0.46	0.18	0.65	0.043	0.37	0.31
46626	cysteine hydrolase	0	0	0	0	0	0	0	1	1	3	3	1	1	0.24	0.011	0.21	0.007	0.11
44756	ATP-binding cassette superfamily protein	2	1	1	0	0	1	0	1	0	0	0	0	0.14	0.19	0.12	0.7	0.63	0.59
44318	N-terminal Histone linker	1	2	2	0	0	1	1	0	0	0	0	0	0.076	0.11	0.072	0.7	0.63	0.59

Table A2 cont.

Protein Id, Description		Spectral Counting Abundance Scores												Fisher Exact Test P values					
		Colim			B12 lim			Fe lim			Replete			Colim vs B12 lim	Colim vs Fe lim	Colim vs replete	B12 lim vs Fe lim	B12 lim vs replete	Fe lim vs replete
		a	b	c	a	b	c	a	b	c	a	b	c						
41702	Tryptophan synthase	3	0	1	0	0	0	1	0	1	0	0	0	0.045	0.35	0.12	0.21	1	0.34
40070	unknown protein, initiation factor domain	0	2	1	0	0	1	0	0	0	0	0	0	0.26	0.13	0.21	0.55	0.63	1
47804	Ribosomal protein L37-like	0	0	2	0	1	0	1	0	1	0	0	0	0.44	0.68	0.35	0.43	0.63	0.34
51245	Propionyl-CoA carboxylase	2	0	0	0	0	0	1	3	1	0	0	0	0.21	0.22	0.35	0.019	1	0.069
26975	translation initiation factor 3	3	1	2	0	0	0	1	0	0	0	0	0	0.0095	0.066	0.043	0.45	1	0.59
32916	imidazoleglycerol-phosphate dehydratase	0	0	0	2	2	1	0	1	0	0	0	0	0.013	0.49	1	0.06	0.039	0.59
54442	alpha-adaptin subunit of the AP1 vesicle coat complex	1	1	0	0	0	0	0	2	0	0	0	0	0.21	0.68	0.35	0.21	1	0.34
9035	Glutaredoxin family protein	0	0	0	2	2	2	0	0	0	0	0	0	0.013	1	1	0.014	0.039	1
51407	pol1-like DNA polymerase	0	1	2	0	0	0	0	0	0	0	0	0	0.097	0.13	0.21	1	1	1
45028	unknown protein	0	0	0	1	1	1	0	0	0	3	2	1	0.16	1	0.028	0.16	0.24	0.03
37959	unknown protein like Tp 261275	1	0	0	2	1	1	0	1	1	0	0	0	0.24	0.49	0.59	0.43	0.16	0.34
43127	unknown transmembrane protein	0	0	1	1	0	1	0	1	1	3	0	0	0.56	0.49	0.37	0.62	0.47	0.55
31339	P450- obtusifoliol 14-alpha demethylase	1	1	1	0	0	0	1	2	1	0	0	0	0.097	0.49	0.21	0.043	1	0.12
YP_874470.1	30S ribosomal protein S5	1	1	1	0	0	0	1	1	2	0	0	0	0.097	0.49	0.21	0.043	1	0.12
45284	Medium chain (mu subunit) of AP4 complex, clathrin protein	1	1	1	0	0	0	1	1	2	0	0	0	0.097	0.49	0.21	0.043	1	0.12
18323	inositol 1-monophosphatase-like protein	0	0	0	1	0	1	0	0	0	1	2	3	0.29	1	0.028	0.3	0.14	0.03
1155	proline dehydrogenase	2	1	0	0	0	0	1	1	1	0	0	0	0.097	0.65	0.21	0.094	1	0.2
YP_874446.1	30S ribosomal protein S16	2	1	0	0	0	1	1	0	1	0	0	0	0.26	0.51	0.21	0.43	0.63	0.34
13382	ribose-5-phosphate isomerase	1	0	2	1	1	0	1	0	0	0	0	0	0.43	0.32	0.21	0.57	0.4	0.59
48058	unknown protein, possible Ni-related domain	1	0	0	1	1	2	0	0	0	0	0	1	0.24	0.51	0.65	0.088	0.39	0.41
9883	possible glutaredoxin	0	1	0	2	1	1	1	0	0	0	0	0	0.24	0.74	0.59	0.25	0.16	0.59
YP_874438.1	50S ribosomal protein L21	2	0	0	1	1	0	1	0	1	0	0	0	0.63	0.68	0.35	0.62	0.4	0.34

Table A2 cont.

Protein Id, Description		Spectral Counting Abundance Scores												Fisher Exact Test P values					
		Colim			B12 lim			Fe lim			Replete			Colim vs B12 lim	Colim vs Fe lim	Colim vs replete	B12 lim vs Fe lim	B12 lim vs replete	Fe lim vs replete
		a	b	c	a	b	c	a	b	c	a	b	c						
40521	hypothetical protein, v-SNARE domain	1	1	1	0	0	0	1	0	2	0	0	0	0.097	0.65	0.21	0.094	1	0.2
49571	unknown protein with leucine-rich repeat	0	1	0	0	1	2	0	0	0	3	2	0	0.37	0.51	0.19	0.16	0.4	0.071
20708	probable aspartyl aminopeptidase	0	0	0	1	1	1	0	0	0	0	2	3	0.16	1	0.068	0.16	0.4	0.071
12379	possible peroxisomal membrane protein-related	2	1	1	0	0	0	2	0	1	0	0	0	0.045	0.51	0.12	0.094	1	0.2
13511	gamma subunit of tetrameric clathrin adaptor complex AP2	1	0	0	0	0	0	0	0	2	1	0	0	0.46	0.49	0.65	0.21	0.37	0.63
44554	unknown protein with HMG box	1	1	2	0	0	1	0	0	2	0	0	0	0.14	0.35	0.12	0.43	0.63	0.34
13662	conserved unknown protein	1	1	0	0	0	0	2	1	2	0	0	0	0.21	0.22	0.35	0.019	1	0.069
47824	conserved unknown like Tp3563 with WD40 domain	0	0	0	1	1	2	0	0	1	0	0	1	0.085	0.49	0.41	0.25	0.39	0.66
13005	Glutathione peroxidase	0	0	0	1	1	2	0	0	0	0	2	0	0.085	1	0.41	0.088	0.39	0.41
3241	LETM1 domain containing protein	1	2	1	0	0	0	0	1	0	0	0	0	0.045	0.19	0.12	0.45	1	0.59
52619	Purine permease	1	1	0	0	0	0	0	1	2	0	0	0	0.21	0.49	0.35	0.094	1	0.2
33356	thioredoxin y	0	0	0	1	2	2	0	0	0	0	2	1	0.046	1	0.17	0.048	0.48	0.17
15777	possible ferredoxin NADP(+) reductase	0	0	0	3	0	2	0	0	0	7	6	5	0.013	1	0.000009	0.014	0.011	0.000011
43348	unknown protein like Tp5394	2	1	1	0	0	0	1	0	0	0	0	0	0.045	0.19	0.12	0.45	1	0.59
bd387	putative ATPase-like zinc transporter	2	1	0	0	0	0	1	1	0	0	0	0	0.097	0.51	0.21	0.21	1	0.34
51703	violaxanthin deepoxidase	0	2	1	1	0	1	0	0	0	0	0	0	0.43	0.13	0.21	0.3	0.4	1
14770	unknown protein with thioredoxin domain	0	1	2	0	0	0	0	1	1	0	0	0	0.097	0.51	0.21	0.21	1	0.34
14762	Isocitrate dehydrogenase	0	2	2	0	0	0	0	1	2	0	0	0	0.045	0.51	0.12	0.094	1	0.2
12620	conserved unknown with AAA domain	1	0	1	0	0	0	2	0	2	0	0	0	0.21	0.33	0.35	0.043	1	0.12
17948	Chromatin assembly factor subunit C	0	0	0	2	0	2	0	0	0	0	2	1	0.085	1	0.17	0.088	0.6	0.17
47962	unknown protein with signal peptide and ubiquitin domain	0	0	1	0	2	0	0	0	0	0	0	0	0.56	0.51	0.59	0.3	0.4	1
YP_874450.1	photosystem II subunit	0	0	0	0	1	2	0	0	0	0	0	0	0.085	1	1	0.088	0.16	1

Table A2 cont.

Protein Id, Description		Spectral Counting Abundance Scores												Fisher Exact Test P values					
		Colim			B12 lim			Fe lim			Replete			Colim vs B12 lim	Colim vs Fe lim	Colim vs replete	B12 lim vs Fe lim	B12 lim vs replete	Fe lim vs replete
		a	b	c	a	b	c	a	b	c	a	b	c						
46212	unknown protein	0	0	0	1	2	1	0	0	0	1	2	0	0.085	1	0.17	0.088	0.6	0.17
bd1870	unknown protein with signal peptide and tryptophan rich domain	0	0	0	0	1	1	1	0	0	3	0	1	0.29	0.49	0.068	0.57	0.27	0.2
50437	C2 domain containing protein	0	0	1	0	1	1	0	2	1	0	0	0	0.56	0.3	0.59	0.42	0.4	0.2
23959	polyadenlyte binding protein	1	0	0	1	1	0	0	0	2	0	2	0	0.56	0.49	0.65	0.62	0.69	0.63
30315	RL18, ribosomal protein 18, 60S	1	0	1	0	0	0	2	1	1	0	0	0	0.21	0.33	0.35	0.043	1	0.12
42504	sec14p-like protein	2	1	1	0	0	0	1	0	1	0	0	0	0.045	0.35	0.12	0.21	1	0.34
47954	conserved unknown with mitochondrial substrate carrier domain	0	1	1	0	0	0	1	1	2	0	0	0	0.21	0.33	0.35	0.043	1	0.12
50034	CTP synthase	1	1	2	0	0	0	0	1	1	0	0	0	0.045	0.35	0.12	0.21	1	0.34
44902	Aspartate--ammonia ligase	1	1	2	0	0	0	1	1	0	0	0	0	0.045	0.35	0.12	0.21	1	0.34
45034	multicopy unknown protein	0	0	0	1	2	1	1	0	0	0	0	0	0.085	0.49	1	0.25	0.16	0.59
47412	possible DEAD/DEAH box RNA helicase	0	1	0	0	0	0	2	0	0	1	0	1	0.46	0.49	0.37	0.21	0.14	0.55
47811	unknown protein	0	1	0	0	0	0	0	2	0	1	0	1	0.46	0.49	0.37	0.21	0.14	0.55
49229	fomate-tetrahydrofolate ligase	2	0	0	0	0	0	0	1	1	0	2	0	0.21	0.68	0.63	0.21	0.37	0.63
46664	D-lactate dehydrogenase	1	0	0	1	0	0	1	0	0	3	0	0	0.71	0.74	0.37	0.7	0.31	0.37
12989	PLP-dependant amidotransferase	0	2	1	0	0	0	0	2	1	0	0	0	0.097	0.65	0.21	0.094	1	0.2
29174	importin alpha 1 subunit-like protein	2	0	1	0	0	0	2	0	1	0	0	0	0.097	0.65	0.21	0.094	1	0.2
48121	unknown protein	0	0	0	1	0	0	2	1	0	0	0	1	0.54	0.12	0.41	0.25	0.6	0.45
24739	glutamate synthase	1	0	2	0	0	0	0	1	1	0	0	0	0.097	0.51	0.21	0.21	1	0.34
23691	RS15A, ribosomal protein 15 40S small ribosomal subunit	1	1	0	0	0	0	2	1	0	0	0	0	0.21	0.49	0.35	0.094	1	0.2
47167	unknown protein with cell wall anchor domain	1	0	0	0	0	2	0	0	0	0	0	0	0.56	0.51	0.59	0.3	0.4	1
4937	unknown protein with AAA+ ATPase domain	0	0	1	0	0	0	1	1	2	0	0	0	0.46	0.18	0.59	0.043	1	0.12
36043	unknown protein with ubiquitin-associated domain	1	0	2	0	0	0	0	0	0	0	0	0	0.097	0.13	0.21	1	1	1

Table A2 cont.

Protein Id, Description		Spectral Counting Abundance Scores												Fisher Exact Test P values					
		Colim			B12 lim			Fe lim			Replete			Colim vs B12 lim	Colim vs Fe lim	Colim vs replete	B12 lim vs Fe lim	B12 lim vs replete	Fe lim vs replete
		a	b	c	a	b	c	a	b	c	a	b	c						
45016	unknown protein like Tp 3932	0	0	0	0	0	1	2	2	0	0	0	0	0.54	0.06	1	0.14	0.63	0.12
10747	flavin-reductase like protein, like Tp25787	0	0	0	0	0	1	0	0	1	0	0	3	0.54	0.49	0.17	0.7	0.31	0.37
30977	possible cell cycle protein like Tp34996	0	0	0	2	0	1	0	0	0	0	0	0	0.16	1	1	0.16	0.25	1
23371	YchF GTP-binding protein, like Tp 39710	0	1	0	0	0	0	2	1	0	0	0	0	0.46	0.3	0.59	0.094	1	0.2
10862	V-ATPase subunit C	0	0	0	0	1	2	1	0	0	0	0	0	0.16	0.49	1	0.38	0.25	0.59
42614	unknown protein	0	0	0	0	0	1	0	2	0	0	0	0	0.54	0.24	1	0.43	0.63	0.34
3140	probable phosphoribosyl-amp cyclohydrolase	0	0	0	0	0	0	0	1	0	4	0	0	1	0.49	0.068	0.45	0.051	0.2
43697	branched chain AA amidotransferase-like	0	0	0	1	0	0	0	0	0	3	2	1	0.54	1	0.028	0.55	0.067	0.03
42904	unknown protein	0	0	0	1	1	2	0	0	0	0	2	0	0.085	1	0.41	0.088	0.39	0.41
19300	Regulatory Proteasome Non-ATPase subunit	0	2	1	0	0	0	1	0	1	0	0	0	0.097	0.51	0.21	0.21	1	0.34
48250	unknown protein	1	0	0	0	0	2	0	1	1	0	0	0	0.56	0.49	0.59	0.62	0.4	0.34
54395	fasciclin domain containing protein	0	1	0	2	1	1	0	0	0	0	0	0	0.24	0.51	0.59	0.088	0.16	1
14715	50S ribosomal protein L10-like	0	0	0	1	2	1	0	0	1	0	0	0	0.085	0.49	1	0.25	0.16	0.59
16840	Gamma carbonic anhydrase-like protein, metal binding site	1	1	1	0	2	0	0	0	0	0	0	0	0.43	0.13	0.21	0.3	0.4	1
YP_874474.1	30S ribosomal protein S11	1	1	0	0	0	0	1	2	0	0	0	0	0.21	0.49	0.35	0.094	1	0.2
31718	possible inosine-5'-monophosphate dehydrogenase	2	0	1	0	0	0	1	0	0	0	0	0	0.097	0.32	0.21	0.45	1	0.59
49377	unknown protein	0	0	0	2	1	0	0	0	0	0	0	0	0.16	1	1	0.16	0.25	1
19152	possible 60S Ribosomal protein L24	2	0	0	0	0	0	1	0	2	0	0	0	0.21	0.49	0.35	0.094	1	0.2
40933	possible Clp protease	0	0	0	0	2	0	1	2	0	0	0	0	0.29	0.12	1	0.42	0.4	0.2
31535	multicopy unknown protein	0	0	1	0	0	0	2	0	1	0	0	0	0.46	0.3	0.59	0.094	1	0.2
47966	unknown protein	0	0	0	0	0	1	0	0	0	3	0	1	0.54	1	0.068	0.55	0.15	0.071
46323	unknown protein	1	1	0	0	0	0	0	0	2	0	0	0	0.21	0.68	0.35	0.21	1	0.34

Table A2 cont.

Protein Id, Description		Spectral Counting Abundance Scores												Fisher Exact Test P values					
		Colim			B12 lim			Fe lim			Replete			Colim vs B12 lim	Colim vs Fe lim	Colim vs replete	B12 lim vs Fe lim	B12 lim vs replete	Fe lim vs replete
		a	b	c	a	b	c	a	b	c	a	b	c						
48524	conserved unknown protein	0	0	0	1	2	1	0	0	0	0	0	0	0.085	1	1	0.088	0.16	1
46005	unknown protein like Tp11085	0	0	1	0	0	0	0	2	0	0	0	0	0.46	0.49	0.59	0.21	1	0.34
43779	unknown protein like Tp21839	1	2	0	0	0	0	0	0	0	0	0	0	0.097	0.13	0.21	1	1	1
42790	unknown protein	0	0	0	0	1	2	0	0	0	0	0	1	0.085	1	0.41	0.088	0.39	0.41
47860	unknown protein	0	0	2	0	0	0	0	0	0	0	0	0	0.21	0.26	0.35	1	1	1
25739	NAD-dependant oxidoreductase	0	0	0	0	0	0	0	0	0	1	2	3	1	1	0.028	1	0.019	0.03
49480	possible gamma-butyrobetaine hydroxylase	0	0	0	0	0	0	0	0	0	1	3	1	1	1	0.028	1	0.019	0.03
18769	unknown protein like Tp 17707	0	0	1	0	0	0	0	2	0	0	2	0	0.46	0.49	0.65	0.21	0.37	0.63
44192	unknown protein	1	0	2	0	0	0	0	0	0	0	0	1	0.097	0.13	0.46	1	0.37	0.41
43856	unknown protein, like Tp24145	0	0	0	0	0	0	2	1	1	0	0	0	1	0.06	1	0.043	1	0.12
44357	unknown protein	0	0	0	0	0	0	1	2	1	0	0	0	1	0.06	1	0.043	1	0.12
45227	unknown protein	0	0	1	0	0	0	1	0	2	0	0	0	0.46	0.3	0.59	0.094	1	0.2
bd1638	WD-40 repeat-containing protein	0	0	0	1	0	0	0	2	1	0	0	0	0.54	0.12	1	0.25	0.63	0.2
16683	putative hydroxyacylglutathione hydrolase	0	0	0	1	2	1	0	0	0	0	0	0	0.085	1	1	0.088	0.16	1
8058	unknown protein with ankyrin repeat	1	0	0	0	0	0	0	0	0	3	0	0	0.46	0.51	0.37	1	0.14	0.17
50546	conserved unknown protei	0	0	0	0	0	0	2	0	0	1	0	0	1	0.24	0.41	0.21	0.37	0.63
17779	nucleosome assembly protein	1	0	2	0	0	0	0	0	0	0	0	0	0.097	0.13	0.21	1	1	1
YP_874456.1	50S ribosomal protein L2	0	0	0	0	0	0	0	1	2	0	0	0	1	0.12	1	0.094	1	0.2
47036	putative protein kinase	0	0	0	0	2	0	0	0	0	0	0	1	0.29	1	0.41	0.3	0.69	0.41
22913	kinase pyruvate kinase 5	0	2	1	0	0	0	0	0	0	0	0	0	0.097	0.13	0.21	1	1	1
50516	unknown protein with Na+/H+ exchange domain	2	0	0	0	0	0	1	0	0	0	0	0	0.21	0.51	0.35	0.45	1	0.59
49420	unknown protein with CorA Metal Ion Transporter domain	0	0	0	0	0	0	1	0	2	0	0	0	1	0.12	1	0.094	1	0.2
42443	WD-40 repeat-containing protein	0	0	0	0	0	2	0	0	1	0	0	0	0.29	0.49	1	0.57	0.4	0.59

Table A2 cont.

Protein Id, Description		Spectral Counting Abundance Scores												Fisher Exact Test P values					
		Colim			B12 lim			Fe lim			Replete			Colim vs B12 lim	Colim vs Fe lim	Colim vs replete	B12 lim vs Fe lim	B12 lim vs replete	Fe lim vs replete
		a	b	c	a	b	c	a	b	c	a	b	c						
40621	l-serine ammonia-lyase	0	0	0	0	0	2	0	0	1	0	0	0	0.29	0.49	1	0.57	0.4	0.59
46550	conserved unknown	0	1	0	0	0	2	0	0	0	0	0	0	0.56	0.51	0.59	0.3	0.4	1
18202	possible atp-dependent serine protease	2	0	0	0	0	0	2	0	0	0	0	0	0.21	0.68	0.35	0.21	1	0.34
55126	PFP Pyrophosphate dependent phosphofructokinase	0	0	2	0	0	0	0	0	2	0	0	0	0.21	0.68	0.35	0.21	1	0.34
55197	oligosaccharyl transferase/asparagine N-glycosyltransferase	0	2	0	0	0	1	0	0	0	0	0	0	0.44	0.26	0.35	0.55	0.63	1
55200	proton-transporting ATPase 3A	0	0	0	0	0	0	1	0	3	0	0	0	1	0.06	1	0.043	1	0.12
47730	contains a Muts domain	0	0	2	0	0	0	0	0	0	0	0	0	0.21	0.26	0.35	1	1	1
46727	unknown protein with NAD-dependant epimerase domain	0	0	0	0	2	0	0	0	0	0	0	0	0.29	1	1	0.3	0.4	1
45782	conserved unknown with choline transporter-like domain	0	0	0	0	0	2	0	0	0	1	0	0	0.29	1	0.41	0.3	0.69	0.41
18228	Triosephosphate isomerase putative	0	0	0	2	1	0	0	0	0	0	0	0	0.16	1	1	0.16	0.25	1
35960	unknown protein	0	0	0	0	1	2	0	0	0	0	0	0	0.16	1	1	0.16	0.25	1
9033	unknown protein with SNARE motif	0	0	0	0	1	2	0	0	0	0	0	0	0.16	1	1	0.16	0.25	1
46448	possible HSP	0	0	0	0	0	0	2	1	0	0	0	0	1	0.12	1	0.094	1	0.2
50971	glutamate dehydrogenase	0	0	0	0	0	0	1	2	0	0	0	0	1	0.12	1	0.094	1	0.2
21821	casein kinase-like protein	1	0	2	0	0	0	0	0	0	0	0	0	0.097	0.13	0.21	1	1	1
32113	unknown protein	1	0	0	0	0	2	0	0	0	0	0	0	0.56	0.51	0.59	0.3	0.4	1
39402	early-response-to-dehydration protein	1	0	0	0	0	0	2	0	0	0	0	0	0.46	0.49	0.59	0.21	1	0.34
46937	unknown protein	1	0	0	0	0	0	0	2	0	0	0	0	0.46	0.49	0.59	0.21	1	0.34
34119	cysteine desulfurase IscS	0	0	0	0	0	0	0	0	2	0	0	0	1	0.24	1	0.21	1	0.34
46767	unknown protein	0	0	0	0	0	0	2	0	0	0	0	0	1	0.24	1	0.21	1	0.34
46582	possible Glycoside hydrolase	0	0	0	2	0	0	0	0	0	0	0	0	0.29	1	1	0.3	0.4	1
36597	possible ATPase	2	0	0	0	0	0	0	0	0	0	0	0	0.21	0.26	0.35	1	1	1
11313	pentapeptide repeat-containing	0	0	0	0	0	2	0	0	0	0	0	0	0.16	1	1	0.16	0.25	1

Table A2 cont.

Protein Id, Description		Spectral Counting Abundance Scores												Fisher Exact Test P values					
		Colim			B12 lim			Fe lim			Replete			Colim vs B12 lim	Colim vs Fe lim	Colim vs replete	B12 lim vs Fe lim	B12 lim vs replete	Fe lim vs replete
		a	b	c	a	b	c	a	b	c	a	b	c						
42832	Superoxide dismutase, Fe/Mn-type	0	0	0	0	0	2	0	0	0	0	0	0	0.29	1	1	0.3	0.4	1
47133	unknown protein	0	0	0	0	2	0	0	0	0	0	0	0	0.29	1	1	0.3	0.4	1
48489	conserved unknown like Tp 21475	0	0	0	0	0	0	0	0	2	0	0	0	1	0.24	1	0.21	1	0.34
48678	unknwon multicopy protein	0	0	0	0	0	2	0	0	0	0	0	0	0.29	1	1	0.3	0.4	1
23314	kinesin-related protein 2 homolog p27 kip1	0	0	0	0	0	0	0	2	0	0	0	0	1	0.24	1	0.21	1	0.34